JANUARY 1984

analytical chemistry

69

ห้าเงิน

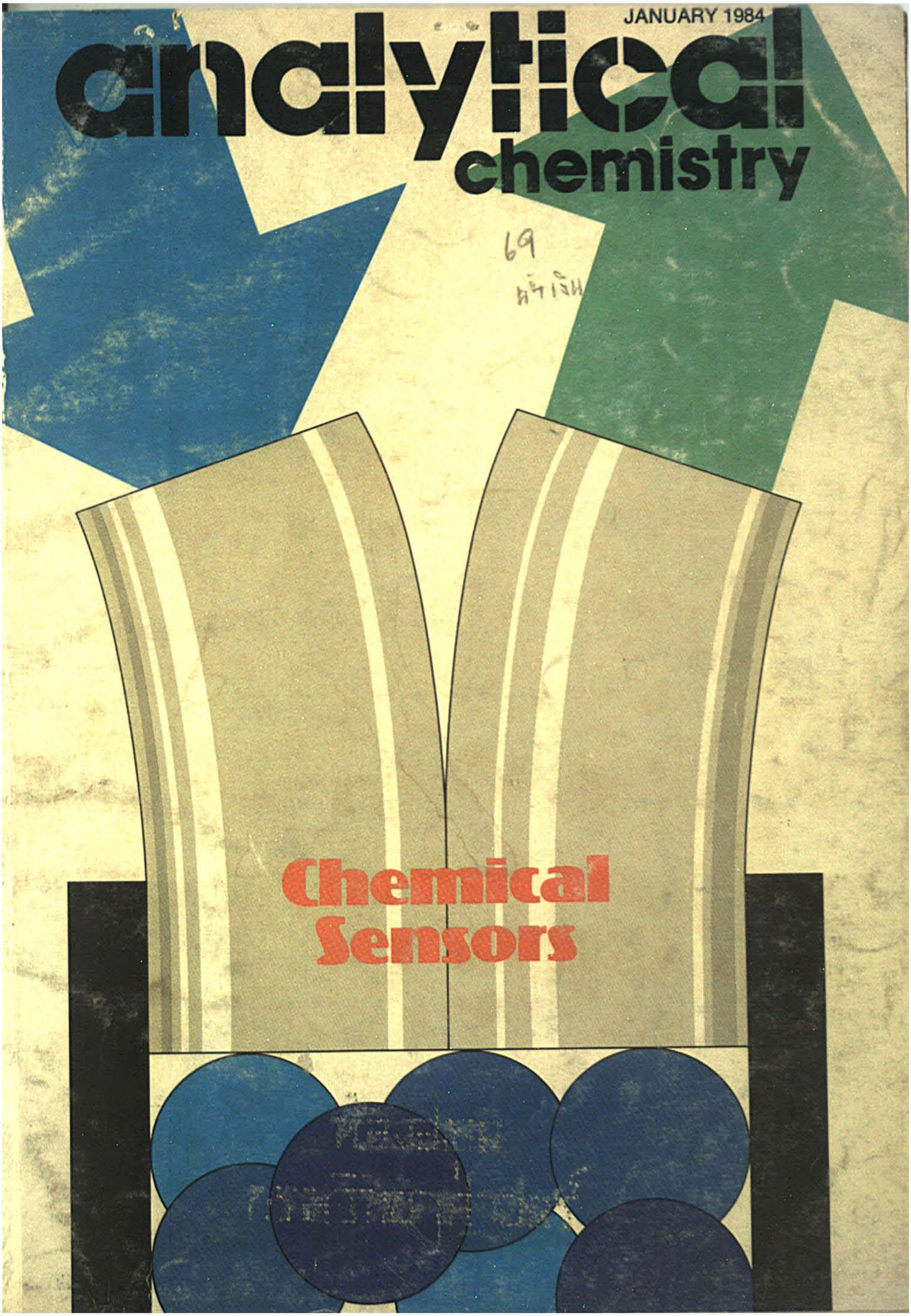

Chemical Sensors

Kevex XRF Deserves a Closer Look.

BA=0.16%
FE=47 PPM
CU= 7 PPM
ZN=0.04%
ZN->
BA
FE
CU

There are a lot of ways to perform quantitative elemental analysis, and you're probably familiar with most of them. Atomic absorption, wet chemistry, arc and spark emission are all standard analytical resources. A more recent development, ICP, is another alternative.

Energy-Dispersive X-Ray Fluorescence

Kevex would like you to take a closer look at one more possibility: energy-dispersive x-ray fluorescence. Because while all these methods perform similar analytical functions, XRF has some outstanding advantages.

Fast, Multi-element Analysis

X-ray fluorescence simultaneously detects all elements heavier than fluorine, allowing complete qualitative and quantitative analysis in a single run. By using multiple-element secondary targets, you can optimize detection limits for several elements at once, when critical results are sought. And analyses typically last only a few minutes.

A Broad Dynamic Range

Because XRF isn't vulnerable to many of the interferences that plague AA and ICP, you can use it to determine elemental concentrations from a few parts per million (or even parts per billion in organic matrices) to one hundred percent. XRF looks at inner-shell atomic structure, so the state of the sample is not important. That means virtually no sample preparation is necessary. Samples can include solids, liquids, powders, aerosols and small particles. And all analyses are nondestructive.

So give Kevex a closer look. We've already installed close to 200 systems in laboratories worldwide, analyzing samples as diverse as metals, ores and petroleum products, industrial chemicals and waste, aerosols, ceramics, forensic samples, food, pharmaceuticals and semiconductor wafers. Kevex XRF may be the right alternative for you, too. Contact Kevex today for literature and applications information.

kevex®

KEVEX CORPORATION
1101 Chess Drive/Foster City, CA 94404
In California: 415/573-5866 Toll Free: 800/227-0277

2 The Howard Estate/Chilton Road
Chesham, Bucks. HP5 2AU/United Kingdom
Tel: (0494) 778877/Telex: 857966 KEVX UK/Fax: (0494) 778185

CIRCLE 124 ON READER SERVICE CARD

Had your fill of sample handling by hand?

Use the Gilson 212 Liquid Handler with Multi-level Interfacing™

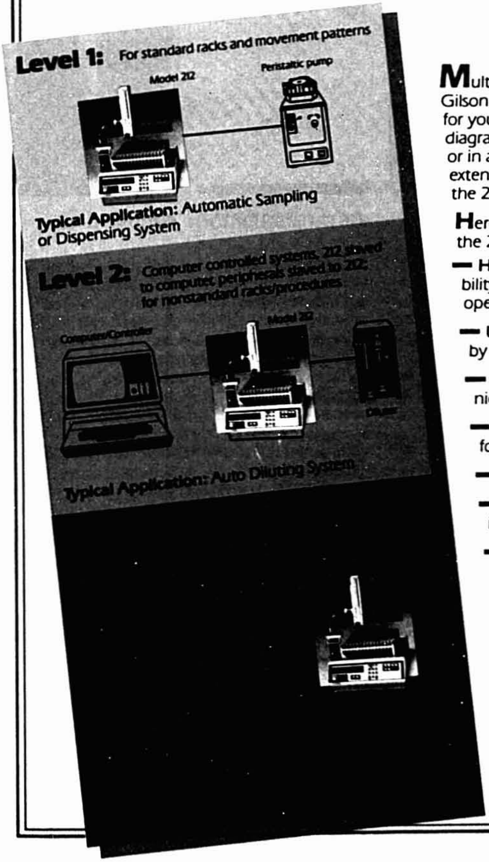

Level 1: For standard racks and movement patterns

Typical Application: Automatic Sampling or Dispensing System

Level 2: Computer controlled systems, 212 slaved to computer, peripheals slaved to 212; for nonstandard racks/procedures

Typical Application: Auto Diluting System

Multi-level Interfacing is a concept developed by Gilson to make the 212 Liquid Handler product specific for your liquid handling application. As shown in the diagrams, the 212 may be used as a stand-alone device or in a variety of other configurations through the extensive input-output capabilities accessible through the 212.

Here are some of the benefits you'll realize by using the 212:

- **High throughput**—large liquid handling capability combined with the potential for 24 hour operation.
- **Unattended operation** increases productivity by freeing personnel for other work.
- **Meaningful data** assured by eliminating technician error on routine repetitive techniques.
- **Simple operation** using prompt/respond format.
- **Easy to read** vacuum fluorescent display.
- **Economically priced;** reduces labor-intensive tasks.
- **Durable construction** assures long operating life for continued value.

For more information, call our 212 product specialist collect at (608) 836-1551.

Box 27, 3000 W. Beltline
Middleton, WI 53562
(608) 836-1551
Telex: 265478

72 rue Gambetta,
B.P. No. 45,95400
Villiers-le-Bel, FRANCE
Tel. (3) 990.54.41
Telex: 696682

GILSON
INTERNATIONAL

Circle #48 for literature. Circle #49 have your representative call on us.

11 เม.ย. 2527
ห้องสมุดกรมวิทยาศาสตร์บริการ

analytical chemistry®

JANUARY 1984

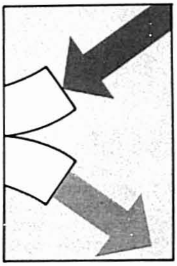

REPORT

Chemical sensors based on fiber optics are similar in use to electrodes but are very different in operating principles. Their applications, advantages, theory, and instrumentation are described by Rudolf Seitz of the University of New Hampshire

16 A

INSTRUMENTATION

Microsensors and microinstrumentation are making it possible to analyze small-volume samples and to improve analysis speed and instrument portability while keeping costs down, according to Hank Wohltjen of the Naval Research Laboratory

87 A

FOCUS

Three Mile Island. Analysts are taking a closer look at the damaged TMI reactor core. ▶ **Center for Process Analytical Chemistry** receives starter grant. ▶ **Academic–industrial cooperation.** ▶ **Three-dimensional elemental analysis**

35 A

Volume 56, No. 1
January 1984
ANCHAM
56(1) 1A–106A
1–128 (1984)
ISSN 0003 2700

Registered in U.S. Patent and Trademark Office; Copyright 1983 by the American Chemical Society

ANALYTICAL CHEMISTRY (ISSN 0003-2700) is published monthly with review issue added in April and Laboratory Guide in August by the American Chemical Society at 1155 16th St., N.W., Washington, D.C. 20036. Editorial offices are located at the same ACS address (202-872-4600; TDD 202-872-8733). Second-class postage paid at Washington, D.C., and additional mailing offices. Postmaster: Send address changes to Membership & Subscription Services, P.O. Box 3337, Columbus, Ohio 43210.

Claims for missing numbers will not be allowed if loss was due to failure of notice of change of address to be received in the time specified; if claim is dated (a) North America: more than 90 days beyond issue date, (b) all other foreign: more than one year beyond issue date, or if the reason given is "missing from files."

Copyright Permission: An individual may make a single reprographic copy of an article in this publication for personal use. Reprographic copying beyond that permitted by Section 107 or 108 of the U.S. Copyright Law is allowed, provided that the appropriate per-copy fee is paid through the Copyright Clearance Center, Inc., 21 Congress St., Salem, Mass. 01970. For reprint permission, write Copyright Administrator, B&J Division, ACS, 1155 16th St., N.W., Washington, D.C. 20036.

Registered names and trademarks, etc., used in this publication, even without specific indication thereof, are not to be considered unprotected by law.

Advertising Management: Centcom, Ltd., 25 Sylvan Road South, Westport, Conn. 06881 (203) 226-7131

Technical Contents/Briefs .... 6 A
Call for Papers .... 47 A
Meetings .... 47 A
For Your Information .... 54 A
New Products .... 60 A
Chemicals .... 65 A
Manufacturers' Literature .... 66 A
Advertising Index .... 104 A
Author Index, Future Articles .... inside back cover

NEWS

Advisory Board members. ANALYTICAL CHEMISTRY announces the appointment of six new members to its Advisory Board. They are William Heineman, Harry Hertz, Atsushi Mizuike, Melvin Redmond, Jr., Martin Rudat, and Charles Wilkins

43 A

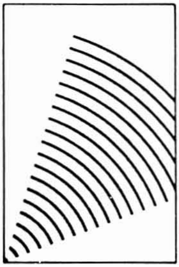

A/C INTERFACE

The laboratory *son et lumière* is coming of age as lab computers are endowed with enhanced capabilities, such as voice input/output, graphics, and image processing and analysis. Ray Dessy reports on the increasing ease of interaction between scientist and instrument

68 A

BOOKS

Critical reviews. A book on HPLC trace analysis and an audio course on GC column selection are reviewed by S. A. Wise and H. L. Gearhart

83 A

EDITORS' COLUMN

EAS 1983. Attendance at the 1983 Eastern Analytical Symposium established a new record. Two FT-IRs, by Perkin-Elmer and Janos, and a Hewlett-Packard GC were among new products on the exhibition floor

14 A

EDITORIAL

Authors, reviewers, and editors are all human and therefore subject to human frailties, but it is not in the author's best interest to mount highly emotional attacks questioning the competence of reviewers or editors

1

1984 subscription rates include surface (and air freight) costs

	1 yr	2 yr
Members		
Domestic	18	30
Canada	37	68
Foreign	37 (103)	68 (200)
Nonmembers		
Domestic	28	48
Canada	47	86
Foreign	74 (140)	132 (264)

Three-year and other rates contact: Membership & Subscription Services, ACS, P.O. Box 3337, Columbus, Ohio 43210, (614) 421-3776.

Subscription orders by phone may be charged to Visa, MasterCard, Barclay card, Access, or American Express. Call toll free at (800) 424-6747 from anywhere in the continental U.S.; from Washington, D.C., call 872-8065. Mail orders for new and renewal subscriptions should be sent with payment to the Treasurer's Office at the Washington address.

Subscription service inquiries and changes of address (include both old and new addresses with ZIP code and *recent mailing label*) should be directed to the ACS Columbus address noted above. Please allow six weeks for change of address to become effective.

ACS membership information: Ann Donahue, Washington address.

Single issues, current year, $7.00 except review issue and LabGuide, $8.00; **back issues and volumes and microform editions available** by single volume or back issue collection. For information or to order, call (800) 424-6747 or write the Sales Department at the Washington address.

Nonmember rates in Japan: Rates at left do not apply to nonmember subscribers in Japan, who must enter subscription orders with Maruzen Company Ltd., 3-10 Nihonbashi 2-chome, Chuo-ku, Tokyo 103, Japan. Tel: (03) 272-7211.

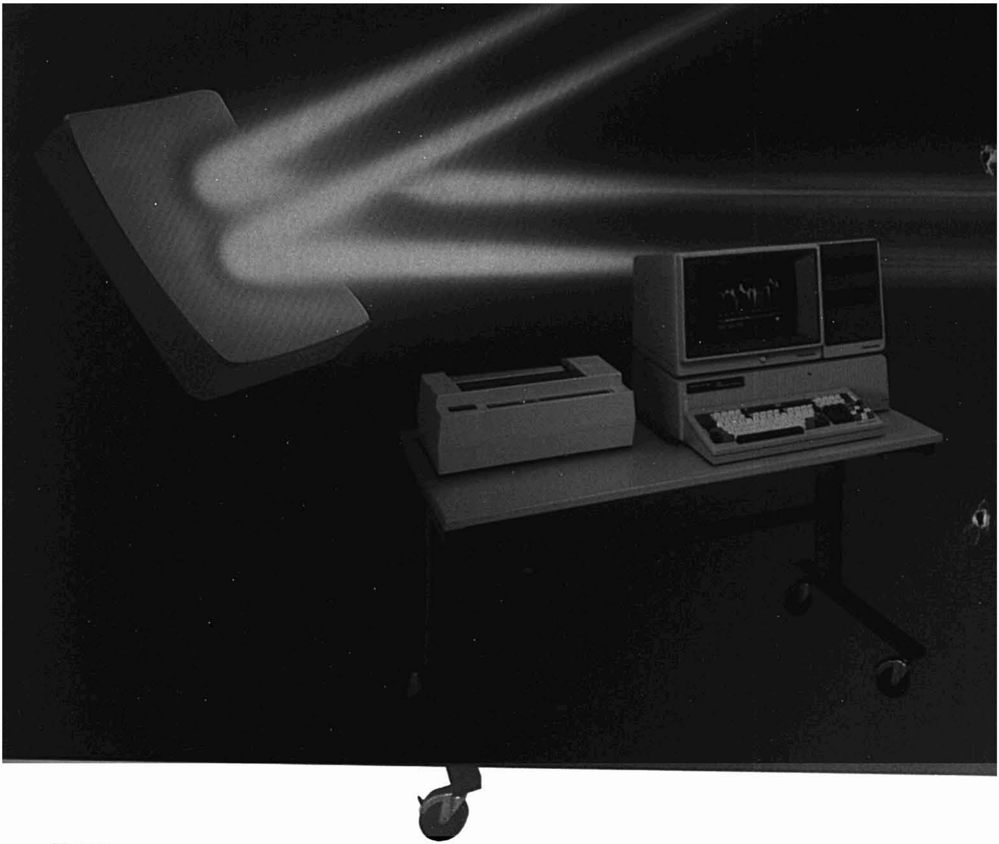

The world's leader in infrared presents the world's most advanced FT-IR.

Introducing the Perkin-Elmer Model 1800 FT-IR.

Perkin-Elmer technology creates a landmark laboratory instrument. Until the Model 1800, the advantages of FT-IR have never been fully realized. Now they have.

It took Perkin-Elmer's combination of expertise in optical systems, analytical instrumentation and computer technology to create a unique system which delivers double beam optical performance at Fourier transform speed.

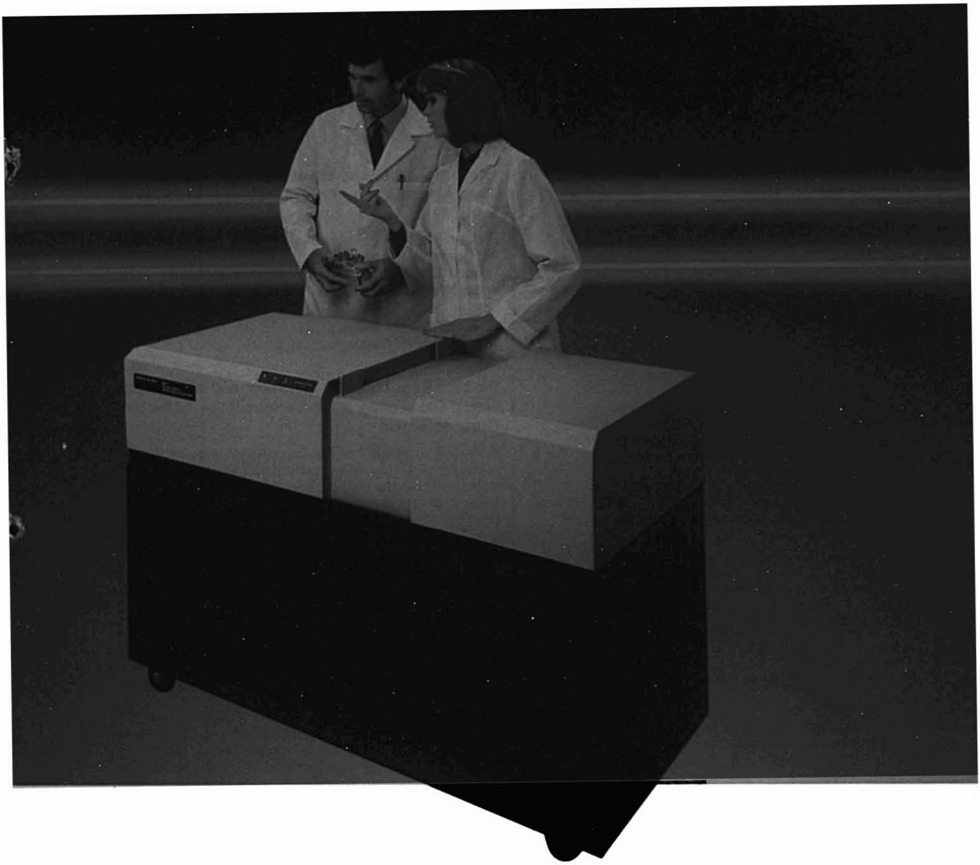

Fast, accurate, detailed spectral generation.

- *Excellent signal to noise ratio.* The Model 1800's unprecedented signal-to-noise ratio, approaching the theoretical limits of FT-IR, allows smaller, more difficult samples to be run at faster speeds.
- *Double beam.* The double beam optical design yields convenient, real-time compensation for instrument background and environmental effects.
- *Superior ordinate linearity.* The Model 1800 allows new, higher levels of accuracy, plus extended flexibility in sample concentration.
- *Array processor speed.* Data transfer, graphic presentation and Fourier transform algorithms are performed at array processor speeds by means of elegant optimized software, fiber optics and IEEE communications.

Computer power to spare.

The Model 1800 has three linked microprocessor systems. The system control processor is a powerful 16-bit Perkin-Elmer 7500 Professional Computer with enough growth potential to let you interface with other instruments and computers throughout your lab and company. And, to make even more use of this computing power, Perkin-Elmer offers the world's largest technical library of applications software. It includes the internationally respected QUANT, SEARCH and CDS programs.

The Perkin-Elmer 7500 can also be used for independent lab computing with such high level languages as BASIC and FORTRAN-77.

There is much more.

Learn how the Perkin-Elmer Model 1800 will solve problems and improve performance in your lab. The details are waiting for your analysis. Call 1-800-762-4000, toll-free. Or write for more information.

Perkin-Elmer Corp., Main Ave. (MS-12),
Norwalk, CT 06856 U.S.A. Tel: (203) 762-1000.
Telex 965-954.

Bodenseewerk Perkin-Elmer & Co., GmbH,
Postfach 1120, 7770 Ueberlingen,
Federal Republic of Germany. Tel: (07551) 811.

Perkin-Elmer Ltd., Post Office Lane,
Beaconsfield, Bucks HP9 1QA, England.
Tel: Beaconsfield (049 46) 6161.

PERKIN-ELMER

Circle #172 for a demonstration. Circle #173 for a sales representative to call.

Briefs

Laser Desorption Mass Spectrometry with Thermospray Sample Deposition for Determination of Nonvolatile Biomolecules 2

Samples are sprayed on-line onto a moving stainless steel belt under partial vacuum with a thermospray vaporizer. The samples are transported through a differentially pumped vacuum lock and ionized in the mass spectrometer source with 45-ns, 10^8-W/cm^2 laser pulses from a Q-switched Nd:YAG laser.

E. D. Hardin, T. P. Fan, C. R. Blakley, and M. L. Vestal*, Department of Chemistry, University of Houston, Houston, Tex. 77004 *Anal. Chem.*, *56* (*1984*)

Analysis of Anionic Surfactants by Mass Spectrometry/Mass Spectrometry with Fast Atom Bombardment 8

A survey of anionic surfactant types by positive and negative FAB MS yields molecular weights; MS/MS is used to confirm structures. Identification of homologues and ethylene oxide-containing polymers is illustrated.

Philip A. Lyon* and William L. Stebbings, 3M Company, Central Research Laboratories, St. Paul, Minn. 55144, and **Frank W. Crow, Kenneth B. Tomer, Dixie L. Lippstreu, and Michael L. Gross**, Midwest Center for Mass Spectrometry, Department of Chemistry, University of Nebraska—Lincoln, Lincoln, Neb. 68588 *Anal. Chem.*, *56* (*1984*)

Liquid Ionization Mass Spectrometry of Nonvolatile Organic Compounds 14

Metastable argon atoms are used to ionize compounds at atmospheric pressure. Mass spectra obtained by this method show ions characteristic of the molecular weight and the structure of the compounds.

Masahiko Tsuchiya*, Department of Industrial Chemistry, Faculty of Engineering, The University of Tokyo, Hongo, Bunkyo-ku, Tokyo 113, Japan, and **Hirofumi Kuwabara**, Department of Industrial Chemistry, Suzuka College of Technology, Shiroko-cho, Suzuka, Mie 510-02, Japan *Anal.Chem.*, *56* (*1984*)

Photothermal Deflection Densitometer for Thin-Layer Chromatography 19

The system is applied to the separation of 1,2-naphthoquinone, phenanthrenequinone, and α-ionone. Detection limits for the compounds range from 30 ng to 7.5 pg, depending on how strongly absorbing the compound is.

Tsuey Ing Chen and Michael D. Morris*, Department of Chemistry, University of Michigan, Ann Arbor, Mich. 48109 *Anal. Chem.*, *56* (*1984*)

Comparison of Suppressed and Nonsuppressed Ion Chromatography for Determination of Chloride in Boric Acid 21

Determination of chloride ion in boric acid solutions by supressed ion chromatography (IC) is complicated by an unidentified matrix effect. With nonsupressed IC and a concentrator column, chloride is determined at concentrations as low as 2 ppb.

H. H. Streckert* and B. D. Epstein, GA Technologies, Inc., P.O. Box 85608, San Diego, Calif. 92138 *Anal. Chem.*, *56* (*1984*)

On-Line Extraction, Evaporation, and Injection for Liquid Chromatographic Determination of Serum Corticosteroids 24

A switching-system model incorporating quantitative solvent extraction, evaporation, and sample injection is developed for the liquid chromatographic determination of serum corticosteroids such as hydrocortisone and prednisolone.

Kitaro Oka, Kazuo Minagawa, and Shoji Hara*, Tokyo College of Pharmacy, Horinouchi, Hachioji, Tokyo 192-03, Japan, and **Makoto Noguchi, Yasuo Matsuoka, Michinori Kono, and Shoichiro Irimajiri**, Kawasaki City Hospital, Kawasaki 210, Japan *Anal. Chem.*, *56* (*1984*)

Preconcentration with Dithiocarbamate Extraction for Determination of Molybdenum in Seawater by Neutron Activation Analysis 27

Extraction of molybdenum from seawater with pyrrolodonedithiocarbamate and diethyldithiocarbamate at pH 1.4 into chloroform is quantitative and eliminates the interferences of uranium and other matrix species for neutron activation analysis.

W. M. Mok and C. W. Wai*, Department of Chemistry, University of Idaho, Moscow, Idaho 83843 *Anal. Chem.*, *56* (*1984*)

Spectrophotometric Determination of Total Gossypol in Cottonseeds and Cottonseed Meals 30

The method is based on the reaction of gossypol with 3-amino-1-propanol and its subsequent reaction with Fe(III). The Fe(III)-bis(aminopropanol)-gossypol complex has a characteristic absorption maximum at 620 nm.

Atnafseged Admasu, Ethiopian Nutrition Institute, P.O. Box 5654, Addis Ababa, Ethiopia, and **B. S. Chandravanshi***, Department of Chemistry, Addis Ababa University, P.O. Box 1176, Addis Ababa, Ethiopia *Anal. Chem.*, *56* (*1984*)

* Corresponding author

NEW ROSS™ CONFIGURATIONS FOR SPECIFIC APPLICATIONS

The ORION Ross™ pH electrodes are not just for clean samples in beakers any more. With the addition of the glass sleeve junction, flat surface, rugged bulb and spear tip electrodes, pH measurements can now be made with the benefits of the Ross Series of electrodes on a whole new range of applications. That means reproducible readings stable to 0.01 pH in 30 seconds even when temperatures vary from one another by 50°C. These results are three to five times more accurate than what conventional electrodes can deliver. And, with less than 0.002 pH drift per day, restandardization is minimal.

Try a new Ross™ electrode yourself. Contact Orion Research to order the Ross™ electrode for your specific application.

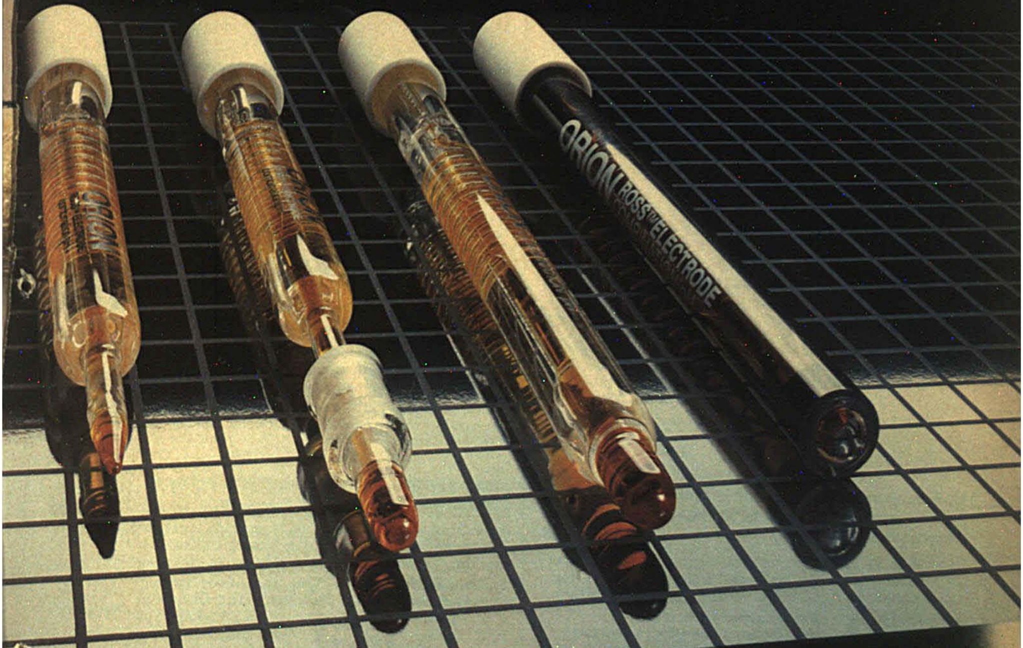

Model 8163
Spear tip
for foods and semisolids

Model 8166
Glass sleeve junction
for viscous samples

Model 8104
Rugged bulb
for field or plant measurements

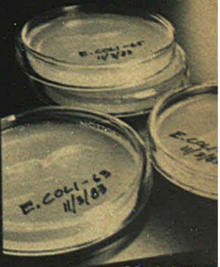

Model 8135
Flat surface
for microbiology samples

ORION

Orion Research Incorporated
840 Memorial Drive, Cambridge, MA 02139 U.S.A.
TEL 800-225-1480 or 617-864-5400. TX 921466 or 4430019.
In Europe: Orion Research AG
Fähnlibrunnenstrasse 5, CH-8700, Küsnacht, Switzerland
Telephone 01-910 7858. Telex 57829.

CIRCLE 156 ON READER SERVICE CARD

Briefs

Elemental Analysis of Estuarine Sediments by Lithium Metaborate Fusion and Direct Current Plasma Emission Spectrometry
33

The method is inexpensive and fast but vulnerable to systematic errors. Coefficients of variation of replicate analyses for major and trace elements are generally in the 2–10% range.

A. Y. Cantillo*, S. A. Sinex, and G. R. Helz, Department of Chemistry, University of Maryland, College Park, Md. 20742
Anal. Chem., *56* (*1984*)

Generalized Internal Reference Method for Simultaneous Multichannel Analysis
37

The internal reference method is expanded to a generalized internal reference method. The generalized method can detect variations in instrumental parameters and compensate for them.

Avraham Lorber and Zvi Goldbart*, Nuclear Research Centre—Negev, P.O. Box 9001, Beer-Sheva 84190, Israel
Anal. Chem., *56* (*1984*)

Correction for Drift by Internal Reference Methods in Inductively Coupled Plasma Simultaneous Multielement Analysis
43

A generalized internal reference method is applied to data obtained from a simultaneous multielement ICP system. The method reduces the noise of spectral lines to the level of electronic shot noise of the detection system.

Avraham Lorber, Zvi Goldbart*, and Michael Eldan, Nuclear Research Centre—Negev, P.O. Box 9001, Beer-Sheva 84190, Israel
Anal. Chem., *56* (*1984*)

Optimization of Electrochemical Atomization Parameters for Simultaneous Multielement Atomic Absorption Spectrometry
48

Conditions for simultaneous electrothermal atomization of Co, Cr, Cu, Fe, Mn, Mo, Ni, V, and Zn are examined using unpyrolyzed and pyrolyzed tubes and a pyrolytic platform.

James M. Harnly* and Jean S. Kane, Beltsville Human Nutrition Research Center, Nutrient Composition Laboratory, U.S. Department of Agriculture, Beltsville, Md. 20705
Anal. Chem., *56* (*1984*)

Sensitivity Factors for Surface Analysis by Ion Scattering Spectroscopy
55

Procedures to determine relative sensitivity factors used in quantitative surface analysis of substitutional alloys by ion-scattering spectroscopy are discussed. A novel procedure involving the physisorption of xenon on elemental substrates is independent of surface roughness.

Dennis G. Swartzfager, E. I. du Pont de Nemours & Company, Central Research & Development Department, Experimental Station, Wilmington, Del. 19898
Anal. Chem., *56* (*1984*)

Determination of Trace Constituents of High-Purity Gallium Arsenide
58

Acceptors are identified by selectively populating acceptor–exciton complexes and observing the subsequent ground and excited final-state relaxations. Interband interferences are reduced, and element-specific splittings are obtained.

P. W. Bohn*, R. Bhat, and T. D. Harris, Bell Laboratories, Murray Hill, N.J. 07974
Anal. Chem., *56* (*1984*)

Fiber-Optic Probe for in Vivo Measurement of Oxygen Partial Pressure
62

A fiber-optic P_{O_2} probe based on fluorescence quenching is described. Physiological P_{O_2} is measured over the range of 1–150 torr.

John I. Peterson* and Raphael V. Fitzgerald, Biomedical Engineering and Instrumentation Branch, Division of Research Services, Building 13, Room 3W13, National Institutes of Health, Bethesda, Md. 20205, and **Delwin K. Buckhold,** Section on Laboratory Medicine and Surgery, National Heart, Lung, and Blood Institute, National Institutes of Health, Bethesda, Md. 20205
Anal. Chem., *56* (*1984*)

Rules for Computerized Interpretation of Vapor-Phase Infrared Spectra
67

Rules for the interpretation of IR vapor-phase spectra are presented and incorporated into existing computerized IR interpretation systems.

Sterling A. Tomellini*, James M. Stevenson, and Hugh B. Woodruff, Merck Sharp & Dohme Research Laboratories, P.O. Box 2000, Rahway, N.J. 07065
Anal. Chem., *56* (*1984*)

Iodometric Method for Determination of Trace Chlorate Ion
71

A modified iodometric method is reported for chlorate ion determination at sub-mg/L levels using hexane as a shielding agent to prevent air oxidation of the iodide ion.

Yasuhisa Ikeda, Tsung-fei Tang, and Gilbert Gordon*, Miami University, Department of Chemistry, Oxford, Ohio 45056
Anal. Chem., *56* (*1984*)

Point-by-Point Matrix Effect Calibration for the Quantitative Analysis of Superlattices by Secondary Ion Mass Spectrometry
74

Using the linear dependence of secondary ion yields and sputtering yields on matrix composition, a point-by-point matrix effect calibration is applied to $Al_xGa_{1-x}As$ multilayer–multimatrix samples.

A. A. Galuska and G. H. Morrison*, Department of Chemistry, Cornell University, Ithaca, N.Y. 14853
Anal. Chem., *56* (*1984*)

VICI

Valco Instruments Co. Inc.
P.O. Box 55603 Houston, Texas 77255
(713) 688-9345
TWX 910-881-5500 Telex 79-0033

Valco Switzerland
Tannberg P.O. Box 13 CH-6214 Schenkon
(045) 216868
Telex 868342 vici ch

ANNOUNCING
NEW FOR GC

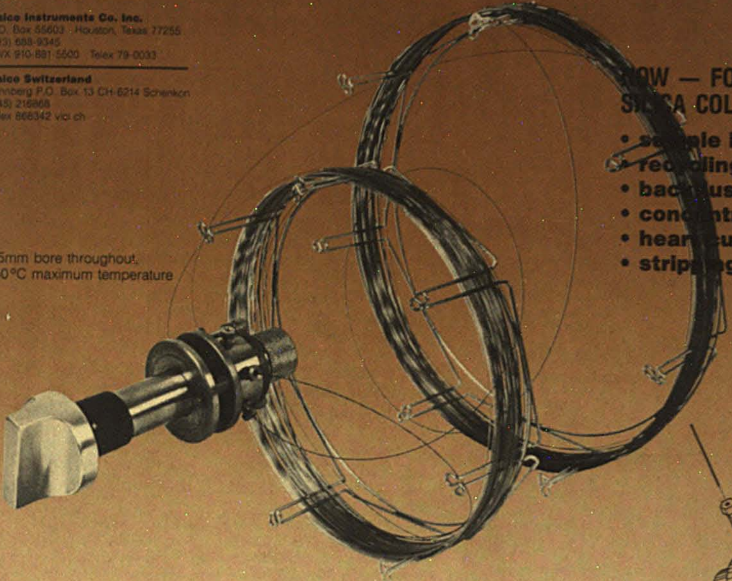

.25mm bore throughout,
350°C maximum temperature

NOW — FOR FUSED SILICA COLUMNS

- **sample injection**
- **recycling**
- **backflushing**
- **concentration**
- **heart cutting**
- **stripping**

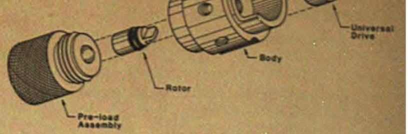

The first devices for direct sampling and switching of fused silica columns are now available from Valco and leading international dealers.

CIRCLE 220 ON READER SERVICE CARD

AND
NEW FOR HPLC

The most advanced "user friendly" HPLC sample injection and switching valves.

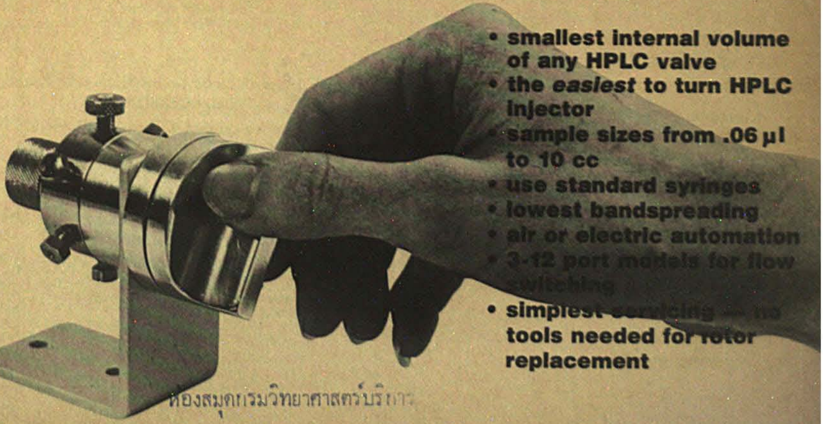

- **smallest internal volume of any HPLC valve**
- **the *easiest* to turn HPLC injector**
- **sample sizes from .06 µl to 10 cc**
- **use standard syringes**
- **lowest bandspreading**
- **air or electric automation**
- **3-12 port models for flow switching**
- **simplest servicing — no tools needed for rotor replacement**

ห้องสมุดกรมวิทยาศาสตร์บริการ

CIRCLE 221 ON READER SERVICE CARD

Briefs

Estimation of Detection Limits in X-ray Fluorescence Spectrometry 77

Experimental X-ray measurements demonstrate the validity of the statistical criterion used to define the minimum detection limit.

John V. Gilfrich* and L. S. Birks, Naval Research Laboratory, Washington, D.C. 20375 *Anal. Chem.*, *56* (*1984*)

Infrared Photoacoustic Spectroscopy of Liquids with an F-Center Laser 80

Infrared photoacoustic spectra of liquids are obtained using a tunable IR laser to excite low-order radial acoustic resonance modes of the sample cell. A $S/N = 1$ for an absorbance of 1×10^{-5} using a 3.5-mW laser is achieved.

Pao-Yuan Chen and James S. Shirk*, Department of Chemistry, Illinois Institute of Technology, Chicago, Ill. 60616 *Anal. Chem.*, *56* (*1984*)

Phase Plane Method for Deconvolution of Luminescence Decay Data with a Scattered-Light Component 82

The phase plane method of deconvoluting luminescence lifetimes in the presence of scattered light is accurate and precise over a wide range of decay parameters, noise levels, and degrees of scatter.

J. C. Love and J. N. Demas*, Department of Chemistry, University of Virginia, Charlottesville, Va. 22901 *Anal. Chem.*, *56* (*1984*)

Optimization of Anion Separation by Nonsuppressed Ion Chromatography 85

Window diagrams are used to optimize separation of Cl^-, Br^-, NO_3^-, SO_4^{2-}, and $S_2O_3^{2-}$ and to predict the elution sequence in nonsuppressed ion chromatography.

Dennis R. Jenke and Gordon K. Pagenkopf*, Department of Chemistry, Montana State University, Bozeman, Mont. 59717 *Anal. Chem.*, *56* (*1984*)

Models for Prediction of Retention in Nonsuppressed Ion Chromatography 88

The agreement between observed and predicted retention times using three models—multiple-species eluent, single-species eluent, and single-interaction sites—is discussed.

Dennis R. Jenke and Gordon K. Pagenkopf*, Department of Chemistry, Montana State University, Bozeman, Mont. 59717 *Anal. Chem.*, *56* (*1984*)

Computer Simulation of Light Transmission through Scattering and Absorbing Chromatographic Media 91

A computer model simulates the Kubelka–Munk differential equations and allows a variable number of iterations. Results from this model are compared with solutions of the same equations obtained by conventional methods of integration.

I. E. Bush* and H. P. Greeley, Research Service, Veterans Administration Medical and Regional Office Center, White River Junction, Vt. 05001 *Anal. Chem.*, *56* (*1984*)

Linear and Helical Flow in a Perfluorosulfonate Membrane of Annular Geometry as a Continuous Cation Exchanger 96

Mass transfer efficiency is studied for linear and helical flow in Nafion membrane-based cation exchangers of annular geometry.

Purnendu K. Dasgupta, Department of Chemistry, Texas Tech University, Box 4260, Lubbock, Tex. 79409 *Anal. Chem.*, *56* (*1984*)

Annular Helical Suppressor for Ion Chromatography 103

Small dead-volume and low-dispersion characteristics of annular helical flow are exploited in the use of a filament-filled helix as an IC suppressor.

Purnendu K. Dasgupta, Department of Chemistry, Texas Tech University, Box 4260, Lubbock, Tex. 79409 *Anal. Chem.*, *56* (*1984*)

Ion Chromatographic Determination of Morpholine and Cyclohexylamine in Aqueous Solutions Containing Ammonia and Hydrazine 106

Column length, eluent flow rate, and eluent ionic strength are optimized for satisfactory resolution of $C_4H_{10}NO^+$, $C_6H_{11}NH_3^+$, NH_4^+, and $N_2H_5^+$ under three analytical modes. Detection limits are 0.1 ppm for both morpholine and cyclohexylamine.

Roland Gilbert* and Reynald Rioux, Institut de recherche d'Hydro-Québec (IREQ), 1800 Montée Sainte-Julie, Varennes, Québec, Canada J0L 2P0, and **Souheil E. Saheb,** Gentilly 2 Nuclear Power Plant, Gentilly, Québec, Canada G0X 1G0 *Anal. Chem.*, *56* (*1984*)

Correspondence

Direct Analysis of Thin-Layer Chromatography Spots by Fast Atom Bombardment Mass Spectrometry 109

Ted T. Chang*, Jackson O. Lay, Jr., and Rudolph J. Francel, Chemical Research Division, American Cyanamid Company, P.O. Box 60, 1937 West Main Street, Stamford, Conn. 06904 *Anal. Chem.*, *56* (*1984*)

Electrokinetic Separations with Micellar Solutions and Open-Tubular Capillaries 111

Shigeru Terabe*, Koji Otsuka, Kunimichi Ichikawa, Akihiro Tsuchiya, and Teiichi Ando, Department of Industrial Chemistry, Faculty of Engineering, Kyoto University, Sakyo-ku, Kyoto 606, Japan *Anal. Chem.*, *56* (*1984*)

Electrodeposition of Actinides in a Mixed Oxalate–Chloride Electrolyte 113

Kenneth W. Puphal*, Terry D. Filer and Gerald J. McNabb, Radiological and Environmental Sciences Laboratory, U.S. Department of Energy, 550 Second Street, Idaho Falls, Idaho 83401 *Anal. Chem.*, *56* (*1984*)

Every powder, crystal, flake, and grain Kodak makes is a solution.

The next time you face a problem in the laboratory, maybe the solution is a chemical from Kodak. We now supply not only organic chemicals, but hundreds of inorganic chemicals too—plus a growing number of biochemicals.

Our new publication—"KODAK Inorganic Chemicals"—lists more than 250 "solutions" available from Kodak Laboratory and Specialty Chemicals. Each one features the same quality, purity, and consistency as our organic chemicals.

What's more, with ON TIME, our new direct-shipment service, your dealer can see that your rush chemical needs get the attention they deserve. When you order a chemical that your dealer doesn't have in stock, the order can be transmitted to us. We'll ship it direct to you—usually within 24 hours.

Find out how our "solutions" can help you become a more creative chemist. Send for your free copy of "KODAK Inorganic Chemicals" today.

KODAK LABORATORY &
SPECIALTY CHEMICALS

The creative source.

Send to: Eastman Kodak Company,
Kodak Laboratory & Specialty Chemicals,
Dept. 412-L, Rochester, NY 14650

KODAK
Inorganic Chemicals

Please send me my free copy of "KODAK Inorganic Chemicals" (JJ-15).

NAME ______________________

TITLE ______________________

FIRM ______________________

ADDRESS ______________________

CITY ______________________

STATE ______________________

ZIP ______________________

The ready source—dealers handling KODAK Laboratory Chemicals: American Scientific & Chemical; American Scientific Products; Bioclinical Laboratories NJ; B.C. Chemicals; Brand-Nu Laboratories, Inc.; Bryant Laboratory, Inc.; CAMX Scientific; Doe & Ingalls, Inc.; Fisher Scientific; Mays Chemical; Midland Scientific, Inc.; North-Strong Division; Preiser Scientific; Sargent-Welch Scientific; Scientific & Industrial Sales & Service, Inc.; Specialty Chemicals, Inc.; Spectrum Chemical Corp.; VWR Scientific Inc.; Ward's Natural Science Establishment, Inc.

© Eastman Kodak Company, 1982. Kodak Laboratory and Specialty Chemicals, Rochester, NY 14650.

CIRCLE 63 ON READER SERVICE CARD

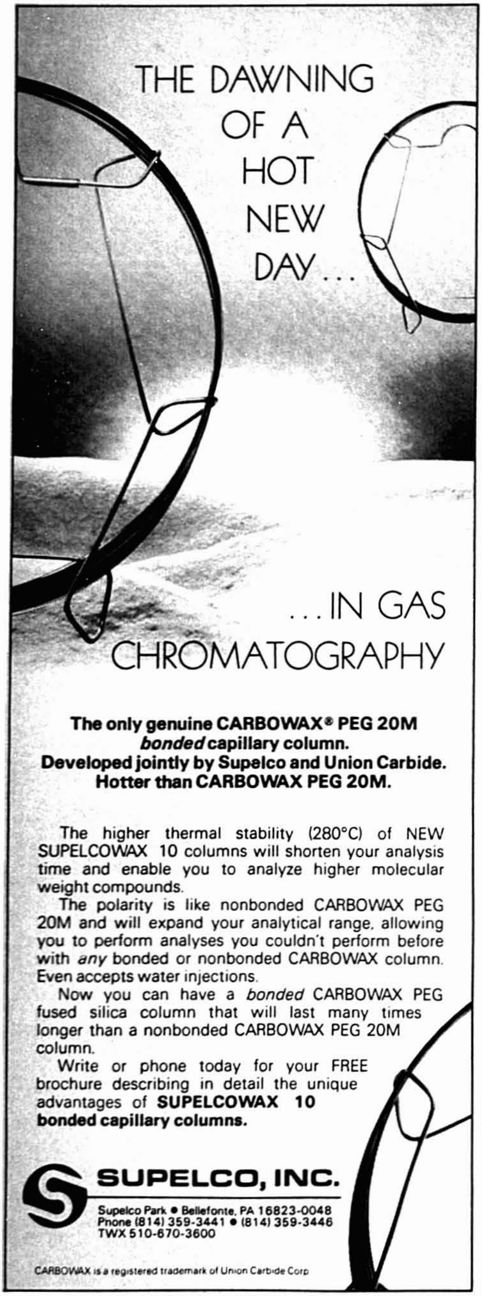

**The only genuine CARBOWAX® PEG 20M *bonded* capillary column.
Developed jointly by Supelco and Union Carbide.
Hotter than CARBOWAX PEG 20M.**

The higher thermal stability (280°C) of NEW SUPELCOWAX 10 columns will shorten your analysis time and enable you to analyze higher molecular weight compounds.

The polarity is like nonbonded CARBOWAX PEG 20M and will expand your analytical range, allowing you to perform analyses you couldn't perform before with *any* bonded or nonbonded CARBOWAX column. Even accepts water injections.

Now you can have a *bonded* CARBOWAX PEG fused silica column that will last many times longer than a nonbonded CARBOWAX PEG 20M column.

Write or phone today for your FREE brochure describing in detail the unique advantages of **SUPELCOWAX 10 bonded capillary columns.**

SUPELCO, INC.

Supelco Park • Bellefonte, PA 16823-0048
Phone (814) 359-3441 • (814) 359-3446
TWX 510-670-3600

CARBOWAX is a registered trademark of Union Carbide Corp

CIRCLE 192 ON READER SERVICE CARD

Briefs

Aids for Analytical Chemists

Modified Polishing Equipment for Voltammetric Electrodes 116

Mary Schreiner, John J. O'Dea, Neal Sleszynski, and Janet Osteryoung*, Department of Chemistry, State University of New York at Buffalo, Buffalo, N.Y. 14214 *Anal. Chem.*, *56* (*1984*)

Rotating Ring-Disk Electrode with Wide Temperature Range 118

David K. Roe* and Mario Aparicio-Razo, Department of Chemistry, Portland State University, Portland, Ore. 97207 *Anal. Chem.*, *56* (*1984*)

Optimization of Electrothermal Atomization-Inductively Coupled Plasma Atomic Emission Spectrometry for Simultaneous Multielement Determination 120

Hassan M. Swaidan and Gary D. Christian*, Department of Chemistry, BG-10, University of Washington, Seattle, Wash. 98195 *Anal. Chem.*, *56* (*1984*)

Correction. Performance Characteristics of a Continuum-Source Wavelength Modulated Atomic Absorption Spectrometer 122

J. D. Messman*, M. S. Epstein, and T. C. Rains, Center for Analytical Chemistry, National Bureau of Standards, Washington, D. C. 20234, and **T. C. O'Haver,** Department of Chemistry, University of Maryland, College Park, Md. 20742

Manuscript Requirements 123

Analysis, Identification, Determination, and Assay 124

Guide for Use of Terms in Reporting Data in ANALYTICAL CHEMISTRY 125

Spectrometry Nomenclature 125

SI Units 126

Copyright Transfer Form 127

Matheson announces the most important gas mixture in 56 years.

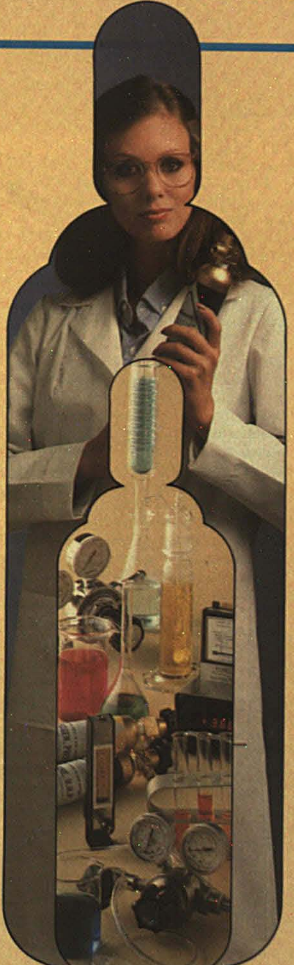

It's today's Matheson, now in partnership with AmeriGas, one of North America's fastest-growing compressed gases suppliers, and Nippon Sanso, Japan's leading supplier of specialty gases and equipment.

Leading from new strengths.

This new alliance means even greater strength for Matheson, world leader in specialty gases and equipment since 1927.

Greater strength in technology, through a sharing of expertise.

And greater strength in distribution through our partners' worldwide network.

Small changes. Big traditions.

You'll see a slight change in our name. In the U.S. we'll be known as Matheson Gas Products, Inc. In Canada, we'll be Matheson Gas Products Canada, Inc.

And wherever you are, you'll know Matheson as the leader.

What will *not* change are the things that have led Matheson to our position of leadership: superior products, outstanding service, comprehensive gas data, and a commitment to innovative specialty gases, gas mixtures, and gas handling equipment.

Try today's Matheson, today.

The name Matheson has always been a symbol of quality. Our cylinders supply the world with more than 100 gases—from specialty, to mixtures, to instrumentation—in a wide variety of purities and sizes.

And our over 2,000 gas handling equipment items—including regulators, flow meters, gas purifiers, detectors, and monitors —permit safe, accurate use of those gases.

So whether you're in a research or industrial control lab, a pilot plant, or a commercial processing plant, today's Matheson is the "new" company for your gases and equipment. No one knows how to serve you better.

For a free Matheson catalog, call: (201) 867-4100. Or contact your Matheson representative.

Call today, and find out how Matheson provides the right mixture of quality, experience, and service for your needs.

Matheson®
Gas Products
World Leader in Specialty Gases & Equipment

CIRCLE 139 ON READER SERVICE CARD

Eastern Analytical Symposium Convenes in New York City

Attendance at the 22nd Eastern Analytical Symposium (EAS), held Nov. 16–18 in New York City, surpassed even the hopeful expectations of symposium officers. The number of conferees and exhibitors registered at this year's meeting was 4509, fully 34% above the 1982 attendance figure.

EAS officials were pleased with the news of well-attended technical sessions, some with standing room only. Over 200 scientific papers were presented.

Award winners at the meeting included Abraham Savitzky, senior scientist in the spectroscopy division of the Perkin-Elmer Corporation, who received the New York Society for Applied Spectroscopy (SAS) Medal for his contributions in IR spectrometry, data processing, and computerized analysis. In addition, Louis Meites of Clarkson College of Technology, Potsdam, N.Y., received the Benedetti-Pichler Memorial Award of the American Microchemical Society, honoring his contributions in the field of electrochemistry. Meites has 204 publications in the field to his credit, including 14 books.

John D. Johnson of SAS (left) presents the 1983 SAS New York section award to Abraham Savitzky

Instruments making their world debuts at EAS included two Fourier transform infrared spectrometers (FT–IRs) and a new gas chromatograph.

Perkin-Elmer's new Model 1800 is the industry's first FT–IR with double-beam capability, a feature that makes it possible for the analyst to do real-time background corrections. According to the company, the precision and accuracy of the instrument are superior to higher priced single-beam FT–IR systems.

Janos Technologies Model 1000 FT–IR contains a rotating optical element, a component that makes it possible for the interferometer to be much smaller than conventional Michelson interferometers. According to Janos, the instrument is also quite insensitive to shock. The moderate-resolution (5 cm^{-1}) instrument can be used for process control and product quality monitoring in industrial settings or in situations where a transportable analyzer is needed.

Hewlett-Packard's new HP 5890A gas chromatograph represents a more efficient manufacturing concept that has enabled the company to offer the instrument at a price it claims is 25% lower than comparable models from other manufacturers. Hewlett-Packard is also offering an optional service contract guaranteeing the user 99% uptime on the instrument.

The EAS committee is looking forward to an expanded meeting in a completely renovated facility in 1984. The New York Penta Hotel (formerly the New York Statler), where the meeting has been held since 1980, was recently acquired by new owners. The Penta management is conducting a major hotel renovation, including redecoration of guest rooms and public areas, an exterior face-lift, and a completely new lobby. That all this will be substantially complete by next November is hard to believe, but that, in fact, is what Penta has promised EAS officers.

The A.A. Benedetti-Pichler Award
LOUIS MEITES

Hercules Felder (left), chairman of the American Microchemical Society, presents the 1983 Benedetti-Pichler award to Louis Meites

According to EAS general chairperson Concetta Paralusz of Permacel/Avery International, the meeting will be extended to four days next year to satisfy a growing demand for exhibit space caused, at least in part, by the departure of the Pittsburgh Conference from the New York–New Jersey area. The largest analytical chemistry meeting in the U.S., the Pittsburgh Conference has been held in Atlantic City, N.J., for the past few years, but will move to New Orleans in 1985. The longer EAS meeting format will free a ballroom formerly used for technical symposia. The number of technical symposia at the 1984 EAS will remain about the same as this year, but the extra day will make it possible to spread them out so there are fewer simultaneous sessions.

Paralusz said she thought that this year's EAS was the best ever—until next year. With registration figures and the number of exhibit booths increasing at a healthy clip, Paralusz's enthusiasm does not seem unfounded.

Stuart A. Borman

Microbore HPLC...
Compromise Isn't
Good Enough.

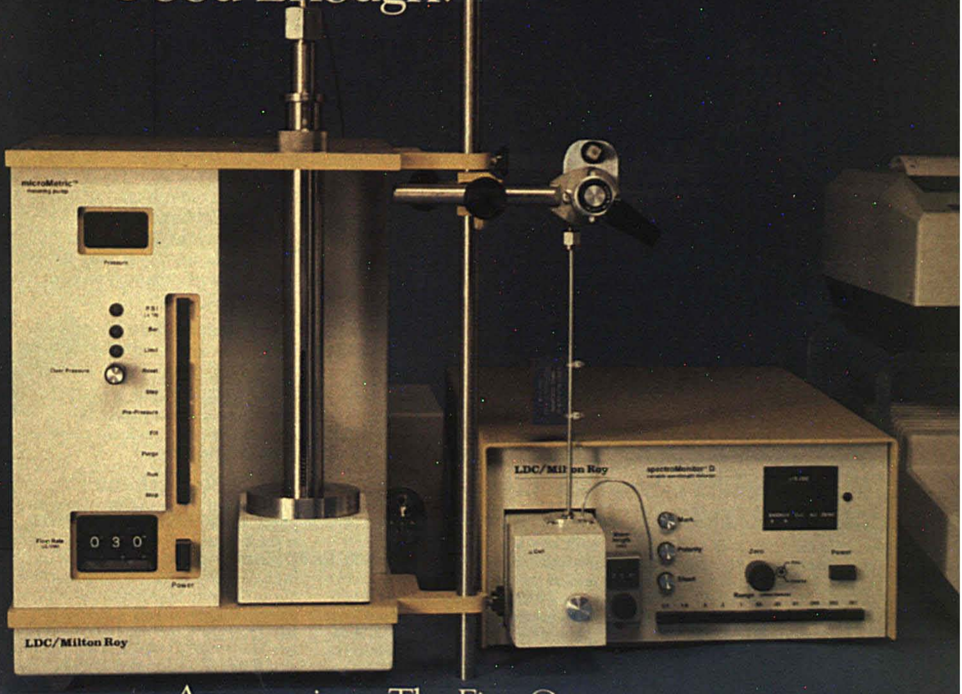

Announcing...The First Components
Specifically Designed For Microbore HPLC

Higher sensitivity and more resolution at very low flow rates — that's the promise of microbore HPLC. Now that promise is met *in full* by LDC/Milton Roy's new components, offering you the first system truly designed for microbore HPLC — *without compromise!* No adaptation of existing components.

LDC/Milton Roy's new microMetric™ Metering Pump offers true pulse-free flow from 1-999 μL/min with better than 1% of thumbwheel setting accuracies. A 5 mL syringe capacity permits multiple chromatograms. Refill is accomplished in one minute. High pressure capability to 10,000 psi for both today's packed columns and tomorrow's capillary columns.

New spectroMonitor® D with microCell™ offers crossflow™ optics to minimize thermal and flow noise without a bulky heat exchanger. A 1 mm tubular quartz fused-silica cell permits direct coupling to microbore columns for maximum efficiency. Unique fiber optics and high performance mirror collect and deflect light to the integral preamplifier circuit board.

Learn more about the marvels of microbore HPLC, and all about how LDC/Milton Roy has packaged all the benefits in one new, uncompromising set of components. Write or call for further information.

LDC/Milton Roy

U.S. HEADQUARTERS, P.O. Box 10235, Riviera Beach, FL 33404 Toll-free: 800-327-6182, In Florida: (305) 844-5241 International Telex: 441098, Domestic Telex: 513479
SUNNYVALE OPERATION, 560 Oakmead Parkway, Sunnyvale, CA 94086 Toll-free: 800-538-1595, In California: (408) 736-0300
UNITED KINGDOM, LDC UK, Milton Roy House, 52 High Street, Stone, Staffordshire ST15 8AR England Phone: 785 81-3542 Telex: 36623
WEST GERMANY, Milton Roy (Deutschland) GMBH Jahnstrasse 22-24 6467 Hasselroth 2, West Germany Phone: 6055-2031 (3386) Telex: 4184357
JAPAN, Milton Roy K.K., Takanawa Dai-Ichi Building 21-41, Takanawa 2-Chome, Minato-Ku, Tokyo 108, Japan Phone: (03) 473-3181 Telex: 242-4296

CIRCLE 125 ON READER SERVICE CARD

W. Rudolf Seitz
Department of Chemistry
University of New Hampshire
Durham, N.H. 03824

Chemical Sensors Based on Fiber Optics

The devices considered in this REPORT involve a reagent phase on the end of a fiber optic. In operation, interaction with analyte leads to a change in optical properties of the reagent phase, which is probed and detected through the fiber optic. Depending on the particular device, the optical property measured can be absorbance, reflectance, luminescence, or something else. An example of such a device would be a pH sensor based on an immobilized dye whose color or fluorescence properties vary with pH.

The term *optrode* is used to describe these devices (*1*). This term, formed by combining "optical" and "electrode," emphasizes that *in use* optical sensors are very similar to electrodes. However, *in operating principles* they are quite different, offering new possibilities relative to electrodes while at the same time being subject to limitations and problems that are not observed with electrodes.

Attractive features of optical sensors relative to electrodes include the following:

- Because the signal is optical, it is not subject to electrical interference.
- No "reference electrode" is required.
- Because the reagent phase does not have to physically contact the fiber optic, it is a simple matter to change reagent phase. In fact, it is possible that in some contexts it will be practical to use reagent phase on a disposable basis. Also, the reagent phase can be in a different environment from the fiber optic. For example, the reagent phase could be in a high-pressure reactor and be probed through a window in the reactor.
- Optical sensors can offer significant cost advantages over electrodes, particularly if a single spectrometer is used with several sensors.
- The most exciting possibility offered by optical sensors is the use of multiwavelength and temporal information. For example, one can envision sensors that respond simultaneously to two or more analytes distinguished by measurements at two or more probe–detection wavelength combinations. If the optical sensor involves luminescence, then time resolution also can be used. In addition, multiwavelength measurements may be used to monitor reagent phase stability or to relate analyte concentrations to intensity ratios at two wavelengths.
- Optical sensors can be developed to respond to analytes for which electrodes are not available.

Optical sensors also are subject to several limitations relative to electrodes:

- Ambient light will interfere with optical sensors. They must either be used in a dark environment, or the optical signal must be encoded (e.g., by modulation) so that it can be resolved from ambient background.
- Long-term stability is likely to be a problem for reagent systems used in optical sensors, although to some extent this can be compensated for by multiple-wavelength detection and by the ease of changing reagent phases.
- Because the reagent and the analyte are in different phases, there is necessarily a mass transfer step before constant response is reached. This, in turn, limits response times of optical sensors.
- For several types of optical measurements, observed intensities are proportional to the amount of reagent phase. If the amount of reagent phase is small, detected intensities can be increased by using more intense probe radiation. However, this will accelerate any reagent photodegradation processes. As a consequence, optical sensors involve a three-way tradeoff between amount of reagent phase, intensity of probe radiation, and stability.
- In general, optical sensors will have limited dynamic ranges compared to electrodes, for reasons that will be considered below.

Optical sensors may be classified as reversible or nonreversible. A sensor is reversible if the reagent phase is not consumed by its interaction with analyte. If the reagent phase is consumed, then the sensor is nonreversible. For such a device to be useful for sensing, the relative consumption of reagent phase must be small or there must be provisions for renewing the reagent. These two categories of devices will be considered separately. This REPORT will not consider systems in which a reagent phase is used on a one-time basis.

Instrumentation

The instrumentation for fiber-optic-based chemical sensors can be simple or complex depending on the

0003-2700/83/0351-016A$01.50/0
© 1983 American Chemical Society

Increase GPC resolution and speed with new MicroPak TSK HXL Columns

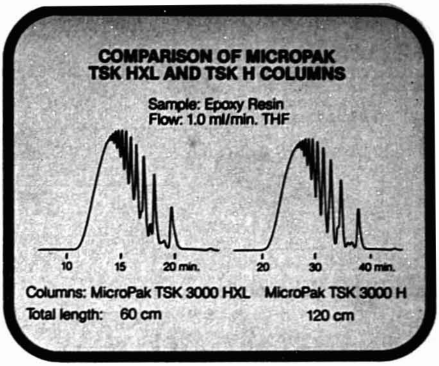

Varian announces a new family of high-resolution GPC columns, manufactured by Toyo Soda, the leader in microparticulate gel technology. Featuring new 5-μm spherical particles, these HXL Gels provide outstanding performance characteristics for GPC analysis.

- **Unexcelled performance for GPC polymer characterization**—Excellent column stability provides highly reproducible calibration for precision of molecular weight distribution calculations.
- **Extremely high resolving power for GPC separation of polymer additives and other small molecules**—Column efficiency specification of 50,000 plates/meter provide twice the efficiency of conventional GPC columns.
- **Increased separation speed**—Higher separation efficiency means equivalent resolving power can be obtained with half the column length of conventional GPC columns. Note the equivalency in separation efficiency with only half the length of the HXL columns as shown in the separation.
Result: Faster Separations.

Varian MicroPak TSK HXL Columns are in stock and available now.

MICROPAK TSK TYPE HXL COLUMNS FOR GPC

Description	Exclusion Limit (MW of PS)	Order Number
MicroPak TSK 1000HXL	1×10^3	00-997149-74
MicroPak TSK 2000HXL	1×10^4	00-997150-74
MicroPak TSK 2500HXL	2×10^4	00-997151-74
MicroPak TSK 3000HXL	6×10^4	00-997152-74
MicroPak TSK 4000HXL	4×10^5	00-997153-74
MicroPak TSK 5000HXL	4×10^6	00-997154-74
MicroPak TSK 6000HXL	4×10^7*	00-997155-74
MicroPak TSK 7000HXL	4×10^8*	00-997156-74
MicroPak TSK GMHXL**	4×10^8*	00-997157-74

* Estimated
** GMHXL = mixed bed packing.
Columns are available packed in ODCB for use in high temperature GPC.

To order call: 800-538-1735 *or in California 800-672-1405 or write: Varian Instrument Group, 220 Humboldt Court, Sunnyvale, CA 94089—ATTN: Order Desk. For further information circle the Reader Service Number.*

varian

Intelligent chromatography . . . from Varian

For assistance contact: • Florham Park, NJ (201) 822-3700 • Park Ridge, IL (312) 825-7772 • Sugar Land, TX (713) 491-7330
In Europe: Steinhauserstrasse, CH-6300 Zug, Switzerland.

CIRCLE 224 ON READER SERVICE CARD

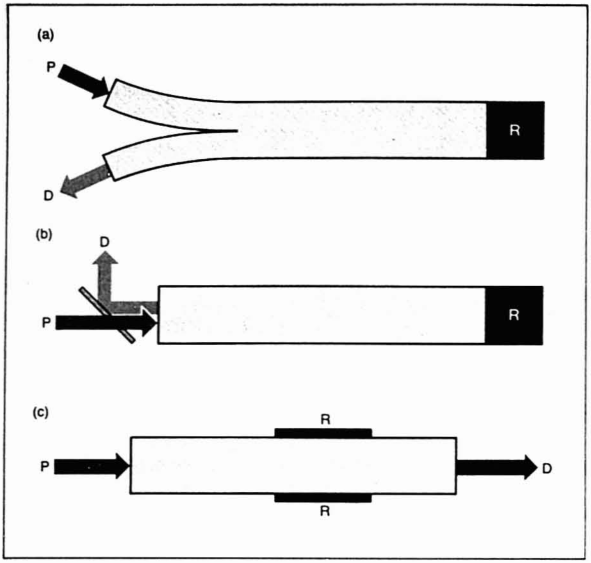

Figure 1. Fiber optic sensors

P = probe radiation, D = detected radiation, R = reagent phase. (a) Sensor based on bifurcated fiber optic in which separate fibers carry probe and detected radiation. (b) Single optic with a beam splitter to separate probe and detected radiation. (c) Single optic sensor in which the reagent phase is coated on the optic

particular application. Laser excitation may be used for long-distance transmission of excitation radiation or to get a useful signal from a small amount of reagent. However, it is also possible to construct devices with incandescent sources that use filters for wavelength selection and phototubes to measure light.

The characteristics of the fiber optic itself are critical in determining the device capabilities. The material of the fiber optic determines the usable range of wavelengths. Fused-silica optics permit measurements in the ultraviolet down to 220 nm, but are relatively expensive. Glass is less expensive and is suitable for measurements in the visible. Plastic fibers are less expensive still, but are restricted to wavelengths above 450 nm.

Devices may involve either bifurcated or single fiber optic bundles as illustrated in Figure 1. A single fiber optic or fiber optic bundle, as shown in Figure 1b, requires that the detected radiation be distinguished from probe radiation either temporally or by wavelength to avoid serious background problems due to scattered probe radiation. Alternatively, the reagent phase can be coated on the outside of a single fiber to modify its transmission characteristics. In bifurcated devices, separate optics transmit probe and detected radiation. These devices observe only the zones of reagent phase that fall within both the cone of emitted probe radiation and the cone of accepted detected radiation.

The diameter of the fiber optic can be on the order of the wavelength of transmitted light. In practice, sensors in the submillimeter size range have already been developed.

Reversible Sensors

Theory of direct sensors. Most reversible sensors involve an equilibrium between analyte and immobilized reagent. If the stoichiometry of this reaction is 1:1 then the reaction may be represented

$$A + R \rightleftharpoons AR \qquad (1)$$

where A is analyte, R is reagent, and AR is the combined analyte–reagent. The equilibrium constant, K_e, may be represented

$$K_e = \frac{\overline{AR}}{\overline{R}\,[A]} \qquad (2)$$

where [A] is analyte concentration and $\overline{R}$ and $\overline{AR}$ are the number of free and combined reagent molecules in the immobilized phase, respectively. It is assumed that activity effects in the immobilized phase are equivalent for $\overline{R}$ and $\overline{AR}$ and thus cancel.

$\overline{AR}$ and $\overline{R}$ vary with analyte concentration as follows:

$$\overline{AR} = \frac{K_e[A]}{1 + K_e\,[A]}\,C_R \qquad (3)$$

$$\overline{R} = \frac{1}{1 + K_e\,[A]}\,C_R \qquad (4)$$

where C_R is the sum of free and combined reagent molecules.

Figure 2a shows response vs. analyte concentration for the case in which the measured optical parameter is proportional to $\overline{AR}$. At low concentrations ($[A] \ll 1/K_e$), response is proportional to [A]. As concentrations increase, response is curved, reaching a limiting value when $[A] \gg 1/K_e$. This corresponds to saturation of the reagent with analyte.

Figure 2b shows the case in which the optical measurement is proportional to $\overline{R}$. In this case, increasing analyte concentration leads to a decrease in the measured parameter. Rather than working with a curve as shown in Figure 2b, it is possible to rearrange Equation 4 to

$$\frac{C_R}{\overline{R}} = 1 + K_e\,[A] \qquad (5)$$

A plot of $C_R/\overline{R}$ vs. [A] will be linear with an intercept of one.

The preferred situation in practice is likely to be the case where the ratio of $\overline{AR}$ to $\overline{R}$ is measured. From Equations 3 and 4

$$\frac{\overline{AR}}{\overline{R}} = K_e\,[A] \qquad (6)$$

The ratio is directly proportional to analyte concentration as well as being independent of C_R and thus insensitive to slow loss of reagent. Ratio measurements frequently have the additional advantage of being less sensitive to instrumental fluctuations as well. The limitation of the ratio approach is that both $\overline{AR}$ and $\overline{R}$ must be present in sufficient amounts to be measured with adequate precision. As a consequence, dynamic range is limited.

It is assumed above that the amount of analyte combining with reagent is small relative to the amount of analyte in the sample, a condition that can be achieved by keeping the amount of reagent small. If this condition is not achieved, the analyte will be depleted in the sample. The response function has to be revised to account for this, and the device is not a true sensor since it is perturbing the sample.

The above discussion emphasizes the importance of the equilibrium constant in determining sensor response. The equilibrium constant is involved in the response function whether one measures $\overline{R}$, $\overline{AR}$, or the $\overline{AR}/\overline{R}$ ratio. In each case, the equilib-

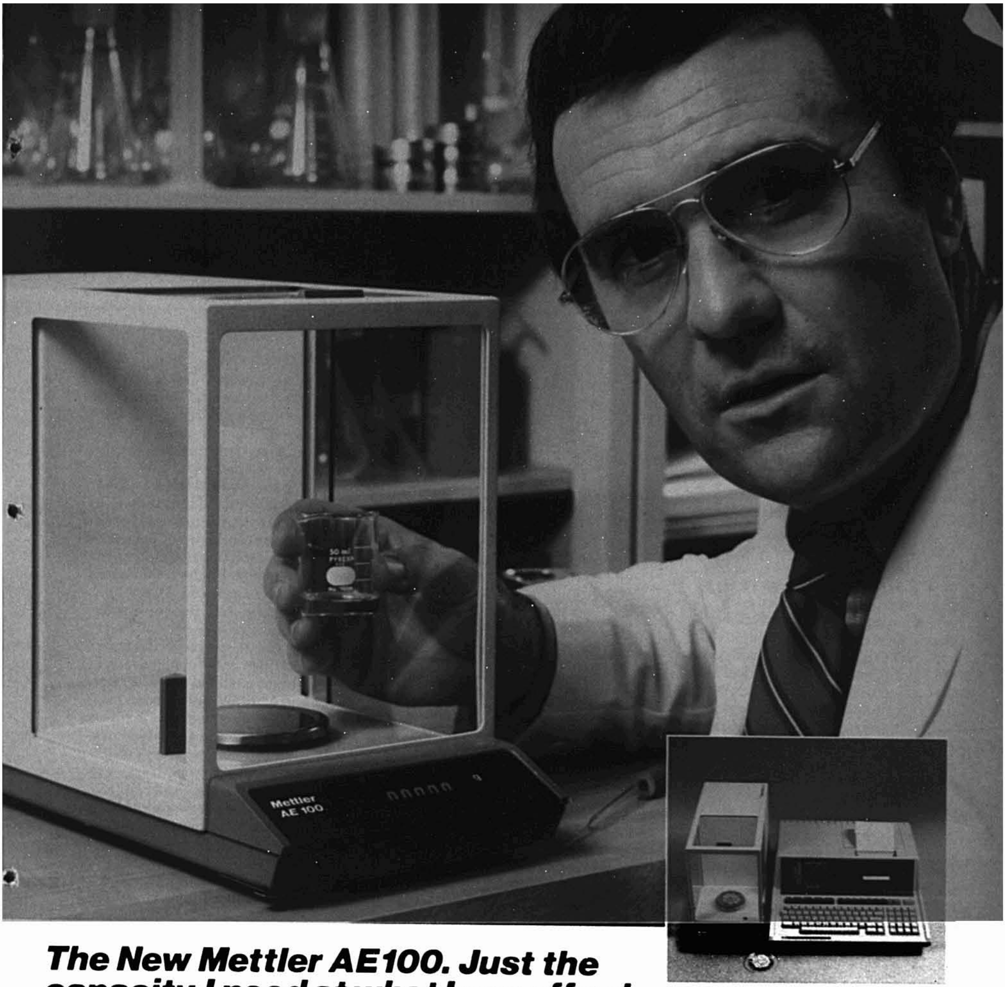

AE balances interface with computers using IEEE-488, 20 mA current loop, RS232C or BCD-parallel standards.

The New Mettler AE100. Just the capacity I need at what I can afford.

Now there's a Mettler electronic analytical balance for weighing 100 grams or less. The new AE100 joins the higher capacity AE163 and AE160 analyticals introduced last year. It has the same big features of the other Mettler AE's. And at a smaller price, just $1995.

Greater productivity with less effort.

The AE's foolproof single control bar design makes it easy to operate. A simple touch on the bar does most of the work for you. From locking in tare to calibration. And the exclusive DeltaDisplay® automatically adjusts itself to your pouring speed until the target weight is reached.

Because it's so easy to use, weighing on an AE goes three or four times faster than on a mechanical balance. And with much more accuracy. It even adjusts itself to environmental changes that would throw off other balances.

Data processing. Another big advantage.

The AE has another great advantage over mechanicals. The ability to interface with computers and other peripherals. Just snap on a Mettler data output option and your AE is ready to transfer information.

Scaled down price.

Like other AE balances, the AE100 is designed with a simplicity of circuitry that keeps the price down. About as affordable as a mechanical. For more information write to Mettler Instrument Corporation, Box 71, Hightstown, NJ 08520. Phone (609) 448-3000.

Mettler

CIRCLE 145 ON READER SERVICE CARD

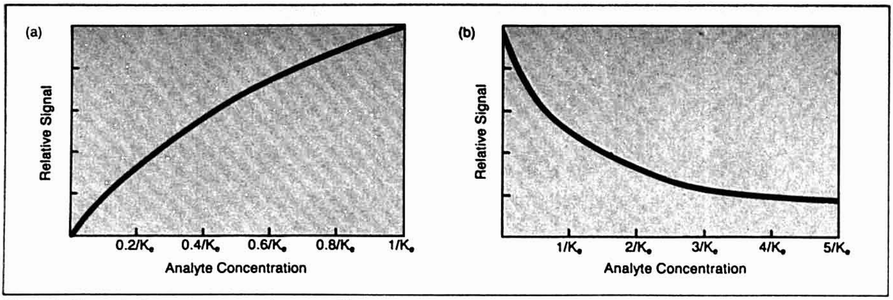

Figure 2. Theoretical response curves for reversible sensors
Analyte concentration is expressed in terms of K_e. (a) Case where $\overline{AR}$ is measured. (b) Case where $\overline{R}$ is measured

rium constant defines the range of analyte concentrations that can be measured with a given reagent phase.

The conditions for optical sensing thus differ from the common analytical situation where large equilibrium constants and reagent excesses are desired to drive an analytical reaction to completion. If that were the case with a sensor, essentially all the analyte would be extracted into the reagent until the point where the reagent phase were saturated. The device would not function as a reversible sensor.

Because the response depends on the equilibrium constant, optical sensors will measure only the concentration of analyte in a form available to interact with reagent. For example, an optical metal ion sensor based on immobilized ligand will measure free metal rather than total metal (just like a potentiometric electrode).

Theory of competitive-binding sensors. A competitive-binding-based sensor includes an immobilized reagent, R, that specifically binds the analyte, A. The reagent phase also includes a ligand, L, which competes with A for binding sites on R. The reactions and associated equilibria are

$$A + R \rightleftarrows AR \quad K_A = \frac{[AR]}{[R][A]} \qquad (7)$$

$$L + R \rightleftarrows LR \quad K_L = \frac{[LR]}{[R][L]} \qquad (8)$$

assuming both R and L are in solution. This can be achieved if L and R are larger molecules than A such that R and L can be confined by a dialysis membrane that allows analyte A to transfer freely between phases. An essential feature of L is that its optical properties change in a measurable way upon binding to R. The detected parameter is based on L, either [L] or [LR].

From mass balance considerations the total concentrations of L and R in the reagent phase, C_L and C_R respectively, are given by

$$C_L = [L] + [LR] \qquad (9)$$

$$C_R = [LR] + [AR] + [R] \qquad (10)$$

Eliminating [R] from Equations 7 and 8 and solving for [A] yields

$$[A] = \frac{[AR]\, K_L\, [L]}{K_A\, [LR]} \qquad (11)$$

If the equilibrium constants K_A and K_L are large enough, then $[R] \ll [LR]$ and [AR], and can be dropped from Equation 10. Substituting for [AR] in Equation 11 yields

$$[A] = \frac{(C_R - [LR])\,[L]}{[LR]} \times \frac{K_L}{K_A} \qquad (12)$$

Using Equation 9 to substitute for either [L] or [LR] yields an expression with a single variable. The K_L/K_A term reflects the fact that response depends on the relative affinity of L and A for reagent R.

Competitive-binding-based sensors make it possible to use analytical reactions that don't directly produce an optical change. The use of antibodies as the specific reagent would allow many possible sensors. However, since more processes and large molecules are involved, response times may be relatively slow. Only one such sensor has been developed to date.

Absorbance-based sensors. The first reversible optical sensor described in the literature is a pH sensor based on the absorbance of phenol red covalently bound to polyacrylamide microspheres (2). Figure 3 shows how the probe is constructed. Two 0.15-mm-diameter plastic fiber optics are inserted into a cellulose hollow fiber that contains the polyacrylamide microspheres plus additional polystyrene microspheres included to scatter light. Radiation from a tungsten source is directed onto the reagent through one fiber optic. Radiation scattered back is detected through the other optic using a filter for wavelength selection. The plug at the end of the fiber keeps incident radiation from interacting with the sample. The wavelength was chosen to measure the basic form of the phenol red.

In the usual absorbance measurement, the reference intensity is mea-

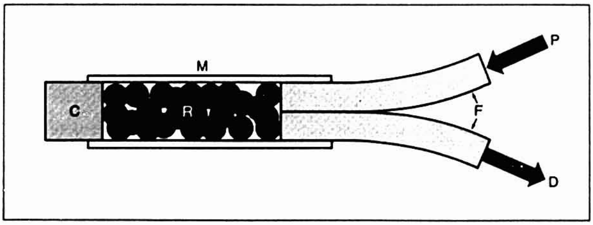

Figure 3. pH sensor based on absorbance

P = probe radiation, F = optical fibers, R = reagent phase immobilized on polyacrylamide spheres, M = cellulose membrane, and D = detected radiation. The reagent phase includes polystyrene spheres to redirect incident probe radiation. A filter wheel is used to sequentially determine transmitted light at two wavelengths, one where the base form of reagent absorbs and the other where no absorption occurs. The cap, C, serves to confine the reagent and prevent incident radiation from entering the sample. The same arrangement is also used for an oxygen sensor based on fluorescence quenching

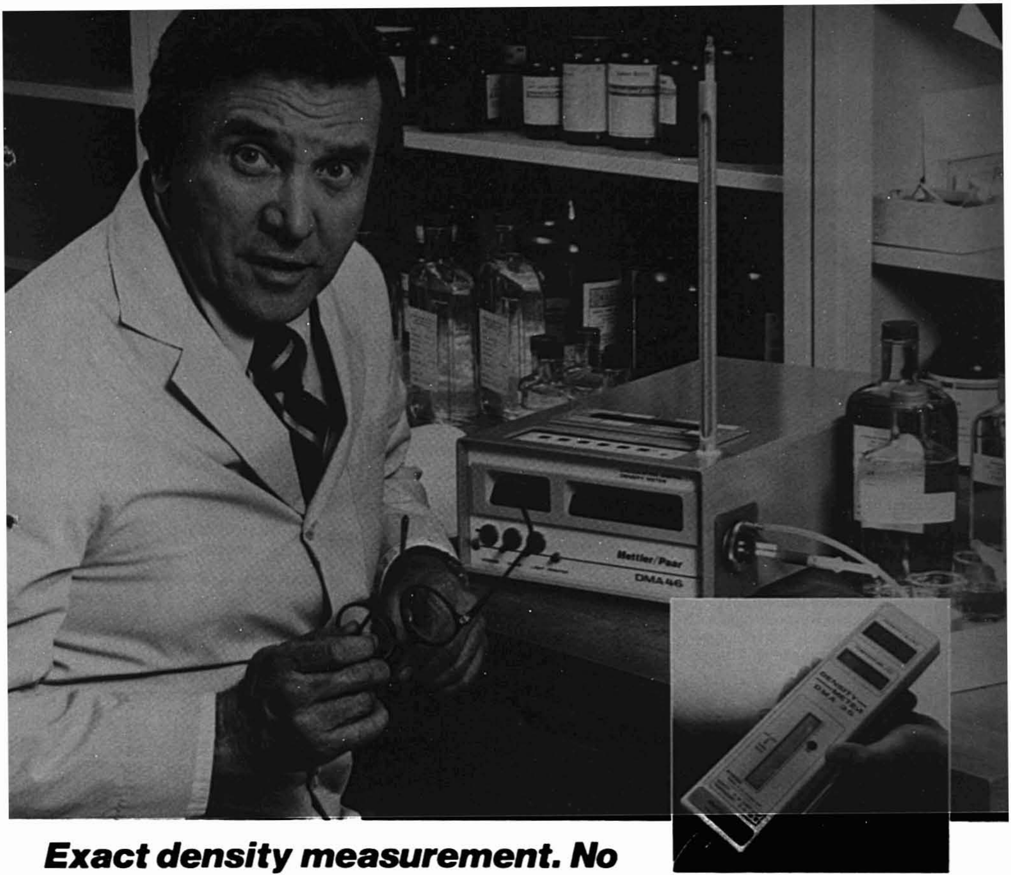

The Mettler/Paar DMA35 is the only totally portable, hand-held density meter.

Exact density measurement. No wait, no error and no pycnometer.

Mettler/Paar Digital Density Meters
All the procedures you're accustomed to, all the time spent on measuring density, specific gravity or concentration, can now be things of the past.

With Mettler/Paar digital density meters, you can obtain identification, characterization and purity measurements in seconds. There's no pycnometer filling, waiting to achieve temperature equilibrium, or weighing procedures. Think how much more quickly you can tighten manufacturing procedures, lower production costs and improve product quality.

Unlimited application
Mettler/Paar density meters are used everywhere. In pharmaceutical and cosmetic labs, in the petrochemical, food and beverage industries, in universities, hospitals and crime labs. For research, quality assurance and process control. And there is one to fit your specific requirements.

The DMA46, for example, has a built-in microprocessor that calculates and displays density, specific gravity, concentration or other density-related values. Its data can be easily transferred to a computer or printer for evaluation or storage. And for work outside the lab, take the portable DMA35 anywhere you need on-the-spot measurements.

Separate models are available to read density, specific gravity or concentration with a precision from 10^{-3}g/cm^3 to 10^{-6}g/cm^3. They are well-suited for quality control or R&D applications, for checking formulation accuracy, and for several ASTM, AOAC and brewing industry methods. Results can be obtained in percent alcohol, Brix or API values.

DMA's meet your needs
Each of our density meters can meet your own special requirements, by itself or with optional accessories. Prices range from under $1,400 to less than $13,000. For more information, or a demonstration of any DMA instrument, write Mettler Instrument Corporation, Box 71, Hightstown, NJ 08520. Or call: (609) 448-3000.

Mettler

CIRCLE 146 ON READER SERVICE CARD

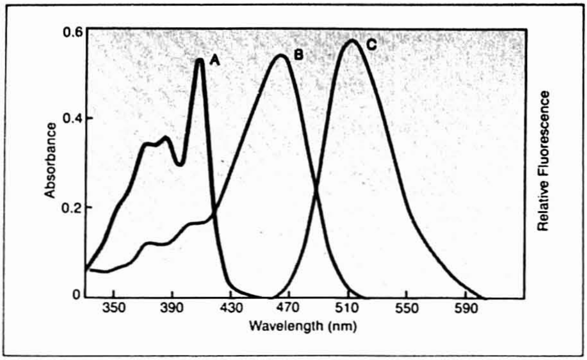

Figure 4. Spectral characteristics of 8-hydroxypyrene-1,3,6-trisulfonate (HOPSA) immobilized on anion exchange membrane

A and B are absorption spectra for acid and base forms of HOPSA, respectively. C is the fluorescence spectrum of the base form. Because HOPSA undergoes rapid excited-state deprotonation at pH > 1, the fluorescence of the base is observed even when the ground state is in the acid form

sured at the same wavelength as the intensity transmitted by the sample. However, in the sensor, it is necessary to measure a reference intensity at a different wavelength where neither the acid nor the base form of the indicator absorb. This intensity is proportional to the reference intensity at the absorption wavelength. The proportionality constant must be accounted for in the calibration procedure.

The resulting probe is small enough to be used for in vivo measurements. The response time is 0.7 min for 63% of maximum response. As is generally true for optical sensors, response time is limited by diffusion of analyte, H^+, into the reagent phase.

Fluorescence sensors. Fluorescence is particularly well suited for optical sensing. It is compatible with a single optic measurement because the detected radiation can be distinguished from probe radiation by wavelength. In addition, fluorescence is an inherently sensitive technique capable of measuring low analyte concentrations. At low fluorophor levels, response to analyte is linear. However, in sensors it may often prove more practical to work at reagent levels where probe radiation is absorbed to a significant extent in the reagent phase. If the absorbance changes with analyte concentration, the response may be affected by the inner filter effect. The geometry of a fluorescence-based sensor corresponds to front-surface detection, a well-characterized situation.

The simplest type of fluorescence sensor involves measuring fluorescence at a single wavelength. An example of this is a pH sensor based on fluoresceinamine covalently coupled to cellulose (*3*). In this sensor, pH is related to an increase in intensity as the acid form of immobilized dye is converted to base. This particular device also illustrates one of the difficulties that can be encountered in preparing fluorescence sensors. Concentration quenching occurs because the immobilized reagent molecules are too close together, causing the intensity from the immobilized reagent to be relatively weak.

Nonfluorescent ligands that form fluorescent complexes with metal ions have been used to prepare sensors that respond to metal ions. Covalently immobilized morin (3,5,7,2′,4′-pentahydroxyflavone) is only weakly fluorescent by itself but forms fluorescent complexes with Al^{+3} and Be^{+2}, and may be used to sense these ions (*4, 5*).

Another metal-ion-sensing system is based on the sodium salt of 8-hydroxyquinoline-5-sulfonic acid immobilized by electrostatic attraction on an anion exchanger (*6*). This form of immobilization is not only convenient but also allows for easy control of the coverage of immobilized reagent on the reagent phase. Leaching of ligand from the anion exchanger does not occur at an observable rate even at high ionic strength when the anion exchanger is undersaturated with respect to ligand. The immobilized salt of 8-hydroxyquinoline-5-sulfonic acid fluoresces only very weakly but forms strongly fluorescent complexes with Mg(II), Zn(II), Cd(II), and Al(III).

In general, metal ions that can be determined fluorimetrically in solution can potentially be sensed optically providing that the appropriate fluorigenic reagent can be immobilized without adversely affecting its fluorescence properties and that the equilibrium constant for complex formation is suitable for sensing (i.e., not too large). The selectivity of sensors based on immobilized fluorigenic ligands will be similar to the selectivity of the ligand in solution. While fluorimetric methods for metals in solution are not widely used at present, adapting them to the two-phase measurement of a sensor may make them the preferred approach to certain problems.

Two-wavelength fluorescence measurements. A more recent pH sensor based on fluorescence illustrates two-wavelength measurements (*7*). The system involves the trisodium salt of 8-hydroxypyrene-1,3,6-trisulfonic acid (HOPSA) immobilized electrostatically on an anion exchange membrane. The absorption spectra for acid and base forms of HOPSA—as well as fluorescence emission of the base form—are shown in Figure 4. As shown below, electronically excited HOPSA undergoes rapid excited-state deprotonation so that $OPSA^-$ fluorescence is observed between pH 1 and 7 even though HOPSA is the dominant ground state species.

$$\begin{tikzcd}
\mathrm{HOPSA}^* \arrow[r] & \mathrm{OPSA}^{-*} \arrow[d, shift left] \\
\mathrm{HOPSA} \arrow[u] \arrow[r, shift left, "\mathrm{p}K_a = 7.3"] & \mathrm{H}^+ + \mathrm{OPSA}^- \arrow[l, shift left] \arrow[u, shift left]
\end{tikzcd}$$

The measured parameter in this sensor is the ratio of fluorescence intensity emitted at 510 nm and excited at 470 nm (specific for base) to intensity excited at 405 nm (selective for acid). The ratio measurement is insensitive to source fluctuations, drift, temperature, quenching, ionic strength, and slow loss of reagent, all of which can affect the single intensity measurement. As a consequence, this type of measurement is likely to be more practical.

Other approaches to ratio measurements are used in pH sensors based on fluorescence from immobilized β-methylumbelliferone (*8*). One approach is to excite at an isosbestic point in the fluorescence excitation spectrum to measure the total amount of indicator present, independent of its form. A second excitation wavelength permits the specific measurement of the base form of the indicator. The ratio of the intensities excited at these two wavelengths is directly proportional to the fraction of β-methylumbelliferone in the base form, which is related to pH and independent of the total amount of indicator.

The second approach is to measure the ratio of fluorescence intensities at two wavelengths, one where the acid form fluoresces and the other where the base form fluoresces. This is possible with fluorescent indicators that do

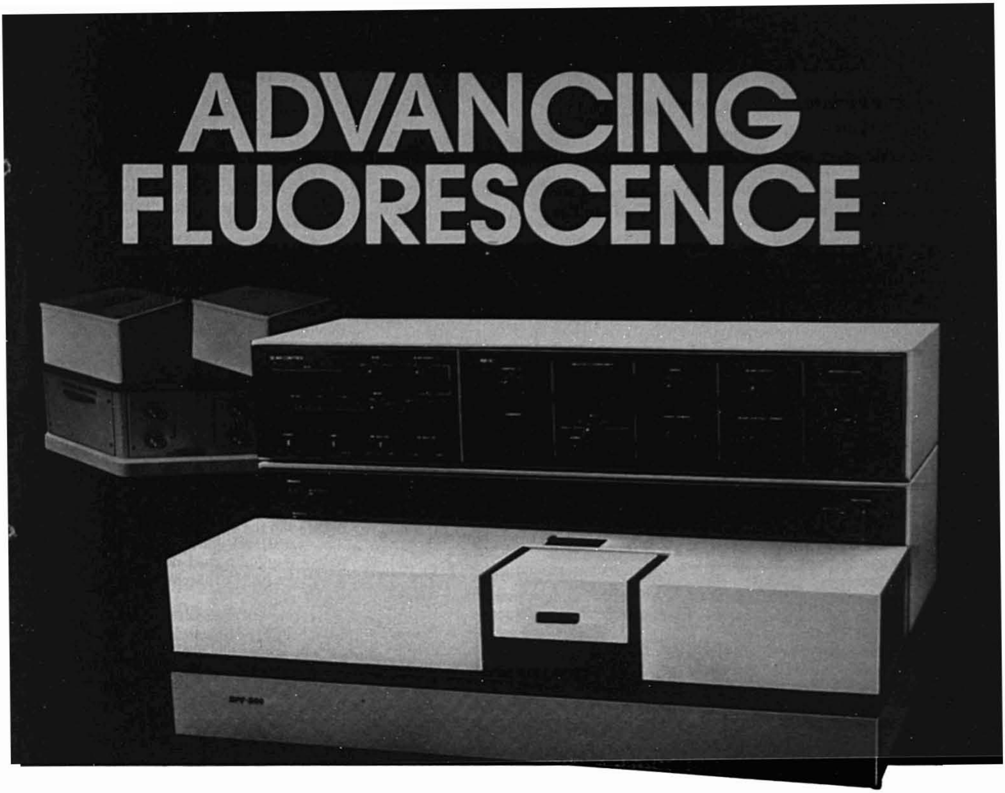

for every fluorometric application.

For over two decades, American Instrument Company has pioneered advances in fluorometry, making instruments which have helped make history.

Today, we make instruments for virtually every fluorescence application. And this experience is part of every instrument we offer.

Consider the SPF-500™ Series Spectrofluorometers, for example; state-of-the-art analytical tools which offer greater sensitivity and resolution, incorporating such features as digital readouts, automatic range selection, and decimal placement for unparalleled operating ease.

And, SPF-500's are versatile. Even without optional accessories, each model includes application capabilities that are simply not available on competitive instruments. These capabilities are further enhanced with our data processing accessory.

For more information about the SPF-500, or any of our other fluorescence instruments, mail this coupon to American Instrument Company, 810 West Anthony Drive, Urbana, IL 61801, U.S.A. or call 800-637-7689 toll-free. TELEX 20-6079.

THE FULL SPECTRUM
FLUORESCENCE INSTRUMENTATION

☐ Send more information on American Instrument's fluorescence instrumentation. **FREE**

My application area is ____________________

Name ____________________

Address ____________________

City ____________ State ______ Zip ______

Phone ____________________

Partners in progress.

SLM·AMINCO T.M.

Copyright 1980, 1982. SLM Instruments, Inc. All rights reserved.

CIRCLE 204 ON READER SERVICE CARD

not undergo excited-state proton transfer like HOPSA. However, it is subject to error if either the acid form or the base form of the indicator is selectively quenched.

The pH sensor based on immobilized β-methylumbelliferone is formulated as a thin layer on a quartz window. The layer is separated from sample by an ion-permeable membrane. The pH sensor also has been used as the internal element of a CO_2 sensor by covering the sensor with a CO_2-permeable membrane and bringing it in contact with HCO_3^-. When the sensing element is a thin layer, it is not optically shielded from the sample. To avoid interferences due to sample fluorescence, it may be necessary to include a layer of a black or reflecting membrane between the sample and the reagent phase. It should be noted that this particular reagent phase was not used with a fiber optic although it easily could be.

Fluorescence quenching. Sensors also can be based on a decrease in reagent phase fluorescence upon association with analyte. Although this is inherently less desirable than systems involving increases in intensity with analyte concentration, it allows access to analytes that could not otherwise be sensed by fluorescence.

An important example of a sensor based on quenching is the O_2 probe developed by Peterson et al. (*9*). The O_2 sensor is similar to the pH probe shown in Figure 3, except that the reagent phase is a dye, perylene dibutyrate, adsorbed on a polymeric support, and the membrane containing the immobilized reagent is porous polypropylene, which is hydrophobic and highly permeable to O_2. Fluorescence is excited through one fiber and observed through the other. Filters are used to measure separately the green fluorescence of perylene dibutyrate and scattered blue excitation radiation. The intensity of fluorescence is ratioed to the intensity of scattered radiation to compensate for changes in source intensity. This sensor is particularly attractive because it is reversible. Unlike the widely used oxygen electrode, it does not require continued mass transfer of oxygen to the sensor surface to maintain a constant signal.

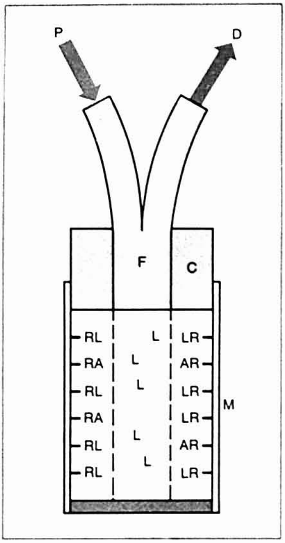

Figure 5. Competitive-binding fluorescence sensor for glucose

F is the bifurcated fiber optic; C is the cladding around the fiber bundle; R is the reagent, concanavalin A immobilized on sepharose and coated on the walls of the hollow fiber, M; L is the competing ligand, dextran labeled with fluorescein; and A is the analyte, glucose

The O_2 sensor is based on dynamic quenching, i.e., an excited-state interaction with the fluorophor. The response follows the form of Equation 5 (Figure 2b) where "free" immobilized reagent is measured as a function of analyte concentration. However, the equilibrium constant is replaced by a quenching constant that depends on the relative rates of fluorescence and nonradiative return to the ground state through interaction with the quencher. One of the reasons perylene dibutyrate was selected as the dye for the O_2 sensor was that its quenching constant was the right magnitude to yield sensitive response to the range of oxygen partial pressures of physiological interest.

A similar device has been based on fluorescence quenching of pyrenebutyric acid by O_2 (*8*). This study demonstrated how the medium of the pyrenebutyric acid affects the rate of quenching by O_2 and how this influences the slope of the response curve. These media effects can serve as a means of tailoring the O_2 sensor to optimally measure a particular O_2 partial pressure range.

A range of quenching-based sensors is possible. In addition to the O_2 sensor, sensors based on transition metal quenching of ligand fluorescence and iodine quenching of rubrene fluorescence have been proposed (*1*).

Competitive-binding sensor based on fluorescence. A fluorescence-based, competitive-binding sensor for glucose has been described (*10*). The specific glucose-binding reagent is concanavalin A immobilized on sepharose. The competing ligand is dextran labeled with fluorescein. A schematic of the device is shown in Figure 5. The fiber optic fits in a hollow fiber with a plug on the end. Glucose can diffuse freely through the hollow fiber but dextran cannot. The immobilized concanavalin A is on the walls of the fiber and thus out of the volume illuminated through the fiber optic. Increasing glucose concentration displaces the labeled dextran from the concanavalin A, causing it to be free to diffuse into the illuminated solution volume. This in turn leads to an increase in fluorescence, which is related to glucose concentration.

Reflectance-based sensors. When dealing with solid phases, it becomes difficult to measure transmitted light satisfactorily. In these cases the intensity of reflected light may be used as a measure of the color of an immobilized reagent phase. In the context of a sensor, a true reference intensity cannot be measured at the analytical wavelength. Instead, an intensity proportional to the reference intensity must be measured at a wavelength other than the analytical wavelength. This wavelength should be chosen so that it is not absorbed either by reagent alone or by reagent combined with analyte.

Because it is difficult to prepare a sensor that truly measures absorbance, reflectance is likely to be the more widely used technique for sensors based on color changes. In fact, it is not clear that the pH sensor developed by Peterson et al. (*2*) truly measures absorbance rather than reflectance, since adherence to Beer's law was not verified. An attractive feature of reflectance is that it can be used to measure the ratio of free and combined reagent if the analytical reaction is accompanied by a change in color. The functional relationship between reflectance and concentration will depend on the nature of the reagent phase and the optical arrangement.

An example of a reflectance-based sensor is an ammonia detector (*11*). In this particular device a layer of oxazine dye is coated on the outside of a fiber optic (see Figure 1c). Interaction with ammonia changes the color of the dye, changing its reflectance and modifying the intensity of light transmitted to the detector. Another example involves a method for monitoring oil in water (*12*).

Nonreversible Sensors

It is possible to design sensors based on analytical reactions that consume reagent. Although such sensors necessarily have finite lifetimes, these lifetimes can be quite long if the rate of reagent consumption is small relative to the total amount of reagent available. Another disadvantage of nonreversible sensors is that they require

(*continued on p. 33 A*)

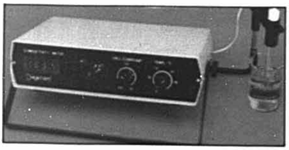

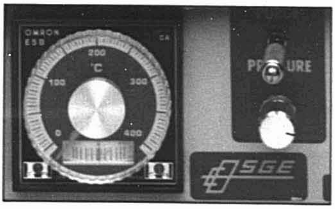
OMRON
E5B
°C
0
100
200
300
400
SGE

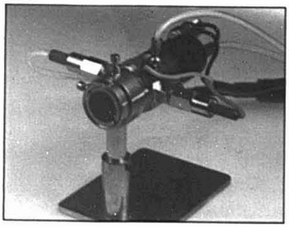

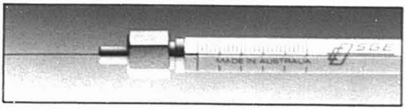
SGE
MADE IN AUSTRALIA

Hi-lights

CAPILLARY PRESSURE SWITCHING SYSTEM

ChronTrol
PM
CIRCUIT
1 2 3 4
ENTER
CLEAR
LOCK
SECOND
WEEK CYCLE
CIRCUIT VARY
AM
PM
PRE-COLUMN
psi
SGE
MID-POINT
INLET SPLIT
MID POINT SPLIT
ON
OFF
REMOTE
BACK-FLUSH
SPLIT BACK-FLUSH
CAPILLARY PNEUMATICS CONTROL MODULE
HEART-CUT
COLD-TRAP

A pneumatic system which permits the relatively simple retrofitting of existing dual detector GC's for multi-dimensional capillary capabilities is available from SGE. A conventional packed or capillary GC can be quickly upgraded to permit capillary column manipulations such as heart-cutting, back-flushing, variable splitting and cold-trapping to be performed. A detailed brochure describing the operation and application of the above system is available upon request.

From a Brilliant Idea to a Brilliant Lamp.

SGE's Demountable Cathode Lamp can be used for all AA analysis. It is no longer necessary to use a special spectral lamp for a particular element—now you can simply plug in an inexpensive interchangeable cathode. Single and multi-element cathodes can be changed quickly and without cross contamination. Multi-element cathodes can be made at short notice by SGE or even by the user. The lamp can be used for AA, fluorescence and emission spectroscopy.

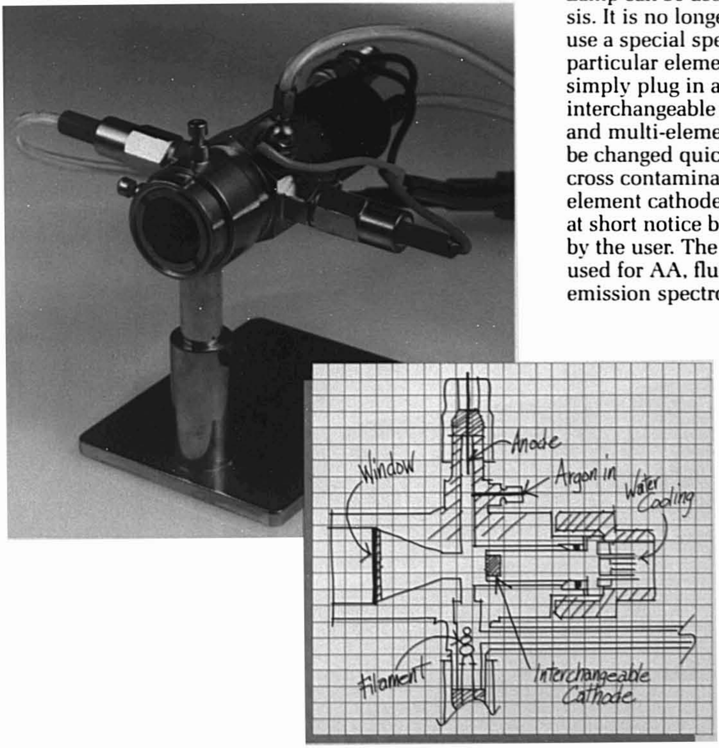
Anode
Window
Argon in
Water Cooling
Filament
Interchangeable Cathode

Circle Reader Service Card No. 195

CONDUCTIVITY METER DIGIMED CD-20

The digital direct reading Conductivity Meter Digimed is specifically built for easy, quick and very accurate measuring of the conductivity of any aqueous sample. Designed for laboratories, it can be used over the entire range of electrolytic conductance from demineralized water to strong acids. It is especially useful in the laboratory for the control of steam boiler water, demineralized water, mine acids, mill waste and in most cases where the determination of the ionic concentration of solutions is required.

It consists basically of an electronic module connected to a special dip-type 12mm O.D. platinum conductivity cell. The cell is dipped in the sample and sends a signal back to the electronic module which amplifies it and transforms it into conductivity units. To avoid the electrolysis effect, the cell is supplied with A.C. current.

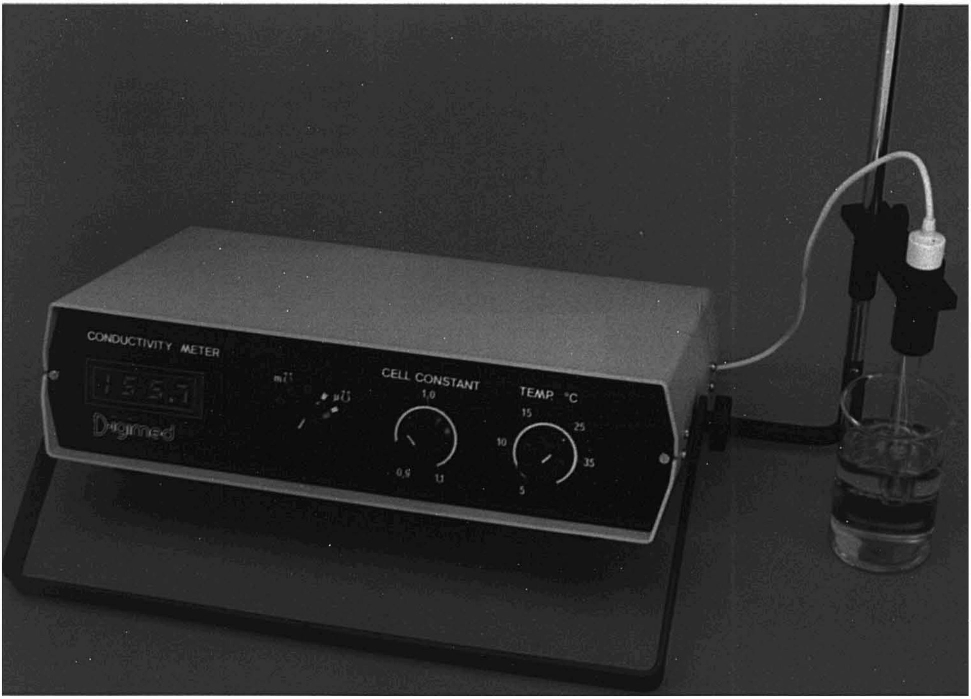

Circle Reader Service Card No. 196

POISON
NOT TO BE TAKEN INTERNALLY
KEEP OUT OF REACH OF CHILDREN
PLEASE FOLLOW ALL DIRECTIONS
SGE
UNITREX

Get the worst out of things.

The SGE Unitrex has been developed as an efficient and economical clean up system for the recovery of pesticides and organic residues from meat fats, butter, cheese and vegetable oils, and a wide range of other samples. The Unitrex can process 10 samples simultaneously and only small amounts of solvents and gas are required. Recoveries for a range of pesticides, both organo-chlorine and organophosphorous compounds, are better than 90% for most samples at ppb levels.

Circle Reader Service Card No. 197

Capillary Chromatography Accessories

Scientific Glass Engineering maintains a complete accessory line for capillary chromatography. Vitreous silica capillary columns in standard liquid phases or bonded phases, narrow or wide bore and three different lengths are in stock for immediate delivery. We manufacture a complete line of inlet splitters, outlet splitters and on-column injectors for converting most commercial GC's to capillary column operation. Also available are ferrules, syringes and low-dead volume unions which the chromatographer may require for system operation. We can fabricate special low-dead volume T's, transfer lines and other similar products if the necessary drawings are sent to us. A catalog is available on the above mentioned items.

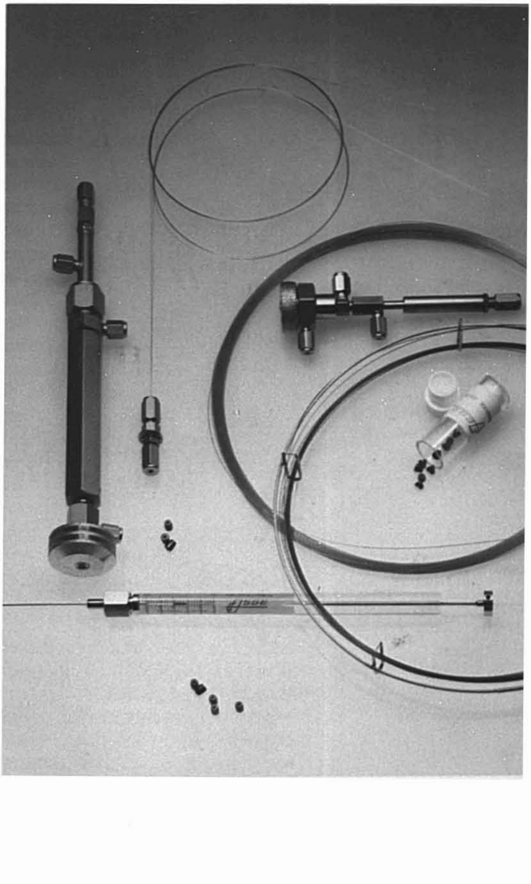

Circle Reader Service Card No. 198

Syringes
Syringes
Syringes

SGE now offers for the first time in the industry a six pack of 10μl-syringes for liquid chromatography. Six packs are available for the Waters, Rheodyne and Valco valves at a savings over a single purchased syringe. Each syringe has a teflon tipped plunger which is interchangeable between syringes, another first in the industry. If the plunger becomes damaged or bent, replacement plungers are available. Since normally the needle is very seldom damaged in LC operation, the life of these syringes is greatly enhanced.

Liquid Chromatography

Ordering

Product/Part #		Description	Price
CAPILLARY PRESSURE SWITCHING SYSTEM			
PCS	093340	Pneumatics Control System	$2,150.00
MRC/.2	093341	Mid-Point Restrictor (Capillary to Capillary, narrow bore)	85.00
MRC/.3	0933410	Mid-Point Restrictor (Capillary to Capillary, wide bore)	90.00
MRP/.2	0933411	Mid-Point Restrictor (Packed to Capillary, narrow bore)	98.00
MRP/.3	0933412	Mid-Point Restrictor (Packed to Capillary, wide bore)	98.00
CTS	093345	Cold-Trap System	150.00
TI-1	093359	Timer (Standard)	259.00
TI-2	093360	Timer (Expanded Capacity)	409.00
ATOMIC ABSORPTION LAMP			
DCL	154150	Demountable Cathode Lamp	1,120.00
MB		Mounting Bracket	Specify Instrument
DCL/PS110	154203	Power Supply	3,380.00
CONDUCTIVITY METER			
CD-20		Digimed (Includes Cell)	790.00
RC-10		Replacement Cell	115.00
UNITREX			
UTX-110	093290	Unitrex 110/120 Volt	3,250.00
CHROMATOGRAPHY ACCESSORIES			
		Request separate catalog and price list	
SYRINGES			
SK-101-R	010004	Six Pack for Rheodyne	110.00
SK-101-W	010007	Six Pack for Waters	110.00
SK-101-V	010006	Six Pack for Valco	110.00

Head Office
Scientific Glass Engineering Pty. Ltd.,
7 Argent Place, Ringwood,
Victoria, 3134 Australia.
Tel: (03) 874 6333

U.S.A. Sales Office:
Scientific Glass Engineering Inc.,
2007 Kramer Lane, Suite 100,
Austin, Texas 78758, U.S.A.
Tel: (512) 837 7190

UK Sales Office:
Scientific Glass Engineering Ltd.,
Potters Lane, Kiln Farm,
Milton Keynes MK11 3LA, Great Britain,
Tel: (0908) 56 8844

German (BRD) Sales Office:
Scientific Glass Engineering GmbH.,
Fichtenweg 15,
D-6108 Weiterstadt 1.
Tel: (06150) 40662

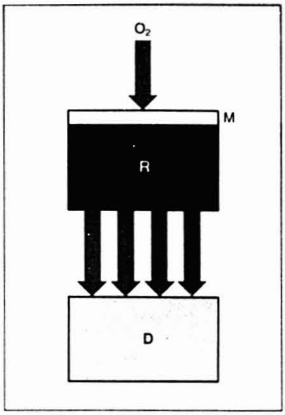

Figure 6. Nonreversible O_2 sensor
O_2 diffuses through Teflon membrane, M, into reagent phase, R, where it reacts to yield chemiluminescence measured by detection system, D

steady-state mass transfer to get a constant signal. Any processes that perturb mass transfer are potential sources of error.

The difference between reversible and nonreversible optical sensors is similar to the difference between potentiometric and amperometric electrodes. Amperometric electrodes, like nonreversible optical sensors, involve a reaction and require mass transfer to an electrode surface.

The use of tetrakis(dimethylaminoethylene) (TMAE) to measure oxygen serves as an example of a nonreversible sensor (*13*). The device is illustrated in Figure 6. Oxygen in the sample diffuses through a hydrophobic O_2-permeable membrane into a reservoir of TMAE. There it reacts with TMAE yielding chemiluminescence, which is measured by a light detection system. (No probe radiation is required for this device.) Steady-state chemiluminescence is proportional to the partial pressure of oxygen. Both the flow rate of O_2 past the membrane and the temperature affect response because they affect the steady-state supply of O_2 into the reagent phase. The lifetime of the sensor is determined by the rate of TMAE consumption relative to the total TMAE available. The lifetime can be quite long—months and even years—if a large TMAE reservoir is used with a low rate of oxygen permeation. Again, it should be noted that this particular reagent was not combined with a fiber optic but readily could be.

Other nonreversible sensors include UO^{2+} and halide sensors (*1*). These devices differ from the O_2 sensor in

VERSATILITY in
ANALYTICAL INSTRUMENTATION
ORIEL'S modular design enables a DO-IT-YOURSELF component approach for
SPECTROFLUORIMETRY
ABSORPTION MEASUREMENTS
TRANSMISSION MEASUREMENTS
SCATTERING MEASUREMENTS
MONOCHROMATIC ILLUMINATION
SPECTRORADIOMETRY
BROADBAND GENERAL ILLUMINATION

For detail information write or call:
ORIEL CORPORATION
250 LONG BEACH BLVD., P.O. BOX 872, STRATFORD, CT 06497 • (203) 377-8282 TWX 710-453-8719

FEDERAL REPUBLIC OF GERMANY
ORIEL GmbH
Darmstadt (06151) 82076

FRANCE
ORIEL S.A.R.L.
Paris 371-00-60

UNITED KINGDOM
ORIEL SCIENTIFIC LTD
Kingston-upon-Thames, Surrey
01 549 4525

ITALY
ORIEL SRL
Milano 02-5392188

SWITZERLAND
ORIEL Bureau Suisse
Morges 21-879509

CIRCLE 157 ON READER SERVICE CARD

CHEMISTRY ...it's the tops!
SAVE 10% TO 20%
FREE CATALOG
Witty and wonderful!
ACS T-shirts
Barbecue/lab aprons
Tote bags
And more!

Experiment with a Chemist! I have Designer Genes! Chemistry Spoken Here! And lots more! Choose your sentiment and wear it close to your heart with ACS sportswear. Sizes for men, women, and children. Quantity discounts, too.

Call (202) 872-4588 or mail coupon below for your free catalog today.

Education Division, American Chemical Society
1155 Sixteenth Street, N.W., Washington, D.C. 20036

Please send free catalog listing ACS T-shirts and other items:

Name ____________________
Address ____________________
City, State, Zip ____________________

that they require that reagent be diffused into the sample. In the UO_2^{2+} sensor, phosphate and nitric acid are diffused into the sample to generate a medium in which UO^{2+} becomes fluorescent. In the halide sensor, Ag-fluorescein is diffused into the sample. Halides combine with Ag^+, rendering fluorescein fluorescent.

The Future

Chemical sensors based on fiber optics are clearly attractive in concept. Success in practice requires the development of appropriate reagent phases. This process is only beginning. However, the devices developed to date already illustrate the wide variety of approaches and systems that are possible.

Interest in optical sensors is certain to intensify in the next few years, and there are some trends that are likely to emerge. Because the dynamic range of sensors is limited and depends on equilibrium constants, a series of reagent phases will be developed for a single analyte in order to respond to different levels of analyte concentration. Other probable trends will be the increased use of measurements at two or more wavelengths and the increased use of reflectance to exploit reactions causing color changes.

Successful development of optical sensors that respond directly to common analytes will inevitably lead to coupled sensors in which a reagent phase "transduces" the analyte of interest to a species measured by the optical sensor. As already mentioned, optical pH sensors in contact with bicarbonate have already served as the internal sensing elements of CO_2 sensors (*8*, *14*, *15*).

References

(1) Borman, S. A. *Anal. Chem.* **1981,** *53,* 1616–18 A.

(2) Peterson, J. I.; Goldstein, S. R.; Fitzgerald, R. V.; Buckhold, D. K. *Anal. Chem.* **1980,** *52,* 864–69.

(3) Saari, L. A.; Seitz, W. R. *Anal. Chem.* **1982,** *54,* 821–23.

(4) Saari, L. A.; Seitz, W. R. *Anal. Chem.* **1983,** *55,* 667–70.

(5) Saari, L. A.; Seitz, W. R., submitted for publication in *Analyst.*

(6) Zhujun, Z., unpublished work.

(7) Zhujun, Z.; Seitz, W. R., submitted for publication in *Anal. Chim. Acta.*

(8) Lübbers, D. W.; Opitz, N. In "Proceedings of the International Meeting on Chemical Sensors"; Fukuoka, Japan; Elsevier: Amsterdam, 1983; pp. 609–19.

(9) Peterson, J. I.; Fitzgerald, R. V.; Buckhold, D. K. *Anal. Chem.*, **1984,** *56,* 62–67.

(10) Schultz, J. S. U.S. Patent 43 444 38, 1982.

(11) Giuliani, J. F.; Wohltjen, H.; Jarvis, N. L. *Opt. Lett.* **1983,** *8,* 54–56.

(12) Kawahara, F. K.; Fiuten, R. A.; Silvus, H. S.; Newman, F. N.; Frazar, J. H. *Anal. Chim. Acta* **1983,** *151,* 315.

(13) Freeman, T. M.; Seitz, W. R. *Anal. Chem.* **1981,** *53,* 98–102.

(14) Zhujun, Z.; Seitz, W. R., submitted for publication in *Anal. Chim. Acta.*

(15) Vurek, G.; Peterson, John; Goldstein, Seth; Severinghaus, John. *Federation Proceedings* **1982,** *41,* 1484.

Rudolf Seitz received his PhD from MIT in 1970. After working at the EPA's Southeast Environmental Research Laboratory and at the University of Georgia, he joined the faculty of the University of New Hampshire in 1976. Although his earlier research dealt with chemiluminescence, he is now primarily interested in fluorescence and the development of optical sensors.

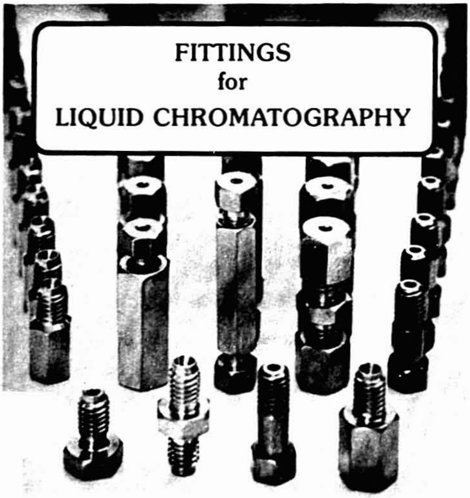

FITTINGS
for
LIQUID CHROMATOGRAPHY

Call or Write for Catalog

Upchurch Scientific, Inc.
2969 North Goldie Road • Oak Harbor, Washington 98277
(206) 679-2528 • (800) 426-0191 • Telex 152-465

CIRCLE 210 ON READER SERVICE CARD

Roger Adams: Scientist and Statesman

by D. Stanley Tarbell and Ann Tracy Tarbell

Examines the life of Roger Adams — a man unparalleled in his contribution to the development of organic chemistry.

A comprehensive biographical sketch of Roger Adams, whose work was important in the development of American chemistry and chemical education. Adams's early years, education, and career achievements in academia, industry, research, and government are described.

CONTENTS

Introduction • Early Years and College • Germany and Harvard, 1912–16 • Illinois, 1916–26 • Academic Progress • Service and Research to 1942 • Government Service, 1940–48 • Illinois and Research, 1943–67 • Broader Horizons • Career Achievements of Roger Adams's Ph.D.s, 1918–58 • Career Achievements of Roger Adams's Postdoctorates, 1936–59

240 pages (1981) Clothbound
US & Canada **$13.95** Export **$16.95**
LC 81-17625 ISBN 0-8412-0598-1

240 pages (1981) Paper
US & Canada **$9.95** Export **$11.95**
LC 81-17625 ISBN 0-8412-0711-9

Order from:
American Chemical Society
Distribution Office — 14
1155 Sixteenth St., N.W.
Washington, D.C. 20036
or CALL TOLL FREE 800-424-6747
and use your credit card.

What Happened at Three Mile Island?

Chemical analysis will help scientists determine the thermal history and chemical composition of the damaged reactor core

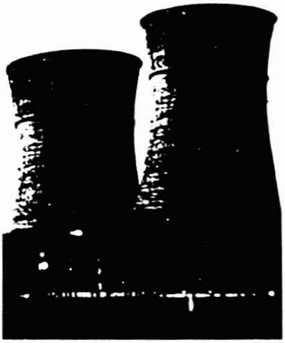

It is nearly five years since the nation's worst nuclear accident occurred at the Three Mile Island (TMI) unit 2 reactor in Middletown, Pa., but only now are scientists beginning to get a close look at what is left of the damaged reactor core. It was this past September that technicians first lowered remote-sampling devices through vacant control rod ports to the rubble bed on top of the TMI core. Sampling was performed from the service structure, a rigid assembly that rests on top of the reactor vessel head. Milton R. Benjamin of the *Washington Post* reported (Sept. 11, 1983, p. A9) that the entry missions looked something like moon walks, with the technicians wearing air-cooled protective suits.

The samples obtained in September were loaded into heavily shielded casks and shipped to the Department of Energy's (DOE's) Idaho National Engineering Laboratory (INEL) for physical and chemical testing. According to Michael R. Martin, program manager for the laboratory's core activities research program, "A good share of the work done here at INEL is related to fuel performance and off-normal or accident-type situations. The technical staff here has been intimately involved with core performance and related safety issues."

INEL has three primary objectives in examining the TMI core material. One objective is to aid in defueling the reactor, "to see what our problems are in taking the core out," explained Willis Young, a nuclear engineer in DOE's Idaho Operations Office. The second aim is to determine the "thermal history" of the reactor, the temperatures experienced by the core during and after the accident. Third, INEL scientists hope to determine what fission products were retained in the core and in what amounts.

The study is divided into two sets of tests: physical testing related to defueling concerns on the one hand, and chemical analysis and other research-oriented activities on the other.

The organizations at TMI that are responsible for plant recovery and defueling, such as General Public Utilities, owner of the damaged unit 2 reactor, are initially interested in obtaining physical and mechanical data on the core debris. Early testing at INEL will thus focus on providing data on physical parameters, such as particle size distribution and leachability.

There are also plans to look at filtration properties of the materials. When the core is defueled, fine particulates will have to be filtered out of the plant water that still covers the core. Smaller particle sizes tend to plug filters, so tests will be run to assist in the design of a filter system that can remove fine particulates and still have a useful lifetime in the plant.

Phase two of INEL's testing program, called the core activities research program, will involve a series of chemical analyses on the core samples. Radioisotopic concentrations will be determined primarily by gamma ray spectroscopy; delayed neutron analysis will be used to determine fissile material content; and elemental composition is being done by emission spectroscopy.

Neutron activation analysis will be used to determine I-129 and Te content, and chemical separation followed by beta counting will be used to obtain Sr concentrations. I-129, Te, and Sr are all fission products of particular interest because they are hazardous to living things.

Perhaps surprisingly, molecular analysis will also play a role in INEL's core activities research. For instance, a molecular optical laser examiner (MOLE) will be used. "I realize the MOLE is generally used in organic chemistry," Martin explains, "and there's no reason to believe there are any organics in the TMI core. But the amount of metallic zirconium that was converted to zirconium oxide in the accident is of interest, and the MOLE will help with those determinations." The zirconium originates in the zircalloy cladding that covers the fuel rods in the TMI reactor core.

According to Martin, analytical testing will probably not be completed until late in 1984, after which a "GEND Report" will be written. The GEND acronym comes from the first initial of each of the four major participants in the cleanup and research at TMI: General Public Utilities, the Electric Power Research Institute, the Nuclear Regulatory Commission, and the Department of Energy. The GEND reports are public documents that are very widely distributed.

0003-2700/83/0351-035A$01.50/0
© 1983 American Chemical Society

Center for Process Analytical Chemistry Receives Planning Grant

On Nov. 1, 1983, the University of Washington received a $52,000 planning grant from the National Science Foundation (NSF) for a proposed Center for Process Analytical Chemistry (CPAC). *Process analytical chemistry* is the use of analytical procedures and instrumentation as an integral part of an automated chemical process. According to CPAC project director Deborah L. Illman, "Continuous analysis is desirable whenever temperature, pressure, chemical composition, product yield, waste product profiles, and quality control are involved."

CPAC plans to conduct basic research on process optimization and control through the application of advanced sensors and state-of-the-art monitoring techniques, and it will serve as a training ground and information clearinghouse on process analytical chemistry. The center will also stress the integration of sophisticated chemometrics techniques, such as multivariate data analysis, into production monitoring technology.

Chemometrics is a field of chemistry involving the use of efficient mathematical methods and optimized experimental design to obtain the greatest possible amount of information on material systems (see *Anal. Chem.* **1982,** *54*, 1379–80 A). The University of Washington has been a center of expertise in chemometrics for some time.

CPAC's prospectus suggests that to compete successfully in world markets the U.S. chemical process industries should pay closer attention to productivity and quality control: "The demand for continuous monitoring and detailed accounting of all process components, including raw materials, . . . products, and effluents will certainly intensify in the future. Moreover, better optimization and control of processes will require more sophisticated on-line sensors that rapidly provide direct chemical information on products and impurities. New powerful algorithms for interpreting this information and utilizing it for process control need to be developed. This is the essence of process analytical chemistry."

CPAC will be an interdisciplinary effort, involving faculty members from the departments of chemistry, chemical engineering, electrical engineering, and laboratory medicine. CPAC principal investigators are Bruce R. Kowalski and James B. Callis, both of whom are professors of chemistry at the University of Washington. Visiting scholars will also augment the center's staff from time to time, including Jaromir Růžička of the Technical University of Denmark, who will be in residence in the spring quarter of 1984.

The NSF planning grant will enable Kowalski and Callis to study possible alternatives for both structure and content of the research to be pursued and to evaluate industry's interest in the proposed center. Industrial sponsors will be asked to contribute $30,000 per year to participate in and benefit from the center's research, with a projected starting date of July 1, 1984.

If sufficient industry support is generated and further NSF funding is obtained, CPAC will become one of a number of NSF-initiated university–industry cooperative research centers, which include the Center for Applied Polymer Research at Case Western Reserve, the Center for Interactive Computer Graphics at Rensselaer Polytechnic Institute, and the Ceramics Cooperative Research Center at Rutgers University. NSF typically provides first a planning grant, such as that recently approved for CPAC, and then a five-year continuing grant to help such centers get on their feet. At the end of five years, the centers are expected to become self-sustaining.

For further information on CPAC, write to the Center for Process Analytical Chemistry, Department of Chemistry (BG-10), University of Washington, Seattle, Wash. 98195, or call the center at 206-543-1655.

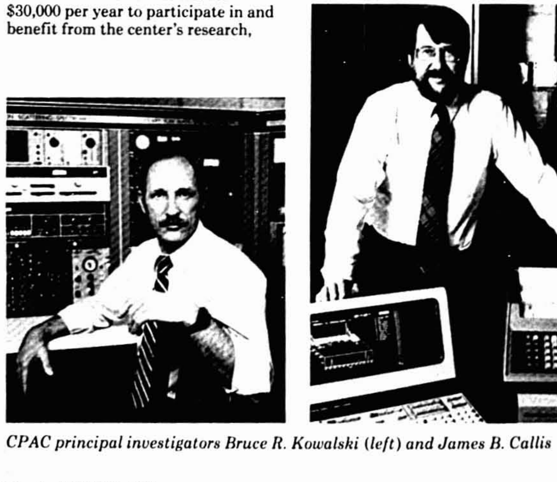

CPAC principal investigators Bruce R. Kowalski (left) and James B. Callis

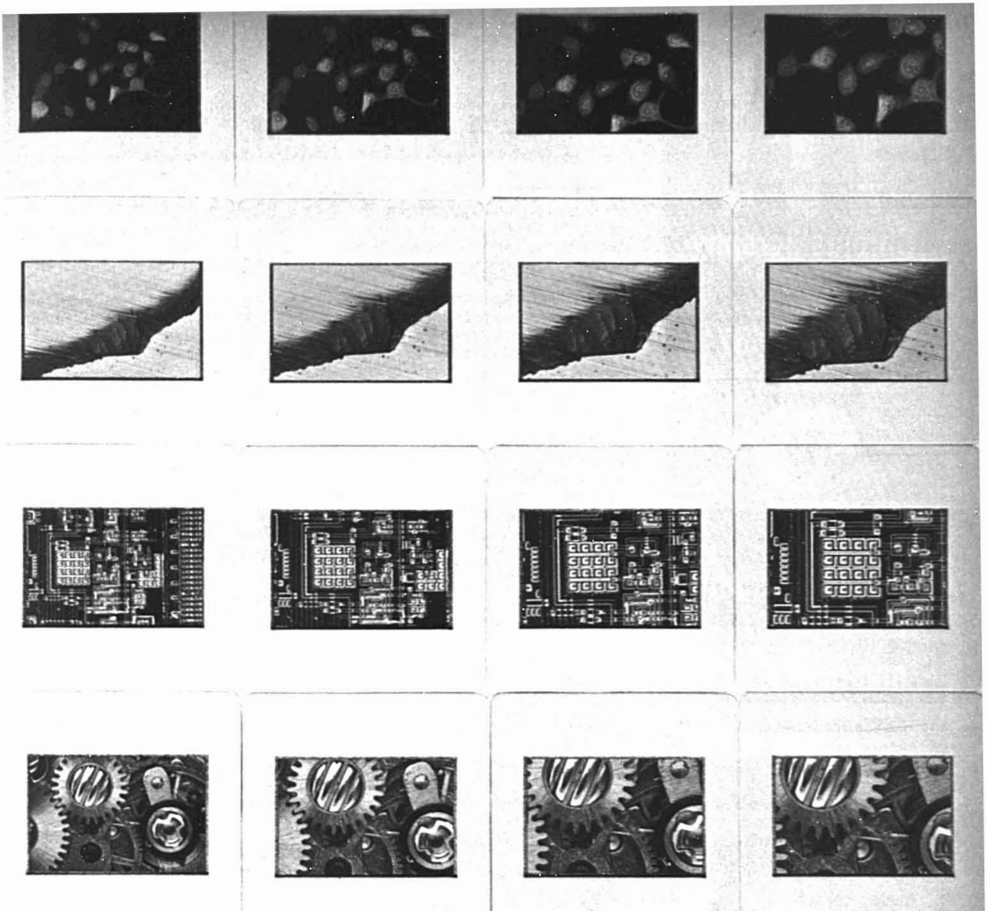

PICTURE PERFECT

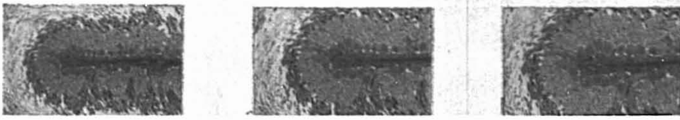

There's a breakthrough in photomicrography that's the image of perfection, the new Nikon UFX photomicrographic system.

An exclusive Direct Projection System transmits 100% of the available light to the film. The result is drastically shorter exposures, greatly enhanced low light sensitivity and a striking improvement in contrast. Computer control assures automatic exposure accuracy in either 1% spot or integrated average metering modes. Yet, this system is astonishingly simple to operate.

For the total picture of Nikon's new FX systems for 35mm, Polaroid® and large format photomicrography, write: Nikon Inc., Instrument Division, 623 Stewart Avenue, Garden City, NY 11530. (516) 222-0200.

Nikon

Extending Man's Vision

Circle #154 for information. **Circle #155 for a demonstration.**

© 1982 Nikon Inc

!!!

Chromatography Problem?
Call
800-526-3687*
for the solution!

?

Chromatography Question?
Call
800-526-3687*
for the answer!

We can help with application advice, we can help with column selection, we can help with technical trouble-shooting or with an accessory that will do the trick, or even a custom made column for your unique needs.

If you're working with HPLC, GC, or Capillary GC (or want to know how to switch over to capillary GC, easily and economically) call 800-526-3687*. You'll reach Chrompack, specialists in chromatography

* In N.J. Call 201-722-8930

chrompack
chromatography specialists

Chrompack, Inc.
PO Box 6795
Bridgewater, NJ 08807
201-722-8930

CIRCLE 32 ON READER SERVICE CARD

Academic–Industrial Cooperation

Can the barriers be overcome?

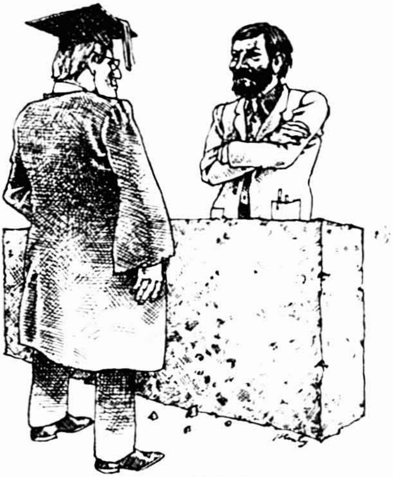

At a recent meeting, L. B. Rogers of the University of Georgia told of a two-week course he and a colleague conducted in the 1950s to teach industrial people how to become "experts" in instrumental analysis—one week on spectroscopy and one week on electrochemistry. "Various manufacturers and distributors," explained Rogers, "brought in equipment for us to use and to show off in the course. One year in the early fifties, an awful-looking contraption called a Technicon AutoAnalyzer was brought in, and I predicted it would never fly. Of course, Technicon only made about $100 million a year on it about 10 or 15 years later, but other than that my prediction was right on. That's why I'm in academia instead of industry."

Rogers spoke at a symposium on academic research and industry, held in October to commemorate the 10th anniversary of the Institute of Chemical Analysis, Applications and Forensic Science at Northeastern University. The institute will now be called the Barnett Institute of Chemical Analysis and Materials Science, in honor of a half-million-dollar endowment, announced at the symposium, from Louis and Madlyn Barnett, longtime supporters of the institute. Northeastern chemistry professor Barry L. Karger has been its director ever since it was established in 1973 with Department of Justice Law Enforcement Assistance Administration seed money. Since then it has grown to a research contract funding level of over $1 million and has attained wide recognition in the scientific community.

As Rogers's anecdote demonstrates, academia and industry represent totally different cultures, and discussion at the symposium centered on ways to bridge the gap. The mechanisms for

Barry Karger

Karl Weiss

academic–industrial interaction have long been in place. Therefore, according to Northeastern University vice-president for research Karl Weiss, innovation will involve "doing new things with mechanisms already described and which we're already using, perhaps not very efficiently at this point."

Personnel exchanges between academia and industry are gaining favor, for example, but the idea is certainly not new. According to Rogers, who has been a consultant since the 1950s for a number of companies, "Consulting has been the basis of the most wonderful educational experience I've ever had or could ever imagine having. And I really think that one of the best things that industry could do if it wants to bridge the academic–industrial interface is to take some of the young faculty members and make them consultants for two or three years to give them a nontrivial exposure to industry."

Personnel exchange goes both ways; the concept also involves academic leave for industrial personnel. But according to Weiss, the movement has been heavily weighted in the other direction. The temporary assignment of industrial people to academia doesn't happen to a large extent because, said Weiss, "American industry is in a hurry. Investors are clamoring for returns, you've got to keep going, so how can you spare a key man?" Weiss would like to see more academic leave for industrial people to pursue short-term academic research projects or to attend specific academic courses and seminars.

What are the benefits of greater academic–industrial cooperation? Weiss stated that industry's primary interest was ensuring itself a continuing supply of trained personnel. And for universities, he said, "There's no question that academic–industrial cooperation provides support for research at a time when enrollments are leveling off and direct institutional support is becoming increasingly difficult." In addition, interaction with industry exposes professors and students to practical research problems of immediate importance to society and to a value system in which attaining goals quickly and efficiently is a prerequisite of economic survival.

According to Weiss, the barriers to greater cooperation spring primarily from a deep disparity between the academic and industrial cultures: "Industry is output-oriented; industrial managers want efficient production and results. By contrast, at universities we see ourselves as elite scholars, somewhat apart from the crowd. In our hearts we feel that the industrials are OK, but we are the cream of it. Creation of knowledge for its own sake is one of our gods—we pray to it.

"Commercialization is sometimes viewed with suspicion. There's a concern that industry will pollute us somehow, that it will influence choice of research direction, prohibit publication, and will do all sorts of dire and terrible things. When you have these kinds of attitudes, perception easily becomes reality.

"Industry and academia have different origins and different cultures," Weiss continued, "and each must respect the other's distinctive role if they are to work together effectively. Industry must recognize that research at the universities has to be open if you're going to get the maximum benefit from the academic environment. On the other hand, academia must realize that applied research involves as much intellect and creativity as does basic research."

FOR THE FIRST TIME—
American Chemical Society offers one catalog covering all Continuing Education Services!

The 1984 ACS Catalog of state-of-the-art courses for chemists and chemical engineers

This new 60-page catalog will give you all the information you need to select the chemistry, chemical engineering and professional development topics you are interested in, and to choose the learning methods that suit your needs and budget best.

To receive your copy, write, use the coupon, or call 202-872-4588—you will find our new catalog bigger, better and more informative than ever!

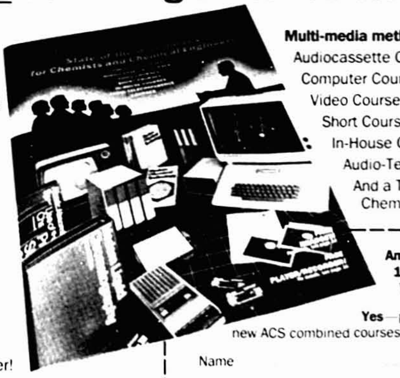

Multi-media methods include:
- Audiocassette Courses
- Computer Courses
- Video Courses
- Short Courses
- In-House Courses
- Audio-Teleconference Courses
- And a Textbook Course on Modern Chemical Technology

American Chemical Society
1155 Sixteenth Street, N.W.
Washington, DC 20036

Yes—please send me a copy of the new ACS combined courses catalog as soon as possible!

Name
Title
Organization
Address
City State ZIP

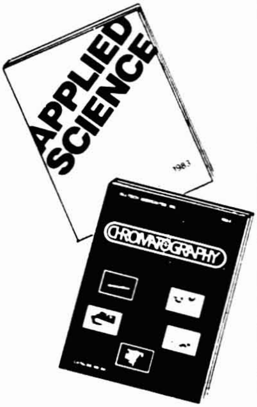

FREE
FOR THE ASKING

The Best In Chromatography Is Here

ALLTECH ASSOCIATES, INC.
APPLIED SCIENCE LABS

2051 Waukegan Road
Deerfield, Illinois 60015
(312) 948-8600
TOGETHER WE'RE BETTER

CIRCLE 2 ON READER SERVICE CARD

Nondestructive Elemental Analysis in Three Dimensions

A nuclear microprobe based on a new type of focusing lens has been constructed at Sandia National Laboratories in New Mexico, and Sandia scientists have been able to perform nondestructive three-dimensional elemental analyses of solid materials with the instrument.

For most MeV ion beam analytical experiments, the beam spot is a few square millimeters or larger. But the recent development of strong focusing lenses for high-energy ion beams has made it possible to obtain beam spot sizes of micrometer dimensions. The signals generated when these ion beams strike sample surfaces contain depth information, making it possible to construct three-dimensional concentration profiles of elements close to the surface.

Other methods used for three-dimensional surface analysis, such as secondary ion mass spectrometry, damage the sample by sputtering away parts of the surface. Nuclear microprobe analysis does introduce some radiation damage, but the sample remains basically intact.

According to Sandia scientist Barney L. Doyle, the nondestructive nature of the nuclear microprobe technique is a significant advantage: "When the amount of sample is extremely limited—small grains of lunar material, for example—it is wise not to exhaust it." Nondestructive analysis also enables the investigator to perform repetitive analytical procedures on the same sample or to place the sample back into service, assuming it is a useful device such as a microchip.

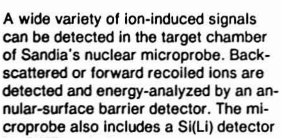

A wide variety of ion-induced signals can be detected in the target chamber of Sandia's nuclear microprobe. Backscattered or forward recoiled ions are detected and energy-analyzed by an annular-surface barrier detector. The microprobe also includes a Si(Li) detector for PIXE analysis

Two analytical techniques are used for three-dimensional profiling—Rutherford backscattering (RBS) and elastic recoil detection (ERD). A combination of these two techniques makes the nuclear microprobe capable of detecting every element in the periodic table. The instrument is also outfitted for proton-induced X-ray emission (PIXE) analysis.

In RBS, lightweight accelerated particles, such as hydrogen or helium ions, collide with heavy atoms in the sample and rebound to a detector, where their energy is measured. In ERD, on the other hand, heavy accelerated atoms, such as silicon, strike less massive atoms in the material, such as hydrogen, and knock them out of the sample. The energies of the detected particles in both cases provide information about the depth at which collisions took place. The PIXE technique, in which surface atoms emit characteristic X-rays in response to proton bombardment, is used primarily for trace elemental analysis.

"One of the biggest problems in three-dimensional microbeam analysis," said Doyle, "is displaying the data in a way that's easy to assimilate, because with RBS you really have five degrees of freedom: the x, y, and z dimensions, concentration, and atomic number. Eventually you have to display this on a two-dimensional matrix. That's one area we're working on."

According to a recent paper written by Doyle and his colleague Norman D. Wing, "The ability to measure nondestructively the three-dimensional concentration of elements ranging from H to U is extremely useful and has provided insight into many material problems which would have been difficult, if not impossible, to study with other techniques."

Stuart A. Borman

We Make Transients Talk.

Transient analysis is a complex job: capture, digitizing, storage, display, analysis and data transfer. It's harder still if you need remote control capability. Most general purpose instruments can't handle more than one or two of these steps. But the Data 6000 Universal Waveform Analyzer does them all...with speed and power you won't find in any other single instrument. In fact, the Data 6000 offers more powerful capabilities than you could obtain from an entire roomful of equipment at many times the cost. Nothing else even comes close to the Data 6000, which offers you:

Faster Data Acquisition

No matter how short-lived the event, you'll capture it with high resolution, thanks to the Data 6000 100 kHz and 100 MHz digitizing modules. Sample times as short as 10 nanoseconds, with full 8-bit resolution, give you the accuracy you need. Only Data Precision, backed by Analogic's leadership in A/D conversion and data acquisition could have offered the Data 6000's powerful acquisition capabilities.

And that's only the front end of the Data 6000's power.

Quicker on the Trigger

Trigger level may be set with minimum 8-bit precision, to eliminate false triggering on noisy signals without sacrificing sensitivity. And event display can begin precisely at the moment you select. View pre- and post-trigger events up to 100% of selected time-base away from the moment of triggering...from milliseconds to months before *and* after. You'll never miss a shot with the Data 6000's smart trigger.

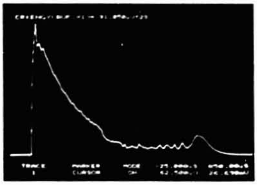

Compute and display a wide variety of functions from the captured signal. Useful functions for transient analysis are Rise, Fall, Settling, and Display Times; Overshoot, Maximum, Minimum, Peak to Peak, Area or Energy under the curve; Real and Complex Magnitude Spectra; Real and Complex Log Magnitude Spectra; and many more...all available with a single keystroke!

More Digital Storage

Up to 56,000 points of data may be stored in on-board storage memory, with unlimited expansion available on accessory floppy disk or your mass storage media. Data acquisition memory holds up to 56,000 points per channel (with the 610 and 611 plug-ins; 16,000 points for the 620).

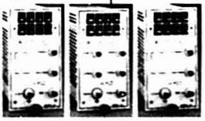

Model 610 2ch 100KHz
Model 611 4ch 100KHz
Model 620 2ch 100MHz

And data storage is accurate, supporting full 5-decimal place readouts. Double precision accumulators are standard. The high resolution CRT display lets you view waveforms as accurately as they are stored, and a comfortable screen angle permits easy use. The large display has full alphanumerics for on-screen labelling and documentation of functions.

On-Board M68000

How does the Data 6000 do so much more than an ordinary A/D converter, digital waveform recorder, digital storage oscilloscope, and engineering microcomputer? The answer is inside: a fast, powerful M68000 microprocessor, armed with the fastest Fast Fourier Transform Algorithm, and capable of quick, user-friendly communications and remarkable computational power. And when you need to go beyond the Data 6000's stand-alone capabilities, versatile data transfer is available through the RS-232 port. And IEEE-488 bus compatibility allows full integration of the Data 6000 with your system.

IEEE-488

Superior. Demonstrably Superior.

The Data 6000's unique capabilities with transient waveforms are reason enough to have it on your bench. But if you need further reasons, the Data 6000 has them. An instrument this powerful can do much more than transient analysis. Consider it as:

☐A Storage Oscilloscope
☐A Spectrum Analyzer
☐An Auto/Cross Correlator
☐A Transient Recorder
☐An RF or Audio Signal Analyzer
☐An ATE Subsystem
☐A Vibration Analyzer

For transient analysis with unprecedented ease, and much more, try the Data 6000. For further information, call:
800-343-8150
Or in Massachusetts,
800-892-0528.

The Data 6000
Universal Waveform Analyzer

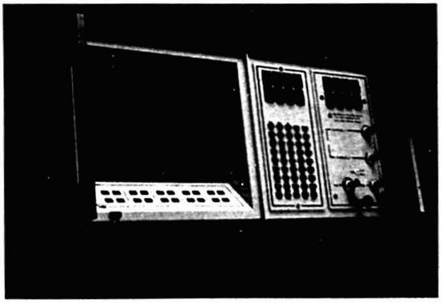

Maintaining The Integrity Of Measurement

ANALOGIC®

DATA PRECISION®

Data Precision Division of Analogic Corporation, Electronics Avenue, Danvers, MA 01923 617-246-1600 TELEX 6817144

Circle #52 for a demonstration. Circle #53 for additional information.

HIRE TECHNOLOGY

PUT ELECTROCHEMISTRY TO WORK!

BAS introduced the first commercial liquid chromatography/electrochemistry instrument in 1974. LCEC has become the fastest growing electrochemical technique. Thousands of our systems are in routine use for environmental, pharmaceutical, biomedical, industrial, and forensic applications. Nitro compounds, phenols, aromatic amines, thiols, and many heterocycles are ideal candidates for trace determination by LCEC. Detection limits of well below 1 picomole can now be achieved in a few minutes using apparatus of very modest cost.

The latest addition to our family is the BAS 100 ELECTROCHEMICAL ANALYZER. This interactive microprocessor based instrument is capable of performing over 25 electroanalytical techniques including cyclic voltammetry, chronocoulometry, differential pulse voltammetry, phase selective AC voltammetry, electrocapillary measurements, and virtually all forms of polarography. The BAS 100 is the first commercial instrument capable of square wave voltammetry, a powerful new technique for both analytical and fundamental studies. The first "smart" iR compensation approach is included, as are various statistical and background subtraction routines. Experimental parameters and data are available on a video screen and publishable figures are rapidly plotted.

The BAS 100 was designed by and for chemists.
It's ready to go to work for you.

WE'LL CHANGE THE WAY YOU
THINK ABOUT ELECTROCHEMISTRY

BAS

2701 Kent Ave
West Lafayette
Indiana 47906

Telex: 276141
(317) 463-4527

CIRCLE 28 ON READER SERVICE CARD

analytical chemistry Appoints New Advisory Board Members

William Heineman

Harry Hertz

Atsushi Mizuike

Melvin Redmond, Jr.

Martin Rudat

Charles Wilkins

Six new members of the Advisory Board of ANALYTICAL CHEMISTRY have been selected to serve three-year terms beginning this month. Each year the membership of the board is rotated, with the new appointees replacing those members whose terms on the board have expired.

The new members joining the board this year are: William R. Heineman, University of Cincinnati; Harry S. Hertz, National Bureau of Standards; Atsushi Mizuike, Nagoya University; Melvin W. Redmond, Jr., Perkin-Elmer Corporation; Martin A. Rudat, E.I. du Pont de Nemours & Company; and Charles L. Wilkins, University of California, Riverside.

The members leaving the board are: Richard Durst, National Bureau of Standards; Shizuo Fujiwara, Chiba University; Wilbur Kaye, Beckman Instruments, Inc.; Janet Osteryoung, State University of New York at Buffalo; Robert E. Sievers, University of Colorado; and Rudolph H. Stehl, Dow Chemical Company.

The following 10 members will continue to serve on the board: Joel A. Carter, Oak Ridge National Laboratory; Richard S. Danchik, Aluminum Company of America; Dennis H. Evans, University of Wisconsin, Madison; Jack W. Frazer, consultant; Helen M. Free, Miles Laboratories; Roland F. Hirsch, Seton Hall University; Csaba Horvath, Yale University; Thomas C. O'Haver, University of Maryland; Herbert L. Retcofsky, Pittsburgh Energy Technology Center; and Wilhelm Simon, Swiss Federal Institute of Technology.

The Advisory Board was established in the 1940s to advise the editors of the JOURNAL. It meets formally once a year at the JOURNAL's editorial offices in Washington, D.C. The board also provides guidance and advice throughout the year with regard to editorial policy and the peer review system. Board members are an invaluable link between the editors and the analytical community.

Brief biographical sketches of the new members follow.

William R. Heineman received his BS degree from Texas Tech University in 1964 and his PhD from the University of North Carolina at Chapel Hill in 1968. He was a research chemist at the Hercules Research Center from 1968 to 1970 and then a research associate at Case Western Reserve University and Ohio State University. In 1972 he joined the faculty at the University of Cincinnati where he is now professor of chemistry and chairman of the analytical division. Heineman's research interests include spectroelectrochemistry, immunoassay with electrochemical detection, polymer-modified electrodes, stripping voltammetry, and analytical chemistry of technetium radiopharmaceuticals. He is the author of 90 research papers, coauthor of "Experiments for Instrumental Methods," and coeditor of "Laboratory Techniques in Electroanalytical Chemistry." Heineman has served the Cincinnati Section of the ACS in many capacities and is currently treasurer of the ACS Division of Analytical Chemistry.

SWAGELOK WHITEY NUPRO CAJON SNO TRIK are Registered Trademarks

New features make VCR® high performance couplings even easier to use

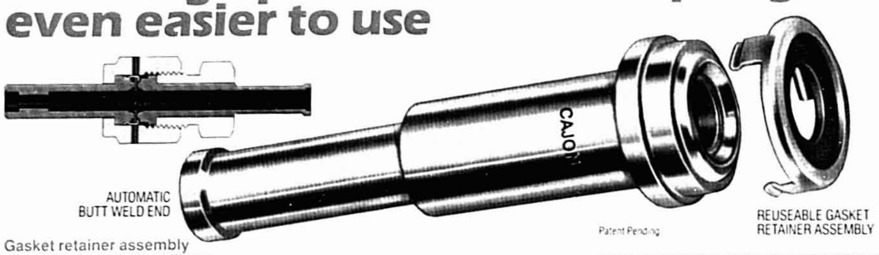

Gasket retainer assembly simplifies installation/allows gasket re-use. The new gasket retainer assembly fits securely over a machined step on VCR glands to hold the gasket in place. Installation will be faster and easier, particularly in difficult locations. Accuracy of positioning permits gasket re-use.

Automatic butt weld gland speeds welding. The weld end of this new gland aligns readily with the tubing to speed both manual and automatic welding set-ups. This end serves as filler material and assures a clean, full penetration weld. The 316L material is not affected by stress corrosion caused by the heat of welding.

New filter gasket. The range of VCR high purity applications is extended with a new .5 micron filter gasket. Other gaskets are available from 2 to 60 microns. Use them to filter particles and dampen surges.

VCR couplings are designed for positive pressure or vacuum applications. Special cleaning and packaging available for high purity applications. Available from local Distributor stocks.

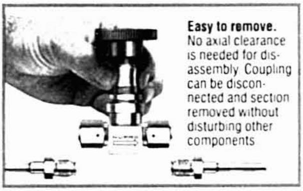

Easy to remove. No axial clearance is needed for disassembly. Coupling can be disconnected and section removed without disturbing other components.

CAJON

CAJON COMPANY
9760 Shepard Road, Macedonia, Ohio 44056

1982 MARKAD SERVICE CO., all rights reserved K-431

CIRCLE 33 ON READER SERVICE CARD

B&J

Superior Purity Water Can Help Improve HPLC Results.

B&J Brand High Purity Water undergoes rigorous purification and quality control to guarantee lot-to-lot uniformity. That's your assurance of its superiority for:

- Reverse phase gradient separations.
- Applications that require purity higher than conventional lab water supplies.

What's more, negligible UV absorbance and extremely low organic carbon and particulates make it the best choice for your critical trace analysis requirements.

Improve your HPLC chromatograms with the consistent quality of B&J Brand High Purity Water. Call us today for a free copy of our high purity water data sheet or for the location of the nearest B&J Distributor. 616-726-3171.

BURDICK & JACKSON LABORATORIES, INC.

1953 South Harvey Street, Muskegon, Michigan U.S.A. 49442 (616) 726-3171

CIRCLE 24 ON READER SERVICE CARD

FREE! MARKSON Catalog of Hard-to-Find Laboratory Equipment

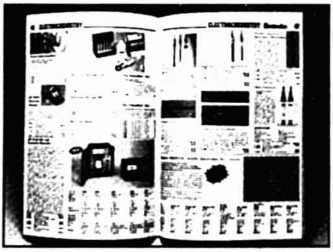

- THERMOMETRY
- SPECTROSCOPY
- PLASTICWARE
- ELECTROCHEMISTRY
- LIQUID HANDLING
- SAFETY SUPPLIES

This new Markson Science catalog is jam-packed with page after page of essential equipment for every type of laboratory . . . research, clinical, medical or analytical. Includes low-cost glassware, pipettes, state-of-the-art multifunction pH and conductivity meters, plus thousands of other hard-to-find items. Call or write for your free catalog today.

MARKSON

Markson Science
7815 S. 46th Street
Phoenix, AZ 85040
(800) 528-5114

CIRCLE 138 ON READER SERVICE CARD

Harry S. Hertz is director of the Center for Analytical Chemistry at the National Bureau of Standards. He received his BS degree in 1967 from the Polytechnic Institute of Brooklyn and his PhD from the Massachusetts Institute of Technology in 1971. From 1971 to 1973 he was an Alexander von Humboldt Fellow at the Institute for Physiological Chemistry at the University of Munich, and in 1973 he joined the staff of the National Bureau of Standards. His research focuses on trace organic analysis, with particular emphasis on organic mass spectrometry. His efforts during the past several years have been devoted to the development of quantitative methods for determination of individual organic compounds in complex matrices. He has served on the board of directors of the National Committee for Clinical Laboratory Standards since 1980 and as the organization's secretary since March 1983. In addition, he is currently secretary of the American Society for Mass Spectrometry.

Atsushi Mizuike is professor of chemistry and director of the Radioisotope Center at Nagoya University. He earned his B. Eng. and Dr. Eng. degrees at the University of Tokyo, where he served on the faculty before assuming his present position in 1965. Mizuike's research interests lie in the area of inorganic micro- and trace analysis. He is the author of over 160 papers and a recently published monograph entitled "Enrichment Techniques for Inorganic Trace Analysis." He is a past recipient of the Japan Society for Analytical Chemistry Award and a former vice-president of the Japan Society for Analytical Chemistry. Since 1971, he has been a member of the IUPAC Commission on Microchemical Techniques and Trace Analysis.

Melvin W. Redmond, Jr., is a senior vice-president with the Perkin-Elmer Corporation in Norwalk, Conn. He earned his BS degree in mechanical engineering from Clarkson College of Technology in 1956. He spent two years at the Army Chemical Center in Edgewood, Md., and joined Perkin-Elmer in 1960 as a project engineer in the Instrument Division, where he developed analytical instruments. In addition to instrumentation, his interests are in computer-aided chemistry. He held management positions in research and development, marketing, and operations prior to assuming his present position as the senior group executive for the Instrument Group.

Martin A. Rudat is a research chemist in the Pioneering Research Laboratory of Du Pont's Textile Fibers Department in Wilmington, Del. He received his BS degree from Harvey Mudd College in 1974 and his MS and PhD degrees from Cornell University in 1976 and 1978, respectively. He then joined the staff at Du Pont and in 1983 assumed his present position in the Textile Fibers Department. His research interests are in mass spectrometry, including secondary ion mass spectrometry and other surface analytical techniques, ion–molecule reaction chemistry, radical–molecule reactions and their analytical utility, ionization mechanisms, the development of new instruments and techniques, and more recently the application of mass spectrometry to life sciences problems and fiber polymers.

Charles L. Wilkins received his BS degree in 1961 from Chapman College and his PhD degree in 1966 from the University of Oregon. He joined the faculty of the University of Nebraska, Lincoln, in 1967 and in 1981 moved to the University of California, Riverside, where he is now professor of chemistry and chairman of the department. Wilkins's research interests are in the area of computer-assisted analysis, including Fourier transform nuclear magnetic resonance, infrared, and mass spectrometry. His recent studies have focused on instrumentation for organic mixture analysis using hyphenated techniques and on development of Fourier transform mass spectrometry for analysis of molecules with masses in the range of 10 000–20 000 amu. Wilkins is the coauthor of two books on computer applications in chemistry and is coeditor of two other books on the same topic. During 1980 he was chairman of the ACS Computers in Chemistry Division and since 1978 has served on the advisory board of the Midwest Center for Mass Spectrometry.

Applications Sought for Pittsburgh Conference College Grants

The Pittsburgh Conference on Analytical Chemistry and Applied Spectroscopy, Inc., the Society for Analytical Chemists of Pittsburgh, and the Spectroscopy Society of Pittsburgh will once again sponsor the Pittsburgh Conference Memorial National College Grants Award Program. Six colleges will be selected to receive $2500 awards to be used for teaching science at the undergraduate level, i.e., for purchase of scientific equipment, audiovisual and other teaching aids, and/or library materials.

To be eligible for an award, a school must have an enrollment of not more than 2500 students and receive less than 25% of its operating budget from national or state governments. Two-year community colleges sponsored by political subdivisions of a state are not bound by these requirements. Previous awardees are ineligible for a three-year period following their award.

Any interested faculty member may participate by requesting an application form from: Raymond P. Bacco, United States Steel Technical Center, Monroeville, Pa. 15146. Deadline for return of application forms and proposals is April 7, 1984.

ALMA Meeting Held at Purdue

Improved productivity through better laboratory management was the theme of the fourth annual conference of the Analytical Laboratory Manager's Association (ALMA), held in October at Purdue University in West Lafayette, Ind. The meeting was cohosted by Purdue University faculty members Jonathan Amy and William Baitinger. ALMA consists of academic, industrial, and government analytical laboratory managers who gather each year to discuss problems and share solutions common to the operation of both large and small analytical laboratories.

Among the topics discussed at the meeting were factors to be considered in instrumentation purchasing decisions, the high costs of laboratory operation, the need to improve productivity, the current trend toward centralization and pooling of expensive instruments, and interfacing existing equipment to laboratory information management systems.

The next ALMA conference will be held in October 1984. Thomas Erickson, analytical laboratory director for Owens-Corning Fiberglas Corporation, is chairman of ALMA for the current year. For information about ALMA, contact Jane Sprouse, Department of Chemistry, University of California at Los Angeles, Los Angeles, Calif. 90024.

Gehrke Named AOAC President for 1984

Charles W. Gehrke has been named 1984 president of the Association of Official Analytical Chemists (AOAC). Gehrke is currently professor of biochemistry and manager of the Experiment Station Chemical Laboratories

The most significant advancement in x-ray microanalysis instrumentation in nearly a decade.

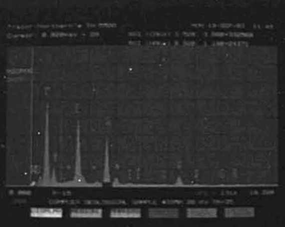

- *Fastest, easiest and most precise quantitative analysis.*

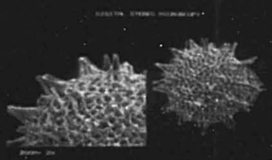

- *Digital Stereo Microscopy including parallax depth measurements.*

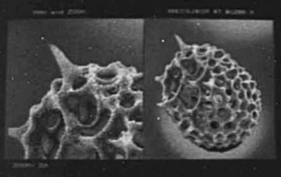

- *Pan and zoom capabilities of a displayed image.*

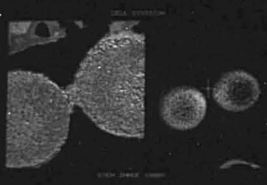

- *Continuous tone gray scale displayed side by side with full color image.*

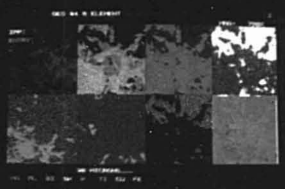

- *True intensity x-ray maps.*

PROOF IS IN PERFORMANCE . . .
NOT PROMISES!

Recently, Tracor Northern introduced the TN-5500 X-Ray Analyzer. It is, unquestionably, the most sophisticated and powerful x-ray microanalysis system available — anywhere.

The TN-5500 speaks for itself. Capabilities such as those demonstrated above outperform any other x-ray microanalysis system by a wide margin. The TN-5500 outperforms even the **promises** of other manufacturers.

We invite you to see for yourself why Tracor Northern continues to be the world leader in x-ray microanalysis.

Tracor Northern

TRACOR NORTHERN 2551 WEST BELTLINE HIGHWAY MIDDLETON, WISCONSIN 53562 (608) 831-6511
TRACOR EUROPA BV P.O. BOX 333 3720 AH BILTHOVEN THE NETHERLANDS (030) 780855
TRACOR NORTHERN — JAPAN 1-18-13 HAMAMATSU-CHO MINATO-KU TOKYO 105, JAPAN 03-434-4866

CIRCLE 202 ON READER SERVICE CARD

at the University of Missouri, Columbia.

Gehrke received his PhD degree from Ohio State University and joined the faculty at the University of Missouri in 1949. His research interests include development of gas and liquid chromatographic methods for determination of amino acids, purines, pyrimidines, nucleosides, fatty acids, and biological markers in cancer; characterization of proteins; and automated analytical methods for nitrogen, phosphorus, and potassium in fertilizers. Gehrke is the author of over 200 publications and is the recipient of a number of awards, including the 1971 AOAC Wiley Award and the 1980 Chromatography Memorial Medal from the Scientific Council on Chromatography of the U.S.S.R. Academy of Sciences.

Call for Papers

26th Rocky Mountain Conference

Denver, Colo. Aug. 5–9. General papers and poster sessions in all areas of chemistry are planned along with the following specific symposia: applications of chromatography to biology, medicine, and biotechnology; atomic spectroscopy; chromatography; computer applications; electrochemistry; environmental; EPR; IR and fluorescence spectroscopy; ion chromatography; mass spectroscopy; NMR; and surface analysis. Abstracts of no more than 200 words must be submitted on a Rocky Mountain Conference or standard ACS abstract form before March 14. To obtain the forms and for additional information contact Jan Gurnsey, 5531 Bitterbush Way, Loveland, Colo. 80537; 303-669-9216.

Symposium on FT–IR Characterization of Polymers

Philadelphia, Pa. Aug. 26–31. The symposium, organized by the ACS Division of Polymer Chemistry, will be held at the 1984 ACS fall national meeting in Philadelphia. Emphasis will be on polymer characterization by sophisticated and unconventional FT–IR techniques that use the unique capabilities of FT–IR instruments. Tentative session topics include reflection spectroscopies, software-dominated spectroscopies, separation techniques/FT–IR combination, emission spectroscopy, photoacoustic spectroscopy, microsampling spectroscopy, and general techniques. For more information on abstract length and format, contact Hatsuo Ishida, Department of Macromolecular Science, Case Western Reserve University, Cleveland, Ohio 44106; 216-368-4285. Deadline for receipt of abstracts is April 15.

9th National Conference on Spectrochemical Excitation and Analysis

Edgartown, Mass. Sept. 4–7. Papers describing practical applications in the field of atomic spectroscopy are solicited. Authors should submit a brief containing the proposed title, author's name and address, and about 50 words describing the content of the paper by Feb. 1 to Hank Griffin, Texas Instruments Inc., 34 Forest St., MS 10–16, Attleboro, Mass. 02703; 617-699-3037. Abstracts for accepted papers are due June 1.

11th Annual Meeting of the Federation of Analytical Chemistry and Spectroscopy Societies

Philadelphia, Pa. Sept. 16–21. The scope of the meeting will encompass all phases of analytical chemistry, applied spectroscopy, chromatographic methods, and allied techniques of instrumental analysis. Prospective authors must submit a title, current address, and telephone number by March 30 to Patricia Roush, Perkin-Elmer, M/S 903, 901 Ethan Allen Highway, Ridgefield, Conn. 06877; 203-797-9481. After receipt of titles, authors will be asked to submit a 250-word abstract by June 15.

Meetings

- **Symposium/Workshop on Low-Dispersion Liquid Chromatography.** Jan. 19–20. Amsterdam, The Netherlands. *Contact: R. W. Frei, Free University, Department of Analytical Chemistry, De Boelelaan 1083, 1081 HV Amsterdam, The Netherlands*
- **Symposium on Sample Preparation and Isolation Using Bonded Silicas.** Jan. 23–24. Philadelphia, Pa. *Contact: Lane S. Yago, Analytichem International, Inc., 24201 Frampton Ave., Harbor City, Calif. 90710; 213-539-6490*
- **1984 Winter Gordon Research Conference on Electrochemistry.** Jan. 23–28. Santa Barbara, Calif. *Contact: Alexander M. Cruickshank, Gordon Research Conferences, University of Rhode Island, Kingston, R.I. 02881; 401-783-4011*
- **31st Annual Conference of the Western Spectroscopy Association.**

We've made the transitions easier (and more sensitive).

We've always been proud of the ability of our Ion Chromatography systems to analyze transition metals at a level of sensitivity and convenience comparable to, and in many cases better than, AA and ICP.

But we still weren't completely satisfied.

So we developed the IonPac™ Membrane Reactor for our Series 2000i Ion Chromatographs™ that not only makes transition metal analysis many times easier, it also provides a five-fold increase in sensitivity over conventional post-column techniques.

Call or write Dionex for information and applications notes on our new Membrane Reactor. We'll show you how easy–and sensitive–transition metal analysis can be.

You'll be happy with the results.

Dionex Corporation • 1228 Titan Way
Sunnyvale, CA 94086 • (408) 737-0700

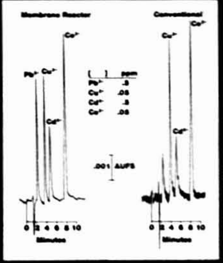

DIONEX
THE ION EXPERTS

CIRCLE 59 ON READER SERVICE CARD

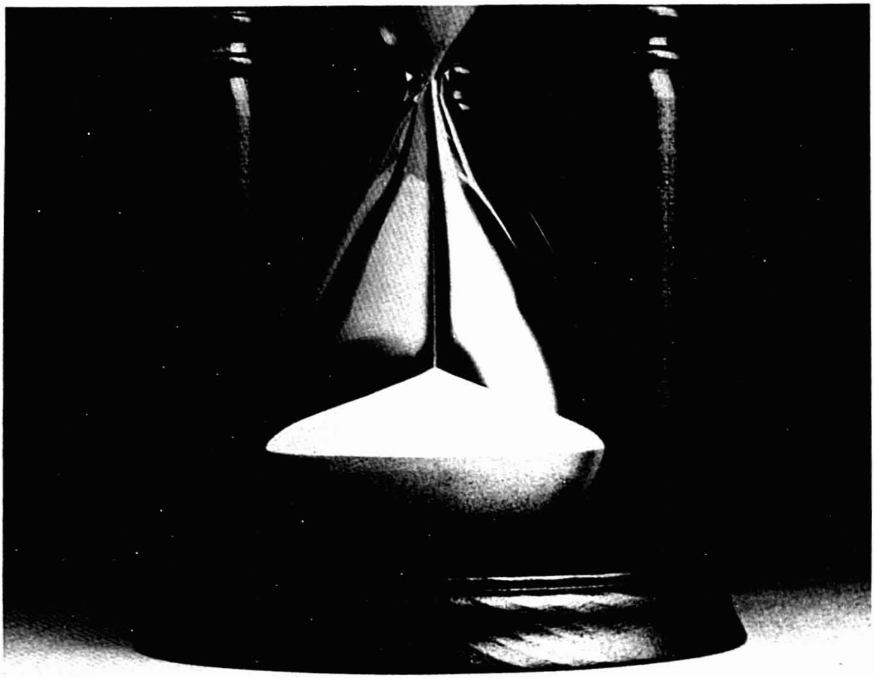

SEND FOR THIS FREE BOOKLET WHEN YOU DON'T HAVE TIME TO EXPERIMENT.

FLORISIL
The Preferred Adsorbent for Chromatography

If you're going to perform chromatography, we may be able to save you time. It's probably already been done with Florisil.

Just send for this free 80-page bibliography on chromatography from Floridin. Find out how Florisil has been used to solve tough separations in column or thin layer chromatography.

The new bibliography includes Florisil's chemical composition, physical and adsorptivity properties, along with a lengthy list of chromatographic procedures performed with Florisil . . . on everything from Alkaloids to Thiosteroids.

For chromatography, consider Florisil, and send for this free bibliography. They both can save you time and money.

Write:
Floridin Company
Department A-4
701 McKnight Park Drive
Pittsburgh, PA 15237
(412) 367-1700

Floridin
A Member of the ITT System

CIRCLE 68 ON READER SERVICE CARD

Jan. 25–27. Pacific Grove, Calif. *Contact: David Saperstein, IBM Instruments, 40 West Brokaw Rd., San Jose, Calif. 95110*

■ **6th Australian Electrochemistry Conference.** Feb. 19–24. Geelong, Australia. *Contact: E. J. Frazer, CSIRO Division of Mineral Chemistry, P.O. Box 124, Port Melbourne, Victoria 3207, Australia*

■ **2nd Topical Meeting on Laser Techniques in the Extreme Ultraviolet.** March 5–7. Boulder, Colo. *Contact: Optical Society of America, 1816 Jefferson Place, N.W., Washington, D.C. 20036; 202-223-8130*

■ **35th Pittsburgh Conference and Exhibition.** March 5–9. Atlantic City, N.J. *Contact: Linda Briggs, 437 Donald Rd., Dept. J-009, Pittsburgh, Pa. 15235; 412-795-7667. July, p. 862 A*

■ **Vacuum '84—Technological Aspects of Surface Treatment and Analysis.** April 1–4. York, U.K. *Contact: J. S. Colligon, Thin Film and Surface Research Center, Department of Electronic and Electrical Engineering, University of Salford, Salford M5 4WT, U.K.*

■ **Symposium on Instrumental Multielement Analysis.** April 2–5. Jülich, F.R.G. *Contact: Helga Bongartz, Tagungsbüro, KFA Jülich, Postfach 1913, D-5170 Jülich, F.R.G.*

■ **5th International Conference on Nuclear Methods in Environmental and Energy Research.** April 2–6. Mayaguez, Puerto Rico. *Contact: James R. Vogt, University of Missouri, 214 Research Reactor, Columbia, Mo. 65211; 314-882-4211. August, p. 973 A*

■ **3rd International Workshop on Trace Element Analytical Chemistry in Medicine and Biology.** April 4–6. Neuherberg, F.R.G. *Contact: P. Schrammel, Gesellschaft für Strahlen und Umweltforschung, Institut für Angewandte Physik, Physikalisch-Technische Abteilung, Ingolstädter Landstrasse 1, D-8042 Neuherberg, F.R.G.*

■ **International Workshop on Chemical Service Analysis.** April 5–6. Aachen, F.R.G. *Contact: Helga Bongartz, Tagungsbüro, KFA Jülich, Postfach 1913, D-5170 Jülich, F.R.G.*

■ **187th ACS National Meeting.** April 8–13. St. Louis, Mo. *Contact: A. T. Winstead, American Chemical Society, 1155 16th St., N.W., Washington, D.C. 20036; 202-872-4397*

■ **International Conference on Biochemical and Instrumental Analysis.** April 10–13. Munich, F.R.G. *Contact: Rosmarie Vogel, Postfach 20 03 24, D-8000 München 2, F.R.G.*

■ **Analytica 84—9th International Exhibition.** April 10–13. Munich, F.R.G. *Contact: Münchener Messeund Ausstellungsgesellschaft mbH, Analytica 84, Postfach 12 10 09, D-8000 München 12, F.R.G.*

■ **16th Annual Symposium on Advanced Analytical Concepts for the Clinical Laboratory,** April 12–13. Knoxville, Tenn. *Contact: AACC, 1725 K St., N.W., Suite 1010, Washington, D.C. 20006. November, p. 1336 A*

■ **IV Brazilian Symposium on Electrochemistry and Electroanalytical Chemistry.** April 15–18. São Carlos, Brazil. *Contact: IV Simpósio Brasileiro de Eletroquímica e Eletroanalítica, Caixa Postal 297, 13.560, São Carlos, SP, Brasil*

■ **2nd Symposium on Resonance Ionization Spectroscopy and Its Applications.** April 16–20. Knoxville, Tenn. *Contact: Henry M. Borella, EG&G, 130 Robin Hill Rd., Goleta, Calif. 93116, 805-967-0456 or G. S. Hurst, Health and Safety Research Division, Oak Ridge National Laboratory, P.O. Box X, Oak Ridge, Tenn. 37830; 615-574-5893*

■ **20th International Symposium on Advances in Chromatography.** April 16–19. New York, N.Y. *Contact: A. Zlatkis, Chemistry Department, University of Houston, Houston, Tex. 77004; 713-749-2623. October, p. 1204 A*

■ **International Symposium on Analytical Methods and Problems in Biotechnology.** April 17–19. Noordwijkerhout, The Netherlands. *Contact: W. A. Scheffers, Delft University of Technology, Laboratory of Microbiology, Julianalaan 67A, NL-2628 BC Delft, The Netherlands*

■ **3rd International Symposium on Analytical Applications of Bioluminescence and Chemiluminescence.** April 17–19. Birmingham, U.K. *Contact: L. J. Kricka, Department of Clinical Chemistry, Wolfson Research Laboratories, Queen Elizabeth Medical Center, Edgbaston, Birmingham B15 2TH, U. K.*

■ **New Orleans Chromatography-Analytical Discussion Group 15th Annual Symposium on Applied Analytical Chemistry.** April 26–27. New Orleans, La. *Contact: Linda Green, P.O. Box 1449, Kenner, La. 70063*

■ **9th Annual AOAC Spring Workshop.** April 29–May 5. Philadelphia, Pa. *Contact: Kathleen Fominaya, AOAC, 1111 N. 19th St., Suite 210,*

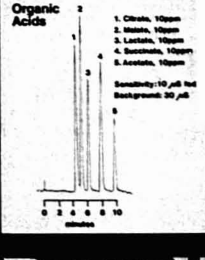

Organic acid analysis–without interferences.

Our new AFS-2 membrane based anion fiber suppressor is a unique, continuous eluant suppression system that provides improved analytical reproducibility for weak acids - such as organic acids, carbohydrates, and borate.

Combined with our Series 2000i Ion Chromatograph, the AFS-2 gives you sensitive and selective detection of weak acids without interference from non-ionic organics present in many sample matrices.

The AFS-2 also significantly improves resolution and sensitivity for inorganic anions (i.e., metal cyanides, etc.)

If you're analyzing organic acids and other hydrophobic ions, you can't afford to be without Dionex Ion Chromatography - and the new AFS-2.

Call or write for complete information and find out how the AFS-2 can give you better results - continuously.

DIONEX
THE ION EXPERTS

Dionex Corporation • [illegible]
[illegible]

CIRCLE 60 ON READER SERVICE CARD

EIGHT GOOD REASONS WHY OUR GC CUSTOMERS CHOOSE S-P OVER H-P.

1 A PICTURE IS WORTH A THOUSAND WORDS.

Nothing beats Spectra-Physics' CRT interface for simplicity. The operator gets a complete, instant picture of status, then follows a simple, menu-assisted setup in everyday English. The other GC engages the user in a lengthy keyboard dialogue which yields information grudgingly and wastes time and reams of paper.

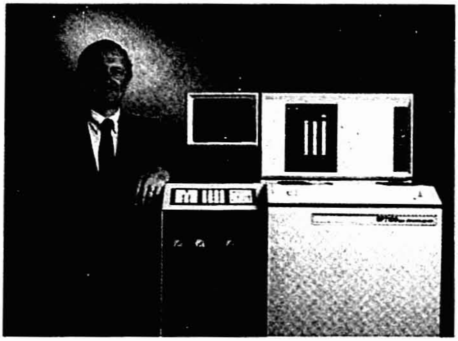

2 OUR KEYBOARD SPEAKS FOR ITSELF.

One look at Spectra-Physics' keyboard and you know how to use it. The simple, universal configuration is constant and self-explanatory. No training is necessary. The other GC's keyboard is so complex and variable that it can only be mastered with hours of training.

3 TEN FILES IN THE HAND MAKE CLOCK-TIME PROGRAMMING A SNAP.

Spectra-Physics' GC's memory stores up to ten files—more than enough for most method-development applications. Mass storage is also available via disk or low-cost tape equipment. The other GC stores one solitary file (a cartridge tape unit for additional file storage comes at a hefty price). Consequently, clock-time programming with our stored files can save you hundreds of hours every year at no added cost.

4 THE DOCTOR IS ALWAYS IN (AND SPEAKS ENGLISH).

The other GC contents itself with performing a startup diagnostic routine. Spectra-Physics' GC pinpoints the source of any problem and communicates it in simple English. No more waiting for a technical expert to solve the mystery. You simply call our toll-free hotline, tell us the problem, and we fix it quickly.

5 CAPILLARY CHROMATOGRAPHY MADE EASY.

Whenever you change a column, you can shave 15-30 minutes off the procedure thanks to the ability to reset conditions effortlessly. Simply dial up flow and pressure and you're ready to go. Spectra-Physics' CRT displays split flow/head pressure parameters (the latter to the nearest 0.2 kPa), assures reproducible retention times, and is included in the base price. The other GC includes only a small gauge—a pressure/flow readout and control is a $3000 option.

6 IN PNEUMATICS, LESS IS MORE.

Spectra-Physics' GC's simplified panel gets top marks for accessibility and ease of use. Furthermore, the unique block construction of the carrier gas control reduces the number of fittings—and possible leaks—to a minimum. The other GC utilizes a cramped configuration with non-standard fittings.

7 OUR OVEN ACCEPTS COLUMNS, NO QUESTIONS ASKED.

Practically every glass packed-column you have in stock will fit into the flexible side-by-side mounting arrangement of Spectra-Physics' GC's large oven. You can even place detectors in injector mounting holes and vice versa. The other GC's mounting can break a lot of glass.

8 AND THE PRICE IS RIGHT.

The SP7100 Gas Chromatograph from Spectra-Physics is the best value in its class. For this and many other reasons, call Spectra-Physics today. In California (408) 946-9682, elsewhere (800) 227-1950. Spectra-Physics, 3333 North First Street, San Jose, California 95134.

THE SP7100 GAS CHROMATOGRAPH.

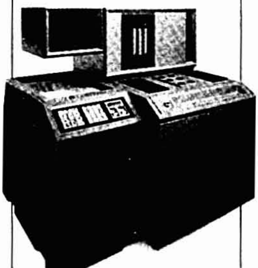

Spectra-Physics

WHERE TECHNOLOGY GIVES YOU MORE FOR LESS.

CIRCLE 188 ON READER SERVICE CARD

Arlington, Va. 22209; 703-522-3032

■ **XII International Congress on Clinical Chemistry.** April 29–May 5. Rio de Janiero, Brazil. *Contact: Sociedade Brasileira de Análises Clinicas, Rua Vicente Licinio, 95, Rio de Janiero, 20270, Brasil*

■ **4th Annual National Symposium on Recent Advances in Measurement of Pollutants in Ambient Air and Stationary Sources.** May 8–11. Raleigh, N.C. *Contact: Seymour Hochheiser, MD 75, EPA Environmental Monitoring Systems Laboratory, Research Triangle Park, N.C. 27711. November, p. 1336 A*

■ **5th International Symposium on Mass Spectrometry in Life Sciences.** May 15–18. Ghent, Belgium. *Contact: A. De Leenheer, Laboratoria voor Medische Biochemie en voor Klinische Analyse, Harelbekestraat 72, B-9000 Ghent, Belgium*

■ **8th International Symposium on Column Liquid Chromatography.** May 20–26. New York, N.Y. *Contact: Cs. Horvath, Yale University, P.O. Box 2159, New Haven, Conn. 06520; 203-436-1271*

■ **18th ACS Middle Atlantic Regional Meeting.** May 21–23. Newark, N.J. *Contact: G. E. Heinze, Jansen Pharmaceutica Inc., 501 George St., New Brunswick, N.J. 08903*

■ **ACS Joint Great Lakes/Central Regional Meeting.** May 23–25. Kalamazoo, Mich. *Contact: L. E. Hines, Upjohn Co., 301 Henrietta St. Kalamazoo, Mich. 49001*

■ **1984 LCEC Symposium on LCEC and Voltammetry.** June 3–5. Indianapolis, Ind. *Contact: Symposium Coordinator, P.O. Box 2206, West Lafayette, Ind. 47906. November, p. 1336 A*

■ **7th ACS Rocky Mountain Regional Meeting.** June 6–8. Albuquerque, N.M. *Contact: Ray Hanson, ITRI, P.O. Box 5890, Albuquerque, N.M. 87185; 505-844-7988*

■ **58th ACS Colloid and Surface Science Symposium.** June 10–13. Pittsburgh, Pa. *Contact G. D. Parfitt, Department of Chemical Engineering, Carnegie-Mellon University, Pittsburgh, Pa. 15213*

■ **14th ACS Northeast Regional Meeting.** June 10–14. Fairfield, Conn. *Contact: D. L. Swanson, American Cyanamid Co., Chemical Research Division, 1937 West Main St., Stamford, Conn. 06904*

■ **37th Annual Summer Symposium of the ACS Analytical Division.** June 12–14. Gaithersburg, Md. *Contact: Harry Hertz, Center for Analytical Chemistry, National Bureau of Standards, Washington, D.C. 20234; 301-921-2851*

■ **Topical Meeting on Ultrafast Phenomena.** June 12–15. Monterey, Calif. *Contact: David H. Auston, Bell Laboratories, 600 Mountain Ave., Murray Hill, N.J. 07974; or Kenneth B. Eisenthal, Department of Chemistry, Columbia University, New York, N.Y. 10027*

■ **ACS Northwest Regional Meeting.** June 13–15. Moscow, Idaho. *Contact: J. L. McHale, Department of Chemistry, University of Idaho, Moscow, Idaho 83843; 208-855-6787*

■ **2nd International Conference on Chromatography and Mass Spectrometry in Biomedical Sciences.** June 18–20. Milan, Italy. *Contact: Alberto Frigerio, Italian Group for Mass Spectrometry in Biochemistry and Medicine, Via Eustachi 36, 20129 Milan, Italy. December, p. 1448 A*

■ **13th International Quantum Electronics Conference.** June 18–21. Anaheim, Calif. *Contact: Optical Society of America, 1816 Jefferson Place, N.W., Washington, D.C. 20036*

■ **Symposium on Liquid Chromatography in the Biomedical Sciences.** June 18–21. Ronneby, Sweden. *Contact: Swedish Academy of Pharmaceutical Sciences, P.O. Box 1136, S-111 81 Stockholm, Sweden*

■ **CLEO '84—Conference on Lasers and Electro-Optics.** June 19–22. Anaheim, Calif. *Contact: Optical Society of America, 1816 Jefferson Place, N.W., Washington, D.C. 20036; 202-223-8130*

■ **International Symposium on Characterization of Heavy Crude Oils and Petroleum Residues.** June 25–27. Lyon, France. *Contact: J. C. Escalier, Centre de Recherche ELF Solaize, BP no. 22, 69360 Saint-Symphorien-D'Ozon, France*

■ **2nd Biennial National Atomic Spectrometry Symposium.** July 10–13. Leeds, U.K. *Contact: F. Buckley, Department of Earth Sciences, University of Leeds, Leeds, W. Yorkshire LS2 9JT, U.K.*

■ **XXIII International Conference on Coordination Chemistry.** July 29–Aug. 3. Boulder, Colo. *Contact: Courtland Pierpont, Campus Box 449, University of Colorado, Boulder, Colo. 80309. October, p. 1204 A*

■ **36th National Meeting of the American Association for Clinical Chemistry.** July 29–Aug. 4. Washington, D.C. *Contact: AACC, 1725 K St., N.W., Suite 1010, Washington, D.C. 20006; 202-857-0717. December, p. 1448 A*

Food analysis problems?

[illegible]

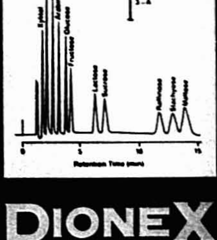

Dionex Corporation • [illegible]

DIONEX

CIRCLE 61 ON READER SERVICE CARD

Determine oxides or nitrides rapidly with LECO® Sepragram Determinators

- **LECO®** RO-316 Oxygen Determinator
- **LECO®** TN-314 Nitrogen Determinator

LECO
RO-316
LECO
EF-100

RO-316 Oxygen Determinator

The LECO® RO-316 Oxygen Determinator and the TN-314 Nitrogen Determinator have proven themselves valuable and reliable tools for the study of materials containing different oxides or nitrides. The relationships between oxygen or nitrogen peaks and the temperatures at which they occur during sample fusion can be used to determine the identity and, to some extent, quantity of different oxides or nitrides in the sample being tested.

These LECO® determinators use the normal inert gas fusion method to determine oxygen or nitrogen released as the sample is heated to successively higher temperatures. The oxygen or nitrogen peaks are plotted against temperature by an integral printer, making analysis fast and easy.

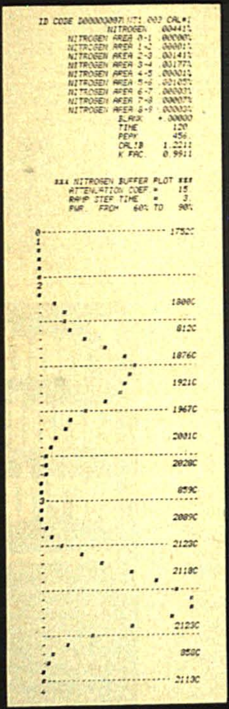

```
ID CODE 0000000097 NT1 003 CAL#1
                 NITROGEN   .00441%
     NITROGEN AREA 0-1 .00000%
     NITROGEN AREA 1-2 .00001%
     NITROGEN AREA 2-3 .00141%
     NITROGEN AREA 3-4 .00177%
     NITROGEN AREA 4-5 .00001%
     NITROGEN AREA 5-6 .00105%
     NITROGEN AREA 6-7 .00003%
     NITROGEN AREA 7-8 .00007%
     NITROGEN AREA 8-9 .00003%
                 BLANK    +.00000
                 TIME        120
                 PEAK        456.
                 CALIB    1.2211
                 K FAC.   0.9911


*** NITROGEN BUFFER PLOT ***
   ATTENUATION COEF =    15.
   RAMP STEP TIME   =     3.
   PWR.  FROM   60% TO   90%
```

Typical TN-314 printout

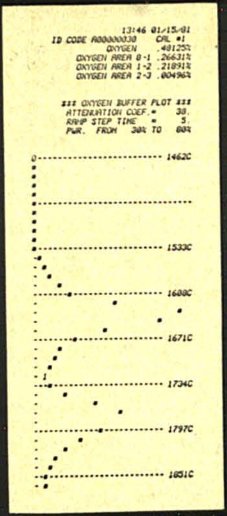

```
               13:46 01/15/81
ID CODE A00000030    CAL #1
             OXYGEN     .48125%
     OXYGEN AREA 0-1 .26631%
     OXYGEN AREA 1-2 .21891%
     OXYGEN AREA 2-3 .00496%


*** OXYGEN BUFFER PLOT ***
  ATTENUATION COEF.=    38.
  RAMP STEP TIME   =     5.
  PWR.  FROM   30% TO   60%
```

Typical RO-316 printout

CONTACT LECO TODAY!

LECO CORPORATION 3000 Lakeview Ave., St. Joseph, MI 49085 U.S.A. • Phone (616) 983-5531
Offices: California (714) 957-8227 • Texas (713) 931-0000 • Pittsburgh (412) 776-4891 • Canada
(416) 270-6610 • Mexico City (905) 658-1877

CIRCLE 126 ON READER SERVICE CARD

■ **International Conference on Luminescence.** Aug. 13–18. Madison, Wis. *Contact: William M. Yen, Department of Physics, 1150 University Ave., Madison, Wis. 53706; 608-263-7475*

■ **Symposium on Concentration Techniques for Biological Testing of Environmental Samples.** Aug. 24–31. Philadelphia, Pa. *Contact: I. H. Suffet, Environmental Studies Institute, Drexel University, Philadelphia, Pa. 19104 or Murugan Malaiyandi, Environmental Health Directorate, Health and Welfare Canada, Tunney's Pasture, Ottawa, Ontario K1A 0L2, Canada. September, p. 1085 A*

■ **188th ACS National Meeting.** Aug. 26–31. Philadelphia, Pa. *Contact: A. T. Winstead, American Chemical Society, 1155 16th St., N.W., Washington, D.C. 20036; 202-872-4397*

■ **5th European Conference on Analytical Chemistry.** Aug. 26–Sept. 1. Krakow, Poland. *Contact: Zygmunt Kowalski, Academy of Mining and Metallurgy, Mickiewicza 30, 30-059 Krakow, Poland*

■ **4th International Meeting of the Electrophoresis Society.** Aug. 27–31. Göttingen, F.R.G. *Contact: Volker Neuhoff, Max-Planck-Institut für experimentalle Medizin, Hermann-Rein-Strasse 3, D-3400 Göttingen, F.R.G.*

■ **4th International Symposium on Isotachophoresis.** Sept. 2–5. Hradec Králové, Czechoslovakia. *Contact: Z. Prusík, Institute of Organic Chemistry and Biochemistry ČSAV, Flemingovo nám.2, 166 10 Praha 6, Czechoslovakia*

■ **International Symposium on Quantitative Luminescence Spectroscopy in Biomedical Sciences.** Sept. 4–5. Ghent, Belgium. *Contact: Willy Baeyens, State University of Ghent, Farmaceutisch Instituut, Harelbekestraat 72, B-9000 Ghent, Belgium*

■ **4th Annual American-Eastern European Symposium on Liquid Chromatography.** Sept. 10–14. Szged, Hungary. *Contact: Huba Kalász, Department of Pharmacology, Semmelweis University of Medicine, P.O. Box 370, Budapest, Hungary 1445*

■ **International Symposium on Thin-Layer Chromatography.** Sept. 10–14. Szeged, Hungary. *Contact: E. Tyihák, Research Institute for Plant Protection, P.O. Box 102, Budapest, Hungary 1525*

■ **10th Triennial Meeting of the International Association of Forensic Sciences.** Sept. 18–25. Oxford, U.K. *Contact: Stuart Kind, International Association of Forensic Sciences, 18A Mount Parade, Harrogate, N. Yorkshire HG1 1BX, U.K.*

■ **6th International Symposium on Analytical and Applied Pyrolysis.** Sept. 24–28. Wiesbaden, F.R.G. *Contact: Fachhochschule Fresenius Wiesbaden, Dambachtal 20, D-6200 Wiesbaden, F.R.G.*

■ **15th International Symposium on Chromatography.** Oct. 1–5. Nürnburg, F.R.G. *Contact: Gesellschaft Deutscher Chemiker, Abteilung Fachgruppen, Postfach 90 04 40, Varrentrappstrasse 40-42, D-6000 Frankfurt (Main) 90, F.R.G.*

■ **2nd International Congress on Automation and New Technology in the Clinical Laboratory.** Oct. 15–18. Barcelona, Spain. *Contact: R. Galimany, Apartado de Correos 543, Barcelona, Spain*

■ **36th Southeastern Regional ACS Meeting.** Oct. 24–26. Raleigh, N.C. *Contact: W. F. Little, Department of Chemistry 045A, University of North Carolina, Chapel Hill, N.C. 27514*

New. Waters QA-1™ Analyzer

The only HPLC for dissolution tests

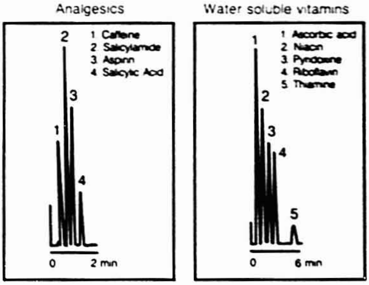

- Reliable three-step push-button operation.
- Simple set-up and changeover with exclusive Method Key™ Cartridge.
- Fastest analysis time. Uses high efficiency, short columns.

Let us prove it. Call or write today — ask for extension 2990.

MILLIPORE **Waters Associates,** 34 Maple Street, Milford, Massachusetts 01757.
Telephone (617) 478-2000.

CIRCLE 232 ON READER SERVICE CARD

- **International Association of Environmental Analytical Chemistry Workshop on LC/MS and MS/MS.** Oct. 24–26. Montreux, Switzerland. *Contact: R. W. Frei, Free University, De Boelelaan 1083, 1081 HV Amsterdam, The Netherlands*

For Your Information

The **University of Florida** at Gainesville is offering a short course entitled **Modern Analytical Chemistry.** The course, to be held March 18–22, is designed principally for scientists who have been out of school for 10 or more years and who may have lost touch with recent advances in the field. The course will provide an overview of modern analytical techniques, along with a discussion of "research fronts" in each area. Enrollment will be limited to 60 participants. Tuition, including room and board, is $800. Purchase orders or checks payable to the University of Florida must be submitted by Feb. 1 to Jill Sanderson, Division of Continuing Education, University of Florida, 1938 W. University Ave., Gainesville, Fla. 32603. For more information, or to indicate your intention to enroll, contact John Dorsey at 904-392-0557.

D14-P, "Proposed Guideline for Enzyme and Fluorescence Immunoassays," a new publication from the **National Committee for Clinical Laboratory Standards,** contains guidelines for enzyme and fluorescence immunoassays of macromolecular analytes. Factors that contribute to reliable and reproducible results are emphasized in sections that describe choosing enzyme fluorescence systems, producing, processing, purifying, and characterizing antibodies and antigens, as well as reagent separation techniques and instrumentation and equipment. Copies are $15 each (plus $1 additional for orders outside the U.S.); discounts are available for multiple copies. For more information contact the National Committee for Clinical Laboratory Standards, 771 E. Lancaster Ave., Villanova, Pa. 19085.

CAS Document Delivery Service provides copies of documents abstracted in *Chemical Abstracts*, *CA Selects*, and *CA Section Groupings*, documents summarized in *Chemical Industry Notes*, and documents cited in *Chemical Titles*. If the service cannot provide a photocopy of the desired document because the copyright status is unclear or because it does not have the publisher's permission to copy, the service will loan you the document from the CAS library. The cost of a photocopy or document loan is $12 if the CA number is provided and $14 without the CA number. For more information contact Chemical Abstracts Service, Customer Service—DDR, P.O. Box 3012, Columbus, Ohio 43210; 614-421-3670 or 614-421-3600, ext. 2956.

"The International Biotechnology Directory 1984" provides a guide to international products, research, and services in biotechnology and covers the traditional and newly emerging genetic engineering technologies. It includes listings of over 2000 companies, universities, and research centers; government agencies and programs; data bases, journals, and newsletters; and products. For ordering information contact The Nature Press, 15 East 26th St., New York, N.Y. 10010; 800-221-2123, or 212-532-4811 in New York.

STEP UP COST-EFFICIENCY
MCI Has Just the Moisture Measurement System You Need.

Performance takes a big step forward in our new microprocessor-control CA-05 Moisture Meter/VA-05 Water Vaporizer system with built-in printer.
Moisture measurement is fully automatic.
High coulometric Karl Fischer titration accuracy and sensitivity combine with wide mode/calculation functions for amazing application versatility.
Advanced features include an airtight titration cell, 16-digit display, automatic calendar and optional electronic balance/computer interfacing.
Write for complete details today.

MITSUBISHI CHEMICAL INDUSTRIES LIMITED
Instruments Dept., Mitsubishi Bldg., 5-2, Marunouchi 2-chome, Chiyoda-ku, Tokyo 100, Japan
Telex: J24901 Cable Address: MBISHICHEMICAL TOKYO Tel: (03)283-6715

CIRCLE 141 ON READER SERVICE CARD

LC problem solvers from Du Pont

Now Zorbax® 3-micron columns make rapid analyses trouble-free

ZORBAX Golden Series 3-micron columns solve the major problems that have plagued rapid analysis separations. With minimal back-pressure and without special instrumentation, Golden Series columns can separate complex mixtures two to three times faster than conventional columns. Samples that take 5 to 6 minutes with a standard 15 cm column can readily be separated in 2 to 3 minutes with a Golden Series column—with no loss of resolution.

Total engineering

The Golden Series column is unique, from the ZORBAX packing to a new column configuration. Particle size is controlled within a narrow distribution range: more than 90% of the particles are within 0.5 microns of the average. The 3-micron particle, made by a patented process, is spherical and mechanically strong; column back-pressure is minimized, and column life is lengthened. Every Golden Series column has a guaranteed minimum of 10,000 theoretical plates.

Optimum column design

The Golden Series column is designed so that its internal configuration (6.2mm ID x 80mm) has a volume equivalent to a standard 4.6mm ID x 150mm column. No new detector, injector, or re-engineering of your LC system is needed. When ZORBAX 3-micron and standard columns are operated at the same linear velocity, resolution and efficiency remain equivalent. However, resolution per unit time is doubled for the 3-micron column because analysis time is halved.

Other advantages

Golden Series columns increase lab productivity. Methods developed on standard ZORBAX columns can be transferred directly to Golden Series columns, because all ZORBAX columns, including the Golden Series, have consistent selectivity; and these 3-micron columns operate effectively from ambient to 60°C.

Three types of packings

Three types of ZORBAX packings are available: ODS, C8 and SIL, meeting more than 80% of chromatographic needs. All columns in the Du Pont line are shipped with a Column Performance Report and guaranteed for 60 days. Only Du Pont makes ZORBAX columns and packings.

Call toll-free

Call us anytime on our 24-hour toll-free number: 800-345-8600 ext. 502, or write: Du Pont Company, Room X40154, Wilmington, DE 19898.

COLUMN COMPARISON

Sample: Water Soluble Vitamins
1. Ascorbic Acid 3. Pyridoxine
2. Niacinamide 4. Riboflavin

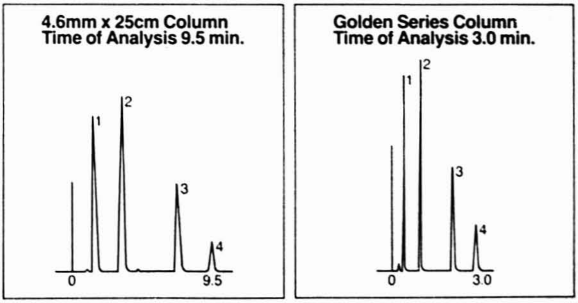

4.6mm x 25cm Column
Time of Analysis 9.5 min.

Golden Series Column
Time of Analysis 3.0 min.

Liquid Chromatography Columns

DU PONT

CIRCLE 55 ON READER SERVICE CARD

OMEGA®

18 Handbooks in one Encyclopedia

OMEGA® 1984 COMPLETE TEMPERATURE MEASUREMENT HANDBOOK AND ENCYCLOPEDIA™
OMEGA ENGINEERING, INC.
TEMPERATURE
PROCESS MONITORS by OMEGA ENGINEERING
NEW! DIGITAL CALIBRATORS for Thermocouples
NEW LOW PRICES
mocouple ector Systems
OMEGA THERMOCOUPLE AND SENSOR COMPUTER INTERFACE HANDBOOK
RECORDER HANDBOOK
OMEGA CL-505 Fast Precision Calibrator with Memory
OMEGA PRESSURE MEASUREMENT HANDBOOK

FREE!
THE BRAND NEW
1984 OMEGA
TEMPERATURE
MEASUREMENT
HANDBOOK AND
ENCYCLOPEDIA™

Over 670 Full-Color pages featuring over 15,000 Sensing and Control Products. Most available "Off-the-Shelf." Prices included.

NEW! FREE!
OMEGA PRESSURE
MEASUREMENT
HANDBOOK
OVER 200 PAGES!

IN A HURRY? CALL!

OMEGA ENGINEERING, INC.

One Omega Drive, Box 4047, Stamford, CT 06907
Telex 996404 Cable OMEGA FAX (203) 359-7700

(203) 359-1660

Send Request Directly to OMEGA;
or Circle Reader Service Number.
© COPYRIGHT 1983 OMEGA ENGINEERING, INC.

CIRCLE 158 ON READER SERVICE CARD

Chemistry and Crime

From Sherlock Holmes to Today's Courtroom

CHEMISTRY AND CRIME
NEW!

Samuel M. Gerber, *Editor*

An illuminating view of forensic science in fact and fiction. Underlines the relationship between detective fiction and the development of modern forensics. Begins with examples of chemistry at work in the novels of crime fiction writers such as Arthur Conan Doyle and Dorothy L. Sayers. Recounts how the sleuthing techniques in detective fiction laid the foundation for the sophisticated analytical methods of modern forensic science. Relates case histories in which modern forensics played a keynote role.

CONTENTS

Medical School Influences on the Fiction of Arthur Conan Doyle • Strong Poison: Chemistry in the Works of Dorothy L. Sayers • A Study in Scarlet: Blood Identification in 1875 • Forensic Science: Winds of Change • Chemistry and the Challenge of Crime • The Elemental Comparison of Bullet-Lead Evidence Specimens • Bloodstain Analysis: Case Histories • Bloodstain Analysis: Serological and Electrophoretic Techniques • Forensic Data in the Judicial Process

Based on a symposium sponsored by the Division of History of Chemistry of the American Chemical Society

135 pages (1983) Clothbound
LC 83-11907 ISBN 0-8412-0784-4
US & Canada **$19.95** Export **$23.95**

Order from:
American Chemical Society
Distribution Office Dept. 54
1155 Sixteenth St., N.W.
Washington, DC 20036
or CALL TOLL FREE 800-424-6747
and use your VISA or MasterCard.

JANUARY 1984

MAY 1984

ADVERTISED PRODUCTS:					1	2	3	4	5	6
7	8	9	10	11	12	13	14	15	16	17
18	19	20	21	22	23	24	25	26	27	28
29	30	31	32	33	34	35	36	37	38	39
40	41	42	43	44	45	46	47	48	49	50
51	52	53	54	55	56	57	58	59	60	61
62	63	64	65	66	67	68	69	70	71	72
73	74	75	76	77	78	79	80	81	82	83
84	85	86	87	88	89	90	91	92	93	94
95	96	97	98	99	100	101	102	103	104	105
106	107	108	109	110	111	112	113	114	115	116
117	118	119	120	121	122	123	124	125	126	127
128	129	130	131	132	133	134	135	136	137	138
139	140	141	142	143	144	145	146	147	148	149
150	151	152	153	154	155	156	157	158	159	160
161	162	163	164	165	166	167	168	169	170	171
172	173	174	175	176	177	178	179	180	181	182
183	184	185	186	187	188	189	190	191	192	193
194	195	196	197	198	199	200	201	202	203	204
205	206	207	208	209	210	211	212	213	214	215
216	217	218	219	220	221	222	223	224	225	226
227	228	229	230	231	232	233	234	235	236	237
238	239	240	241	242	243	244	245	246	247	248
249	250	251	252	253	254	255	256	257	258	259
260	261	262	263	264	265	266	267	268	269	270
271	272	273	274	275	276	277	278	279	280	281
282	283	284	285	286	287	288	289	290	291	292
293	294	295	296	297	298	299	300	301	302	303
304	305	306	307	308	309	310	311	312	313	314

NEW PRODUCTS				401	402	403	404	405	406	407
408	409	410	411	412	413	414	415	416	417	418
419	420	421	422	423	424	425	426	427	428	429
430	431	432	433	434	435	436	437	438	439	440
441	442	443	444	445	446	447	448	449	450	451
452	453	454	455	456	457	458	459	460	461	462
463	464	465	466	467	468	469	470	471	472	473
474	475	476	477	478	479	480	481	482	483	484
485	486	487	488	489	490	491	492	493	494	495

ONE ENTRY FOR EACH CATEGORY BELOW:

Intensity of product need:
☐ 1. Have salesman call
☐ 2. Need within 6 mos
☐ 3. Future project

Primary field of work
☐ A. Energy
☐ B. Environmental
☐ C. Medical/Clinical
☐ D. Drug/Toiletries
☐ E. Forensic/Narcotic
☐ F. Biotechnology
☐ G. Metals
☐ H. Pulp Paper Wood
☐ I. Soaps Cleaners
☐ J. Paint Coating Ink
☐ K. Electrical Electronic
☐ L. Instrument Dev. Des
☐ M. Plastic Polymer Rub
☐ N. Agricultural Food
☐ O. Inorganic Chemicals
☐ P. Organic Chemicals

Primary area of employment.
INDUSTRIAL
☐ A Research Development
☐ B Quality Process Control
MEDICAL HOSPITAL
☐ C Research Development
☐ D Clinical Diagnostic
GOVERNMENT
☐ E Research Development
☐ F Regulate Investigate
COLLEGE UNIVERSITY
☐ G Research Development
☐ H Teaching
INDEPENDENT CONSULTING
☐ I Research Development
☐ J Analysis Testing

CIRCLE 314 FOR SUBSCRIPTION FORM TO ANALYTICAL CHEMISTRY

NAME ____________________
TITLE ____________________
FIRM ____________________
STREET ____________________
CITY ____________________
STATE ____________ ZIP ____________
PHONE ( )

NEED MORE INFORMATION?

CIRCLE a key number. . .

SEND IN the postage paid reply card. . .

AND GET free data on any product advertised in this issue. . .

NO POSTAGE
NECESSARY
IF MAILED
IN THE
UNITED STATES

BUSINESS REPLY CARD

FIRST CLASS Permit #27346 Philadelphia, Pa.

POSTAGE WILL BE PAID BY ADDRESSEE

analytical
chemistry

P.O. BOX #7826
PHILADELPHIA, PA 19101

NO POSTAGE
NECESSARY
IF MAILED
IN THE
UNITED STATES

BUSINESS REPLY CARD

FIRST CLASS Permit #27346 Philadelphia, Pa.

POSTAGE WILL BE PAID BY ADDRESSEE

analytical
chemistry

P.O. BOX #7826
PHILADELPHIA, PA 19101

NEED MORE INFORMATION?

CIRCLE a key number. . .
SEND IN the postage paid
reply card. . .
AND GET free data on any product
advertised in this issue. . .

JANUARY 1984

VALID THROUGH
MAY 1984

ADVERTISED PRODUCTS:					1	2	3	4	5	6
7	8	9	10	11	12	13	14	15	16	17
18	19	20	21	22	23	24	25	26	27	28
29	30	31	32	33	34	35	36	37	38	39
40	41	42	43	44	45	46	47	48	49	50
51	52	53	54	55	56	57	58	59	60	61
62	63	64	65	66	67	68	69	70	71	72
73	74	75	76	77	78	79	80	81	82	83
84	85	86	87	88	89	90	91	92	93	94
95	96	97	98	99	100	101	102	103	104	105
106	107	108	109	110	111	112	113	114	115	116
117	118	119	120	121	122	123	124	125	126	127
128	129	130	131	132	133	134	135	136	137	138
139	140	141	142	143	144	145	146	147	148	149
150	151	152	153	154	155	156	157	158	159	160
161	162	163	164	165	166	167	168	169	170	171
172	173	174	175	176	177	178	179	180	181	182
183	184	185	186	187	188	189	190	191	192	193
194	195	196	197	198	199	200	201	202	203	204
205	206	207	208	209	210	211	212	213	214	215
216	217	218	219	220	221	222	223	224	225	226
227	228	229	230	231	232	233	234	235	236	237
238	239	240	241	242	243	244	245	246	247	248
249	250	251	252	253	254	255	256	257	258	259
260	261	262	263	264	265	266	267	268	269	270
271	272	273	274	275	276	277	278	279	280	281
282	283	284	285	286	287	288	289	290	291	292
293	294	295	296	297	298	299	300	301	302	303
304	305	306	307	308	309	310	311	312	313	314

NEW PRODUCTS:				401	402	403	404	405	406	407
408	409	410	411	412	413	414	415	416	417	418
419	420	421	422	423	424	425	426	427	428	429
430	431	432	433	434	435	436	437	438	439	440
441	442	443	444	445	446	447	448	449	450	451
452	453	454	455	456	457	458	459	460	461	462
463	464	465	466	467	468	469	470	471	472	473
474	475	476	477	478	479	480	481	482	483	484
485	486	487	488	489	490	491	492	493	494	495

TO VALIDATE THIS CARD, PLEASE CHECK
ONE ENTRY FOR EACH CATEGORY BELOW:

Intensity of product need:
- ☐ 1. Have salesman call
- ☐ 2. Need within 6 mos.
- ☐ 3. Future project

Primary field of work:
- ☐ A. Energy
- ☐ B. Environmental
- ☐ C. Medical/Clinical
- ☐ D. Drug/Toiletries
- ☐ E. Forensic/Narcotic
- ☐ F. Biotechnology
- ☐ G. Metals
- ☐ H. Pulp/Paper/Wood
- ☐ I. Soaps/Cleaners
- ☐ J. Paint/Coating/Ink
- ☐ K. Electrical/Electronic
- ☐ L. Instrument Dev./Des
- ☐ M. Plastic/Polymer/Rub
- ☐ N. Agricultural/Food
- ☐ O. Inorganic Chemicals
- ☐ P. Organic Chemicals

Primary area of employment.

INDUSTRIAL
- ☐ A. Research/Development
- ☐ B. Quality/Process Control

MEDICAL/HOSPITAL
- ☐ C. Research/Development
- ☐ D. Clinical/Diagnostic

GOVERNMENT
- ☐ E. Research/Development
- ☐ F. Regulate/Investigate

COLLEGE/UNIVERSITY
- ☐ G. Research/Development
- ☐ H. Teaching

INDEPENDENT/CONSULTING
- ☐ I. Research/Development
- ☐ J. Analysis/Testing

CIRCLE 314 FOR SUBSCRIPTION FORM TO ANALYTICAL CHEMISTRY

NAME: ______________________
TITLE: ______________________
FIRM: ______________________
STREET: ______________________
CITY: ______________________
STATE: ______________ ZIP: __________
PHONE: (___ ___ ___) ___ ___ ___ ___ ___ ___ ___

Polymer Characterization
Spectroscopic, Chromatographic, and Physical Instrumental Methods

Polymer Characterization
203

Clara D. Craver, *Editor*
Chemir Laboratories

Reports significant advances in polymer characterization and analytical procedures and automation. Discusses different techniques and applications of seven major analytical methods. Also covers new or highly specialized techniques.

CONTENTS

Physical Properties: Torsional Braid Analysis; Dynamic Mechanical Analysis; Viscoelastic Solids; Triblock & Multiblock Copolymers • Thermal Methods: DSC and the Single Dynamic Temperature Scan Method; Thermogravimetry Applied to Degradation Kinetics • Chromatographic Methods: Fractionation; Orthogonal Chromatography; Size Exclusion Chromatography • Electron Microscopy: Scanning Electron Microscopy; Molecular Optical Laser Examiner; Transmission Electron Microscopy; Electron Crystal Structure Analysis • Nuclear Magnetic Resonance: ^{13}C and ^{19}F NMR; Variable Temperature Magic Angle Spinning; Fluoropolymer Semicrystalline Polymers; Poly(styrene-co-chloromethylstyrene) Gels • IR Spectroscopy: Vibrational; Time-Resolved and Photoacoustic FTIR; Polyacrylonitrile Copolymers; Polymer Degradation • Analytical Pyrolysis/GC/MS: Pyrolysis/GC (glass capillary); Laser Desorption Mass Spectrometry; Pyrolysis/MS Pattern Recognition; Biopolymers • Special Topics: Scattering Studies; Excimer Fluorescence

Based on a symposium sponsored by the Macromolecular Secretariat of the American Chemical Society

Advances in Chemistry Series 203
793 pages (1983) Clothbound
LC 82-24496 ISBN 0-8412-0700-3
US & Canada **$69.95** **Export $83.95**

Order from:
American Chemical Society
Distribution Office Dept. 34
1155 Sixteenth St., N.W.
Washington, DC 20036
or CALL TOLL FREE 800-424-6747
and use your VISA or MasterCard.

MPF-66 fluorescence combines superior optical performance and powerful data handling.

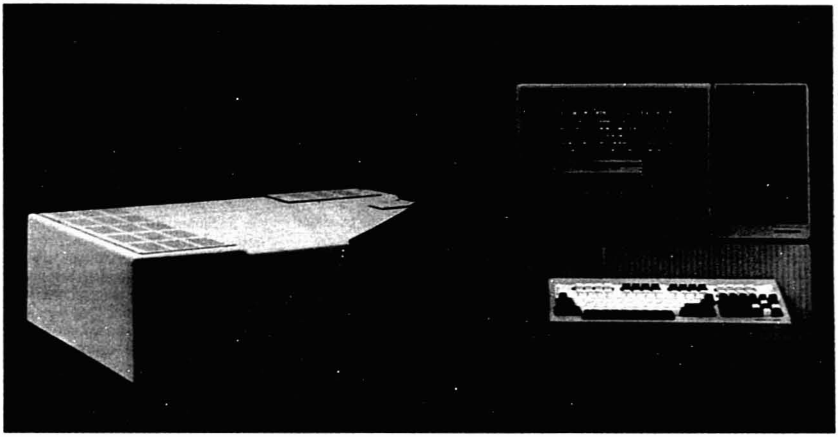

The new Perkin-Elmer MPF-66 Fluorescence Spectrophotometer combines the superior optical performance that you have come to expect from the MPF Series with the state-of-the-art Perkin-Elmer Series 7000 Professional Computer. A powerful, yet easy-to-use, software program provides simple instrument operation and data manipulation.

The MPF-66 provides excellent optical performance.
The MPF-66 optimizes both sensitivity and resolution, the two most important considerations in fluorescence. A new optical design which includes continuously variable slits allows you to select the largest slit width that provides the desired resolution, maximizing the sensitivity of your analysis.

A versatile microcomputer.
All instrument commands are entered via the Series 7000 Professional Computer, a unit specifically designed for the analytical laboratory. Soft keys on the computer make instrument operation simple. The Series 7000 Computers also support BASIC and FORTRAN, word processing and electronic spreadsheets.

Data manipulation-data you need in the format you want.
Perkin-Elmer's Computerized Luminescence Spectroscopy Software (PECLS) program, regarded as the most complete and flexible data manipulation program available for fluorescence, can be used with the MPF-66. PECLS includes an interactive viewing feature to let you see the part of the spectrum that you really need. The "OBEY" programming feature is included so you can automate your analysis and format the output.

Find out more!
For more information about Perkin-Elmer's new Model MPF-66 Fluorescence Spectrophotometer, call (800) 323-7155 (in Illinois, call (312) 887-0770). If you prefer, contact one of the offices below.

Perkin-Elmer Corp., Analytical Instruments,
Main Ave. (MS-12), Norwalk, CT 06856
U.S.A. Tel: (203) 762-1000. Telex 965-954

Bodenseewerk Perkin-Elmer & Co., GmbH,
Postfach 1120, 7770 Ueberlingen, Federal
Republic of Germany. Tel: (07751) 811

Perkin-Elmer Ltd., Post Office Lane,
Beaconsfield, Bucks HP9 1QA, England.
Tel: Beaconsfield (049 46) 6161

PERKIN-ELMER

Circle 170 For Literature. **Circle 171 For Sales Call.**

New Products

Ion Chromatograph

System IC 1000 is a compact modular system. Its compact nature makes it useful for analysis in extremely difficult situations such as in mobile labs under desert, tundra, or arctic conditions. Two basic systems are available: IC 1001 for the determination of organic acids and IC 1002 for the determination of anions and cations, Biotronik **404**

Humidity Chambers

Chamber models 435300 and 435310 can provide almost 444 ft^2 of load area and can accommodate 10 shelves. Temperature ranges from ambient to 95 °C or 5 °C to 95 °C ± 0.2 °C with controlled relative humidity from 20% to 98% ± 2%. They feature a solid, insulated outer door with an inner glass door, all stainless steel construction, mechanical convection, and solid-state proportional controls for both wet- and dry-bulb control systems. Hotpack Corp. **405**

Digital Polarimeter

P10 Solid-State Polarimeter offers the user reliable angular degree measurements to 0.02° by reading directly from a digital display. A null meter replaces the traditional half-shadow matching technique, thereby reducing human error and eyestrain. It has a range of ±85° angular. Sample tubes up to 200 nm in length can be used. Kernco Instruments Co. **406**

IR Spectrophotometer

9510 Series microprocessor-controlled, ratio-recording IR comes in three versions based on wavelength range. Options include a built-in Quant/Printer package and an RS232C interface that allows interfacing to any computer. It is capable of a 1-min hard-copy spectrum. The microprocessor is keyboard controlled, and interaction with the instrument is through the 16-character display. Sargent-Welch Scientific Co. **407**

Centrifuges

AccuSpin features digital controls that provide an accuracy superior to that of analog models. Programmed acceleration provides optimum acceleration speeds for fast processing while offering a gentle start to protect gradients. A digital integrator allows precise speed control, accurate to 10 rpm, with no overshoot. Beckman **408**

Far-IR Lenses

TPX, a methylpentene polymer, has good transmission properties in the submillimeter and millimeter region from about 100 μm to 5 mm; it is transparent in the visible with about the same refractive index as in the far-IR. Boston Electronics Corp. **421**

Data-Handling System

CFA-85 system incorporates a computer and interface designed specifically to collect, analyze, and correct data from segmented-flow, continuous-analysis, wet-chemical systems. In selecting peak responses, it uses a combination of peak detection and time windows, which allows the data system to account for abnormal responses that can occur in any chemical analysis system. Scientific Instruments Corp. **409**

Developing Chamber

Vega-T 10X Developing Chamber is precision manufactured of white PTFE with a lab glass cover. HPTLC and TLC plates developed in the chamber have exhibited excellent R_f reproducibility. The chamber has two solvent compartments, one at either end, each of 5.0-mL capacity. This permits simultaneous development from either end of the TLC plate or sequential development. Advanced Separation Technologies Inc. **410**

Model G-8R Moisture Analyzer is designed for lab or production line analysis of moisture content. It obtains homogeneity by applying pressure to the sample to bring it to a compressed condition that eliminates particle variations and air pockets. A hydraulic jack with a pressure gauge allows fast testing. Data Tech **401**

For more information on listed items, circle the appropriate numbers on one of our Readers' Service Cards

CONFIDENCE:

Don't let the buying decision scare you!

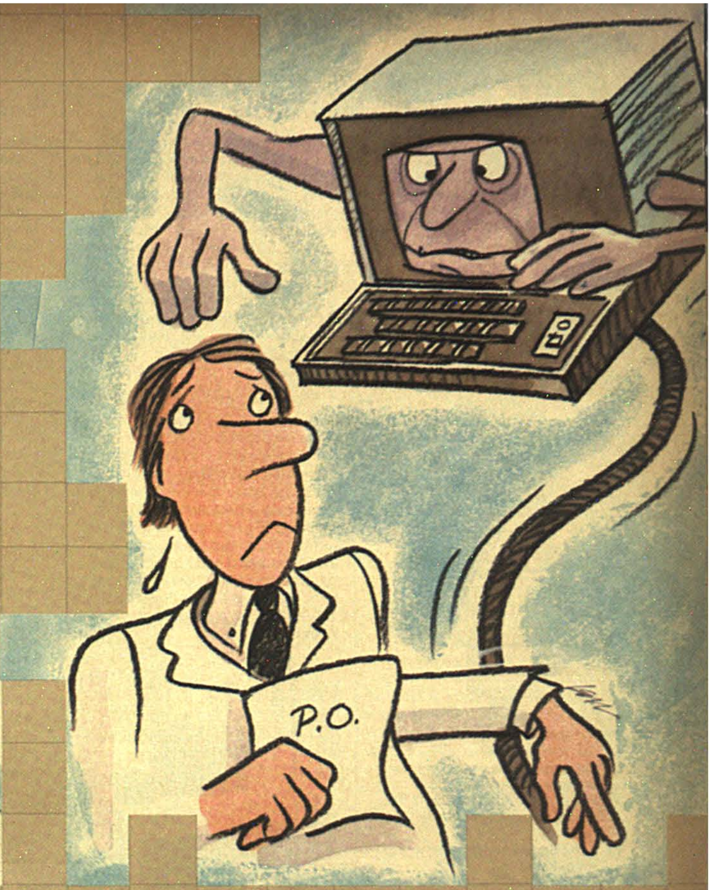

It's understandable that there are still a few decision makers out there who are scared when it comes to choosing atomic spectroscopy equipment. At Beckman we take that purchasing fear away. Users choose Beckman for experience. They know that Beckman has the elemental analysis expertise and long standing world leadership that means confidence.

Beckman makes the finest spectrometers ever. They are easy to use, allow more comprehensive analysis than atomic absorption, and save you money.

SpectraSpan™IV:
- 20+ more elements than AA for the cost of an AA
- wider linear dynamic range
- reduced sample preparation time
- no explosive gases
- quantitative and qualitative analysis capabilities

SpectraSpan™ V:
- worldwide industry standard for simultaneous multi-element analysis
- cost effective operation
- most flexible instrument on the market (quantitative and qualitative capabilities)
- high sample throughput

Need more convincing? Come for a free demonstration! Our chemical specialists will be happy to work with you personally and demonstrate how easy plasma emission analysis can be. Call them now for an appointment (In Europe, contact your local specialist). There's nothing to be scared of when you join the world leader in plasma emission.

Beckman Instruments Inc.:
Anaheim, CA (714)634-4343 - Jerold Kacsir
Arlington Heights, IL (312)398-2440 - Ray Derler
Houston, TX (713)781-0810 - Paul Watson
Somerset, NJ (201)560-0076 - Gerald DeMenna
Spectroscopy Instruments Operation, Beckman Instruments, Inc.
Irvine, CA (714) 833-0751 - Pat Carpenter

BECKMAN

CIRCLE 193 ON READER SERVICE CARD

A NEW ANION SEPARATOR FOR SUPPRESSOR IC

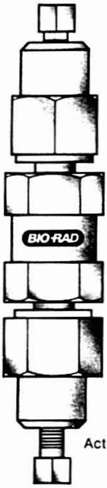

Actual Size

At last, a true replacement for the anion separator column in your suppressor ion chromatograph: the Bio-Rad PW Anion Separating Column.

- Acrylate polymer for chemical ruggedness.
- Macroporous 10 μ particles for high efficiency at low operating pressure.
- Wide pH range (0.5–13).
- Usable in new or old suppressor instruments.

For further information, call **800-4BIORAD ext. 575.**

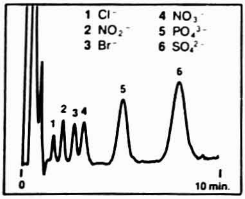

BIO-RAD

Chemical Division *2200 Wright Ave., Richmond, CA 94804*
Digilab Division *237 Putnam Ave., Cambridge, MA 02139*

CIRCLE 22 ON READER SERVICE CARD

New Products

UV/VIS

Lambda 7 Spectrophotometer offers exceptional sample throughput by providing a fast scan capability of up to 1440 nm/min. To enhance sample throughput, the Lambda 7 employs eight soft keys, each with multiple designations depending upon the method, mode, or parameter selected. The instrument's optical system reduces stray light to $<0.0002\%$ and thereby permits accurate and linear measurements of samples at values as high as four absorbance. Perkin-Elmer 411

Vacuum Spectrometer

Model VM-510 is designed for high-resolution spectral analysis. It uses a computer-optimized 1.0-m-focal-length optical system to produce symmetrical, coma-corrected spectral lines and a flat focal plane. Resolution is 0.004 nm with a 3600 g/mm grating, 0.007 nm with a 2400 g/mm grating, and 0.014 nm with a 1200 g/mm grating (10-μm-wide slits). Operational range is from 100 nm to the far-IR with available 110 × 110-mm gratings. Acton Research Corp. 412

Coat 95 Nondestructive Analyzer is based on energy-dispersive analysis of X-ray-excited emissions. It can analyze coatings of thicknesses ranging from a few angstroms up to multielement or multilayer finishes extending well into the micrometer range. Measurements can be made on silicon wafers, lead frames, or any other device. Philips 402

Opacity Combiner

Model 1100M is able to accept various inputs proportional to duct velocity. Velocity sensors can be used, but other parameters such as fan speed, fan motor current, or steam flow can be substituted. There is a simple conversion from one input to another. Dynatron 413

Digital Hygrometer

Model AY-21 allows precision reading and monitoring of temperature and humidity in ranges from 0 °C to 100 °C and from 10% to 95% RH. The unit, which is totally solid state, is capable of operation whether it is used in a lab, factory, office, production line, or in the field. The sensor is made of porous sintered Al_2O_3 and ceramic. Yamato USA, Inc. 414

Spectrophotometer

Model 390 features 8-nm bandwidth and convenient digital readout of concentration, factor, absorbance, and transmission. The instrument may be standardized by dialing in the concentration of the standard or a factor from 1 to 19 990. It has a continuous-wavelength range of 330 nm to 1000 nm to cover all routine colorimetric tests. This wide range is achieved by a monochromator using a plane diffraction grating in an f7 Ebert mounting. Sequoia-Turner Corp. 415

HPLC Detector

Model 87.00 features servo selection, which enables wavelength to be digitally set from 190 to 600 nm in 1-nm steps. Key front-panel features include event mark, auto and manual zero offset, and 11 measuring ranges (from 2.56 to 0.0025 au in binary steps). The design incorporates a high-pressure flow cell that is quickly and easily exchanged and cleaned. Sonntek, Inc. 416

Materials-Testing Automation

PC Series software–hardware system is modular and inexpensive and features data acquisition, critical instrument control, display, analysis, and data storage. The hardware, TESTMATE, acquires data and provides instrument control. The menu-driven materials-testing automation programs test specific to ASTM standards, analyze tests, display the data in graphic and statistical form, store the results, and print hard copy for permanent recordkeeping. Laboratory Technologies Corp. 417

HERE'S THE MODEL 344M

Now Beckman can put you into micro-gradient HPLC

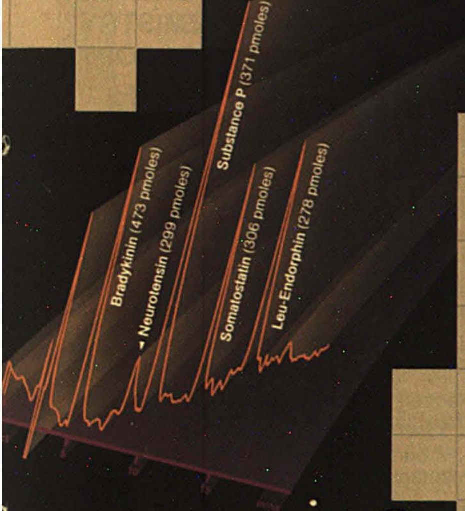

With separations like this!

Micro-gradient chromatography is today's most dynamic HPLC technique.

Increased sensitivity. Substantial solvent savings. The ability to analyze micro samples. All these advantages are yours with the new Beckman Model 344M Micro-Gradient System. And that's just the start!

Separations you hardly thought possible
The Model 344M is fully optimized for 2mm micro-gradient chromatography. Your detection limits are increased by as much as five times over conventional HPLC, depending on the detector flow cell you use. This is due in part to a new low-volume mixer, providing stable baselines even at high sensitivities. Even difficult to mix solvents can be used. In fact, the peptide separation exhibited here was obtained using a solvent gradient of methanol, TFA and water! Sensitivity was a low 0.02 AUFS while monitoring at 214nm.

Fine-tuned components mean high performance
Every component is specifically designed to process small samples at low flow rates. The Model 114M Pump, for example, controls solvent flow to 0.001 mL/minute. The zero-dead volume injector assures plug injections of samples ranging in volume from 0.5 to 5.0 μL. Detectors for the Model 344M System are fitted with a micro flow cell to maximize performance. What's more, a column compartment shields the column against sudden changes in ambient temperatures. Beckman offers you a choice of *three* micro columns—C_{18}, C_8 and Cyano—for a wide range of separations. You can even add our Model 504 Autosampler, combining unattended operation with micro sampling.

Micro-gradient HPLC . . . today and tomorrow
This is the system that can get you into micro-gradient HPLC *right now.* Beckman's strong support program of on-going applications, training and service means that you'll be getting the separations you want right from the start. And our dedication to system modularity means that your instrument will never become obsolete or anything less than the best. Start by calling your Beckman sales representative for complete details. Or simply request our brochure on the Model 344M.

Call toll free for detailed brochure

Continental U.S.: (800) 556-1234, extension 503
California: (800) 441-2345, extension 503
Or write Beckman Instruments, Inc., 1716 Fourth Street, Berkeley, CA 94710 (415) 527-5900

© 1983 Beckman Instruments, Inc.

BECKMAN

CIRCLE 20 ON READER SERVICE CARD

20 ACS INTENSIVE SHORT COURSES

Pre-meeting courses increase benefits of one of the most significant chemistry meetings of the year!

PRECEDING THE 35TH PITTSBURGH CONFERENCE AND EXPOSITION ON ANALYTICAL CHEMISTRY AND APPLIED SPECTROSCOPY

in ATLANTIC CITY, NJ • MARCH, 1984

Friday-Saturday, March 2-3

Electronics for Laboratory Instrumentation

Friday-Sunday, March 2-4

Applied Optical Microscopy for Chemists
Atomic Absorption and Plasma Emission Spectrometry
Interpretation of NMR Spectra
Practice of Modern Liquid Chromatography
X-Ray Fluorescence Spectrometry

For a free brochure giving full details on all courses, write, use the coupon below, or CALL COLLECT (202) 872-4508

American Chemical Society, Education Division,
1155 Sixteenth Street, NW, Washington, DC 20036

Yes! Please send me the free brochure describing ACS Short Courses to be held preceding the Pittsburgh Conference in Atlantic City in March 1984.

Name ______________________

Title ______________________

Organization ______________________

Address ______________________

City/State/ZIP ______________________

Saturday-Sunday, March 3-4

Analytical Infrared Spectroscopy: Techniques, Applications, Computer Methods
Capillary Gas Chromatography: Techniques and Problem Solving
Effective Management Techniques for Scientists and Engineers
Electron Spectroscopy and Surface Analysis
Environmental Analysis—Priority Pollutants
Gas Chromatography/Mass Spectrometry
Laboratory Automation: Micro-, Mini-, and Midicomputers
Liquid Chromatography/Mass Spectrometry
Maintaining and Troubleshooting Chromatographic Systems
Modern Techniques in Gas Chromatography
Quality Assurance of Chemical Measurements
Statistics for Experimental Design
Thermal Analysis
Writing for Results

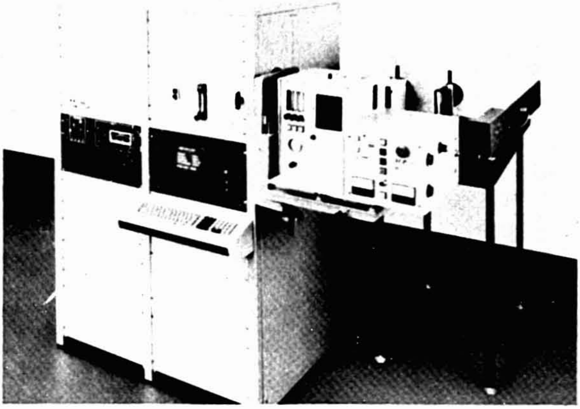

JY-70 Combination Spectroanalyzer features a sequential unit capable of analyzing for almost any element and a simultaneous unit with preset detectors for specific elements. Advantages of the system include push-button operation, one software package for both units, and one printout from either or both systems. Instruments SA **403**

X-ray Microanalyzer

System 5000 energy-dispersive spectroscopy system for electron column instruments uses advanced microcomputer technology to enable quantitative and qualitative elemental analysis at a fraction of the price of previous energy-dispersive spectrometers. It has a 16-bit microcomputer with 256 kbytes of internal memory plus 384 kbytes of display memory. Data storage is 2 Mbytes on dual floppy disks. EG & G Ortec **418**

UV/VIS

Response UV/VIS scanning spectrophotometer combines ease of use with flexibility and uses a 16-bit microprocessor. An autoranging photometric system provides up to 40 readings/s and a wide dynamic range. The standard software package includes wavelength scanning, kinetics, gel scanning, multiwavelength, and time-scanning routines. Gilford **419**

TLC Scanner

Features of the TLC Scanner II include scanning in both the absorption and fluorescence mode, built-in light sources, nine memories to store frequently used scanning programs, and a wide range of peripherals with varying degrees of sophistication for further processing of raw data. CAMAG **420**

Chemicals

Silica Gel

Flash chromatography silica gel is use tested and quality controlled for average particle size, particle size distribution, mean pore diameter, moisture, pore volume, specific surface area, and pH. J.T. Baker Research Products **422**

pH Papers

Type CF pH 4.5–10 advanced pH indicator papers consist of plastic support strips onto which are mounted three specifically impregnated test papers. The papers contain chemically bonded dyes that will not leach into test solutions. Solution pH values can be determined rapidly and accurately without ambiguous readings. The papers can also be used to read weakly buffered solutions, as they can be immersed for 5 to 15 min to allow final color change to take place. Whatman **423**

Silane

Silane capable of 10 000 ohm-cm resistivity is available. Each cylinder of silane is tested and certified by outside independent labs to meet or exceed the resistivity specification. The actual wafer used in the testing is provided along with the formal resistivity report. Matheson Gas Products **424**

J.T.Baker® RESEARCH PRODUCTS

Separate thousands of racemic mixtures by chromatography

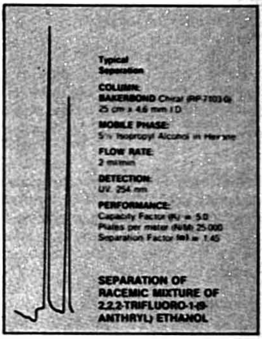

J.T. Baker Research Products can supply all the appropriate materials you need for chromatographic chiral separations.

BAKERBOND™ Chiral Phase HPLC Columns use high purity DNBPG ((R)-N-3,5-dinitrobenzoylphenylglycine) bonded to aminopropyl silica to separate a wide range of optical isomers. Up to 10 mg of sample can be applied to the column in a single injection.

Preparative chiral sorbents, in 40 μm particle size, are also available for scale-up of separations. In addition, longer column life can be achieved with our Chiral Column Regenerating Solution. For more information, call or write today.

J.T. BAKER RESEARCH PRODUCTS

222 Red School Lane
Phillipsburg, NJ 08865 USA
(201) 859-2151
Outside New Jersey (800) 526-0239

Gross Gerau, W. Germany • Deventer, Holland
Mexico City, Mexico • Singapore • Sydney, Australia

©J.T. Baker Chemical Co. 1983

Manufacturers' Literature

GC Troubleshooting Guide. Publication explains symptoms, probable causes, and remedies that relate to GC equipment, including such problems as isolating the problem source, testing for leaks, checking the carrier gas system, and sample injection. 32 pp. Supelco, Inc. **425**

Instruments. Product selection guide describes precision digital instruments used for problem solving in science and industry. Graphics plotters, logic analyzers, and digital oscilloscopes are included. 10 pp. Nicolet **426**

Gel Scanning. Bulletin T-1535 discusses the use of the DU-8B Slab Gel Scanning System to compare the relative sensitivity of stained and unstained slab gels. The system can scan a 20 × 20-cm slab gel, autoradiogram, or TLC plate at any wavelength in the UV or visible range. Beckman **427**

Nermag Newsletter. Vol. I, Issue 3 features news items on corporate matters as well as an article on a GC/MS method for analysis of neutral-sterols biosynthesis and bile acids in derivation of epithelial cells in rat liver. 5 pp. Nermag **428**

Floating-Ball Blankets. Applications bulletin details the industrial uses of hollow plastic balls including effective reduction of evaporation, minimization of heat loss, and containment of fume and odor emission from exposed-liquid areas. 27 pp. Techne Inc. **429**

Determination of Uranium. A procedure for the determination of uranium as UO_2^{2+} by IC is described in application note 48. The analysis is performed on a Series 2000i IC using cation exchange separation, postcolumn chemistries, and UV/VIS detection. 2 pp. Dionex **430**

Water-Treating System. Brochure describes the Petreco Air Flotation System, an induced-gas flotation machine that separates oil and particulate matter from oil field, refinery, and industrial wastewaters. System reduces operating costs by eliminating devices that typically cause maintenance problems and downtime. Petrolite Corp. **431**

Resin-Based Coatings. Booklet describes durable coatings based on UCAR phenolic resins. Twenty phenolic resins are listed in a table of physical properties; an applications table matches these coatings with their uses. FDA status is discussed. 32 pp. Union Carbide **432**

The Supelco Reporter. Vol. II, No. 5 includes articles on Supelcowax 10 columns, monitoring chlordane with Orbo-44 tubes, and analyzing enzymatic reaction products using HPLC. 12 pp. Supelco, Inc. **433**

Computer Interface. Thermocouple and sensor handbook is complete with a glossary and various tutorial aids to help the user understand the products and relate them to specific needs. 56 pp. Omega Engineering, Inc. **434**

Catalogs

Lab Chemicals. Special sections list dessicants, oxidation–reduction indicators, standard solutions, colorimetric reagents, very high purity acids, and the Royer catalysts. 198 pp. GFS Chemicals **435**

Lab Supplies. Catalog features timers, pipettors, pumps, balances, cleaners, cells, and a variety of lab accessories. 32 pp. Lux Scientific Instrument Corp. **436**

Stepping-Motor-Driven Positioning Devices. Catalog features the Stepper Mike micrometer drive system, Stepper-Mike-equipped and manually operable translators, rotators, optical mounts, and mirror mounts. 64 pp. Oriel Corp. **437**

Balances and Scales. Products described include balances for specific purposes such as check weighing, quality control sampling, field or job site tests, heavy-duty industrial weighing, moisture determination, and classroom teaching. 32 pp. Ohaus Scale Corp. **438**

Gas Products. Catalog features products such as pure gases, research gases, gas mixtures, electronic gases and gas mixtures, regulators, flow meters, filters, detectors, and tubings. 120 pp. Scientific Gas Products **439**

Chemicals. 84–85 catalog features monomers/polymers, biologicals, standards, dyes, stains, and chemicals for microscopy, chromatography, and electrophoresis. 231 pp. Polysciences **440**

Lab Supplies. Products listed include DO and temperature meters, pH electrodes, safety cans, mixers, evaporators, heating tape, illuminators, dry-ice makers, and flasks. 47 pp. Cole-Parmer Instrument Co. **441**

Lab Instruments. New instruments presented include a clamp DMM meter, multimeters, oscilloscopes, a pH/ORP controller, tachometers, calibrators, and thermometers. 35 pp. Extech **442**

Stable Isotopes. Along with a listing of stable isotopes, other products such as biochemicals, books, lab accessories, and NMR solvents and reagents are given. 83 pp. KOR Isotopes **443**

For more information on listed items, circle the appropriate numbers on one of our Readers' Service Cards

---

Shimadzu. Three gateways to one-touch analysis

Each one is feature packed.

1 GCMS-QP1000 Gas Chromatograph—Mass Spectrometer System

Measurements are stable even in the high-mass range with Shimadzu's GCMS-QP1000 Gas Chromatograph—Mass Spectrometer System, a quadrapole type GCMS with a mass range of 1000. Data processing functions for tabulations, graphics and area calculations are standard and standard floppy disc capacity is 1M bytes. Also standard for easy and cost-efficient monitoring is display of auto repeat scanning. Conversational dialog using the keyboard and CRT assures easy gas and mass chromatography, mass spectrometry, mass fragmentography (MF), direct-inlet mass spectrometry, multiple mini-range mass profile, mass number calibration and mass peak catching in mass fragmentography.

CIRCLE 159 ON READER SERVICE CARD

2 VF-320 X-Ray Fluorescence Spectrometer

Shimadzu's compact VF-320 Fluorescence Spectrometer with Rhodium target 3kW X-ray tube is user friendly. Just load the sample and touch a button for quantitative and qualitative analysis of metals, oxides, electronic materials, treatment solutions, chemicals, furnace products and other products. Easy key operation combined with CRT answers speeds an operator to accurate analysis in research as well as quality-control applications. High analytical accuracy and a wide dynamic range are assured by Shimadzu's advanced pulse-counting electronics.

CIRCLE 160

3 VXQ-150 Multi-Channel X-Ray Fluorescence Spectrometer

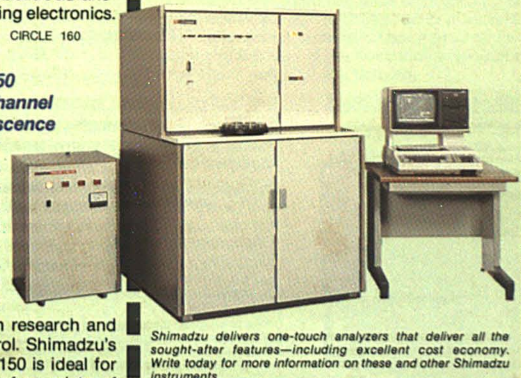

Simultaneous quantitative analysis of 24 elements at a touch of a button and complete data on all elements in just one minute—in research and in quality control. Shimadzu's compact VXQ-150 is ideal for rapid analysis of a variety of samples. A curved crystal monochromator assures high sensitivity. Pulse-counting electronics for all elements provide a wide dynamic range. And a gas-sealed detector is assurance of long-term reliable performance.

CIRCLE 161 ON READER SERVICE CARD

Shimadzu delivers one-touch analyzers that deliver all the sought-after features—including excellent cost economy. Write today for more information on these and other Shimadzu instruments.

Shimadzu

SHIMADZU (EUROPA) GMBH Acker Strasse 111, 4000 Düsseldorf,
F.R. Germany. Phone: (0211) 666371 Telex: 08586839
SHIMADZU CORPORATION INTERNATIONAL MARKETING DIV.
Shinjuku-Mitsui Building, 1-1, Nishishinjuku 2-chome, Shinjuku-ku,
Tokyo 160, Japan. Phone: Tokyo 03-346-5641 Telex: 0232-3291 SHMDT J.

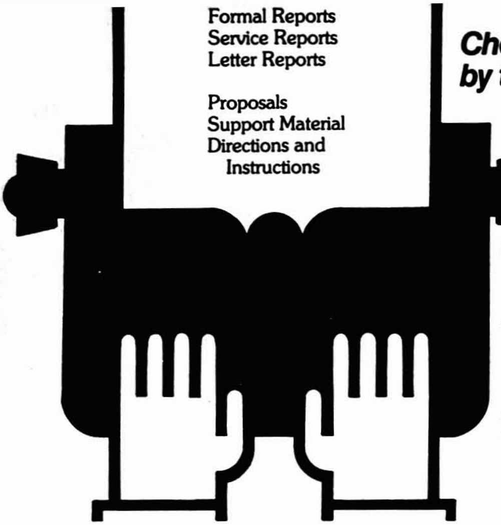

Chemists are often judged by the papers they write

AMERICAN CHEMICAL SOCIETY'S AUDIO COURSE

PRACTICAL TECHNICAL WRITING

SHOWS HOW TO WRITE TECHNICAL PAPERS WITH EASE, CLARITY AND CONFIDENCE

The successful chemist writes a good many technical papers in a lifetime . . . some in-house, some for publication, some for clients or potential clients. In any case, careers are often helped—or hindered—by the caliber of those papers.

Fortunately, writing good, sound technical papers is a skill that can be mastered. The ACS Audio Course, PRACTICAL TECHNICAL WRITING, is designed to help scientists and engineers express themselves clearly, convincingly, and professionally.

Combining the ease of listening with the challenge of doing, the course consists of eight audiotape cassettes, with a total playing time of 5.3 hours, and an integrated manual which includes examples and exercises covered in the lecture, as well as additional information and instructions.

NO RISK: 10-DAY FREE TRIAL

Order your course in Practical Technical Writing now. Look over the manual . . . listen to some of the cassettes . . . see how comprehensively the manual and cassettes complement each other. Read the examples of sound technical writing. Notice the clear Do's and Don'ts spelled out in the easy-to-read sections. Then start the course. Try some of the exercises. If you are not satisfied, return it to us within ten days and all billing will be cancelled, or your money will be returned.

Practical Technical Writing
Practical Technical Writing

THE INSTRUCTOR: Professor Jay R. Gould, for many years Director of the Technical Writers' Institute and Master's Program in Technical Writing at Rensselaer Polytechnic Institute, is the author of "Opportunities in Technical Writing" and a revision of "Technical Reporting." While Professor of English and Communication at RPI, Professor Gould conducted in-house writing seminars for many companies and government agencies.

INDIVIDUAL OR GROUP USE

Individuals intent on improving their communications skills will find this course a worthwhile investment in their futures.

Groups, including companies, government agencies, universities, and professional clubs and associations will find that it lends itself to multi-person use, since individual manuals can be ordered for each participant.

THE COST:

The complete unit, including eight cassettes and a manual in a handsome, sturdy case . . . $265.00.
Additional manuals: $17.50 each.

Be prepared to write your next paper easily, quickly, confidently. Order your course under our no-risk, 10-day trial offer. Call TOLL FREE 1-800-424-6747 (Credit card orders only) or mail coupon.

ACS Audio Courses
1155 Sixteenth Street, N.W., Washington, D.C. 20036

Please send me ______ Practical Technical Writing Courses @ $265.00
Please send ______ additional manuals at a total cost of ______
☐ Please send me information on other available Audio Courses.
☐ Payment enclosed
Charge my ☐ VISA ☐ MasterCard ☐ ACCESS ☐ Barclay Card
Acct. No. ______
Exp. Date ______ Interbank Code ______ (MasterCard Only)
Name ______
Place of Employment ______
Address ☐ Home ☐ Business ______
City ______ State ______ Zip ______

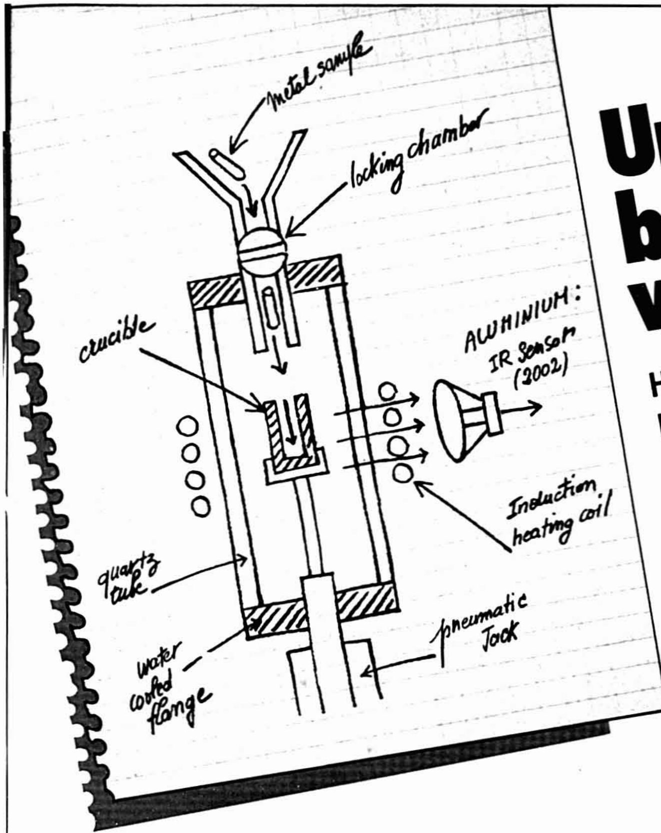
metal sample
locking chamber
crucible
ALUMINIUM:
IR Sensor
(2002)
Induction
heating coil
quartz
tube
water
cooled
flange
pneumatic
Jack

Unique but versatile

H_2YDROGEN
IS H_2ARMFUL
FOR YOUR METALS...
DON'T BE DISARMED
THA$_2$NKS
TO ITHA$_2$C 2000!

ITHAC 2000
Main features:
- Solid or liquid phase extraction capabilities
- Either ferrous (steel) or non-ferrous metals (Al - Ti - Zr - Cu...)
- Automatic analysis sequence for routine control
- Fully manual procedure for research application
- Conversational computer

ADAMEL LHOMARGY
DIVISION d'INSTRUMENTS SA

15, AVENUE JEAN-JAURES - B.P. 238
94203 IVRY-SUR-SEINE CEDEX - FRANCE
PHONE : (1) 670.11.80 - TELEX : ALJYINS 204342 F
Branch offices and distributors all over the world

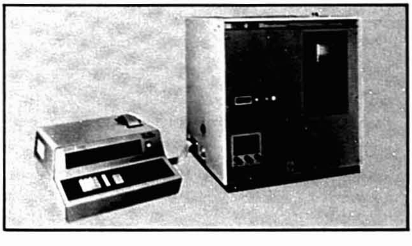

Principle:	Nitrogen carrier gas extraction method
Measurement range:	0.005 to 1000 ppm H_2
Heating range:	0 to 2000 °C
Sample weight:	10 mg. to 15 g.

CIRCLE 3 ON READER SERVICE CARD

LIQUID CHROMATOGRAPHY
NEW POWER
NEW SCOPE
NEW DEAL

Update your ideas on Liquid Chro

PHILIPS

Scientific &
Analytical Equipment

Start with the total automation and supreme flexibility of Pye Unicam's mighty PU4002 methods development liquid chromatography system. It stores up to ten methods files with complex combinations of gradient elution, column switching and flow programming. It automatically records, integrates and compares results from different detectors. It features the most sophisticated autosampler available.

Add the new Pye Unicam video chromatography control centre, PU4850, a twin floppy disk system that gives simultaneous data handling and control of four independent channels, with full graphic display, and increases storage, speed and capacity to unprecedented levels.

Reader inquiry no. 70

Take a look at the Pye Unicam PU4001 gradient liquid chromatograph and you'll see a first-class instrument that provides a fully automated gradient elution and column switching facility for the analytical laboratory. Its performance is proven. Its versatility is found in compatibility with a wide range of detector options – including the new, intelligent PU4021 diode-array multichannel detector.

Look closer and the new PU4810 computing integrator will be revealed as an easy to use, flexible and readily expandable data processor that provides optimum performance at a realistic price. Upgrading is a simple process with this modular unit, which in its standard form incorporates a tactile 32-key functional keypad, a high speed printer-plotter, and 16K of RAM and BASIC programming.

Reader inquiry no. 71

Just because Pye Unicam's PU4000 isocratic liquid chromatograph is a fully integrated system that offers reliable, repeatable high performance, day after day, you needn't think it's going to cost you the earth.

Admittedly, it's precision engineered, designed specifically for the demanding world of the modern quality control laboratory, and readily expandable. It incorporates all the lasting features and benefits you'd expect from a leading manufacturer like Pye Unicam. But even so, we think you'll be pleasantly surprised at the price.

Take the time to find out more. After all, it's hardly fair that anyone should be denied the excellence of the PU4000 because of a little thing like a budget.

Reader inquiry no. 72

matography

NEWS FROM PHILIPS AND PYE UNICAM

PU8800: eminent and affordable

Despite being endowed with one of the world's finest UV/Visible optical systems; offering ease of use and a level of information display beyond that of any other video UV/VIS spectrophotometer; and being capable of astonishing performance with or without a wide range of accessories – Pye Unicam's PU8800s are still within reach of the majority of budgets.

For details of how the four models available can each extend your purchasing power,

Reader inquiry no. 73

Autojector offers more

Pye Unicam's PU4700 chromatography Autojector offers more control than any competitive system.

Skilful microprocessor control of all operating parameters, including program storage, keeps the PU4700 easy to use and highly reliable while giving the operator great flexibility during the injection sequence.

Reader inquiry no. 75

Peak performance at any price

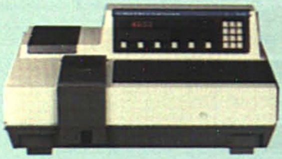

Performance and reliability – just what you'd expect from Pye Unicam's world-beating single beam UV/VIS range.

	SP6	PU8600
Low-cost	●	●
Microprocessor/keypad operation		●
Remote control		●
VIS or UV/VIS	●	
10 program storage		●
Meter or digital	●	
Automatic peak seeking		●
Many accessory options	●	●
Self-test		●
Master holographic grating	●	●
Kinetics option		●
Built-in printer option		●

Circle **reader inquiry no. 74** for a copy of the new Pye Unicam single beam UV/VIS brochure.

	Inquiry no.
PU4002 LC system	**70**
PU4001 LC system	**71**
PU4000 LC system	**72**
PU8800 UV/VIS spectrophotometer	**73**
Single beam UV/VIS spectrophotometers	**74**
PU4700 chromatography Autojector	**75**
IR spectrophotometers	**76**
SP9 AA systems	**77**
PU9000 multi-element AA spectrophotometer	**78**
Gas chromatography	**79**
pH meters	**80**
Conductivity meters	**81**
Ion selective meters	**82**

Pye Unicam Ltd

A SCIENTIFIC AND INDUSTRIAL COMPANY OF PHILIPS

York Street Cambridge Great Britain CB1 2PX
Telephone (0223) 358866 Telex 817331

PHILIPS

SAVE

UP TO 80% ON THESE SELECTED AUDIO TITLES

Quantities of these selected audio cassette tape programs are limited. Orders will be filled on a first-come, first-served basis. All titles will go back to list price after sale ends.

Affinity Lables in Drug Design
5 tapes 140 visual illustrations (1981)
List $59.95 **Sale $39.00**

NMR in Chemistry and Biology
6 tapes 150 visual illustrations (1981)
List $79.95 **Sale $39.00**

Innovative Approaches to Clinical Analytical Chemistry
7 tapes 218 visual illustrations (1980)
List $89.95 **Sale $29.00**

Innovation and Research in the United States
10 tapes 96 visual illustrations (1980)
List $99.95 **Sale $19.00**

Unusual Hydrocarbons: Synthesis and Properties
7 tapes 200 visual illustrations (1981)
List $89.95 **Sale $39.00**

Approaches to Solving Industrial Toxicology Problems
7 tapes 30 visual illustrations (1981)
List $139.00 **Sale $69.00**

Automating Your Laboratory
6 tapes 57 visual illustrations (1981)
List $149.00 **Sale $79.00**

Melvin Calvin: Impact on Bio-Inorganic Chemistry
8 tapes 167 visual illustrations (1981)
List $99.00 **Sale $29.00**

Each audio tape program comes packed in a protective album with the illustrations bound in a three-ring binder. Prices include shipping and handling. The order form below must accompany your payment or purchase order to take advantage of these sale prices.

AUDIO TAPE SALE ORDER FORM

Send to:

American Chemical Society
Distribution Office
1155 16th Street, N.W.
Washington, D.C. 20036
Phone 800-424-6747

☐ Payment Enclosed ☐ Invoice Company/Purchase Order # ____________

☐ Invoice Me ☐ VISA Account Number: ____________

☐ Master Card/Interbank Code: ____________

Expiration Date: ____________ Signature: ____________

Your Name ____________ Title ____________

Company ____________

Address ____________

Billing Address ____________

City ____________ State ____________ Zip ____________

California residents add 6% state use tax.

INFRARED SPECTROPHOTOMETRY

Captured!

The new high speed performance of FD-IR

Put the old ideas and prejudices out of your mind. All the qualities anyone ever sought in an IR spectrophotometer have been incorporated without compromise in the new PU 9510 Series from Pye Unicam.

Accuracy, speed and reproducibility are phenomenal (a high quality survey scan of a 1mm disc microsample takes just a minute).

Ease of use is exceptional (English language commands and RS 232C interface option for control by personal computer or IR data centre).

Data handling facilities are virtually limitless (the elaborate menu will stimulate any appetite).

Send today for more details and let the outstanding qualities of FD-IR capture your imagination.

	Inquiry No
PU 9510 FD-IR Series	83
SP3 Series	84

Pye Unicam Ltd

A SCIENTIFIC AND INDUSTRIAL COMPANY OF PHILIPS

York Street Cambridge Great Britain CB1 2PX
Telephone (0223) 358866 Telex 817331

PHILIPS Scientific & Analytical Equipment

PHILIPS

Choosing Your Graduate School?
Find out which departments have
specializations in your area of interest.

Involved in Research?
Learn what papers your colleagues
are publishing in your field.

The ACS Directory of Graduate Research 1983

The ACS Directory of Graduate Research is a comprehensive listing of U.S. and Canadian universities offering doctoral and master's degrees in chemistry, chemical engineering, biochemistry, pharmaceutical/medicinal chemistry, clinical chemistry, and polymer science. Included within each department's listing are names and biographical information for all faculty members, their areas of specialization, titles of all papers published in the last two years, and individual telephone numbers. A Statistical Summary in the front of the book provides information by department on numbers of full-time and part-time faculty, postdoctoral appointments, graduate students, and M.S. and Ph.D. degrees granted. For added convenience, an alphabetical index of faculty members is included.

The 1983 Directory lists information that is current as of the 1983-84 academic year and includes 715 departments, 9,285 faculty members, and 57,833 publication citations. The cost for this hard cover, 1231-page volume is $43.00. To order a copy, **Call Toll Free 1-800-424-6747** or mail the coupon below.

Special Note: The entire 1983 Directory, including a concordance of the research interests of each faculty member listed in the Directory, will soon be available as an on-line computer-readable file. Write to the ACS Office of Professional Training, 1155 16th Street, N.W., Washington, D.C. 20036, for further details.

American Chemical Society, Department 706, P.O. Box 57136, West End Station, Washington, DC 20037

Please send ________ copies of the **1983 ACS Directory of Graduate Research** @ $43 per copy.

On prepaid orders (including credit card orders) ACS pays shipping and handling charges. On purchase orders, shipping and handling fees will be added. For single orders of 20 or more copies, a 5% discount is available.

☐ Payment enclosed (payable to American Chemical Society) ☐ Bill me ☐ Bill company
Charge my ☐ MasterCard ☐ VISA ☐ Barclay Card ☐ ACCESS

Card # ________________ Interbank # ________________ Expiration Date ________________
(MasterCard Only)
Signature ________________ Telephone # ________________
(Area Code)
Name ________________ Organization ________________
Ship To Address ________________
City ________________ State ________________ ZIP ________________
Billing Address ________________
City ________________ State ________________ ZIP ________________

Can your G.C. isolate an important group of peaks and transfer them to a second column for better analysis?

MAN FILE 3
SiCHROMAT 2
SIEMENS

The Siemens SiCHROMAT 2 Can

Valvelessly.

With the patented, valveless "live" column switching system important trace components can be "heart-cut" from a multi-component sample and transferred to a second column for further analysis. By reducing the ratio between the trace and main components and utilizing a second column of different polarity, substantially increased resolution and optimized separations can be achieved.

Valveless "live" column switching is an exclusive feature of the Siemens SiCHROMAT 2 Double Oven Gas Chromatograph. Valveless means the sample does not come in contact with any switching valves. It is a pulseless, low dead volume system with extremely short (<1 second) switching times. The "live" principle allows switching times for transfer to be determined directly and the effect is immediately seen.

For more information and a demonstration of how the features of the new Siemens SiCHROMAT 2 can improve your chromatography contact:
ES Industries, Inc., 8 South Maple Avenue, Marlton, New Jersey 08053, 609/983-3616.

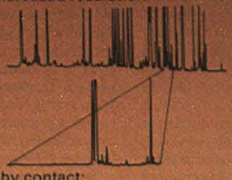

"Expanding the parameters of chromatography . . . for chromatographers"

ES
INDUSTRIES
MARLTON, NEW JERSEY
8 SOUTH MAPLE AVENUE

CIRCLE 67 ON READER SERVICE CARD

A/C Interface

Edited by Raymond E. Dessy

A Laboratory *Son et Lumière*

Part I

Sound and light are the sources of our two most important senses. In the human–machine dialogue so essential to effective use of computers in the analytical environment the *son et lumière* approach expands our capabilities and increases our awareness. This tutorial will examine some of the techniques being used to provide computers with voice output, voice input, image generation, and image analysis. These capabilities merge the scientist with his instrument, and immerse him, with increased awareness, in the data produced.

Imagine controlling instruments with both our hands *and* voices, receiving prompts and information back audibly while our eyes are occupied with other tasks, then seeing the data in graphic form, with color highlighting and color animation. Or imagine capturing images in the lab and eliminating spurious noise, increasing contrast, detecting edges, converting to pseudo-3-D images, and measuring areas. This world already exists. To use these tools effectively analytical chemists must know how they work, so that they can have models on which to build new techniques.

Son

The computer-generated voice is often monotonous. Male voices may predominate. Voice input commands to computers have a limited vocabulary, and more errors occur with female speakers. Why? To answer these questions let us explore the source of human speech.

The human voice is created by a mechanism akin to the whistle created by air escaping from the gently pinched throat of a balloon. The rapidly escaping air creates a low-pressure area that causes the throat to constrict. Internal pressure forces the throttled opening to expand. This rapidly alternating set of events creates a whistle. Muscle-controlled vocal cords provide a similar reed that produces various sounds. However, a tubular resonator (the throat) and a variety of tunable resonant cavities and muscle-controlled "stops" are essential to create the harmonic structures present in the human voice. The glottis, oral cavity, tongue, teeth, and lips all function interactively to produce recognizable speech.

Languages are cleverly constructed with respect to vocabulary and grammar so that a complete thought can be expressed by voicing speech units in "puffs" of vocal energy, with soft or silent intervals embedded. This mechanism conserves the air supply. Our speech apparatus generates about 100 basic sounds, or phonemes (like the *p* in pat). These are interconnected to form words. Depending on the surroundings, each phoneme can take on one of several variant forms, called allophones (like the *p* in pin or spin).

Equipment that produces a spectral analysis of speech as a function of time provides important information. From such studies, the complex, burst nature of speech is obvious, and speech scientists can abstract the several basic frequencies used in generating speech elements, called formant frequencies (Figure 1). These are the resonant frequencies of the vocal tract. The quality of speech is carried in the harmonic frequencies. Utterances can be broken down into short time segments and each subjected to an analysis that reflects all the frequency components involved during the period. This can simply involve subjecting the speech segment to a series of frequency-sensitive filters. The output of each filter represents the energy content in each passband during that segment. Alternatively, the data can be digitized and subjected to Fourier transform to provide similar data. Another approach views the speech process as a noise source that is subjected to a series of filters. This speech analysis process entails calculating the filter parameters.

Voice Output. Speech can be created via computers by several techniques. The simplest method requires that the sound stream be digitized at a rate twice that of the highest frequency components required for intelligibility or acceptability. The digital data are then sent to a digital-to-analog converter (DAC) to recreate the sound (Figure 2a). Given a 4-kHz upper limit and a dynamic intensity range of 256, this generates 64 kbits of information per second. Storage of

0003-2700/83/0351-068A$01.50/0

© 1983 American Chemical Society

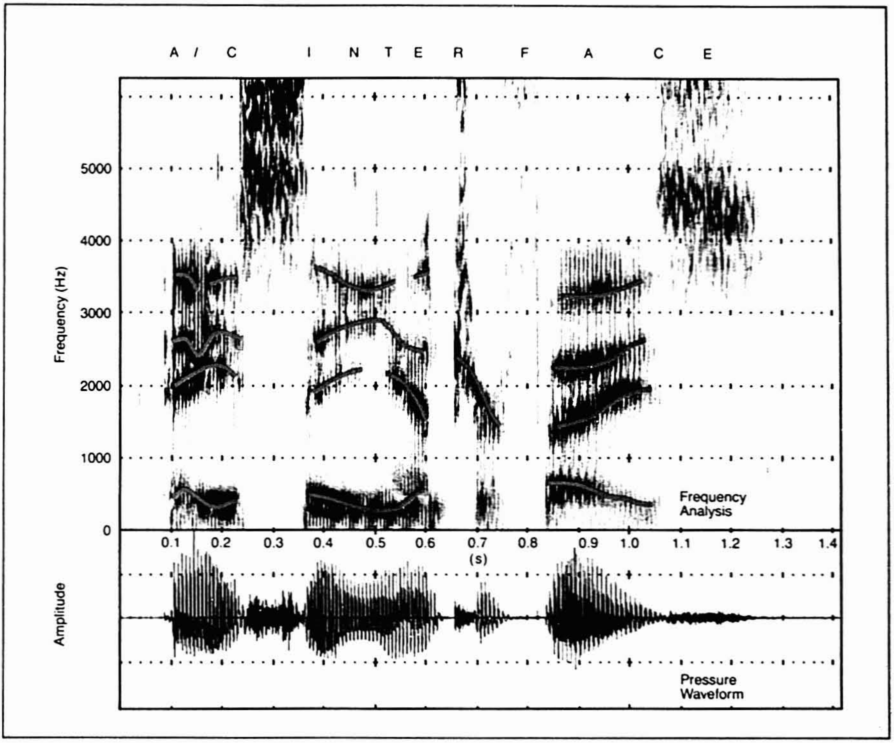

Figure 1. A frequency analysis of the words "A/C Interface"

The formant frequencies are centered around 500, 2000, 2500, and 3500 Hz. The burst nature of speech is very evident, as is the large amount of information speech contains. Courtesy of George R. Doddington, Texas Instruments, Inc., Dallas, Tex.

such a large amount of data is currently impractical, and some very imaginative techniques are used to compress the data.

Moser encoding, popular in some hand-held products, combines a number of techniques, all of which reduce the amount of necessary data. First, the speech is differentiated, lowering the dynamic range. Then, the burst pattern of speech is used to eliminate the silent areas, which carry no information. Subunits that recur require a single storage of the repeating unit. The bursts are then aligned so that the wave pattern is symmetrical about zero. Since the burst has little amplitude at the beginning and end these are "chopped off." The burst can be considered symmetrical, and only half of the remaining information need be stored. Finally, instead of storing each amplitude as an 8-bit digital number, only the differences between each succeeding value are stored. With proper techniques this *delta* encoding can quarter the storage requirements. All of these techniques are multiplicative, and the result is speech that can be stored at a cost of about 1 kbit/s. The speech produced from the digital data is rather flat, but acceptable in restricted environments.

Frequency analysis encoding (Figure 2b) is also used to generate speech. A digital table of energies associated with each passband in the sound segments can be created by filter or Fourier transform techniques. Since the human ear is relatively insensitive to phase relationships between the various required frequencies, the regener-

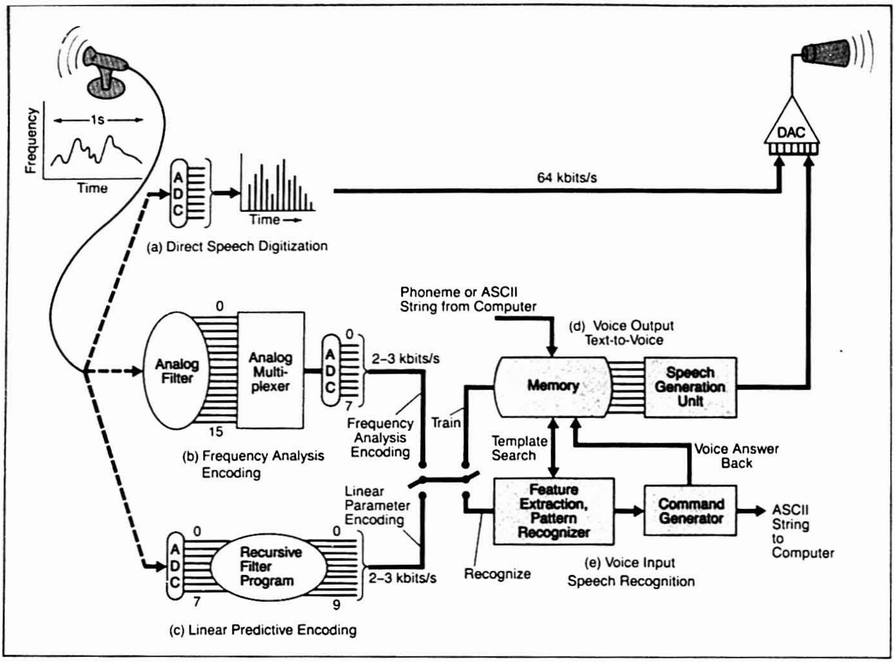
Frequency
1s
Time
A
D
C
Time →
64 kbits/s
DAC
(a) Direct Speech Digitization
Phoneme or ASCII String from Computer
(d) Voice Output Text-to-Voice
0
Analog Filter
Analog Multi-plexer
15
A
D
C
0
7
2–3 kbits/s
Frequency Analysis Encoding
Train
Memory
Speech Generation Unit
Template Search
Voice Answer Back
(b) Frequency Analysis Encoding
Linear Parameter Encoding
Feature Extraction, Pattern Recognizer
Command Generator
ASCII String to Computer
A
D
C
0
7
Recursive Filter Program
0
9
2–3 kbits/s
Recognize
(e) Voice Input Speech Recognition
(c) Linear Predictive Encoding

Figure 2. Various ways to implement voice input and voice output

ation process involves summing the individual components.

Linear predictive encoding is the most viable approach. The parameters describing the filter coefficients of the modeled vocal tract, with a suitable noise source, are used. Because of the linear nature of the time-dependent recursive filters the technique is termed linear predictive encoding (Figures 2c and 3).

These latter two techniques require about 2 to 3 kbits of information/s to produce acceptable voice sounds via DACs (Figure 2b, 2c). The voice quality is excellent.

Text-to-voice stores phonemes and/or allophone sounds in read-only memory (ROM), using one of the techniques described above. Supported vocabulary is also stored in ROM, along with pointers to the allophones that would be used to generate the spoken word. ASCII character strings (where seven bits of information are used to encode each letter or number in the text) are sent to the speech device from a host computer (Figure 2d). These character strings are interpreted, and if the word is found in the vocabulary ROM the corresponding sound is heard. Rules are available in some implementations that allow unlisted words to be pronounced. A program chooses the correct phoneme from the letter sequence and selects the correct allophone depending upon the surroundings. If the rules fail, the word is spelled out. Languages that do not exhibit numerous anomalies, such as Spanish, are served well by this approach.

Voice Input. Peering through a microscope you identify a new cell type in a biological sample. How can you enter the datum into a computer without breaking away from the eyepiece? Running an electron microprobe occupies both hands with sample movement. How can you change a gain setting? Simple, just talk to the device.

Speech input is more difficult to implement than voice output. In principle, direct digitization, frequency analysis, or linear predictive techniques could all be used to characterize a speech waveform. Search–match techniques would then be used to scan a previously stored library for equality (Figure 2e). If a "hit" occurred, the speech identification device would transmit a predetermined ASCII sequence to the host computer. In practice there are difficulties.

Direct digitization of the speech waveform envelope by analog-to-digital converters (ADCs) does not work well, since the envelope characteristics are very phase sensitive. Two sounds will "hear" the same, but have quite different envelopes due to phase differences in the sources.

Frequency analysis and linear predictive techniques are often limited to applications involving discrete utterances. These consist of speech of a few seconds in length with embedded pauses that do not exceed about 100 ms. The utterances may be words or short phrases. The utterance is divided into 20–50-ms windows and analyzed. The first step produces a series of descriptors for each window using the techniques already described.

A set of frequency-sensitive analog filters can produce a set of 16 numbers that represents the integral of the energy content of each passband (Figure 2b). A related technique digitizes the entire utterance and then sends it, via DACs, through a single filter repetitively, at faster and faster rates. The single filter produces the same spectral energy information. Fourier transform techniques can produce a similar set of numbers that represents the

Our new Model 6000 Chromatography Data System mates our unique and highly successful software with the new Micro 26 member of the Hewlett-Packard 1000 family of computers. This processor is designed for true foreground/background multitasking with multiple user terminals, all operating simultaneously . . . and for a starting price of only $29,500.

Up to 20 chromatographs, each generating up to 100 points per second of data, can be run simultaneously. And up to seven terminals and four disc drives can be tied to this computers, including a 132 megabyte Winchester.

You can network the 6000 System. For example, three processors networked would permit 60 chromatographs to be run on the same net, allowing all to share discs, files, methods, software and other facilities.

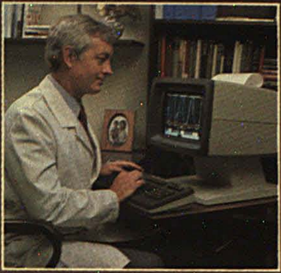

Our 4400 Systems can pass files to the 6000, thus tying the workhorse laboratory desktop system to the central 6000 System for reprocessing, archiving, and database management.

Nelson Analytical's sophisticated software teamed with powerful HP hardware lets you do extensive batch processing, complex graphics and reconstruction, as well as quantitative analysis.

Please call or write to 10061 Bubb Road, Cupertino, CA 95014. (408) 725-1107.

CIRCLE 152 ON READER SERVICE CARD

Multiuser, multitasking chromatography data system that grows and grows . . . and

nelson ANALYTICAL

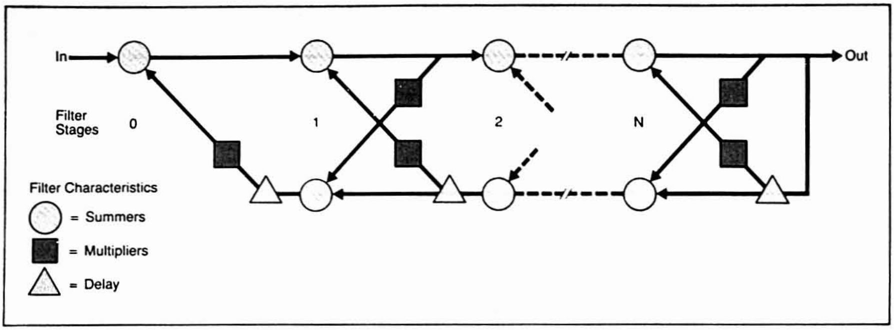

Figure 3. Recursive lattice filter used in linear predictive encoding voice synthesis

power spectrum magnitude in certain passband regions.

Alternatively, relatively inexpensive microchips can analyze the utterance by linear predictive techniques, which produce a set of 10 filter parameters (Figures 2c and 3). Such devices can even compress continuous speech in real time! These digital data must be compared with a library of stored utterances.

Templates are created in a training process in which the user is asked by the computer to say the various words in the vocabulary randomly and repeatedly (Figure 2e). The parameters are "averaged" in a process that also normalizes both the amplitude and time variables. These library parameters are then tested. The testing utterance cannot be compared to the templates in a direct search-match manner. The human voice is too variable; it changes the duration and stress of each phoneme according to the human condition. The most successful approach locates pronounced areas of similarity between the test utterance and a template and then compresses and expands the unknown accordingly. A summation is made of the differences that exist between the two. All vocabulary candidates are treated this way, and a list is made of the best "hits," along with their scores. The goal is to make the uttered word and the identified word agree, and have a score much better (lower) than any other candidate. If this fails, other words must be chosen for the voice control function. At the end of this iterative process the system is trained for a single person and may be switched to recognize mode (Figure 2e). Speaker independence is not commonly found in the lab because of speed and cost factors.

The discrete-utterance speaker-dependent systems currently available for the lab can handle vocabularies of a few hundred words. The user may still be faced both with failures (no identification) and errors (incorrect substitutions). The better systems recognize that at any moment in the human-machine dialogue only a few words from the entire vocabulary need to be distinguished from one another. Other utterances included in the user's vocabulary would be nonsense. Only acceptable library templates are scanned in the search-match process, so that the comparison process involves only about 10 words at any one time. Such systems work well even in noisy environments.

We now have a tool that allows users to train systems to respond to their own voices, employing any words they choose. Each user command results in the transmission of an ASCII string to a host computer to activate a required function (Figure 2e). The voice utterance and the ASCII command string need not be the same. In systems that can store speech, using the techniques described above, the instrument can respond vocally in prechosen words with a "personality" that can be determined by the user. Such personalized systems are not a luxury. They can provide security, since speaker-dependent systems are oriented to one person. They provide technicians with a mode of control that does not require a knowledge of the arcane ASCII command strings required by most operating systems. They provide a control mode that can augment and assist busy hands. Finally, they can provide an aural output that permits the eyes to continue performing other tasks.

Lumière

Traditional computer output is a list of numbers. Graphic presentation of data is more effective. Color graphics are capable of communicating even more information (Figure 4). Multidi-

Figure 4. A three-dimensional color view of chemical data

One frame of a stereo pair. Courtesy of Stanley Grotch, Lawrence Livermore National Laboratory, Livermore, Calif.

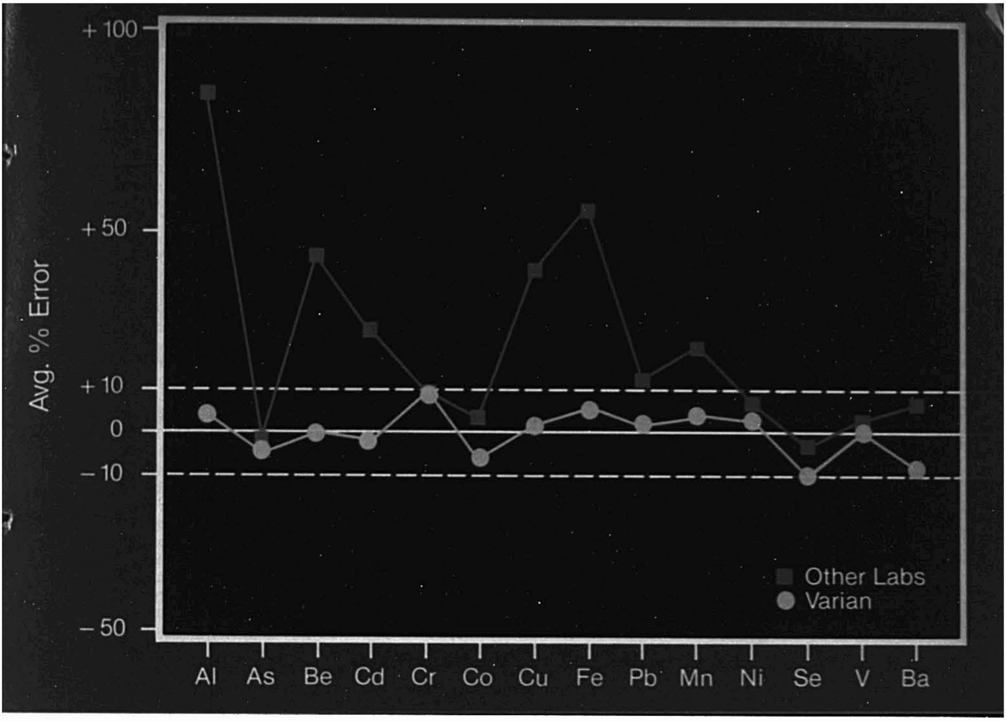

The test that proved beyond a doubt:

Varian AA gives the best results!

Varian AA delivers results unmatched by anyone, and here's the proof. The traces show the results of a round-robin study of 14 metals in seven different samples. Our results fit to within ±10% of true values at levels ranging from 200 ppb Al to as low as 1.3 ppb Cd.

Compare these results to the wide variances reported by labs using other makes of equipment!

How does Varian outperform all other makes of atomic absorption instruments? By letting intelligent automation take on the critical analytical operations; by eliminating contamination errors and dilution problems; by spiking samples for calibration by standard additions; by dispensing chemical modifiers to reduce matrix interferences. You get accurate, repeatable analytical results every time. And you save time and money per analysis in the bargain!

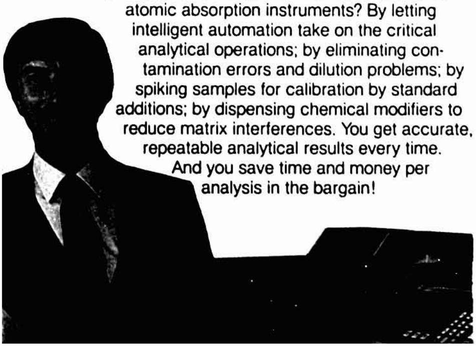

Whether your needs call for a basic instrument or an automated furnace system capable of running in a completely unattended mode, you make your best decision when you choose Varian AA. The reason is simple. Because Varian has established itself as the Number One company in the fields of trace metals analysis and automation, as the above tests have clearly demonstrated.

You owe it to yourself and your operation to join the growing trend toward intelligent instrumentation from Varian.

For more information about Varian intelligent AA spectrophotometer systems, circle Reader Service No. 222 to discuss your AA needs with a Varian representative, circle No. 223.

varian

Intelligent automation . . . from Varian

For immediate assistance contact: Florham Park, NJ (201) 822-3700
Park Ridge, IL (312) 825-7772 • Sugar Land, TX (713) 491-7330
Georgetown, Ontario (416) 873-1611
Or write: 611 Hansen Way, Palo Alto, CA 94303
In Europe: Steinhauserstrasse, CH-6300 Zug, Switzerland

See us at the
Pittsburgh Conference
Atlantic City March 5-9!

mensional plotting and 3-D images of objects are often the only way a human can comprehend the data message. How do computers create such images?

The gamut of color sensations can be created by adding together varying amounts of three-colored light sources, each covering a selected passband in the short, medium, and long wavelength region between 380 and 780 mμ. Classically, the primary additive colors are red, blue, and green.

CRT Terminals. Black-and-white cathode ray tubes (CRTs) have only a single electron gun and a phosphor-coated screen that emits visible light when struck by electrons. White or green phosphors are common. Color CRTs use three electron guns, one for each of the primary colors. The screen is coated with phosphor triads composed of a red-, blue-, and green-emitting phosphor dot at the corners of an equilateral triangle. A shadow mask located in front of the phosphor screen has a small hole located over each triad to help direct the electron beams. The CRT display is a rectangular array of visual points created by selectively exciting phosphor areas. Although it is possible to build displays in which individual points are randomly addressable, or displays in which images are created by vector strokes oriented at any angle, the most common displays are raster scan devices.

Driven by scan electronics, the electron beam moves (rasters) across the tube face through one horizontal line at a time, retracing rapidly to the left at end-of-line. At end-of-frame the beam vertically retraces to the top left.

The minimum picture element is called a pixel. (Typically there are about 2.5 triads/pixel in a high-resolution display.) Each pixel area is excited by electron guns controlled by DACs, which in turn receive their digital input from computer memory. A row of pixels is called a scan line. A collection of scan lines is a raster frame. If a frame is displayed at a rate of 60 Hz the human eye fuses separate frames into a continuum. This generates the need to handle a very large bandwidth (60 MHz). A 30-Hz rate reduces bandwidth, but leads to flicker. This flicker can be reduced by dividing the raster frame into odd- and even-numbered lines and alternately displaying each set (a field). Such displays are termed *interlaced*. There are trade-offs in cost, brightness, and flicker between interlaced and noninterlaced displays.

Bit-Mapped Displays. The raster frame is driven from a high-speed frame buffer memory that can be viewed as a matrix whose planar array dimensions, in bits, are determined by the number of pixels on the screen; e.g., 512 × 512 or 1024 × 1024 bits. If the picture is "sampled" at 512 pixels/line the time to generate and display one pixel is 100 ns! If the horizontal and vertical resolution is increased by two the display time/pixel would be just 25 ns. But resolution is the key to acceptable displays. Two hundred fifty-six elements of resolution lead to displays in which "smooth" curves appear with very jagged edges, referred to as granularity or aliasing. This can be not only visually distracting, but the data may be misrepresented or distorted by the lack of resolution. Low-resolution displays (256 × 256) are suitable for peer distribution. Presentation graphics requires 515 × 512 to 1024 × 1024 displays. Picture quality is delivered by 2048 × 2048 high-resolution CRTs. Commonly a rectangular frame is involved, rather than a square one.

Depth gives a third dimension, z, to the matrix. This depth, expressed in bit-planes, is determined by the color characteristics required. If this is one bit deep (one bit-plane) only monochrome black-and-white information can be displayed; the single electron gun is turned off or on by the binary bit pattern stored in this bit-plane (Figure 5a). A monochrome display having three bit-planes could support eight levels of gray scale, since the DAC driving the electron gun could be set at eight beam current levels. The simplest eight-color display would also have three bit-planes: one bit for each color gun. A logic 1 would turn that color beam on; a logic 0 would leave it off. Such a display mixes the primary colors in an off–on manner giving very saturated colors (Figure 5b). A more versatile approach allocates two bits to each color gun allowing four energy levels for each (six bit-planes). This system can create 64 different colors by properly mixing the primary additive colors. Allocating eight bits to each color gun gives a palette of 16 million colors, but requires 24 bit-planes and a total of 3 Mbyte of memory.

The intent of these palettes is not to encourage concurrent use of such a panorama. Rather the scientist can use color texture to describe surfaces, where shadows and three-dimensional character must be expressed or use related hues to express chemical connec-

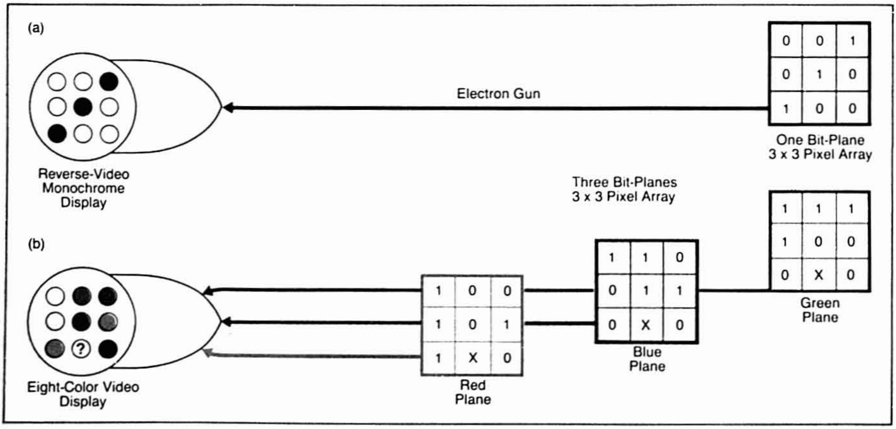

0	0	1
0	1	0
1	0	0

1	0	0
1	0	1
1	X	0

1	1	0
0	1	1
0	X	0

1	1	1
1	0	0
0	X	0

Figure 5. The number of bit-planes in the matrix determines the color variations that can be output to the screen

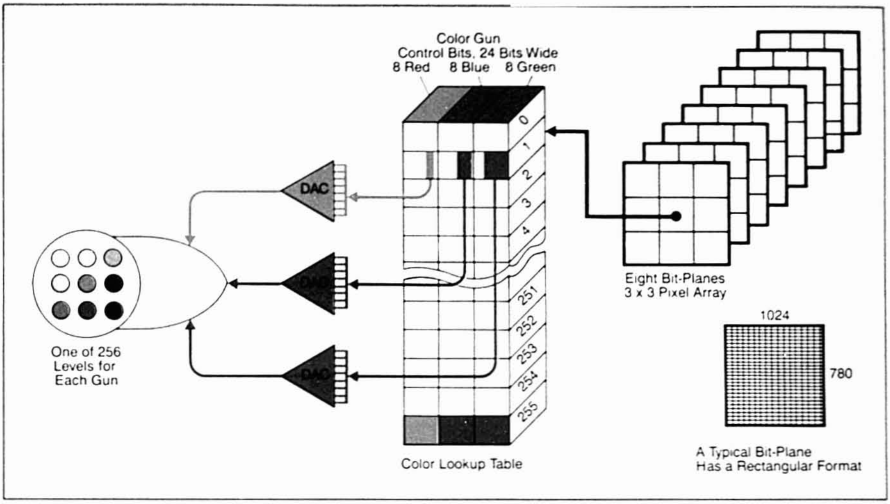
Color Gun
Control Bits, 24 Bits Wide
8 Red 8 Blue 8 Green
DAC
DAC
DAC
0
1
2
3
4
251
252
253
254
255
One of 256
Levels for
Each Gun
Color Lookup Table
Eight Bit-Planes
3 x 3 Pixel Array
1024
780
A Typical Bit-Plane
Has a Rectangular Format

Figure 6. Bit-planes map through a lookup table to determine colors output to the display, thus reducing memory requirements

tions. Since even the shallowest matrix involves megabits of memory, and all palette colors will never be used concurrently, most systems "map" from this matrix, through a color lookup table, to the CRT screen. The binary word describing each pixel in the matrix points to an address in the color map lookup table. The contents of this memory cell determine the values output to the DAC associated with each color gun. An 8-bit-deep matrix can address one of 256 different locations in the lookup table. Each word in this table might contain 24 bits, eight for each primary color. We can now display 256 colors chosen from a palette of 16 million (Figure 6)!

It is possible to alter the contents of the lookup table in a very short time. Changing certain memory cells during vertical retrace will then change all pixels referenced through that cell during the next scan. (Imagine rewriting every affected cell in the memory matrix!) The array maps to the tube surface geometrically; the bit-planes map through the lookup table to color. This allows the chemist to change colors rapidly, illustrating connections within a data set. Simple animation can be done by changing the values in the lookup table.

Character vs. Graphics CRTs. ASCII characters occupy seven bits (128 possible characters). Their display requires many more pixels, e.g., a 5 × 7 or 9 × 15 matrix. It is possible to map from ASCII code through a character generator, conserving considerable memory space (Figure 7). Alpha-

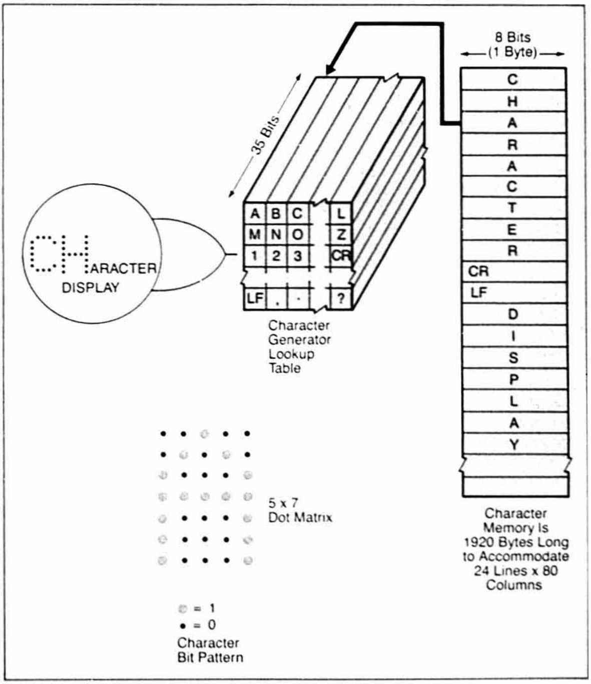
8 Bits
(1 Byte)
C
H
A
R
A
C
T
E
R
CR
LF
D
I
S
P
L
A
Y
35 Bits
A B C L
M N O Z
1 2 3 CR
LF . · ?
CHARACTER
DISPLAY
Character
Generator
Lookup
Table
5 x 7
Dot Matrix
○ = 1
• = 0
Character
Bit Pattern
Character
Memory Is
1920 Bytes Long
to Accommodate
24 Lines x 80
Columns

Figure 7. Letters and numbers are bit-mapped through a character generator to conserve memory
CR = carriage return, LF = linefeed

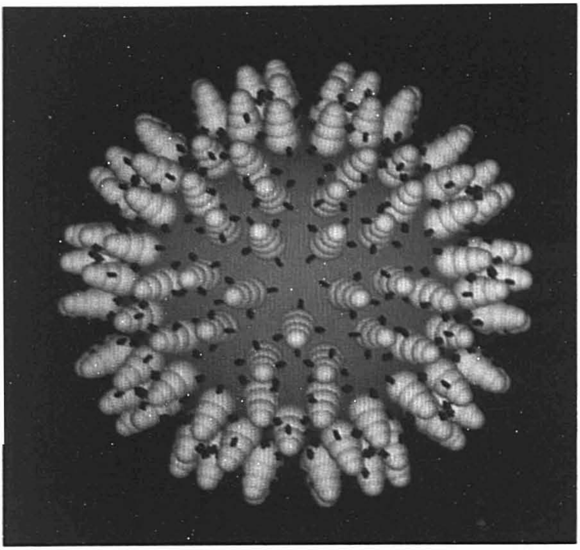

Figure 8. The use of related colors, light reflection, and perspective to provide a sense of depth
Courtesy of Richard Feldmann, Molecular Graphics Lab, National Institutes of Health, Bethesda, Md.

numeric terminals possess *only* this capability. They can draw graphs only by using symbols in the 24-line × 80-character/line positions. Some of these terminals can have options added that allow bit-mapped addressing. Good bit-mapped displays can superimpose alphanumeric information over graphs and drawings. Often one or more bit-planes are reserved for such overlay functions. Overlays also allow simple animation over a fixed background.

3-D Plotting. With an extensive color palette it is possible to produce pseudo three-dimensional representations of data and objects (Figure 8). The perspective problem in Cartesian space is easily solved. The outlines of solid objects can be generated by sweeping out in "space" volumes defined by rotating polygons. Clever algorithms solve the hidden line and surface problem, so that acceptable visual surfaces remain. The fundamental laws of reflectance of light are then used to generate color and shading information that draws on the color palette for implementation. Both diffuse reflectance (cosine-dependent, Lambert's law) and specular reflection (mirror reflection) models have been developed. The eye then sees depth by perspective, shadow, and color differences. The result is very lifelike images.

Stereo views can easily be created by changing the angle of view between two frames of the same subject, photographing the two images, and using the appropriate stereo viewers (Figure 4). Even more startling, 3-D images can be created by interlacing stereo images on the screen or by using side-by-side presentation. These may be viewed in relevant time.

Graphics Standards. Unfortunately, software is the most difficult problem. The user would like to use powerful graphic commands without having to know the steps taken in high-level languages to accomplish his/her goal. Standard graphic functions include drawing vectors, generation of conics and wire frame polygons, and filling these structures with accent and color. Advanced functions include zoom, rotate, translate, and scale operations. Application programs deal with the geometric and topographical description of objects by graphic primitives and Cartesian transformations. A viewing package translates these descriptions into image data suitable for the bit-mapped matrix of a display device. Then, a device driver, written in machine code, outputs the data to a particular device. Incompatibilities in coordinate systems, scaling, graphic primitives, and display protocols make transportation of graphics from one system to another a nontrivial task.

The International Standards Organization (ISO) has adopted a Graphics Kernel Standard (GKS) that addresses the application and viewing levels. The American National Standards Institute (ANSI) has endorsed GKS. Although GKS supports only 2-D displays, the Core Standard, developed by the American Association for Computing Machinery Special Interest Group on Graphics (SIGGRAPH), does address 3-D graphics.

The North American Presentation Level Protocol Syntax (NAPLPS) has been developed because of the intense interest in videotex, which involves text–graphics exchange between central data bases and terminals via commercial communication channels. AT&T has adopted and enhanced this standard.

Vendors provide a wide range of offerings, from enhanced graphic boards that plug into standard buses of microcomputers to turnkey systems. In addition to resolution and interlacing specifications, the buyer should examine the speeds at which oblique vectors can be drawn (100 000 to 4 000 000 pixels/s) and polygons filled (4 000 000 to 40 000 000 pixels/s). Some of these terminals will emulate industry standard terminals (Tektronix 4010, 4014, the DEC VT family, or IBM 3270), which provides flexibility. The speeds supported by serial ports range from 9600 to 39.2 kbaud. Some devices have standard printer ports that allow direct attachment to color ink jet printers that provide color hard copy.

Image Processing and Analysis

Technology is moving so rapidly that the rigid distinctions between graphics and image manipulation are blurring. Peter Jansson of Du Pont has defined computer graphics as a "numbers-in/picture-out" technology. Image processing is "picture-in/picture-out," and image analysis involves "picture-in/numbers-out" (Figure 9). A chemical example? 2-D electrophoresis plates, in which molecules are separated by molecular weight and polarity, often produce fuzzy, hard-to-decompose images. Boolean/algebraic manipulation of the image by techniques called erosion and dilation, with background subtraction, can create pseudo-3-D views that are umbral (moon crater shadow) in nature. Important features are easily seen. Then quantitative numbers can be abstracted from the display.

Image processing usually implies capture of the image of an object by a 256 × 256, or larger, solid-state camera device. As each pixel in the captured image is scanned out it is digitized (eight-bit resolution) and stored in memory. Imagine a very large

Shimadzu. Three approaches to wide-ranging LC

All are modular designs

1 SPD-M1A Photodiode Array UV-VIS Spectrophotometric Detector for HPLC

An advance in HPLC that achieves simultaneous detection through the full UV-VIS wavelength range. Shimadzu's SPD-M1A Photodiode Array Spectrophotometric Detector for liquid chromatography is designed for simultaneous quantitative and qualitative analyses. It offers the advantage of three-dimensional spectro-chromatograms, easily identifiable peaks, spectrum memory on-flow and single and double wavelength range chromatograms. The photodiode array sensor covers the full UV and VIS spectrum range and all detector signals in the UV/VIS wavelength range are processed by dedicated microprocessor combined with a dialog system on the CRT for easy operation.

CIRCLE 162

2 RF-530 Fluorescence HPLC Monitor

Shimadzu's RF-530 Fluorescence HPLC Monitor with xenon lamp and concave holographic gratings offers a wide range of excitation and emission wavelengths.

The corrected excitation energy and sensitivity to give a detection limit for quinine sulphate is 0.45pg/12μl. An off-plane optical system and aberration-corrected concave holographic gratings decrease noise. All connections are made with standard 1/16″ O.D. tubing for connection to all HPLC systems.

CIRCLE 163

3 SPD-2A UV Spectrophotometric Detector for HPLC

Shimadzu's SPD-2A is equipped with a high-performance grating monochromator having a wavelength range from 195 to 350nm. To ensure high stability, the SPD-2A has a double beam optical system which cancels drifts caused by fluctuation in the intensity of the light source. Available with 8μl flow cell and 0.5μl micro flow cell.

CIRCLE 164

Shimadzu delivers modular design, versatile components and full automation. Write today for more information on these and other Shimadzu instruments.

Shimadzu

SHIMADZU SCIENTIFIC INSTRUMENTS, INC. 7102 Riverwood Drive, Columbia, Maryland 21046, U.S.A. Phone: (301) 997-1227
SHIMADZU (EUROPA) GMBH Acker Strasse 111, 4000 Düsseldorf, F.R. Germany. Phone: (0211) 666371 Telex: 08586839
SHIMADZU CORPORATION INTERNATIONAL MARKETING DIV. Shinjuku-Mitsui Building, 1-1, Nishishinjuku 2-chome, Shinjuku-ku, Tokyo 160, Japan. Phone: Tokyo 03-346-5641 Telex: 0232-3291 SHMDT J.

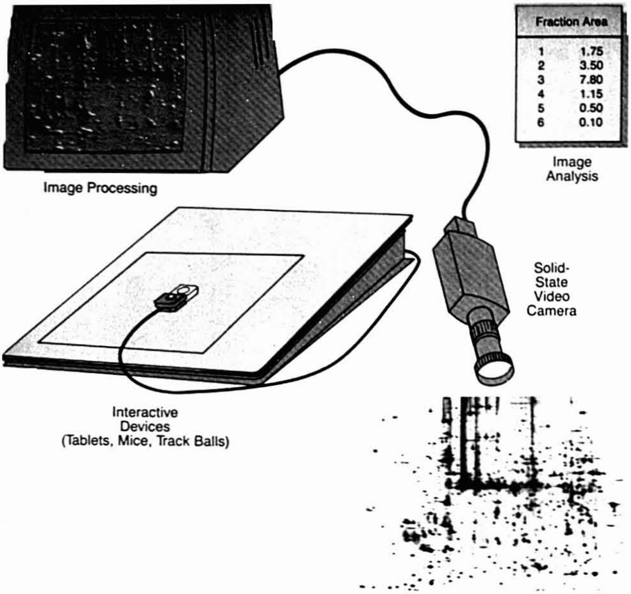
Image Processing
Fraction Area
1 1.75
2 3.50
3 7.80
4 1.15
5 0.50
6 0.10
Image Analysis
Solid-State Video Camera
Interactive Devices (Tablets, Mice, Track Balls)

Figure 9. Image processing and analysis of a 2-D electrophoresis gel

Photographs courtesy of N. Leigh Anderson, Molecular Anatomy Program, Argonne National Laboratory, Argonne, Ill.

graphics memory capable of storing many such frames. Imagine that many such frames can be stored in a virtual manner so that a prospective user need only specify a size, coordinate system, origin, and name. A small window of a frame can be viewed by specifying name, size of window, and origin. Several windows may be viewed simultaneously by "splitting" the screen, or frame windows can overlay one another. Screens can be manipulated algebraically or in a Boolean fashion.

Successive images of the same object can be added together, and the result normalized, yielding a less noisy image. This is similar to ensemble averaging. A region of interest can be brought into our display and viewed. By panning left/right or up/down the desired area can be found. To zoom in on this area, take a section and move the adjacent pixel values into even-numbered positions, and then replicate each value into the adjacent odd position. Unfortunately, the result is a jagged image. To correct this, take the entire filled frame and replicate it; then move it horizontally one pixel position; replicate the original and move it vertically one pixel position; then again diagonally. Add them together, and divide by four (Figure 10a). The

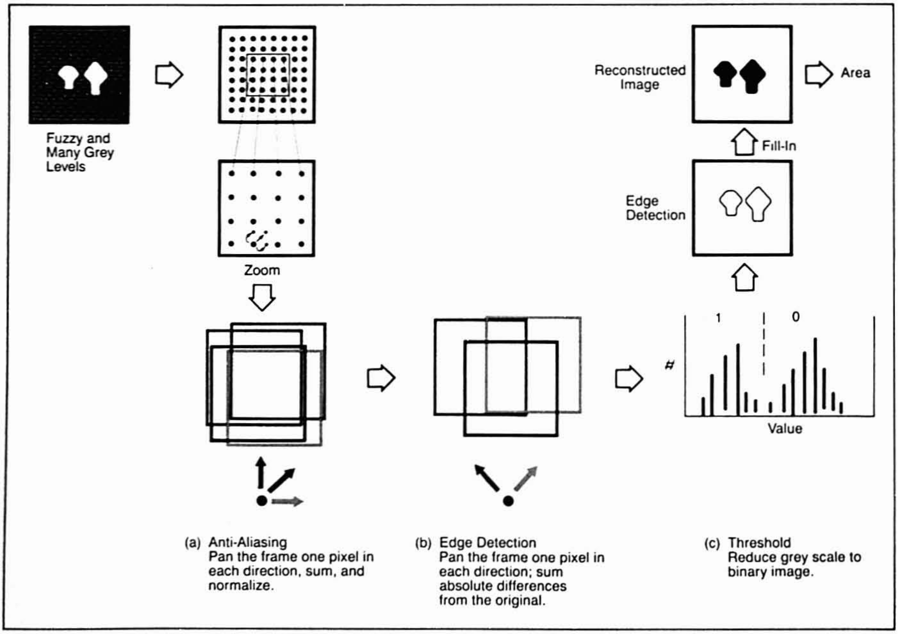
Fuzzy and Many Grey Levels
Zoom
Reconstructed Image
Area
Fill-In
Edge Detection
1
0
#
Value

(a) Anti-Aliasing
Pan the frame one pixel in each direction, sum, and normalize.

(b) Edge Detection
Pan the frame one pixel in each direction; sum absolute differences from the original.

(c) Threshold
Reduce grey scale to binary image.

Figure 10. Zoom, smooth, edge detection, and area operations in image processing/image analysis

Shimadzu. Two short cuts to expedient quantitative TLC

Both are data-processor equipped

1 CS-930 Dual-Wavelength TLC Scanner

The Shimadzu CS-930 Dual-Wavelength TLC Scanner is a refined microcomputerized version of the Shimadzu CS-910 Dual-Wavelength Scanner, a winner of the 1977 I-R Competition. The CS-930 with parallel line printer is a low cost complete microprocessor controlled system for quantitative, highly sensitive, high-speed densitometry.

The features are outstanding:

- **Dual-wavelength method** eliminates baseline drifts caused by local irregularities of layer thickness.
- **Zigzag scanning method with a very small light beam** eliminates errors caused by irregular shape of developed spots.
- **Working curve linearization** according to the Kubelka-Munk's equations.

Built-in microprocessor provides:

- **Signal averaging-smoothing** permits the quantitation of nanogram quantity level.
- **Automatic lane changing** up to 30 lanes of chromatogram spots.
- **Automatic detection of chromatogram spots.**
- **Quantitative calculation** with the external or internal standard method. The concentration values are directly printed out.
- Storage of operational parameters.

CIRCLE 165 ON READER SERVICE CARD

2 CS-920 High-Speed TLC Scanner

The first instrument to make direct quantitation of TLC spots available, Shimadzu's CS-920 High-Speed TLC Scanner has a built-in integrator,printer and other technical refinements to ensure excellent quantitative analysis. Many valuable features:

- **The automatic lane changing mechanism permits rapid analysis of a large number of samples.** Up to seven samples a minute can be scanned.
- **The built-in microprocessor provides automatic detection of chromatogram spots.** Fused spots are separated and determined automatically.
- **Unique high-speed zigzag scanning, working curve linearization, background correction, and reflection absorption ensure concentration-linear output.** Thus excellent quantitativeness is provided.
- Quantitative calculation with either the external or internal standard method.
- **Direct printout of concentration values.**

CIRCLE 166 ON READER SERVICE CARD

Shimadzu delivers densitometers equipped for new dimensions in quantitative TLC. Write today for more information on these and other Shimadzu instruments.

Shimadzu

SHIMADZU SCIENTIFIC INSTRUMENTS, INC. 7102 Riverwood Drive,
Columbia, Maryland 21046, U.S.A. Phone: (301) 997-1227
SHIMADZU (EUROPA) GMBH Acker Strasse 111, 4000 Düsseldorf,
F.R. Germany. Phone: (0211) 666371 Telex: 08586839
SHIMADZU CORPORATION INTERNATIONAL MARKETING DIV.
Shinjuku-Mitsui Building, 1-1, Nishishinjuku 2-chome, Shinjuku-ku,
Tokyo 160, Japan. Phone: Tokyo 03-346-5641 Telex: 0232-3291 SHMDT J.

ISCO's new well sampler: 1.75" small, 2 gal/min big.

ISCO's new Model 2600 Well Sampler features a flow rate sufficient to bail four to five casing volumes prior to sampling wells with up to 150-foot head in a minimum amount of time. This sampler is ideal for sampling test wells for groundwater contamination. Besides its high flow rate, the sampler's submersible, gas-operated pump:

- alleviates sample contamination
- is lightweight
- is simple to use

A tank of compressed gas or a portable air compressor is used to operate the sampler. Rapid inflation and deflation of the pump's elastic silicone rubber bladder efficiently displaces water through check valves at flow rates up to 2 gal/min. Gas does not contact the sample, eliminating the major objection to other types of gas-operated pumps.

The control box monitors the direction and velocity of gas flow, compensating for varying gas supply pressure, pumping head, and sample line length.

For more information, contact your local ISCO representative, write ISCO, or dial toll-free (800) 228-4373.

® DuPont

ISCO
P.O. Box 82531
Lincoln, NE 68501
[800] 228-4373

CIRCLE 105 ON READER SERVICE CARD

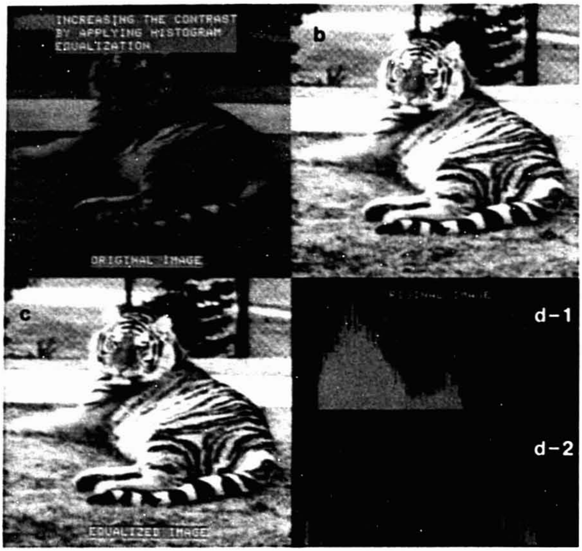

Figure 11. Image processing

(a) Original image; (b,c) improved contrast images derived by expanding the pixel histogram as shown in d; (d-1) pixel histogram of a; (d-2) pixel histogram of b,c. Courtesy of Lexidata, Billerica, Mass.

result is a perfect zoom. The process is sometimes called anti-aliasing because it tends to remove the granularity of digital video displays. Some displays have anti-aliasing hardware.

How is the area of an enclosed space determined? The original must be replicated and the origin shifted one pixel position in both the x and y direction into the first quadrant; subtract the two images. Repeat this by a motion into the fourth quadrant. Sum the absolute values of the difference arrays. This Robert's cross gives information as to the location of edges in the image (Figure 10b). Then a histogram plot of pixel values is made. This plots the number of pixels having a common value. Often this is bimodal and allows the image to be "thresholded" into a black-white binary image (Figure 10c). Now duplicate this binary image and move it in four directions (left, diagonally left, up, diagonally right) applying Boolean operations (ANDing and ORing) between the intermediate images. This directional filter yields a final image that is a clean representation of the edges of the object. The area within the edge can now be easily established.

The pixel values within an image can be multiplied or divided by a constant to change the contrast of the image. Addition or subtraction of a constant can change the brightness (Figure 11). In cases of nonuniform lighting a "blank" can be taken and this image used to correct a subsequent image so that it has a uniform background. This involves multiplying images. Much of this can be performed in real time with inexpensive hardware. Plug-in cards for several standard buses are available, providing image-processing capabilities in microcomputer packages. The price of fully implemented work stations is also dropping.

Interactive Graphics

And now the action of the *son et lumière* begins. Simple graphic tools allow the user to move the cursor about the screen with function keys (up, down, right, and left). More human-oriented interactive techniques are available. These allow rapid manipulation and choice of objects on the screen.

Light Pens. As the light beam rasters across the surface of the CRT a photocell held in front of the tube experiences a change of light intensity as the beam passes in front of it. This can be used to activate circuitry that records the x,y position of the beam at that moment. What does this allow us to do? The cursor can be moved to this new position. A vector can be drawn from a previously selected point to the new position. A segment of a line can be picked up and stretched or bent. Or the computer can be instructed to select the operation displayed on the CRT screen in the area of the beam. This is interactive graphics with a light pen.

Touch Screens. With a matrix of light-emitting diodes (LEDs) and photodetectors arranged around the screen periphery, a finger can block one horizontal and one vertical beam, establishing the x,y position. This touch screen can be used like the light pen. The same effect can be created with a transparent electrical conducting sheet placed in front of the CRT screen. This sheet is a resistive element that can serve as a voltage divider for an imposed potential. A second transparent conducting screen is supported one mil in front of the first. When a finger depresses this it "taps" the voltage divider like a potentiometer wiper. The potential gradient is rapidly applied, first in the x, then in the y direction. ADCs are used to produce x,y coordinates.

Tablets. Off-screen devices can be used for digitizing spectra or drawing pictures and letters, as well as manipulating the cursor and choosing screen images. A tablet consists of a grid system of horizontal and vertical wires embedded in a plastic body. A detector coil is placed above the grid. All of the columns are successively pulsed with an ac signal source. Then all of the rows are sequentially pulsed. The detector coil will produce pulses that can be time correlated with particular transmitting wires, providing x,y coordinate data.

Mice and Track Balls. Imagine a reflective sheet with a grid of finely spaced horizontal and vertical nonreflective lines. The detector assembly consists of an LED and a four-quadrant photodetector. The light from the LED is bounced off the surface of the grid and strikes the four-quadrant assembly. As the detector is moved across the surface the photodetector pairs pulse on and off, providing a pulse for every line crossed and directional information. The x,y pulse strings are used to interact with the display. This is an optical mouse.

An electrical mouse has two orthogonal shafts and two idler shafts that form a nest for a ball. As the ball is pressed against a friction surface it turns in the nest, causing the active shafts to rotate. As these revolve they generate pulse trains proportional to the ball's rotational component along the Cartesian coordinates, as well as directional information. If such a device is turned over, so that the ball is seen nestling in the shaft cradle, we have a track ball. These are manipulated with the palm of the hand.

Joysticks. These devices have a vertical shaft gimble connected to two orthogonally mounted potentiometers. The wipers of the potentiometer indicate an x,y displacement. ADCs are used to convert the analog potentials to digital numbers for coordinate purposes. Alternatively, binary up–down counters and DACs may be used to null the potential, providing a type of digital servo. Coordinate position is read directly from the counters.

All of these devices have one or more push buttons or capacitively coupled switches that signal the computer to read the x,y position and/or take other actions.

Selection of an interactive device should involve careful consideration of the accuracy, reproducibility, and resolution of the system, particularly if digitization from hard copy or drawing is the goal. A resolution of 1 to 5 mil is quoted for tablets, with accuracies of 10 to 25 mil. Reproducibility is seldom specified. For screen-located selection devices, the distances are much larger.

Next month's A/C INTERFACE will describe typical laboratory examples of these interactive techniques.

The Analytical Approach

Jeanette G. Grasselli, *Editor*

Brings together 52 papers from *The Analytical Approach* column in ANALYTICAL CHEMISTRY. Provides unique approaches to analytical science and focuses on real-world problems. Discusses topical and interesting subjects such as the analysis of the JFK assassination bullets, Mt. St. Helens ash, flavor changes in food, and failure mechanisms in spacecraft parts. Written in a "popular" style yet is highly informative. Will serve as a teaching aid in higher education or as a guide in corporate training programs on analytical capabilities.

CONTENTS

Sections include:

- Production Processes
- Products
- Environmental
- Toxicity
- Forensic
- Miscellaneous

240 pages (1983) Clothbound
LC 82-22618 ISBN 0-8412-0753-4
US & Canada **$29.95** Export **$35.95**
A paperbound student edition is available in bulk quantity. For price and ordering information, call toll free 800-424-6747.

Order from:
American Chemical Society
Distribution Office — 50
1155 Sixteenth St., N.W.
Washington, DC 20036
or CALL TOLL FREE 800-424-6747
and use your credit card.

SCIENTIFIC WRITING FOR GRADUATE STUDENTS

This manual is a "must" for those who would introduce courses of instruction in scientific writing into university graduate schools. The first nine chapters provide the essentials for "Writing a Journal Article," and the remaining five chapters cover "Related Topics" in scientific communication.

CONTENTS: 1. Clearing Away the Underbrush • 2. The Ground Plan • 3. The Master Plan • 4. The First Draft • 5. The First Revision: Structural Alterations • 6. Further Revision: Polishing the Style • 7. Editing Assignments • 8. The Final Steps • 9. Responding to the Editor • 10. Design of Tables and Figures • 11. Preparation for Writing the Doctoral Thesis • 12. Writing a Research Project Proposal • 13. Oral Presentation of a Scientific Paper • 14. Principles and Practices in Searching the Scientific Literature

Paperbound; ISBN: 0-914340-01-8; Published 1968, reprinted 1983; Trim size: 6 × 9 inches; 190 pages

Regular Price: $9.75 (10% discount on 10 or more copies delivered to one address)
CBE Member Discount Price: $8.75 (single copy paid by personal check)

Terms of Sale: All sales final; no returns.
Prepayment required; U.S. currency drawn on a U.S. bank.
Price includes BOOK RATE postage.
For faster delivery--first class, air mail, or UPS available at additional charge (book weight, 11.5 oz).
Maryland residents, please add 5% sales tax.

COUNCIL OF BIOLOGY EDITORS, INC.
9650 Rockville Pike, Bethesda, MD 20814

Three Good Reasons for Checking With the Number Two Company in Ion Chromatography

WESCAN

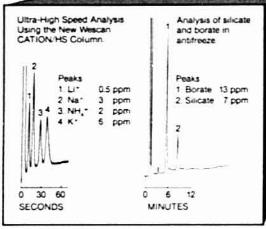

FLEXIBILITY...
In applications.

We pioneered the Single Column Ion Chromatography technology that has been applied to the analysis of over 125 ions in virtually any imaginable matrix.

FLEXIBILITY...
In hardware.

Whether you need an upgrade to existing equipment, a simple manual system, or full dual channel automation, our systems and components provide you with the ion analysis capability you NEED at a price you can AFFORD. And, our Ion Analyzers are fully compatible with standard HPLC hardware!

FLEXIBILITY...
In technical support.

Because we are a small company, we can respond to YOUR needs, not to OUR ego. The result? You get a solution tailored to your analytical problem, not a standard package.

THE BOTTOM LINE: We can help you analyze for virtually any ionic species:
☐ Anions ☐ Cations ☐ Organic Acids ☐ Surfactants ☐ Metals
With sensitivity down to the parts-per-billion level, and analysis times measured in seconds.
Want to find out how WE can help YOU save time, effort, and money in ion analysis?
Just contact the Wescan Applications Group.

WESCAN *we are something special*

WESCAN INSTRUMENTS, INC.
3018 Scott Blvd., Santa Clara, CA 95050
(408) 727-3519, TELEX 171627 ATTN: WESCAN

CIRCLE 235 ON READER SERVICE CARD

Books

Selected Topics in Trace Analysis by HPLC

Trace Analysis. Vol. 2. James Lawrence, Ed. xi + 275 pp. Academic Press, 111 Fifth Ave., New York, N.Y. 10003. 1982. $35

Reviewed by Stephen Wise, National Bureau of Standards, Center for Analytical Chemistry, Bldg. 222, Room A-113, Washington, D.C. 20234

This is the second in a proposed multivolume series devoted to "state-of-the-art critical discussions of selected topics in organic and inorganic chemistry. These include detection, identification, and quantitation of trace quantities of substances in a large variety of sample materials."

> *. . . each contribution is generally a detailed, up-to-date review of the particular topic . . .*

This volume contains selected topics in the use of high-performance liquid chromatography (HPLC) in trace analysis. Since Vol. 1 also focused on HPLC topics, these two volumes together "provide the reader with a great deal of information that will be extremely helpful for the development of trace analytical methodology by high-performance liquid chromatography." Vol. 2 consists of five individual contributions that discuss the following areas: trace analysis of vitamins by HPLC, liquid chromatography-mass spectrometry (LC/MS), size exclusion chromatography in trace analysis, trace enrichment techniques, and use of unmodified silica for LC analysis of polar substances. As in Vol. 1, each contribution is generally a detailed, up-to-date review of the particular topic (ranging from 30 to 70 pages).

The first contribution provides a comprehensive review (over 260 references) of the application of HPLC to the measurement of vitamins in foods and tissues. This chapter is similar in format to the excellent contribution in Vol. 1 on the LC analysis of mycotoxins. It is divided into two categories of vitamins—fat soluble and water soluble—with individual sections for each vitamin of interest (e.g., vitamins A, D, E, K, B_6, and B_{12}). Each section provides background information on the particular vitamin and then reviews the methods of analysis. In the introduction to this chapter, the author points out that many of the methods described in the literature will not survive the "era of rapid change that is upon us," particularly in LC analysis, but that the information in the literature should be used only as the basis for the development of better and more convenient methods. The author has succeeded in providing an excellent summary of the existing literature with additional comments from his own experience to support particular advantages or disadvantages of a method.

The second contribution, entitled "Combining Liquid Chromatography with Mass Spectrometry," focuses on the mechanics of the various approaches employed in using a mass spectrometer as an LC detector. Diagrams illustrating the design of each interface type are provided, and the advantages and disadvantages of each interface type are discussed. The discussion of applications of LC/MS is limited to an extensive table summarizing sample type, LC/MS mode, and literature references.

In the third chapter, "Applications of Steric Exclusion Chromatography (SEC) in Trace Analysis," the authors' purpose was to demonstrate that SEC (traditionally used for the determination of polymer molecular weight distributions and polymer additives) can lend itself to trace analysis. After a brief description of the basics of SEC, the authors present advantages and disadvantages of the technique followed by the various approaches to using SEC in trace analysis. A variety of recent applications are described, including a number of chromatograms, to illustrate this technique. The final section in this chapter ("Problems and Trouble-Shooting") provides useful practical experience in the use of SEC and describes typical problems that may be encountered.

"Trace-Enrichment Techniques for Organic Analysis" reviews three areas of applications of trace enrichment—environmental, clinical, and pharmacological—with the majority of the discussion focused on environmental applications. In the discussion of these applications, the author has often provided excessive details relating to the procedure (e.g., column length, mobile-phase composition, flow rate, injection volume, etc.), but he provides little comment on reasons for certain experimental conditions, advantages, or problems.

The final chapter, "HPLC Analysis of Polar Substances on Unmodified Silica," has a somewhat different format and content than the other contributions in this or the previous volume. In this chapter, the authors briefly review the literature concerning the use of mobile-phase additives in liquid-solid chromatography (LSC); this is followed by three sections of original work by the authors on carboxylic acid and amine additives in LSC. These three sections are presented as one would expect to see a journal research paper, with an experimental section followed by results and discussion. The experimental section describes the apparatus (including commercial names), materials, and procedures in great detail. The results of this research are of interest; however, they should be published as a research paper (with peer review). In my opinion, they are out of place in a volume such as this.

Column Selection in Gas Chromatography. Harold McNair. 4.2 hours playing time, 140-page manual. ACS Audio Courses, Suite 809-D, 1155 16th St., N.W., Washington, D.C. 20036. 1982. $265

Reviewed by Harry Gearhart, Conoco, P.O. Box 1267, Ponca City, Okla. 74603

This ACS audio course is a comprehensive but concise, practical treatment of selection criteria for choosing the proper GC system to perform a given separation. The title of the

FOR THE FIRST TIME—
American Chemical Society offers one catalog covering all Continuing Education Services!

The 1984 ACS Catalog of professional development courses for chemists and chemical engineers

Multi-media methods include:
Audiocassette Courses
Computer Courses
Video Courses
Short Courses
In-House Courses
Audio-Teleconference Courses
And a Textbook Course on Modern Chemical Technology

This new 60-page catalog will give you all the information you need to select the topics you are interested in, and to choose the learning methods that suit your needs and budget best.

To receive your copy, write, use the coupon, or call 202-872-4588 —you will find our new catalog bigger, better and more informative than ever!

American Chemical Society
1155 Sixteenth Street, N.W.
Washington, DC 20036

Yes—please send me a copy of the new ACS combined courses catalog as soon as possible!

Name ______

Title ______

Organization ______

Address ______

City ______ State ______ ZIP ______

course may lead some to believe that the subject material might be limited to measurement and comparison of retention indexes. In fact, the scope of the course is quite broad, covering measurement of various types of column performance, characteristics and selection of the proper liquid phase and solid support, criteria for choosing porous polymers and adsorbents, use and characteristics of special column types, including capillary columns, and consideration of column and instrument operating parameters (e.g., carrier gas, flow rate, temperature, length, diameter, and liquid loading).

McNair very effectively highlights the course presentation by interjecting personal insights and relevant examples from his substantial career experience in the field of gas chromatography. Short problem sets are presented at the end of each section. However, "correct" answers to a number of the problems require more information and background than are presented in the course. An obvious deficiency in the course material is inadequate editing. There are numerous typographical errors, and a list of cited references was omitted from one section. Dubbing or editing the audio portion when appropriate would have provided a better delivery.

Overall, however, this is a very good audio course for practicing gas chromatographers. It should be beneficial in training or updating operators in a wide variety of settings, including industrial, contract analysis, and biomedical laboratories.

Books Received

Solid Phase Biochemistry—Analytical and Synthetic Aspects. William Scouten, Ed. xiv + 779 pp. John Wiley & Sons, Inc., 605 Third Ave., New York, N.Y. 10016. 1983. $75

Instrumentation of Environmental Monitoring. Vol. 1. 2nd ed. Robert Budnitz et al. xix + 1130 pp. John Wiley & Sons, Inc., 605 Third Ave., New York, N.Y. 10016. 1983. $150

Industrial Applications of Surface Analysis. Lawrence Casper, Cedric Powell, Eds. 438 pp. American Chemical Society, 1155 16th St., N.W., Washington, D.C. 20036. 1982. $56.95

The Technobyte Microcomputer Program Compendium for Chemical Engineering and Chemistry. Hal Abbott, Richard Bigda. ii + 149 pp. RJB & Associates, 6216 South Lewis Ave., Tulsa, Okla. 74136. 1983. $42

ENVIRONMENTAL SCIENCE & TECHNOLOGY
ES&T

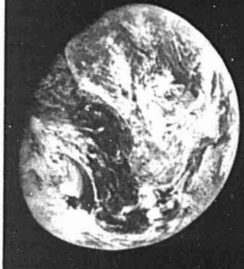

The premiere research publication in the environmental field.

Environmental science continues to be one of the fastest growing fields. And ES&T has grown right along with it!

ES&T continues to give you the practical, hard facts you need on this science . . . covering research, techniques, feasibility, products and services.

Essential reading for environmental scientists both in the business and academic world . . . ES&T has increased its emphasis on peer-reviewed research dealing with water, air, and waste chemistry in addition to adding critical reviews of important environmental science issues—all relevant to understanding the management of our natural environment.

Also included are discussions on environmental analyses, governmental regulations, current environmental lab activities, and much more!

For rate information, and to subscribe, call toll free:
(800) 424-6747

The VISTA 402 LC/GC Data System handles all these samples fully automatically.

And it's still only loafing.

peptide hormones in mouse brain
halocarbons in drinking water
fragrances in perfume
hydrocarbons in burned wood
preservatives in skin cream
vitamins in vitamin tablet
diazepam in plasma
phenols in shale oil
LC automation-assisted methods development
GC automation-assisted methods development
pesticides in soil
caffeine and theobromine in chocolate

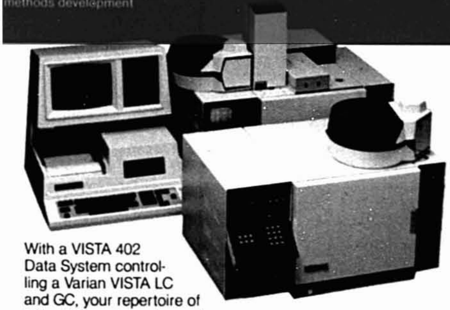

With a VISTA 402 Data System controlling a Varian VISTA LC and GC, your repertoire of LC or GC analyses is nearly unlimited. Using the unique intelligence of a single VISTA 402, all the samples shown can be analyzed using a VISTA LC and GC. And you can instruct the system to orchestrate this impressive array of analyses in your absence.

VISTA 402-initiated LC and GC automation is much more than just repetitive injections, more than merely adding an autosampling device. The key is our concept of "user emulation," an approach that strives to simulate the actions you would perform if you were running the system manually.

A VISTA system will choose chromatography/data handling parameters based on the identity of the sample. It will perform a prep run for equilibration, control all GC and/or LC parameters, check on resolution, and optimize data processing.

It will "look" at the peaks as they are eluted and control signal/noise, tangent skim, horizontal or valley baselines, and other data handling parameters. It will perform all result calculations—calibrations and analyses, area or height calculation, auto calibration, and check for instrument, resolution, and calibration errors.

The VISTA system will plot the chromatogram with or without baselines and print the results, including relative retention time, peak widths at half height, and a run log and error logs. Data and results storage are automatic, of course!

In a nutshell: A VISTA 402-controlled LC or GC emulates all your actions and decisions as closely as non-humanly possible. That's what we mean by user emulation!

And here's the best part: the VISTA LC/GC shown above is only working at half its capacity! The 4-channel VISTA 402 can still handle two more LCs or GCs with autosamplers, plus data system options—which means you can double your laboratory's throughput whenever the time is right.

To learn more about the unique intelligence and expandability of the VISTA system, circle Reader Service Number 218; circle No. 219 to have a Varian rep convince you.

For assistance contact: • Florham Park, NJ (201) 822-3700 • Park Ridge, IL (312) 825-7772 • Sugar Land, TX (713) 491-7330 • Georgetown, Ontario (416) 457-4130. Or write 611 Hansen Way, Palo Alto, CA 94303. In Europe: Steinhauserstrasse, CH-6300 Zug, Switzerland.

See us at the
Pittsburgh Conference
in Atlantic City, March 5-9!

varian

Intelligent Chromatography . . . from Varian

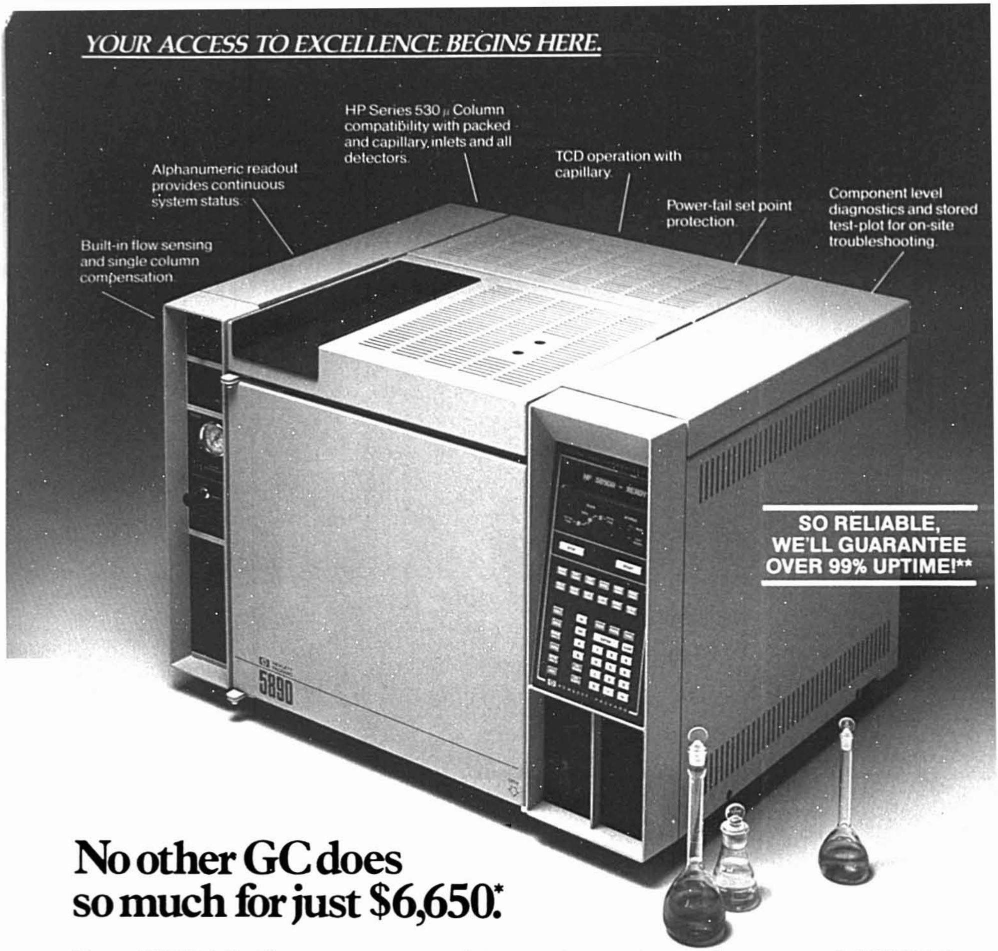

YOUR ACCESS TO EXCELLENCE BEGINS HERE.
HP Series 530 μ Column compatibility with packed and capillary, inlets and all detectors.
Alphanumeric readout provides continuous system status.
TCD operation with capillary.
Power-fail set point protection.
Component level diagnostics and stored test-plot for on-site troubleshooting.
Built-in flow sensing and single column compensation.
SO RELIABLE, WE'LL GUARANTEE OVER 99% UPTIME!**
5890

No other GC does so much for just $6,650.*

The new HP 5890A Gas Chromatograph combines an exceptional price with the exceptional performance and productivity you need to meet today's laboratory demands.

Consider this: the 5890A offers you the choice of split/splitless, split-only, and on-column capillary inlets, as well as a universal packed injection port. It lets you choose from a range of rugged detectors including FID, NPD, TCD and ECD. And, to complete the system, optional communications capabilities permit networking to the HP 3392A Integrator for method storage and print-out or incorporation in a full HP laboratory automation system.

The 5890A has also been designed to be extremely user-friendly, bringing a new level of convenience and simplicity to the entire analysis procedure.

Your ongoing cost of ownership stays low too. The many innovations and design improvements incorporated into the 5890A make it the most reliable GC HP has ever built, with a parts count that has been reduced by a factor of three. (A case in point: the entire keyboard uses only two parts!)

In every respect, the HP 5890A Gas Chromatograph is designed to be your laboratory's next benchtop standard. To get the complete story on this exceptional value, call your local HP office listed in the telephone directory white pages and ask for the Analytical representative. Or, write: Hewlett-Packard, Analytical Group, 1820 Embarcadero Rd., Palo Alto, CA 94303.

*U.S. domestic price only, single FID packed column, temperature-programmable configuration.
**Customers may purchase a Guaranteed Uptime Maintenance agreement. If an instrument fails to meet the guarantee, the agreement will be extended at no charge.

AG 04312

HEWLETT PACKARD

Circle #96 for literature. Circle #97—have and H-P representative contact us.

Hank Wohltjen
Naval Research Laboratory
Surface Chemistry Branch
Code 6170
Washington, D.C. 20375

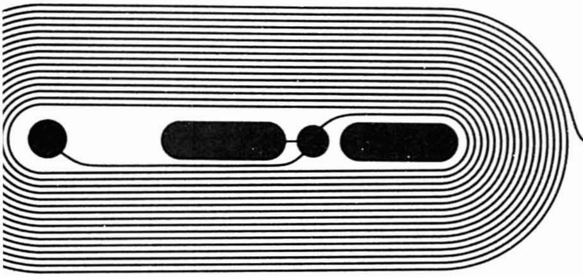

Chemical Microsensors and Microinstrumentation

Progress in analytical chemistry has often been led by progress in instrumentation. In recent times analytical instrumentation has undergone a metamorphosis as a result of extraordinary advances in microelectronics. The advent of inexpensive computing power has dramatically changed the way experiments are controlled and data are acquired, manipulated, displayed, and stored. In many respects a tremendous gap has developed between the size, cost, and performance of modern microcomputers and the corresponding size, cost, and performance of the instruments they control. The size and cost of microcomputers have dropped precipitously while performance has soared. The same cannot be said for the measurement instrumentation. This article will describe several approaches aimed at closing the technology gap between instruments and computers. Perhaps it is not surprising that the most promising approach for reducing the gap derives from the same technology used in the microelectronics industry, namely, microfabrication and microlithography.

Microsensors and microinstrumentation are relative newcomers to the analytical scene. Virtually unheard of a decade ago, microsensor research has grown steadily, driven perhaps by the tantalizing array of opportunities afforded by small low-cost sensors. Such areas as clinical chemistry, environmental monitoring, process control, and automobile emission control are all heavily dependent on sensor technology. If pocket calculators can be made small and inexpensive, it is exciting to think of the possibilities of a comparably sized sensor system. Suddenly it becomes feasible to measure things that have not previously been routinely measured. Thus, the cost of information can be reduced, and knowledge can increase at a quicker pace.

All of the devices described in this article have one thing in common—they are fabricated, at least partially, using microlithographic techniques. Thus, a chemical microsensor is broadly defined as a microfabricated device that provides a reproducible electronic output signal when exposed to a chemical stimulus. Work being conducted on small electrodes (e.g., coated wires [*1*] or carbon fibers [*2*]) or optical fiber sensors will not be considered here since they are not microfabricated. A chemical microinstrument is defined in a similarly broad fashion, as a small, chemically sensitive system whose components can be microfabricated.

Since microlithography is the key to understanding present and future microsensor approaches, it is appropriate to quickly review some of the fundamental concepts in microfabrication technology.

Lithography

The technique of lithography (which means, literally, writing on stone) was first developed over 100 years ago by the graphic arts industry. In recent times, the microelectronics industry has refined the technology nearly to the physical limits of perfection. Transistors and integrated circuits consist of layers of patterned thin films of metals, dielectrics, and semiconductors on a substrate, usually silicon (*3*). The patterns are defined in the thin film by a process shown in Figure 1. A radiation-sensitive *resist* layer (usually a sensitized organic polymer) is coated on top of the thin film to be patterned. Radiation, in the form of visible, UV, or X-ray photons, electron beams (E-beams), or ion beams, is permitted to strike the resist wherever a thin-film pattern is (or is not) desired. After this "mask" expo-

This article not subject to U.S. Copyright
Published 1983 American Chemical Society

sure, the resist is developed in an appropriate solvent that leaves some areas of the thin film still protected with resist and other areas bare. A positive resist becomes more soluble after irradiation, and exposed areas are rinsed away in the developing step. Negative resists become insoluble in the areas of exposure. The areas of the thin film that are not protected by resist can then be etched away (e.g., in acid solution or a reactive plasma) to yield the desired pattern. Processing of additional levels by evaporation of new thin films etc. can be conducted after the resist layer is stripped away with a solvent.

The sizes of patterns that can be defined using lithographic techniques are breathtakingly small. Optical mask exposure can mass produce devices having 2-μm geometries. Today's X-ray and E-beam lithography systems routinely produce patterns with 0.5-μm geometries. Laboratory researchers have successfully patterned structures (using E-beam techniques) having 0.005-μm (50 Å!) feature sizes. It is important to note that at these size scales many macroscopically important physical phenomena (e.g., gravity) become irrelevant and other phenomena (e.g., surface diffusion) become increasingly significant (4). Besides small feature sizes, microlithography also yields exquisite precision and dimensional control. This permits enormous numbers of patterns to be replicated with incredibly small batch-to-batch variations in pattern size.

The microlithographic method is applicable to a very wide range of situations and materials. Several very general observations can be made about the present technology. Most microlithography is conducted on optically smooth substrate surfaces, deposited films of metals, or insulators with thicknesses less than about 1 μm. Etched grooves most often have aspect ratios less than 2:1 (i.e., the depth of the groove is seldom greater than two times as large as the width of the groove). Thus, the overwhelming feature of microfabricated structures is that they are planar since the lithographic images are two-dimensional, and vertical topography is only achieved slowly as more and more layers of thin films are added. Higher aspect ratio structures are rapidly emerging as progress is made in X-ray lithography, multilayer resists, and anisotropic etching techniques, but for the near future, the landscape of most conventionally microfabricated structures will have a rather flat appearance. These realities inspire microsensor enthusiasts to think small and to think in two dimensions rather than three.

Clearly there is enormous potential for using microlithography to produce structures and devices that are useful for many applications beyond microelectronics (5). For analytical chemistry, microlithography has been employed to make not only sensors and detectors but also other common instrument components such as valves and capillary tubes. It is obvious that this is only the beginning. As chemists become more aware of microfabrication methods, it is likely that many other parts of common instruments will be microfabricated and new techniques, not practical with macroscopic systems, will appear.

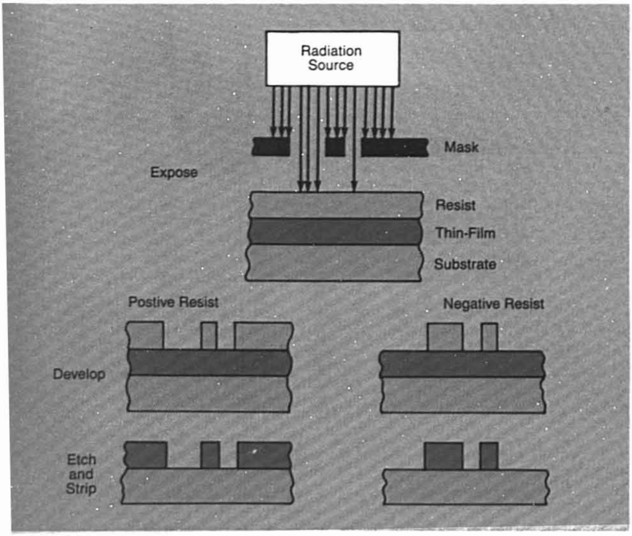

Figure 1. Typical lithographic processing steps
Positive resists become more soluble upon irradiation. Negative resists become less soluble

Present Microsensor Technologies

Clearly, microfabrication offers some very attractive advantages for making small, rugged, and inexpensive sensors. The primary obstacle to using it more extensively is the constraint that the devices be planar. This forces designers to think about analytical problems from a smaller and flatter perspective and to consider physical–chemical interactions that might be considered unimportant in the macroscopic world. Chemical microsensor research is therefore a multidisciplinary endeavor requiring a synergistic combination of chemistry, physics, materials science, and electrical engineering.

All chemical microsensor devices fall into two categories. The first category consists of devices that sense chemical species whose presence modulates the transport of electronic charge in the device. Examples of microsensors in this category include CHEMFETs, ion-controlled diodes, Schottky diodes, thin-film tin oxide gas sensors, chemiresistors and microdielectrometers. The second category consists of all microsensor devices that do not fit into the first category. These devices, which are based on a number of unique techniques, include surface acoustic wave devices, potentiometric gas sensors, and pyroelectric enthalpimetric sensors.

In their most general form, all chemical microsensors consist of at least two elements: a microfabricated

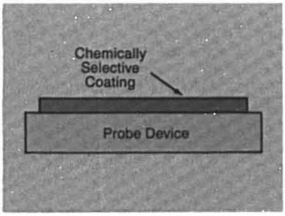

Figure 2. Chemical microsensors typically involve a microfabricated electronic probe device in contact with a chemically selective coating whose properties are altered by the species to be detected

Microbore sample injection poses new problems in HPLC.

And Rheodyne solves them.

People using microbore columns want to inject miniscule samples–typically only a fraction of a microliter.

It's not easy to form a sample that small with high precision. And it's even harder to convey it to the column with low dispersion.

Rheodyne solved these problems with the micro sample injection valve pictured below. The sample holding chamber is a tiny hole bored through the valve's rotor. You load the sample through a built-in needle port–that's the easy way–then turn the valve to inject a precisely repeatable sample of 0.2, 0.5 or 1.0μL. You change sample size by changing the rotor, a simple 3-minute task.

To minimize dispersion Rheodyne formed a flow passage to the column only 0.13 mm (0.005 inch) in diameter. Incredibly small!

For the whole story on the Model 7520 injector, contact Rheodyne, Inc., P.O. Box 996, Cotati, California 94928, U.S.A. Phone (707) 664-9050.

LOAD
RHEODYNE

RHEODYNE
THE LC CONNECTION COMPANY
CIRCLE 185 ON READER SERVICE CARD

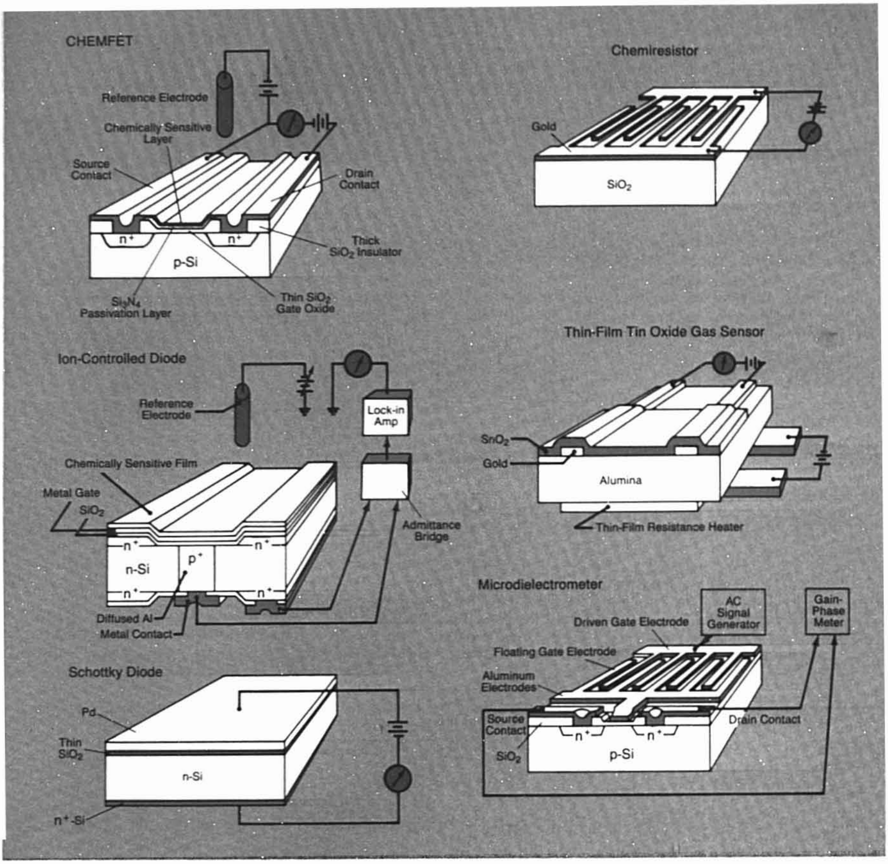
CHEMFET
Reference Electrode
Chemically Sensitive Layer
Source Contact
Drain Contact
n^+
n^+
p-Si
Thick SiO_2 Insulator
Si_3N_4 Passivation Layer
Thin SiO_2 Gate Oxide
Chemiresistor
Gold
SiO_2
Thin-Film Tin Oxide Gas Sensor
SnO_2
Gold
Alumina
Thin-Film Resistance Heater
Ion-Controlled Diode
Reference Electrode
Lock-in Amp
Chemically Sensitive Film
Metal Gate
SiO_2
n^+
n^+
n-Si
p^+
n^+
n^+
Admittance Bridge
Diffused Al
Metal Contact
Microdielectrometer
AC Signal Generator
Gain-Phase Meter
Driven Gate Electrode
Floating Gate Electrode
Aluminum Electrodes
Source Contact
Drain Contact
n^+
n^+
SiO_2
p-Si
Schottky Diode
Pd
Thin SiO_2
n-Si
n^+-Si

Figure 3. Microsensors based on modulation of electron transport through the device by chemical interactions
Conventional silicon electronic device technology is often employed. The p-Si regions consist of Si doped with an electron acceptor. The n-Si regions are doped with an electron donor

physical probe device and a chemically selective coating (Figure 2). The probe device contacts the coating and provides an electrical signal whose characteristics reflect the state of the coating. The coating is in physical contact with the medium in which chemical species are to be detected. Thus, the nature of the coating interaction with the chemical species determines the type of physical transduction mechanism required of the probe. For example, if the dielectric properties of a coating respond strongly to exposure to a particular vapor, then the microdielectrometer is the probe of choice. It is safe to predict that the ultimate performance of chemical microsensors will be determined by the coating chemistry.

CHEMFETs. Probably the best-known chemical microsensor is the CHEMFET illustrated in Figure 3. First reported by Bergveld in 1970 (*6*), the CHEMFET is essentially a conventional insulated-gate field effect transistor that has its metallic gate contact replaced by a chemically sensitive coating and a reference electrode. Excellent reviews of CHEMFET technology can be found in References 7 and 8. In normal operation a current is made to flow by the application of a voltage across the source and drain contacts. Variations in the electric field in the gate region, located between the source and drain, produce corresponding variations in the observed drain current. The CHEMFET can be used in a variety of ways. In solution, the gate region can be coated with an ion-sensitive membrane. Interaction of ions in solution with the membrane results in a change of the interfacial potential and a corresponding alteration of drain current. Numerous cations and anions have been sensed (e.g., H^+, K^+, Ca^{2+}, Cl^-, I^-, and CN^-), and near Nernstian responses are commonly observed. The ion-sensing CHEMFET (or ISFET as it is often called) has advantages in its small size (e.g., less than 1 mm^2 area) and low output impedance, which

The world of XRF will never be the same again.
X-RAYS ON
28
Ni
29
Cu
46
Ag
47
48
Cd
In
78
79
80
81

Announcing the all new SPECTRACE™4000 XRF Analysis System from Tracor Xray.

Energy dispersive x-ray fluorescence (EDXRF) revolutionized elemental analysis. Now, Tracor Xray revolutionizes EDXRF, with the SPECTRACE 4000 — a compact XRF analysis system that puts the power and versatility of EDXRF to work for you with a combination of hardware, software and performance features you won't find on any other system. And it does it all at a price that makes EDXRF a cost effective alternative or complement to other elemental analysis methods.

A simpler world

The SPECTRACE 4000 takes the confusion out of instrumental analysis. It uses menu-driven commands to help you select and set-up the analysis methods best suited to your objectives and provides a comprehensive set of programs ranging from the classical empirical methods to the simplest element identification. And once you've established procedures for your applications, the SPECTRACE 4000 makes it easy, by automatically storing them for future use.

A more flexible world

Use the SPECTRACE 4000 in the laboratory, in the warehouse or on the production line. Its modular design lets you convert the system from a fully programmable, multi-sample, laboratory configuration to a simple push-button, single-sample QC system in minutes. You can even remove the keyboard when all you need is mistake-proof, push-button operation.

A world of new possibilities.

When you're not using the SPECTRACE 4000 for XRF analysis, use it as a general purpose computer. The software operating system is CP/M-86 based, so you can use off-the-shelf programs for word processing and data base management, as well as programming.

Contact Tracor Xray for complete information on the SPECTRACE 4000. We'll show you what's new in the world of XRF.

Tracor Xray
345 East Middlefield Road
Mountain View, CA 94043, USA
(415) 967-0350.

Tracor Xray

CIRCLE 200 ON READER SERVICE CARD

FOR OPTICAL PURITY ANALYSIS AND SEPARATION OF OPTICAL ISOMERS

A Proven HPLC Method...

Developed by Pirkle*, the method is

- **Sensitive**...Only nanograms of sample required
- **Unequivocal**...Trace amounts of one enantiomer determinable in presence of great excess of the other
- **Insightful**...Chiral separations observable even in complex mixtures
- **Preparative**...Up to 100 mg per-pass with 10 mm I.D. column

From A Reliable Column Source...

Regis is a pioneer and leader in developing HPLC columns based on the Pirkle* concept of chiral separation. Regis chiral columns are

- **Efficient**...Average 40 000 plates per meter
- **Versatile**...Separate many classes of aromatic compounds such as alcohols, hydroxyls, sulfoxides, hydantoins, and succinimides
- **Guaranteed**...If, for any reason, you are not satisfied with the performance of your Regis column, simply return it for a full refund

HOW SUPPLIED:
Ionic D-Phenyl Glycine
(Either 25 cm x 4.6 mm I.D. or
25 cm x 10 mm I.D.)

Covalent D-, L-, or D, L-Phenyl
Glycine (Either 25 cm x 4.6 mm I.D.
or 25 cm x 10 mm I.D.)

Ionic L-Leucine (25 cm x 4.6 mm I.D.)

Covalent L-Leucine
(25 cm x 4.6 mm I.D.)

***Dr. W.H. Pirkle, University of Illinois**

Literature available upon request

REGIS
CHEMICAL COMPANY
8210 Austin Avenue
Morton Grove, Illinois 60053 USA
Phone: 1 (312) 967-6000
Telex: 910-223-0808

CIRCLE 183 ON READER SERVICE CARD

make it ideal for in vivo monitoring or analysis of small sample volumes. The small size can also be used to advantage in making multiple-ion sensor arrays. The main technological problem that has prevented wide-scale use of CHEMFETs is related to encapsulation of the device. No traces of moisture or ionic contaminants can be allowed to penetrate beyond the ion-selective coating or instability results. Problems with ion-selective coating adhesion and device encapsulation continue to be studied by numerous groups, and steady progress is being made.

A very sensitive detector for hydrogen can be made if the chemically sensitive coating of the CHEMFET is a thin film of palladium. The Pd-gate CHEMFET was first reported by Lundstrom et al. in 1975 (*9*). Hydrogen can reversibly adsorb into the hot palladium (~150 °C), which causes a shift in the work function difference between the palladium and the silicon of the transistor. The change in work function results in an altered electric field in the transistor's gate region and a corresponding shift in observed drain current. Detection of hydrogen at levels well below 1 ppm is possible. The detection of other gases such as H_2S, NH_3, and CO has also been reported.

In addition to detecting ions in solution and reducing gases, CHEMFETs offer tremendous potential for immunological and enzymatic assays. Janata (7) has conducted several very interesting investigations in this area. While several mechanisms of interaction are possible between the immobilized enzyme or antibody coating and the CHEMFET, interactions that cause a change in interfacial charge density generally provide measurable interactions. The small size of the CHEMFET is particularly attractive if expensive enzymes or antibodies are to be used in a disposable device.

Ion-controlled diodes. The ion-controlled diode (or gate-controlled diode as it is sometimes called) was first described by Zemel in 1975 (*10*). This device is a combination of a p–n junction and a metal oxide semiconductor capacitor in which the junction makes contact with the inversion layer of the capacitor. Like the CHEMFET, the device can be used as an ion sensor by application of a suitable ion-selective coating to the gate surface. Variations in the effective gate voltage resulting from the interaction of solution ions with the membrane produce changes in the properties of the inversion layer. In operation, the ion-controlled diode behaves as a variable distributed RC element, so that changes in the inversion layer can be followed with an admittance bridge. A more detailed discussion of the operating mechanism of this device can be found in Reference 11.

The ion-controlled diode has several interesting features in addition to being small, rugged, and inexpensive. The electrical contacts to this device are on the side opposite the selective coating. This means that encapsulation of the device to protect all but the selective coating from the solution is greatly simplified. Furthermore, the device can be used in a mode whereby the gate voltage is held constant (with respect to the reference electrode) and the driving frequency is varied to keep the inversion layer capacitance constant. In this mode, a digital output signal is obtained. Measurements of potassium and hydrogen ion concentrations with this device have been reported (*11*).

Schottky diodes. A device that has shown considerable sensitivity as a gas sensor is the Schottky diode (Figure 3). In its simplest form a Schottky diode consists of a small area of metal in contact with a semiconductor. This contact exhibits a rectifying behavior and a characteristic nonlinear current–voltage dependence. It has been demonstrated that if the metal used in the Schottky diode is palladium, then a very sensitive detector of hydrogen results. As in the case of the Pd-gate CHEMFET, the mechanism of operation relies on a change in the work function of the metal caused by the adsorption of hydrogen. Gas-sensitive metal–semiconductor Schottky diodes have been made with Pd–TiO_2, Pd–CdS, Pd–ZnO, and PbS–Si. Metal–insulator–semiconductor Schottky diodes also have been made with Pd–SiO_2–Si structures (*12*). In operation, the reverse-bias diode current exhibits significant variation with exposure to ppm levels of hydrogen gas. Although these devices are very small (e.g., 1 mm^2), simple, and sensitive, the palladium devices seem to be restricted to detecting low-molecular-weight gases such as H_2, H_2S, NH_3, and CO with poor selectivity. The use of organic semiconductors offers considerable untapped potential for fabrication of vapor-sensitive Schottky diodes, which can be functionalized and made selective to higher-molecular-weight organic vapors.

Chemiresistors. It has been known for some time that semiconductors exhibit characteristic electronic conductivities that are strongly affected by ambient gases and vapors (*13, 14*). In the case of organic semiconductors the use of such compounds as vapor sensors has been hindered by the rather high resistivities of the material (e.g., 10^8–10^{15} ohm-cm). To obtain measurable electronic current flow it was sometimes necessary to apply hun-

When HPLC, GC and AA don't.
When wet chemistry can't.
When electrochemistry won't.

Dionex Ion Chromatography will!

Many chemists are surprised to find out just how much Dionex Ion Chromatography can do—and how much time and money it can save!

If you think of Ion Chromatography in terms of simple inorganic anion and cation analysis, it's a little startling to discover that it can analyze organic acids and amines, sequestering agents, heavy and transition metals, amino acids and carbohydrates as well—in just about any sample matrix.

Watch a Dionex system in action

In many cases, a Dionex Ion Chromatograph is the only instrument you need to perform both complex and routine analysis on inorganic and organic anions and cations. And, thanks to the extraordinary selectivity of our advanced post column chemistries, usually all you have to do is "dilute and shoot."

For example, with a Dionex Ion Chromatograph, you can detect ppm levels of polyphosphates, polyphosphonates, EDTA and other sequestering agents, even in brines in as little as 20 minutes. A Dionex system also lets you determine a complete range of alcohols and carbohydrates, including large polysaccharides—faster and more efficiently than any other technique.

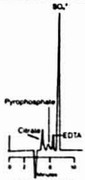

Analysis of polyvalent ions in lemon dishwashing liquid

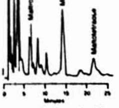

Analysis of polysaccharides in beer

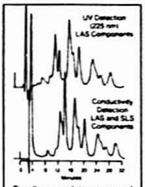

Simultaneous determination of aliphatic sodium lauryl sulfate (SLS) and aromatic linear alkyl benzene sulfonate (LAS) surfactants.

The same holds for organic acids and surfactants. Dionex column and detector technology makes Ion Chromatography a sensitive and specific alternative to GC and HPLC, whether the sample is oil recovery fluids, cosmetics, or detergents.

Of course, when it comes to inorganic ions and metals in samples such as chlor-alkali brines, plating baths, or even food, nothing—not even AA or wet chemistry—can compete with the sensitivity and convenience of a Dionex system.

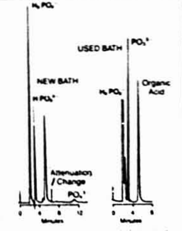

Analysis of electroless nickel plating bath.

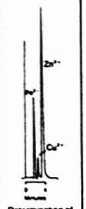

Determination of transition metals in infant formula.

Advanced technology only comes from experience

The key to Dionex versatility is proprietary column technology and superior detection based on advanced membrane post column chemistries.

Over the years, this technology has solved some of the toughest analysis problems in laboratories throughout the world.

But that doesn't mean you have to have unsolvable analysis problems to take advantage of Dionex Ion Chromatography. Dionex offers a complete line of high performance systems for applications ranging from routine sample analysis to the most demanding research.

That's only part of it.

To give you the whole story, we'd have to fill this magazine with our application notes and details about our technical assistance program, training courses, and worldwide service network.

Your own samples can tell you more than we can

Tell us about your applications needs so we can show you how Dionex Ion Chromatography can meet them. Call the Dionex applications chemist at the regional office nearest you, or contact Dionex Corporation, 1228 Titan Way, Sunnyvale, CA 94086, (408) 737-0700.

We have some pleasant surprises in store for you.

DIONEX.
ION CHROMATOGRAPHS™

Regional Offices: Marlton, NJ (609) 596-0600; Chicago, IL (312) 860-1030; Houston, TX (713) 847-5652.
In Europe: Dionex (UK) Ltd. Camberley, England (0276) 29771; Dionex GmbH, Darmstadt, W. Germany 06150-12258; Dionex S.r.l., Rome, Italy (06) 536130.

CIRCLE 58 ON READER SERVICE CARD

dreds of volts across a thin, metal–semiconductor–metal sandwich. Such devices were prone to drift induced by irreversible electrochemical reactions at the semiconductor–metal interface and were not easily accessible to ambient gas exposure. By using a microfabricated surface conductivity measurement cell having the semiconductor film coated onto an interdigitated electrode structure (Figure 3), these problems can be prevented. Because the "fingers" of the interdigital electrode are very long relative to their close spacing, the electrode array has a very high ratio of electrode perimeter distance to interelectrode distance, and measurable ohmic currents can often be obtained from typical organic semiconductors with low applied bias voltages (e.g., 1 V). The electrodes are frequently made of gold to form an ohmic contact and occupy a few square millimeters of area or less. Metal-substituted phthalocyanine films, which are less than 1 μm thick, are interesting chemiresistor coatings because they respond to a variety of vapors in a sensitive and often reversible fashion (*15*). Furthermore, the central metal atom has a significant effect on the selectivity exhibited to various vapors. The mechanism of operation is not well understood, but it is believed to involve the formation of a weak charge transfer complex between the vapor and semiconductor, which alters the number of charge carriers and hence the measured resistance. Chemiresistors are attractive because of their very low cost and size and their high sensitivity (ppm detection limits are common) to a number of organic and inorganic vapors.

Thin-film tin oxide gas sensors. Tin oxide and other metal oxide semiconductors are sensitive to low concentrations of vapors (*16*). In operation a sintered block of the semiconductor is heated to several hundred degrees centigrade and its electrical conductivity is monitored. Reducing or oxidizing gases that interact with adsorbed oxygen on the hot surface can cause a dramatic change in the device conductivity. Tin oxide is the basis for the Taguchi gas sensor manufactured by Figaro Engineering in Japan, which is used extensively for explosive vapor monitors, combustion hazard alarms, and breath alcohol meters.

Recently, this technology has been applied to microfabricate a sensor (*17*) (shown in Figure 3). A thin film of tin oxide is formed over a set of lithographically defined electrodes deposited on a thermally conductive substrate. The reverse side of the substrate has electrodes with a resistive film deposited over them. This film can be used as a heater for the device. Thus, the complete sensor–heater package can be made quite small, which is of great value in conserving heater power consumption. Many organic vapors are detectable at the 1–10-ppm level. The primary disadvantage of this technology is the relatively poor selectivity exhibited for specific vapors. Numerous partially successful attempts have been made to modify the selectivity of the tin oxide with empirically derived additions of noble metals or other metal oxides. Indeed such modifications have formed the basis of dozens of patents (primarily from Japan) focused toward specific detection of ethanol, methane, carbon monoxide, and other gases of interest. More details of the operational characteristics of metal oxide semiconductor gas sensors can be found in References 18 and 19.

Microdielectrometer. The microdielectrometer is a direct descendant of the charge flow transistor microsensor first described by Senturia and coworkers in 1977 (*20*). The device, presently manufactured by Micromet, consists of a planar interdigital microelectrode array, one side of which is attached as a floating gate to an on-chip FET charge amplifier (Figure 3). The other side of the microelectrode array is driven with a sinusoidal voltage. By measuring the amplitude and phase differences of the signal applied to the driven gate and the signal produced by the floating gate, it is possible to determine the complex impedance (i.e., the resistance and capacitance) of the medium in contact with the electrode. The integration of the FET amplifier and microelectrode permits extremely weak currents to be measured easily. Thus, the device can provide dielectric information over a frequency range not readily accessible by any other technique. Microdielectrometers are capable of monitoring the cure of epoxy resins and have an on-chip temperature sensor to permit use at elevated cure temperatures (*21*). The device can also be used to monitor the impedance of thin films coated onto the microelectrode. Measurements of the ac conductivity of coatings that are poor insulators (e.g., most undoped organic semiconductors) can be obtained quite readily. Thus, chemical microsensors can be made with this device if one coats it with a material that undergoes a change in either conductivity or dielectric constant when it is exposed to the species of interest. Microdielectrometers coated with aluminum oxide have been studied as humidity sensors (*22*).

Other Microsensor Approaches

Surface acoustic wave sensors. Chemical microsensors using the surface acoustic wave (SAW) phenome-

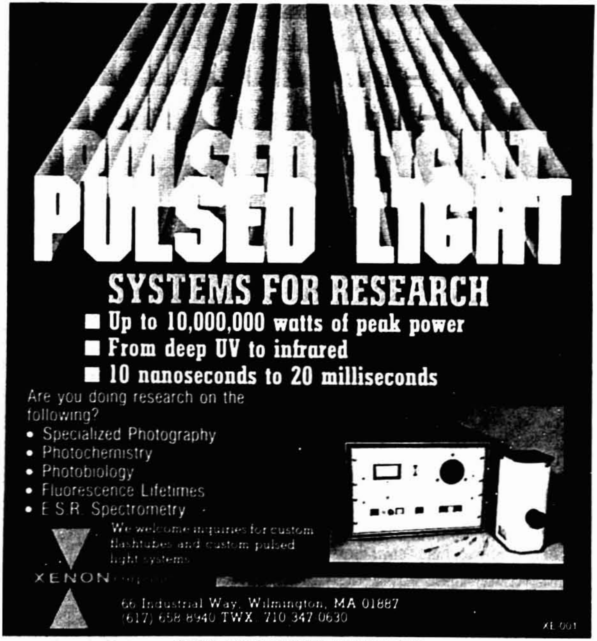

PULSED LIGHT

SYSTEMS FOR RESEARCH

- Up to 10,000,000 watts of peak power
- From deep UV to infrared
- 10 nanoseconds to 20 milliseconds

Are you doing research on the following?

- Specialized Photography
- Photochemistry
- Photobiology
- Fluorescence Lifetimes
- E.S.R. Spectrometry

We welcome inquiries for custom flashtubes and custom pulsed light systems.

XENON

66 Industrial Way, Wilmington, MA 01887
(617) 658-8940 TWX: 710 347 0630

XE 001

CIRCLE 240 ON READER SERVICE CARD

Chemists-How's this for user friendly?

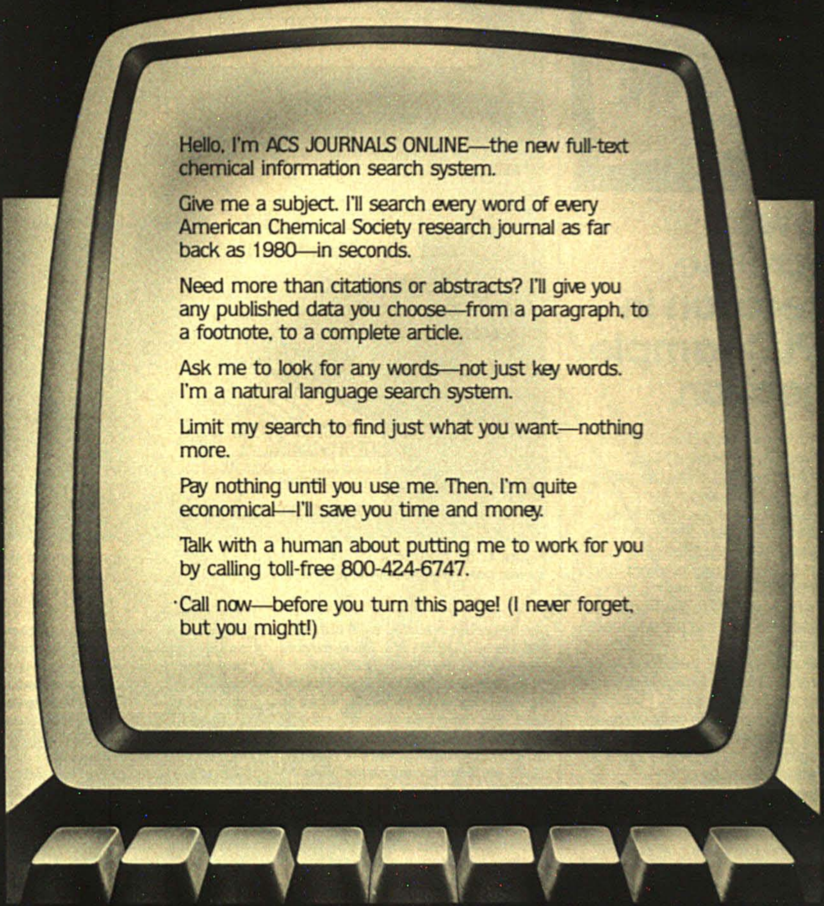

Hello, I'm ACS JOURNALS ONLINE—the new full-text chemical information search system.

Give me a subject. I'll search every word of every American Chemical Society research journal as far back as 1980—in seconds.

Need more than citations or abstracts? I'll give you any published data you choose—from a paragraph, to a footnote, to a complete article.

Ask me to look for any words—not just key words. I'm a natural language search system.

Limit my search to find just what you want—nothing more.

Pay nothing until you use me. Then, I'm quite economical—I'll save you time and money.

Talk with a human about putting me to work for you by calling toll-free 800-424-6747.

Call now—before you turn this page! (I never forget, but you might!)

ACS JOURNALS
ONLINE

The Computer-Powered
Full-Text Search System
From The American
Chemical Society

TECHNICAL NOTES 5

How to increase precision in HPLC sample injection.

Rheodyne's Tech Note 5 shows how you can maximize HPLC precision by using skillful sample injection techniques.

The information is drawn from hundreds of closely controlled experiments using different types of sample injectors and different loading methods. The 6-page summary of results is written to help both the beginner and the experienced chromatographer.

The experiments yielded some surprising answers to highly practical questions. One question:

How much sample must you waste to fill a sample loop "completely"? (It's more than you are likely to think.)

Another question:

When you are reading a syringe to judge the amount of sample being loaded, how much sample can you inject without impairing accuracy? (It's less than you may think.)

Get the answers to these and other salient questions now.

Send for Tech Note #5.

Contact Rheodyne, Inc.,
P.O. Box 996, Cotati, California 94928,
U.S.A. Phone (707) 664-9050.

RHEODYNE
THE LC CONNECTION COMPANY
CIRCLE 186 ON READER SERVICE CARD

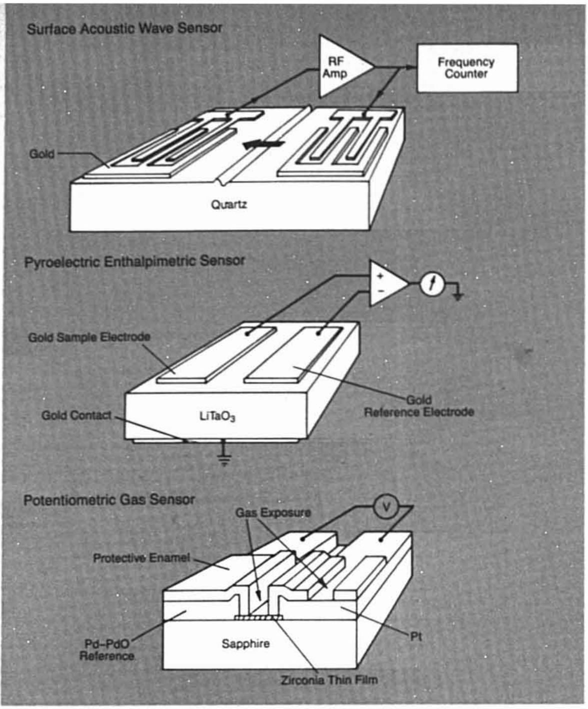

Figure 4. Microsensors using other probe techniques such as mechanical surface waves, heat flow, and electrochemical potential

non were first reported by Wohltjen and Dessy in 1979 (*23*). These devices consist of a piezoelectric substrate that has interdigital electrode arrays microfabricated at each end. When excited by a radio frequency (rf) voltage of the appropriate frequency, a synchronous mechanical wave is created in the piezoelectric substrate. This Rayleigh surface wave then propagates from the transmitting electrode array across the surface to an identical receiving electrode array where the mechanical energy is converted back into an electrical rf voltage. Because the Rayleigh wave energy is confined to about one acoustic wavelength (100 μm or less) of the surface, any material present on the surface will produce large changes in the wave characteristics (e.g., amplitude, velocity). The most sensitive response is obtained when the device is used as a delay line oscillator (Figure 4). Here the input and output transducers are connected to each other through an rf amplifier. In this configuration the device oscillates at a characteristic frequency determined by the electrode geometry and Rayleigh wave velocity. Small perturbation in the mass or elastic modulus of a thin, selective coating on the device surface will produce substantial shifts in the device's resonant frequency. Thus, in this mode, the device behaves in a fashion similar to the bulk wave piezoelectric crystal microbalance first described by King (*24*) and investigated extensively by Guilbault and Hlavay (*25*). The SAW device has several fundamental differences from the bulk wave device, including smaller size, more sensitive response, and the fact that it can be microfabricated. SAW vapor sensors have been used to detect a wide variety of vapors including water, ethanol, SO_2, H_2, and organophosphorus compounds at low (e.g., ppm or less) concentrations (*26*). A recent study suggests that immunological coatings may be possible (*27*).

SAW devices can also be used to study the rheological characteristics of polymer coatings as a function of temperature. Polymers can undergo a va-

THIS IS THE ONE!

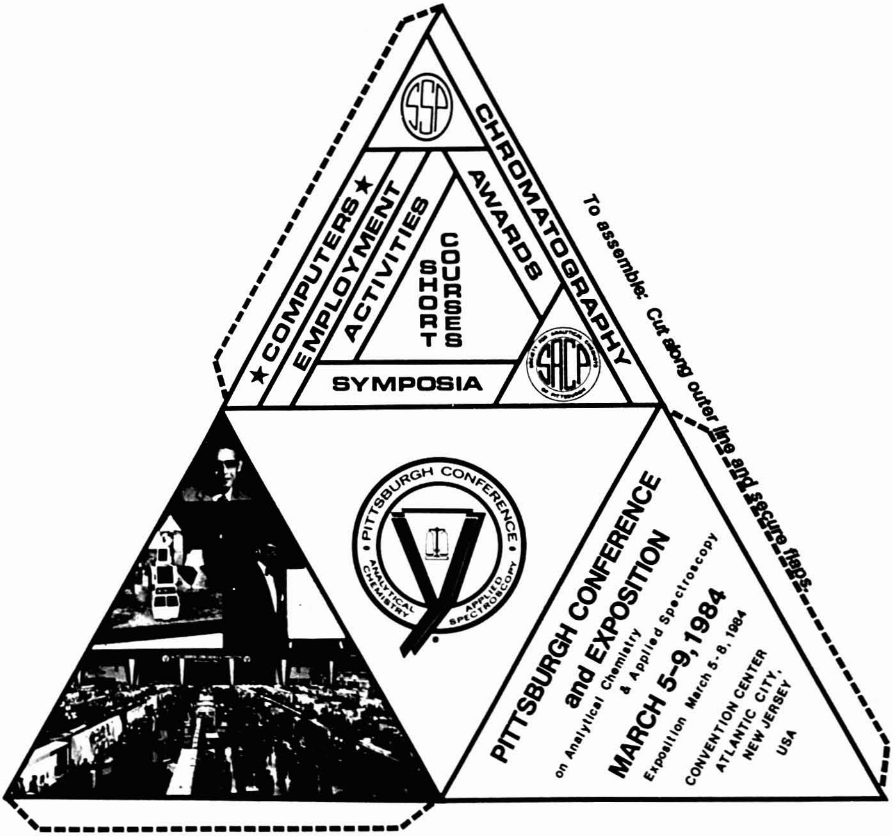
SSP
CHROMATOGRAPHY
AWARDS
★ COMPUTERS ★
EMPLOYMENT
ACTIVITIES
SHORT COURSES
SYMPOSIA
SACP
To assemble: Cut along outer line and secure flaps.
PITTSBURGH CONFERENCE
ANALYTICAL CHEMISTRY
APPLIED SPECTROSCOPY
PITTSBURGH CONFERENCE and EXPOSITION
on Analytical Chemistry & Applied Spectroscopy
MARCH 5–9, 1984
Exposition March 5-8, 1984
CONVENTION CENTER
ATLANTIC CITY, NEW JERSEY
USA

For information:
The Pittsburgh Conference
on Analytical Chemistry and Applied Spectroscopy
437 Donald Road
Pittsburgh, PA. 15235
U.S.A.
CIRCLE 175 ON READER SERVICE CARD

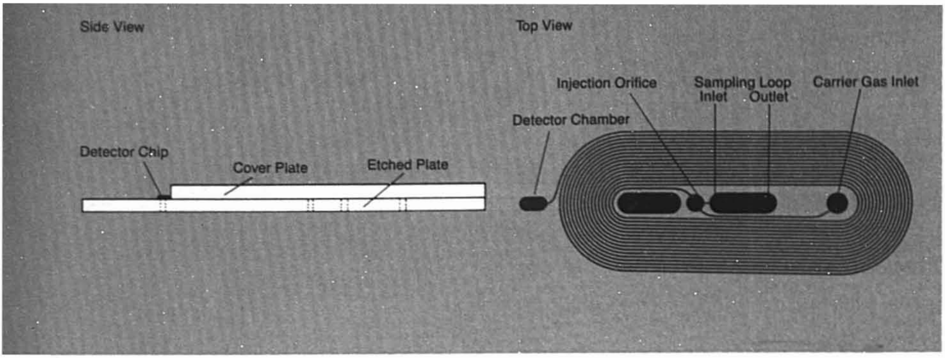

Figure 5. An experimental micro gas chromatograph developed at NRL

A lithographically defined spiral capillary was fabricated on a glass microscope slide. Samples are injected from a pressurized sampling loop onto the column through a small orifice that is always open. Injection occurs when the column pressure is momentarily turned off by a miniature solenoid valve connected to the carrier gas supply

riety of phase transitions that are easily detected as changes in SAW amplitude.

Pyroelectric enthalpimetric sensor. The principle of operating a pyroelectric microsensor for chemical vapors based on thermally programmed desorption was first described by Zemel et al. in 1980 (*28*). The same technique has been used by Rahnamai to perform differential thermal analysis (*29*). Pyroelectric microsensors are quite simple to fabricate (Figure 4). It is also possible to include a thin-film heater on the pyroelectric substrate. When the device is heated, any difference in heat flow between the sample and reference surfaces will produce a differential output voltage. Thus, coatings can be applied to the sample electrode surface, which will adsorb vapors. Heating of the device will desorb the molecules, which results in a transient change in heat flow and a corresponding output signal shift. Some selectivity based on desorption temperature may be possible. Alternatively the device can be used to study various thermal processes (e.g., phase transitions and decomposition) in extremely small samples.

Potentiometric gas sensor. It is well-known that an electrochemical concentration cell can be used to potentiometrically measure the partial pressure of a gaseous species. Oxygen sensors using zirconia-based solid electrolytes have been used for many years in metallurgical and combustion process monitoring and more recently in automotive air–fuel mixture control. Today microfabrication techniques are being employed to make potentiometric microsensors for oxygen, hydrogen, SO_2, and other gases (*30, 31*). The devices operate at a temperature of several hundred degrees centigrade in order to obtain reasonable conductivity from the solid-state electrolyte. Planar configurations of this technology (Figure 4) have been shown to be quite robust and able to withstand the extreme stresses caused by thermal cycling. In addition, the miniaturized device yields a substantial reduction in electrolyte resistance that translates into improved performance at lower operating temperatures. Nernstian responses are often obtained over many orders of magnitude of gas partial pressure.

This same approach can be used to make miniature electrochemical pumps that can add oxygen to a flowing gas stream at a rate determined by the pump current. The combination of an oxygen pump and an oxygen sensor on the same "chip" results in an oxygen regulation system that can control oxygen partial pressure over an extremely wide range (*31*).

Present Microinstrumentation Technology

Microlithography can be used not only to make sensing devices but to make other components of a conventional analytical instrument as well. The best example of this approach is the micro gas chromatograph developed at Stanford by Terry and coworkers (*32*) and first suggested by Karasek (*33*). Microfabrication techniques were employed to make three critical components of the system, namely, the capillary column, injection valve, and thermal conductivity detector. It is well-known to gas chromatographers that reduction of the capillary diameter can result in a greater separation efficiency per unit length of column. Thus, good separation can be achieved with a relatively short column of small diameter. This is very attractive if a lightweight, portable system is desirable. Furthermore, the reduced column diameter means that the carrier gas flow requirements are similarly reduced, and small gas reservoirs can supply the carrier gas needs of the system for a long period of time. The short column lengths allow very rapid analyses to be conducted. Thus, the gas chromatograph appeared to be an instrument that scales down beautifully, except for two major problems. These problems are a result of the small sample size (e.g., nanoliters) that must be reproducibly injected into the small column. How does one make a valve that can inject such small samples in a few milliseconds, and how does one build a sensitive detector with the incredibly small dead volume and fast response required? The Stanford group answered all of these questions with some very elegant silicon micromachining.

The capillary column was made by etching a lithographically defined spiral groove into a silicon wafer and covering the wafer with an electrostatically bonded glass plate. The resulting 1.5-m-long capillary tube had a rectangular cross section approximately 30 μm deep and 200 μm wide. The lithographic technique permits much smaller capillaries to be produced if desired. Coupled to the column on the same wafer, a solenoid-actuated-diaphragm injection valve was also microfabricated. A valve seat was etched into the silicon and covered with a flexible nickel diaphragm that could be pressed against the seat with the external solenoid actuator. Energizing the solenoid releases pressure on the diaphragm, allowing higher pressure gas from a sampling loop to flow into the column. Reproducible injections of

JOIN THE EXCITEMENT!

PLASMA-SPEC

ICP

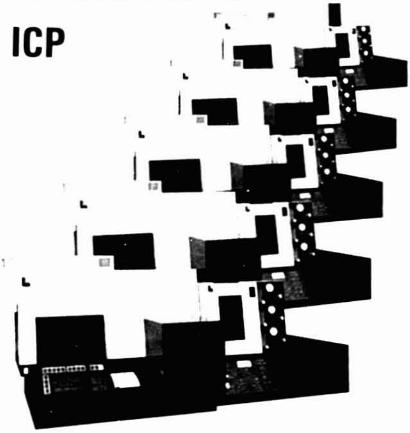

Accuracy, stability, reliability, easy operation in a state-of-the-art design.

Why is the newest ICP getting so much attention? Because the PLASMA-SPEC:

- **Is easily operated.** Instructions on the CRT display guide you through methods development and analysis programs.
- **Never gets lost.** A patented technique assures accurate wavelength selection.
- **Is unmatched in versatility.** Multiple operating modes include sequential, simultaneous, qual/semiquant, and investigative in the same package.
- **Interference free measurement.** Easily handles a wide variety of sample types.
- **Stable, reliable operation.** Ease of operation and maintenance through careful design.

The bench-top PLASMA-SPEC combines the high resolution of an echelle grating spectrometer with a tuned-cavity ICP to provide the state-of-the-art instrument at the price you can afford. Call or write today to get the complete story of the newest ICP that's creating all the excitement.

LEEMAN LABS, INC.
600 Suffolk Street / Lowell, MA 01854
(617) 454-4442

Sales and service offices in Boston; Pittsburgh; Houston; Detroit; Golden, Colorado; Huntsville, Alabama; Research Triangle Park, N. Carolina; Lake Stevens, Washington; Los Gatos, California; W. Jordan, Utah; and world wide.

CIRCLE 130 ON READER SERVICE CARD

A Breakthrough in Spectrophotometers...

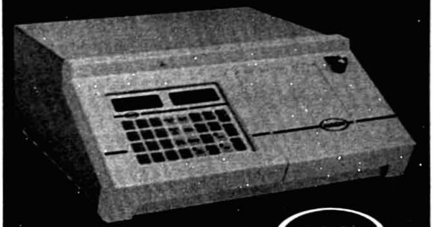

HACH

...Microprocessor Control For Only $2995

The new DR/3000 Spectrophotometer brings greater accuracy and convenience to colorimetric analysis with these outstanding features:

Versatile Testing: Prompting software lets you read colorimetric test results directly in concentration with four operating modes:

- Manual programs easily establish linear calibrations from routine absorbance and %T measurements
- A "best fit" program computes a linear calibration from multiple data points
- Other stored programs assist in performing nonlinear calibrations
- Plus, pre-programmed calibrations are included for over 60 important water quality tests using Hach reagents

Microprocessor Control: Precise and rapid keyboard control of operations insures user accuracy while reducing analysis time. Audible tones distinguish between accepted and unacceptable commands.

Digital Readout: Select from three readout modes—absorbance, % transmittance or concentration—all in 4-digit display.

Advanced Single Beam Optics: A unique double-pass grating monochromator yields a full 325 to 1000-nm wavelength range, ±1-nm accuracy, 9-nm spectral bandwidth and less than 0.1% stray light.

Call or write for more information.

U.S. domestic list price

Hach Company
P.O. Box 389
Loveland, CO 80539

HACH

Call toll-free
800-525-5940
(Colo. 800-227-4224)

CIRCLE 98 ON READER SERVICE CARD

nanoliter-size samples were demonstrated. The reader should consult References 32 and 34 for more details. An alternative micro gas chromatograph system developed at the Naval Research Laboratory (NRL) (*35*) is illustrated in Figure 5.

The micro gas chromatograph detector offered another formidable fabrication problem. The detector was required to have a dead volume less than a few nanoliters, be sensitive enough to detect trace constituents in this sample volume, and have a response time of a few milliseconds, since peak widths from the microcapillary column were often less than 100 ms wide. The Stanford group determined that a concentration-sensitive detector would be required since the sensitivity would therefore be size independent. The thermal conductivity detector is a concentration-sensitive device that scales down nicely. It can be microfabricated on a surface, thus allowing minimal sampling volume, since it can lie face down in a shallow groove through which the column output flows. In addition, the time response (limited by the thermal mass of the hot wire and substrate) goes down along with size. The actual detector consisted of a lithographically patterned zigzag "wire" of nickel (1000 Å thick) on a thinned silicon substrate. The wire was heated with a current source, and resistance changes—caused by heating of the sensor as sample peaks eluted—were used to produce the chromatogram. Detection of air contaminants in the ppm concentration range has been demonstrated, and analysis times of less than 60 s for many organic vapors are typical. The instrument is available commercially from Microsensor Technology Inc.

Technical Challenges

Microsensors and microinstruments are a reality today, but numerous technical challenges must be met before they will be used extensively in routine analysis. For chemical microsensors, the leading challenge is to develop reproducible coatings that are compatible with the sensor device and selective to the chemical species of interest. Undoubtedly a considerable amount of basic research will be required to examine reversible interactions with immobilized films on the microsensor. Interactions that turn out to be irreversible but still selective can be used to make throwaway dosimeters. Because selectivity will be degraded by the complex matrices to be analyzed (e.g., ambient air and urine) the use of pattern recognition techniques with microsensor arrays will be essential. Considerable work will be required to develop suitable algorithms to provide qualitative and quantitative analytical information from an array of sensors that responds in a reproducible but probably nonlinear way to the target molecule and known interferences. Such an approach would have been considered absurd by most analytical chemists a decade ago. The ever-diminishing cost of computation power is changing that opinion.

Packaging is another area that will require a major commitment before mass-produced sensors will be viable. The chemical microsensors that perform so well in the laboratory are often plagued by fragile chip connections and contamination of sensor elements not intended for exposure to the medium being analyzed. This is because researchers have often relied on conventional microelectronic packaging techniques that were never intended for sensing applications.

The elucidation of new physical–chemical interactions that are compatible with planar devices will offer many research opportunities. Thus, effects such as surface plasmon resonance (*36*) or adsorption-induced surface potential changes (*37*) could be used as the basis for new chemical microsensors. As new sensing interactions are elucidated and refinements are made on existing devices, it will be necessary to develop fundamentally new microstructures using new microfabrication techniques. For the immediate future, however, the existing lithographic and etching techniques will probably have more capabilities (e.g., resolution) than microsensor designers will require.

Future Prospects

The research and development of chemical microsensors has been growing steadily in recent years. The trends that have been established in this field allow one to make some conservative predictions about the kinds of devices and systems that will probably emerge in the next decade.

In the device area, integrated optical components will undoubtedly be explored as chemical microsensors. Much interesting work has already been done on optical-fiber-based sensors such as optrodes (*38*) and optical waveguide vapor sensors (*39*). An integrated optics approach involving evanescent wave interactions in thin-film waveguides on small solid substrates should be quite feasible.

The use of etched capillary tube technology with its associated microvalving will see other applications beyond gas chromatography. Indeed, Růžička has recently described how microcapillary technology can be used in flow injection analysis (*40*). Wide but shallow etched capillary tubes could be very useful for field flow fractionation. In addition, it may be possible to build a miniature fluid pump on the same substrate as the capillary tube by using piezoelectric technology similar to that used in ink jet printing (*5*). Capillary tubes will also be used in conjunction with thin-film heaters to provide temperature control. When such a capillary tube is coated with a suitable sorbent material it could be used as a miniature sample preconcentrator with fast thermal desorption capability. Sample manipulation such as flow metering and switching with fluidic logic is another possibility. Etched capillary technology may also benefit chemical analysis in the form of miniature Joule–Thomson cryogenic refrigerators, such as those developed by Little and co-workers and MMR Technologies (*41*). Future refrigerators may operate at temperatures of a few degrees Kelvin, which would permit sensors based on superconducting technology to be used without elaborate refrigeration equipment. One can imagine an inelastic tunneling spectrometer fabricated from a superconducting interdigital electrode array on a substrate cooled by a microrefrigerator. Such technology might constitute a practical approach for sensitive detection and identification of adsorbed materials with a true microinstrument.

New opportunities in electrochemistry will result from use of E-beam fabricated planar disk electrodes such as those investigated by Aoki and Osteryoung (*42*).

Lithographic and thin-film techniques may also be applicable to mass spectrometry and ion mobility spectrometry. Ion sources, ion optical components, and detector arrays have been proposed that could be microfabricated and possibly used in a miniature low-resolution fixed-sector mass spectrometer (*43*).

It should be clear that microfabrication techniques offer an enormous range of opportunities in chemical analysis. Microsensors and microinstrumentation are more than cute gimmicks. Rather they afford fundamentally new capabilities in terms of usable sample volumes, analysis speed, robustness, portability, and cost. The engineering community has developed a very powerful set of tools and techniques for creating microstructures and devices. It is now up to the chemistry community to take advantage of this capability. A revolution in microcomputer technology produced a dramatic change in the way analytical information is processed. This new wave of analytical technology is sure to produce a dramatic change in the way analytical information is obtained.

(continued on p. 103 A)

ACS Membership Application 1984

AMERICAN CHEMICAL SOCIETY • 1155 Sixteenth Street, N.W., Washington, D.C. 20036/(202) 872-4600
TTY: (202) 872-8733

Applicant

Mr., Mrs. (Name) ______________________________
Dr., Miss, Ms. (Please type or print) Family Name First Middle

Mailing Address ______________________________
Number and Street

______________________________ Telephone ______________
City State Zip Code / Country Area Code

Academic Training

Name of College or University (Including current enrollment)	City and State	Curriculum Major	Years of Attendance	Title of Degree(s) Received or Expected	Date Degree Received or Expected

Courses Completed

Please list completed courses (by title) in the chemical sciences (Attach separate sheet or transcript if more space is needed.) *Not required of those with a bachelor's, masters or doctor's degree in a chemical science or those with a doctor's degree in a science closely related to chemistry with demonstrated significant experience in the practice of a chemical science.*

Quarter hour credits should be multiplied by two-thirds. If school did not use a credit hour system, please estimate credits on basis of 15 lecture clock hours or 45 laboratory clock hours as equivalent to one semester hour credit.

Course Title	Semester Hours	Course Title	Semester Hours	Course Title	Semester Hours

Nomination

Nomination by two ACS members (not necessary for former members; student affiliation does not constitute former membership). If this presents difficulty, please contact the Washington office.

We recommend ______________________________ for membership in the American Chemical Society.
(Name of Applicant)

ACS Member: ______________________________
(Signature) (Printed Name)

ACS member: ______________________________
(Signature) (Printed Name)

This space for use of
ADMISSIONS COMMITTEE

1 2

3 4

Statistical Information

Mr., Mrs. (Name) ______________________________
Dr., Miss, Ms. (Please type or print) Family Name First Middle

Mailing Address ______________________________
Number and Street

____
City State Zip Code/Country

Date of Birth ______________________________ Sex ☐ F ☐ M
(Information needed for statistical purposes)

Previous Membership

I have ☐ have not ☐ previously been a member.

I have ☐ have not ☐ previously been a student affiliate.

[illegible]
[illegible]
[illegible]
DEL ______
MED ______
CST ______
PIN ______
CLD ______
GNS ______
CNR ______
TEC ______
WTD ______

Professional Experience

Employer	Job Title	Functions	% Time on Chemical Work	Inclusive Dates of Employment (Mo. & Yr.)

ues/Subscriptions/Divisions

There are four start dates for membership: 1 January, 1 April, 1 July and 1 October. We are anxious to begin your membership as soon as possible and will therefore enroll you immediately upon approval by the Admissions Committee. Dues for 1984 are $65.00. Your membership will begin at the nearest quarter and you will be billed accordingly. *Please send no money now.*

Student Dues

If you are a student majoring in the chemical sciences a 50% reduction on membership is available. To apply you must be registered for at least six credit hours as an undergraduate or be enrolled as a full-time graduate student.

I am ☐ an undergraduate student enrolled as described above.
☐ a graduate student enrolled as described above.

____
Name of College or University

National Affiliation

National affiliates pay three-quarters dues (i.e. $48.75) and likewise will receive a prorated bill based on the quarter national affiliation begins.

Husband/Wife Dues

If you are the spouse of a member receiving C&EN, 23% (or the prorated amount) will be deducted from your bill. This is the portion that is allotted for C&EN. If you are eligible, please give the name of your spouse and his/her membership number.

____
Spouse's Name Membership Number

If you wish to subscribe to an ACS publication or join an ACS division please list the publication(s)/division(s) below.

______________________ ______________________
______________________ ______________________

Remember, send no money now.

Agreement

I agree to restrict for my own personal use all publications to which I subsribe at member rates. I understand that membership dues are payable annually unless my signed resignation is received by the Executive Director before January 1 of the year for which the resignation is to take effect.

____
(Date) (Signature of Applicant)

Acknowledgment

I wish to express my gratitude to my colleagues, specifically, N. Lynn Jarvis, Arthur Snow, John F. Giuliani, William Barger, Dawn Dominguez, and John Lint for stimulating discussions and many significant scientific contributions to the chemical microsensor research program at NRL.

References

(1) Freiser, H. In "Ion Selective Electrodes in Analytical Chemistry"; Plenum Press: New York, N.Y., 1980; Vol. 2, Chapter 2.
(2) Dayton, M. A.; Brown, J. C.; Stutts, K. J.; Wightman, R. M. *Anal. Chem.* 1980, 52, 946–50.
(3) Glaser, A. B.; Subak-Sharpe, G. E. "Integrated Circuit Engineering"; Addison-Wesley: Reading, Mass., 1979.
(4) Hirschfeld, T. Presented at 185th ACS National Meeting, March 22, 1983, Seattle, Wash.
(5) Petersen, K. E. *Proc. IEEE* **1982,** *70(5)*, 420–57.
(6) Bergveld, P. *IEEE Trans. Biomed. Eng.* **1970,** *17*, 70–71.
(7) Janata, J.; Huber, R. J. In "Ion Selective Electrodes in Analytical Chemistry"; Plenum Press: New York, N.Y., 1980; Vol. 2, Chapter 3.
(8) "Workshop on Theory, Design and Biomedical Application of Solid State Chemical Sensors"; Cheung, P.; Fleming, D. G.; Ko, W. H.; Neuman, M. R., Eds.; CRC Press: Cleveland, Ohio, 1978.
(9) Zemel. J. N. *Anal. Chem.* **1975,** *47*, 255–68 A.
(10) Lundstrom, I.; Shivaraman, M. S.; Svensson, C. *J. Appl. Phys.* **1975,** *46*, 3876.
(11) Zemel, J. N. *Sensors and Actuators* **1981,** *1*, 31–75.
(12) Ruths, P. F.; Ashok, S.; Fonash, S. J.; Ruths, J. M. *IEEE Trans. Electron Devices* **1981,** *ED-28(9)*, 1003–9.
(13) Gutman, F.; Lyons, L. E. "Organic Semiconductors"; Wiley: New York, N.Y., 1967.
(14) Young, J. J.; Zemel, J. N. *Thin Solid Films* **1976,** *31*, 25.
(15) van Ewyk, R. L.; Chadwick, A. V.; Wright, J. D. *J. Chem. Soc., Faraday Trans. 1* 1980, *76*, 2194–2205.
(16) Seiyama, T.; Kato, A.; Fujishi, K.; Nagatani, M. *Anal. Chem.* **1962,** *34*, 1502.
(17) Chang, S. C. *IEEE Trans. Electron Devices* **1979,** *ED-26(12)*, 1875–80.
(18) Morrison, S. R. *Sensors and Actuators* **1982,** *2*, 329–41.
(19) Clifford, P. K.; Tuma, D. T. *Sensors and Actuators* **1982/83,** *3*, 233–81.
(20) Senturia, S. D.; Sechen, C. M.; Wishneusky, J. A. *Appl. Phys. Lett.* **1977,** *30*, 106.
(21) Sheppard, N. F.; Day, D. R.; Lee, H. R.; Senturia, S. D. *Sensors and Actuators* **1982,** *2*, 263–74.
(22) Garverick, S. L.; Senturia, S. D. *IEEE Trans. Electron Devices* **1982,** *ED-29(1)*, 90–94.
(23) Wohltjen, H.; Dessy, R. E. *Anal. Chem.* **1979,** *51*, 1458–75.
(24) King, W. H. *Anal. Chem.* **1964,** *36*, 1735.
(25) Hlavay, J.; Guilbault, G. G. *Anal. Chem.* **1978,** *49*, 1890–98.
(26) Bryant, A.; Lee, D. L.; Vetelino, J. F. Proc. 1981 Ultrasonics Symposium, IEEE Cat. 81-CH1689-9, p. 1735.
(27) Roederer, J. F.; Bastians, G. J. Presented at the Pittsburgh Conference, March 8, 1983, Atlantic City, N.J.; Paper 274.
(28) Zemel, J. N.; Keramati, B.; Spivak, C. W. *Sensors and Actuators* **1981,** *1*, 427–73.
(29) Rahnamai, H. *Anal. Chem.* **1982,** *54*, 142–43.
(30) Velasico, G.; Schnell, J. Ph.; Croset, M. *Sensors and Actuators* **1982,** *2*, 371–84.
(31) Fouletier, J. *Sensors and Actuators* **1982/83,** *3*, 295–314.
(32) Terry, S. C.; Jerman, J. H.; Angell, J. B. *IEEE Trans. Electron Devices* **1979,** *ED-26(12)*, 1880–86.
(33) Karasek, F. W. U.S. Patent No. 3 538 744, 1970.
(34) Angell, J. B.; Terry, S. C.; Barth, P. W. *Sci. Am.* **1983,** *248(4)*, 44–55.
(35) Wohltjen, H.; Giuliani, J.; Jarvis, N. L., unpublished work, 1980–82.
(36) Nylander, C.; Liederberg, B.; Lind, T. *Sensors and Actuators* **1982/83,** *3*, 79–88.
(37) Bregman, J. I.; Dravnieks, A. "Surface Effects in Detection"; Spartan Books: Washington, D.C., 1965.
(38) Hirschfeld, T.; Wong, F.; Deaton, T. Presented at the Pittsburgh Conference, March 9, 1983, Atlantic City, N.J.; Paper 382.
(39) Giuliani, J. F.; Wohltjen, H.; Jarvis, N. L. *Opt. Lett.* **1983,** *8(1)*, 54–56.
(40) Růžička, J. *Anal. Chem.* **1983,** *55*, 1040 A.
(41) Hollman, R.; Little, W. A. Proc. NBS Conf. Refrigeration for Cryogenic Sensors and Electronics Systems, 1980; Special Publication 607, p. 160.
(42) Aoki, K.; Osteryoung, J. *J. Electroanal. Chem.* **1981,** *122*, 19–35.
(43) Campana, J.; Wohltjen, H., unpublished work, 1981.

Hank Wohltjen is a research chemist at the U.S. Naval Research Laboratory (NRL). He received his undergraduate education—a BS in chemistry in 1972 and a BS in engineering science (electrical) in 1974—from the City University of New York, and his PhD (chemistry) from Virginia Polytechnic Institute. From 1978 to 1979 he was an IBM postdoctoral fellow in the E-beam lithography group at the T. J. Watson Research Laboratory in Yorktown Heights and was later employed in the New Devices group at IBM's research laboratory in Zurich, Switzerland, where he worked on microfabrication of Josephson effect superconducting memory circuits. Since joining NRL in 1981 he has focused on development of new chemical microsensors and microinstrumentation.

Plutonium Chemistry

William T. Carnall, *Editor*
Argonne National Laboratory

Gregory R. Choppin, *Editor*
Florida State University

Reviews recent progress in plutonium chemistry. Reports on fundamental research as well as applied environmental and process chemical research. Covers physical–inorganic chemistry and spectroscopy, solution chemistry and behavior of plutonium in the aquatic environment, and separations chemistry. Includes introductory chapter by Glenn T. Seaborg, Nobel laureate and co-discoverer of element 94 and numerous radioactive isotopes.

CONTENTS

Plutonium Chemistry: The Beginnings • Magnetic Properties of Organometallic and Coordination Compounds • Reaction of Pu Metal with Diiodoethane • Bis(μ-hydroxo)tetraaquadiplutonium(IV) Sulfate • Superconductivity and Magnetism in Metallic Pu Systems • Pu Halides and Halogeno Complexes • Thermodynamics of Pu–Noble Metal Compounds • Thermodynamic Aspects of Pu–O System • Hypostoichiometric Pu Dioxide • x-Ray Photoemission Spectroscopy • PuF_6 Gas Photophysics and Photochemistry • Measurement and Interpretation of Pu Spectra • Stability and Electronic Spectrum of $CsPuF_6$ • Pu Solution Chemistry • Pu(IV) Hydrous Polymer Chemistry • Pu Ions and Products of H_2O Radiolysis • Stability Constants, Enthalpies, and Entropies • Photochemistry of Aqueous Pu Solutions • Behavior of Pu in Natural Waters • Aquatic Chemistry of Pu • Pu(IV) Ion in Carbonate–Bicarbonate Solutions • Ground-Water Composition and Pu Transport Processes • Overview of Pu Process Chemistry • Pu Process Chemistry at Rocky Flats • Pyrochemical Processing of Pu • Pu Production and Purification at Los Alamos • Carbamoylmethylphosphoryl Derivatives • Appendixes: Round Table Discussion; Pu Isotopes

Based on a symposium jointly sponsored by the Divisions of Nuclear Chemistry and Technology and Analytical Chemistry of the American Chemical Society

ACS Symposium Series No. 216
480 pages (1983) Clothbound
LC 83-6057 ISBN 0-8412-0772-0
US & Canada **$51.95** Export **$62.95**

Order from:
American Chemical Society
Distribution Office Dept. 24
1155 Sixteenth St., N.W.
Washington, DC 20036
or CALL TOLL FREE 800-424-6747
and use your VISA or MasterCard.

LABORATORY SERVICE CENTER

Acetyl thiourea • Benzohydroxamic acid • Biuret • tert-Butyl chloride
Cesium chloride • Dibenzoylmethane • Diethyl adipate • Dipropyl ketone
2,2'-Dipyridyl • Disodium phenyl phosphate • Glutaric acid & anhydride
2,5-Hexanediol • Imidazole • Iminodiacetic acid, disodium salt
Malonic acid • Melibiose • Methyl-2-furoate • Methyl tert-butyl ether
Nitroso R salt • Orcinol • Phenyl thiourea • Phenylurea • Pimelic acid
Sarcosine • Sodium malonate • Sodium succinate • Sodium tetraphenylboron
Taurine • Triphenyl phosphine • o-Vanillin • Veratraldehyde • Xanthone

Write for our Products List of over 3000 chemicals

Tel: 516-273-0900 • TOLL FREE: 800-645-5566 TWX: 510-227-6230

EASTERN CHEMICAL
A Division of UNITED-GUARDIAN, INC.
P. O. Box 2500
DEPT. AC
SMITHTOWN, N. Y. 11787

Laboratory Service Center (Equipment, Materials, Services, Instruments for Leasing). Maximum space — 4 inches per advertisement. Column width, 2-3/16"; two-column width, 4-9/16". Artwork accepted. No combination of directory rates with ROP advertising. Rates based on number of inches used within 12 months from first date of first insertion. Per inch: 1" — **$115; 12" — $112; 24" — $108; 36" — $105; 48" — $102.**

CALL OR WRITE BARBARA AUFDERHEIDE

ANALYTICAL CHEMISTRY
25 Sylvan Road South
P.O. Box 231
Westport, Ct. 06881
203-226-7131

USE
LABORATORY
SERVICE CENTER

INDEX TO ADVERTISERS IN THIS ISSUE

CIRCLE INQUIRY NO.	ADVERTISERS	PAGE NO.
3	** **Adamel Lhomargy** Groupe 4/Marais	66D
2	* **Alltech Associates** Chromad	40A
26	**J. T. Baker Chemical Company** Stiegler & Wells	65A
20	* **Beckman Instruments** La Pointe, Schott & Smith, Inc.	63A
28	* **Bioanalytical Systems** Kissinger Advertising Associates	42A
22	* **Bio-Rad Digilab Division** Pan & Associates	62A
30	* **Sybron/Brinkmann** Lavey/Wolfe/Swift	OBC
24	* **Burdick & Jackson Laboratories, Inc.** Nordstrom/Cox Marketing	44A
33	* **Cajon** Falls Advertising	44A
32	* **Chrompack, Inc.** Lohmeyer Simpson	38A
52-53	**Data Precision** Allied Advertising Agency, Inc.	41A
58-61	* **Dionex Corporation** LaPointe, Schott & Smith, Inc.	47A, 49A, 51A, 93A
55	* **DuPont Clinical Labs** Barnum Communications, Inc.	55A
63	**Eastman Kodak Company** Rumrill-Hoyt, Inc.	11A
67	**ES Industries** Scientific Marketing Services, Inc.	67A
68	* **Floridan** Marsteller, Inc.	48A
48-49	* **Gilson Medical Electronics** LaPointe, Schott & Smith, Inc.	1A
98	* **Hach Chemical Company** Art Service/Technical Promotion	99A
96-97	* **Hewlett Packard Company** Pinne, Garvin, Herbers & Hock, Inc.	86A
105	* **ISCO, Inc./Environmental Div.** Farneaux Associates	80A

INDEX TO ADVERTISERS IN THIS ISSUE

CIRCLE INQUIRY NO.	ADVERTISERS	PAGE NO.
124	* **Kevex** Commart Communications	IFC
125	* **LDC/Milton Roy** HRS Communications	15A
126	**Leco Corporation** LECOM	52A
130	**Leeman Labs., Inc.** James F. Balderson & Associates	99A
139	**Markson Science** Arcadia Advertising	13A
139	* **Matheson Gas Products** Schaefer Advertising, Inc.	13A
145–146	**Mettler Instrument Corporation** McKinney, Inc.	19A, 21A
141	* **Mitsubishi Chemical** Global Advertising	54A
152	**Nelson Analytical** Moran, Lanig & Duncan	71A
154–155	**Nikon, Incorporated** Jarman, Spitzer & Felix	37A
158	* **Omega Engineering** Media Business House	56A
157	**Oriel Corporation** Oriel Advertising	33A
156	**Orion Research** OBC Advertising	7A
170–171	**PE/Oakbrook Instrument Division**	59A
172–173	* **Perkin-Elmer Corporation** AC&R Advertising, Inc.	4A–5A
175	**Pittsburgh Conference**	97A
70–84	** **Pye Unicam, Ltd.** Connors Publicity, Ltd.	66E–66F, 66H
183	**Regis Chemical Company**	92A
185–186	* **Rheodyne, Incorporated** Bonfield Associates	89A, 96A
194–198	* **Scientific Glass Engineering Pty, Inc.** Arden Advertising	25A–32A
162–166	* **Shimadzu Scientific Instruments, Inc.** General Advertising-Sagami	77A, 79A
159–161	** **Shimadzu Scientific Instruments, Inc.** General Advertising-Sagami	66B
204	**SLM/AMINCO** Grubb, Graham & Wilder	23A
188	* **Spectra-Physics**	50A
193	**Spectrametrics** McKinney, Inc.	61A
193	**Supelco** Supelco Park	12A
202	**Tracor Northern**	46A
200	**Tracor X-Ray** LaPointe, Schott & Smith, Inc.	91A
210	**Upchurch Scientific** Oak Harbor Advertising	34A
220–221	* **Valco Instruments Co., Inc.** Technical Advertising Associates	9A
218–224	* **Varian** Moran, Lanig & Duncan Advertising	17A, 73A, 85A
232	**Waters Associates**	53A
235	* **Wescan Instruments** Webb & Associates	82A
240	**Xenon Corporation**	94A

** See ad in ACS Laboratory Guide*
*** Company so marked has advertisement in Foreign Regional edition only.*

Advertising Management for the American Chemical Society Publications

CENTCOM, LTD.

Thomas N. J. Koerwer, President
James A. Byrne, Vice President
Alfred L. Gregory, Vice President
Clay S. Holden, Vice President
Benjamin W. Jones, Vice President
Robert L. Voepel, Vice President
Joseph P. Stenza, Production Director

25 Sylvan Rd. South
P.O. Box 231
Westport, Connecticut 06881
(Area Code 203) 226-7131
telex no. 643310

ADVERTISING SALES MANAGER
James A. Byrne

ADVERTISING PRODUCTION MANAGER
Barbara Aufderheide

SALES REPRESENTATIVES

Philadelphia . . . Dean A. Baldwin, Patricia O'Donnell, CENTCOM, LTD., GSB Building, Suite 425, 1 Belmont Avenue, Bala Cynwyd, Pa. 19004. Telephone: 215-667-9666

New York . . . Dean A. Baldwin, Edward M. Black, CENTCOM, LTD., 60 East 42nd St., 212-972-9660, New York, N.Y. 10165

Westport, CT . . . Edward M. Black, CENTCOM, LTD., 25 Sylvan Rd. South, P.O. Box 231, Westport, Ct. 06881. Telephone: 203-226-7131, Telex 643310

Cleveland . . . Bruce E. Poorman, CENTCOM, LTD., 325 Front St., Suite 2, Berea, Ohio 44017, 216-234-1333

Chicago . . . Michael J. Pak, CENTCOM, LTD., 540 Frontage Rd., Northfield, Ill. 60093, 312-441-6383

Houston . . . Dean A. Baldwin, CENTCOM, LTD., 215-667-9666

San Francisco, CA . . . Paul M. Butts, CENTCOM, LTD., Suite 112, 1499 Bayshore Hwy, Burlingame, CA 94010. Telephone: 415-692-1218

Los Angeles . . . Clay S. Holden, CENTCOM, LTD., Newton Pacific Center, 3142 Pacific Coast Highway, Suite 200, Torrance, CA 90505, 213-325-1903

Boston, MA . . . Edward M. Black, CENTCOM, LTD. Telephone: 203-226-7131

Atlanta, GA . . . Edward M. Black, CENTCOM, LTD. Telephone: 203-226-7131

Denver . . . Paul M. Butts, CENTCOM, LTD., 415-692-1218

United Kingdom

Reading, England . . . Malcolm Thiele, Technomedia Ltd., Wood Cottage, Shurlock Row, Reading RG10 0QE. Berkshire, England. Telephone: 0734-343302

Lancashire, England . . . Technomedia Ltd., c/o Meconomics Ltd., Meconomics House, 31 Old Street, Ashton Under Lyne, Lancashire, England. Telephone: 061-308-3025

Continental Europe . . . Andre Jamar, International Communications, Inc., Rue Mallar 1, 4800 Verviers, Belgium. Telephone: (087) 22-53-85, Telex #49263

Tokyo, Japan . . . Shuji Tanaka, International Media Representatives Ltd., 2-29 Toranomon, 1-Chome Minato-ku Tokyo 105 Japan. Telephone: 502-0656

ORGANOMETALLICS

The ACS Journal You've Been Hearing About

Edited by Dietmar Seyferth
Published by the American Chemical Society

ORGANOMETALLICS is the journal introduced in 1982 for organic chemists, inorganic chemists, polymer chemists — all scientists needing the most current research worldwide in the highly active field of organometallic chemistry.

Monthly issues of the journal will bring you articles, communications, and occasional reviews in all aspects of organometallic chemistry. Specifically, ORGANOMETALLICS covers—

Synthesis

Structure and Bonding — experimental and theoretical studies

Chemical Reactivity and Reaction Mechanisms — of the metal-carbon bond as well as of other inorganic and organic functionality present in the molecule

Applications — organometallic reagents in organic synthesis and in polymer synthesis; catalytic processes in which an organometallic compound is the catalyst or in which organometallic species are intermediates; and applications of organometallic compounds in the synthetic aspects of materials science and solid state chemistry

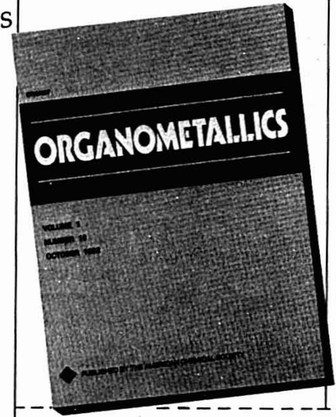

Don't delay — Use the coupon below to enter your subscription to the impressive new journal, ORGANOMETALLICS!

Cable Address: JIECHEM
Telex: 440159 ACSPUI or
892582 ACSPUBS

American Chemical Society 1984
1155 Sixteenth St., N.W. / Washington, D.C. 20036 U.S.A.

Yes, please enter my 1983 subscription to ORGANOMETALLICS at the rate checked below:

	U.S.	**Foreign** (Surface Postage Included)	**Foreign** (Air Freight Included)
ACS Members	☐ $ 34.00	☐ $ 48.00	☐ $ 74.00
Nonmembers	☐ $195.00	☐ $209.00	☐ $235.00

☐ Payment enclosed (Payable to American Chemical Society) ☐ Bill me ☐ Bill company

Charge my ☐ MasterCard ☐ VISA ☐ Barclaycard ☐ Access

Card No. __________

Interbank No. _____ (MasterCard only) Expires _____

Signature __________

Name __________

Organization _____ Title _____

Address ☐ Home ☐ Business __________

City _____ State/Country _____ Zip _____

Journal subscriptions start January 1984.

Subscriptions at ACS member rates are for personal use only. Foreign payment must be made in U.S. currency, by international money order, UNESCO coupons, U.S. bank draft, or through your subscription agency.

2752H

analytical chemistry

EDITOR: **GEORGE H. MORRISON**

EDITORIAL HEADQUARTERS
1155 Sixteenth St., N.W.
Washington, D.C. 20036
Phone: 202-872-4570 Teletype: 710-8220 151

Executive Editor: Josephine M. Petruzzi
Managing Editor: Barbara Cassatt
Associate Editors: Stuart A. Borman, Marcia S. Vogel
Assistant Editor: Rani A. George
Editorial Assistant: Louise Voress
Production Manager: Leroy L. Corcoran
Art Director: Alan Kahan
Designer: Sharon Harris Wolfgang
Production Editor: Gail M. Mortenson
Circulation Manager: Cynthia G. Smith

Journals Dept., Columbus, Ohio
Associate Head: Marianne Brogan
Associate Editor: Rodney L. Temos

Advisory Board: Joel A. Carter, Richard S. Danchik, Dennis H. Evans, Jack W. Frazer, Helen M. Free, William R. Heineman, Harry S. Hertz, Roland F. Hirsch, Csaba Horvath, Atsushi Mizuike, Thomas C. O'Haver, Melvin W. Redmond, Jr., Herbert L. Retcofsky, Martin A. Rudat, Wilhelm Simon, Charles L. Wilkins

Instrumentation Advisory Panel: M. Bonner Denton, Raymond E. Dessy, Larry R. Faulkner, Michael L. Gross, F. James Holler, Peter N. Keliher, Curt Reimann, D. Warren Vidrine, Andrew T. Zander

Contributing Editor, A/C Interface: Raymond E. Dessy

The Analytical Approach Advisory Panel: Edward C. Dunlop, Robert A. Hofstader, Wilbur D. Shults

Regulatory Affairs, Analytical Division Committee: Curt W. Reimann (Chairman)

Published by the
AMERICAN CHEMICAL SOCIETY
1155 16th Street, N.W.
Washington, D.C. 20036

Books and Journals Division
Director: D. H. Michael Bowen
Journals: Charles R. Bertsch
Production: Elmer Pusey, Jr.
Marketing & Sales: Claud K. Robinson
Research and Development: Seldon W. Terrant

Manuscript requirements are published in the January 1984 issue, page 123. Manuscripts for publication (4 copies) should be submitted to ANALYTICAL CHEMISTRY at the ACS Washington address.

The American Chemical Society and its editors assume no responsibility for the statements and opinions advanced by contributors. Views expressed in the editorials are those of the editors and do not necessarily represent the official position of the American Chemical Society.

Authors, Editors, and Reviewers Are All Human

High-quality research should be the goal of all scientists. And since the measure of high quality is directly related to the quality of the publication medium, the journals with a reputation for rigorous standards are always under great pressure. As a journal strives to maintain high standards, however, the rigor of the peer review process inevitably results in a large number of disappointed authors. Behind each rejected paper there may be an author who believes he has been unfairly treated, that those who reviewed his manuscript were either incompetent or were competitors out to "steal" his ideas. Rejected authors often perceive that papers of poorer quality than theirs are regularly published by the journal in question. This perception leads to the conclusion that the editors share a mindless hostility to new ideas and are in collusion with the reviewers.

ANALYTICAL CHEMISTRY has over the years maintained an excellent reputation for quality. Much of this success can be attributed to the tireless efforts of experienced and objective staff editors and an invaluable group of expert reviewers. Maintaining this position in conjunction with a limited page budget means that marginally acceptable papers are turned down. Although authors are entitled to offer rebuttal arguments in those cases where criticisms are incorrect, a small number tend to resent even constructive criticism. This is unfortunate, since the reviewers serve as an unusually well-informed microcosm of the readership, and their comments can help authors present their work in the best light. Nearly every manuscript can benefit from constructive criticism.

It should be noted also that although great efforts are made by the staff to identify the best reviewers, sometimes the best reviewers are not available because of the pressure of other work or other reasons. Furthermore, in recent years many new and highly specialized areas of research have evolved; as a result tremendous pressure has been placed on the staff to identify expert reviewers from a small but evolving pool. We always welcome suggestions for new reviewers, but we must continue to make our own judgments regarding their competence and impartiality. I want to assure all our authors that no manuscript is ever rejected without my personal attention. The disappointed author should realize that in each and every case the Editor evaluates the comments of the reviewers as well as their competence.

Authors, reviewers, and editors are all human beings and therefore are subject to human frailties. However, it is not in the author's best interest to mount highly emotional attacks questioning the competence of reviewers or the editorial staff. In those cases where a rejection is based on "faulty review" or lack of understanding, the resubmission of a revised manuscript accompanying an objective rebuttal would be more appropriate. An emotional attack on the reviewers or the staff does not change the weakness of the manuscript.

G. H. Morrison

Laser Desorption Mass Spectrometry with Thermospray Sample Deposition for Determination of Nonvolatile Biomolecules

E. D. Hardin, T. P. Fan, C. R. Blakley, and M. L. Vestal*

Department of Chemistry, University of Houston, Houston, Texas 77004

A new laser desorption mass spectrometer has been interfaced to a liquid chromatograph using a moving stainless steel belt. Samples are sprayed on-line onto the belt under partial vacuum with a thermospray vaporizer. These samples are transported through a differentially pumped vacuum lock and ionized in the source of the mass spectrometer with 45 ns, 10^8 W/cm^2 laser pulses from a Q-switched Nd:YAG laser. Data on the performance of this new LC/LDMS are presented for several classes of nonvolatile, thermally labile biomolecules.

An area of great analytical importance to organic and biomedical research is the development of mass spectrometric techniques for determination of high molecular weight (>1000 daltons), nonvolatile, thermally labile biomolecules (see reviews in ref 1–3). Some of the most successful approaches to this problem involve the use of desorption–ionization (DI) techniques where energetic beams of fission fragments, ions, atoms, or photons are used to desorb molecular ions from solid samples present in the source of a mass spectrometer. These DI techniques include plasma desorption mass spectrometry (PDMS) (*4*), secondary ion mass spectrometry (SIMS) (*5, 6*), fast atom bombardment (FAB) (*7, 8*), and laser desorption mass spectrometry (LDMS) (*9–19*).

In 1978 Kistemaker and co-workers showed that LDMS could be used to analyze representative samples from many major classes of nonvolatile biomolecules such as amino acids, nucleosides, peptides, nucleotides, and saccharides. Much of the current LDMS research has focused on elucidating the ionization mechanisms involved in the LD process. In LDMS submicrosecond laser pulses with power densities on the order of 10^6–10^8 W/cm^2 are used to desorb molecular ions. Proton transfer, alkali attachment, and desorption of "preformed ions", e.g., organic salts, have been studied by LDMS. Cationization by silver ion attachment has been studied in laser desorption experiments by Cooks and co-workers (*13*), and attachment of many other metal cations was also observed. Cluster formation with metastable dissociation has been observed (*12*). With magnetic instruments large cluster ions formed in semifluid chemical ionization type reactions of sucrose have been observed (*14*). Cotter has determined the temporal distribution of laser desorbed neutrals and ions (*15, 16*). Laser desorbed neutrals have been ionized by CI (*17*), EI, and alkali ion attachment from a crossed alkali ion beam (*18, 19*). Cationized molecular ions have been shown to be formed in gas-phase ion/molecule reactions between neutrals desorbed around the periphery of the laser hot spot and co-desorbed alkali ions thermionically desorbed from the center of the beam (*19*). Intense, long-lasting molecular ion beams have been laser desorbed from samples diluted in an ammonium chloride matrix (*13*). Cationized molecular ions and "preformed ions" have been desorbed from bulk samples and salt mixtures upon irradiation with CW lasers (*20*). These experiments have helped to isolate and identify ionization mechanisms involved in LDMS, some of which may be shared by all of the energetic beam DI techniques.

Our research involves both understanding the LD process and developing its analytical potential. In our view, a practical technique should provide both molecular weight and structural information on a wide range of nonvolatile and/or thermally labile compounds, it should be compatible with conventional rapid scanning mass analyzers, both magnetic and quadrupole, and it should be suitable for combination with the techniques commonly used for separating and purifying mixtures of involatile compounds such as liquid chromatography (LC) and thin-layer chromatography (TLC). With these criteria in mind, we have coupled a liquid chromatograph to a LD mass spectrometer using a moving stainless steel belt sample introduction system for continuously supplying sample to the source of a LD quadrupole mass spectrometer. SIMS has previously been used as an on-line LC detector utilizing the moving belt interface (*21, 22*) and PDMS has also been used as a detector in combined LCMS (*23*) with an on-line rotating disk sample collection device. We are using a new approach for sample deposition in which a thermospray vaporizer (*24*) is used to spray the LC effluent onto the moving belt under partial vacuum. The advantage of this approach is that most of the solvent (~95%) is removed before sample deposition onto the belt. This prevents backmixing on the belt and also eliminates the need for strip heaters and extra differential pumping stages.

INSTRUMENTAL METHODS

The mass spectrometer used in this work (see Figure 1) consists of a hyperbolic rod quadrupole mass filter, an Extranuclear Model QPS quadrupole controller, an rf-only quadrupole filter, an off-axis electron multiplier, a PAR CW-1 boxcar integrator, and a Finnigan INCOS data system. Ions are focused into the quadrupole entrance aperture by using two ion extraction cones and an einzel lens. The source lenses and quadrupoles are usually operated at a potential of 10–15 V with respect to the grounded belt. Differential pumping is supplied by a 1000 L/min mechanical pump on the thermospray region, a 2-in. diffusion pump on the intermediate region, and a 4-in. diffusion pump on the analyzer region. A source pressure of 2×10^{-6} torr and a thermospray region pressure of approximately 400 mtorr is maintained when an LC flow rate of 1 mL/min of water is used. Samples are introduced into the system with a Valco LC injector valve backed by a Waters M-45 HPLC solvent delivery system. The belt (Ebtec Corp.) is 304 alloy stainless steel, 120 cm × 3.19 cm × 0.05 nm, and is normally operated from 0.20 to 1.0 cm/s. We have found that belts darkened by mild oxidation at 450 °C in a furnace give better results, presumably due to more efficient laser power absorption.

The thermosprayer (see Figure 2) consists of a 0.15 mm i.d. stainless steel capillary tube brazed into a copper block heated by two cartridge heaters. The thermosprayer has been operated in two modes, with and without the transfer tube. In

0003-2700/84/0356-0002$01.50/0 © 1983 American Chemical Society

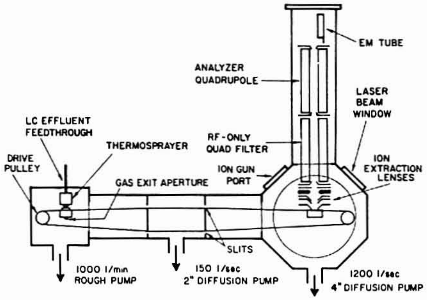

Figure 1. Schematic diagram of the laser desorption mass spectrometer showing the thermospray deposition apparatus and sample transport system. The laser beam enters through the window at the right and intersects the belt at a 45° angle.

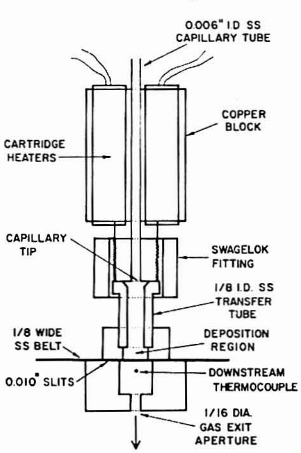

Figure 2. Schematic diagram of the enclosed thermospray deposition assembly. The internal pressure is optimized by varying the gas exit aperture diameter.

the open arrangement (without the transfer tube) the thermosprayer is positioned about 1 cm above the belt and approximately 220–240 °C is necessary to produce a fine, visible mist covering the belt when using 1 mL/min of water. The thermospray temperature is used to adjust the degree of solvent vaporization, and the temperature at which a visible mist is produced without liquid buildup on the belt gives the best results. With the transfer tube in place (see Figure 2) slightly lower temperatures can be used. In this mode the thermosprayer is adjusted to a temperature just high enough to prevent ice formation on the belt or on the downstream thermocouple. With this approach there is a more gradual desolvation and less thermal energy loss than when spraying directly into the vacuum. This arrangement has only recently been installed but preliminary results show better sample deposition efficiency than the open arrangement. We are currently optimizing the pressure of the enclosed thermospray assembly to further increase the sample deposition efficiency.

Some samples were prepared by the electrospray deposition method (*25*). This is accomplished by removing the entire belt assembly (which conveniently slides out in one piece) followed by electrospraying at ambient pressure. Replacement of the belt assembly and evacuation of the mass spectrometer take approximately 20 min.

Energy deposition into the sample is provided by a Quantronix Model 210 Q-switched Nd:YAG laser which can operate from 100 to 50 000 Hz. The unfocused output of the 1.06 μm, 0.5 mm diameter beam has a power density of 2×10^8 W/cm^2 during a 45-ns pulse. This beam is expanded to 5 mm diameter and then refocused with a cylindrical lens (f = 10 cm) and a spherical lens (f = 50 cm) to produce a line image (3.1 mm × 0.11 mm) across the full width of the belt. From the lens equations the power density delivered to the belt during normal operation is calculated to be on the order of 10^8 W/cm^2 at the center and 10^6 W/cm^2 at the ends. The lenses are mounted on a translation stage (f_{total} = 10.4 cm) which allows the central power density to be varied from 10^5 W/cm^2 to above 10^9 W/cm^2. It should be noted that these are calculated power densities; the actual power density absorbed by the sample and belt is the important parameter and cannot be easily measured directly.

When operating in the on-line LC/MS mode several parameters, quadrupole scan rate, laser pulse rate, and belt speed are coordinated and some compromises must be made. We have found experimentally that over the normal range of belt speeds used, 0.2–1.0 cm/s, a laser pulse rate of 100–200 Hz gives the best molecular ion yields, presumably because there is less overlap on the belt between consecutive laser pulses causing less local heating. At 100 Hz this limits our quadrupole scan rates to 100 daltons/s, which allows for 1 pulse/dalton. At a belt speed of 0.25 cm/s a flat thermocouple placed under the belt measures a belt temperature of 31 °C at 100 Hz, but at 1000 Hz the temperature of the belt is raised to 125 °C. More pulses per dalton give more reproducible mass spectra but this requires either higher pulse rates or slower mass scans. Local heating produced by the higher pulse rates may cause some sample pyrolysis or premature desorption, while slower scan rates limit the mass range available for rapidly eluting chromatographic peaks.

RESULTS AND DISCUSSION

All of our laser desorption studies have been carried out by using a stainless steel belt as the substrate and source pressures in the 10^{-6} torr range. Under these conditions there are many contaminants adsorbed on the belt. Figure 3 shows two summed background spectra from a well-used belt obtained at different power densities but at otherwise normal operating conditions. In the 10^7 W/cm^2 range there is little ionization except for Na$^+$, K$^+$ (not shown), and a few clusters such as KCl·K$^+$ and CsCl·K$^+$. There are also unidentified mass peaks, presumably from previously pyrolyzed samples or vacuum pump oil contaminates. Above approximately 1.4×10^8 W/cm^2 there is a sharp rise in total ion current as atomic ion emission, Cr$^+$ and Fe$^+$, from the stainless steel itself now dominates the spectrum. There are also more cluster ions and more low mass unidentified ions at this power density. This high power density range has been called the laser desorption plasma mode (*11, 26*) and its use results in formation of visible craters on the surface. We generally operate at an experimentally determined power density just above that necessary for atomic ion emission from the stainless steel; this gives the best trade off between background interference, sample fragmentation, and molecular ion intensity. One must keep in mind that only the power density at the center of the beam image is 10^8 W/cm^2; the outer ends of the line image have a power density 100 times less than the center. Whatever the power density used there is no discernible background above 375 daltons, the K(CsCl)$_2^+$ ion. In the positive ion mode cluster ions are practically unavoidable but generally not a problem except in the low mass range (below 150 daltons)

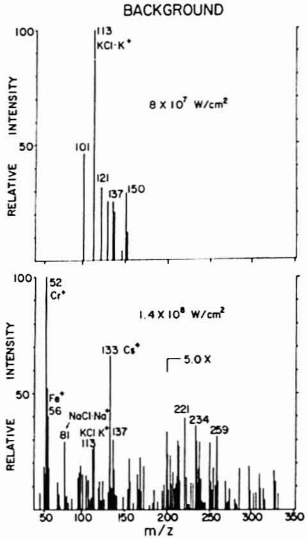

Figure 3. Summed background spectra from the "clean" belt at 8 × 10^7 W/cm² and 1.4 × 10^8 W/cm². Not shown is the K^+ ion peak which is at least 2 orders of magnitude larger than the peaks shown. These spectra were taken at the following operating conditions: belt speed, 0.25 cm/s; laser repetition rate, 100 Hz; and quadrupole scanning rate, 100 daltons/s.

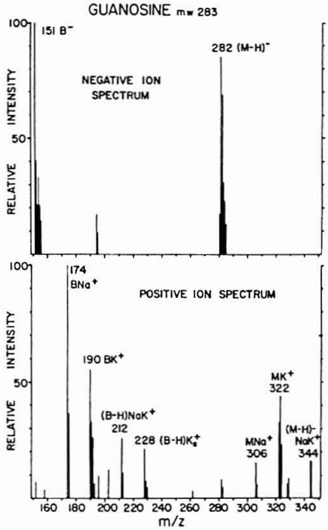

Figure 4. Positive and negative ion spectra of guanosine taken at normal operating conditions. Not shown is the $(M - H)K_2^+$ ion peak in the positive ion spectrum.

where they are quite intense. The negative ion background spectrum is substantially less intense. In the negative ion background intense peaks at 63 and 79 are observed.

The nucleoside guanosine is a thermally labile, nonvolatile biomolecule that has frequently been used as a test sample for soft ionization techniques. Figure 4 shows the LD positive and negative ion spectra of guanosine taken at normal operating conditions using an LC flow rate of 1 mL/min of water. The positive ion spectrum shows alkali-attached molecular ions and double alkali-attached deprotonated molecular ions as well as corresponding guanine base fragment ions. The degree of fragmentation is dependent on the power density as has been noted by others (*11*). The negative ion spectrum shows only $(M - H)^-$ and B^- ions. These results are typical of our laser desorption mass spectra from nucleosides and amino acids; MH^+ ions are usually weak or absent. Some samples tested always yield MH^+ ions, however, most notably the basic amino acids arginine and histidine, but alkali-attached positive molecular ions are by far the most frequently observed species in the LD process. Also, samples with the highest positive molecular ion yields give the lowest negative molecular ion yields and vice versa.

It would seem that alkali ion attachment would be enhanced and variability suppressed by using an alkali salt matrix containing the sample, and in fact this does yield an increase in cationized molecular ion production, but unfortunately this also caused a high increase in background from many different salt clusters and adducts. There is also a long lasting memory effect on the belt when using pure alkali halide salts. For these reasons we are presently not using a salt matrix with our samples.

All of the common nucleosides and amino acids we have tested thus far yield strong alkali-attached molecular ion signals. We have also been testing samples of higher molecular weights with similar results. Figure 5a shows the LD mass spectrum obtained from a 1 μg injection of the antibiotic erythromycin into the LC sample loop. This sample yields intense MNa^+ and MK^+ ions as well as structurally significant fragments at 583 and 599 daltons. The peaks at 739 and 755 daltons may be due to loss of water from the molecular ion.

Figure 5b shows the LD mass spectrum obtained from 1 μg of the cyclic peptide antibiotic, gramicidine S hydrochloride. This spectrum also shows intense MNa^+ and MK^+ ions. The excessive peak broadening at the base of the molecular ion peaks is partly due to incomplete resolution by the quadrupole mass filter, but there appears to be an additional contribution, particularly at higher masses, which is not yet understood. This result demonstrates the high mass potential of LDMS, but it should be noted that desorption of alkali-attached molecular ions from cyclic compounds has been shown to occur by purely thermal methods (*27*) even at temperatures below that necessary for alkali ion emission.

Figure 5c shows the LD mass spectrum obtained from 1 μg of the peptide trp-met-asp-phe-amide HCl. The spectrum shows a strong MH^+ ion signal but uncharacteristically little signal from alkali-attached molecular ions. This may be due to the fact that the sample is a hydrochloride salt. Again there appears to be loss of water or ammonia from the protonated molecular ion.

All of the spectra shown here were taken by use of on-line thermospray sample deposition LC/LDMS. We have also prepared many samples by using off-line electrospray sample deposition onto the moving belt. The electrospray method can be used to provide relatively smooth sample coverages of known surface concentration. It would not make a suitable sprayer in an on-line moving belt interface, however, in that it requires high voltage, atmospheric pressure, 80% alcohol solutions, and low flow rates. We use the electrospray method as a comparison tool for studying relative thermospray sample deposition efficiency and homogeneity. Figure 6a shows the reconstructed ion chromatogram (RIC) from an electrosprayed

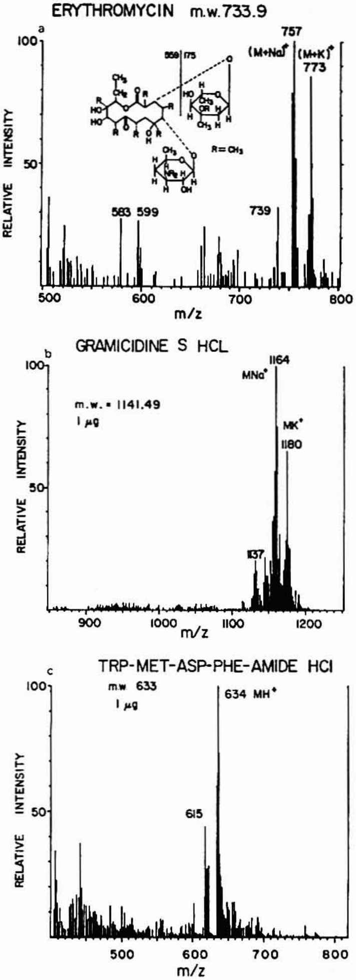

Figure 5. (a) Positive ion LD mass spectrum taken from a 1-μg injection of erythromycin into the LC sample loop. (b) Positive ion LD mass spectrum taken from a 1-μg injection of gramicidine S hydrochloride. (c) Positive ion LD mass spectrum of the peptide trp-met-asp-phe-amide HCl. With this sample the MH^+ ion is the major molecular ion produced.

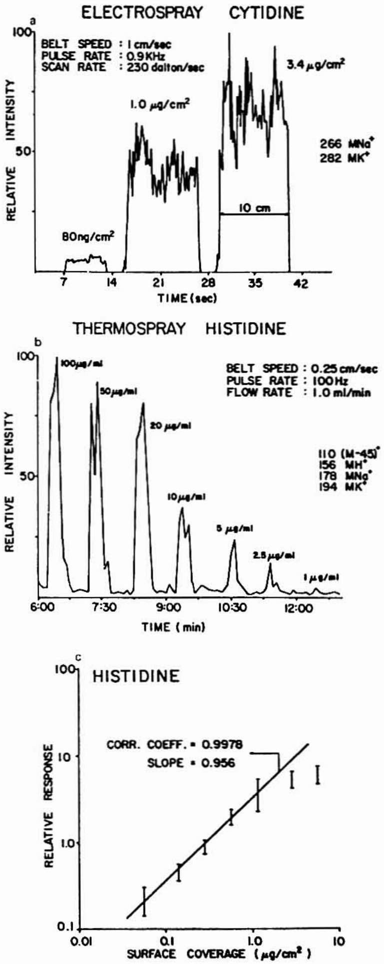

Figure 6. (a) Reconstructed ion chromatogram of the summed MNa^+ and MK^+ ion intensities from a series of electrosprayed surface coverages of approximately 80 ng/cm², 1 μg/cm², and 3.4 μg/cm². In this case the operating conditions are as follows: belt speed, 1 cm/s; laser repetition rate, 900 Hz; and scan rate, 230 daltons/s. (b) Reconstructed ion chromatogram from thermosprayed histidine obtained by using 250-μL sample injections and the concentrations shown. A 150 dalton mass range was scanned in 3 s which allows for 2 pulses/dalton. (c) log–log plot of peak area response vs. sample surface coverage obtained from four replicates of the experiment illustrated in Figure 6b. A least-squares plot is shown for data up to and below a nominal monolayer. The bars indicate the upper and lower limits of the mean ± standard deviation at each data point.

series of different surface concentrations. This RIC of the summed intensities of the MNa^+ and MK^+ ions of cytidine, a particularly stable nucleoside, was obtained at a 900 Hz laser repetition rate, a 230 daltons/s scan rate, and a 1 cm/s belt speed. It characterizes the relative ion yields from above and below nominal monolayer (~1 μg/cm²) surface coverages. Below a monolayer, the response is approximately proportional to the surface coverage, but above a monolayer, the response increases only slightly with increasing surface concentration. This may be due to attenuation of the laser intensity by the sample preventing good energy deposition, or it may be an artifact of bulk vs. surface ionization reactions. This RIC also shows the scan to scan fluctuations involved in the laser desorption measurement. We are not sure if these fluctuations are primarily from sample coverage inhomogeneity induced in the electrospray process or from differences in local substrate condition. Darker areas on the belt have a higher capacity for laser power absorption usually resulting in higher molecular ion yields. Also, at this pulse rate and belt speed there is overlap of the consecutive laser pulse images on the belt surface which may induce localized heating and sample pyrolysis. In experiments at different belt speeds, we have determined that sample ionization efficiency is better when every laser pulse impinges on a fresh surface area.

Figure 6b shows the RIC obtained from on-line thermosprayed histidine (mol wt 155) in various concentrations to show the response from above and below nominal monolayer surface coverages. The RIC is a summation of all the major molecular ions that are observed from histidine, $(M - COOH)^+$, MH^+, MNa^+, and MK^+. Figure 6c shows the data from Figure 6b along with three other replicates in terms of relative peak areas vs. sample surface concentration. Surface coverages are estimated assuming a 40% thermospray sample deposition efficiency and average peak widths of 30 s. Mean and standard deviations were calculated for each data point and are shown on the graph. As can be seen, the response is linearly proportional to surface coverage up to slightly over a monolayer ($\sim 0.5\ \mu g/cm^2$ for histidine), but at higher surface concentrations the response increases only slightly. This agrees with results obtained by electrospray deposition.

Although all experimental conditions were carefully controlled to be identical in each repeated experiment, the absolute response still may vary by as much as ±30% between experiments. This variation can be attributed to several factors. Liquid flow modulation inherent in the LC pump operation is one factor; while thermospray deposition is observed, the mist spot formed under the spray on the belt can be seen to grow and shrink in phase with the LC pump piston operation. This effect can be effectively eliminated, however, with a column in place. Another difficulty is in regenerating a reproducibly clean belt surface between experiments. Nonhomogeneous pump oil accumulations and local surface discolorations almost certainly contribute to variations in response. In spite of these uncontrolled factors, the relationship between relative response and surface coverage is still apparently linear.

The relative thermospray sample deposition efficiency was obtained from detailed comparisons with electrospray sample deposition. In these experiments it was assumed that electrospray deposition provided 100% transfer efficiency. Comparisons between the open and closed thermosprayer arrangements have shown the closed arrangement to have a transfer efficiency 40% that of electrospray and approximately twice the transfer efficiency of the open arrangement. These comparisons were based on the intensity of the LD response; it is assumed that differences in response are due to actual surface concentration and that the response is not strongly influenced by the size of aggregates which may be formed on the belt. Also, in our comparisons using the two sample deposition techniques we have seen no evidence for sample decomposition induced by the thermospray process. For example, the apparent fragmentation of a thermally labile sample such as guanosine is the same with thermospray deposition as with electrospray deposition.

Figure 7 shows a series of 12 injections of cytidine ranging from 2 to 100 ng using a 20-μL injection loop. Only the MNa^+ peak at 266 daltons is shown in the reconstructed ion chromatograph. As can be seen, the chromatographic peak shapes are good and the response is approximately proportional to sample size. The peaks are approximately 3 s wide at the base and there is no apparent peak broadening induced by the thermospray deposition process. To catch these rapidly eluting peaks, 1 s mass scans were taken covering a range of 100 daltons each. A representative mass spectrum covering 100 daltons can be obtained with a 10-ng sample in this way.

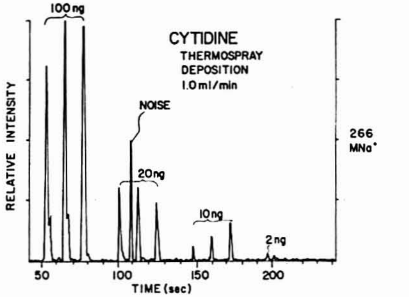

Figure 7. Reconstructed ion chromatogram from a series of 12 injections of cytidine ranging from 100 ng to 2 ng each. A 20-μL sample loop was used with a flow rate of 1 mL/min. The RIC of the MNa ion of cytidine is shown. The noise peak is from a sample deposited during a previous run.

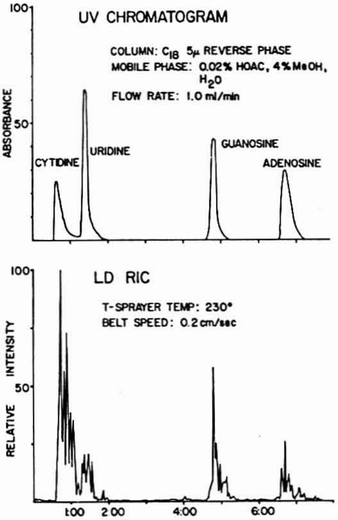

Figure 8. UV trace and LDMS reconstructed ion chromatogram from an on-line separation of 1 μg each of four nucleosides. The RIC is a summation of all the molecular and fragment ions that these nucleosides have been observed to yield.

A small number of LC separations have been carried out to test the capability of the LD mass spectrometer as an LC detector. For these tests we chose a mixture of four common nucleosides, cytidine, guanosine, uridine, and adenosine. Figure 8 shows the UV trace and the LD reconstructed ion chromatogram taken from an on-line separation of a mixture containing 1 μg each of these four nucleosides. The RIC is a summation of the molecular ions and fragments these molecules are known to yield. As can be seen, the RIC follows the UV trace very closely. There is little or no peak broadening induced by the thermosprayer because there is no liquid or ice build up on the belt. The RIC also shows the relative molecular ion yields of the different nucleosides; at the power density used in this experiment guanosine and cytidine have a somewhat higher ionization efficiency than uridine and adenosine. Compared to UV detection at 254 nm the LD mass spectrometer is about 100 times less sensitive for nucleosides. The mass spectrometer does provide molecular weight and, in some cases, structural information where the UV detector does not. For samples that do not have strong UV absorptions, the LD mass spectrometer may be more sensitive. A time-of-flight (TOF) mass spectrometer with simultaneous ion detection would greatly improve our sensitivity; with the scanning quadrupole mass spectrometer we are sampling only a small portion of the total ions produced.

A major limitation of our present moving belt system is that the LC separations must be accomplished in less than 9 min in order to prevent eluting sample components from overlapping each other on the belt. With the belt operating at 0.25 cm/s small sample amounts (less than a monolayer) are over 95% removed after one pass under the laser but larger sample amounts or faster belt speeds leave more residue. We do not, as yet, have a good method for on-line belt cleanup. Our approach thus far has been to clean off the belt after each revolution. This is accomplished by allowing the belt to rotate under the laser while operating at high repetition rate and high power density. Cleanup by conventional heaters has not proven satisfactory because their use causes nonvolatile samples to pyrolyze leading to localized discoloration of the belt and uneven laser power absorption. It appears that either a solvent scrubber combined with heating or using a single-pass disposable belt may be better approaches.

Preliminary results with the new LC/LDMS are promising. Currently, we are attempting to optimize the enclosed thermospray deposition apparatus, experimenting with darkened belt surfaces, studying the effects of different sample matrices on molecular ion yields, and measuring the effects of different belt speeds. An ion gun has recently been installed for direct comparisons between SIMS and LDMS from the moving stainless steel belt. More detailed studies will be necessary before the analytical utility of these techniques can be established. Such studies are presently in progress.

Registry No. Guanosine, 118-00-3; erythromycin, 114-07-8; gramicidin S hydrochloride, 57572-76-6; Trp-Met-Asp-Phe-amide-HCl, 5609-49-4; cytidine, 65-46-3; histidine, 71-00-1; uridine, 58-96-8; adenosine, 58-61-7.

LITERATURE CITED

(1) Vestal, M. L. *Mass Spectrom. Rev.*, in press.
(2) Benninghoven, A., Ed. "Ion Formation from Organic Solids"; Springer-Verlag: New York, 1983.
(3) Busch, K. L.; Cooks, R. G. *Science* **1982**, *218*, 247.
(4) Macfarlane, R. D.; Torgerson, D. F. *Science* **1976**, *191*, 920.
(5) Benninghoven, A.; Sichtermann, W. K. *Anal. Chem.* **1978**, *50*, 1180.
(6) Unger, S. E.; Day, R. J.; Cooks, R. G., *Int. J. Mass Spectrom. Ion Phys.* **1981**, *39*, 231.
(7) Barber, M.; Bordoli, R. S.; Sedgwick, R. D.; Tyler, A. N. *Nature (London)* **1981**, *293*, 270.
(8) Rinehart, K. L., Jr. *Science* **1982**, *218*, 254.
(9) Posthumus, M. A.; Kistemaker, P. G.; Meuzelaar, H. L. C.; Ten Noever de Brauw, M. C. *Anal. Chem.* **1978**, *50*, 985.
(10) Kaufmann, R.; Hillenkamp, F.; Nitsche, R.; Schurmann, M.; Wechsung, R. *Microsc. Acta* **1978**, *2*, 297.
(11) Heinen, H. J. *Int. J. Mass Spectrom. Ion Phys.* **1981**, *38*, 309.
(12) Hardin, E. D.; Vestal, M. L. *Anal. Chem.* **1981**, *53*, 1492.
(13) Zakett, D.; Schoen, A. E.; Cooks, R. G. *J. Am. Chem. Soc.* **1981**, *103*, 1295.
(14) Heresch, F. *Int. J. Mass Spectrom. Ion Phys.* **1983**, *47*, 27.
(15) Van Breeman, R. B.; Snow, M.; Cotter, R. J. *Int. J. Mass Spectrom. Ion Phys.* **1983**, *49*, 35.
(16) Cotter, R. J.; Tabet, J. C. *Int. J. Mass Spectrom. Ion Phys.*, in press.
(17) Cotter, R. J. *Anal. Chem.* **1980**, *52*, 1767.
(18) Stoll, R.; Rollgen, F. W. *Z. Naturforsch, A* **1982**, *37A*, 9.
(19) Van der Peyl, G. J. Q.; Isa, K.; Haverkamp, J.; Kistemaker, P. G. *Org. Mass Spectrom.* **1981**, *16*, 416.
(20) Stoll, R.; Rollgen, F. W. *Org. Mass Spectrom.* **1979**, *14*, 642.
(21) Smith, R. D.; Burger, J. E.; Johnson, A. L. *Anal. Chem.* **1981**, *53*, 1603.
(22) Benninghoven, A.; Eicke, A.; Junack, M.; Sichtermann, W.; Krizek, J.; Peter, H. *Org. Mass Spectrom.* **1980**, *15*, 459.
(23) Jungclas, Hartmut; Danigel, Harald; Schmidt, Lothar; Dellbrugge, Jorg *Org. Mass Spectrom.* **1982**, *17*, 499.
(24) Blakley, C. R.; Carmody, J. J.; Vestal, M. L. *Anal. Chem.* **1980**, *52*, 1636.
(25) McNeal, C. J.; Macfarlane, R. D.; Thurston, E. L. *Anal. Chem.* **1979**, *51*, 2036.
(26) Schueler, B.; Krueger, F. R. *Org. Mass Spectrom.* **1979**, *14*, 439.
(27) Stoll, R.; Rollgen, F. W. *Org. Mass Spectrom.* **1981**, *16*, 72.

RECEIVED June 30, 1983. Accepted October 3, 1983. This work was supported by the Institute of the General Medical Sciences (NIH) under Grant GM 29451 and the Robert A. Welch Foundation.

Analysis of Anionic Surfactants by Mass Spectrometry/Mass Spectrometry with Fast Atom Bombardment

Philip A. Lyon* and William L. Stebbings

3M Company, Central Research Laboratories, St. Paul, Minnesota 55144

Frank W. Crow, Kenneth B. Tomer, Dixie L. Lippstreu, and Michael L. Gross

Midwest Center for Mass Spectrometry, Department of Chemistry, University of Nebraska—Lincoln, Lincoln, Nebraska 68588

Fast atom bombardment (FAB) in conjunction with mass spectrometry/mass spectrometry (MS/MS) was applied to the analysis of anionic sufactants for the first time. Pure materials and commercial products were investigated. Molecular weight distributions of commercial surfactants could be obtained from either the positive or negative FAB spectra. Collisionally activated dissociation (CAD) spectra of selected ions were used to confirm strutural identification. Classes successfully characterized include alkyl and alkylaryl sulfates and sulfonates, alcohol ether sulfates, α-olefin sulfonates, fatty acid salts, sulfosuccinate diesters, and N-acylated amino acids. The FAB MS/MS technique permits the rapid analysis of these ionic surfactants without any derivatization or preseparation.

Two developments in the past few years which have significantly advanced the capabilities of mass spectrometry for chemical analysis are tandem mass spectrometry (MS/MS) and fast atom bombardment (FAB). Although the multisector instruments used in MS/MS have existed for many years, their capability for unaided separation (MS-I) and identification of single components (MS-II) in complex mixtures has only recently been explored. Analysis by MS/MS required that little sample pretreatment or preparation be done. MS/MS also provides a level of sensitivity and specificity not afforded by other instruments. The reader is referred to many fine articles which have been published on the theory and application of MS/MS (*1–7*).

Fast atom bombardment has become recognized as the preferred method of ionization for ionic or multifunctional molecules (*8–11*). The use of FAB has grown tremendously over the last 2 years. A great many substances not amenable to ionization by conventional MS methods have now been analyzed sucessfully making use of FAB (*12–15*). Anionic surfactants and surfactant mixtures are a class of such substances, and this paper is the first report of their analysis by FAB and FAB combined with MS/MS.

The analytical methods presently used for anionic surfactants cover a range from classical colorimetric determinations through chromatographic techniques, sometimes preceded by chemical modification (*16, 17*). Applications involving mass spectrometry are seldom seen except for methods involving field desorption (*18–21*), laser ionization (*22, 23*), and heated filament in-beam electron impact (*24, 25*). In fact, the first application of MS/MS in surfactant analysis was worked out by Levsen and co-workers (*18*) using FD as the ionization method.

Even if the surfactant molecules or ions can be brought into the gas phase, the problem is still not solved. This is because the functional properties of anionic surfactants do not require commercial products to be pure. The raw materials are invariably mixtures of fatty acids, alcohols or hydrocarbon precursors. The resulting surfactants are primarily water soluble salts.

The ability of MS/MS to deal with mixtures such as commercial anionic surfactants and the ability of FAB to desorb nonvolatile sample ions make the combination of the techniques a logical choice for the analysis of these materials. This paper describes the application to alkyl sulfates and sulfonates, alkylbenzenesulfonates, xylenesulfonates, alkyl ether sulfates, α-olefin sulfonates, fatty acid salts, N-acylated amino acids, and sulfosuccinates. Both positive and negative ion FAB spectra have been taken, and CAD spectra are presented for the major components.

EXPERIMENTAL SECTION

The pure chemicals were obtained from Eastman Kodak and were used without further purification. The sources of the commerical surfactants are listed in Table I.

The mass spectra were obtained with a Kratos MS-50 triple analyzer mass spectrometer (*26*). The instrument is comprised of a high-resolution MS-I (a standard Kratos MS-50) followed by an electrostatic sector, MS-II. An Ion Tech atom gun and a standard Kratos FAB source were used. The samples were analyzed neat or dissolved in a glycerol or triethanolamine matrix. A small drop of the sample solution was placed on the copper target of the FAB direct insertion probe. The sample was bombarded with 8-keV xenon atoms, and the ions produced were accelerated through 8 keV. CAD spectra were obtained by selecting the appropriate ion in MS-I and then introducing sufficient helium into the collision cell (third field-free region) between MS-I and MS-II to result in a 50% reduction of the intensity of the selected ion. CAD spectra were obtained by scanning MS-II and were signal averaged and processed with a standard DS-55 data system using software written in this laboratory.

RESULTS AND DISCUSSION

Alkyl Sulfates and Alkylsulfonates. As a group, salts of primary alkylsulfonates rank as the oldest (1830s) anionic surfactants after soap. They remain an important class of surfactants despite trends in the mid 1960s away from their use in favor of the use of biodegradable surfactants (*27*).

Positive and negative mass spectra and CAD spectra of FAB-generated negative ions were easily interpretable and very informative for alkylsulfonate surfactants. The typical mass spectrum of positive ions (see Table II) shows a series of ions of the formula $L_nNa_{n+1}^+$, where n varies from 1 to 7 and L is the subject anion. The negative ion data, also in Table II, show L^- and NaL_2^+ ions. The CAD spectra of FAB-generated negative ions allow one to verify that the material is a sulfate and to obtain the lengths of the carbon chains by counting peak manifolds from m/z 96 to the molecular ion (see Figure 1). CAD spectra of 2-ethylhexyl sulfate (Figure 2A) and octyl sulfate (Figure 2B) illustrate the effect of chain branching. The position of the branch point in the

© 1983 American Chemical Society

Table I

compound type	trade name	manufacturer
sodium dodecylbenzenesulfonate	Siponate DS-4	Alcolac Inc.
sodium α-olefinsulfonate	Siponate A-168	Alcolac Inc.
ammonium lauryl ester sulfonate	Sipex EA	Alcolac Inc.
sodium 2-ethylhexyl sulfate	Sipex BOS	Alcolac Inc.
sodium isodecyl sulfate	Sipex CAV	Alcolac Inc.
sodium cetyl sulfate	Sipon GW	Alcolac Inc.
sodium oleyl sulfate	Sipon OS	Alcolac Inc.
sodium dioctylsulfosuccinate	Aerosol OT	American Cyanamid
ammonium xylenesulfonate	Ultrawet 40AX	Arco Chemical Co.
sodium octyl sulfate	Standard	Eastman Kodak
sodium octanesulfonic acid	Standard	Eastman Kodak
sodium decyl sulfate	Standard	Eastman Kodak
sodium tetradecyl sulfate	Standard	Eastman Kodak
sodium lauryl sulfate	Standard	Eastman Kodak
sodium laurylsarcosinate	Hamposyl	Grace
sodium 2-ethylhexyl sulfate	NAS 08	Niacet Corp.
sodium heptadecyl sulfate	NAS 07	Niacet Corp.
sodium tetradecyl sulfate	NAS 04	Niacet Corp.
sodium dioctylsulfosuccinate	Triton GR-5	Rohm and Hass Co.
ammonium stearate	Purified	Whitco

Table II. Fast Atom Bombardment of Alkyl Sulfates

		mass of ion						
		positive $[L_nNa_{n+1}]^+$				negative[c] $[L_{n+1}Na_n]^-$		
		n				n		
compound	mass of ligand, daltons	1	2	3	4	1	2	3
Na 2-ethylhexyl sulfate[a]	209	255	487	719	951	441		
Na isodecyl sulfate[b]	237	283	543	803	1063	497		
Na lauryl sulfate	265	311	599	887	1175	553		
Na tetradecyl sulfate	293	339	655	971	1287	609	925	1241
Na heptadecyl sulfate	335	381	739	1097				

[a] Same numbers for sodium octyl sulfate. [b] Same numbers for sodium decyl sulfate. [c] Ligand also observed in FAB spectrum negative ions.

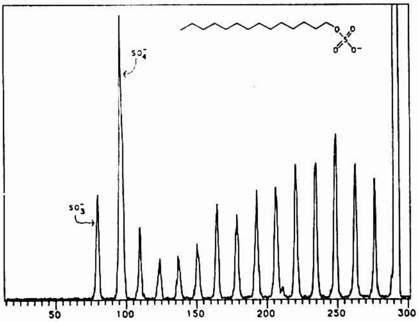

Figure 1. CAD spectrum of the negative ion *m/z* 293, the molecular anion of pure tetradecyl sulfate.

2-ethylhexyl compound is detectable by the missing peak manifold for chain length = 2 (*m/z* 124) which would require the cleavage of two C–C bonds at the same carbon atom (i.e., carbon 2). Unfortunately, detection of the branch point in the iso- form was not possible. The spectrum of octylsulfonate shows the absence of the 96 (SO_4^-) peak and presence of the 80 peak (SO_3^-), indicative of a sulfonate rather than a sulfate.

Most of the materials run in this series were fairly pure except NAS-4 (sodium tetradecyl sulfate), EK sodium lauryl sulfate, and NAS-7 (sodium heptadecyl sulfate). These contained homologous impurities which were readily seen in the FAB spectrum.

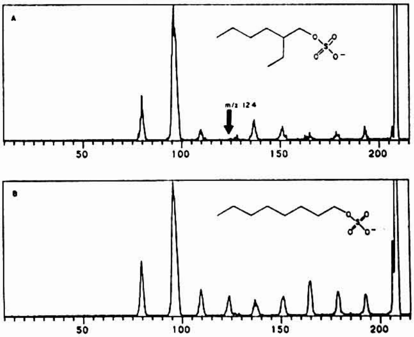

Figure 2. CAD spectra of the negative ions: (a) *m/z* 209, the molecular anion of sodium 2-ethylhexyl sulfate (NAS 08), and (b) *m/z* 279, the molecular anion of pure sodium octyl sulfate.

Occasionally unsaturated alcohol sulfates are used as surfactants. These may arise when hydrolysis products of certain fats are used as feedstock in the sulfation process. Sipon OS was studied as an example. The negative ion FAB spectra clearly show that Sipon OS is a mixture of saturated and unsaturated alcohol sulfates. The main component *m/z* 321 appears to be sodium palmityl sulfate, with lesser amounts of sodium stearyl sulfate *m/z* 349 and sodium oleyl sulfate *m/z* 347 together with a minor amount of the C_{14} sodium sulfate. The CAD spectrum of each component was used to

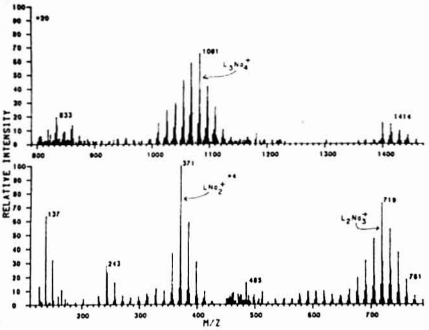

Figure 3. Sodium dodecylbenzenesulfonate (Siponate DS-4): FAB spectrum of positive ions.

Table III. Relative Intensities of Sodium Dodecylbenzenesulfonate Homologues

ionization mode	homologue					
	C_{10}	C_{11}	C_{12}	C_{13}	C_{14}	C_{15}
positive	12	23	100	55	29	16
negative	10	36	100	59	30	9

confirm the identity of that component by matching its spectrum with those of authentic samples. The length of the carbon chain of each consistuent was readily determined by simple inspection of the spectrum as discussed above.

Alkylbenzenesulfonates. Another class of hydrocarbon based anionic surfactants is the alkylbenzenesulfonates. They are commonly described as either linear (LAS) or branched (ABS) alkylbenzenesulfonates. The branched chain types were used extensively as detergents between World War II and 1965, when manufacturers voluntarily discontinued their use. The ABS surfactants are not biodegradable, and their heavy use resulted in environmental accumulation. To overcome the environmental impact of these hard detergents, manufacturers reformulated and utilized the less persistent LAS types (a biodegradable or soft detergent alkylate).

The product selected for this study was sodium dodecylbenzenesulfonate (Siponate DS-4), a classic example of the ABS type. The alkylation of benzene with an olefin tetramer to generate the dodecylbenzene alkylate eventually leads to a mixture of products. The mass spectrum of positive ions (see Figure 3) suggests that the material is a mixture of 17 substituted benzenes over a molecular weight range of 230–430. The most abundant of these compounds (based on the relative abundance of the parent ion) is the dodecylbenzene species with a molecular weight of 371 for the disodium salt cation. This sulfonate salt behaves like the sodium sulfate surfactants by combining with a second sodium atom under FAB conditions, forming ligand clusters $L_nNa_{n+1}^+$ as previously described. This spectrum contains clusters up to L_4Na_5 at m/z 1415 (that can be observed with reasonable certainty).

The corresponding anion of each mixture constituent is visible in the negative ion FAB spectrum. The relative ratios of the components in the mixture observed in the positive ion mode agree reasonably well with those found in the negative ion mode (see Table III).

The CAD spectra of the negative molecular ions at m/z 311, 325, 339, and 353 confirm that there are homologues differing by 14 daltons (a branch methyl or additional methylene group). These sulfonates show a much less intense peak at mass 80 in their CAD spectra compared to other similar sulfonates (e.g., xylenesulfonate). All the spectra contain a stable and abundant ion at m/z 197, which probably has structure 1, and is consistent with the two methyl branches at the carbon atom attached to the aromatic ring.

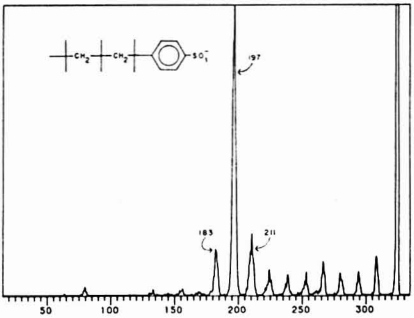

Figure 4. CAD spectrum of the negative ion m/z 325, the molecular anion of sodium dodecylbenzenesulfonate (Siponate DS-4).

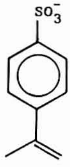

m/z 197

1

The remainder of the spectra consists of ions at intervals corresponding to the carbon number of the alkyl substituent. For the C_{12} compound, see Figure 4 (molecular ion at m/z 325), there are three carbon atoms in the fragment at m/z 197 and nine peaks above that mass, totaling 12 carbons in the molecule. This pattern is found in the other CAD spectra of mixture constituents.

Xylenesulfonates. Another alkylarylsulfonate investigated was ammonium xylenesulfonate (Ultrawet 40AX). Although classed as a surfactant, its principal use is as a hydrotrope (a material added to solubilize other less soluble surfactants). This formulation appears to contain predominantly the title species.

The mass spectrum of positive ions contains a single major peak at m/z 204 corresponding to the protonated ammonium salt $[L(NH_4)H]^+$. The mass spectrum of negative ions has predictably the xylenesulfonate anion at m/z 185 and few other significant ions. It is worth noting that there is some ligand cluster formation observed in the desorption to give the positive ion FAB spectrum. These clusters in the region of 400, 600, and 800 daltons represent various proton bound clusters involving two to four xylenesulfonic acids with varying numbers of ammonia molecules. The clustering appears similar to that observed for the sodium alkyl sulfates, but the number of ammonium cations incorporated in these clusters is variable. Less intense higher mass ions were present for the series $[L_n(NH_4)_nH]^+$ where $n = 2$ (m/z 407), $n = 3$ (m/z 610), and $n = 4$ (m/z 813). However, the cluster type $[L_n(NH_4)_{n+1}]^+$ was seen for only the $n = 2$ (m/z 424) and $n = 4$ (m/z 830).

Table IV. Parent Ions for Alkyl Sulfate Ester Adducts

alkyl alcohol	ion mode	sulfate ester	NH_4 sulfate	EO adduct (no. of moles) 1	2	3	4	5	6	7	8
dodecyl C_{12}	+		283	327	371	415	459	503	547		
	−	265		309	353	397	441	485	529	573	617
tridecyl C_{13}	+		297	341	385	429	473	517	561	605	649
	−	279									
tetradecyl C_{14}	+		311	355	399	443	487	531	575	619	663
	−	293		337	381	425	469	513	557		
pentadecyl C_{15}	+		325	369	413	457	501	545	589		
	−	307		351							

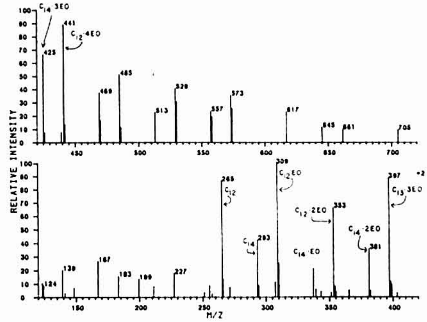

Figure 5. FAB spectrum of positive ions from ammonium lauryl ester sulfate (Sipex EA). This product contains 3.5 mol of ethylene oxide.

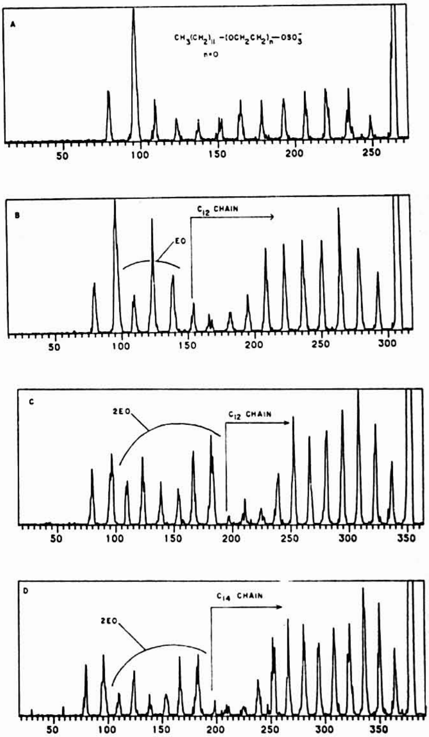

Figure 6. CAD spectra of negative ions from ammonium lauryl ester sulfate: (a) *m/z* 265, the molecular anion containing no EO units; (b) *m/z* 309, the ligand with one EO; (c) *m/z* 353, the ligand containing two EO units; and (d) *m/z* 381, the tetradecyl homologue containing 2 mol of EO in the structure.

The CAD spectra of negative ions are also quite simple. The parent anion (*m/z* 185) cleaves at the sulfonate yielding the characteristic SO_3^+ ion at *m/z* 80 (96% relative abundance). Other ions are observed for methyl losses from the intact sulfonate (170, 155; relative abundance 100% and 13%, respectively) and a rearrangement to lose molecular SO_2, resulting in the ion at *m/z* 121 (relative abundance 50%), probably a phenoxide $(C_8H_9O)^-$. Similar fragmentations were observed for the negative ion of toluene sulfonic acid (*m/z* 190) where, again, the anion loses methyl to give a daughter ion at *m/z* 156 and undergoes a rearrangement to lose SO_2 giving *m/z* 107. Both processes occur with almost equal probability.

Alkyl Ether Sulfates. The ethoxy alkyl sulfates as surfactants have grown in usage to rival their predecessors, the alkyl sulfates. The addition of oxyethyl groups to the molecule enhances its water solubility and improves the foaming quality. Major uses of this anionic surfactant type are light duty liquid detergents, shampoo, and bath preparations. Ammonium lauryl ether sulfate (Sipex EA) is an example of the ethoxy alkyl sulfate group with the general formula $(OCH_2CH_2)_nOSO_3^-NH_4^+$. Lauryl alcohol has been modified with the addition of ethylene oxide (EO) units and finally sulfated to give the desired product.

The mass spectrum of FAB-produced positive ions shows molecular ions for compounds (adducts and homologues) upward from *m/z* 300. The series consists of compounds differing by 44, the mass of an ethylene oxide unit. The sample did not solubilize well in glycerol, and the spectral quality was not as good as observed in the negative ion mode (Figure 5) where the matrix was triethanolamine. The lauryl ester ammonium sulfate anion without any EO unit ($C_{12}H_{29}NSO_4$) has a mass of 265 and is the lowest significant mass ion of the series (95% relative abundance). The incorporation of a single mole of EO results in the species observed at *m/z* 309 ($C_{14}H_{29}SO_5$); additional units of EO give *m/z* 353, etc., up to at least *m/z* 705 (ten units of EO), where the abundance of the anion drops to less than 5% of the base peak. The most abundant constituents (based on the intensities of the parent ion) contain one to four units of EO.

Superimposed on the lauryl (dodecyl) series are other series based on the tridecyl, tetradecyl, and pentadecyl moieties. The ions representing each homologue are also shown in Table IV. The relative abundances of these series point to a mixture containing predominantly dodecyl > tetradecyl with minor amounts of tridecyl and pentadecyl.

The CAD spectra of major constituent ions provide confirmation of the structures inferred from the positive and negative FAB spectra (see Figure 6A for a spectrum of m/z 265). The sulfate moiety is seen by the characteristic ions at m/z 80 ($SO_3^{-}\cdot$) and 96 ($SO_4^{-}\cdot$). The mass of the molecular anion indicates that no ethylene oxide groups have been incorporated. As expected, we see fragments at 14 dalton intervals indicative of the aliphatic structure; the length can be deduced by counting the peaks between the main beam and the sulfate fragment at m/z 96. In the CAD spectrum of m/z 265, there are 12 peaks representing a lauryl group. Thus, the constituent giving m/z 265 is a dodecyl sulfate ester and is present as an NH_4^+ salt as deduced from the mass spectrum of positive ions.

The number of units of EO incorporated can be verified from the CAD spectra of the higher mass ions at m/z 309, 353, and 397. The spectra of these ions exhibit the basic sulfate and alkyl portions, now separated by peaks which correspond to various EO units which have been inserted into the structure. There is a group of low intensity peaks in the CAD spectra of these molecules, which indicate the end of the alkyl portion (the higher mass portion) and the beginning of the EO unit. The series continues downward to m/z 96 where we see the terminal sulfate group. The number of EO molecules incorporated can be determined by counting the number of peaks differing by 44 mass units ($-CH_2CH_2O-$) starting at m/z 96 upward. For example, the CAD spectrum of the negative ion m/z 309 (Figure 6B) shows that the molecule contains one EO unit and m/z 353 (Figure 6C) contains two. The CAD spectra (Figure 6D) of a m/z 381 homologue in this product shows an alkyl chain length of C_{14} and two EO units.

The combination of mass spectra of positive and negative ions and the information from CAD spectra permit a rapid identification of the cation and structural determination of the anion for compounds of this nature.

α-Olefin Sulfonates. A smaller class of the hydrocarbon-based surfactants is know commercially as the α-olefin sulfonates (AOS). These are usually mixtures whose composition is dependent on the α-olefin feedstock used and the reaction used to achieve sulfonation. If the feedstock is produced by cracking of paraffin wax, the product will consist of homologues of both odd and even carbon number chains. The Ziegler process for ethylene polymerization produces a mixture of hydrocarbons with only even numbers of carbon atoms.

The mass spectrum of positive ions from Siponate A-168, a sodium α-olefin sulfonate, shows predominantly an equal abundance of C_{16} and C_{18} alkenesulfonates ($LNa_2^+ = m/z$ 349 and m/z 377, respectively) and a small amount of C_{20} (less than 10% relative abundance). Minor peaks for the C_{16} and C_{18} hydroxyalkanesulfonates (m/z 367 and 395) can be observed. Products with odd numbered carbon chains were not detected. The anions $[C_{16}H_{31}SO_3]^-$ and $[C_{18}H_{35}SO_3]^-$ (m/z 303 and 331) were observed as the predominant peaks in the negative ion FAB spectrum. Clusters of the type $[(RSO_3)_2Na]^-$ were also found as $[(C_6H_{31}SO_3)_2Na]^-$, $[(C_{16}H_{31}SO_3)(C_{18}H_{35}SO_3)Na]^-$, and $[(C_{18}H_{35}SO_3)_2Na]^-$ in a ratio of 1:1.7:1, which approximates the statistical pattern for a 1:1 mixture of C_{16}– and C_{18}–sulfonates. The CAD spectra of negative ions are similar to those of other sulfonates discussed above. They contain the sulfonate peak at m/z 80 and the C_nH_{2n-2}/SO_3^- series starting at $n = 2$ and extending up to the main beam.

Fatty Acid Salts. Hydrolysis of the glycerides from animal and vegetable fats and oils is an excellent source of fatty acids for surfactants. Sodium and potassium salts of these fatty acids (especially those with C_{12}–C_{18} chain lengths) account for a signficant portion of the surfactants used in soap manufacturing. Ammonium stearate, a C_{18} fatty acid salt, was analyzed by FAB mass spectrometry, but failed to give signals in the positive ion mode corresponding to the intact salt or higher mass clusters. The negative ion spectra, however, contained a strong signal for the stearate anion at m/z 283. Smaller amounts of the C_{16} and C_{14} saturated fatty acids were observed at m/z 255 and 227, respectively.

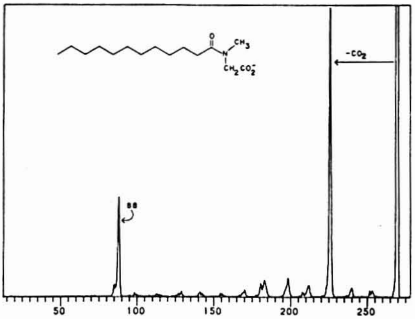

Figure 7. CAD spectrum of the negative ion at m/z 270, the.molecular anion of sodium laurylsarcosinate (Hamposyl L-95).

The CAD spectra of either the C_{16} or C_{18} anion result in the characteristic linear alkyl carbon series at 14-dalton intervals (beginning at m/z 43).

The highest small ion fragment in the CAD spectra of these two samples is 44 daltons less than the parent, suggesting decarboxylation. The intensities of the daughter ions decrease smoothly toward the low mass end of the spectrum.

N-Acylated Amino Acids. Surfactants of the N-fatty acyl amino acid type have been extensively used in specialized applications, but, due to the cost of manufacturing, have not been used in bulk cleaning products. The sarcosinates, derivatives of *N*-methylglycine, are useful in toothpaste (under the trademark Gardol), hair shampoos, and hand cleaners, as rust inhibitors, and as antifogging agents in silver halide X-ray film.

N-Laurylsarcosine can be easily prepared by an S_N2 displacement reaction of the lauryl acid chloride with the sodium salt of *N*-methylglycine (eq 1). The mass spectrum of positive

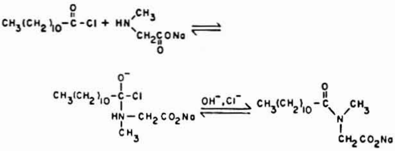

$$CH_3(CH_2)_{10}-\overset{O}{\overset{\|}{C}}-Cl + HN(CH_3)CH_2\overset{\|}{\underset{O}{C}}ONa \rightleftharpoons CH_3(CH_2)_{10}-\overset{O^-}{\underset{HN(CH_3)-CH_2CO_2Na}{C}}-Cl \xrightleftharpoons{OH^-, Cl^-} CH_3(CH_2)_{10}-\overset{O}{\overset{\|}{C}}-N(CH_3)CH_2CO_2Na \qquad (1)$$

ions from sodium laurylsarcosinate shows a protonated molecular ion at m/z 294 (relative intensity 40%) for the sodium salt $(LNa)H^+$. The ion at m/z 317 comes from the addition of a second sodium atom: $[LNa_2]^+$. Clustering of the form L_nNa_{n+1} where $L = RCO_2^-$ yields ions at m/z 609 for $[L_2Na_3]^+$ and m/z 902 for $[L_3Na_4]^+$ (relative intensities 18% and <2%, respectively). The sulfate and sulfonic acid salts cluster in a similar manner, and the relative intensities of alkyl sulfate clusters are greater than those observed for the laurylsarcosinates.

The mass spectrum in the negative ion mode consists of the laurylsarcosinate anion at m/z 270 and a dimer (m/z 563) corresponding to $[L_2Na]^-$ in an abundance ratio of 3:1.

The CAD spectrum of the anion $[C_{15}H_{28}NO_3]^-$ (m/z 270) shows two major fragmentation pathways (eq 2). As expected, the most intense fragment (m/z 226) results from decarboxylation of the parent anion (see Figure 7). An alternate

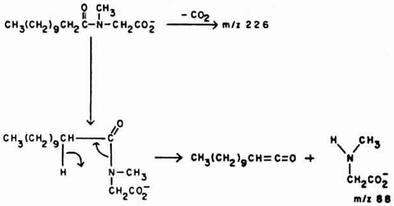

(2)

decomposition pathway involves loss of the lauryl portion of the molecule via hydrogen rearrangement, leaving the sarcosine moiety at m/z 88. A series of less intense ions indicates the presence of an alkyl moiety (viz., m/z 85, 99, 113, 127, 141, 155, ...).

The predominant ion for decarboxylation may be a diagnostic aid in identifying surfactants of the carboxylate class.

Sulfosuccinates. The sulfopolycarboxylate surfactants are widely used commercially. The predominant type are the sulfosuccinates, which exhibit excellent wetting properties, can be used in a diversity of applications and are readily available commerically.

Aerosol OT and Triton GR, both 2-ethylhexyl diesters, were analyzed by making use of FAB mass spectrometry. The positive and negative mass spectra are very simple with only the disodium species at m/z 467 (positive) and anion at m/z 421 (negative). There is apparently a small amount of the monoester sulfosuccinate as evidenced by the ions at m/z 355 in the positive and m/z 309 in the negative ion mass spectrum. The sulfosuccinates as sodium salts form ligand clusters about an additional sodium atom $(L_nNa_{n+1})^+$, resulting in the ions observed at m/z 911 and 1355.

The CAD spectrum of m/z 421 is consistent with the known structure, verifying the presence of an SO_3^- moiety (m/z 80) and the 2-ethylhexyl ester function (fragments between m/z 309 and 421). These spectra were considerably different from those discussed previously, lacking the characteristic alkyl patterns of the alkylsulfates or LAS and ABS surfactants.

ACKNOWLEDGMENT

The authors are indebted to Richard Guenthner of the 3M Commercial Chemical Division for this helpful discussions and advice and for providing the samples of commerical surfactants used in this study.

LITERATURE CITED

(1) Kruger, T. L.; Litton, J. F.; Kondrat, R. W.; Cooks, R. G. *Anal. Chem.* **1976**, *48*, 2113–2119.
(2) McLafferty, F. W.; Bockhoff, F. M. *Anal. Chem.* **1978**, *50*, 69–76.
(3) Kondrat, R. W.; Cooks, R. G. *Anal. Chem.* **1978**, *50*, 81A–92A.
(4) Cooks, R. G. *Am. Lab.* (*Fairfield, Conn.*) **1978**, *7*, 111–123.
(5) McLafferty, F. W. *Acc. Chem. Res.* **1980**, *13*, 33–39.
(6) Russell, D. H.; McBay, E. H.; Mueller, T. R. *Am. Lab.* (*Fairfield, Conn.*) **1980**, *9*, 50.
(7) Cooks, R. G.; Glish, G. L. *Chem. Eng. News* **1981**, *59*, 40–52.
(8) Williams, D. H.; Bradley, C.; Bojesen, G.; Santikarn, S. Taylor, L. C. E. *J. Am. Chem. Soc.* **1981**, *103*, 5700–5704.
(9) Barber, M.; Bardoli, R. S.; Sedgwick, R. D.; Tyler, A. N. *Nature* (*London*) **1981**, *293*, 270–275.
(10) Barber, M.; Bardoli, R. S.; Sedgwick, R. D.; Tyler, A. N. *J. Chem. Soc., Chem. Commun.* **1981**, 325–327.
(11) Rinehart, K. L., Jr. *Science* **1982**, *218*, 254–260.
(12) Gross, M. L.; McCrery, D.; Crow, F.; Tomer, K. B.; Pope, M. R.; Ciufetti, I. M.; Knoche, H. W.; Daly, J. M.; Dunkle, L. D. *Tetrahedron Lett.* **1982**, *23*, 5381–5384.
(13) Monaghan, J. J.; Barber. M.; Bardoli, R. S.; Sedgwick, R. D.; Tyler, A. N. *Org. Mass Spectrom.* **1982**, *17*, 569–574.
(14) Cotter, R. J.; Hansen, Gordon; Jones, T. R. *Anal. Chim. Acta* **1982**, *136*, 135–142.
(15) Grotjahn, L.; Frank, Ronald; Blocker, Helmut *Nucleic Acids Res.* **1982**, *10*, 4671–4678.
(16) Cross, J., Ed. "Anionic Surfactants—Chemical Analysis"; Marcel Dekker: New York, 1977.
(17) Llenado, R. A.; Jamieson, R. A. *Anal. Chem.* **1981**, *53*, 174R–182R.
(18) Weber, R.; Levsen, K.; Louter, G. J.; Boerboom, A. J. Henk; Haverkamp, J. *Anal. Chem.* **1982**, *54*, 1458–1466.
(19) Daehling, P.; Roellgen, F. W.; Zwinselman, J. J.; Fokkens, R. H.; Nibbering, N. M. M. *Fresenius' Z. Anal. Chem.* **1982**, *312*, 335–337.
(20) Sanders, R. A.; DeStefano, A. J.; Keough, T. *Org. Mass Spectrom.* **1980**, *15*, 348–350.
(21) Keough, T.; DeStefano, A. J.; Sanders, R. A. *Org. Mass Spectrom.* **1980**, *15*, 351–354.
(22) Mumma, R. O.; Vastola, F. J. *Org. Mass Spectrom.* **1972**, *6*, 1373–1376.
(23) Vastola, F. J.; Mumma, R. O.; Pirone, A. J. *Org. Mass Spectrom.* **1970**, *3*, 101–104.
(24) Kosugi, Y.; Matsumoto, K. *Fresenius' Z. Anal. Chem.* **1982**, *312*, 317–318.
(25) Matsumoto, K.; Kosugi, Y. *Fresenius' Z. Anal. Chem.* **1980**, *303*, 18–19.
(26) Gross, M. L.; Chess, E. K.; Lyon, P. A.; Crow, F. W. *Int. J. Mass Spectrom. Ion Phys.* **1982**, *42*, 243–254.
(27) Lindfield, Warner M., Ed. "Anionic Surfactants"; Marcel Dekker: New York, 1976.

Received for review June 20, 1983. Accepted September 22, 1983. This work was supported by 3M and the Midwest Center for Mass Spectrometry, a National Science Foundation Regional Instrumentation Facility (Grant No. CHE8211164).

Liquid Ionization Mass Spectrometry of Nonvolatile Organic Compounds

Masahiko Tsuchiya*

Department of Industrial Chemistry, Faculty of Engineering, The University of Tokyo, Hongo, Bunkyo-ku, Tokyo 113, Japan

Hirofumi Kuwabara

Department of Industrial Chemistry, Suzuka College of Technology, Shiroko-cho, Suzuka, Mie 510-02, Japan

Characteristics of a technique termed liquid ionization mass spectrometry for organic compounds are described. In particular the use of additives (solvent, matrix, and reagent) for nonvolatile compounds and ease of sample handling are reported. Metastable argon atoms are used to ionize compounds at atmospheric pressure. Samples are placed on a needle tip positioned near an aperture leading to the mass analyzer. The needle is heated and a high voltage (about 1 kV) is applied to the needle. Mass spectra obtained by this method showed ions characteristic of the molecular weight and the structure of the compounds. Liquid alkane(s) is a good matrix for nucleosides, while glycerol is good for phosphatidylcholines. A minute amount of a reagent such as ethanolamine increases the abundance of MH^+ ions of sucrose, resulting in reproducible mass spectra. The use of several reagents (e.g., D_2O) for one compound is suggested in order to obtain additional structural information. The advantages of the method are also described.

In recent years, nonvolatile and/or thermally labile organic compounds have been successfully investigated by several soft methods of ionization such as field desorption (FD) (*1*), laser desorption (*2*), plasma desorption (*3*), secondary ion mass spectrometry (SIMS) (*4*), fast atom bombardment (FAB) (*5*), atmospheric pressure ionization (API) (*6, 7*), and direct exposure techniques such as direct CI (*8*), in-beam EI and CI (*9, 10*), emitter CI (*11*), and so on. There are, however, many compounds whose mass spectra cannot be obtained satisfactorily by using any of these techniques, especially when such compounds are present in an actual sample. The influence of coexisting compounds has to be investigated not only for obtaining a good mass spectrum of a compound but also for applying the rapidly developing method termed mass spectrometry/mass spectrometry (MS/MS) (*12*) to nonvolatile compounds.

Many efforts to combine a liquid chromatograph with a mass spectrometer (LC/MS) have been made in recent years (*6, 13–16*) and commercial instruments are now available. There is, however, still difficulty in measuring nonvolatile compounds reliably by LC/MS combinations presently available. Therefore, it is important to understand the mechanism of ionization and desorption (*17*) and the effects of experimental parameters in order to develop new techniques in mass spectrometry.

We have developed a method which we call "liquid ionization" (referred to as LI in this paper) for ionizing organic compounds present as a liquid or in solution at atmospheric pressure (*18, 19*). Thus, the method (LI) is a variation of the atmospheric pressure ionization (API) developed by Horning and his co-workers (*13*). The main differences in the principles of the method (LI) from that of Horning and other API methods (*6, 7*) involve the technique of ionization and the sample introduction system. There are two techniques of ionization in the LI method, one of which utilizes proton transfer reactions from cluster ions of water, $(H_2O)_nH^+$, to sample molecules (a kind of chemical ionization) used in early studies (*18, 19*). In this paper (as described previously (*20*)), the other technique utilizing metastable argon atoms produced at atmospheric pressure was used as the ionizing species in an ion source. One of the purposes of using metastable argon was to apply a high electric field to a sample holder in order to increase the ion abundance.

The objectives of developing the LI method have been (a) to obtain a good mass spectrum showing the characteristic of molecular weight and the structure of a compound, (b) to analyze a liquid sample, e.g., a fraction of effluent in liquid chromatography and of a reaction product, (c) to investigate the mechanisms of ionization and desorption of solutes and the effect of additives (solvent, matrix, and reagent) in order to develop new analytical techniques, and (d) to obtain information about chemical and physical properties of a molecule, such as proton affinity, bond energy, and reactivity, in a condensed phase as well as in a gas phase at atmospheric pressure. This paper characterizes the LI method especially for nonvolatile compounds, including the effect of additives.

EXPERIMENTAL SECTION

The principle of ionization and the experimental setup of the instrument used in this paper are similar to those reported previously (*20, 21*) but will be described again briefly. A modified quadrupole mass spectrometer (ANELVA TE 600 GC/MS) equipped with the ion source shown in Figure 1 was used. In the previous paper, a port (G) for introducing a sample and a port for a sample holder (E) were both perpendicular to the axis of the ion source. These are tilted in this paper in order to place a sample closer to a pinhole (25 μm in diameter (I) of Figure 1) of an aperture, because the transmission of ions of involatile compounds through the pinhole is critically affected by the distance between the pinhole and the sample holder.

Argon (carrier gas, 300 mL/min) at atmospheric pressure was ionized by a corona discharge between a needle electrode (A) and a counterelectrode (B). Charged species were eliminated by connecting the electrodes (B) and (C) to ground, so that only excited argon (metastable argon, Ar^*, $^3P_{0,2}$) produced in the carrier gas can flow into the ionization chamber and ionize a liquid sample deposited on the sample holder. When a metal rod or a silicon emitter (ordinarily used in FD MS) is used as the sample holder, 1–2 μL of a sample solution is deposited on the holder. When a needle ((E) sewing needle commercially available) is used, 1–10 μg of solute (or 1 μL of solution) is mixed well with 1 μL of a matrix such as glycerol used in FAB and about one-tenth of the mixture is deposited on the needle tip (E) which is heated by direct current through a tungsten wire (F) surrounding it and kept at a high voltage (V_E).

0003-2700/84/0356-0014$01.50/0 © 1983 American Chemical Society

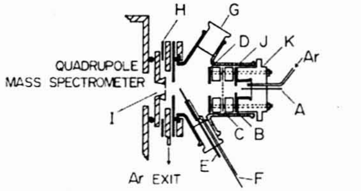

Figure 1. Schematic diagram of an ion source of a liquid ionization mass spectrometer: (A) needle electrode for corona discharge; (B) counterelectrode (connected to the ground); (C) gauze electrode (ground); (D) repeller; (E) sample holder (needle); (F) heater wire; (G) Teflon plug; (H) Teflon plate; (I) aperture with a pinhole (30 μm in diameter); (J) glass envelope of the ion source; (K) Teflon body for discharge block.

Compounds whose ionization energies are below the excitation energy (11.72 eV) of Ar* ($^3P_0$) are ionized according to

$$\mathrm{Ar} + e^- \xrightarrow{\text{(corona discharge)}} \mathrm{Ar}^* + e^- \tag{1}$$

$$\mathrm{Ar}^* + \mathrm{M} \rightarrow \mathrm{M}^+ + e^- + \mathrm{Ar} \tag{2}$$

$$\mathrm{M}^+ + \mathrm{M} \rightarrow (\mathrm{M} + \mathrm{H})^+ + (\mathrm{M} - \mathrm{H}) \tag{3}$$

$$\mathrm{Ar}^* + n\mathrm{M} \rightarrow (k\mathrm{M} + \mathrm{H})^+ + (m\mathrm{M} - \mathrm{H})^- + (n - k - m)\mathrm{M} + \mathrm{Ar} \tag{4}$$

$$\mathrm{S}_x\mathrm{H}^+ + n\mathrm{M} \rightarrow (k\mathrm{M} + \mathrm{H})^+ + (n - k)\mathrm{M} + x\mathrm{S} \tag{5}$$

Reaction 2 is well-known as Penning ionization and should be followed by reaction 3 to produce MH^+ ions, because the major ions observed in this method are MH^+. In general, the number k in reaction 4 is 1 and 2 for involatile compounds. The main processes in the method are thought to be reactions 4 and 5 for several reasons; i.e., the method involves soft ionization producing MH^+ and M_2H^+ ions of nonvolatile compounds, and there are the significant effects of a high electric field (V_E), the position of the sample, and additives on the MH^+ ion abundance. Reaction 4 could be called "soft atom bombardment". When a solvent is used (or matrix, i.e., S), SH^+ ions from the solvent (or matrix) are produced by reactions 2, 3, and 4 where M should be replaced by S. In the case of hydrocarbons, however, ions formed are generally M^+ for aromatics and $(M + 13)^+$ for alkanes, instead of MH^+. Reactions will be discussed in detail in the future.

Sample ions are observed when an adequate heater current and a high voltage (V_E) are applied to the sample holder. These ions flow into the vacuum region ($(2–4) \times 10^{-5}$ torr) through the pinhole (I) and are analyzed in the quadrupole filter. Usually the voltage applied to the pinhole, V_p, is kept at +20 V for MH^+ measurements. If V_p is increased, fragment ions produced by so-called "collisionally activated dissociation" (CAD) (*12, 19*) can be obtained. A Shimadzu microcomputorized data processing system (GCMSPAC 90) and a pen recorder were used for recording mass spectra. A mass spectrum between m/z 10 and 800 is scanned in 7 s with the former. The largest mass measurable was about 1000 using an Extranuclear Laboratories quadrupole power supply (No. 011-15). Unit resolution was obtained up to m/z 600 with lower resolution at higher m/z. Since mass descrimination in ion collection efficiency was not corrected, the actual abundances of high mass ions may be greater than those shown in this paper. Argon (99.99%) was purchased from the Takachiho Trading Co. and reagent chemicals were used as purchased from Tokyo Kasei Co. (Japan). Phosphatidylcholines were the products of Sigma Chemicals, St. Louis, MO.

RESULTS AND DISCUSSION

Effect of Temperature and Electric Field. Mass spectra of compounds such as dimethyl phthalate (bp 284 °C) can be measured even at room temperature, but moderate heating of the sample holder is required to observe ions from less volatile and nonvolatile compounds. Abundant MH^+ ions have been obtained from most amino acids by heating with a metal rod type sample holder (*19*), but it was not easy to obtain stable MH^+ ions from nonvolatile and thermolabile compounds such as saccharides. Ionization of such nonvolatile compounds must occur even without heating, because the ionization energies (7–10 eV) of such compounds are lower than the internal energy of metastable argon. Therefore we supposed that ions of such compounds produced on the sample holder could not desorb without heating or hardly desorb even by heating and a high electric field would assist the desorption of the ions produced. Then, we used metastable argon as the ionizing species. Since metastable argon is neutral, a high voltage (V_E, referred to as emitter voltage) can be applied to the sample holder without any loss of the ionizing collisions. Thus, we observed a remarkable increase in the ion abundances for nonvolatile compounds by applying the high voltage V_E (*20*).

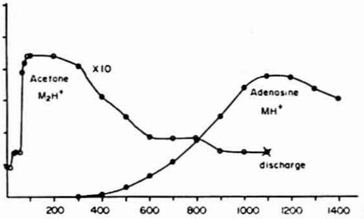

Figure 2. Effects of emitter voltages (V_E) on the ion abundance of adenosine in comparison with that of acetone.

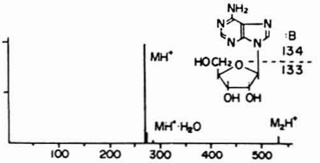

Figure 3. Mass spectrum of adenosine: matrix, Nujol; V = 1000 V; 140 °C;

The effect of the emitter voltage (V_E) on the ion intensity is shown in Figure 2 for adenosine as an example, compared with that for acetone. The maximum ion current was obtained at V_E of 100–200 V for a very volatile compound like acetone. In contrast, the maximum ion current for adenosine was obtained at ~1100 V and was about 2 orders of magnitude higher than that obtained at ~200 V. In general, the optimum V_E which provides the maximum ion current of a less volatile compound is ~1100 V and varies about ±100 V according to the sharpness and cleanliness of the needle tip. Acetone molecules are ionized by Ar* to form positive ions and electrons in the gas phase; then a V_E of +200 V is probably enough to remove electrons (negative charges) in the gas phase and to repell the positive ions to the pinhole. Molecules of nonvolatile (and probably less volatile) compounds are thought to be ionized at the sample surface (boundary of liquid phase and gas phase). A strong electric field (V_E) may have three functions: one is to assist desorption of ions from the needle tip (*22*), another is to capture electrons at the needle tip, and the other is to focus the ions to the pinhole. The high V_E slightly lowers the temperature required to desorb ions, resulting in more abundant stable MH^+ ions (*22*).

Adenosine and Guanosine. Adenosine and guanosine are known as two nucleosides which decompose thermally at temperatures required for vaporizing them. Soft ionization methods have produced an MH^+ ion of adenosine with a fragment at m/z 136 (BH_2^+). Guanosine has been detected as MH^+ by emitter CI (*11*) and API (*7*) or as cationized

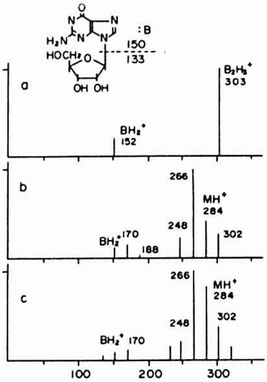

Figure 4. Mass spectra of guanosine: (a) glycerol matrix; (b) Nujol matrix; (c) *n*-hexadecane matrix.

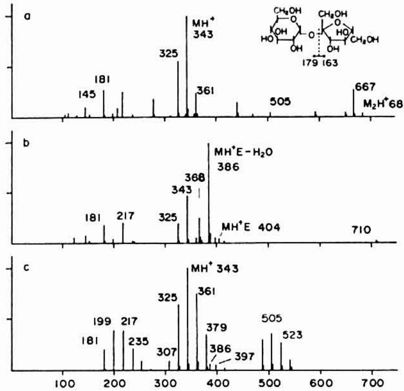

Figure 5. Mass spectra of sucrose: (a) matrix is Nujol; (b) ethanolamine (0.2 μL of 10^{-1} M aqueous solution) was added; (c) a trace of ethanolamine was added.

molecule $(M + Na)^+$ by laser desorption (*23*) and SIMS (*24*). All mass spectra have shown the protonated base (BH_2^+, *m/z* 152) as the dominant peak.

In this method (LI), using the needle and Nujol (liquid paraffins, d = 0.88–0.89, used commonly in infrared spectrometry), adenosine gives very stable MH^+ ions with no fragments (Figure 3). Sometimes M_2H^+ and MH^+H_2O ions were observed as shown. Therefore the protonated molecule (MH^+) of adenosine produced by the LI method is thought to be stable. In contrast, guanosine gives much fragmentation, since the MH^+ ion of guanosine is less stable than that of adenosine. The stability of cytidine has been found somewhere between these two nucleosides (*21*). Three spectra of guanosine obtained by the LI method (about 170 °C) are shown in Figure 4 to indicate the effect of a matrix. Without a matrix or with glycerol, $(BH)_nH^+$ ions (n = 1–4, although 3 and 4 are not shown in Figure 4a) were observed as the dominant peak, but no MH^+ ion. When guanosine was examined with the Nujol and with *n*-hexadecane as the matrix, MH^+ ions were obtained as shown in Figure 4b,c, respectively, although $(MH^+ - H_2O)$ was the base peak. A similar effect of Nujol has been obtained for adenosine, cytidine, and creatine (*21*). We concluded that alkanes are better matrices than glycerol for these compounds which have less proton affinities. The compounds may be partly soluble or suspended in alkanes. As hexadecane gave more abundant MH^+ ions than Nujol did, another alkane might be a better matrix than hexadecane. The interaction between glycerol molecules and a ribose of guanosine (also for adenosine or cytidine) is thought to be large, so that the bond cleavage between the base (B) and the ribose occurs when glycerol is used.

It is interesting to note that the relatively intense peaks at *m/z* 302 and 320 (Figure 4) corresponding to the MH^+H_2O and MH^+2H_2O ions, respectively, were observed, even when no water was used, because the composition of guanosine used was $M{\cdot}xH_2O$. An intense MH^+H_2O peak has been observed also for creatine (*21*) and a synthetic compound, both of which contain one water molecule of crystallization.

Sucrose. Sucrose is a well-known nonvolatile compound and has been extensively studied by numerous investigators with a variety of soft ionization methods (*2*, *25–28*). A field desorption spectrum exhibits the MH^+ ions as the base peak (*25*), but the cationized molecule such as $(M + Na)^+$ was reported also as the dominant peak (*2*, *26*). Severe temperature (and heating rate) dependence of the mass spectrum has been reported (*17*, *27*). Therefore sucrose was examined by the LI method in order to clarify the characteristics of the method and to investigate the effects of a high electric field and additives. At first, a silicon emitter was tested as the sample holder, and we found that a good spectrum was obtained by rapid heating, especially during the early period of heating. During continual heating, however, a variety of fragment ions were produced from sucrose and their abundances increased (*20*). The spectral pattern changes so rapidly that it is not easy to obtain a reproducible good mass spectrum. It was later found that the needle sample holder was much better than the silicon emitter due to better focusing of ions as mentioned in the Experimental Section. Mass spectra in Figure 5 were obtained with the needle, indicating the effects of the needle and additives which were water (solvent), Nujol (matrix), and ethanolamine (reagent or stabilizer). The mass spectrum (Figure 5a) was obtained from an aqueous solution of sucrose (about 1 $\mu g/\mu L$ H_2O) mixed with Nujol (1 μL) and recorded in one scan (7 s). The abundance of fragment ions increased with time, but slower than that observed by using the silicon emitter. Although the aqueous solution without a matrix gave a similar mass spectrum, the $(MH^+ - H_2O)$ ion was generally more abundant than the MH^+ ions. The mass spectrum of Figure 5b was obtained from the same sample as used in Figure 5a, with 0.2 μL of aqueous solution of ethanolamine (10^{-1} M) which was deposited on the wall inside the ion source when the mass spectrum was recorded. The peak at *m/z* 386 of the adduct ion, $MH^+E - H_2O$ (E, ethanolamine), was obtained as the dominant peak which was two to five times more intense than the MH^+ in the case of Figure 5a. The mass spectrum shown in Figure 5c was obtained the same way as was that in Figure 5b, except only a trace of ethanolamine (10^{-2} M aqueous solution) was used in the ion source. Each mass spectrum in Figure 5b and Figure 5c is the summed spectrum of four and five scans, respectively.

The dimeric ions, M_2H^+, and their fragments (*m/z* 505: $M_2H^+ - 180$, etc.) are often observed for sucrose. The time and temperature dependencies of the main ions from sucrose under similar conditions of Figure 5c are shown in Figure 6 which indicates that the M_2H^+ and its fragment ions appear soon after the sample loading on the needle (within 10 s); then the abundant MH^+ ion group (MH^+H_2O, $MH^+ - H_2O$ etc.) increased up to their maximum and finally fragment ions (*m/z*

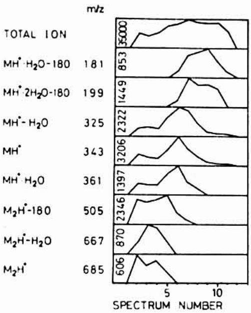

Figure 6. Time (temperature) dependences on the abundances of main ions from sucrose.

181 etc.) from the MH$^+$ ion group are produced. Each spectrum was recorded every 10 s. The time dependencies of main ions are reproducible at an optimum heater current (150–180 °C, the heater current was fixed). In many cases, the M$_2$H$^+$ ion appears earlier than the MH$^+$ ion does and there is no relation between the abundances of MH$^+$ and M$_2$H$^+$ ions. The results are considered as another proof of liquid surface ionization. The results also indicate that a minute amount of ethanolamine in water has a beneficial effect on producing the abundant MH$^+$ ion and a reproducible mass spectrum. There is also the possibility of finding some better additives for sucrose. Fragment ions like (A$^+$ − 180) may be produced by the bond cleavage (accompanied by a hydrogen rearrangement) at both sides of the center oxygen, although only one side is indicated in Figure 5.

Phospholipids. Recently FD (*29*) and FAB (*30, 31*) were reported as powerful techniques for obtaining molecular ions of phospholipids which are well-known thermolabile compounds. However, only a few fragment ions have been obtained by FD (*29*) and the interpretation of the FAB and SIMS spectrum (*30*) is not easy due to the existence of complexed ions.

Several phosphatidylcholines (PC) such as 1,2-dimyristoyl-*sn*-glycero-3-phosphocholine, 1,2-dipalmitoyl-*sn*-glycero-3-phosphocholine, 1,2-distearoyl-*sn*-glycero-3-phosphocholine, 1,2-dioleoyl-*sn*-glycero-3-phosphochiline, and their mixtures were examined by the LI method. A sample containing 1–10 μg of PC in 1–5 μL of methanol (or methanol–chloroform) solution was mixed well with 1 μL of a matrix and deposited on the needle tip with a glass rod. For a comparison, the sample solution, concentrated by warming it, was also examined to obtain a mass spectrum without a matrix. Liquid paraffins were found to be useless for PC, because such a matrix did not dissolve (nor suspend) the sample. Glycerol was found to be a moderately good matrix; therefore the proton affinities of the phospholipids are greater than that of glycerol. The mass spectrum obtained from the concentrated solution was similar to that with glycerol. If the amount of PC was less than 1 μg, glycerol should be used.

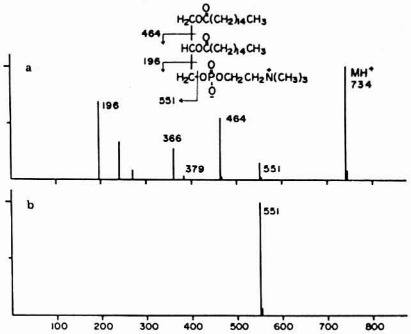

Figure 7. Mass spectra of 1,2-dipalmitoyl-*sn*-glycero-3-phosphocholine (matrix, glycerol): (a) at lower heater current (around 150 °C); (b) at higher heater current (around 180 °C).

As an example, the mass spectrum of 1,2-dipalmitoyl-*sn*-glycero-3-phosphocholine is shown in Figure 7. The MH$^+$ ion was observed as the base peak soon (within 5 s) after the sample introduction at an optimum heater current (1.25 A, a needle temperature of ~150 °C). Then fragment ions increased in abundances as shown in Figure 7a, that is, the summed mass spectrum of four scans. If the heater current was increased slightly (1.30 A, ~180 °C), the peak at m/z 551 corresponding to (M − phosphocholine)$^+$ ions became dominant as shown in Figure 7b. The diacyl ions (m/z 551) are abundant and stable at the higher temperatures, but sparse at the lower temperatures. Therefore diacyl ions may be produced from thermal decomposition products of the parent molecules. The FD spectrum of this compound showed dominant peaks at m/z 734 (MH$^+$), sometimes m/z 756 (M + Na)$^+$, and m/z 551 (*29*). The FAB and SIMS mass spectrum showed peaks at m/z 550, 496, 480, and 224 (and 184) (*30*). It is not easy to elucidate the structure of the compound from these peaks. In contrast, major fragment ions in the LI spectrum were observed at m/z 551 (diacyl ion), m/z 464 (M − RCOOCH$_2$)$^+$, and at m/z 196 (CH$_2$OPO$_3$CH$_2$CH$_2$N$^+$(CH$_3$)$_3$), indicating good correlation between the mass spectrum and the structure. An intense fragment peak at m/z 328 (weak in Figure 7) was observed for this compound in the mixture and the same type of fragment ions (one acyl + 59) were observed for other components. As the relative abundances of these ions change rapidly with temperature, a data processing system with a computer should be used for accurate measurements. The MH$^+$ and mass 551 ions give information about the sum of two acyl groups. The fragment ion of mass 464 includes one acyl group whose position has not been determined, but is assumed to be at position 2 from its mass. The ion of mass 328 also includes one acyl group. Mass spectra of other standard compounds and their mixtures showed similar fragmentations, suggesting the possibility of analyzing for phosphatidylcholines in a mixture. Such results will be reported in detail elsewhere.

Application of a Labeling Compound for Determination of Active Hydrogens and CAD Spectrum. Structure elucidation of a complex product is often aided considerably by knowledge of the number of active (or acidic) hydrogens present in the molecule. The qualitative determination of active hydrogen is accomplished by equilibrating the sample with D$_2$O and measuring the resulting change in molecular weight (*32, 33*).

This technique is applicable to nonvolatile compounds by the LI method. Since the ion source for LI is at atmospheric pressure, the LI method provides easy sample handling. Since the production of ions from a few micrograms of a sample like an amino acid lasts generally for 2–5 min, a labeling compound such as D$_2$O can be introduced even when a mass spectrum of the sample is being measured. Besides, only a small amount (1–5 μL) of D$_2$O is required in order to observe the change in molecular weight.

As an example, a part of the mass spectrum of alanine is shown in Figure 8. At first, the mass spectrum around the MH$^+$ peak (m/z 90) was being recorded repeatedly (one scan

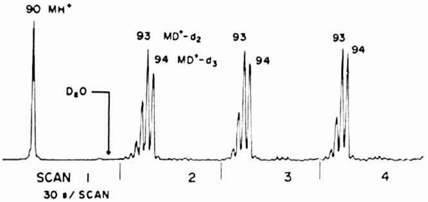

Figure 8. Increase in mass number of protonated molecule of D,L-alanine.

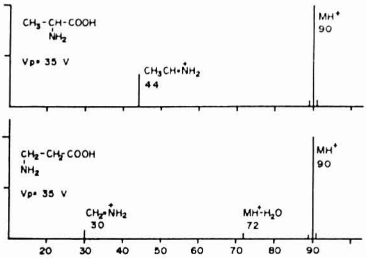

Figure 9. Mass spectrum of D,L-alanine and β-alanine at V_p of 35 V (partly CAD).

per 30 s) using about 1 μg of alanine (10^{-1} M aqueous solution) without D_2O.

Then 1 μL of D_2O was deposited on the glass wall near the port for sample introduction inside the ion source. Soon after the D_2O introduction, the mass spectrum changed as shown in Figure 8. The increase in the number of peaks and in their mass number (91 to 94) indicates that three hydrogens in the molecule are replaced (MH^+ (90) → MD^+-d_3 (94)) by deuterium atoms. This number, 3, corresponds to the N–H_2 and COO–H groups of alanine.

D,L-Alanine, β-alanine, proline, valine, serine, threonine, cysteine, and lysine were examined by the same procedure and showed the expected changes in the mass number for each MH^+ ion. In the case of lysine, however, one small extra peak was observed at m/z 154, although the peak was small enough to distinguish the number of active hydrogens. These results suggest that the number of active hydrogens for most amino acids could be measured by this technique with D_2O. In the case of adenosine and cytidine, however, one extra peak was clearly observed, indicating that some hydrogen atom(s) attached to carbon atom(s) exchange with deuterium. Although the phenomena are still under investigation, it suggests that such reactions occur at the liquid surface, because the CI (D_2O) spectrum for adenosine has shown no extra H–D exchange (*33*).

The mass spectra of D,L-alanine and β-alanine shown in Figure 9 indicate a good correlation with the structure of the compounds. As these amino acids gave abundant MH^+ ions with no fragment ions, the spectra were measured at a pinhole voltage (V_p) of 35 V at which a few fragment ions were produced by a kind of collisional activation (CAD) (*19*). The peak at m/z 44 of alanine (Figure 9a) corresponds to $CH_3CHNH_2^+$. The peaks at m/z 72 and 30 of β-alanine (Figure 9b) correspond to ($MH^+ - H_2O$) and $CH_2NH_2^+$, respectively, and if the V_p is increased to 70 V, the peak at m/z 45, $(COOH)^+$, is observed. Thus these two isomers can be distinguished easily. The number of active hydrogens in the fragment ions of alanine and proline measured by our technique agreed with the expected number. When a sample compound was unknown, the most probable structure of fragment ions of mass 44 and 30 having two active hydrogens may be $CH_3CHNH_2^+$ and $CH_2NH_2^+$, respectively. These data should be accumulated not only for analytical purposes but also for study of chemical reactions.

CONCLUSION

Use of a matrix and a reagent (e.g., ethanolamine) increases the abundance of MH^+ ions. The matrix has to be a proton donor to a sample molecule similar to the reagent gas in CI. It holds (and solvates or suspends) a sample on the needle tip, and lowers the activation energies for desorption of ions and molecules.

The mass spectrum obtained by this method is somewhat different from those obtained by other methods of ionization as seen in Figures 4–7, probably due to a slightly different mechanism, namely, liquid surface ionization and field assisted thermal desorption at atmospheric pressure. We can obtain several different mass spectra for one compound in a short period of time by using several reagents such as ethanolamine, D_2O, and any compounds with less proton affinities than that of a sample compound. Systematic studies on properties of compounds (sample and additives) by the method should be done not only for analytical purpose but also for other chemical fields.

The method has several advantages: (1) soft ionization and a simple rule for molecular weight estimations; (2) a useful mass spectrum, correlation between the structure of a compound and its mass spectrum is good (better than EI spectrum), CAD spectrum can be obtained easily; (3) ease of sample handling, either a microsyringe, a rod, or a tube can be used for introducing a sample and additives; (4) free use of additives, additives can be used even while a mass spectrum is being measured; (5) low background, no background ion is produced in vacuum, it is easy to clean the ion source (the only problem is plugging of the pinhole, although it occurs rarely when using a solvent or a matrix); (6) high sensitivity, useful mass spectra can be obtained with 10^{-7}–10^{-9} g of a sample, detection limit (single peak) is 10^{-13} g.

The method gives information about the structure of a compound, the reaction mechanism, and the properties of compounds probably in a condensed phase as well as in a gas phase. Such information must be useful not only for further development of our method but also for FD, FAB, MS/MS, and LC/MS.

ACKNOWLEDGMENT

We wish to thank K. Saito for his helpful discussion and his kind gifts of phospholipid standards and T. Taira for his help.

Registry No. Argon, 7440-37-1; glycerol, 56-81-5; ethanolamine, 141-43-5; sucrose, 57-50-1.

LITERATURE CITED

(1) Schulten, H.-R. *Int. J. Mass Spectrom. Ion Phys.* **1979**, *32*, 97.
(2) Posthumus, M. A.; Kistemaker, P. G.; Meuzelaar, H. L. C. *Anal. Chem.* **1978**, *50*, 985.
(3) Macfarlane, R. D.; Torgerson, D. F. *Science* **1976**, *191*, 920.
(4) Benninghoven, A.; Sichtermann, W. *Anal. Chem.* **1978**, *50*, 1180.
(5) Barber, M.; Bordoli, R. S.; Sedgwick, R. D.; Tyler, A. N. *Nature (London)* **1981**, *293*, 270.
(6) Kambara, H. *Anal. Chem.* **1982**, *54*, 143.
(7) Thomson, B. A.; Iribarne, J. V.; Dziedzic, P. J. *Anal. Chem.* **1982**, *54*, 2219.
(8) Baldwin, M. A.; McLafferty, F. W. *Org. Mass Spectrom.* **1973**, *7*, 1353.
(9) Ohashi, M.; Nakayama, N.; Kudo, H.; Yamada, S. *Mass. Spectrosc. (Tokyo)* **1976**, *24*, 265.
(10) Hansen, G.; Munson, B. *Anal. Chem.* **1978**, *50*, 1130.
(11) Hunt, D. F.; Shabanowitz, J.; Botz, F. K.; Brent, D. A. *Anal. Chem.* **1977**, *49*, 1160.
(12) McLafferty, F. W.; Kornfeld, R.; Haddon, W. F.; Levsen, K.; Sakai, I.; Bente, P. F., III; Tsai, S.-C.; Schuddenmage, H. D. R. *J. Am. Chem. Soc.* **1973**, *95*, 3886.

(13) Carroll, D. I.; Dzidic, I.; Stillwell, R. N.; Haegele, K. D.; Horning, E. C. *Anal. Chem.* **1975**, *47*, 2369.
(14) McFadden, W. H. *J. Chromatogr. Sci.* **1980**, *18*, 97.
(15) Dedieu, M.; Juin, C.; Arpino, D. J.; Guiochon, G. *Anal. Chem.* **1982**, *54*, 2372.
(16) Blakely, C. R.; Vestal, M. L. *Anal. Chem.* **1983**, *55*, 750.
(17) Cotter, R. J. *Anal. Chem.* **1980**, *52*, 1589A.
(18) Tsuchiya, M.; Taira, T. *Int. J. Mass Spectrom. Ion Phys.* **1980**, *34*, 351.
(19) Tsuchiya, M.; Seita, K.; Taira, T. *Mass Spectrosc. (Tokyo)* **1980**, *28*, 235.
(20) Tsuchiya, M.; Nonaka, T.; Taira, T. 30th Annual Conference on Mass Spectrometry and Allied Topics, Honolulu, 1982; paper WPB-06.
(21) Kuwabara, H.; Tsuchiya, M. *Mass Spectrosc. (Tokyo)* **1982**, *30*, 313.
(22) Tsuchiya, M.; Nonaka, T.; Taira, T.; Tanaka, S. *Mass Spectrosc. (Tokyo)* **1982**, *30*, 95.
(23) Schueler, B.; Krueger, F.R. *Org. Mass Spectrom.* **1980**, *15*, 295.
(24) Eicke, A.; Sichtermann, W.; Benninghoven, A. *Org. Mass Spectrom.* **1980**, *15*, 289.
(25) Moor, J.; Waight, E. S. *Org. Mass Spectrom.* **1974**, *9*, 903.
(26) Schulten, H.-R. *Methods Biochem. Anal.* **1979**, *51*, 317.
(27) Hansen, G.; Munson, B. *Anal. Chem.* **1978**, *50*, 1130.
(28) Carroll, D. I.; Dzidic, I.; Horning, M. G.; Montgomery, F. E.; Nowlin, J. G.; Stillwell, V. N.; Thenat, J. P.; Horning, E. C. *Anal. Chem.* **1979**, *51*, 1858.
(29) Sugatani, J.; Kino, M.; Saito, K.; Matsuo, T.; Matsuda, H.; Katakuse, I. *Biomed. Mass Spectrom.* **1982**, *9*, 293.
(30) Aberth, W.; Straub, K.M.; Burlingame, A. L. *Anal. Chem.* **1982**, *54*, 2029.
(31) Ohashi, Y.; Heller, D.; Fenselau, C., submitted for publication in *Biomed. Mass Spectrom.*
(32) Biemann, K. "Mass Spectrometry"; McGraw-Hill: New York, 1962; Chapter 5.
(33) Hunt, D. F.; McEwen, C. N.; Upham, R. A. *Anal. Chem.* **1972**, *44*, 1292.

RECEIVED for review June 6, 1983. Accepted October 5, 1983.

Photothermal Deflection Densitometer for Thin-Layer Chromatography

Tsuey Ing Chen and Michael D. Morris*

Department of Chemistry, University of Michigan, Ann Arbor, Michigan 48109

Photothermal deflection is used as the basis of a sensitive densitometer for thin-layer chromatography. An argon ion laser delivering 20 mW at 488 nm is used as the source and a 2-mW He–Ne laser is used as the probe. The system is applied to separation of 1,2-naphthoquinone, phenanthrenequinone and α-ionone. Detection limits for the compounds range from 30 ng to 7.5 pg, depending upon how strongly absorbing the compound is.

Thin-layer chromatography (TLC) is a simple, rapid, and versatile separation technique. In recent years, TLC technology has benefited from the introduction of "high-performance" plates, coated with very uniform layers of 5 or 10 μm diameter silica (*1–3*). High-performance thin-layer chromatography (HPTLC) requires both improved sample introduction techniques and improved detection systems. In this paper we describe a laser-based densitometer suited to HPTLC.

Diffuse reflectance spectrometry is probably the most popular TLC detection technology. The principles and limitations are well understood (*4, 5*) and commercial instruments are available. Detection limits for this technique are typically in the low nanogram range (*5*). However, there is a need for more sensitive detectors. Fluorescence detection is the most common alternative to reflectance measurements (*5*). Detection limits are often in the 1–10 pg range. Fluorescence detection is limited to those compounds which fluoresce or for which suitable fluorescent derivatives can be conveniently prepared.

Photoacoustic spectroscopy has been suggested as an alternative for nonfluorescent compounds (*6–10*). The first qualitative use of photoacoustic spectroscopy (PAS) in TLC was demonstrated by Rosencwaig and Hall in 1975 (*6*). More recently, Castleden and co-workers (*7*) have proposed quantitative photoacoustic determinations of fluorescein compounds separated by TLC. Fishman and Bard (*9*) have developed an open-ended PAS cell that can be placed directly on a TLC plate. Lloyd et al. (*10*) have reported PAS studies of TLC plates themselves by using Fourier transform infrared (FTIR) PAS with both gas-microphone and piezoelectric transducer detection. In these studies the detection limit of photoacoustic spectroscopy on TLC plates has been reported to be the range of low nanograms to high picograms.

Recently, thermal lens spectroscopy has been proposed as an alternative to photoacoustic spectroscopy (*11–16*). The change in the index of refraction of a sample caused by absorption of light and subsequent heat generation is measured. The conventional thermal lens experiment is not directly applicable to opaque solids. However, a thermal lens can be formed in a coupling gas, such as air, over a solid sample and probed as the deflection of a low power laser (*17–20*). This experiment is called photothermal deflection, or the "mirage effect". Photothermal deflection has been used as the detection scheme for Fourier transform infrared spectrometry of solids (*20*).

In this paper, we report first results on the development of a simple photothermal deflection system for quantitation of thin-layer chromatograms.

EXPERIMENTAL SECTION

The photothermal deflection system used for these experiments is based on our earlier thermal lens designs (*21*) and is shown in Figure 1. As the light source, we used the 488.0-nm laser line from an argon ion laser (Coherent, Inc., CR-6) loosely focused on the TLC plate. The laser could not be operated stably at low enough powers for this experiment. Therefore, the power was maintained at 40 mW at the laser head and attenuated to 20 mW with a neutral density 0.3 filter. A periscope and a 90° prism were used to aim the laser beam onto the sample. A 73-mm focal length lens was used to control beam size. Reflection losses along the transmission optics train reduced the power to about 15 mW at the sample.

A mechanical chopper (Laser Precision, CTX-534) operated at 11 Hz was used to modulate the argon laser beam. A 2-mW He–Ne laser (Uniphase, 1103P) was used as the probe laser. A razor blade in the light path was used to detect beam deflection.

0003-2700/84/0356-0019$01.50/0 © 1983 American Chemical Society

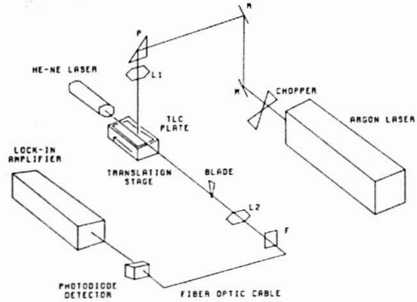

Figure 1. Photothermal deflection system: M, aluminum mirror; P, right angle prism; L_1 and L_2, 73 mm focal length lens; F, 3-66 filter.

The blade was fastened to a lens mount so that the fraction of the probe beam passed could be adjusted. The light passed by the blade was focused into a 4-m length of 400-μm diameter Pifax optical fiber to a photodiode (EG&G DT-25) located close to the remainder of the electronics. In order to avoid the noise due to room air currents, the entire optical system from the prism to the fiber was enclosed in an aluminum case.

A lock-in amplifier (EG&G/PARC 5101) was used to demodulate the photothermal deflection signal. The output filter had a 1-s time constant and 12 dB/octave attenuation. A small computer equipped with a 12-bit A/D converter was used to sample and store the lock-in amplifier output. It also performed peak height and area measurement and smoothing operations. On occasion, a strip chart recorder was used to take data.

The chromatogram was scanned by placing the plate on a translation stage driven by a motorized micrometer (Oriel). Provision was made to adjust the height of this stage to maximize the signal. With the system, a 50 mm length of a plate could be scanned. Typically, scan speed was 11 mm/min.

Precoated 10 cm × 10 cm HPTLC plates were obtained from Whatman. The test compounds α-ionone, phenanthrenequinone, and 1,2-naphthoquinone were obtained from Aldrich and used as received. Compounds were initially diluted in acetone to about 10 mg/mL and stock solutions were stored below 4 °C. Stock solutions were further diluted with acetone just before use. Ceric sulfate prepared by adding 42 g of $(NH_4)_4Ce(SO_4)_4$ and 56 mL of concentrated H_2SO_4 in 1000 mL of distilled water was used as a chromogenic reagent.

Mixtures of the test compounds were applied as 0.05 μL volumes with a 0.5-μL Hamilton microsyringe equipped with a no. 3 needle. The chromatograms were developed with a solvent system of benzene/ethyl acetate (5:1, v/v) 3 to 4 cm in a Regis SB/CD chamber. Plates were dried in air first and then on a hot plate at 86 °C for 2 to 3 min. As soon as the plates cooled to ambient temperature, they were sprayed with ceric sulfate and heated on a hot plate at 92 °C for 8–10 min. The HPTLC plates were scanned after they cooled to ambient temperature.

RESULTS AND DISCUSSION

Under our experimental conditions, solvent development was about 36 mm and the separation between spot centers was about 3–4 mm. Samples were applied as spots of less than 1 mm diameter. Development increased this to become 1 and 2 mm. R_f values were 0.51 for 1,2-naphthoquinone, 0.63 for phenanthrenequinone, and 0.71 for α-ionone. Ceric ion oxidation produced spots which were brown (1,2-naphthoquinone and α-ionone) or yellow (phenanthrenequinone).

We have examined the dependence of signal/noise ratio on chopping frequency and on fraction of the probe beam passed by the razor blade. In agreement with our earlier thermal lens work (*21*), we found that although the signal decreased with increasing chopper frequency, signal/noise ratio remained constant over the test region 10–100 Hz. For this work a chopper frequency of 11 Hz was chosen.

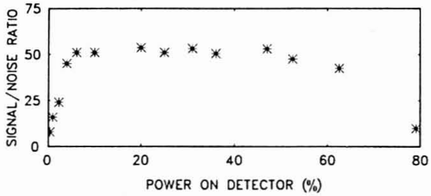

Figure 2. Dependence of signal/noise ratio on the fraction of the probe laser power passed by the razor blade.

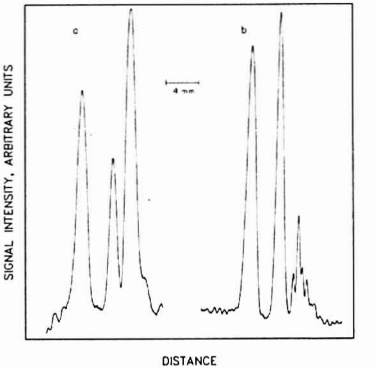

Figure 3. Photothermal deflection chromatograms of test compounds: (a) 144 ng of 1,2-naphthoquinone, 93 ng of phenanthrenequinone, and 149 pg of α-ionone; (b) 144 ng of 1,2-naphthoquinone, 186 ng of phenanthrenequinone, and 14.9 pg of α-ionone.

Figure 2 shows the dependence of signal/noise ratio on the fraction of the probe laser power passed by the razor blade. The signal/noise ratio maximizes over a very broad range, 6–45% passed. Thus, adjustment of the razor blade is not critical if an internal standard is used. Absolute measurements are satisfactory if the positions of the optical elements are fixed throughout a series of measurements.

Figure 3 shows a typical chromatograms for the compounds used. Chromatogram A shows all three compounds well above detection limits. In chromatogram B, the quantity of α-ionone is approaching the detection limits, and the peak is breaking up. The source of the breakup of peaks at very low concentrations is still uncertain. It may be due to irregularities in the coating of the TLC plate.

Peak areas are reproducible to about 2.5% and are linear in amount of analyte over almost 2 orders of magnitude. Negative deviations from linearity occur at high values of analyte. This deviation is expected, since the quantity measured is proportional to the percentage of the incident light absorbed and must reach a limit as the sample becomes more opaque. Similar working curves are obtained in photoacoustic spectrometry (22) and fluorimetry. Curvature is also predicted by the Kubelka-Munk equation for diffuse reflectance (*4, 5*). What is measured here is not strictly described by a Kubelka-Munk equation, since the heat evolution depends on heat conduction back to the surface (22) as well as on absorption.

Detection limits for the three compounds are as follows: α-ionone, 7.5 pg; 1,2-naphthoquinone, 2.3 ng; phenanthrenequinone, 31 ng. This disparity of 3 orders of magnitude arises because the laser line used is not really near an absorption maximum of the latter two compounds.

Shielding the detector from laboratory air currents is quite important. Noise levels are more than ten times greater when the apparatus is operated in the open air than when it is enclosed in a box. However, no special vibration isolation is necessary. We have successfully operated the system on a wooden table and on a honeycomb optical table. The flexibility of a wooden table is undesirable, but any rigid metal base is apparently adequate. Photothermal deflection is not sensitive to scattered light, unlike conventional densitometry or fluorescence.

The detector has not been optimized for laser spot size. Photothermal deflection and dual beam thermal lens systems operate best if both beams have approximately the same diameter. In these experiments we have reduced the argon ion laser beam size to match the helium–neon beam. This approach requires only one lens but produces a detector which samples only a small fraction of the cross section of the chromatographic spot. In future experiments we will explore the effects of expansion of both beams to more closely match spot diameters. The use of cylindrical lenses or prisms as beam expanders suggests the possibility of making a detector with slit-like cross section which approximates the ideal shape of a densitometer for thin-layer chromatography.

Photothermal deflection has been shown to be a simple and sensitive method for quantitation of thin-layer chromatograms. The detector is easy to align and stable for long periods. Only modest laser powers are needed to reach picogram sensitivity. Further reduction in laser power is possible with some refinement of the system. Thus, the device should be operable with inexpensive lasers, including devices which operate in the ultraviolet. Experiments toward these goals are under way in our laboratories.

Registry No. 1,2-Naphthoquinone, 524-42-5; phenanthrenequinone, 84-11-7; α-ionone, 127-41-3.

LITERATURE CITED

(1) Fried, B.; Sherma, J. "Thin-Layer Chromatography: Techniques and Applications"; Marcel Dekker: New York, 1982; pp 15–16.
(2) Fenimore, D. C.; Davis, C. M. *Anal. Chem.* **1981**, *53*, 252A–266A.
(3) Zlatkis, A., Kaiser, R. E., Eds. "High Performance Thin Layer Chromatography"; Elsevier: New York, 1977.
(4) Pollak, V. "Advances in Chromatography"; Giddings, J. C., Grushka, E., Cazes, J., Brown, P. R., Eds.; Marcel Dekker: New York, 1979; Vol. 17, pp 1–52.
(5) Coddens, M. E.; Butler, H. T.; Schuette, S. A.; Poole, C. F. *LC* **1983**, *1*, 282–289.
(6) Rosencwaig, A.; Hall, S. S. *Anal. Chem.* **1975**, *47*, 548–549.
(7) Castleden, S. L.; Elliott, C. M.; Kirkbright, G. F.; Spillane, O. E. M. *Anal. Chem.* **1979**, *51*, 2152–2153.
(8) Burggraf, L. W.; Leyden, D. E. *Anal. Chem.* **1981**, *53*, 759–764.
(9) Fishman, V. A.; Bard, A. J. *Anal. Chem.* **1981**, *53*, 102–105.
(10) Lloyd, L. B.; Yeates, R. C.; Eyring, E. M. *Anal. Chem.* **1982**, *54*, 549–552.
(11) Harris, J. M.; Dovichi, N. J. *Anal. Chem.* **1980**, *52*, 695A–706A.
(12) Kliger, D. S. *Acc. Chem. Res.* **1980**, *13*, 129–134.
(13) Haushalter, J. P.; Morris, M. D. *Appl. Spectrosc.* **1980**, *34*, 445–447.
(14) Fujiwara, K.; Lei, W.; Uchiki, H.; Shimokoshi, F.; Fuwa, K.; Kobayashi, T. *Anal. Chem.* **1982**, *54*, 2026–2029.
(15) Mori, K.; Imasaka, T.; Ishibashi, N. *Anal. Chem.* **1982**, *54*, 2034–2038.
(16) Miyaishi, K.; Imasaka, T.; Ishibashi, N. *Anal. Chem.* **1982**, *54*, 2039–2044.
(17) Jackson, W. B.; Amer, N. M.; Boccara, A. C.; Fournier, D. *Appl. Opt.* **1981**, *20*, 1333–1344.
(18) Aamodt, L. C.; Murphy, J. C. *J. Appl. Phys.* **1983**, *54*, 581–591.
(19) Murphy, J. C.; Aamodt, L. C. *J. Appl. Phys.* **1980**, *51*, 4580–4588.
(20) Low, M. J. D.; Lacroix, M.; Morterra, C. *Appl. Spectrosc.* **1982**, *36*, 582–584.
(21) Buffett, C. E.; Morris, M. D. *Anal. Chem.* **1982**, *54*, 1824–1825.
(22) Rosencwaig, A. "Photoacoustics and Photoacoustic Spectroscopy"; Wiley: New York, 1980.

RECEIVED for review June 6, 1983. Accepted October 3, 1983. This work was supported by Research Grant GM28484 from the National Institutes of Health.

Comparison of Suppressed and Nonsuppressed Ion Chromatography for Determination of Chloride in Boric Acid

H. H. Streckert* and B. D. Epstein

GA Technologies, Inc., P.O. Box 85608, San Diego, California 92138

A comparison was made of suppressed and nonsuppressed ion chromatography (IC) to determine chloride ion in boric acid solutions. On first inspection, it appears that good separation between borate and chloride is obtained with suppressed IC. However, quantitation of chloride is complicated by an unidentified matrix effect. This determination can be accomplished with nonsuppressed IC. Chloride is concentrated on a small precolumn prior to separation on a silica-based anion exchange resin. Chloride can be determined at concentrations as low as 2 ppb in boric acid solutions.

Ion chromatography (IC) is attracting considerable interest as an analytical technique for the determination of ions in solution (*1–3*). Small et al. (*4*) developed the method of using conductometric detection to monitor ion-exchange separations. Ions are separated on a column containing a low-capacity ion-exchange resin. The effluent from the separator column is subsequently passed through a suppressor column which converts the highly conducting eluent to one of much lower conductance. With the high background conductivity thus reduced, the ions of interest are detected conductometrically.

Fritz et al. (*5, 6*) described a method of IC which does not require the use of a suppressor column. A low-capacity resin is employed in conjunction with a low conductivity eluent which can be passed directly through the conductivity detector. Both suppressed and nonsuppressed techniques have been employed for anion analyses in water samples (*1–6*).

Quantitative determination of chloride ion impurity in boric acid solutions is an important requirement in the nuclear reactor industry. Boric acid is added to the primary coolant in pressurized water reactors to aid in the control of reactivity. Chloride ion can lead to stress corrosion of reactor components. Typical procurement specifications allow a maximum of 0.4 μg of chloride/g of boric acid (ppm) (*7*). Due to the limited solubility of boric acid in water (~50 g/L), a maximum solution concentration of ~20 μg/L (ppb) chloride will be obtained by dissolving boric acid at ambient temperature.

Chloride can be determined at the parts-per-billion level in aqueous media by a spectrophotometric technique (*8*). Solutions of ferric ammonium sulfate and mercuric thio-

0003-2700/84/0356-0021$01.50/0 © 1983 American Chemical Society

cyanate are added to the sample. The chloride ion reacts with the mercuric thiocyanate to liberate thiocyanate ion. Thiocyanate complexes with ferric ion to form red ferric thiocyanate which has been shown to obey Beer's law.

This method has several disadvantages. One drawback arises from high blank readings produced by the ferric ammonium sulfate and mercuric thiocyanate reagents. A high blank coupled with a low incremental absorbance due to the ferric thiocyanate complex at low chloride levels limits the usefulness of this technique.

Two methods of IC, suppressed and nonsuppressed, for the determination of chloride in boric acid are compared in this paper. It is demonstrated that suppressed IC can give erroneous results for the impurity chloride concentration. Nonsuppressed IC yields adequate sensitivity and specificity for the analysis. Boric acid solutions have been analyzed successfully for low ppb concentrations of chloride with nonsuppressed IC.

EXPERIMENTAL SECTION

Apparatus. A Dionex Model 2010i ion chromatograph, modified as described below, was used throughout the study. Chromatograms were recorded either on a Hewlett-Packard Model 3390A recording integrator or a Linear Instruments Corp. Model 255 strip chart recorder. In all cases the detector response parameter used was peak height.

Suppressed IC. A 3 × 50 mm anion guard column was used in series with a 3 × 150 mm anion separator column (Dionex, HPIC-AS2) and a fiber suppressor (Dionex). The eluent consisted of a solution of 3×10^{-3} M Na_2CO_3 and 2×10^{-3} M NaOH. The flow rate was 2.3 mL/min. The fiber suppressor was continuously regenerated with 0.025 N H_2SO_4. A Dionex Model CDM-1 conductivity detector was employed. Injection volumes ranged from 50 to 150 μL.

Nonsuppressed IC. A 4.6 × 250 mm standard anion column (Wescan) was used with a 3.9×10^{-3} M potassium acid phthalate (pH 4.1) eluent. The flow rate was 2.3 mL/min. A concentrator column consisting of a 4.6 × 30 mm Ion-Guard Anion Cartridge in an Ion-Guard Holder (Wescan) replaced the sample loop in the injection valve and was loaded "on-line" in order to avoid sample contamination. Samples were loaded either manually with a plastic syringe or with a Cole-Parmer Model 7013 peristaltic pump at a rate of ~1 mL/min. A Wescan Model 213A conductivity detector was employed. A calibration curve was obtained by injecting freshly prepared standards containing 4, 8, 16, 32, and 64 ppb chloride, respectively.

Reagents. Chemicals which were used as received were NaOH (Baker), Na_2CO_3, and potassium acid phthalate (Mallinckrodt). NaCl (Baker) was dried at 120 °C for 3 h prior to use. Chloride standard solutions were prepared from a 1000 mg/L stock solution. Boric acid samples were obtained from Southern California Edison, San Onofre Nuclear Generating Station. Water used throughout the study was distilled water which was subsequently passed through a Barnstead Ultrapure mixed bed resin. It was analyzed by IC to contain ≲0.5 ppb chloride. All eluents were made from this water after boiling.

RESULTS AND DISCUSSION

Suppressed Ion Chromatography. Most of the work was performed with a pellicular anion-exchange resin containing partially sulfonated polystyrene/divinylbenzene beads and an eluent consisting of a 3×10^{-3} M Na_2CO_3 and 2×10^{-3} M NaOH. Initially, we sought to determine whether chloride can be detected with adequate sensitivity in the presence of a large excess of boric acid. A 150-μL sample loop proved sufficient to obtain a good chloride response.

A typical chromatogram of the impurity chloride in boric acid is shown in Figure 1. The negative peak, A, commonly referred to as a "water dip", results from the dilution of the eluent by the water sample. The large peak B, having an elution time of ~1.3 min from the point of injection, is due to borate. After nearly base line resolution the chloride elutes at ~3.8 min, peak C. Peak D is due to sulfate and is observed at ~13 min. For this comparison only the chloride was considered. At first inspection it appears that good separation between borate and chloride is obtained under the chromatographic conditions employed in this study.

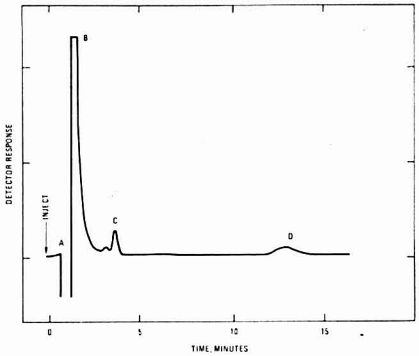

Figure 1. Chromatogram of a 3% boric acid solution obtained under suppressed IC conditions (see Experimental Section). Peak A is the "water dip". Peaks B, C, and D are due to borate, chloride, and sulfate, respectively.

Table I. Chloride Analysis in Boric Acid

sample (% boric acid)[a]	detector response for chloride: suppressed IC	detector response for chloride: nonsuppressed IC
0.5	62	—[b]
1.0	120	10
2.0	40	18
4.0	47	45

[a] Four grams of boric acid was dissolved in 100 mL of water. Successive dilutions of this sample were made to obtain the other samples. [b] No peak above the noise level was observed for this sample.

The good sensitivity and apparently adequate separation obtained in these chromatograms seemed to allow the quantitative analysis of chloride. However, the chloride response depends not only on the chloride concentration but also on the boric acid concentration as evidenced by the following experiment. Samples containing 40, 20, 10, and 5 g of boric acid per liter were analyzed. Eliminating adventitious sources of chloride contamination, the chloride response should be in proportion to the boric acid content. The results given in Table I show that a matrix effect is occurring. As the boric acid concentration increases the chloride response increases initially but then declines. This type of behavior prevents quantitation of chloride by a calibration curve obtained in the absence of boric acid.

Attempts to quantify the chloride concentration by the standard additions method were also limited by this type of matrix effect. As the chloride concentration is purposely increased by spiking the sample with a standard chloride solution, a "leveled" chloride response is obtained. Plotting chromatographic response vs. standard added results in a straight line with a slope which is too low and an apparent chloride concentration which is artificially high. This can be demonstrated with a recovery study. Spiking a sample with 0.8 μg of chloride yielded a recovery in excess of that of an unspiked sample of ~1.2 μg of chloride. It should be noted that during the course of these experiments no change in retention times was observed, indicating that the capacity of

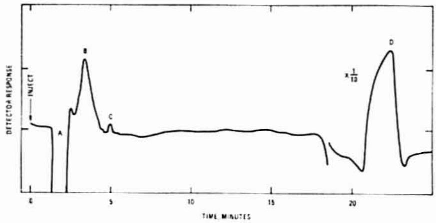

Figure 2. Chromatogram of a 4% boric acid solution obtained with nonsuppressed IC (see Experimental Section). Peak A is the "water dip". Peak B is attributed to be a solvent front disturbance. Peak C represents ~8 ppb chloride. Peak D has been identified as carbonate which coelutes with sulfate at the pH employed. Note the scale change for this peak. Borate is not retained under the conditions used to obtain this chromatogram.

the column was not exceeded and the column did not change with time.

In an attempt to minimize these matrix effects we diluted the eluent incrementally up to a factor of 2. This change resulted in better peak separation but did not improve the quantitation. Dissolving boric acid in the eluent, in the hopes of preequilibrating the sample, gave the same type of response. Adding 10^{-2} M mannitol to the eluent, in order to form a boric acid–mannitol complex also did not eliminate the matrix effects.

Nonsuppressed Ion Chromatography. Further investigation demonstrated that nonsuppressed IC could also be used to analyze for chloride in boric acid solutions. Good separation results with use of a low-capacity bonded-phase silica anion exchanger and a 3.9×10^{-3} M potassium acid phthalate eluent. To obtain the required sensitivity 10 mL of sample was preconcentrated on a small column containing the same ion-exchange resin as the analytical column. Because the boric acid itself is not retained on this type of column at the pH employed it is not concentrated and does not interfere with the chloride loading. The use of a preconcentrator column was precluded in this application of suppressed IC because the pellicular resin employed concentrates both chloride and borate. The preconcentrator column used for nonsuppressed IC cannot be employed for the suppressed IC because the silica-based resin in that column is not compatible with the eluent used for suppressed IC.

The concentrator column is substituted for the sample loop in the injection valve. After the sample is loaded onto the concentrator column, the ions that were retained are swept into the analytical column by directing the eluent flow through the concentrator column. It has been demonstrated previously that sample ions are quantitatively retained on the concentrator column during the loading process (*9*).

A typical chromatogram of a boric acid sample under these conditions is shown in Figure 2. The chloride elutes at ~5 min adjacent to a large peak attributed to be a solvent front disturbance. Sulfate and carbonate coelute at ~22 min. Varying the boric acid concentration has no adverse effect on the chloride response as demonstrated in Table I. No significant chloride peak was detected for the most dilute solution under our chromatographic conditions. However, at the 1% boric acid level a chloride peak was observed. The chloride peak increased monotonically as the boric acid content was increased to 4%.

A calibration curve was established which was linear from 4 ppb to 64 ppb in chloride with a correlation coefficient of 0.993. The detection limit in solution was determined to be about 2 ppb. This limit could be lowered by loading more sample onto the concentrator column. The absence of matrix effects and analytical utility of this technique was demonstrated by adding known amounts of chloride to a solution of boric acid. Three 50-mL samples of a 4% boric acid solution were spiked with 0.4, 0.8, and 1.6 μg of chloride. The results in Table II show that the recoveries ranged from 95 to 106%. The relatively consistent chloride recovery data indicate that there were no major interferences in the analysis.

Table II. Recovery Study for Nonsuppressed IC

μg of Cl^- added[a]	total μg of Cl^- found[b]	net μg of Cl^- found[c]	% recovery
0	0.24	—	—
0.40	0.62	0.38	95
0.80	1.05	0.81	101
1.60	1.94	1.70	106

[a] Amount of chloride added to 50 mL of 4% boric acid sample; 50-μL aliquots of an 8 ppm chloride standard were added incrementally. [b] Sample peak height was converted to concentration via interpolation of the calibration curve. The total chloride was then calculated from the sample volume and chloride concentration. [c] Amount of chloride found in excess of the amount found in the unspiked sample.

Table III. Chloride Analysis in Boric Acid

	chloride, ppm in solid[a]	
sample[b]	nonsuppressed IC[c]	spectrophotometric method[d]
842C-1	0.20	0.27
842C-13	0.18	0.16
842C-9	0.14	0.16
652C-73	0.09	0.13

[a] Concentration of chloride in 4% boric acid sample was determined by the indicated technique and then converted to micrograms of chloride per grams of solid boric acid. [b] Samples of boric acid obtained from Southern California Edison, San Onofre Nuclear Generating Station. [c] Measurements made by nonsuppressed IC are estimated accurate to ±10% based on recovery data. [d] The ferric ammonium sulfate/mercuric thiocyanate method was employed. Chloride was quantified by standard additions. Table entries are estimated to be accurate to ±30%.

The results of chloride analyses for boric acid solutions are presented in Table III. The values obtained are compared with data from the ferric ammonium sulfate/mercuric thiocyanate spectrophotometric method. Relatively good agreement between the two techniques is observed; the two determinations generally differ by less than 30% and are well within the error bars associated with each technique. These samples, obtained from Southern California Edison, San Onofre Nuclear Generating Station, are also in compliance with the procurement specifications (vide supra).

The absence of certified standards for chloride in boric acid makes it difficult to evaluate the absolute accuracy of the technique. However, the recovery data indicate that the accuracy of the quantitation of chloride can be in the range of 5–6% relative to the chloride present in excess of background. This finding coupled with the comparison to the spectrophotometric technique indicates that nonsuppressed IC could serve as a routine method for the determination of chloride in solid boric acid at the 0.4 ppm level.

In summary, while apparently good separation of chloride from borate can be obtained by using suppressed IC, quantitation of low level chloride is complicated by an unidentified matrix effect under the chromatographic conditions employed in this study. Quantitation of impurity chloride in boric acid can be accomplished by using nonsuppressed IC and a concentrator column to ensure the necessary sensitivity.

ACKNOWLEDGMENT

We thank John Dixon for performing the spectrophotometric chloride analyses. We are also grateful to Southern California Edison for providing boric acid samples and verification test plans.

Registry No. Boric acid, 11113-50-1.

LITERATURE CITED

(1) Rocklin, R. D.; Johnson, E. L. *Anal. Chem.* **1983**, *55*, 4-7.
(2) Green, L. W.; Woods, J. R. *Anal. Chem.* **1981**, *53*, 2187-2189.
(3) Pohlandt, C. *S Afr. J. Chem.* **1982**, *35*, 96-100.
(4) Small, H.; Stevens, T. S.; Bauman, W. C. *Anal. Chem.* **1975**, *47*, 1801-1809.
(5) Gjerde, D. T.; Fritz, J. S.; Schmuckler, G. *J. Chromatogr.* **1979**, *186*, 509-519.
(6) Gjerde, D. T.; Schmuckler, G.; Fritz, J. S. *J. Chromatogr.* **1980**, *187*, 35-45.
(7) Verification Test Procedure for Safety Related Boric Acid; Southern California Edison Co., San Onofre Nuclear Generating Station, San Onofre, CA.
(8) Iwasaki, I.; Utsumi, S.; Ozawa, T. *Bull. Chem. Soc. Jpn.* **1952**, *25*, 226-229.
(9) Wetzel, R. A.; Anderson, C. L.; Schelcher, H.; Crook, G. D. *Anal. Chem.* **1979**, *51*, 1532-1535.

RECEIVED for review June 30, 1983. Accepted September 19, 1983.

On-Line Extraction, Evaporation, and Injection for Liquid Chromatographic Determination of Serum Corticosteroids

Kitaro Oka, Kazuo Minagawa, and Shoji Hara*
Tokyo College of Pharmacy, Horinouchi, Hachioji, Tokyo 192-03, Japan

Makoto Noguchi, Yasuo Matsuoka, Michinori Kono, and Shoichiro Irimajiri
Kawasaki City Hospital, Kawasaki 210, Japan

To construct an on-line system for cleanup of biological fluids, closed-bed columns packed with fine diatomaceous earth granules were developed. Three cascaded columns were coated with neutral water, aqueous sodium hydroxide, and sulfuric acid since the extraction of neutral components with a high degree of selectivity is possible by such stationary phase liquids. The recovery of steroid solutes from sera was almost quantitative, using aqueous diethyl ether as the carrier. The effluent from the aqueous liquid-liquid partition columns was introduced into a line evaporator made of glass tubing. The injection of the sample into a liquid chromatography column was performed by inserting a steel stick for eliminating the dead space in the evaporator to resolve the residue. A model of an on-line equipped extraction, evaporation, and injection system was constructed by the incorporation of a valve switching procedure. This technique was applied to a clinical assay of corticosteroids in sera and was found suitable as a highly sensitive method for monitoring steroidal drugs.

For determination of constituents in biological fluids such as serum and urine samples, preliminary fractionation and/or enrichment of target compounds is usually recommended. Elimination of contaminants from the fluids consisting of a complex matrix enhances the sensitivity of analysis of the compounds under consideration. In many instances, the cleanup of biological fluids has been carried out by manual batch operation prior to high-performance liquid chromatography (HPLC) analysis. Recently, two new procedures have been introduced: (1) liquid-liquid distribution using columns packed with diatomaceous earth support and (2) prechromatography involving either a normal or reversed phase system employing a silica gel or octadecylsilyl silica columns. Commercially available disposable short columns such as Extrelut by Merck, Darmstadt, and Sep-PAK cartridges by Waters, Milford, MA, are being widely accepted by analytical chemists. However, it is difficult to transfer the effluent from the cleanup column directly into the main analytical system. Sample preparation by collecting the fraction and evaporation of the solvent is often necessary. Hence these prechromatographic techniques require off-line processes.

At our laboratory, column switching extraction and chromatography for programmed flow preparation (PFP) have been developed (*1*, *2*). PFP has improved the preparation system and avoids the defects encountered in former procedures using batch processing in chemical laboratory experiments. Through the PFP concept, an attempt has been made to develop an on-line technique for fractionation, evaporation, and injection in microchemical analysis. First, a suitable design for the liquid-liquid distribution column system for on-line procedure was investigated. Instead of the open-bed cartrige columns commonly employed in the laboratory, the closed-bed columns slurry packed by fine diatomaceous earth granules were introduced (*3*, *4*). These cleanup columns were found to have high efficiency and could be used repeatedly if the columns are flushed by water soon after the injection of certain amounts of biological fluids. Secondly, a new type of evaporator made by glass tube was developed to afford quantitative recovery of small amounts of solutes. There was hardly loss of any sample when the residue in the evaporator was injected into the analytical column (*3*). As a result, construction of the on-line system for switching extraction, evaporation, and injection into the HPLC column (LEEI system) was achieved. Several applications of this system revealed high sensitivity and efficiency for HPLC analysis of biological samples. In this paper, the application of this technique to the clinical analysis of serum corticosteroids is reported.

EXPERIMENTAL SECTION

LEEI System. A model for a switching fractionation and chromatography system is illustrated in Figure 1. This sytem is integrated by four functional operations: (a) presaturation of water for the mobile phase solvent; (b) sample application and extraction of the constituents; (c) evaporation of the effluent; (d)

0003-2700/84/0356-0024$01.50/0 © 1983 American Chemical Society

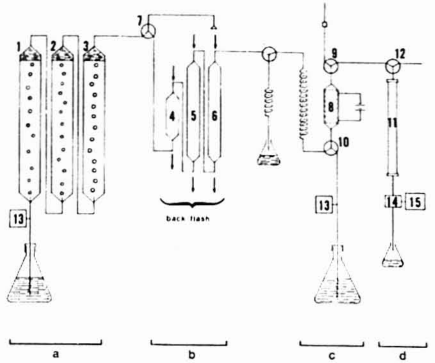

Figure 1. Schematic diagram of the on-line extraction–evaporation–injection (LEEI) system equipped with HPLC. See text for details.

HPLC analysis. The construction materials of the system consist of glass tubes, PTFE plugs and tubes, valves, pumps, and detectors. Thick-wall pressuretight glass tubes were connected by PTFE plugs so designed as to be easily inserted into the inside of the glass tubes and removable by hand (5). The upper pressure limit of the glass tube and PTFE plug connection with a metal clip is 50 kg/cm^2 and the PTFE plugs are connected by PTFE tubing.

System Operation (a). The solvent was pumped into glass tubes 1, 2, and 3 (2.2 cm i.d. × 30 cm) filled with water and an aqueous solution for equilibration of the solvent and water. The solvent was passed through the three cascaded tubes by a droplet current. Carrier solvent used was a commercial product of diethyl ether containing phenol derivatives as a stabilizer. Tube 1 was filled with a 15% sodium hydroxide solution to remove the phenolic additives. Tube 2 was filled with 25% sodium chloride solution for washing and tube 3 with distilled water to obtain a water-saturated mobile phase. The outlet of the solvent flow was connected to valve 7 of operation b using PTFE tubes (1 mm i.d.).

System Operation (b). Crude sample fluid was applied by use of a glass syringe and valve 7. A 0.5 mL, or a lesser amount, of serum sample was introduced into the cascaded columns (excolumns 4, 5, and 6) for fractional extraction of the constituents. These columns, provided with thin PTFE filters, were packed with fine diatomaceous earth granules (particle size, 10 μm, AquEx-10, DSD, Tokyo) by a slurry packing procedure using a gastight syringe. The column efficiency was determined by using caffeine as the standard sample and aqueous diethyl ether as the carrier. Excolumns 5 (4 mm × 20 cm) and 6 (4 mm × 20 cm) afforded approximately 300 theoretical plates. The packing support in the excolumn 4 (1 cm i.d. × 7 cm) was coated with distilled water. Water was injected into the column with a gastight syringe. The aqueous phase of excolumn 4 was washed out after each analytical run to remove any hydrophilic substances distributed in the aqueous phase, such as serum proteins, by injecting about 5 mL of distilled water from the top of the column. A subsequent fast flow of diethyl ether (10 mL/min) in a direction from top to bottom to remove excess water was required for conditioning prior to the next run. This backflash procedure is indicated by the arrow lines in Figure 1. In this figure, several valves for the conditioning process are abbreviated for clarity.

Diatomaceous earth in excolumn 5 was coated with 1% sodium hydroxide solution as the stationary phase. Support material in excolumn 6 was coated with 1% sulfuric acid. The aqueous stationary phases in these columns were conditioned by adding the corresponding aqueous solution from the top of the column and a fast flow of diethyl ether to remove the excess aqueous solution. Reconditioning of excolumn 5 was required for each 1 mL of serum injected.

After the serum was fed into excolumn 4, aqueous diethyl ether was injected to extract the ether-soluble components in the column. The mobile phase solvent was then moved through the cascaded columns step by step to eliminate acidic and basic contamination and to fractionate the neutral components at a flow rate of 0.8 mL/min.

System Operation (c). Evaporator 8 was constructed of a single glass tube (4 mm i.d. × 7 cm). Evaporation of the effluent was achieved in the inside wall of the tube at a reduced pressure (20 mmHg and 40 °C). The pressure was regulated by a water aspirator via valve 9. The temperature was maintained by an electric heater attached to the outer surface of the glass tube. Evaporator 8 was connected to excolumn 6 via valve 10 and a thin PTFE tube (0.1 mm i.d. × 1 m) which allowed switching to the higher pressure site of system operation b and the lower pressure site of operation c. At specified switching times of valve 10, the effluent containing neutral components was introduced into the evaporator and concentrated to dryness. Monitoring of the effluent by a UV detector was necessary for the pilot run, using a larger amount of authentic samples added to the serum. Following stipulation of the extraction time, it was conventional and sufficient to evaporate the proper amount of effluent containing all the desired materials without UV monitoring. The effluent emerging from the column within 5 to 17 min was collected for corticosteroid fractionation.

In order to minimize the diffusion of the fractionated solute, the inner dead volume of evaporator 8 was reduced. It was found that insertion of a stick within the glass tube served this purpose quite well. Consequently, a mechanically driven steel stick (3.9 mm i.d. × 6.9 cm) was attached to evaporator 8. On completion of the evaporation, the inner dead volume of the glass tube was reduced by insertion of this steel stick. The outlet of the tube was connected to HPLC column 11 (Lichrosorb S-100, 4 mm i.d. × 25 cm) via valve 12. The mobile phase solvent for HPLC was then introduced into the evaporator 8 via valve 10 at a flow rate of 0.1 mL/min and the inner air was pushed out through valve 12. When the solvent reached valve 12, it was directly switched to analytical column 11.

System Operation (d). The HPLC equipment consisted of a reciprocal pump (13) (Twincle, Jasco, Tokyo), a UV detector (14) (Uvidec 100-III, Jasco, Tokyo) set at 240 nm, and a pen recorder (15) (RC-150, Jasco). Generation of gasified solvent at the plunger site of the pump caused base line waving unfavorable for high sensitive nano-level analysis. Insertion of a glass tube (1 cm i.d. × 7 cm) as a damper between the pump and evaporator eliminated this line waving completely. Furthermore, the reciprocal pump generated other types of base line wavings owing to pressure pulse in the plunger. This noise could be reduced remarkably by a condensed air damper functioning as a neutralizer of pressure change. Base line stabilization was necessary for sensitive analysis within a detection range of 0.005 and recorder range of 2 mV.

Glass and PTFE components were supplied by Kusano Scientific, Tokyo.

Reagents and Solvents. Reagent grade chemicals were used. Diatomaceous earth (AquEx-10) for the column extraction was supplied from DSD, Tokyo. Authentic steroid hormones were supplied from Teikoku Zoki Co., Kawasaki, Japan).

HPLC Procedure. The eluent was a mixture of 0.1% water, 4% methanol, and 30% dichloromethane in *n*-hexane (v/v). The solvent system was designed according to ref 6.

The silica gel column was washed with 1% sulfuric acid and then methanol. This treatment was suitable for analysis of acidic or polar neutral compounds such as corticosteroids and related substances. Results similar to ours have been reported recently by Engerhart and co-worker (7).

Calibration for Quantitative Analysis. Calibration curves of cortisol and prednisolone were made on the basis of peak height measurements using sample quantities between 1 ng and 100 ng/mL serum. The peak heights were reproducible with the coefficient of variation (CV) values being less than 4%, using the authentic samples injected from evaporator 8. Cortisol was recovered from the sera in a 102 ± 6.8% yield and prednisolone, in a 93.3 ± 1.4% yield, when known amounts of the authentic specimens (1–100 ng) were added to the sera.

Analysis of Sera. A blood sample (5 mL) was centrifuged for 5 min at 3000 rpm. A 0.5-mL sample of the supernatant was injected into excolumn 4 through valve 7. The mobile phase for the extraction was introduced into the column system at a flow rate of 0.8 mL/min. The eluate, collected between 5 and 17 min, was then introduced into evaporator 8. After insertion of the stick into the evaporation tube, HPLC solvent was introduced into the evaporator at a flow rate of 0.1 mL/min followed by switching valve 12 to HPLC column 11. The HPLC flow rate was 1 mL/min.

RESULTS AND DISCUSSION

In order to formulate an on-line cleanup procedure for the analysis of biological fluids, a system of a closed-bed column packed with fine diatomaceous earth powder was developed (*3, 4*). This column-packing material was found to support an aqueous stationary phase and was capable of constructing a two layer aqueous liquid–liquid distribution system for a water-saturated organic solvent. It was also found that protein and other high molecular polar components in serum were trapped in the aqueous stationary phase on the diatomaceous earth support and that contaminants in the fluid were almost completely eliminated from the column by a flushing out procedure using a fast flow of water following injection of a certain amount of serum. Hence, this cleanup column is reusable. To achieve efficient extraction and fractionation of serum corticosteroids, an extraction column system comprised of three diatomaceous earth columns was introduced. The first column contained a water-coated support, the second and third, aqueous stationary phases of sodium hydroxide solution and dilute sulfuric acid. In the neutral column (excolumn 4 in Figure 1), lipophilic substances in human serum were distributed within the carrier solvent. Diethyl ether was the most conventional extracting solvent because of its low boiling point and high solubility toward various solutes except for high molecular and high polar compounds such as proteins, peptides, amino acids, and carbohydrates. Although diethyl ether is inflammable, its use poses a slight safety problem since our apparatus is a totally closed system. The manner of distribution was consistent with the partition coefficients of substances mentioned earlier, using an acid-treated silica gel column and aqueous diethyl ether system (*8*). Even a nearly insoluble compound in diethyl ether could be quantitatively distributed within the mobile phase on using an extraction column with a wide surface area.

The effluent from neutral excolumn 4 was introduced into the next alkaline excolumn 5 in which the acidic solutes were distributed in the basic stationary phase and retained there. In the third excolumn 6, organic bases still present in the mobile phase were removed to the acidic stationary phase. Thus, the effluent from the third column consisted of only neutral diethyl ether soluble materials. For a highly sensitive analysis of the neutral components in sera, a cleanup process incorporating three columns was found to be useful.

The durability of each excolumn was maintained completely except for changes in the pH of the stationary phase. The pH was easily measured by the fast flow of the mobile phase from the top to the bottom of the column, resulting in the extrusion of droplets of the stationary phase. A new stationary phase liquid was supplied from the top of the column and the subsequent fast flow of the carrier solvent, diethyl ether, created a condition of column control for the next run. This condition was necessary occasionally even when the pH remained unchanged, since the stationary phase liquid moved slowly, eventually flowing over the top of the column during analysis. An overflowed aqueous phase may result in an uncontrolled column condition and technical difficulties in the following evaporation stage.

The excolumn 4 loaded with human sera should be conditioned for each analytical run. This is also necessary for the extrusion of serum protein from the stationary phase, which degenerates slowly on the support surface and gradually clogs the column. Thus, a neutral column can be used repeatedly for hundreds of runs without any technical problems.

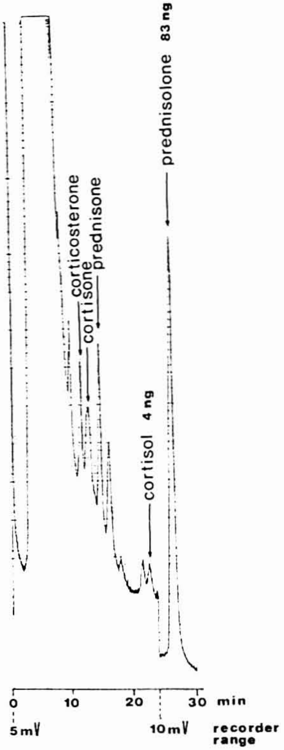

Figure 2. Chromatogram of serum corticosteroids obtained by the LEEI technique using 0.5 mL of serum from a systemic lupus erythematosus patient. The flow rate was 1 mL/min.

The effluent from the excolumns was concentrated in the line evaporation system connected to excolumn 6 through a fine PTFE tube functioning as a pressure converter between the high and low pressure sides. In the glass evaporator, 8, the effluent was concentrated to dryness at 40 °C, at which all corticosteroids tested were intact and stable. The residue was redissolved in a chromatographic solvent and introduced via an attached valve after reducing the dead space in the glass evaporator by the insertion of a steel stick, causing the resulting dead volume to be no more than about 50 μL. The quantitative amount of neutral components derived from the serum was injected into the HPLC column.

Solvent system was optimized for HPLC equipped with a silica gel column. A multicomponent system consisting of *n*-hexane and dichloromethane as diluents and methanol and water as stronger solvents was employed for the simultaneous analysis of several corticosteroids. The results suggest that unfavorable diffusion of the solutes does not occur in the process of resolving a residue in the evaporator and transferring the solution to the analytical column.

The all-unit operations such as extraction, evaporation, and injection were completely linearized with good reproducibility and efficiency, resulting in no need for an internal standard, usually indispensable for HPLC clinical analysis.

The calibration curves for the determination of prednisolone and hydrocortisone were made on the basis of the peak heights of the corresponding steroids. Recovery of these steroids from the sera was approximately quantitative and reproducible as shown by a comparison of the injection of the standard sample solutions and sera containing known amounts of steroids (1–100 ng/mL serum).

We applied the technique presented in this paper to the nano level analysis of serum corticosteroids such as hydrocortisone suppressed by prednisolone therapy for colagen disease and especially SLE patients. The results in Figure 2 show that our method is quite adequate for clinical assay before the use of prednisolone therapy or medication design determined by pharmacokinetics.

ACKNOWLEDGMENT

The authors express their appreciation of M. Shibuya, Nippon Medical College, for his suggestions and comments.

Registry No. Cortisol, 50-23-7; prednisolone, 50-24-8; prednisone, 53-03-2; corticosterone, 50-22-6; cortisone, 53-06-5.

LITERATURE CITED

(1) Hara, S.; Oka, K.; Dobashi, Y.; Ohkuma, T. *Yakugaku Zasshi* **1982**, *102*, 107–109.
(2) Oka, K.; Dobashi, Y.; Ohkuma, T.; Hara, S. *J. Chromatogr.* **1981**, *217*, 387–398.
(3) Hara, S.; Ijitsu, T.; Oka, K. *Yakugaku Zasshi* **1982**, *102*, 895–897.
(4) Hara, S.; Ijitsu, T.; Dobashi, Y.; Oka, K. *Yakugaku Zasshi* **1982**, *102*, 1036–1040.
(5) Hara, S. U.S. Patent 4 289 620, 1981.
(6) Rose, J. Q.; Jusko, W. J. *J. Chromatogr.* **1979**, *162*, 273–280.
(7) Engelhardt, H.; Mueller, H. *J. Chromatogr.* **1981**, *218*, 395–407.
(8) Hara, S.; Dobashi, Y.; Oka, K. *J. Chromatogr.* **1982**, *239*, 677–685.

RECEIVED for review October 13, 1982. Resubmitted June 28, 1983. Accepted September 9, 1983.

Preconcentration with Dithiocarbamate Extraction for Determination of Molybdenum in Seawater by Neutron Activation Analysis

W. M. Mok and C. M. Wai*

Department of Chemistry, University of Idaho, Moscow, Idaho 83843

Molybdenum in seawater can be quantitatively extracted with pyrrolidinedithiocarbamate and diethyldithiocarbamate at pH 1.4 into chloroform, for neutron activation analysis. Uranium in seawater cannot be extracted at this pH, and hence eliminates the interference from the ^{235}U(n,f)^{99}Mo reaction. Interferences from matrix species in seawater, such as sodium and bromine, are also removed during the extraction. The proposed method, with good accuracy and sensitivity, is suitable for the determination of molybdenum in natural waters.

The determination of certain trace elements has become important in studies of marine environments. Among these, molybdenum, as a biologically active element for growth and as a micronutrient in the aquatic environment, is often measured. Because of the low levels of molybdenum involved, neutron activation analysis (NAA) appears to be a suitable technique. Molybdenum can be identified in NAA through ^{99}Mo ($t_{1/2}$ = 66 h) or its daughter ^{99m}Tc ($t_{1/2}$ = 6.05 h). Direct application of NAA for trace element determination in complex systems is generally difficult because of serious matrix interferences. Chemical separation methods have been used either before or after neutron irradiation to eliminate such interferences. Besides matrix interferences, another complication in the molybdenum determination by NAA is the contribution of ^{99}Mo from the ^{235}U(n,f)^{99}Mo reaction, which is significant in systems with high uranium contents. Separation before neutron irradiation has the advantage of avoiding this complication if the method is selective for molybdenum.

Kulathilake and Chatt reported a preconcentration method for the NAA determination of molybdenum in seawater by cocrystallization with β-naphthoin oxime (*1*). This method is selective for molybdenum but requires a couple of days to complete the separation. Molybdenum has also been determined in seawater after preconcentration on activated charcoal in the presence of ammonium pyrrolidinedithiocarbamate (APDC), followed by neutron activation of the charcoal sample (*2*). Since activated charcoal is an efficient adsorber, a significant fraction of the uranium in seawater was also found with the molybdenum in the charcoal. Consequently, a correction for the uranium contribution to ^{99}Mo must be considered in this charcoal adsorption method.

This paper describes a simple solvent extraction method using dithiocarbamates for preconcentration of molybdenum in seawater. The solvent extraction method not only is fast and efficient but also eliminates the interferences caused by uranium and other matrix species in the determination of molybdenum by NAA.

EXPERIMENTAL SECTION

Ammonium pyrrolidinedithiocarbamate (APDC) and sodium diethyldithiocarbamate (NaDDC) were obtained from the Fisher Scientific Co. Chloroform used in the extraction was Baker Analyzed Reagent. Nitric acid used in the experiments was of Ultrex grade from Baker Chemical Co. Deionized water was obtained by treatment of distilled water through an ion exchange column (Barnstead Ultrapure Water Purification Cartridge) and a 0.2-μm filter assembly (Pall Corporation Ultipor DFA).

A stock solution containing 1000 μg/mL molybdenum was prepared by dissolving 1.8401 g of dry ammonium molybdate (analytical reagent grade) in deionized water and diluted to a liter in accordance with the EPA's instructions (*3*). Standard working solutions were prepared by appropriate dilution of the stock solution. Surface seawaters were collected from the southwest corner of Discovery Park in western Seattle. The salinity of the seawater was 27‰. The seawater was filtered through a 0.45-μm membrane filter, acidified to pH 2, and stored in precleaned polyethylene bottles. All containers used in this study were

0003-2700/84/0356-0027$01.50/0 © 1983 American Chemical Society

washed with 10% nitric acid, rinsed with deionized water, and stored in a class 100 clean hood equipped with a vertical laminar flow HEPA filter.

The extraction solution was prepared by dissolving 1 g of APDC and 0.5 g of NaDDC in 100 mL of deionized water. In all cases, the extraction solution was prepared fresh daily, filtered to remove the insoluble material, and shaken for 30 s with chloroform to remove bromine and other impurities.

In the determination of molybdenum in seawater, a 100-mL sample of the filtered seawater was poured into an Erlenmeyer flask, equipped with a ground stopper. The sample was adjusted to pH 1.4 ± 0.1 before 2 mL of the extraction solution and 5 mL of chloroform were added. The mixture was shaken for 15 min, and then was allowed to sit for 10 min for phase separation. After the waiting period was up, 3 mL of the organic phase was collected and placed in a polyethylene vial. The solution was evaporated to dryness before heat-sealing the vial for neutron irradiation. The preconcentration factor attained with this procedure is 60. Standards were made of 1-mL solutions containing proper concentrations of molybdenum, sealed in the same kinds of vials as the samples. One hundred milliliters of deionized water that went through the same extraction procedure was used as a blank for seawater analysis.

All samples and standards were normally irradiated for 2 h in a 1-MW TRIGA reactor at a steady neutron flux of 6×10^{12} n cm^{-2} s^{-1}. After irradiation, the samples were allowed to decay for about 48 h, to allow ^{99}Mo and ^{99m}Tc to reach equilibrium before counting. The following sample transfer procedure was used to avoid the interferences of ^{24}Na and other radioactivities produced in the plastic material of the irradiated vials. To each vial, 1 mL of a 3 N HNO_3 solution was injected by means of a 5-mL disposable syringe. After shaking for about 1 min, the acid solution, containing any molybdenum present, was transferred, using the same syringe, into a new $^{2}/_{5}$-dram vial for γ counting. Less than 1% of the molybdenum was found to remain in the irradiated vial after sample transfer. Standards were also transferred into new $^{2}/_{5}$-dram vials with disposable syringes. Each sample was counted 2×10^3 s with a large volume coaxial ORTEC Ge(Li) detector with a resolution of about 2.3 keV for the 1332-keV γ-ray of ^{60}Co, a peak-to-Compton ratio of 35:1, and an efficiency of 11%. The detector output was fed into a Nuclear Data 4096-channel pulse-height analyzer. The 140-keV γ-ray of ^{99m}Tc was used in this work to determine the molybdenum concentration. Data analysis was carried out by using the SPAN program with an IBM 370 computer.

Experiments were also carried out to determine the extracted molybdenum by graphite furance atomic absorption spectrometry (GFAAS). In this case, the dried sample was first dissolved in 1 mL of concentrated nitric acid, and then diluted to about 2% of the acid. A Perkin-Elmer HGA 2100 graphite furnace and a Model 603 AA spectrometer were used for this study. Perkin-Elmer pyrolytically coated graphite tubes were used, and a deuterium-arc background correction was applied. The operation conditions for molybdenum determination followed that prescribed by the EPA (3). A 25-μL Eppendorf micropipet was employed for injecting samples into the furnace. All samples and standards were injected in triplicate, or more if triplicates disagreed significantly. Standards spanning the sample absorbance range were run between each series of samples as a regular check.

RESULTS AND DISCUSSION

Conditions for the Extraction of Molybdenum from Seawater. Extraction of metal ions by dithiocarbamate depends on several factors, such as type of solvent, amount of dithiocarbamate, pH of a solution, and shaking time. The advantages of using a mixture of APDC + NaDDC, and chloroform as solvent, to extract trace metals from seawater have been described in the literature (4). APDC is more stable than NaDDC in acid solution, but the mixture provides a better working pH range and appears to have a stabilizing effect on metal complexes. In this study, a mixture of 2:1 APDC to NaDDC, at a total concentration of 0.03% or greater, was used for molybdenum extraction. To test the effect of pH on the extraction, a synthetic seawater whose composition was described in a previous paper was spiked with 48 μg/L of molybdenum (4). Ten-milliliter aliquots of this spiked seawater were taken, with the pH adjusted to different values. The spiked molybdenum in each sample was extracted with the dithiocarbamate solution into 2 mL of chloroform for NAA. A blank of unspiked synthetic seawater was run in the same manner as the samples in each irradiation. In all cases, the blanks showed less than 1% of molybdenum activities relative to the samples. After correction for the background activities, the percentages of molybdenum recovery for the spiked seawater samples are shown in Figure 1.

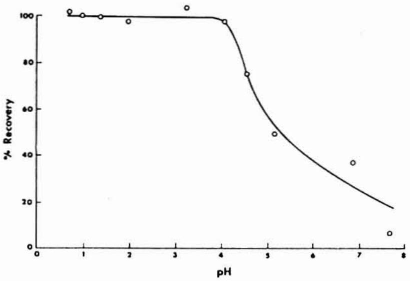

Figure 1. pH dependence of the extraction of molybdenum from seawater by APDC + NaDDC into chloroform.

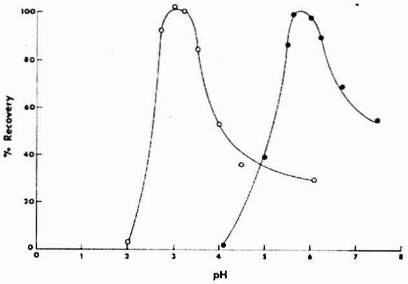

Figure 2. pH dependence of the extraction of uranium from seawater by APDC (open circles) and by NaDDC (closed circles).

Near total recovery of molybdenum was observed from pH 0.7 to 4.0. At pH 4.6, recovery of molybdenum was found to decrease to about 75%. Further increase in pH resulted in very poor recovery of molybdenum. Similar experiments with the natural seawater spiked with 48 μg/L of molybdenum showed almost identical pH dependence. Extraction of molybdenum at very low pH is not practical because of the accelerated decomposition of dithiocarbamates in acid solution (5). On the other hand, extraction at pH >2 is also not satisfactory because uranium in seawater can be extracted above this pH (Figure 2). Therefore, a pH range of 1.3 to 1.5 was chosen as the standard condition for this method.

Under our experimental conditions, extraction of molybdenum for seawater is kinetically a very fast process. For 10 mL of the spiked seawater with 1 mL of the APDC + NaDDC solution and 2 mL of chloroform, extraction of molybdenum is virtually complete in 1 min of vigorous shaking. With a large volume of seawater, e.g., 100 mL of sample with 2 mL of the extraction solution and 5 mL of chloroform, several minutes of shaking is sufficient to complete the extraction.

Extraction of Uranyl Dithiocarbamate Complexes. The interfering nuclear reactions in the molybdenum determination by NAA are ^{120}Ru(n,α)^{99}Mo and ^{235}U(n,f)^{99}Mo.

However, the amount of ruthenium in natural waters is so low that its contribution to ^{99}Mo is negligible. The ^{235}U(n,f)^{99}Mo reaction is important in samples in which the ratio of Mo:U is close to one (*2, 6*). The average uranium concentration in seawater is about 3.2 ppb, comparable to that of molybdenum in seawater (*7*). Therefore, the contribution from fission of ^{235}U needed to be investigated under the proposed extraction conditions for molybdenum.

The various effects of pH on the extraction of uranium in seawater by APDC and by NaDDC are shown in Figure 2. The experiments were carried out with a synthetic seawater spiked with 50 μg/L of uranium, extracted with either APDC or NaDDC into chloroform, following a procedure similar to that described for molybdenum. The extracted uranium was determined by NAA, utilizing the 228-keV γ-ray from the decay of ^{239}Np (daughter of ^{239}U, $t_{1/2}$ = 2.36 days). As shown in Figure 2, extraction of uranium with either APDC or NaDDC depends strongly on pH. At pH <2, no significant amount of uranium can be extracted by APDC. At pH 2, about 2% of the spiked uranium can be extracted. The extraction efficiency increases rapidly to a maximum around pH 2.8–3.4 and then begins to decrease at higher pH values. In the case of NaDDC, the extraction efficiency for uranium becomes significant at pH >4 and reaches a narrow maximum at a pH of around 5.5–6.0. The uranyl–PDC complex is apparently stable in slightly acidic solutions, whereas the corresponding DDC complex is stable in near neutral solutions. In either case, extraction of uranium is insignificant at a pH of around 1.3–1.5. This is also true when a mixture of APDC and NaDDC, in a ratio of 2:1, was used in the extraction. The recommended pH for molybdenum extraction should be totally free of uranium interference.

Determination of Molybdenum by NAA. One advantage of using dithiocarbamate for preconcentration of trace metals in seawater is that matrix species such as the alkali metals, the alkaline earth metals, the halogens, and phosphorus can be simultaneously eliminated during extraction. In a previous study of preconcentrating gold and mercury from seawater for NAA, it has been shown that sodium and bromine in the system can be essentially all removed with dithiocarbamate extraction (*8*). The large amount of ^{24}Na and ^{82}Br produced in seawater upon neutron irradiation would otherwise mask the low-energy peaks from radioisotopes such as ^{99}Mo or ^{99m}Tc. Removing these matrix species, as well as uranium, from the system enables accurate determination of molybdenum in seawater without spectral interference.

The procedures for molybdenum extraction and NAA described in this paper have been applied to the analysis of NBS Standard River Water (SRM 1643a), which is certified to contain 95 ± 6 ng/g of molybdenum. Based on four replicate analyses, the average molybdenum content determined by this extraction method and NAA was 102 ± 4 μg/L, which agrees well with the certified value. The precision of this method for seawater analysis was tested by individually preparing seven samples, all at pH 1.4 ± 0.1 and each containing 48 μg/L of molybdenum. The average recovery was 100.2%, and the average coefficient of variation for the series of replicates was ±3.5%. With 100 mL of seawater treated by the described procedure, the detection limit, based on three standard deviations of the background under the 140-keV peak, in a counting period of 2×10^3 s and the specified irradiation conditions, was estimated to be 0.35 μg/L. This is sensitive enough for molybdenum determinations in seawaters. The detection limit can be further improved by increasing the preconcentration factor, the irradiation time, and the counting time.

The molybdenum content in the seawater collected from the Seattle coast was determined by NAA, after preconcentration with this extraction method, to be 8.8 ± 0.3 μg/L. The ratio of molybdenum concentration (in μg/L) to salinity (in ‰) for this sample is 0.33, which is consistent with the average ratio of 0.32–0.34 found in open ocean waters (*9, 10*).

Determination of Molybdenum by GFAAS. Four replicate analyses of NBS Standard River Water (SRM 1643a) were also carried out using this extraction method and GFAAS. The average molybdenum content was found to be 97 ± 6 μg/L, in good agreement with the value obtained by NAA. The average molybdenum concentration in the seawater from Seattle was determined by GFAAS to be 9.0 ± 0.4 μg/L, which again is in good agreement with the value of 8.8 ± 0.3 μg/L determined by NAA. In this GFAAS study, samples and standards were all kept in 2% nitric acid solution. Our experiments indicate that the effect of acid concentration on the signal of molybdenum absorbance is small (<10%) in the acid range of 2–10%. However, to obtain reproducible results, it is still recommended to keep all samples and standards in the same acid concentration. This experiment has shown that the results of molybdenum determinations obtained by the NAA technique are consistent with those obtained by GFAAS. It is unlikely that any significant interferences would be present in the extracted seawater for molybdenum determination by NAA.

CONCLUSION

Direct determination of molybdenum in seawater by instrumental NAA is not preferable, mainly due to the presence of interferences in the seawater matrix that seriously impair the sensitivity and detection limit. The proposed solvent extraction method with APDC + NaDDC and chloroform provides a fast and efficient way of preconcentrating molybdenum from seawater for NAA. Interferences from the matrix species and from uranium in seawater are effectively removed during the extraction. Evaluation of the procedure with seawater spiked with molybdenum, natural seawater, and NBS Standard River Water shows that the extraction is quantitative and that the sensitivity is suitable for the determination of molybdenum in open ocean waters.

Registry No. Mo, 7439-98-7; U, 7440-61-1; APDC, 5108-96-3; NaDDC, 148-18-5; water, 7732-18-5.

LITERATURE CITED

(1) Kulathilake, A. I.; Chatt, A. *Anal. Chem.* **1980**, *52*, 828–833.
(2) Sloot, H. A. v. d.; Wals, G. S.; Das, H. A. *Anal. Chim. Acta* **1977**, *90*, 193–200.
(3) "Methods for Chemical Analysis of Water and Wastes", U.S. Environmental Protection Agency: Cincinnati, OH, 1979.
(4) Lo, J. M.; Yu, J. C.; Hutchison, F. I.; Wai, C. M. *Anal. Chem.* **1982**, *54*, 2536–2539.
(5) Bajo, S.; Wittenbach, A. *Anal. Chem.* **1979**, *51*, 376–378.
(6) Nadkarni, R. A.; Morrison, G. H. *Anal. Chem.* **1978**, *50*, 294–296.
(7) Brewer, P. G. In "Chemical Oceanography"; Riley, J. P., Skirrow, G., Eds.; Academic Press: New York, 1975; Vol. 1, pp 415–496.
(8) Yu, J. C.; Lo, J. M.; Wai, C. M. *Anal. Chim. Acta*, in press.
(9) Head, P. C.; Burton, J. D. *J. Mar. Biol. Assoc. U.K.* **1970**, *50*, 439–448.
(10) Wedepohl, K. H., Ed. "Handbook of Geochemistry"; Springer-Verlag: Berlin, 1978; Vol. II-4, pp 4217–4218.

RECEIVED for review July 19, 1983. Accepted September 13, 1983. Neutron irradiations were performed at the Washington State University Nuclear Radiation Center, under the Reactor Sharing Program supported by DOE.

Anal. Chem. **1984**, *56*, 30–32

Spectrophotometric Determination of Total Gossypol in Cottonseeds and Cottonseed Meals

Atnafseged Admasu

Ethiopian Nutrition Institute, P.O. Box 5654, Addis Ababa, Ethiopia

B. S. Chandravanshi*

Department of Chemistry, Addis Ababa University, P.O. Box 1176, Addis Ababa, Ethiopia

A new spectrophotometric method for the determination of total gossypol content in cottonseeds and cottonseed meals has been developed. The method is based on the reaction of gossypol with 3-amino-1-propanol and its subsequent complexation with iron(III). The green colored iron(III)–bis(aminopropanol)–gossypol complex has a characteristic absorption maximum at 620 nm. The colored system obeys Beer's law in the concentration range of 4–80 ppm of gossypol. The effects of several experimental variables on the determination of gossypol have been studied and the stoichiometric composition of the complex has been determined. The new method has been found to be simple, rapid, and precise and to yield results comparable with the standard AOCS method. The method has been applied for the determination of total gossypol in several cottonseed and cottonseed meal samples.

Cottonseed products in the forms of oil and meal are widely used for human and animal food. However, the utilization of cottonseed products in human nutrition is limited by the presence of a phenolic compound, gossypol. This undesirable constituent is toxic to different animal species (*1–3*). The toxicity of gossypol also limits its own application in many areas (*4–9*).

Gossypol and its analogues are found primarily in the pigment glands of cottonseed. The structures of the three tautomeric forms of gossypol itself are given in Figure 1. Analogues of gossypol have a similar structure and can either occur naturally in cottonseeds or form as a result of storage and processing of cottonseed. The actual pigment composition of cottonseed pigment glands varies with the genetic type of the cotton plant and with environmental conditions during the development of cottonseed.

Several methods have been reported for the determination of gossypol in a variety of samples (*10*). The results of the analysis are reported in terms of percent of free gossypol, percent of bound gossypol, i.e., gossypol that is bound to protein, and percent of total gossypol by weight. Methods used for the analysis of gossypol include spectrophotometric methods (*11–16*), an NMR method (*17*), a chemiluminescent method (*18*), a gas–liquid chromatographic method (*19*), polarography, thin-layer chromatography, and paper chromatography (*20*). Most of these methods are tedious, time-consuming, and suffer from interferences due to the presence of the other pigments. Therefore, it is necessary to look for the development of a simple and precise method for the routine analysis of gossypol in cottonseed materials.

The reactions of gossypol with several metal ions including iron(III) have been reported in the literature (*21–23*). However, no fundamental investigation has been made on the application of such reactions for the quantitative determination of gossypol. Hence, it is worthwhile to study the complexation of gossypol with iron(III) in detail and, if possible, to develop a new method for the determination of gossypol in cottonseed samples.

The present investigation deals with the development of a new spectrophotometric method for the determination of total gossypol in cottonseeds and cottonseed meals. The method is based on the reaction of gossypol with 3-amino-1-propanol and its subsequent complexation with iron(III). The composition of the complex has been determined and the method has been applied successfully for the analysis of total gossypol in several cottonseeds and cottonseed meals. The results obtained by the new method have been compared with the AOCS method.

EXPERIMENTAL SECTION

Apparatus and Equipment. A Beckman Model 26 UV-VIS spectrophotometer equipped with a pair of 1-cm path length quartz cuvettes was used for absorbance measurements. A Beckman Expandometric SS-2 pH meter was used for pH measurements.

Reagents and Standards. All the chemicals used were of analytical reagent grade. A 1.79×10^{-2} M iron(III) solution was prepared by dissolving hydrated ferric nitrate ($Fe(NO_3)_3{\cdot}9H_2O$, BDH AnalaR) in 40:60 (v/v) hexane–isopropyl alcohol containing a few drops of concentrated hydrochloric acid. The complexing agent solution was prepared by mixing 2 mL of 3-amino-1-propanol (E. Merck) with 10 mL of glacial acetic acid. The solution was cooled to room temperature and diluted to 100 mL with dimethylformamide in a volumetric flask.

A 4.821×10^{-3} M standard solution of gossypol was prepared by dissolving gossypol acetic acid (Sigma Chemical Co.) in complexing agent solution. A working solution of gossypol was prepared by diluting a 10-mL aliquot of standard solution to 100 mL with 40:60 (v/v) hexane–isopropyl alcohol in a volumetric flask.

Procedure for Extraction of Gossypol from Cottonseeds and Cottonseed Presscakes. Samples of seven varieties of cultivated cottonseeds, commonly grown under different conditions in Ethiopia, belonging to the *hirsutum* species of the genus *Gossypium* were collected from the Institute of Agricultural Research, Addis Ababa. Samples of cottonseed presscakes were collected from Addis Ababa Oil Mills. The dehulled cottonseeds and cottonseed presscakes were ground in a laboratory mill (Max Luscher AG Seon, Type 12E8) to pass through a 2-mm screen.

A weighed quantity of the sample containing 2–20 mg of total gossypol was transferred into a 100-mL Erlenmeyer flask and 10 mL of complexing agent solution was added to it. The mixture was heated in a boiling water bath for 30 min, cooled, and diluted to about 30 mL with 40:60 (v/v) hexane–isopropyl alcohol. The solution was filtered and diluted to 50 mL with hexane–isopropyl alcohol in a volumetric flask.

Procedure for Determination of Gossypol. An aliquot of the solution containing 0.2–2.0 mg of gossypol was transferred into a 25-mL volumetric flask and 2 to 4 drops of 5 M hydrochloric acid were added to it. A 5-mL aliquot of iron(III) solution was added to the flask, the solutions were mixed well and then allowed to stand for 5 min. One milliliter of distilled water was added to the flask, and the solution was immediately diluted to volume

0003-2700/84/0356-0030$01.50/0 © 1983 American Chemical Society

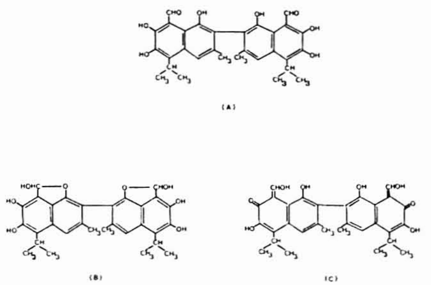

Figure 1. The three tautomeric forms of gossypol: (A) hydroxy aldehyde; (B) lactol; (C) cyclic carbonyl.

with 40:60 (v/v) hexane-isopropyl alcohol. The absorbance of the colored solution was measured at 620 nm against the hexane-isopropyl alcohol mixture as a reference. Calibration curves were prepared by measuring the absorbance of the solutions containing known amounts of gossypol by the same procedure.

RESULTS AND DISCUSSION

Colorimetric Reaction. Gossypol reacts with 3-amino-1-propanol to form bis(aminopropanol)gossypol. The bis(aminopropanol)gossypol reacts with iron(III) in the acidic medium to form a stable, green colored complex, freely soluble in hexane-isopropyl alcohol mixture. This sensitive color reaction forms a basis for the development of a new spectrophotometric method for the determination of gossypol.

Absorption Spectra. The green bis(aminopropanol)-gossypol-iron(III) complex showed an absorption maximum around 620 nm while iron(III) and 3-amino-1-propanol showed negligible absorption in the region of 450-700 nm. Thus, excess quantities of iron(III) and 3-amino-1-propanol did not interfere with the determination of gossypol. The absorption spectra are given in Figure 2.

Effect of pH. To obtain a complete complexation reaction with constant and maximum absorbance, the pH of the final solution should be in the range of 1.0-1.5. At higher and lower pH values the solutions exhibit no fixed absorption maxima in the visible region.

Effect of Concentration of Iron(III). A 1:10 molar ratio of gossypol to iron(III) was found to be necessary for the maximum color development. A large excess of iron(III) up to 500-fold molar excess has no adverse effect on the determination of gossypol.

Effect of Amount of Water. It has been found that a stable color intensity is developed only in the presence of a small amount of water. The amount of water can vary from 0.8 to 1.5 mL in the reaction mixture without any change in the color intensity for a total volume of 25 mL. The role of water may be to satisfy the coordination number of iron(III) in the complex.

Effect of Time and Temperature. It was found that the optimum color intensity is obtained within 5 min of reaction time and the absorbance of the colored solution remains constant for at least 3 h. Variation in the temperature of the colored solution from 20 to 30 °C did not produce any measurable change in the absorbance of the solution. At higher temperature, absorbance of the colored solution decreases slowly.

Beer's Law, Optimum Concentration Range, Sensitivity, and Molar Absorptivity. The colored system obeys Beer's law in the concentration range of 4-80 ppm of gossypol at 620 nm. The optimum concentration range for the determination as evaluated from the Ringbom plot (*24*) was found to be 8-64 ppm of gossypol. The effective molar absorptivity in terms of gossypol was found to be 6480 L mol^{-1} cm^{-1} and the photometric sensitivity (*25*) of the color reaction was found to be 0.08 μg of gossypol cm^{-2} at 620 nm.

Table I. Determination of Total Gossypol by Weight in Cottonseed Samples

type of cottonseed variety	% total gossypol by wt new method	 AOCS tentative method
Acala 1517/70	0.489	0.483
Albar 637	0.613	0.616
AMS 1.74	0.331	0.329
Acala 1517c	1.069	1.063
Acala 63-64 glandless	0.029	0.032
Frago glandless	0.415	0.411
Frago Bract glandless	0.168	0.166

Table II. Determination of Total Gossypol by Weight in Cottonseed Presscakes

type of sample	% total gossypol by wt new method	 AOCS tentative method
Nazrawi Oil Mills	0.689	0.685
Arsina Mertu Oil Mills	0.518	0.519
Teramaj Oil Mills	0.962	0.952
Akaki Oil Mills	0.850	0.845
United Oil Mills	0.758	0.757

Composition of Complex. The composition of the complex was determined by the continuous variations (*26*) and molar ratio (*27*) methods. In the continuous variations method the mole fractions of bis(aminopropanol)gossypol (BAPGP) and iron(III) were varied with a constant total molarity. The absorbances were plotted against the mole fractions of BAPGP. Maximum absorption occurred at a mole fraction of 0.33 (Figure 3). This suggests that the combining ratio of BAPGP to iron(III) in the complex is 1:2. This result was also supported by the molar ratio method.

These results are similar to the result obtained by Haas and Shirley (*23*) in which they have reported that the aldehyde groups and the adjacent 7-hydroxyl groups of the gossypol are the site of complexation. In the present investigation the bis(aminopropanol)gossypol was used for the complexation with iron(III); hence, the structure of the complex may be as given in Figure 4.

Precision. The precision of the newly developed method has been evaluated in terms of relative standard deviation. Ten independent analyses on samples each containing 36 ppm of gossypol gave a mean absorbance value of 0.450. The standard and relative standard deviations were found to be ±0.0030 and 0.67%, respectively. These results indicate that the method is precise and gives reproducible results.

Application of the Method. The validity of the newly developed method has been tested by determining the total gossypol content of cottonseed and cottonseed presscake samples. These results have been compared with the results obtained by the AOCS tentative method which is based on the extraction of gossypol with 3-amino-1-propanol in dimethylformamide, its subsequent reaction with aniline to form dianilinogossypol, and measurement of the colored reaction product at 440 nm (*11*). The data given in Tables I and II clearly indicate that the two methods give almost identical results.

To test the effect of interferences, known concentrations of pure gossypol, treated with 3-amino-1-propanol, were added to the gossypol extracts from cottonseeds and cottonseed presscakes. The total gossypol was then determined by the

Table III. Recovery of Gossypol Added to Cottonseed and Cottonseed Presscake Extracts

type of sample extract	amt of gossypol, g in extract	added	total	found	% recovery of gossypol
cottonseed variety	0.513	0.302	0.815	0.809	99.3
cottonseed presscake	0.497	0.160	0.657	0.654	99.5

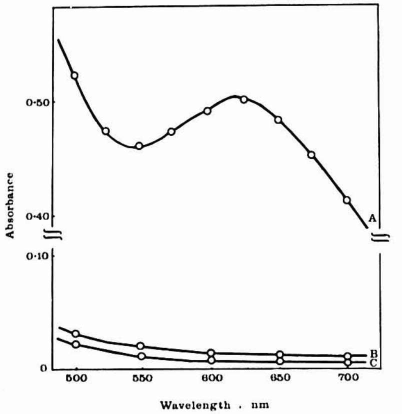

Figure 2. Absorption spectra of: (A) bis(aminopropanol)-gossypol-iron(III) complex (6.94×10^{-5} M gossypol); (B) iron(III) solution (1.79×10^{-2} M); (C) reagent blank in 40:60 (v/v) hexane-isopropyl alcohol.

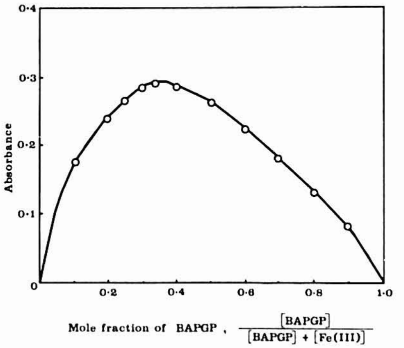

Figure 3. Job's method of continuous variations.

procedure described earlier. The results of the analysis of two samples are given in Table III. These results show satisfactory recovery of gossypol and establish the precision of the method. It has also been found that there is no shift in the absorption maximum of the iron(III) complex by the presence of other consituents in the gossypol extracts from the samples.

The precision of the method was also tested on the cottonseed meal extract containing a mean total gossypol content of 0.705%. Ten independent analyses gave a standard deviation of ±0.005 with a relative standard deviation of 0.71%.

Thus, the proposed method is sensitive, selective, and free from the interferences of other constituents present in cottonseeds. The method is simple, rapid, precise, and accurate. The reagents involved are cheap and readily available and the analysis can be completed within a short period of time. The method can be applied for the determination of total gossypol in a variety of cottonseed and cottonseed product samples.

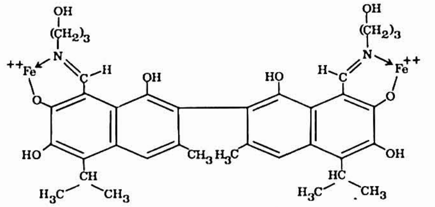

Figure 4. Structure of the bis(aminopropanol)-gossypol-iron(III) complex.

LITERATURE CITED

(1) Abou-Donia, M. B. *Residue Rev.* **1976**, *16*, 125–160.
(2) Liener, I. E. "Toxic Constituents of Plant Food-Stuffs"; Academic Press: New York, 1969; p 251.
(3) Qian, Shao-Zhan; Xu, Ye; Jing, Quang Woi *Yao Hsueh Hsueh Pao* **1979**, *14*, 116–119. *Chem. Abstr.* **1980**, *92*, 33909*f*.
(4) Askarov, M. A.; Dzhalilov, A. T.; Fatkhullaev, E.; Sukhinina, L. A. *Otkrytiya, Izobret., Prom. Obraztsy, Tovarnye Znaki* **1980**, *8*, 99–100. *Chem. Abstr.* **1980**, *92*, 216236*d*.
(5) Bickford, W. G.; Pack, F. C.; Castillon, L. E.; Mack, C. H. *J. Am. Oil Chem. Soc.* **1954**, *31*, 91–93.
(6) Bailey, A. "Cottonseed and Cottonseed Products"; Interscience: New York, 1948; p 148.
(7) Markman, A. L.; Rzhekhin, V. P. "Gossypol and its Derivatives"; Israel Program for Scientific Translations: Jerusalem, 1968; p 148.
(8) Wang, Nai-Gong; Lei, Hai-Peng *Chung-hua I Hsueh Tsa Chih (Peking)* **1979**, *59*, 402–405. *Chem. Abstr.* **1980**, *92*, 174961*d*.
(9) Liener, I. E. "Toxic Constituents of Plant Food-Stuffs"; Academic Press: New York, 1969; p 255.
(10) Pons, W. A. *J. Assoc. Off. Anal. Chem.* **1977**, *60*, 252–259.
(11) American Oil Chemists Society "Official and Tentative Methods"; American Oil Chemists Society: Champaign, IL, 1978; Tentative Method Ba 8-58.
(12) Crouch, Floyd W.; Bryant, Melton F. *Anal. Chem.* **1982**, *54*, 242–246.
(13) Pons, W. A.; Guthrie, J. D. *J. Am. Oil Chem. Soc.* **1949**, *26*, 671–676.
(14) Pons, W. A.; Hoffpauir, C. L.; O'Connor, R. T. *J. Am. Oil Chem. Soc.* **1951**, *28*, 8–12.
(15) Storherr, R. W.; Holley, K. T. *J. Agric. Food Chem.* **1954**, *2*, 745–747.
(16) Mathur, J. M. S.; Sharma, N. D.; Singh, M. *J. Food Sci. Technol.* **1972**, *9*, 138–140.
(17) Waiss, A. C.; Chan, B. G.; Benson, M.; Lukefahr, M. J. *J. Assoc. Off. Anal. Chem.* **1978**, *61*, 146–149.
(18) Aver'yanov, A. A.; Merzlyak, M. N.; Rubin, B. A. *Biokhimiya (Moscow)* **1978**, *43*, 1594–1601. *Chem. Abstr.* **1978**, *89*, 211079*h*.
(19) Raju, P. K.; Cater, C. *J. Am. Oil Chem. Soc.* **1967**, *44*, 465–466.
(20) Markman, A. L.; Rzhekhin, V. P. "Gossypol and Its Derivatives"; Israel Program for Scientific Translations: Jerusalem, 1968; Chapter 8.
(21) Ramaswamy, H. N.; O'Connor, R. T. *J. Am. Oil Chem. Soc.* **1968**, *45*, 841–844.
(22) Jonassen, H. B.; Demint, R. J. *J. Am. Oil Chem. Soc.* **1955**, *32*, 424–426.
(23) Haas, R. H.; Shirley, D. A. *J. Org. Chem.* **1965**, *30*, 4111–4113.
(24) Ringbom, A. *Z. Anal. Chem.* **1938**, *115*, 332–343.
(25) Sandell, E. B. "Colorimetric Determination of Traces of Metals", 3rd ed.; Interscience: New York, 1959; p 83.
(26) Job, P. *Ann. Chim. (Paris)* **1928**, *9*, 113–203.
(27) Yoe, J. H.; Jones, A. L. *Ind. Eng. Chem., Anal. Ed.* **1944**, *16*, 111–115.

RECEIVED for review April 19, 1983. Accepted September 1, 1983. The authors are thankful to the Chairman, Department of Chemistry, Addis Ababa University, Addis Ababa, Ethiopia, and Director of Ethiopian Nutrition Institute for providing the facilities. They are also thankful to the Swedish Agency for Research Cooperation with Developing Countries for the financial assistance.

Anal. Chem. **1984**, *56*, 33-37

Elemental Analysis of Estuarine Sediments by Lithium Metaborate Fusion and Direct Current Plasma Emission Spectrometry

A. Y. Cantillo,*[1] S. A. Sinex,[2] and G. R. Helz

Department of Chemistry, University of Maryland, College Park, Maryland 20742

The elemental analysis of sediments and related materials by lithium metaborate fusion and DC plasma emission spectrometry has been evaluated during the course of a major geochemical survey. Coefficients of variation of replicate analyses for major and trace elements were mostly in the 2–10% range, comparable to reproducibility in routine atomic absorption work but poorer than reported in the best inductively coupled plasma emission work. Evaluation of systematic errors by use of geochemical standards indicated good agreement with the published results for Si, Ti, V, Mn, Ni, Cu, and Zn. The results for Al, Cr, and Fe were slightly low, and those for Yb and Zr were substantially low. Poor correlations with published data were obtained for La, Ce, and Zr. This method possesses many features that make it attractive for geochemical monitoring, but analysts will have to exercise great care to avoid systematic errors.

Several groups interested in geological samples have described multichannel, inductively coupled plasma (ICP) emission spectrometric systems that are capable of high sample throughput and accuracy, using on-line corrections for spectral interferences (*1–4*). However, the instrumentation costs for these systems are large and therefore they are likely not to be economical in small laboratories. Commercial direct current plasma (DCP) emission systems are now available for a small fraction of the cost of multichannel ICP systems. They share some of the advantages of ICP, including often competitive detection limits (*5*). Single-channel versions of these systems are free from interelement interferences resulting from contamination of one channel by light from the slit of another (*6*). Also, because there is no photomultiplier crowding problem, single channel units permit greater freedom than multichannel systems in selecting analytical wavelengths to minimize spectral interferences. Obviously, single channel units do not have the same high sample throughput capacity that multichannel systems do. However in the analysis of rocks, soils, and sediments, this disadvantage can be partly offset by greater efficiency in sample preparation because of the ability of the DC plasma source to tolerate samples with a high dissolved solids content. Some ICP sources are intolerant of such samples (*7*), and previous workers who have analyzed geologic materials with ICP instruments have usually used acid digestion procedures in preference to faster fusion procedures (*2–4*).

Because of a favorable earlier report (*8*) on the analysis of geological materials by a procedure involving lithium metaborate fusion followed by measurement with a single-channel DCP emission spectrometer, we adopted this approach in a large-scale study of major and minor elements in estuarine sediments (*9–11*). This paper contains an appraisal of our experiences with this method.

Table I. Geochemical Reference Standards: Descriptions and Sources

std rock designation	description	source	ref^a
BIR-1	Icelandic basalt	USGS^b	27
BCSS-1	marine sediment	NRC^c	34
MAG-1	marine mud	USGS	19–23, 27–29
MESS-1	marine sediment	NRC	34
SDC-1	mica schist	USGS	19–21, 23, 25, 27
SL-1	lake sediment	IAEA^d	26
SRM-1645	river sediment	NBS^e	35
SRM-1646	estuarine sediment	NBS	35
QLO-1	quartz latite	USGS	19–21, 23, 25, 27, 28
W-2	Centerville diabase	USGS	27

^{a} More extensive compilations of data are also available (ref 32, 33, and others). ^{b} U.S. Geological Survey, Reston, VA 22902. ^{c} National Research Council, Chemistry Division, Montreal Road, Ottawa, Ontario K1A OR9, Canada. ^{d} International Atomic Energy Agency, Laboratory Seibersdorf, Vienna, Austria. ^{e} U.S. National Bureau of Standards, Washington, DC 20234.

EXPERIMENTAL SECTION

Procedure. A modification of the lithium metaborate fusion method developed by Suhr and Ingamells (*12, 13*) was used in the analysis. Approximately 0.2 g of sample was weighed to the nearest tenth of a milligram into a 7.5 cm^3 drill point graphite crucible (Ultra Carbon Corp., Bay City, MI) containing 1.0 g of lithium metaborate. The sediment was placed in a small depression made in the borate flux to prevent incomplete fusion problems that are encountered when sediment is in direct contact with graphite.

The sediment–flux mixture was fused in a muffle furnace at 950 ± 50 °C for 15 min. The liquid borate bead was poured into a 150-mL Teflon FEP beaker containing 100 mL of 5% nitric acid (measured from a graduated cylinder). The beaker was then placed on a magnetic stirrer, and the contents were stirred for approximately 10 min. The resulting solution was transferred to an acid-washed 125-mL linear polyethylene bottle. Blanks containing only lithium metaborate were also fused in the manner described above.

Reagents. Throughout the analytical work, deionized, distilled water was used. The lithium metaborate ($LiBO_2$) was Baker analyzed grade. The nitric acid used was analytical grade meeting American Chemical Society specifications. All linear polyethylene and Teflon FEP labware was washed in concentrated nitric acid and rinsed with deionized distilled water following a procedure similar to that recommended by Moody and Lindstrom (*14*).

Stock standard solutions were prepared in a manner similar to that in Dean and Rains (*15*) or purchased from Alfa Inorganics (Danvers, MA). Working standards were prepared by dilution of the stock solutions with a solution of $LiNO_3$ in 5% nitric acid such that the lithium concentrations of both the standards and

---

[1] Present address: Office of Oceanography and Marine Services, National Oceanic and Atmospheric Administration, Rockville, MD 20852

[2] Present address: Department of Physical Sciences, Prince Georges Community College, Largo, MD 20772.

0003-2700/84/0356-0033$01.50/0 © 1983 American Chemical Society

Table II. Emission Lines (nm) and Lowest Detectable Concentrations in Sediments (μg/g Except Where mg/g)

	emission line,[a] nm	lowest detectable concn in sediments[b]		emission line, nm	lowest detectable concn in sediments
Al	396.2	3 (mg/g)	Ga	417.2	2
Si	288.2	3 (mg/g)	Y	371.0	2
Ti	334.9	0.04 (mg/g)	Zr	339.2	6
V	347.9	5	Nb	408.0	
Cr	357.9	2	Mo	379.8	
Mn	403.1	10	La	394.9	5
Fe	373.7	0.4	Ce	418.7	10
Co	340.5	7	Dy	353.2	1
Ni	341.5	2	Yb	369.4	1
Cu	324.8	2	W	400.9	
Zn	213.9	5	Tl	351.9	

[a] Wavelengths are reported only to 0.1 nm because of the physical limitations of setting the monochromator. [b] Composition on a dry weight basis that will produce a solution by the described procedure with a concentration that will produce a signal twice the average standard deviation after subtraction of the blank.

the sample solutions matched. The geochemical standards used and their sources are listed in Table I.

Apparatus. Analysis of the borate solutions was done by direct current argon plasma emission spectrometry with a Spectraspan IV Echelle spectrometer equipped with the Spectrajet III DC plasma source (Spectrametrices, Andover, MA). Conditions for analysis were as recommended by the manufacturer, and the smallest available slits were used. The emission wavelengths used are listed in Table II. The spectral band-pass in the worst case was 0.02 nm. Tables of emission lines were checked for possible interferences before selecting analytical wavelengths (*10*). Analysis of the sediment–borate solutions commenced as soon as possible after fusion. Concentrations were calculated from three 5-s integrated emission signals.

The detection limit will be defined as the concentration of an element in 0.2 g of sample that, after being fused with 1 g of $LiBO_2$ and dissolved in 100 mL of aqueous solution, gives an emission signal, less blank, equal to twice the standard deviation of the background (*16*). Detection limits per unit weight of solid sample are listed in Table II. These detection limits are specific for our procedure. Doubling the sample weight or halving the final volume will halve the detection limits assuming no change in standard deviation. Lowering the flux to sample weight ratios, however, can result in recovery problems for some elements.

The graphite crucibles lose up to 10% of their initial mass during the fusion process and their surfaces are thus continuously degraded. Part of the mass of graphite lost during firing is trapped in the molten borate bead and is transferred to the nitric acid–borate solution. This results in the presence of black particles in the solution which are insoluble in acid, nonmagnetic, and range in size from fractions of a millimeter to millimeters. The formation of these particles showed no correlation with sample characteristics or fusion time. Fusion temperatures above 1100 °C appeared to decrease the formation of particles. Comparison between two fusions of the same sample, one in which particles appeared and one in which particles did not, showed no significant differences in the concentrations of the elements determined (*10*).

RESULTS AND DISCUSSION

Development and Testing. The lithium enhancement of the emission signal previously reported in the literature (*17*) was observed in this work. The concentration of Li^+ was kept constant for both the standard and sample solution to minimize this effect. The calibration curves of all the elements analyzed were found to be linear up to 1000 μg/L, except for those of Mn, Al, Si, Ti, and Fe which were linear up to 200 μg/L, 200, 800, 10, and 200 mg/L, respectively.

The effect of variations in the time of fusion was investigated by using two samples of sediment from the Chesapeake Bay and the NBS river sediment standard (SRM-1645). Four samples of each of the above were fused for 15, 30, 45, and 60 min, and the resulting molten borate bead dissolved and was analyzed as previously described. No significant differences due to variations in the time of fusion were noted (*10*).

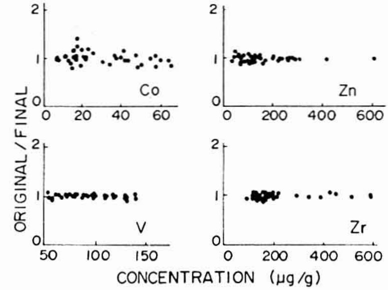

Figure 1. Comparison of results obtained within 1 month of fusion and during reanalysis of the same solutions 2 to 10 months later (μg/g dry weight). Sediment–borate solutions were stored at room temperature before reanalysis.

To determine whether the ACS reagent grade nitric acid used to dissolve the molten borate bead contributes significantly to the blanks, blanks were prepared with ultrapure nitric acid (G. Frederick Smith Chemical Co., Columbus, OH). All the values were comparable except in the case of Mn and La, which were higher in the ACS reagent grade nitric acid blank, and Ni and Zn, which were higher in the ultrapure acid blank. It was concluded that use of ultrapure acid offered no particular advantage over reagent grade acid.

The possibility of contaminating samples during fusion was investigated by comparing blanks prepared from fused $LiBO_2$ with blanks prepared by simply dissolving $LiBO_2$ reagent. Differences were negligible, indicating that this type of contamination was not a problem for the elements under study.

The stability of the solutions was tested by reanalysis several months after original preparation, of a randomly selected set of 30 solutions prepared from a suite of more than 300 sediment samples from the Chesapeake Bay. Typical results are shown in Figure 1. The newly determined concentrations were within 10% or better of the original values. The largest differences were observed for Co and Cu (not shown in Figure 1). In all cases, the reproducibility of the measurements was worse in solutions with concentrations close to the lower limit of detection. No evidence for systematic loss with time beyond the 10% range was observable of any for the elements discussed in this paper.

Precision and Accuracy. The precision of the analytical method was evaluated by performing replicate analysis (n = 6) of the USGS marine mud (MAG-1), the IAEA lake sediment (SL-1), the NBS estuarine sediment (SRM-1646)

Table III. Comparison of Replicate Analysis of the USGS Marine Mud (MAG-1) (µg/g Dry Weight Except Where Percent)

	analyzed simultaneously $(n = 6)$[a]	analyzed over 10 months $(n = 15)$[b]
Al (%)	7.6 (<1)[c]	7.0 (10)[c]
Si (%)	24 (< 2)	23 (5)
Ti (%)	0.48 (4)	0.49 (6)
V	140 (<4)	140 (4)
Cr	89 (1)	94 (6)
Mn	690 (3)	670 (3)
Fe (%)	4.4 (2)	4.1 (8)
Co	26 (12)	28 (24)
Ni	53 (4)	53 (6)
Cu	33 (10)	32 (9)
Zn	120 (4)	120 (8)
Ga	28 (3)	27 (11)
Y	11 (7)	13 (19)
Zr	98 (2)	110 (7)
La	41 (2)	42 (17)
Ce	130 (6)	110 (13)
Dy	3.0 (10)	3.6 (22)
Yb	1.6 (6)	2.3 (23)

[a] Mean values of six samples analyzed together as a batch. [b] Mean values of 15 samples analyzed one at a time over a period of 10 months. [c] Coefficient of variation (%) = 100σ/mean.

Table IV. Fusion Results of Duplicate Analyses of the NBS Estuarine Sediment (SRM-1646) (µg/g Except Where Percent)

	analyst I $(n = 6)$[a]	analyst (II) $(n = 6)$	F[c]	t[c]
Al (%)	5.3 (2)[b]	5.4 (1)	5.2*	
Si (%)	30 (3)	30 (1)	1.6	0
Ti (%)	0.36 (2)	0.37 (2)	6.4*	
V	89 (3)	91 (3)	1.4	1.4
Cr	74 (1)	70 (4)	9.0*	
Mn	280 (2)	280 (2)	1.0	0
Fe (%)	2.9 (2)	3.0 (0)		
Co	17 (18)	20 (14)	1.2	1.8
Ni	31 (5)	37 (6)	2.1	5.5*
Cu	28 (9)	28 (6)	5.6*	
Zn	130 (0)	120 (13)		
Ga	19 (8)	19 (6)	1.9	0
Y	17 (8)	15 (4)	5.0	3.2*
Zr	270 (4)	300 (4)	1.4	4.0
La	36 (2)	36 (3)	2.5	0
Ce	110 (4)	110 (7)	3.3	0
Dy	2.8 (7)	3.1 (14)	4.1	1.6
Yb	2.2 (4)	2.0 (5)	1.5	3.8*

[a] Number of samples. [b] Coefficient of variation (%) = 100σ/mean. [c] F and t test statistics, asterisk denotes a difference at the 5% level of significance.

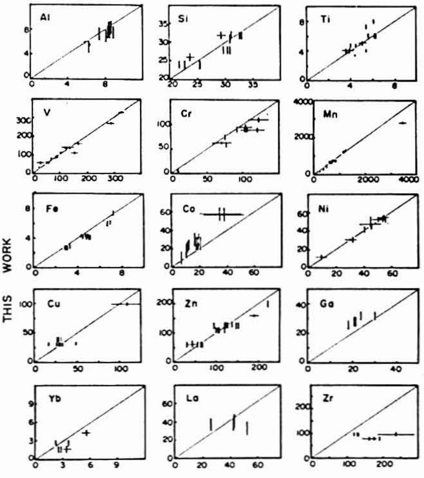

Figure 2. Experimental vs. certified and reported values of various geochemical standards (µg/g dry weight except for Al, Si, Ti, and Fe which are reported as percent). To improve clarity, horizonal error bars, representing uncertainty in the literature values, are shown only when they substantially exceed the vertical error bars. Vertical error bars are ±σ.

standard, and a Chesapeake Bay mud sample. The average results and coefficient of variation of these sets of replicates were similar (*10, 11*), the coefficients of variation being below 10% for all elements except Cu, Co, and Dy.

Marine mud (MAG-1) samples were also reanalyzed on a number of occasions over a period of 10 months as a quality control precaution during the analysis of sediment samples from the Chesapeake Bay. The average results and coefficient of variation of this set of 15 widely spaced determinations are compared to the simultaneously analyzed replicates ($n = 6$) in Table III. Use of the F test (*18*) indicated that most of the elements (Al, Si, V, Cr, Fe, Ga, Y, Zr, La, Dy, Yb) have variances that are significantly different at the 5% level. In all cases (except Mn and Cu), the coefficients of variation of the analyses performed over a period of months were moderately higher (i.e., higher variances), as would be expected.

Operator bias was investigated by independent analysis of the NBS estuarine sediment (SRM-1646) by two of the authors. The means and coefficients of variation ($n = 6$) are shown in Table IV. The F test results indicated that Al, Ti, Cr, and Cu have significantly different variances at the 5% level. This is also true for Fe and Zn, as the F test balloons to infinity because of identical replicate values observed by one of the analysts. The actual results, except for Cu, do not seem to be very different, especially since the coefficients of variation for all the elements involved are less than 5%. Low levels of Cu were a problem and the % CV's are somewhat higher (*10*).

For the elements with similar variances (i.e., those that satisfied the F test) the t test (*18*) was applied to test the similarity of the mean values. The results indicated that Ni, Y, Zr, and Yb have a difference in their means at the 5% level of significance. The difference for Zr is considered later in the paper.

In addition to the geochemical standards mentioned above, several others were analyzed by using this method to evaluate the accuracy. These standards are listed in Table I. The results obtained in this work and the values reported in the literature (*10, 11, 19–29*) are shown in Figure 2. Some analytical results obtained for the NBS river sediment (SRM-1645) and the NRC marine sediment (MESS-1) were included in Figure 2 although experimental problems were encountered which will be discussed below.

Fusion of the NBS river sediment standard (SRM-1645) yielded a black, insoluble magnetic phase which is believed to be chrome magnetite. This sediment has certified Cr and Fe contents of 2.96% and 11.3%, respectively, concentrations which are much higher than those normally found in typical uncontaminated estuarine and coastal sediments. The magnetic phase was not observed during the fusion of any of the other standards and may have formed due to the high contents of Cr and Fe present. Thus, the Cr and Fe recoveries obtained by using the fusion method are 71% and 68%, respectively. The certified Zn content of the SRM-1645, 1720 μg/g, is also higher than could be expected in typical uncontaminated sediments. The recovery obtained by using the fusion method is 93%. The results of the Cr, Fe, and Zn analyses of the SRM-1645 are not included in Figure 2. The results obtained for the other elements for this standard were comparable to values published in the literature and are included in Figure 2.

Part of the molten borate bead that formed during the fusion of the NRC marine sediment (MESS-1) remained undissolved in the nitric acid solution. This insoluble residue was hard, opaque, black and nonmagnetic. The MESS-1 borate solutions were analyzed only for Al, Si, Ti, V, Cr, Mn, Fe, Co, Ni, and Zn. The recoveries based on the Canadian NRC certified values were within the range 80–120%, or better, for these elements except for Ti and Co which were 76 and 190%, respectively.

It is generally agreed that, whenever possible, standards as similar in concentration as possible to the sample being analyzed should be used in order to evaluate the effectiveness of a given method for that particular sample matrix. In sediment analysis work, six standards are now available, the NBS SRM-1645 and SRM-1646, the USGS MAG-1, the IAEA SL-1, and the Canadian NRC BCSS-1 and MESS-1. Difficulties were encountered in fusing two of these standards, MESS-1 and SRM-1645.

In addition to the elements already mentioned, the determination of several others was attempted. Preliminary comparison of the amounts present and found in several of the geochemical standards suggested that the results for Mo, Nb, and Tl might be anomalous. Sediment–borate solutions of a geological standard, a Chespeake Bay sediment sample, and a blank were sent to the Applications Laboratory of Spectrametrics for wavelength scanning at the analytical wavelengths of these elements.

The Mo analytical line (379.8 nm) was found to overlap with other unidentified lines. Since the values determined for Mo were higher than those reported in the literature, it appears that background and/or matrix emission rather than Mo emission was being measured. The Nb line (407.9 nm) was free of visible background and/or matrix emission. The Nb values determined by using the method, however, were substantially higher than those reported in the literature. A good correlation between amounts of Ti and Nb in Chesapeake Bay sediments suggested that Ti may be interfering with Nb. This was investigated by analyzing a sediment–borate solution for Nb before and after increasing the Ti content of the solution by 20%. No change was observed in the apparent Nb concentration. The Nb concentration of this solution was then increased by 20 and 50%, but this increase likewise did not change the observed emission signal at the Nb wavelength. During the experiment, the location of the spectrometer on the analyte line was confirmed by using aqueous Nb standards. Emission from an unidentified component appears to coincide with the Nb emission line resulting in misleading Nb results.

The Tl analytical line (351.9 nm) was free of background and/or matrix emission, according to the results of wavelength scanning, but the data obtained for the geochemical standards were nearly 10-fold higher than those reported in the literature. Sample splits were sent to the U.S. Geological Survey for an independent analysis. The values determined by the Survey were indeed almost an order of magnitude lower than those determined in this work.

The determination of W was also attempted. The standard deviation of the concentrations determined was high and erratic. Stray light interference from the W cathode is possible although the cathode is physically about 2 cm away from the region of maximum emission of the plasma. During the reanalysis of the borate–sediment solutions months after the original analysis, it was found that the newly determined W values did not agree well with the ones previously determined, indicating loss of W from the solution with time.

Analytical reproducibility for the elements studied in this work, as measured by coefficients of variation in Tables III and IV, was mostly in the 2–10% range. Coefficients of variation for Co and some of the rare earths tended to be higher. Varations in the 2–10% range have been deemed acceptable by numerous analysts who do routine atomic absorption spectrometry. However, these variations are considerably larger than those that have been obtained with state-of-the-art multielement ICP (e.g., ref 4).

As judged by the results of analysis of geochemical standards (Figure 2), the accuracy of this method for most elements is not as good as its reproducibiliy. For seven of the sixteen elements in Figure 2 (Si, Ti, V, Mn, Ni, Cu, and Zn), there appears to be no systematic deviation of our results from those in the literature and the scatter is consistent with the estimated error determined from evaluating reproducibility. For five elements (Al, Cr, Fe, Yb, and Zr), our results appear to be systematically lower than those reported in the literature. However in the first three cases (Al, Cr, and Fe), the amount of systematic deviation is mostly in the 10% range.

Systematic underdetermination may be largely a defect of the $LiBO_2$ fusion rather than of the DC plasma emission determinations. In the worst case of this type, we observed a constant concentration of Zr in the standards (Figure 2) regardless of the amount present; this strongly suggests that the $LiBO_2$ flux had become saturated with a refractory phase such as $ZrSiO_4$. This kind of problem could be reduced by increasing the flux to sample ratio, but this strategy can lead to other problems including less favorable detection limits, higher noise, and clogging of the plasma torch system.

In the case of Co and Ga, our results appear to be systematically higher than those in the literature. This suggests the possibility of spectral interferences. For La as well as Zr, our results obviously are quite poor (Figure 2).

In summary, the lithium metaborate fusion–DC plasma emission method for the elemental analysis of sediments has several advantages. The fusion procedure is fast and does not require expensive laboratory equipment. In many cases, the method measures approximately the total element present in a sample. The amount of sample required is small. Although this can be a disadvantage in the analysis of sands and coarse grained materials (*10, 30*), it can be advantageous in the study of small geological features or in cases where sample size is limited. Perhaps the greatest frustration in this work was our inability to predict interference problems by inspecting standard wavelength tables (*31*) at wavelengths in the vicinity of the analytical lines we selected. These problems became apparent only after considerable work had been done with the geochemical standards. A wavelength scanning capability, not available on our instrument, would have greatly facilitated early discovery of interference problems.

ACKNOWLEDGMENT

The authors acknowledge F. J. Flanagan, Harry Rose, and William d'Angelo of the U.S. Geological Survey for some of the geological standards and for obtaining the thallium analysis, Donald Bankston, J. B. Willis, and Andrew Zander for their comments, and Spectrametrics Applications Laboratory for the spectral scans. This work was supported the Environmental Protection Agency's Chesapeake Bay Program (R 80594010).

Registry No. Al, 7429-90-5; Si, 7440-21-3; Ti, 7440-32-6; V, 7440-62-2; Cr, 7440-47-3; Mn, 7439-96-5; Fe, 7439-89-6; Co,

7440-48-4; Ni, 7440-02-0; Cu, 7440-50-8; Zn, 7440-66-6; Ga, 7440-55-3; Y, 7440-65-5; Zr, 7440-67-7; Nb, 7440-03-1; Mo, 7439-98-7; La, 7439-91-0; Ce, 7440-45-1; Dy, 7429-91-6; Yb, 7440-64-4; W, 7440-33-7; Tl, 7440-28-0; lithium metaborate, 13453-69-5.

LITERATURE CITED

(1) Ronan, R. J.; Kunselman, G. In "Methods and Standards for Environmental Measurement"; Kirchoff, W. H., Ed.; U.S. National Bureau of Standards: Washington, DC, 1977; Special pub. 464, pp 107–111.
(2) McQuaker, N. R.; Kluckner, P. D.; Chang, G. N. *Anal. Chem.* **1979**, *51*, 888–895.
(3) Walsh, J. N.; Howie, R. A. *Min. Management* **1980**, *43*, 967–974.
(4) McLaren, J. W.; Berman, S. S.; Boyko, V. J.; Russell, D. S. *Anal. Chem.* **1981**, *53*, 1802–1806.
(5) Skogerboe, R. K.; Urasa, I. T. *Appl. Spectrosc.* **1978**, *32*, 527–532.
(6) Johnson, G. W.; Taylor, H. E.; Skogerboe, R. K. *Appl. Spectrosc.* **1979**, *33*, 451–456.
(7) Burman, J.-O.; Pouter, C.; Bostrom, K. *Anal. Chem.* **1978**, *50*, 679–680.
(8) Bankston, D. C.; Humphris, S. E.; Thompson, G. *Anal. Chem.* **1979**, *51*, 1218–1225.
(9) Sinex, S. A.; Cantillo, A. C.; Helz, G. R. *Anal. Chem.* **1980**, *52*, 2342–2346.
(10) Cantillo, A. Y. Ph.D. Thesis, University of Maryland, College Park, MD 1982.
(11) Sinex, S. A.; Helz, G. R. *Environ. Sci. Technol.* **1982**, *16*, 820–825.
(12) Suhr, N. H.; Ingamells, C. O. *Anal. Chem.* **1966**, *38*, 730–734.
(13) Ingamells, C. O. *Anal. Chem.* **1966**, *38*, 1228–1234.
(14) Moody, J. R.; Lindstrom, R. M. *Anal. Chem.* **1977**, *49*, 2264–2267.
(15) Dean, J. A., Rains, T. C., Eds. "Flame Emission Atomic Absorption Spectrometry: Components and Techniques"; Marcel Dekker: New York, 1971; Vol. 2.
(16) Nygaard, D. D. *Anal. Chem.* **1979**, *51*, 881–884.
(17) Decker, R. J. *Spectrochim. Acta, Part B* **1980**, *35B*, 19–31.
(18) Davis, J. C. "Statistics and Data Analysis in Geology"; Wiley: New York, 1973.
(19) Fabbi, B. P.; Espos, L. F. *Geol. Surv. Prof. Pap.* (*U.S.*) **1976**, *No. 840*, 89–93.
(20) Katz, A.; Grossman, L. *Geol. Surv. Prof. Pap.* (*U.S.*) **1976**, *No. 840*, 49–57.
(21) Machavek, V.; Rubeska, I.; Sixta, V.; Sulcek, Z. *Geol. Surv. Prof. Pap.* (*U.S.*) **1976**, *No. 840*, 73–77.
(22) Manheim, F. T.; Hathaway, J. C.; Flanagan, F. J.; Fletcher, J. D. *Geol. Surv. Prof. Pap.* (*U.S.*) **1976**, *No. 840*, 25–28.
(23) Thomas, J. A.; Mountjoy, W.; Huffman, C. *Geol. Surv. Prof. Pap.* (*U.S.*) **1976**, *No. 840*, 119–112.
(24) Walker, G. W.; Flanagan, F. J.; Sutton, A. L.; Bastron, H.; Berman, S.; Dinnin, J. I.; Kenkins, L. B. *Geol. Surv. Prof. Pap.* (*U.S.*) **1976**, *No. 840*, 15–20.
(25) Weigand, P. W.; Thoreson, K.; Griffin W. L.; Heier, K. S. *Geol. Surv. Prof. Pap.* (*U.S.*) **1976**, *No. 840*, 79–81.
(26) Dybczynski, R.; Suschny, O. "Final Report on the Intercomparison Run SL-1 for the Determination of Trace Elements in a Lake Sediment Sample"; International Atomic Energy Agency: Vienna, 1979; IAEA/RL/64, 79-10306.
(27) Failey, M. P. Ph.D. Thesis, University of Maryland, College Park, MD, 1979.
(28) Quisefit, R. D.; DeLaBatie, R. D.; Faucherre, J.; Malingre, G.; Vie Le Sage, R. *Geostands. Newsl.* **1979**, *3*, 181–184.
(29) Bothner, M. H.; Aruscavage, P. J.; Ferrebee, W. M.; Baedecker, P. A. *Estuarine Coastal Mar. Sci.* **1980**, *10*, 523–541.
(30) Sinex, S. A.; Helz, G. R. *Environ. Geol.* (*N. Y.*) **1981**, *3*, 315–323.
(31) Meggers, W. F.; Corliss, C. H.; Scribner, B. F. "Tables of Spectral-Line Intensities"; U.S. National Bureau of Standards: Washington, DC, 1975; Mongraph 145.
(32) Abbey, S., *Geostands. Newsl.* **1980**, *4*, 163–190.
(33) Gladney, E. S.; Goode, W. E. *Geostands. Newsl.* **1981**, *5*, 31–64.
(34) Certificate of Analysis, 1981; National Research Council, Chemistry Division, Montreal Road, Ottawa, Canada.
(35) Certificates of Analysis, 1978 and 1982; U.S. National Bureau of Standards, Washington, DC.

RECEIVED for review September 29, 1982. Resubmitted September 12, 1983. Accepted September 27, 1983.

Generalized Internal Reference Method for Simultaneous Multichannel Analysis

Avraham Lorber and Zvi Goldbart*

Nuclear Research Centre—Negev, P.O. Box 9001, Beer-Sheva 84190, Israel

The applicability of the internal reference method is limited by the need to find a reference channel that will mimic the fluctuations of the analytical channel. A generalized internal reference method (GIRM) is suggested, that enables compensation of nonrandom fluctuations in analytical channels, regardless of the parameters affecting them. In the generalized method several internal standard channels, that respond differently to variations of the parameters of the analytical system, are measured simultaneously. The criteria for selecting internal standards and the calculation procedure are described. The GIRM is applicable to systems that are flicker noise limited and that perform multichannel (or multiplex) measurements simultaneously.

Inductively coupled plasma (ICP) atomic emission spectrometry (AES) is now one of the most important analytical methods for the accurate determination of minor elements and features very low limits of detection for trace elements. Both precision and limits of detection are signal to noise limited.

Noise characteristics for optical spectrometry sources were investigated by Winefordner et al. (*1*). Two major types of noise were considered: shot noise and fluctuation noise (flicker noise). Shot noise is due to the statistical nature of photon arrival at the detector and electron emission in the detector and amplifying electronics. Shot noise follows the Poisson distribution with the standard deviation proportional to the square root of the number of events. The second type of noise is the low-frequency noise called fluctuation (flicker) noise. This arises from changes caused by slow drift of analyte supply rate and light source drift. Analysis of the limiting noise in the ICP source (*2, 3*) showed that the source flicker noise contribution was dominant and limited the precision to 1%. This limit applies to other optical spectrometry methods as well (*1*).

A well-known method to reduce the nonrandom fluctuations is the internal standard method (ISM) (now known as the internal reference method) (*4*), which has been applied successfully in direct current (DC) arc spectrometry. Extensive theoretical and experimental studies of ISM in analytical emission spectrometry were performed by Barnett, Fassel, and Kniseley (*5, 6*). Their aim was to set criteria for a systematic procedure for choosing the right internal standard for each analytical line. Their list of criteria is copied here for convenience of discussion:

(1) The internal standard's concentration should be negligibly low.

(2) The internal standard should be very pure compared to the elements being determined.

(3) Both internal standard and analyte lines should have the same excitation energies.

(4) When photographic methods of recording are used, both

0003-2700/84/0356-0037$01.50/0 © 1983 American Chemical Society

lines should be of approximately the same wavelength.

(5) The volatilization rate of the internal standard element and the analyte element should be similar.

(6) The ionization energies of the internal standard and the analyte element should be similar.

(7) The atomic weights of the two elements should be roughly the same.

(8) Both lines should be free of self-absorption.

(9) Both lines should be of approximately the same intensity, especially when photographic methods are used.

Conditions 1, 2, 8, and 9 can easily be achieved; the other conditions constitute the ideal case.

The internal reference method has been used widely in spark and DC arc analytical emission spectrometry. These sources are characterized by time dependence of the analyte feed rate to the excitation zone and temporal and spatial fluctuations. The advantage of the IRM in these cases is in meeting criterion 5 mentioned above, when appropriate match of line pair is achieved. Other criteria for selecting the internal standard are of less importance as the mass transfer rate from sample to excitation zone is responsible for most intensity changes and source dependent noise. The reproducibility of a DC arc signal can be improved by this method from 40% deviation to 10%, and to 2% for the spark source.

Barnett et al. (*5*, *6*) checked the validity of the IRM for the ICP and found only limited success. The absence of a valid model for the source and the inapplicability of local thermodynamic equlibrium (LTE) conditions were the reasons for the unsuccessful application of IRM to the ICP. The problem of the applicability of the IRM to ICP was discussed at the second ICP conference at Noordwijk (*7*). It was noted there that many lines that were chosen showed negative response. To overcome this limitation it was suggested having one standard line for each analytical line. A recent note by Belchamber and Horlick (*2*) concluded that as a standard, one must choose the parameter that mimics in as many ways as possible the fluctuation behavior of the analyte. It is suggested there, that this parameter may be a spectral line, flow, pressure, or acoustic emission.

It is the aim of this work to present a mean for generalizing the internal reference concept and using it for drift correction. The generalized method may be applied without regard to the five restrictions (criteria 3 to 7) mentioned above. The method applies to all simultaneous multichannel methods and not only to emission spectrometry.

THEORY

In contrast to the traditional internal reference method that cannot be applied to systems violating criteria 3 to 7 (mentioned in the former section), the generalized internal reference method (GIRM) uses information on the variations of signals gathered simultaneously from channels having different physical parameters, to correct for variations in signals.

The calculation procedure that includes three steps is described schematically in Figure 1. The temporal characteristics of p internal standards signals (signals that are not affected by change of analytical sample concentration) serve as sensors to detect variation of the instrumental parameters. Rotation of the fluctuation data from the spectral line space to the instrumental parameter space is performed in the first step. In the second step the determined instrumental parameters are used to find the fluctuations of the analytical signals (signals produced by a species whose concentration is to be determined). In the last stage the calculated variations in the analytical signals are compared to the measured analytical signals variations to obtain information on the concentrations. When both calculated and measured variations are equal, the variation is attributed merely to system parameter variation from the "set point" (the system's condition at the time in which the analytical calibration function has been determined).

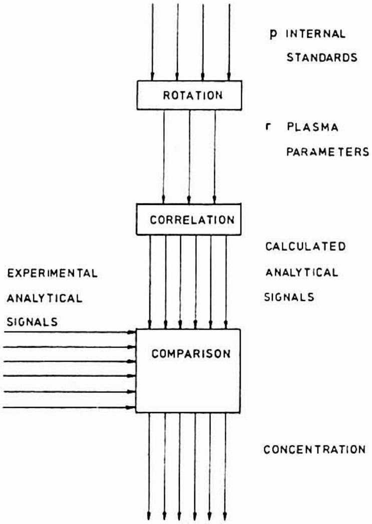

Figure 1. Mnemonic diagram illustrating the GIRM.

To illustrate the GIRM's calculation procedure, we assume that the fluctuation of ith spectral signal, y_i, is described by a linear sum of fluctuations of r ($r \le p$) system parameters, d_j. The assumption is valid both for the internal standard and for the analytical signals. Therefore we can write for the internal standard signals the set of equations given by (1). u_{ij}

$$\begin{aligned} u_{1,1}d_1 + u_{1,2}d_2 + \dots + u_{1,j}d_j + \dots + u_{1,r}d_r &= y_1 \\ u_{2,1}d_1 + u_{2,2}d_2 + \dots + u_{2,j}d_j + \dots + u_{2,r}d_r &= y_2 \\ &\vdots \\ u_{i,1}d_1 + u_{i,2}d_2 + \dots + u_{i,j}d_j + \dots + u_{i,r}d_r &= y_i \\ &\vdots \\ u_{p,1}d_1 + u_{p,2}d_2 + \dots + u_{p,j}d_j + \dots + u_{p,r}d_r &= y_p \end{aligned} \tag{1}$$

are the linear coefficients describing the variation of the ith internal standard signal due to fluctuation in the jth instrumental parameter. In matrix notation eq 1 is written as

$$\mathbf{Ud} = \mathbf{y} \tag{2}$$

where $\mathbf{U}$ is a $p \times r$ matrix, $\mathbf{d}$ is the vector of instrumental parameter fluctuations with r elements, and $\mathbf{y}$ is the internal standard fluctuation vector with p elements. In cases that ($p > r$) a least-squares solution of the matrix equation is given by

$$\mathbf{d} = (\mathbf{U}^{\mathrm{T}}\mathbf{U})^{-1}\mathbf{U}^{\mathrm{T}}\mathbf{y} \tag{3}$$

The calculated value of any analytical signal is computed by an equation similar to eq 1 with the aid of the vector $\mathbf{d}$.

The linear model of the GIRM presented in eq 1–3 may serve as a possible model for a rough approximation as will

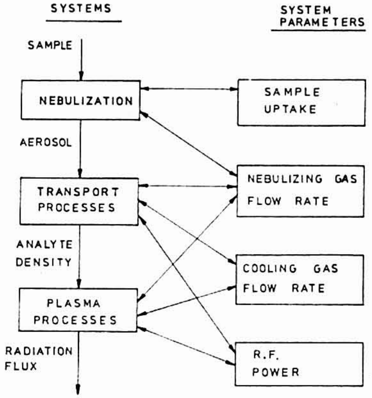

Figure 2. Block diagram illustrating the compound system concept and the alternative system parameters representation. Inductively coupled plasma is used as a model.

be shown later. However, the actual relations describing the signal fluctuation cannot be described as a summation of the system parameter fluctuations. In order to form a suitable basis to develop the method, one must define some terms and analyze the compound system involved.

System Consideration. The ICP, which serves as a popular light source for atomic emission spectrometry is used to demonstrate the concept of the compound system and its analysis. The compound system of the ICP, shown in Figure 2, transforms the sample, which is the input signal, to an output light signal. The light detection and electronic readout system is not considered, as it is assumed that its main contribution to the noise is shot noise which is negligible. Each system is characterized by an individual transfer function that is the ratio of the output signal to the input signal. The transfer function is time dependent but its value is controlled by external system parameters shown at the right side of the figure. A change in the transfer function of one system will result in the proportional change of its output signal which is the input signal for the following system. The transfer function of the compound system will therefore be the product of the transfer functions of the individual systems.

In terms of system theory the impulse response of a compound system $h_c(t)$ fully characterizes a linear system. Provided that the impulse response is known, the output signal $\xi(t)$ can be calculated from the input signal $\chi(t)$ with the convolution interal (8)

$$\xi(t) = \int_0^\infty h_c(\tau)\chi(t-\tau)\,\mathrm{d}\tau \equiv h_c(t)*\chi(t) \qquad (4)$$

If the impulse response $h_i(t)$ of each of the individual system processes is known, the impulse response of the complete linear system of three components can be expressed as

$$\xi(t) = h_3(t)*\{h_2(t)*[h_1(t)*\chi(t)]\} = h_3(t)*h_2(t)*h_1(t)*\chi(t) \qquad (5)$$

The systems that comprise the compound transfer function are more practically represented by system parameters that are measurable quantities, while the impulse response of the systems cannot usually be measured, especially during an analytical run. The analytical functions describing the systems in terms of system parameters are usually unknown. However, we can describe the transformation of the input signal to the output signal by system parameters directly when the following requirememts are fulfilled: (a) all system parameters that affect the signal have been included; (b) the changes in system parameters are mutually independent; (c) each functional relationship, g_j, describing the dependence of the output signal on the ratio, l_j, of the present jth system parameter value to its value at the "set point", can be found experimentally.

We observe that a change in one parameter changes the output signal, which is the input signal for the following parameter change. The transfer function of the compound system is therfore the product of the individual functional relationship values.

In order to omit time dependence, we notice that the time lag between the entrance of the sample and the exit of radiation is short when compared to the integration time. The output signal therefore represents the sample which enters the system within the same time interval. The time dependence of the response function can be replaced by a serial integration index, m. To further simplify the notation we notice that the exact number of a measurement in a sequence is of no importance. The ratio of the present measurement value to the value at the point referred to as the "set point", is the quantity of importance. Thus, the integration index is omited.

The preceding assumptions and observations allow us to write the dependence of the output signal on system parameters as

$$\xi = \prod_{j=1}^{r} g_j(l_j)\cdot\chi \qquad (6)$$

where the product is taken over the r system parameters and χ and ξ are integrations of the input and output signals, respectively, taken over an arbitrary period.

The explicit presentation of the plasma parameters in eq 6 sets a limitation on the precision that may be obtained from the method. In order to achieve high precision, the precision in measuring system parameters, when calibrations are performed, should be at least as high as that in measuring analytical signals. This is not the case in instrumental analytical systems (if gas flow rates are assigned to system parameters, they can be measured within a relative error of 1%, which is 2 orders of magnitude higher than a 12 bit A/D converter resolution). Therefore, the system parameters fluctuation measurements should be replaced by sensors that have the same precision as those of analytical signals. The replacement is done by an alternative definition of the IRM.

Defining the Internal Reference Method. "The internal reference method (IRM) is a method of correction for system fluctuations by measuring reference signals that emerge from the same source as analytical signals".

The term signal will be limited to the output signals of the system, I_i ($i = 1, ..., s$). Deviation in signal is expressed by a relative signal, I_i^{R}, defined as the ratio of the instantaneous signal to its value at the "set point".

Reference signal is an internal standard signal that serves as a scale for measuring the values of the system parameters at a specific integration period. The reference signal, $I_{\mathrm{ref}}^{\mathrm{R}}$, is a product of r components, each of which, $I_{\mathrm{ref},j}^{\mathrm{R}}$, varies due to the jth parameter while all other parameters are held constant according to

$$I_{\mathrm{ref},j}^{\mathrm{R}} \equiv I_{\mathrm{ref}}^{\mathrm{R}}(l_j) \quad (\text{all } l_k \neq l_j \text{ held constant}) \qquad (7a)$$

and the total reference signal is

$$I_{\mathrm{ref}}^{\mathrm{R}} = \prod_{j=1}^{r} I_{\mathrm{ref},j}^{\mathrm{R}} \qquad (7b)$$

With this definition of the internal reference signal, it is obvious that the components of the reference signal replace the instrumental parameters and the compound reference signal described by eq 7b acts in the same way as the compound transfer function in eq 6, thus providing a means to avoid the presentation of the parameters explicitly. For a single internal standard, the internal standard signal serves as the reference signal.

The IRM Calculation Procedure. The calculation procedure is as described in Figure 1: p internal standard signals are measured ($p \geq r$) and used to calculate the components $I_{\mathrm{ref},j}{}^{\mathrm{R}}$ of the reference signal by solving the set of equations (8a). The first equation in this set is equivalent to eq 7b.

$$\begin{aligned} I_{\mathrm{ref}}{}^{\mathrm{R}} &= \prod_{j=1}^{r} I_{\mathrm{ref},j}{}^{\mathrm{R}} \\ I_2{}^{\mathrm{R}} &= \prod_{j=1}^{r} f_{2,j}(I_{\mathrm{ref},j}{}^{\mathrm{R}}) \\ &\;\;\vdots \\ I_i{}^{\mathrm{R}} &= \prod_{j=1}^{r} f_{i,j}(I_{\mathrm{ref},j}{}^{\mathrm{R}}) \\ &\;\;\vdots \\ I_p{}^{\mathrm{R}} &= \prod_{j=1}^{r} f_{p,j}(I_{\mathrm{ref},j}{}^{\mathrm{R}}) \end{aligned} \qquad (8a)$$

The rest of the equations that describe the functional relationships $f_{i,j}$ are determined by

$$I_{i,j}{}^{\mathrm{R}}(l_j) = f_{i,j}(I_{\mathrm{ref},j}{}^{\mathrm{R}}) \quad (\text{all } l_k \neq l_j \text{ held constant}) \qquad (8b)$$

The components of the reference signal can now be used to calculate the "calculated analytical signal"—$I*_i{}^{\mathrm{R}}$ for analytical signals i ($i = q, ..., s$). The calculated analytical signal is the signal that is obtained if the analyte concentration is held constant. The set of equations for the calculated analytical signals is given in eq 9.

$$\begin{aligned} I*_q{}^{\mathrm{R}} &= \prod_{j=1}^{r} f_{q,j}(I_{\mathrm{ref},j}{}^{\mathrm{R}}) \\ &\;\;\vdots \\ I*_i{}^{\mathrm{R}} &= \prod_{j=1}^{r} f_{i,j}(I_{\mathrm{ref},j}{}^{\mathrm{R}}) \\ &\;\;\vdots \\ I*_s{}^{\mathrm{R}} &= \prod_{j=1}^{r} f_{s,j}(I_{\mathrm{ref},j}{}^{\mathrm{R}}) \end{aligned} \qquad (9)$$

When there is no change in the concentration of the analyte, the ratio $I_i{}^{\mathrm{R}}/I*_i{}^{\mathrm{R}}$ should equal unity. Therefore, any variation in this ratio indicates a variation in the concentration C_i

$$C_i = \psi_i(I_i{}^{\mathrm{R}}/I*_i{}^{\mathrm{R}}) \qquad (10)$$

where ψ_i is the analytical calibration function. Considering the concentration as the input signal to the system, one observes that eq 10 acts in the same way as eq 6.

In the following section the sets of eq 8, 9, and 10 will be solved for three degrees of complexity as follows: (a) solving eq 10 assuming $I*_i{}^{\mathrm{R}} = I_{\mathrm{ref}}{}^{\mathrm{R}}$; (b) solving eq 9 and 10 assuming the response of $I*_i{}^{\mathrm{R}}$ to all components of the reference signal is the same; (c) the general case, solving all three equations.

Schemes for Solution. *Line Ratio Internal Reference Method* (*LRIRM*). This is the well-known IRM, which is the simplest case of the full method. Let eq 8 be $I*_i{}^{\mathrm{R}} = I_{\mathrm{ref}}{}^{\mathrm{R}}$ for all analytical signals, regardless of the fluctuation in system parameters. Inserting it into eq 10 results in

$$C_i = \psi_i(I_i{}^{\mathrm{R}}/I_{\mathrm{ref}}{}^{\mathrm{R}}) \qquad (11)$$

This solution shows the same dependence for all analytical lines, as the reference line has only one component. The physical interpretation is that the change in analytical signal is related to the compound system and cannot be related to any specific system or to its corresponding system parameter.

Analyte–Internal Reference Correlated Method (*AIRCM*). This method assumes that each calculated analytical signal is correlated to the reference signal by its specific equation

$$I*_i{}^{\mathrm{R}} = f_i(I_{\mathrm{ref}}{}^{\mathrm{R}}) \qquad (12)$$

Using this assumption we still observe a compound system that cannot be divided into systems and that reacts with the same response to all system parameters. Equation 12 is superior to eq 11, as it permits a specific functional relationship, f_i, of the ith relative analytical signal to the reference signal. These functions must be found experimentally and may even have a negative response. There are two experimental methods to find the functional relations. The first is to collect random analytical and reference signals and correlate them by a common statistical regression. The second is to perform a predetermined change in system parameters. Each method has its advantages and limitations. The first method is superior to the second in that the measured changes are representative of the fluctuations that usually occur in the compound system. It is limited, however, as there is no guarantee that the fluctuations that have occurred represent the fluctuations in the measuring interval. The advantage of the second method is that the coefficients are determined by taking measurements throughout the whole range of possible fluctuations. This approach may cause inaccurate determination of coefficients as the weight it applies to each change in any parameter is the same, while the first approach represents the right weight proportions.

Generalized Internal Reference Method (*GIRM*). In GIRM, eq 8, 9, and 10 are solved by assuming that the functions $f_{i,j}$ can be written as a power series

$$y_{i,j} = a_{i,j}x_j + b_{i,j}x_j{}^2 + ... \qquad (13)$$

where $y_{i,j}$ is the relative fluctuation in the ith signal caused by variation of the jth instrumental parameter and x_j is the fluctuation of the jth component of the reference signal. The fluctuation terms are connected to the relative signal by $y_i = I*_i{}^{\mathrm{R}} - 1$ and $x_j = I*_{\mathrm{ref},j}{}^{\mathrm{R}} - 1$. Each equation in the set of equations (8) then becomes

$$I_i{}^{\mathrm{R}} = \prod_{j=1}^{r}(1 + a_{i,j}x_j + b_{i,j}x_j{}^2 + ...) \qquad (14)$$

Equation 14 is a nonlinear equation. However, by assuming small fluctuations we may neglect all terms of order higher than 1 and obtain

$$y_i \simeq \sum_{j=1}^{r} a_{i,j}x_j \qquad (15)$$

which connects the fluctuation in the signal to fluctuations in the components of the reference signal linearly. This equation is the same as eq 2 except that the instrumental parameters are now replaced by x_j. The set of eq 8 and 9 now becomes eq 16. The reasons for deriving the linear approximation are the following: It presents a simple method for solving the GIRM and a first approximation for a more accurate solution of eq 8 by nonlinear methods. It serves to describe new criteria for selection of internal standards and to estimate the error propagation involved in the method.

$$\begin{pmatrix} 1 & 1 & \cdots 1 & \cdots 1 \\ a_{2,1} & a_{2,2} & \cdots a_{2,j} & \cdots a_{2,r} \\ \vdots & & & \\ a_{r,1} & a_{r,2} & \cdots a_{r,j} & \cdots a_{r,r} \\ \vdots & & & \\ a_{p,1} & a_{p,2} & \cdots a_{p,j} & \cdots a_{p,r} \\ a_{q,1} & a_{q,2} & \cdots a_{q,j} & \cdots a_{q,r} \\ \vdots & & & \\ a_{s,1} & a_{s,2} & \cdots a_{s,j} & \cdots a_{s,r} \end{pmatrix} \begin{pmatrix} x_1 \\ x_2 \\ \vdots \\ x_r \end{pmatrix} = \begin{pmatrix} y_1 \\ y_2 \\ \vdots \\ y_r \\ \vdots \\ y_p \\ y_q \\ \vdots \\ y_s \end{pmatrix} \qquad (16)$$

We can describe eq 16 by means of matrix notation as

$$\mathbf{A}\mathbf{x} = \binom{\mathbf{y}_1}{\mathbf{y}_2} \qquad (17)$$

where **A** is the $s \times r$ matrix composed of $a_{i,j}$ components, **x** is the vector of r components of the fluctuations of the reference signal, and $\mathbf{y}_1$ is an upper subvector of measured fluctuations in the internal standard signals. $\mathbf{y}_2$ is a lower subvector of $(s - p)$ elements, of the calculated analytical signal fluctuations. Considering the upper $p \times r$ submatrix $\mathbf{A}_1$, which corresponds to the coefficients of internal standard signals and the lower $(s - p) \times r$ submatrix $\mathbf{A}_2$, which corresponds to the coefficients of the analytical signals, the solution of the GIRM method is performed according to the following steps:

The vector **x** is found by solving the equation

$$\mathbf{A}_1\mathbf{x} = \mathbf{y}_1 \qquad (18)$$

which has a least-squares solution

$$\mathbf{x} = (\mathbf{A}_1^{\mathrm{T}}\mathbf{A}_1)^{-1}\mathbf{A}_1^{\mathrm{T}}\mathbf{y}_1 \qquad (19)$$

The vector $\mathbf{y}_2$ is then simply

$$\mathbf{y}_2 = \mathbf{A}_2(\mathbf{A}_1^{\mathrm{T}}\mathbf{A}_1)^{-1}\mathbf{A}_1^{\mathrm{T}}\mathbf{y}_1 \qquad (20)$$

More accurate solutions of eq 8 are obtained by taking into account higher orders of the term x_j. For example, by adding second-order terms to eq 14, we get

$$y_i \equiv \sum_{j=1}^{r} a_{i,j}x_j + \sum_{j=1}^{r} b_{i,j}x_j^2 + \sum_{j=1}^{r-1}\sum_{k=j+1}^{r} a_{i,j}a_{i,k}x_jx_k \qquad (21)$$

The higher order terms are added to the right-hand side of eq 16 and the system is solved iteratively by one of the methods described in ref 9. The linear system (eq 16) serves as an initial approximation.

A generalized approach is the solution of the nonlinear system (eq 8) by one of the methods of unconstrained optimization. We solve the objective function

$$F = \min \sum_{i=1}^{p} \left| \frac{(I^{*}{}_i^{\mathrm{R}} - I_i^{\mathrm{R}})^2}{w_i} \right| \qquad (22)$$

where w_i values are the weights. The objective function minimizes the least-squares sum of the differences between the calculated values of the relative internal standard signals, $I^{*}{}_i^{\mathrm{R}}$, and its measured value, I_i^{R}. The sum is taken over the internal standard signals. A first estimate for $I_{\mathrm{ref},j}^{\mathrm{R}}$ can be obtained by eq 19. Methods for solving unconstrained optimization problems can be found in ref 10.

The determination of the coefficients in eq 14, can be done in one of the following ways: variation of each system parameter separately; variation of all system parameters simultaneously.

The experimetnal design for the first approach is easier, but the second method has an advantage of having more statistical information for each parameter change (for the same number of experiments). It is easier to examine the benefits of each method when using the linear approximation. Equation 16 can then be written for a set of m experiments as

$$\mathbf{A}\mathbf{X} = \mathbf{Y} \qquad (23)$$

where **X** is the $r \times m$ matrix for m changes in the r components of the reference signal and **Y** is the $s \times m$ matrix for m changes in s signals. The problem of solving eq 23 is similar to the problem of finding the concentrations of several components in a set of multicomponent solutions with an array of detectors, each of which is interfered by all accompanying components. Such a problem was analyzed by Kowalski et al. (*11, 12*) for the generalized standard additon method (GSAM), who found that the first method is preferable as its error propagation is minimal. This will, of course, be even more important for our nonlinear system. Therefore, it is highly recommended to vary one parameter for determination of each coefficient.

DISCUSSION

In the simple internal reference method, since the mathematical relationship is a simple ratio, the "rules" for selecting an appropriate standard are mainly physical. In the GIRM, since the signals are correlated to system parameters, the physical criteria are not important, except that the signals of the standard channels must be large enough to avoid shot noise limited precision. Instead of physical criteria we have the following mathematical demands: The rank of the coefficient matrix should be sufficient to avoid singularity, and the number of internal standards must be equal or greater than the number of considered parameters. The error in internal standard signals should be limited to a level that will be stated in the following section. The standard channels should be selected for minimum error propagation.

Rank Deficiency in the GIRM. It has been stated that for r instrumental parameters we must have p internal standard signals so that $p \geq r$. More precisely, p should be larger than or equal to the rank (**A**). A matrix whose rank is smaller than r is singular. This can happen for the following reasons:

(a) The rows of the matrix **A** are multiples of other rows. This is the case when some internal standards respond in the same manner to instrumental parameter variations, so that they behave according to the criteria for internal standards mentioned by Barnett et al. (*5*). This can also occur if one internal standard is correlated to another internal standard.

(b) The rows of the matrix are linear combinations of each other. This case is very unlikely to happen and has not yet been observed in cases of analytical applications.

(c) A column of the matrix is a multiple of another one. This happens when two instrumental parameters affect the same system and thus only one column is needed to define the system change; the change in signal cannot be related to either of the instrumental parameters alone. This can also occur if the signal is affected similarly by two different system parameters, not necessarily the same system.

(d) A column of the matrix is a linear combination of other columns. In this case the number of systems affecting the signal is exceeded by the number of assumed instrumental parameters. To avoid singularity and permit solution of the matrix, one system parameter should be excluded. With this principle the analytical system can be analyzed for the minimum number of systems that can define the analytical output.

In principle, the rank of the matrix **A** can be calculated by the Gaussian process of elimination. However, experimental errors destroy the elegance of this process, and statistical methods of decision must be brought for rank determination. A few methods have been developed and applied to the determination of the number of species in multicomponent systems (*13–17*). The application of rank (factor) analysis to chemistry has been reviewed by Malinowski and Howery (*18*).

Error Propagation in the GIRM. Solving eq 16, one finds two extreme cases of accuracy: In the first case (the "well conditioned" case), each coefficient of the equation is related to one plasma parameter and thus the coefficient matrix (except the internal reference row) is diagonal. This leads to a solution in which each equation is solved independently. The uncertainty in determination of each variable is, therefore, not affected by the others. The opposite case (the "ill conditioned" case) leads to a singular matrix that cannot be inverted in order to find a solution. Therefore, the error in solving it tends to infinity. Between those two extremes lies the general case in which the errors in the experimental data are propagated. An example for error propagation is quoted here (*12*).

$$\begin{pmatrix} 3.56 & -1.92 \\ -1.92 & 2.44 \end{pmatrix} \begin{pmatrix} x_1 \\ x_2 \end{pmatrix} = \begin{pmatrix} -20 \\ 15 \end{pmatrix} \quad (24)$$

The solution of this sytem is $x = (-4.0, 3.0)^{\mathrm{T}}$ as is easily verified. Suppose the right-hand side, b, is perturbed by the error vector $\delta b = (0.3, 0.4)^{\mathrm{T}}$ which produces a relative error $||\delta b||/||b||$ of 2% ($||\cdot|| \equiv$ the Euclidian norm of the vector, defined by the square root of the sum of the squared elements of the vector). The corresponding solution for the perturbed vector $\bar{x} = x + \delta x$ is; $\bar{x} = (-3.7, 3.4)^{\mathrm{T}}$ which corresponds to a relative solution error of 10%. Thus an error amplification factor of 5 results. This fact should be considered when a set of internal standard signals is selected. The set should give the minimum error amplification possible. There are two methods for determining the condition of a matrix (*19*). One is an analytical method that determines the "condition number", that can be calculated by

$$\mathrm{cond}\ (\mathbf{A}) = (\lambda_1/\lambda_k)^{1/2} \quad (25)$$

where λ_1 is the largest eigenvalue of the matrix $\mathbf{A}^{\mathrm{T}}\mathbf{A}$ and λ_k is the smallest significant eigenvalue. The second method is the "sensitivity analysis".

Errors due to the Extraction of the Signals from the Background. The measured gross signal, I_{G_i}, is composed of

$$I_{\mathrm{G}_i} = I_{\mathrm{c}_i} + I_{\mathrm{d}} + I_{\mathrm{s}} \quad (26)$$

where I_{c_i} is the signal due to the concentration of species i, I_{d} is a background signal that is dominated by drift noise (source background), and I_{s} is a background signal that is dominated by shot noise (electronic components in the detection system). Let us assume no drift components and deal only with shot dominated noise. If we require that the relative error not exceed e_1, we get the condition

$$e_1 > [\sum_{i=1}^{r} I_{\mathrm{G}}(p-r)]^{-1/2} \quad (27)$$

This is the ideal case. When an attempt is made to solve eq 8, one begins with I_{c_i}, which includes the drift noise in the background, I_{d}. For this case we have the condition

$$e_2 > S_{\mathrm{d}}{*}[\sum_{i=1}^{p} (I_{\mathrm{d}}/I_{\mathrm{c}_i})^2/(p-r)]^{1/2} \quad (28)$$

where S_{d} is the drift component value in the background.

The signal from the drift dominated background may be corrected by considering it as an analytical signal, given that its correlation to the various instrumental parameters is known. This calculated value of the background is inserted in calculating I_{c}. Successive approximations will result in a background that is free of drift. In order that convergence will occur, the following condition should be satisfied:

$$e_2 \gg e_1 \quad (29)$$

The criterion for stopping the iteration is

$$||\mathbf{y}_1^{n+1} - \mathbf{y}_1^{n}|| \simeq e_1 \quad (30)$$

where $\mathbf{y}_1^n$ is the value of the vector of internal standard signals at the nth iteration. The final result will be free of drift. This iteration procedure can be applied to problems of analyzing small signals in high background spectra, in which the background noise is dominated by drift noise.

CONCLUSIONS

The GIRM takes full advantage of the multidimensional data obtainable in the multichannel analytical system, in order to improve the performance of analytical instruments. This is an alternative to the common approach of improving the stability of the analytical instrument components. Application of the GIRM to existing analytical signal sources results in the following benefits:

The characterization of nonrandom noise can be accomplished (*20*), to find the contribution of various components of an instrumental system. Systems of different firms can thus be compared and improvement in components performance can be quantitatively evaluated. This concept can be further extended to detect possible differences between sampling techniques and between different sample preparation methods.

The precision of simultaneous multielement analysis can be improved (*21*) up to the limit of shot noise.

In high background spectra, the GIRM can be used to determine precisely the background at the analytical channels during the data collection period. The limit of detection, which is inversely proportional to the background noise, can thus be improved.

The method as presented here does not include correction for spectral interelement interferences, though extention of this case is possible by the generalized standard addition method (*11*) or by multivariate calibration.

The motivation for generalizing the internal reference method was due to problems encountered in applying the method to the ICP source as mentioned above. However, other multichannel systems also may be considered. Of particular interest is the application of the GIRM to isotopic dilution mass spectrometery (IDMS). Successful application will result in reducing the number of isotopes (acting as internal standards) in multielement analysis and precision improvement.

In a following publication the suggested method will be applied to an ICP source (*21*).

ACKNOWLEDGMENT

The authors wish to thank A. Levin and S. Adar for carefully reading this manuscript.

LITERATURE CITED

(1) Winefordner, J. D.; Avni, R.; Chester, T. L.; Fitzgerald, J. J.; Hart, L. P.; Johnson, D. J.; Plankey, F. W. *Spectrochim. Acta, Part B* **1976**, *31B*, 1–19.
(2) Belchamber, R. M.; Horlick, G. *Spectrochim. Acta, Part B* **1982**, *37B*, 71–74.
(3) Boumans, P. W. J. M.; McKenna, R. J.; Bosveld, M. *Spectrochim. Acta, Part B* **1981**, *36B*, 1031–1058.
(4) Boumans, P. W. J. M. "Theory of Spectrochemical Excitation"; Hilger & Watts: London, 1966.

(5) Barnett, W. B.; Fassel, V. A.; Kniseley, R. N. *Spectrochim. Acta, Part B* **1968,** *23B,* 643–664.
(6) Barnett, W. B.; Fassel, V. A.; Kniseley, R. N. *Spectrochim. Acta, Part B* **1970,** *25B,* 139–161.
(7) Greenfield, S. *ICP Inf. Newsl.* **1978,** *4,* 199–220.
(8) Duursma, R. P. J.; Smit H. C.; Maessen, F. J. M. J. *Anal. Chim. Acta* **1981,** *133,* 393–408.
(9) Carnahan, B.; Luther, H. A.; Wilks, J. O. "Applied Numerical Methods"; Wiley: New York, 1969.
(10) Murray, W. "Numerical Methods for Unconstrained Optimization"; Academic Press: London, 1972.
(11) Saxberg, Bo E. H.; Kowalski, B. R. *Anal. Chem.* **1979,** *51,* 1031–1038.
(12) Jochum, C.; Jochum, P.; Kowalski, B. R. *Anal. Chem.* **1981,** *53,* 85–92.
(13) Wallace, R. M. *J. Phys. Chem.* **1960,** *64,* 899–901.
(14) Wallace, R. M. J.; Katz, S. M. *J. Phys. Chem.* **1964,** *68,* 3890–3892.
(15) Katakis, D. *Anal. Chem.* **1965,** *37,* 876–878.
(16) Hugus, Z. Z., Jr.; El-Awady, A. A. *J. Phys. Chem.* **1971,** *75,* 2954–2957.
(17) Wernimont, G. *Anal. Chem.* **1967,** *39,* 554–557.
(18) Malinowski, E. R.; Howery, D. G. "Factor Analysis in Chemistry"; Wiley: New York, 1980.
(19) Rice, J. R. "Matrix Computation and Mathematical Software"; McGraw-Hill: New York, 1981.
(20) Lorber, A.; Goldbart, Z. *Spectrochim. Acta, Part B* **1983,** *38B,* 211 (Supplements).
(21) Lorber, A.; Goldbart, Z.; Eldan, M. *Anal. Chem.* **1984,** *56,* 43–48.

RECEIVED for review September 20, 1982. Accepted September 2, 1983.

Correction for Drift by Internal Reference Methods in Inductively Coupled Plasma Simultaneous Multielement Analysis

Avraham Lorber, Zvi Goldbart,* and Michael Eldan

Nuclear Research Centre—Negev, P.O. Box 9001, Beer-Sheva 84190, Israel

The internal reference method (IRM) is a common method for the correction of nonrandom fluctuations in atomic emission spectrometry (AES). A generalized form of the IRM (GIRM) is presented in this paper, which enables the detection of variations in discrete plasma parameters, through internal standards. An inductively coupled plasma (ICP) system was used to evaluate the GIRM. Changes with time in net line intensity, of various spectral lines, over 30-min periods were recorded by a photodiode array system and then corrected for the drift by the GIRM. It was found that the remaining noise exceeded that of the detection system (0.07%) by 30% to 100% only, whereas without this treatment the drift was a 100 times higher than that of the detection system.

There are three common approaches to the stabilization of output signals that are affected by nonrandom noise: (a) the noise characteristics of the signal generating system are improved; (b) the physical parameters of the system are kept constant by a measuring and feedback system; (c) the signal is corrected by computational techniques only.

The first approach was applied to an ICP system and succeeded in reducing noise to less than 0.5% by using an improved nebulizer and stabilized flow (*1*).

The application of the second approach to ICP-AES was proposed by Ohls and Koch (*2*) and was tested by Dorn (*3*). A certain degree of improvement in the stability of the argon signal was achieved at the cost of considerable complication of the measurement and control system and the requirement that the accuracy in measuring the variable parameters of the analytical system be at least as high as that in measuring the analytical signals. This requirement becomes especially rigorous in cases where small changes in the experimental variable parameters cause amplification of the instability of the analytical signals. This approach is especially important and common for cases in which the deviations in the output signal are caused by changes in system parameters such as chemical processes, which are irreversible.

The third approach has become more attractive in recent years, with the rapid advance and the miniaturization of computers and the tendency to incorporate them in modern analytical apparatus.

In a recent note Belchamber and Horlick (*4*) suggested that changes in one variable parameter—the pressure in the spray chamber—are representative of most of the plasma parameters. Correlating the measured changes of this parameter to changes in the analytical signal allows its correction. This treatment has the same limitation as the second approach, with respect to the accuracy in measuring the plasma parameter.

Others have suggested that the drift of the output signal is a simple function of time and thus can be corrected either by prior calibration (*5*) or by measuring a number of standards before and after the analytical run (*6*). This treatment can be applied only to sources for which this assumption is valid.

A well-known method for correcting nonrandom fluctuations in AES is the IRM (7). A spectral line with physical parameters similar to those of an analytical line is selected as a reference, and it is assumed that both lines are affected to the same degree by various parameters, so that the ratio of their signal intensities is constant. This method does not provide the sought for correction of output signal for the relatively new emission sources such as ICP and direct current plasma, and therefore its use is limited mainly to atomic emission sources such as DC arc, sparks, and glow discharge. The reason that the IRM does not hold for ICP is that the observed changes in the internal reference line do not necessarily mimic those in the analytical lines (*8*).

The IRM can be used for plasma sources that are in local thermodynamic equilibrium even though the line pair is not similar, on condition that the temperature change is known (7). Barnett et al. (*9*) checked experimentally and concluded that an ICP source is dominated by non-LTE mechanisms.

Three versions of the IRM were presented in detail in a separate paper (*10*). In the present work the compatibility of the three versions was tested experimentally.

THEORY

The line ratio internal reference method (LRIRM) correlates variations in concentration C_i of the ith element in a sample to variations of the ratio I_i^R/I_{ref}^R, where I_i^R is the relative intensity (≡intensity at present measurement divided

0003-2700/84/0356-0043$01.50/0 © 1983 American Chemical Society

Table I. Experimental Facilities and Operating Conditions

aerosol generator	Meinhard concentric glass nebulizer, type T-230-A2, with average sample uptake rate of 2.3 mL/min
spray chamber	Plasma-Therm, Scott type
plasma torch	semimountable, as described in Figure 1, all of fused quartz
plasma power supply	27.12 MHz rf generator, Plasma-Therm Model HFP-2500D, normally operated at 1.25 kW incident power; inductor, 27 mm i.d., made from 2 turns of 5 mm o.d. silver coated copper tubing
gas flows	plasma gas, 15 L/min argon; aerosol carrier gas, 1.0 L/min argon; no intermediate gas was used
spectrometer	0.5 m Czerny-Turner Spex, Model 1870
grating	Jobin-Yvon holographic grating with 3000 grooves/mm, 58 × 58 mm, blazed for the 170–450 nm region
entrance slit	30 μm
observation zone	15 mm above the top of the induction coil; zone height, 0.4 mm
data acquisition system	
detector head	detector: Reticon, Model RL1024C/17, self-scanned photodiode array, consisting of 1024 elements. The dimensions of each element: height, 0.4 mm; width, 25.4 μm. Preamplifier: Tracor Northern, Model TN-1223. Full scale output, 4 V
multichannel analyzer	Tracor Northern, Model TN-1710; combined with Tracor Northern Model 1710-21 optical spectrometer module

by a previous one) of the ith analytical signal (≡a signal produced by an element whose concentration is unknown) and $I_{\text{ref}}^{\text{R}}$ is the relative intensity of the reference signal (≡a signal produced by an element whose concentration is constant) by

$$C_i = \psi_i(I_i^{\text{R}}/I_{\text{ref}}^{\text{R}}) \qquad (1)$$

where ψ_i is the analytical calibration function.

According to the LRIRM model both lines are affected to the same degree by various variable parameters. Assuming that each analytical line has a specific correlation to the internal reference line, a less restrictive model can be obtained

$$C_i = \psi_i[I_i^{\text{R}}/f_i(I_{\text{ref}}^{\text{R}})] \qquad (2)$$

where f_i is a functional relationship that compensates for nonuniform responses of the ratio $I_i^{\text{R}}/I_{\text{ref}}^{\text{R}}$. The value of f_i is found by fitting a set of experimental values to a power series. This model is the analyte–internal reference correlated method (AIRCM).

It is of common knowledge to ICP analysts that different plasma parameters affect the ratio $I_i^{\text{R}}/I_{\text{ref}}^{\text{R}}$ to a different degree. Therefore, a model that will take these effects into account will remove most of the nonrandom fluctuations, a feat that cannot be accomplished by the AIRCM model. A generalization of the IRM may be presented by

$$C_i = \psi_i[I_i^{\text{R}}/f_i(I_{\text{ref},1}^{\text{R}}, I_{\text{ref},2}^{\text{R}}, ..., I_{\text{ref},j}^{\text{R}}, ..., I_{\text{ref},r}^{\text{R}})] \qquad (3)$$

where $I_{\text{ref},j}^{\text{R}}$ values are the variations caused in the reference line by the jth plasma parameter only (there are r plasma parameters). Equation 3 is too general and some assumptions should be made in order to put it in a form that will be of practical use.

The suggested model of the generalized IRM (GIRM) is based on the following observations and assumptions: (a) fluctuations in a signal are caused by variations in individual plasma parameters; (b) each plasma parameter varies independently of the others; (c) fluctuations caused by changes in any parameters are the input for the successive variation caused by another parameter, therefore, the compounded fluctuation may be described as a multiple of fluctuations caused by the individual parameters; (d) the measuring interval is sufficiently long so that the transient values of the fluctuations do not have to be taken into account.

This set of observations and assumptions is the basis of the GIRM model and permits the replacement of eq 3 by

$$C_i = \psi_i[I_i^{\text{R}}/\prod_{j=1}^{r} f_{i,j}(I_{\text{ref},j}^{\text{R}})] \qquad (4)$$

where $f_{i,j}$ is a functional relationship that compensates for nonuniform responses of the ratio $I_i^{\text{R}}/I_{\text{ref},j}^{\text{R}}$. The values of $f_{i,j}$ are found by fitting to a power series a set of experimental values taken when all parameters except the jth are constant.

In order to solve eq 4 the values of $I_{\text{ref},j}^{\text{R}}$ have to be determined during the measurement interval. This is accomplished by measuring a set of p internal standard lines (whose number should be greater than, or equal to, the number of the considered plasma parameters), that can be solved by any unconstrained optimization method.

Computational Procedure. The functional relationships $f_{i,j}$ in eq 4 were calculated by regression to a quadratic equation that passes through the origin. Only one variable was changed at a time, and insertion in eq 4 gives

$$y = a_{i,j}x + b_{i,j}x^2 \qquad (5)$$

where $y = I_i^{\text{R}} - 1$ and $x = I_{\text{ref},j}^{\text{R}} - 1$.

Solution of the normal equations that result from the least-squares regression provides the following coefficients:

$$b_{i,j} = \frac{\sum x^2 \cdot \sum x^2 y - \sum xy \cdot \sum x^3}{\sum x^2 \cdot \sum x^4 - (\sum x^3)^2} \qquad (6)$$

$$a_{i,j} = \frac{\sum xy - b_{i,j} \cdot \sum x^3}{\sum x^2}$$

where the sum is take over all the measurements.

Equation 4 was solved by the conjugate gradient method of Powell (*11*) for the objective function

$$f = \min \sum_{i=1}^{p} (I^*{}_i^{\text{R}} - I_i^{\text{R}})^2 \qquad (7)$$

Where $I^*{}_i^{\text{R}}$ denotes the calculated relative signal at the kth iteration. The convergence criterion is that the norm of the difference vector $\|x^{k+1} - x^k\|$, is less than 10^{-4}.

EXPERIMENTAL SECTION

The experimental facilities and operating conditions are given in Table I. Each experimental point was recorded over a 30 s integration time. The actual scanning of the photodiode array was done at intervals of 1 s.

The multichannel analyzer is capable of simultaneously measuring over 10 nm of continuous spectral information in the range 190–450 nm. The solutions to be tested were prepared in concentrations to give 3200 counts at line center for each exposure; 3200 counts is 80% of the saturation current (4096 counts). The resulting concentration range was 2–100 mg/L.

Plasma parameters were controlled and changed separately over the following ranges: incident power, 1.2–1.3 kW; plasma gas flow rate, 13–17 L/min; aerosol carrier gas flow rate, 1.0–1.1 L/min.

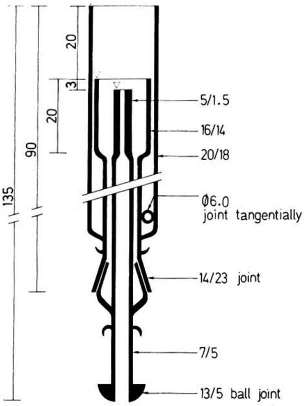

Figure 1. The semimountable ICP torch.

The solution uptake rate was varied by changing the position of the hydraulic head relative to the nebulizer from +10 cm to −10 cm.

The experimental data were processed by the Cyber 170-720 computer of the Ben-Gurion University of the Negev. The computation time for correcting 64 measurements by the GIRM was 15 s.

RESULTS AND DISCUSSION

Noise Characteristics of the System. The internal reference method compensates for noise that arises from the plasma source but does not compensate for shot noise due to the electronics of the detection system.

Evaluation of the IRM requires knowledge of the residual noise (after IRM correction) and of how close it is to the net electronic noise.

A spectral line can be extracted accurately from the continuous plasma radiation only when the exact value of the background is known. A photodiode array simultaneously determines the intensity of both a spectral line and the background in its vicinity. The significant contribution to the RSD in such a system is thus the noise in the photodiode array system. Salin and Horlick (*8*) evaluated the noise in the photodiode array system and, for signals of about 2.0×10^5 counts, found the RSD to be 0.07%.

The RSD of a spectral line signal (of 2×10^5 counts) was determined in our photodiode array system by the intensity ratio of two Cr spectral lines: Cr I 425.4/Cr I 427.4. Both lines arise from the same spectral transition and therefore suggest themselves as an ideal internal standard. It follows that the noise measured in the determination of this ratio is the noise that is not compensated for by the IRM.

Figure 2 depicts the cumulative distribution of the normalized line ratio for 50 measurements. The distribution is normal, with an RSD of 0.07%, which fits well with the findings of Salin and Horlick.

Selection of Spectral Lines and Spectral Region. To achieve minimum error propagation in the use of a series of spectral lines as internal standards, their response to various instrumental parameters should be different (*10*). It is a well established fact that atomic and ionic spectral lines, as well as argon's atomic line, respond differently to changes in various parameters of the ICP system (*12*). Two pairs of atomic lines and two pairs of ionic lines, each with similar values of excitation and of ionization energies, and one line of each type with different values were chosen, together with an argon atomic line. The pairs chosen allow us to compare the GIRM method to the common line ratio one.

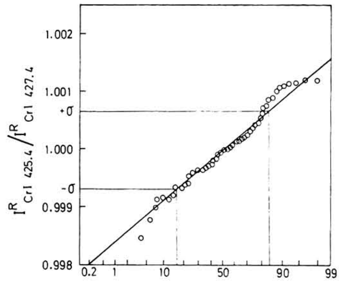

Figure 2. Cumulative distribution of the relative signal ratio of the line pair Cr I 425.4/Cr I 427.4 nm.

Table II. Relevant Parameters of the Elements Chosen for This Study

element and state	wavelength, nm	excitation potential, eV	ionization potential, eV	$E_{ex} + E_i$, eV
Ga I	417.21	3.07	6.00	
Ar I	419.83	14.74	15.76	
Eu II	420.51	2.95	5.64	8.59
Sr II	421.55	2.94	5.69	8.63
Ca I	422.67	2.93	6.11	
Sc II	424.68	3.23	6.54	9.77
Cr I	425.43	2.91	6.76	

Since the efficiency of the diode array is low below 350 nm, a spectral region above 350 nm should be selected in order to achieve large *S*/*N*. The selected spectral region was 416–426 nm. The spectral lines that were chosen and their relevant physical parameters are given in Table II.

Selection of Plasma Parameters. The intensities of spectral lines are affected by the following plasma parameters (*13*): plasma and aerosol carrier gas flow rate; incident power of the plasma generator and the coupling efficiency; sample uptake rate; efficiencies of nebulization, aerosol transport, desolvation, volatilization, atomization, and ionization; rate of collisions; excitation and deexcitation mechanisms.

We narrowed our treatment to the following parameters: sample uptake rate, incident power, and plasma and aerosol carrier gas flow rates. The flow rates of the carriers are affected by the fact that both of them flow in a common gas line, but they are considered separately as the spectral lines respond differently to their variations. Our experience is that only these parameters are independent of all the others (the rest are either related to one or more parameters, or cannot be measured), and therefore only those four parameters can be considered for the GIRM treatment.

Drift of the Spectral Line Intensities. Figure 3 shows the intensity of the various spectral lines relative to the first in each series of 64 measurements. The measurements started half an hour after plasma ignition. Considerable drift of the relative intensities was recorded, up to 10%. The intensities of the atomic lines drifted down with time, while the ionic intensities increased. During about the eighth minute of measurement, some unknown disturbances occurred, causing rather large changes in the measured line intensities. An exception to all the above is the Ar line, whose intensity rises monotonously with time. These observations disagree with the hypothesis of Kalivas and Kowalski (*5*), that the drift of the spectral line intensities can be expressed as a simple function of time.

Line Ratio Method. Figure 4 illustrates intensity ratios, normalized to the first measurement, of the atomic pairs Cr I 425.43/Ca I 422.67 nm and Ga I 417.20/Ca I 422.67 nm and

Table III. Results of the Regression to Quadratic Equation for the AIRCM (a, b, ρ) and the Resulting Improvement (μ, RSD)

	correlation to Cr line					correlation to Eu line				
element	a	b	ρ	μ	RSD	a	b	ρ	μ	RSD
Ar	−0.428	−1.110	0.585	0.9940	0.0106	0.437	−0.515	0.717	0.9919	0.0093
Eu	−1.086	−2.531	0.880	1.0067	0.00541					
Sr	−1.274	−2.803	0.887	1.0067	0.00631	1.178	0.102	0.999	0.9988	0.0012
Ca	1.103	−0.192	0.998	1.0014	0.00246	−0.917	−1.553	0.779	1.0174	0.0100
Sc	−1.560	−2.966	0.898	1.0064	0.00731	1.474	0.578	0.997	0.9976	0.0015
Ga	0.300	−1.518	0.916	1.0054	0.00325	−0.274	−1.529	0.553	1.0106	0.0060
Cr						−0.877	−1.386	0.834	1.0122	0.0070

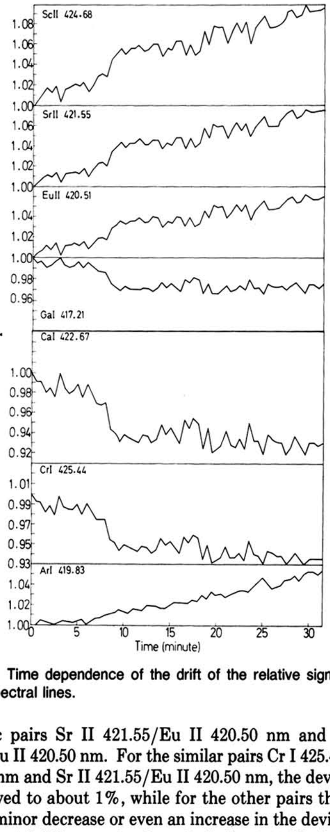

Figure 3. Time dependence of the drift of the relative signals for various spectral lines.

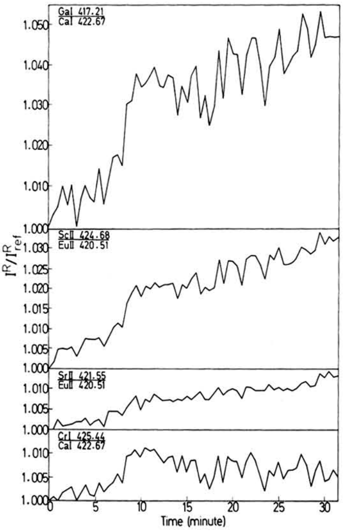

Figure 4. Time dependence of relative line ratios for various line pairs.

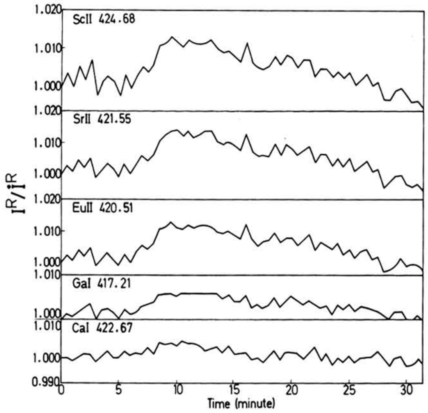

Figure 5. Time dependence of the ratios of the measured relative signals to those calculated by the AIRCM.

the ionic pairs Sr II 421.55/Eu II 420.50 nm and Sc II 424.68/Eu II 420.50 nm. For the similar pairs Cr I 425.43/Ca I 422.67 nm and Sr II 421.55/Eu II 420.50 nm, the deviation is improved to about 1%, while for the other pairs there is either a minor decrease or even an increase in the deviation. The potential difference for the pair Ga I 417.20/Ca I 422.67 nm is much smaller than that of Sc II 424.68/Eu II 420.50 nm (0.14 eV vs. 1.16 eV). Contrary to expectations the deviation for the pair Ga I 417.20/Ca I 422.67 nm was found to increase, while that of Sc II 424.68/Eu II 420.50 nm decreased. This finding is consistent with the conclusion of Barnett et al. (*9*), that "choosing ideal line pairs is quite difficult because the process is more involved than matching numbers easily derived from tables".

Analyte–Internal Reference Correlation Method. The regression was performed for 20 measurements, both for the Cr I 425.43 nm and the Eu II 420.50 nm spectral lines, that serve as internal standards. One of the plasma parameters was changed by up to 5% at a time, and the effect of each of the four plasma parameters was measured five times. The correlation coefficients, ρ, and the quadratic equation constants, a and b, are presented in Table III. From Table III it is clear that the Cr I 425.43 nm line as an internal standard is highly correlated to all the other lines except that of argon. The correlation was found to be very good for all the atomic lines. Eu II 420.50 nm as an internal standard gave good correlations only for the ionic lines. Figure 5 shows the reduction in deviation obtained by correlating the Cr I 425.43 nm line to some measured atomic and ionic spectral lines. The

Table IV. The Effects of Four Plasma Parameters on the Quadratic Equation Constants (a, b) and Correlation Coefficient (ρ) for GIRM, Eu as Reference Element

	sample uptake rate			incident power to plasma			aerosol carrier gas flow rate			cooling gas flow rate		
element	a	b	ρ	a	b	ρ	a	b	ρ	a	b	ρ
Ar	0.412	1.215	0.995	1.284	0.707	0.999	0.208	0.042	0.999	1.124	−5.420	0.995
Ca	−2.821	−3.760	0.997	−0.198	−0.028	0.988	−0.737	0.141	0.999	−0.423	−1.692	0.980
Ga	−1.503	−4.242	0.995	0.210	−0.222	0.996	−0.124	−0.423	0.978	0.004	−0.868	0.572
Sr	1.258	0.440	0.998	1.187	0.148	0.999	1.157	0.023	0.999	1.141	−0.244	0.999
Sc	1.708	1.863	0.997	1.431	0.472	0.999	1.418	0.356	0.999	1.377	0.401	0.999
Cr	−2.334	−4.023	0.996	−0.369	−0.304	0.998	−0.691	−0.137	0.999	−0.384	−0.730	0.989

figure shows that the AIRCM succeeded in eliminating the eighth minute disturbance only partially, but contrary to the line ratio method, it did improve the signal ratio and caused it to return to its original level following the transient disturbance. The mean signal ratio, μ, and the RSD are given in Table III for all the correlated spectral lines. For the similar pairs, Ca I 422.67 vs. Cr I 425.43 nm and Sr II 421.55 vs. Eu II 420.50 nm, the mean deviation is 0.15% and the RSD has the same value, while for the other pairs the mean deviation is 0.54% for Ca I 417.20 vs. Cr I 425.43 nm and 0.25% for Sc II 424.68 vs. Eu II 420.50 nm. The correlation of the ionic lines to the atomic Cr I 425.43 nm line reduced the mean deviation to 0.67% or less, while the correlation of the atomic lines to the Eu II 420.50 nm ionic line reduced the mean deviation only to 1.7% or more.

Even though the spectral lines that were selected do not represent all the types of spectral lines that are encountered in ICP, the results in Table III lead us to conclude that two spectral lines, one "hard" and the other "soft" (*12*), may suffice to calculate the correlations for all the analytical signals in an ICP source. These two internal standard lines will help reduce the drift of analytical signals by a large factor (in some cases by as much as an order of magnitude).

The AIRCM has not as yet been applied to AES despite its simplicity. Our results suggest that this method should be prefered to LRIRM, significantly improving the stability of the analytical signal.

Generalized Internal Reference Method. The same data that were processed by the AIRCM served as raw material for the GIRM, with the difference that in the latter the regressions were calculated for series of experiments in which one plasma parameter was changed at a time. Table IV gives the results of the regression calculations with Eu II 420.50 nm as reference line. It is clear from this table that for most of the cases, including argon, there is a good degree of correlation, higher than 0.995. Close scrutiny of the values of the quadratic parameters given in Table IV shows that low values of a result in relatively poor correlation coefficients. This is due to the rather low accuracy of the calculations of low a values and not because of any inherent limitation of the GIRM.

The fact that the correlation coefficients that are evaluated for the variation of each plasma parameter separately are close to unity means that our assumption is correct, i.e., a good correlation can be obtained between any two spectral lines if the correlation is subjected to the variation of only one plasma parameter. Therefore, the compounded signal fluctuation is well described by the contribution of the individual plasma parameters in eq 4. The calculated coefficients were inserted into eq 7 and thus served to eliminate the drift from the experimental data in Figure 3.

Figure 6 shows the ratio of the relative experimental to calculated signals for both the Cr I 425.43 and Sc II 424.68 nm analytical lines. The other five lines served as internal standards. It is obvious that the residual drift is random. The distribution of the signal ratio for the data presented in Figure 6 was tested and verified for normality. The RSD for Sc II 424.68 nm is 0.09% and 0.14% for Cr I 425.43 nm. The median for Sc II 424.68 nm falls exactly at the mean, while that of Cr I 425.43 nm deviates by only 0.01% from the mean.

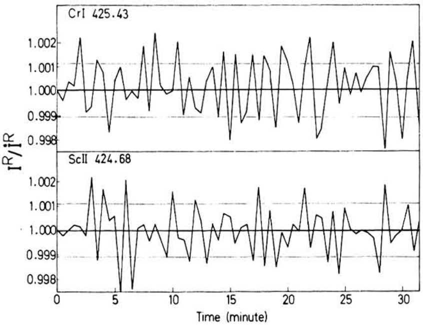

Figure 6. Time dependence of the ratios of the measured relative signals to those calculated by the GIRM.

The number of spectral lines serving as internal standards was checked for its effect on the distribution of the signal ratio. The RSD and the mean are the same for four, five, and six internal standards. (In the case of four internal standards Cr I 425.43 nm Sc II 424.68 nm and Sr II 421.55 nm serve as analytical signals. The RSD for the Sr II 421.55 nm is 0.10% and no deviation from the mean is observed.) The only effect of the number of internal standards is that the higher the number of internal standards, the better the fit to a straight line.

CONCLUSIONS

Stabilization of spectral signals by the GIRM is achieved by the fulfilment of two requirements: numerous internal standards and considerable computing power.

The internal standards do not necessarily constitute a complication in comparison to the LRIRM, as spectral lines arising from different transitions of a single element may qualify as separate internal standards for the GIRM. Moreover, even the spectral lines of argon can serve as internal standards for the GIRM. The GIRM requires considerable computing power for a number of reasons: fast processing of the experimental results measured by the analytical apparatus permits the final results to be displayed in real time; measurements should be repeated many times to improve the estimate of the mean value; finally, in commercial equipment for AES where direct reading spectrometers are used, the measurement of the background in the vicinity of the spectral line demands its profiling, which causes loss of information. Accurate subtraction of the background can be performed by the GIRM through successive iterations. The iteration scheme is outlined elsewhere (*10*).

The RSD of the photodiode array system exceeds the shot noise by only 30% for the Sc II 424.68 nm line and by 100% for the Cr I 425.43 nm line. These results demonstrate the high potential of the GIRM for the provision of extremely

Anal. Chem. 1984, 56, 48–54

accurate values, which could not be obtained by any other instrumental analytical method.

The number of analytical lines corrected in the present work is limited by the spectral window of the detector; therefore, the GIRM was applied to two analytical lines. However, its application to a real multielement analysis (>10 elements) does not require extra computation time, due to the fact that most of the time was needed to determine the components of the reference signal. The same components can serve to correct all analytical signals within a relatively very short time. The potential of the GIRM has been demonstrated in the present work, but its application in routine analytical determinations requires further investigation of internal standard lines so as to find the minimal number of lines required and the development of fast computer codes that will enable the solution of the GIRM in real time.

ACKNOWLEDGMENT

The authors wish to thank A. Levin for critical reading of the manuscript.

LITERATURE CITED

(1) Anderson, H.; Kaiser, H.; Meddings, B. "Developments in Atomic Plasma Spectrochemical Analysis"; Barnes, R. M., Ed.; Heyden: Philadelphia, PA, 1981; pp 251–277.
(2) Ohls, K.; Koch, K. H. *ICP Inf. Newsl.* **1977**, *5*, 192–200.
(3) Dorn, G. "Developments in Atomic Plasma Spectrochemical Analysis"; Barnes, R. M., Ed.; Heyden: Philadelphia, PA, 1981; pp 369–382.
(4) Belchamber, R. M.; Horlick, G. *Spectrochim. Acta, Part B* **1981**, *36B*, 581–583.
(5) Kalivas, J. H.; Kowalski, B. R. *Anal. Chem.* **1982**, *54*, 560–565.
(6) Svehla, G.; Dickson, E. L. *Anal. Chim. Acta* **1982**, *136*, 369–372.
(7) Barnett, W. B.; Fassel, V. A.; Kniseley, R. N. *Spectrochim. Acta, Part B* **1968**, *23B*, 643–664.
(8) Salin, E. D.; Horlick, G. *Anal. Chem.* **1980**, *52*, 1578–1582.
(9) Barnett, W. B.; Fassel, V. A.; Kniseley, R. N. *Spectrochim. Acta, Part B* **1970**, *25B*, 139–161.
(10) Lorber, A.; Goldbart, Z. *Anal. Chem.* **1984**, *56*, 37–43.
(11) Powell, M. J. D. *Comput. J.* **1964**, *7*, 155–162.
(12) Blades, M. W.; Horlick, G. *Spectrochim. Acta, Part B* **1981**, *36B*, 861–880.
(13) Strasheim, A. *Pure Appl. Chem.* **1981**, *53*, 1913–1952.

RECEIVED for review November 15, 1982. Accepted September 2, 1983.

Optimization of Electrothermal Atomization Parameters for Simultaneous Multielement Atomic Absorption Spectrometry

James M. Harnly* and Jean S. Kane[1]

Beltsville Human Nutrition Research Center, Nutrient Composition Laboratory, U.S. Department of Agriculture, Beltsville, Maryland 20705

The effect of the acid matrix, the measurement mode (height or area), the atomizer surface (unpyrolyzed and pyrolyzed graphite), the atomization mode (from the wall or from a platform), and the atomization temperature on the simultaneous electrothermal atomization of Co, Cr, Cu, Fe, Mn, Mo, Ni, V, and Zn was examined. The 5% HNO_3 matrix gave rise to severe irreproducibility using a pyrolyzed tube unless the tube was properly "prepared". The 5% HCl matrix did not exhibit this problem, and no problems were observed with either matrix using an unpyrolized tube or a pyrolyzed platform. The 5% HCl matrix gave better sensitivities with a pyrolyzed tube but the two matrices were comparable for atomization from a platform. If Mo and V are to be analyzed with the other seven elements, a high atomization temperature (2700 °C or greater) is necessary regardless of the matrix, the measurement mode, the atomization mode, or the atomizer surface. Simultaneous detection limits (peak height with pyrolyzed tube atomization) were comparable to those of conventional atomic absorption spectrometry using electrothermal atomization above 280 nm. Accuracies and precisions of ±10–15% were found in the 10 to 120 ng mL^{-1} range for the analysis of NBS acidified water standards.

A simultaneous multielement atomic absorption continuum source spectrometer (SIMAAC) has been developed which is compatible with either flame or electrothermal atomization (*1*). To date, the characterization of SIMAAC has been limited almost completely to flame atomization (*2–4*). However, the greatest potential for SIMAAC lies with electrothermal atomization.

Preliminary results indicate that, with electrothermal atomization, simultaneous multielement detection limits can be achieved for SIMAAC which are comparable to those for conventional single element atomic absorption spectrometry (AAS) for most elements (*1*). In addition, SIMAAC offers simultaneous detection for 16 elements, background correction equivalent to the Zeeman (*5, 6*) or Smith-Hieftje (*7*) methods, a response time as short as 0.018 s for each element, simultaneous determination of peak heights and peak areas, and, most importantly, calibration ranges of 4–6 orders of magnitude of concentration for each element.

The optimization of parameters for effective electrothermal atomization of more than one element has not been examined. The initial SIMAAC electrothermal atomization results were based on only a single set of parameters (*1*). Other multielement (three or more elements) spectrometers using electrothermal atomization have been reported (*8–10*). However, each study, like the initial SIMAAC study, dealt with the development of the instrumentation and did not investigate the atomization parameters.

This paper will present an investigation of the simultaneous determination of nine elements (Co, Cr, Cu, Fe, Mn, Mo, Ni, V, and Zn) as a function of: (1) the acid matrix (5% HNO_3 and 5% HCl), (2) the measurement mode (peak height and peak area), (3) the atomizer surface (unpyrolyzed and pyrolyzed graphite), (4) the atomization mode (from the tube wall and from a platform), and (5) the atomization temperature. Optimized parameters were then used to analyze acidified water reference materials, SRM 1643 and 1643a from the

---

[1] U.S. Geological Survey, Reston, VA.

This article not subject to U.S. Copyright. Published 1983 by the American Chemical Society

Table I. Atomization Parameters[a]

	ramp time, s	hold time, s	temp, °C
dry	10	20	110
char	10	20	500
atomize[b]	0	7	2700
clean out	1	4	2700

[a] 20-μL sample sizes used in all cases. [b] Ar sweep gas reduced to a flow of 20 mL min^{-1} (from 300 mL min^{-1}) during atomization.

National Bureau of Standards (NBS). It is recognized that the problems presented by actual sample matrices will be different from the relatively pure acid matrices used in this study. These acid matrices, however, offer realistic analytical problems and permitted some fundamental questions to be answered as a basis for future investigations.

EXPERIMENTAL SECTION

Instrumentation. The SIMAAC system has been previously described (*1, 2*). For these studies, an HGA-500 electrothermal atomizer, power supply/controller, and AS-1 autosampler (Perkin-Elmer Corp., Norwalk, CT) were used. All drying, charring, and atomization temperatures are the nominal temperatures displayed by the HGA-500, not measured temperatures. Unpyrolyzed graphite tubes, pyrolyzed graphite tubes, and pyrolyzed tubes with pyrolyzed platforms, constructed from unfired tubes in the manner described by Koirtyohann et al. (*11*), were used in the HGA-500.

The computer programs used for data acquisition and reduction have been previously described (*12*).

Elements Determined. The elements for which the original multielement cassette was aligned have been listed previously (*1*). Recently, the cassette was updated to correct elements improperly aligned and to replace undesired elements with new ones. The current suite of elements and wavelengths are Al (396.2 nm), Ca (422.7 nm), Cd (228.8 nm), Co (240.7 nm), Cr (357.9 nm), Cu (324.8 nm), Fe (248.3 nm), In (303.9 nm), K (404.4 nm), Li (610.4 nm), Mg (285.2 nm), Mn (279.5 nm), Mo (313.3 nm), Na (589.6 nm), Ni (232.0 nm), Pb (283.3 nm), Se (196.0 nm), Sn (224.6 nm), V (318.4 nm), and Zn (213.9 nm).

Calibration Standards. High-purity stock standards were prepared in the laboratory (*4*) or purchased from a commercial source (Spex Industries, Metuchen, NJ). Stock standard solutions were prepared containing 120 ng mL^{-1} of Mo and V and 100 ng mL^{-1} of Co, Cr, Cu, Fe, Mn, Ni, and Zn in three matrices: 5% HCl, 5% HNO_3, and 5% HNO_3 plus 25 μg mL^{-1} Ca. The standards in 5% HNO_3 and 5% HNO_3 plus 25 μg mL^{-1} Ca were further diluted in 5% HNO_3 and 5% HNO_3 plus 25 μg mL^{-1} Ca, respectively, to give standards of 75 (90 for Mo an V), 50, 25, and 10 ng mL^{-1}. The 25 μg mL^{-1} Ca plus 5% HNO_3 matrix was used to match the matrix of the NBS acidified water SRM.

Atomization Parameters. The atomization parameters used for these studies are listed in Table I. The charring temperature was dictated by the most volatile element, Zn. For the atomization temperature study the atomization temperature was varied and shorter integration times were employed. All other parameters were held constant. For all studies, a 20-μL sample size was used. Ar was used as the sweep gas with a flow of 20 mL min^{-1} during the atomization cycle.

Analytical Signal Ratios. The strengths of the analytical signals of elements in 5% HNO_3 and 5% HCl were compared by using all three atomizers (an unpyrolyzed and pyrolyzed tube and a pyrolyzed platform) and mixed standards containing 100 ng mL^{-1} of Co, Cr, Cu, Fe, Mn, Ni, and Zn, and 120 ng mL^{-1} Mo and V. The data represent the average of three determinations each obtained on a different day with different tubes and platforms. Peak areas were obtained by integrating over the whole 7-s atomization period and peak heights were obtained by using a 0.09-s response time (a five-point sliding average filter).

Atomization Temperature Studies. The peak heights and areas were determined by using the 100 ng mL^{-1} standards, 5% HCl and 5% HNO_3, all three atomizers, and atomization temperatures of 1500, 1800, 2100, 2300, 2500, 2700, and 2900 °C. For the 5% HNO_3 matrix, the studies were repeated four times, each with the pyrolyzed tube and the pyrolyzed platform and twice with the unpyrolyzed tube. The studies were performed only once with 5% HCl, using a pyrolyzed tube and a pyrolyzed platform. Each study was performed on a different day using a different tube or platform and was conducted as follows: The appropriate temperature calibration settings on the HGA-500 were determined for stepped atomization to each temperature. An appropriate acid blank was atomized at 2900 °C until a reproducible signal was obtained. The standard was then atomized twice at 2900 °C and twice at each of the other temperatures in descending order. Peak areas were obtained by integrating over the entire 7-s atomization period and over shorter intervals to minimize carry-over contamination from previous firings. In addition, a 5-s clean-out step at 2900 °C was used after each firing to minimize carry-over contamination. The shorter integration intervals were 0–1.8 s for Zn, 0–2.7 s for Co, Cr, Cu, Fe, Mn, and Ni, and 0–3.6 s for Mo and V for atomization from the wall. For atomization from a platform, the shorter intervals were 0–2.7 s for Zn and 0–4.5 s for Co, Cr, Cu, Fe, Mn, and Ni. No shorter integration limits were possible for Mo and V with platform atomization. All peak heights were determined with a 0.09-s response time.

Analysis of NBS SRM's. The NBS acidified water standard reference materials (1643 and 1643a) were atomized at 2700 °C by using the program in Table I. A set of calibration standards, six replicates of each of the acidified waters, and then a repeat set of calibration standards were atomized, in that order. Standards in both 5% HNO_3 and 5% HNO_3 plus 25 μg mL^{-1} Ca (to match the Ca content of the acidified waters) were used. Both 7-s integrations and the shortened integration intervals described above were used with the pyrolyzed tube and the pyrolyzed platform. Only 7-s integrations were used with an unpyrolyzed tube.

Detection Limits. The detection limits, X_{DL}, were computed according to Currie (*13*)

$$X_{DL} = ts\sqrt{\frac{1}{n_s} + \frac{1}{n_B}} \qquad (1)$$

where t is Student's t, s is the standard deviation of the base line, and n_s and n_B are the number of sample and blank measurements, respectively. For the instrumental detection limits, s was determined without firing the furnace. For method detection limits, s was determined from multiple atomizations of the reagent blank. For these studies n_s and n_B were 2 and 10, respectively, and a value of 3 was used for t as specified by IUPAC (*14*). Thus

$$X_{DL} = 2.3s \qquad (2)$$

RESULTS AND DISCUSSION

Acid Matrices. Five percent HNO_3 and 5% HCl were used as diluents for the standards in these studies. Nitric acid, at lower concentrations (1% or less), is generally the preferred matrix for electrotherml atomization. Chloride matrices are avoided because of the well-documented chloride suppression interferences (*15*). It is generally accepted that suppression of the analytical signal by the chloride matrix is brought about by the escape of monochlorides from the atomizer prior to dissociation of the molecule. It must be noted, however, that it is metal chlorides in 100-fold excess or greater, not hydrochloric acid, which cause the reported suppressions. It has been shown that chloride interferences are sensitive to the heating rate and can be reduced or eliminated by atomization into a more isothermal atmosphere (*16–18*).

Atomization of standards in 5% HNO_3, using a pyrolyzed tube, produced extremely erratic results. Relative standard deviations, for both peak height and area, ranged from 20% to 40%, varying from tube to tube and independent of the number of firings. The precisions were observed to be equally poor for all elements and were independent of the atomization temperature. The lack of precision was observed to be worse when longer temperature ramp times were used in the drying step.

Table II. Analytical Signal Ratios: Pyrolyzed Tube/Unpyrolyzed Tube[a]

element	peak area	peak height
Co	3.5	4.9
Cr	1.8	1.4
Cu	2.4	1.5
Fe	1.1	1.3
Mn	1.1	1.5
Mo	2.6	2.7
Ni	2.2	3.2
V	3.3	3.8
Zn	4.3	1.2

[a] 2700 °C atomization temperature, 5% HNO_3 matrix.

Table III. Analytical Signal Ratios: 5% HCl/5% HNO_3[a]

	pyrolyzed tube		pyrolyzed platform	
	height	area	height	area
Co	3.7	2.9	1.7	1.2
Cr	2.4	1.4	1.1	1.0
Cu	1.6	1.4	1.2	1.0
Fe	2.3	1.3	1.0	0.8
Mn	2.5	1.0	1.1	0.9
Mo	4.4	3.5	1.5	1.3
V	5.3	3.2	2.0	1.4
Zn	3.5	1.8	1.2	0.7

[a] 2700 °C atomization temperature.

The lack of the precision was unique to the atomization of 5% HNO_3 from a pyrolyzed tube. Acceptable relative standard deviations (1-3%) were obtained for all elements for the atomization of the same standards using an unpyrolyzed tube and a pyrolyzed platform. In each of the three cases, the surfaces on which the standards were deposited were different, chemically or physically. The unpyrolyzed graphite surface is physically more porous and chemically much more active than the pyrolyzed graphite. The pyrolyzed platforms were constructed from the grooved portion of the tube and thus offered physical barriers to contain the solution as compared to the smooth surface of the pyrolyzed tubes. Acceptable relative standard deviations were obtained for all elements in 5% HCl atomized from all three atomizers, unpyrolyzed and pyrolyzed tubes and pyrolyzed platforms.

The observed poor precision for the atomization of 5% HNO_3 from a pyrolyzed tube agrees with the results reported by Dabeka (*19*) and Routh et al. (*20*). They attributed their poor results to "running" of the nitric acid on the pyrolyzed surface, i.e., the movement, or spreading, of the acid droplet on the tube surface during the drying step. Dabeka observed that the problem was peculiar to the pyrolyzed tubes and that HNO_3 exhibited a greater tendency for "running" than 5% HCl (*19*). Neither author reported on the behavior of HNO_3 on a pyrolyzed platform or a structured pyrolyzed surface. Our own observations have shown that the drying of a droplet of 5% HNO_3 proceeds smoothly with a slight diminishing of the droplet size until a critical temperature is reached around 100 °C. At this temperature, the droplet collapses and there is an outward spreading of solution.

Acceptable relative standard deviations could only be obtained for pyrolyzed tubes, if the tubes were "prepared" prior to running samples or standards. "Preparing" the tube consisted of atomizing a dozen blanks of 5% HNO_3 from a new, pyrolyzed tube. Subsequent atomization of standards and samples yielded precisions comparable to those obtained by using an unpyrolyzed tube and a pyrolyzed platform. Atomization of the blanks roughened the pyrolytic surface coating where the solution was deposited. It was not determined whether the preparation process penetrated the pyrolytic coating. The observed analytical signals (2700 °C atomization temperature) for a "prepared" pyrolyzed tube were greater than those for an unpyrolyzed tube (Table II). The remaining results reported in this study for pyrolyzed tubes were obtained with "prepared" pyrolyzed tubes.

Table III lists the signal ratios of the multielement standards in 5% HCl and 5% HNO_3 atomized at 2700 °C from a pyrolyzed tube and from a pyrolyzed platform. The ratios were the average of three separate determinations. The precision of the individual results was typically ±10% around the mean. The data for Ni have been omitted because the signal-to-noise ratios were less than 5. It can be seen that the analytical signals of the elements in 5% HCl were greater than those in 5% HNO_3. In general, the enhancement of the signals in 5% HCl was more pronounced in the peak height mode for both atomizers and for the less volatile elements. Since each ratio is computed from results obtained on a common atomizer, it appears that the difference in signal strengths arises from the acid matrices. Salmon et al. (*21*) have suggested that the thermal decomposition of oxyanions can chemically alter the carbon surface, producing shifts in the appearance temperature. For Cd, Pb, and Zn, the appearance temperature shifts by O_2 were accompanied by reduced signal intensities. In this study, the decrease in the signals of metals in 5% HNO_3 was more pronounced for the less volatile elements. More comparable signal strengths, for both height and area, using platform atomization, suggest that higher gas phase temperatures, at the time of atomization, partially alleviate the signal suppression by 5% HNO_3.

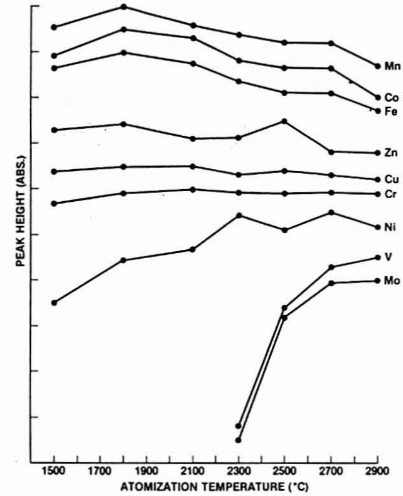

Figure 1. Peak heights of nine elements, atomized from a pyrolyzed tube, as a function of the atomization temperature.

In all cases, the analytical signals for the 5% HCl matrix were greater than or comparable to those for 5% HNO_3. There was no indication of a suppression of the analytical signals by the chloride matrix. However, no cation was present at a greater than 10-fold excess of any other cation. For low metal concentrations (100 ng mL^{-1}, or less) 5% HCl is a more attractive matrix.

Signal vs. Atomization Temperatures. Peak height and area as a function of the atomization temperature are shown in Figures 1–4 for atomization of a mixed standard in 5%

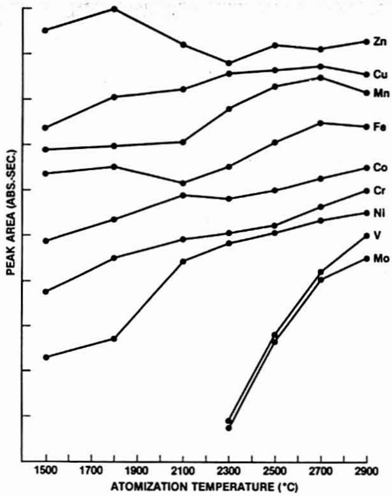

Figure 2. Peak area of nine elements, atomized from a pyrolyzed tube, as a function of the atomization temperature.

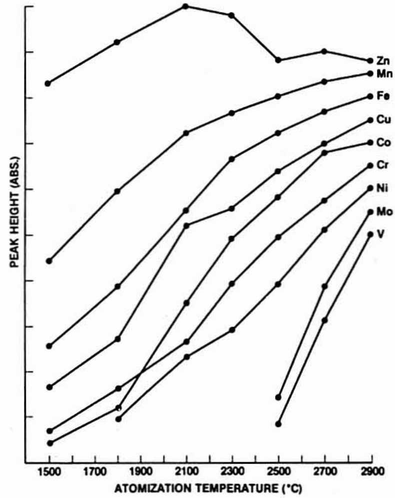

Figure 3. Peak height of nine elements, atomized from a pyrolyzed platform, as a function of the atomization temperature.

HNO_3 from a pyrolyzed tube and from a pyrolyzed platform. In each figure, the plot for each element has been individually scaled to provide adequate spacing for easy inspection. Consequently, the relative signal strengths between elements are arbitrary. Of primary interest are the plot shapes, the relative change in the signal of each element with the atomization temperature. Each plot represents the average of two or four sets of data obtained on different days by using different tubes as described in the Experimental Section. Data were taken for all nine elements simultaneously. Signal vs. temperature plots are shown only for 5% HNO_3 since similar responses were seen for 5% HCl.

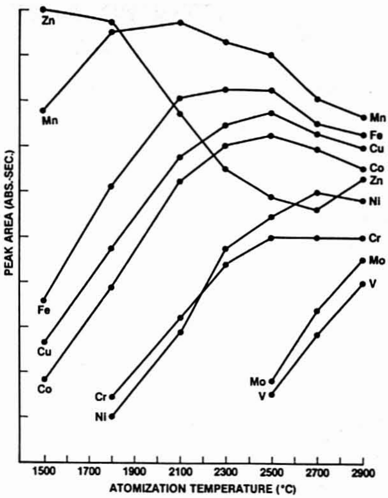

Figure 4. Peak area of nine elements, atomized from a pyrolyzed platform, as a function of the atomization temperature.

In general, the nine elements examined in this study can be divided into three categories according to their volatility and their response to the atomization temperature. The categories are (1) the volatile elements, Zn, (2) the intermediate elements, Co, Cr, Cu, Fe, Mn, and Ni, and (3) the nonvolatile elements, Mo and V.

The nonvolatile elements are the easiest to characterize. Regardless of the atomization mode or the atomizer surface, the maximum peak height and peak area were observed at 2900 °C, the highest atomization temperature. Due to the faster heating rate of the tube wall, compared to the platform, larger relative signals were observed at lower temperatures with a pyrolyzed tube; i.e., the slopes of the plots are not as steep between 2500 and 2900 °C for atomization from the wall as they are for atomization from a platform.

The signal for the most volatile element, Zn, was relatively independent of the atomization temperature for a pyrolyzed tube. The variation between temperatures appears to be random with no tendency to increase or decrease. When atomized from a platform, peak height measurements showed a distinct maximum at 2100 °C. The peak areas decreased significantly (40%) with increasing atomization temperature.

The elements of intermediate volatility were relatively insensitive to the atomization temperature when atomized from a pyrolyzed tube. In general, the peak heights and areas changed by less than 30% over the range of atomization temperatures. Only Ni proved an exception. The peak heights for Co, Fe, and Mn (Figure 1) showed a slight decrease (15–20%) with increasing temperature, while Cr and Cu showed no change with temperature. Ni increased (56%) with increasing temperature. The peak areas for Co, Cu, Fe, and Mn increased from 16–33% with increasing atomization temperature (Figure 2). Cr and Ni showed increases of 60% and 139%, respectively, with increasing temperature.

The peak height and area responses observed for the intermediate elements with atomization from a platform were considerably different from those for a pyrolyzed tube. The

Table IV. Average Multielement Signals[a]

	pyrolyzed tube		unpyrolyzed tube		pyrolyzed platform	
	height	area	height	area	height	area
2900	93 ± 6	98 ± 2	94 ± 2	94 ± 9	99 ± 4	90 ± 12
2700	95 ± 4	95 ± 6	92 ± 8	91 ± 11	86 ± 12	85 ± 15
2500	91 ± 8	86 ± 16	86 ± 18	81 ± 26	69 ± 28	80 ± 27
2300	74 ± 42	74 ± 32	81 ± 28	72 ± 42	59 ± 34	72 ± 36
2100	74 ± 42	67 ± 38	70 ± 41	66 ± 40	50 ± 35	62 ± 39
1800	75 ± 43	63 ± 38	59 ± 40	53 ± 36	34 ± 31	47 ± 38
1500	71 ± 42	58 ± 36	52 ± 44	42 ± 34	23 ± 28	34 ± 36

[a] Average for all nine elements. Largest signal for each element is assigned a value of 100. Signals at all other temperatures are expressed as a ratio to the maximum signal.

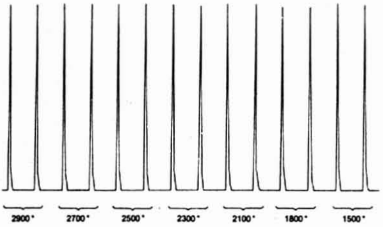

Figure 5. Tracings of Cu, in 5% HNO_3, atomized from a pyrolyzed tube at different temperatures.

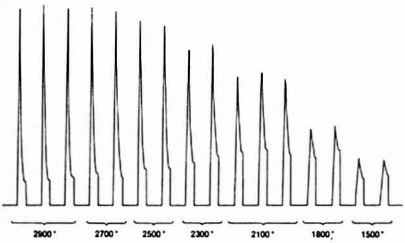

Figure 6. Tracings of Cu, in 5% HNO_3, atomized from a pyrolyzed platform at different temperatures.

peak heights increased almost linearly with the atomization temperature (Figure 3) while the peak areas increased rapidly with temperature initially, reached a maximum, and then decreased at higher temperatures (Figure 4). The extent of the deviation between platform and pyrolyzed tube atomization can be seen for Cu in Figures 5 and 6. The peak locations, heights, and areas for atomization from a pyrolyzed tube (Figure 5) show little variation with temperature. However, for platform atomization (Figure 6), the changes with temperature are quite marked: peak height decreases significantly with temperature, the peak maximum occur later in time with decreasing temperature (from 1.5 s at 2900 °C to 2.8 s at 1500 °C), and tailing (as indicated by the ratio of the absorbance at the end of the integration period, 4.5 s, to the maximum absorbance) increases with decreasing temperature. It is well established that the heating rate of the HGA-500 is related to the final temperature (the higher the final temperature, the faster the heating rate). The variation in the heating rate, however, had little effect on the peak heights obtained for atomization from the wall, while the normally slower heating rate of the platform appears to have been significantly reduced at lower temperatures. The peak shapes of Cu atomized from a platform at lower temperatures are similar to Mo and V atomized at higher temperatures from the wall.

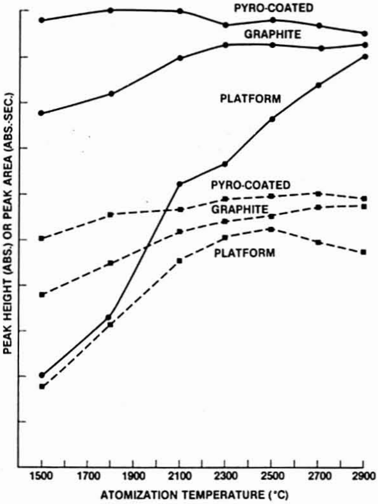

Figure 7. Peak height (—) and area (– – –) for Cu (in 5% HNO_3) atomized from an unpyrolyzed and pyrolyzed tube and from a pyrolyzed platform at different temperatures.

Peak height and area as a function of temperature were also examined for all nine elements atomized by use of an unpyrolyzed tube. The height and area plots were similar to those obtained from pyrolyzed tube atomization as shown in Figure 7 for Cu. Again, the signals have been arbitrarily scaled for easy comparison. A comparison of sensitivities, for pyrolyzed and unpyrolyzed tubes (at 2700 °C), was presented in the first section of the discussion.

The data in Figures 1–4 make it obvious that the compromise atomization temperature for the simultaneous determination of all nine elements will be dictated by the nonvolatile elements. With either an unpyrolyzed or pyrolyzed tube, an atomization temperature greater than 2500 °C is necessary, and with a platform, 2700 °C is the minimum temperature.

A more quantitative evaluation of the best compromise atomization temperature is presented in Table IV. The plots for each element in Figures 1–4 (and unpyrolyzed tubes as well) have been normalized with the maximum values being taken as 100%. The average signal and standard deviation for all nine elements were computed for each temperature, atomizer, and measurement mode. The average signal indi-

Table V. Graphite Furnace Instrumental Detection Limits (ng mL^{-1})[a]

element	wavelength, nm	pyrolyzed tube		pyrolyzed platform		Perkin-Elmer[b]
		area	height	area	height	
Co	240.7	6.0	0.9	12	2	0.2
Cr	357.9	0.6	0.3	0.9	0.5	0.08
Cu	324.7	0.7	0.1	1	0.3	0.2
Fe	248.3	0.5	0.7	1	2	0.2
Mn	279.5	0.8	0.1	1.4	0.3	0.08
Mo	313.3	5	0.7	8	2	0.2
Ni	232.0	6	2	7	5	2
V	318.5	10	0.9	9	2	2
Zn	213.8	1	0.4	0.9	1	0.008

[a] Based on 20 μL sample size and computed as shown in the Experimental Section. [b] Reference 22 multiplied by 5 to correspond to a 20-μL sample size and by 1.5 to correspond to 3σ.

cates the extent of compromise involved while the standard deviation quantifies the distribution of the results. Thus the values in each column can be compared. A comparison between columns is not valid. For unpyrolyzed and pyrolyzed tube atomization, a temperature of 2700 °C or greater gives optimum compromise signal responses for area and height. For peak height measurements with a pyrolyzed tube, 2500 °C is sufficiently high. Atomization from a platform is optimum at 2900 °C for both height and area measurements. However, continuous atomization at 2900 °C has been found to severely shorten the life of the tubes. Consequently, an atomization temperature of 2700 °C is the most desirable compromise temperature for all three modes of atomization. If nonvolatile elements are not to be determined, then significantly lower temperatures can be used. Omitting Mo and V would allow temperatures as low as 2500 °C to be used without significantly compromising the signal strength of the remaining elements. The lower atomization temperature would significantly increase the tube life.

Detection Limits. The simultaneous instrumental detection limits for the HGA-500 are shown in Table V for atomization at 2700 °C. Instrumental detection limits, as described in the Experimental Section, were based on the precision of a blank signal obtained without firing the atomizer. This "optical" blank reflects the continuum source noise, electronic noise, and any wavelength or order drift in the echelle polychromator which produces a shift in the base line absorbance. The instrumental detection limit defines the ability of the spectrometer to detect any analytical signal during atomization, whether it arises from a standard, sample, blank, or carry-over contamination from previous firings. The method detection limit is based on the precision of replicate firings of the reagent blank signal. Thus the method limit is also dependent on the purity of the reagents. The method limit is more useful to the analyst for evaluating the suitability of a method while the instrumental limit allows a more accurate comparison of spectrometers.

The method and instrumental detection limits should be comparable provided the reagent blank is reasonably pure and there is no carry-over contamination. This proved to be the case for most elements in this study after the tube was fired a sufficient number of times (5–10 times) to remove contamination resulting from dust and handling. For some elements (Ca, Mg, and Na and to a lesser extent Fe), however, a reproducible signal could not be obtained for atomization of the reagent blank. The height and area showed a positive bias which slowly and systematically decreased toward zero over a series of 40 atomizations. Since the solution was not changed (an autosampler was used) and because of the accuracy of the background correction system (*23*), it could only be concluded that the material was coming from the tube. While this contamination is analytically insignificant, the consistent drift served to inflate the computed standard deviation and to give a high bias to the method detection limit. The standard deviation of the reagent blank signals about a linear least-squares fit to the data agreed well with the standard deviation of the optical blanks. Thus, residual material on the atomizer can give rise to a drifting base line and different detection limits.

The optical blank gives an accurate estimate of the random error of the spectrometer but it is questionable whether it has any value other than for comparing instrumental operation from day-to-day or for comparing different instruments. The reagent blank reflects the random error plus any changing bias or systematic error resulting from atomization. Since the rate of change of the bias varies over the course of a series of determinations, the usefulness of the reagent blank is also questionable. Close attention must be paid to the stability of the base line analytical signal.

The peak height detection limits for SIMAAC, using a pyrolyzed tube, agree well with those reported by the Perkin-Elmer Corp. for the HGA-500. The exceptions lie below 280 nm where the lower intensity of the continuum source results in detection limits which grow worse with decreasing wavelength. The peak area detection limits (for a pyrolyzed tube and a pyrolyzed platform) are conservative since they are based on integration over the entire atomization cycle (7 s). Integration over a 1-s interval optimized for the peak location would provide detection limits a factor of $7^{1/2}$ better. Slightly poorer detection limits are also expected for peak height and area measurements with a pyrolyzed platform since at 2700 °C, the average signals are 15% less than the maximums (Table IV). The platform height limits are slightly worse due to the slower heating rate.

SRM Water Analyses. Tables VI and VII summarize the results for the simultaneous determination of nine elements in the NBS acidified waters, SRM 1643 and 1643a, using peak

Table VI. Analysis of NBS SRM 1643 Acidified Water (ng mL^{-1})

element	NBS certified value and confidence limit	pyro tube		platform	
		height	area	height	area
Co	17 ± 2	16 ± 3[a]	18 ± 3	18 ± 6	20 ± 5
Cr	15 ± 1	16 ± 2	17 ± 2	19 ± 5	16 ± 2
Cu	16 ± 1	16 ± 2	16 ± 2	16 ± 2	15 ± 2
Fe	75 ± 1	72 ± 3	78 ± 5	74 ± 3	78 ± 3
Mn	29 ± 1	29 ± 7	28 ± 2	30 ± 5	31 ± 2
Mo	105 ± 3	102 ± 18	95 ± 17	118 ± 25	113 ± 18
Ni	49 ± 1	50 ± 5	52 ± 6	44 ± 5	51 ± 3
V	50 ± 1	52 ± 7	50 ± 7	51 ± 7	55 ± 6
Zn	65 ± 3	55 ± 7	62 ± 5	61 ± 12	62 ± 7

[a] Values expressed as $\overline{X} \pm ts/N^{1/2}$, where $t = 2.571$ ($\nu = 5$, $\alpha = 95\%$) and $N = 5$.

Table VII. Analysis of NBS SRM 1643a Acidified Water (ng mL^{-1})

element	NBS certified value and confidence limit	pyrolyzed tube		pyrolyzed platform	
		height	area	height	area
Co	19 ± 2	22 ± 3[a]	21 ± 3	22 ± 3	21 ± 3
Cr	17 ± 2	16 ± 2	18 ± 2	19 ± 2	20 ± 2
Cu	18 ± 2	18 ± 2	18 ± 2	18 ± 3	17 ± 1
Fe	88 ± 4	78 ± 9	86 ± 7	83 ± 6	88 ± 7
Mn	31 ± 2	34 ± 6	30 ± 2	32 ± 2	32 ± 3
Mo	95 ± 6	106 ± 24	98 ± 12	94 ± 16	95 ± 9
Ni	55 ± 3	51 ± 8	54 ± 7	52 ± 6	55 ± 7
V	53 ± 3	56 ± 9	55 ± 10	54 ± 8	52 ± 5
Zn	72 ± 4	58 ± 9	77 ± 7	62 ± 16	70 ± 12

[a] Values expressed as $\overline{X} \pm ts/N^{1/2}$, where $t = 2.571$ ($\nu = 5$, $\alpha = 95\%$) and $N = 5$.

Table VIII. Analysis of Cr (ng mL^{-1}) in NBS SRM 1643a[a]

standard matrix	unpyrolyzed tube		pyrolyzed tube		pyrolyzed platform	
	height	area	height	area	height	area
5% HNO_3	8.6	8.9	9.2	9.3	9.2	9.2
5% HNO_3 + 25 μg mL^{-1} Ca			16 ± 2	18 ± 2	19 ± 2	20 ± 2

[a] Certified value is 17 ng mL^{-1} ± 1.

height and area measurements and atomization from a pyrolyzed tube and a pyrolyzed platform. Multielement calibration standards were made up in 5% HNO_3 plus 25 ppm Ca as described in the Experimental Section. An atomization temperature of 2700 °C was used. For each experiment, the standards were run in duplicate, while the SRMs were determined six times. The average results from five experiments were used to compute the results reported in Tables VI and VII.

In almost every case, for both atomizers and for both measurement modes, the NBS certified values fell within the 95% confidence limits of the SIMAAC determinations. The notable exceptions were the low recoveries of Zn for both the pyrolyzed tube and platform using the peak height measurement mode. Although not shown here, the unpyrolyzed tube atomizer demonstrated accuracies and precisions comparable to the other two atomizers. Low recoveries for Zn, in the peak height mode, were also observed for the unpyrolyzed tube.

The 95% confidence limits ($st/N^{1/2}$, where s is the standard deviation, t is the Student t value for 95%, and N is the number of determinations), expressed as percentages of the means, fell between 4% and 33% with 65 of the 72 reported values falling between 4% and 20%. The average recovery and the average 95% confidence limit (as a percentage of the mean) were 102% and ±13%, respectively, for the determination of the nine elements simultaneously.

There is no evidence, with the exception of Zn, to suggest that either the peak height or area measurement mode or that either the unpyrolyzed or pyrolyzed tube or the pyrolyzed platform offers advantages with regard to accuracy and/or precision. On the basis of the confidence limits established for each element in this study, with the exception of Zn, there were no significant matrix effects. It is possible that better precision will reveal biases which are presently hidden in the uncertainty of the measurements. However, interferences greater than 15% to 20% were not observed. This lack of interferences may in part be due to the matrix matching of the standards. Every element determined was present in each of the multielement standards as well as 5% HNO_3 and 25 μg mL^{-1} of Ca. Although the elemental ratios are not identical with the water reference materials, they are a much better approximation than the use of fairly pure, single element standards. The use of Ca for matrix matching was found to aid only in the determination of Cr. As shown in Table VIII, the determination of Cr by using mixed standards without Ca produced recoveries of approximately 50%.

Registry No. Co, 7440-48-4; Cr, 7440-47-3; Cu, 7440-50-8; Fe, 7439-89-6; Mn, 7439-96-5; Mo, 7439-98-7; Ni, 7440-02-0; V, 7440-62-2; Zn, 7440-66-6.

LITERATURE CITED

(1) Harnly, J. M.; O'Haver, T. C.; Golden, B. M.; Wolf, W. R. *Anal. Chem.* **1979**, *51*, 2007.
(2) Harnly, J. M.; O'Haver, T. C. *Anal. Chem.* **1981**, *53*, 1291.
(3) Harnly, J. M.; Kane, J. S.; Miller-Ihli, N. J. *Appl. Spectrosc.* **1982**, *36*, 637.
(4) Kane, J. S.; Harnly, J. M. *Anal. Chim. Acta* **1982**, *139*, 297.
(5) Koizumi, H.; Yasuda, K. *Anal. Chem.* **1975**, *47*, 1679.
(6) Fernandez, F. J.; Myers, S. A.; Slavin, W. *Anal. Chem.* **1980**, *52*, 741.
(7) Smith, S. B., Jr.; Schleicher, R. G.; pfeil, D. L.; Hieftje, G. M. Pittsburgh Conference and Exposition on Analytical Chemistry and Applied Spectroscopy, Atlantic City, NJ, 1982; Paper 442.
(8) Alder, J. F.; Alger, D.; Samuel, A. J.; West, T. S. *Anal. Chim. Acta* **1976**, *87*, 301.
(9) Lundberg, E.; Johnson, G. *Anal. Chem.* **1976**, *48*, 1922.
(10) Salin, E. D.; Ingle, J. D., Jr. *Appl. Spectrosc.* **1978**, *32*, 596.
(11) Koirtyohann, S. R.; Kaiser, M. L. *Anal. Chem.* **1982**, *54*, 1515A.
(12) Harnly, J. M.; Miller-Ihli, N. J.; O'Haver, T. C. *J. Autom. Chem.* **1982**, *4*, 54.
(13) Currie, L. A. *Anal. Chem.* **1968**, *40*, 586.
(14) IUPAC Commission of Spectrochemical and Other Optical Procedures, Nomenclature, Symbols, Units and Their Usage in Spectrochemical Analysis—II Data Interpretation, *Pure Appl. Chem.* **1976**, *45*, 99.
(15) Slavin, W.; Manning, D. C. *Prog. Anal. At. Spectrosc.* **1982**, *5*, 243.
(16) Slavin, W.; Manning, D. C. *Spectrochim. Acta., Part B* **1980**, *35B*, 701.
(17) Chakrabarti, C. L.; Wan, C. C.; Hamed, H. A.; Bertels, P. C. *Anal. Chem.* **1981**, *53*, 444.
(18) Giri, S. K.; Littlejohn, D.; Ottaway, J. M. *Analyst (London)* **1982**, *107*, 1095.
(19) Dabeka, R. W. Pittsburgh Conference on Analytical Chemistry and Applied Spectroscopy, Atlantic City, NJ, 1981; Paper No. 68A.
(20) Routh, M. W.; Doidge, P. S.; Wiseman, A. G.; McKenzie, T. N. Pittsburgh Conference on Analytical Chemistry and Applied Spectroscopy, Atlantic City, NJ, 1981; Paper No. 68.
(21) Salmon, S. G.; Holcombe, J. *Anal. Chem.* **1982**, *54*, 630.
(22) "Technique and Applications of Atomic Absorption"; Perkin-Elmer Corp.: Norwalk, CT, July 1980; No. L655.
(23) Harnly, J. M.; O'Haver, T. C. *Anal. Chem.* **1977**, *49*, 2187.

RECEIVED for review May 31, 1983. Accepted September 22, 1983.

Anal. Chem. **1984**, *56*, 55–58

Sensitivity Factors for Surface Analysis by Ion Scattering Spectroscopy

Dennis G. Swartzfager

E. I. du Pont de Nemours & Company, Central Research & Development Department, Experimental Station, Wilmington, Delaware 19898

A surface analysis by ion scattering spectroscopy (ISS) is fundamentally different from an analysis by electron spectroscopy because of its extreme surface sensitivity. For substitutional alloys, an accurate analysis of the outermost surface can be obtained when proper analytical procedures are followed. In this work, the fundamentals of quantitation by ISS will be reviewed and procedures for obtaining relative sensitivity factors will be illustrated and discussed. One of these procedures, which involves the physical adsorption of xenon on pure element surfaces, is extremely flexible and should be generally applicable.

Conceptually, ion scattering spectrometry is a very simple technique. The surface of interest (see Figure 1) is bombarded with ions characterized by an energy E_0 and mass M_1; some of these are backscattered from the surface through an angle ϕ defined by a slit or aperture, energy analyzed, and detected to produce a spectrum such as the one shown at the bottom of Figure 1. The position of the elastically scattered ion peaks on the reduced energy scale (E/E_0) is given by eq 1 where M_2 is the mass of the surface atom involved in the collision.

$$E/E_0 = \left(\frac{M_1}{M_1 + M_2}\right)^2 \left[\cos\phi + \left(\left(\frac{M_2}{M_1}\right)^2 - \sin^2\phi\right)^{1/2}\right]^2 \tag{1}$$

The important advantage which ISS has over other surface analysis techniques such as Auger electron spectroscopy (AES) and X-ray photoelectron spectroscopy (XPS or ESCA) is its extreme surface sensitivity. In AES or ESCA, the surface being analyzed is always defined as the volume from which a particular signal arises, but this varies from element to element within a given sample as a result of the different kinetic energies of the emitted electrons. Procedures to correct this situation are known in theory, but they require poorly known estimates of the elastic mean-free path and other correction factors (such as the electron backscattering correction). Even when these corrections are made, the final result is critically dependent on the assumption that there is, or is not, an in-depth concentration gradient of a given element within the sampling depth.

In ISS, only the outermost surface atoms contribute significantly to the scattered ion intensity, but this extreme surface sensitivity is both a blessing and a curse. If a meaningful surface analysis is to be obtained, the surface must be accurately defined: this can only be done if the surface structure is known or can be inferred. This problem is not unique to the ion scattering technique; the same problem arises in electron spectroscopy, but as a result of the deeper sampling depth, the problem is less severe. This problem will be ignored in this study by confining it to the analysis of substantial alloys.

Powell (*1*) has pointed out that there are three approaches to the quantitative analysis of the surface that use (a) a first-principles model, (b) standards, and (c) relative elemental sensitivity factors.

In ISS, the peak intensity of an element "A" is related to its surface concentration by the following equation:

$$I_a = I_p{}^+ K_a N_a R \tag{2}$$

where

$$K_a = C(TD\Delta\Omega)\sigma_a P_a \tag{3}$$

where I_a is the scattered ion intensity, $I_p{}^+$ is the primary ion current density, T is the transmission of analyzer, D is the efficiency of the detector, $\Delta\Omega$ is the acceptance angle of the detector, σ_a is the differential scattering cross section for "A" atoms, P_a is the ion survival probability, C is a constant, dependent on the quantity being measured (peak height, peak area, or first derivative peak to peak), N_a is the surface atom density of element "A", and R is the surface roughness parameter

The product of terms T, D, and $\Delta\Omega$ is a constant of the instrument, and the conditions under which it is being operated in principle can be determined. The differential scattering cross section can be computed provided the proper interatomic potential is employed. Unfortunately, the ion survival probability cannot be computed; although several models have been proposed (*2, 3*), none is quantitative. This factor alone prohibits any practical attempt at a first-principles calculation of either the absolute scattered ion intensity or the relative intensities of the two peaks. Whether or not this term is dependent, to whatever extent, on the electronic or chemical environment of the surface atom involved in the collision is an important question that is yet to be answered. This will be discussed later, but for the moment, it will be assumed that the ion survival probability is constant for a given ion-atom pair at a given scattering angle and incident ion energy.

The surface roughness hinders but does not preclude the use of standards. The effect of surface roughness on the scattered ion yield has been described by Nelson (*4*), but a description of the problem is not a solution to it.

For certain types of samples (sputtered, evaporated, or electrodeposited films on smooth substrates) elemental standards could easily be prepared such that R(standard) = R(unknown); when this is the case, eq 4 can be employed to give reasonably accurate results.

$$N_a(\text{unk}) = \left[\frac{I_a(\text{unk})}{I_a(\text{std})}\right]\left[\frac{I_p(\text{std})}{I_p(\text{unk})}\right] N_a(\text{std}) \tag{4}$$

It should be pointed out that this procedure is independent of the nature and number of the other atomic species present on the surface on the unknown. This could be advantageous in certain circumstances.

Unfortunately for most of the practical samples that must be analyzed, it will be impossible to match the surface roughness of the unknown and a suitable standard. The practical way of circumventing the surface roughness problem is the relative sensitivity factor approach.

0003-2700/84/0356-0055$01.50/0 © 1983 American Chemical Society

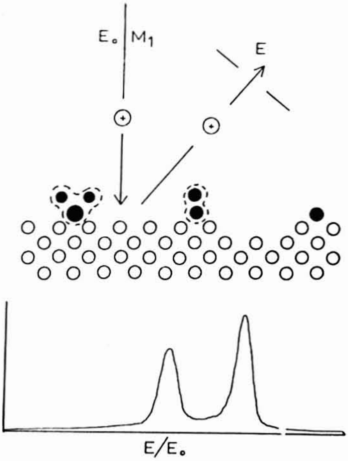

Figure 1. Schematic of the ion scattering process.

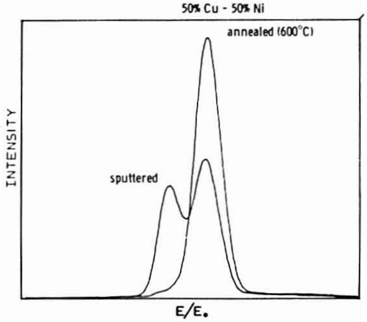

Figure 2. ISS spectra of an annealed and sputter etched surface of a 50/50 Cu-Ni alloy.

The primary intent of this study is to illustrate and critically compare several procedures for obtaining accurate, relative sensitivity factors.

EXPERIMENTAL SECTION

The alloys used in this study were prepared as previously described (5). The alloys and pure palladium and gold samples were polished with alumina and ultrasonically cleaned with methanol before loading them into the spectrometer.

The ion scattering spectrometer is a modified 3M Model 525B, which has been interfaced to a PDP 11/34 minicomputer. All measurements were performed with a normally incident beam at 2.0 keV ion energy with ^{20}Ne as the probe ion. Typically, the ion beam was rastered over 0.1 cm^2, and the scattered ion signal was electronically gated so that only the center portion of the rastered area was observed. The nominal static beam diameter was 120 μm. The specimens could be heated with a resistance heater and rapidly cooled by contacting them (from the back side) with a liquid-nitrogen-cooled cold finger. The temperature was measured with a chromel-alumel thermocouple spot-welded to the back of the specimen.

RESULTS AND DISCUSSION

Relative sensitivity factors have always been used in Auger electron spectroscopy. Traditionally, they are determined by suitably preparing (usually by polishing and sputter etching) elemental samples, placing them, side-by-side, in the spectrometer, and measuring the signals of interest under identical instrumental conditions. This same procedure was followed for ISS measurements on gold and palladium and yielded a value of 2.47 for the relative sensitivity factor $K_{\mathrm{Au}}/K_{\mathrm{Pd}}$. However, this one measurement does not provide any check on the suitability of the surface preparation. For this type of measurement, suitable surface preparation means not only cleaning the surface to remove foreign contaminants but also treating the surfaces of the two elemental standards so that these roughness parameters are identical or at least have very similar values.

A procedure that is unique to the ion scattering technique involves measurements on a series of binary alloys between the elements of interest. This procedure can be described as follows. The scattered ion intensities due to the elements A and B in a binary alloy are given in equations 5 and 6.

$$I_{\mathrm{a}} = I_{\mathrm{p}}^{+}K_{\mathrm{a}}N_{\mathrm{a}}R \tag{5}$$

$$I_{\mathrm{b}} = I_{\mathrm{p}}^{+}K_{\mathrm{b}}N_{\mathrm{b}}R \tag{6}$$

Then one may define the surface atom fraction of species A and B (θ_{A} and θ_{B}, respectively) as

$$\theta_{\mathrm{A}} = N_{\mathrm{a}}/N_{\mathrm{t}} \qquad \theta_{\mathrm{B}} = N_{\mathrm{b}}/N_{\mathrm{t}}$$

where $N_{\mathrm{t}} = N_{\mathrm{a}} + N_{\mathrm{b}}$ and, of course, $\theta_{\mathrm{A}} + \theta_{\mathrm{B}} = 1$.

Combining eq 5 and 6 yields eq 7

$$I_{\mathrm{a}} = I_{\mathrm{p}}^{+}K_{\mathrm{a}}N_{\mathrm{t}}R - (K_{\mathrm{a}}/K_{\mathrm{b}})I_{\mathrm{b}} \tag{7}$$

which explicitly illustrates that there is a linear relationship between scattered ion intensities due to each of the surface species. Therefore, the term $(K_{\mathrm{a}}/K_{\mathrm{b}})$, which is the relative sensitivity factor, can easily be determined by plotting the scattered ion intensity I_{a} vs. the intensity I_{b}.

Utilizing data from four different Pd-Au alloys and pure Pd and Au samples, the procedure gave a value of 2.37. As before, the accuracy of this value is dependent on the suitability of the surface preparation, but in this instance, we may use the average deviation of the points from the straight line as a measure of that surface preparation. A more important facet of this procedure is its independence of any knowledge of either the surface or bulk compositions of the alloys.

Equation 7 may also be employed with only a single alloy sample provided that its surface composition can be significantly altered in some fashion. Shown in Figure 2 are two ISS spectra, obtained from a 50/50 Cu-Ni alloy. One was obtained after annealing the alloy at 600 °C, which caused the surface to be enriched with Cu (*5, 6*). The other was obtained after sputter removing the Cu-rich outer layer of the sample. Measuring the intensities and plotting them according to eq 1 give two-point line from which the relative sensitivity factor between Cu and Ni may be determined. This procedure assumes that the roughness parameter does not change significantly during the sputter removal of the Cu-rich outer layer. Of course, there is no reason to restrict the data analysis to just two points.

Shown in Figure 3 are the Pd and Au peak intensities obtained from an 80/20 Pd-Au alloy vs. sputtering time. Prior to time zero, the alloy was annealed at 600 °C which produces a gold-rich surface (*5, 7*). The intensity changes that occur between 0 and 270 s are the result of the sputter removal of this Au-rich layer. At this point, the temperature of the alloy was quickly raised to 600 °C, again causing the surface to become gold rich. For this experiment, time is a superficial variable; therefore the data were replotted as suggested by eq 7. This produced a linear plot from which a value of 2.67 was obtained for the relative sensitivity factor, $K_{\mathrm{Au}}/K_{\mathrm{Pd}}$.

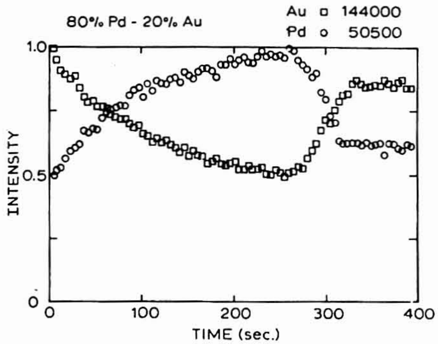

Figure 3. Sputter profile of an annealed Pd-Au alloy. At τ = 270 s, the sample was rapidly heated to 600 °C.

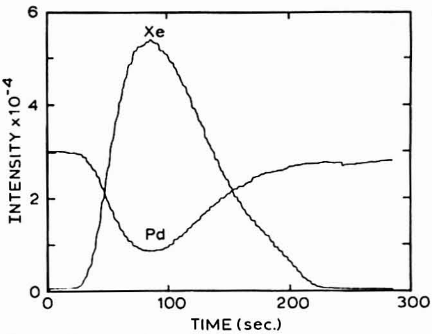

Figure 4. Time dependence of the Xe and Pd peak intensities as Xe is adsorbed and then thermally desorbed from a pure Pd surface.

The previously mentioned procedures involving measurements on binary alloys may not be feasible in many cases; so a more general method which still allows the surface roughness problem to be circumvented is necessary. One such procedure involves the physisorption of Xe on the surfaces of elemental samples.

The ion intensity due to element "A" obtained from a sample of pure "A" is

$$I_a = I_p{}^+K_aN_aR_A \tag{8}$$

and the scattered ion intensity for physisorbed Xe on the surface of the pure "A" sample is as follows:

$$I_{Xe} = I_p{}^+K_{Xe}N_{Xe}R_A \tag{9}$$

Furthermore, the intensity due to species A when Xe is present on the surface in the submonolayer coverage is given in eq 10, which was first introduced by Heiland and Taglauer (*8*)

$$I_a = I_pK_a(N_a - \lambda N_{Xe})R_A \tag{10}$$

where λ is the shadowing coefficient.

Combining eq 8, 9, and 10 gives eq 11, which is identical in form with eq 7.

$$I_a = I_p{}^+K_aN_aR - \lambda(K_a/K_{Xe})I_{Xe} \tag{11}$$

Figure 4 shows a plot of the Pd and Xe peak intensities vs. time as Xe was being absorbed on and then desorbed from a Pd metal surface whose initial temperature was approximately −180 °C. Xenon was admitted to the system at t = 25 s and at t = 95 s, the xenon valve was closed, and the Pd was heated slowly to desorb the xenon. Here, as in the third procedure, time is a superficial variable, and the Pd intensity was replotted vs. the Xe intensity giving a value of −0.387 for the slope [$=\lambda(K_{Pd}/K_{Xe})$]. A similar experiment with Au as the substrate yielded a slope [$=\lambda(K_{Au}/K_{Xe})$] of −0.964. The ratio of these two values, 2.49, is the sensitivity factor K_{Au}/K_{Pd}.

The relative sensitivity factors (K_{Au}/K_{Pd}) for each method were as follows: pure metals, 2.47; binary alloys (*4*), 2.37; single alloy, 2.67; and Xe physisorption, 2.49. The agreement among these values is very good; the relative mean deviation is only 3.4%. At first glance, it may seem that the precision of these measurements would be improved simply by obtaining more and better experimental data, but this is not the case. The accuracy with which the values can be determined by any procedure is ultimately dependent on the validity of the assumptions or approximations which are necessarily a part of the analysis. For each of the procedures discussed, assumptions were made concerning the roughness parameter R; it was assumed either that R had the same value for two or more surfaces or that it was invariant on a single surface, although a change in the composition of the surface was induced either by adsorption from the gas phase or by exchange with the bulk material. Judging by the results, these assumptions must have been very good for all of the procedures, but this will not always be the case.

The xenon adsorption is clearly the most generally applicable procedure of those discussed. The shadowing coefficient λ may be dependent on the surface atom density and crystal structure of the substrate, but this is expected to be a minor problem. The method might even be used on high-vapor-pressure materials. Multilayers of Hg, S, Rb, or I could be condensed on a Au substrate followed by Xe or perhaps Kr adsorption.

Earlier, the question was raised whether or not the electronic or chemical environment of an atom affected the ion survival probability. Judging by results and considering the different methods by which they were obtained, it is quite clear that the ion survival probabilities for the $^{20}Ne^+$–Pd and $^{20}Ne^+$–Au ion–atom collisions are independent of one another and constant for the Au–Pd alloy system. Other results obtained in this laboratory indicate that this is also true for the Ag-Au, Cu-Ni, Au-Ni, and Cu-Au alloy systems; however, it should be noted that none of these ion–atom pairs falls into the resonant charge exchange category (*9*). There is evidence (*9, 10*) to suggest that the resonant charge exchange phenomenon is somewhat chemical-state dependent, but the extent of the dependence is difficult to ascertain because the effect of the surface structure was not taken into account.

CONCLUSIONS

Accurate relative sensitivity factors for quantitative surface analysis of substitutional alloys by ISS can be determined by several different procedures. When binary alloys are employed together with pure-element standards, an independent check of the suitability of the surface preparation of the materials can be obtained. The surface roughness problem can be circumvented by restricting the measurements to a single surface whose composition can be altered either by exchange with the bulk material or by the adsorption of a suitable reference element from the gas phase. Xenon physisorption appears to be the most general method and should be applicable to high-vapor-pressure materials.

Registry No. Xe, 7440-63-3; 50/50 Cu–Ni alloy, 11101-29-4; 80/20 Pd–Au alloy, 37319-92-9.

LITERATURE CITED

(1) Powell, C. J. *ASTM Spec. Tech. Publ.* **1978**, *STP 643*, 5–30.
(2) Bloss, W.; Hone, D. *Surf. Sci.* **1978**, 72, 277.

(3) Woodruff, *Surf. Sci.* **1982**, *116*, L219.
(4) Nelson, G. C. *J. Appl. Phys.* **1976**, *47*, 1253.
(5) Swartzfager, D. G.; Kelley, M. J.; Ziemicki, S. B. *J. Vac. Sci. Technol.* **1981**, *19*, 185.
(6) Brongersma, H. H.; Sparnaay, M. J.; Buck, T. M. *Surf. Sci.* **1978**, *71*, 657.
(7) Joblonski, A.; Overbury, S. H.; Somorjai, G. A. *Surf. Sci.* **1977**, *65*, 578.
(8) Taglauer, E.; Heiland, W. *Surf. Sci.* **1975**, *47*, 234.
(9) Rusch, T. W.; Erickson, R. L. *J. Vac. Sci. Technol.* **1976**, *13*, 374.
(10) Christensen, C. L.; Mossotti, V. G. Rusch, T. W.; Erickson, R. L. *J. Nucl. Inst., Methods* **1978**, *149*, 587.

RECEIVED for review July 25, 1983. Accepted September 14, 1983.

Determination of Trace Constituents of High-Purity Gallium Arsenide

P. W. Bohn,*[1] R. Bhat, and T. D. Harris

Bell Laboratories, Murray Hill, New Jersey 07974

Various schemes for the determination of unintentionally introduced impurities in high-purity GaAs are discussed. The identification of acceptor species is accomplished by measuring the $1s_{3/2}$–$2s_{3/2}$ splitting of hydrogen-like acceptors. This measurement is made possible by an excited final state relaxation process which is manifested in the luminescence spectrum by a red-shifted replica of the acceptor bound exciton doublet. A technique is described for enhancing this process with respect to the free to bound transitions which make up the background. It involves selectively exciting only those initial states which can give rise to the desired process. Laser excitation wavelength and power density affect the emission intensities of various bound exciton peaks. The implications of these results for quantitative determinations of acceptors are discussed.

Among the problems encountered in growing high-purity group 3–group 5 semiconductor materials, the dearth of reliable analytical schemes for determination of trace impurities is one of the most serious. The materials in question are characterized by free electron densities in the 10^{13} to low 10^{14} cm^{-3} region and compensation ratios ranging from 0.1 to 0.9 which suggest impurity concentrations near 10^{14} cm^{-3}. These concentrations are near 10 ppb by weight for dopants in GaAs and, thus, pose special problems for nondestructive elemental determinations of either qualitative or quantitative nature.

At higher concentrations the problem of identification of impurities is alleviated by knowing the dopant used in the growth process. However, at the lower concentrations present in high-purity unintentionally doped material, impurities arise from the elements present in the ambient. Indeed several elements may contribute to this background leading to the incorporation of more than one donor or acceptor at comparable concentrations. Therefore, the qualitative analysis problem is composed of resolving the contributions of the several background impurities and identifying their sources. This is a task which must be completed before considering how to quantitatively determine the impurity in question.

Previously identifications have been made by far-infrared absorption spectrometry of Zeeman split hydrogenic energy levels for both acceptors (*1*) and donors (*2–5*) and by far-red luminescence for acceptors (*6, 7*). The far-infrared measurements, although useful as an identification tool, are not promising as a means of making quantitative determinations of impurity elements. This is partly due to the difficulties inherent in making quantitative measurements in the infrared and partly due to the additional level of complexity introduced by requiring the levels to be split by a magnetic field. Therefore, visible light induced luminescence emerges as the method of choice for the analysis of semiconductor samples with the goal of making both qualitative and quantitative elemental determinations of trace level impurities.

Chemical identification of specific acceptor species can be made by measuring energy differences between hydrogen-like energy levels which are characteristic of that element. When an exciton becomes bound to a neutral acceptor in GaAs, the resulting four particle complex denoted (A°, X) gives rise to three states with total angular momenta of $^1/_2$, $^3/_2$, or $^5/_2$ (*8, 9*). Relaxation of this four-particle acceptor bound exciton complex to the two-particle ground ($j = {}^3/_2$) state of the hydrogen-like acceptor is accompanied by annihilation of the exciton. Other possibilities exist, however. If the acceptor atom is left in the first excited state ($2s_{3/2}$) instead of the ground state ($1s_{3/2}$), the transition is denoted $(A^\circ, X)^*$, and the observed energy difference between (A°,X) and $(A^\circ,X)^*$ transitions may be used to identify the impurity. The energy level scheme used is shown in Figure 1. The identification is made based on extensive effective mass theory calculations of the splitting in different acceptor atoms and back doping experiments (*7, 10*). This method of identifying acceptor atoms is especially important because the direct transition is Laporte forbidden, and the absorption process cannot be observed without some form of perturbation.

After an elemental assignment has been made, the question of concentration of the impurity may be addressed. Several attempts have been made to correlate various luminescence properties with chemical concentration in GaAs (*11*) and Si (*12–14*). These have been made on a strictly empirical basis and are characterized by limited dynamic range and poor precision. They do, however, separately address two issues important to any workable quantitative analysis scheme for epitaxial semiconductor samples. The silicon studies use the free exciton intensity as an internal standard by which to ratio the impurity related bound exciton peaks. This is an attempt to remove the intrinsic crystal quality related factors which affect luminescence intensity and, consequently, concentration estimates. The GaAs work addresses the removal of some of the instrumental factors which affect reproducibility and accuracy. In neither case, however, is a satisfactory analytical

---

[1] Present address: Department of Chemistry, University of Illinois, Box 62, Roger Adams Laboratories, 1209 W. California St., Urbana, IL 61801.

0003-2700/84/0356-0058$01.50/0 © 1983 American Chemical Society

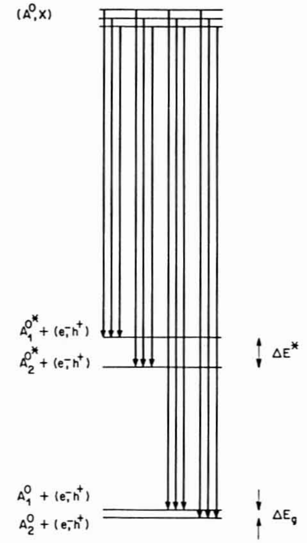

Figure 1. Energy level diagram showing the triplet manifold of (A°,X) states and the internal levels of the hydrogen-like acceptor atoms. Asterisks denote excited atomic states and subscripts refer to different elements. The notation (e^-,h^+) refers to a recombined electron-hole pair while X refers to the exciton. ΔE^* and ΔE_g refer to chemical splittings in the excited and ground states, respectively.

method fully demonstrated. Only by obtaining an understanding of both instrumental and sample related factors can a true concentration measurement be approached. The present work sought to understand how matrix related interferences could be eliminated as problems in qualitative work and how the resulting instrumental changes might affect future quantitative experiments.

EXPERIMENTAL SECTION

Samples used in this study were prepared by organometallic chemical vapor deposition (OMCVD) using $Ga(CH_3)_3$ and $Ga(C_2H_5)_3$ as the group 3 source and AsH_3 as the group 5 source. The high-purity nature of these samples was demonstrated by free electron densities ranging from 2×10^{14} to 5×10^{14} cm^{-3}. Samples were mounted for spectral work on a specially designed mechanical finger. This new mount allowed the stress of mounting to be dissipated over the 2 mm width of the sample rather than the 0.35 mm thickness. Such strain relief greatly reduces strain broadening contributions to spectral line width and is very important in high-resolution or quantitative measurements. Spectra were obtained at 2 K by introducing the sample into the cold region of an immersion type optical cryostat. This temperature was chosen for the bulk of the quantitative and high-resolution work because the Schlieren effect noise of boiling liquid He is eliminated below the superfluid transition temperature. No special surface preparation was used.

In experiments in which above band gap radiation was desired for excitation the 647.1-nm output of a 2-W Kr^+ ion laser was used. For experiments in which a variable energy excitation source was needed, the combined 647/676 nm output of the Kr^+ laser was used to pump a three mirror cavity employing a flowing jet of 3,3′-diethyloxatricarbocyanine (DEOTC) perchlorate. Typically 1.0 W of pump radiation produced 70 mW of dye laser radiation at the peak wavelength with an attendant tuning range from approximately 780 to 825 nm. Laser radiation was focused to an approximately 125-μm spot size at the sample by *f*/6 optics. Luminescence was collected at an oblique angle by *f*/1 optics and then matched to the *f*/7.8 optics of the 0.85-m Czerny-Turner double monochromator. The full width at half maximum of the instrument function was approximately 0.008 nm at 10 μm slit width at 647 nm. Radiation was detected by a C31034A photomultiplier and measured by using either phase sensitive or photon counting electronics. A MINC 11/23 (Digital Equipment Corp., Maynard, MA) microcomputer was employed to control data acquisition and to reduce raw spectral data.

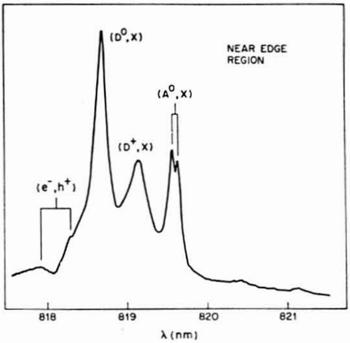

Figure 2. Medium resolution spectrum of the near edge region in GaAs.

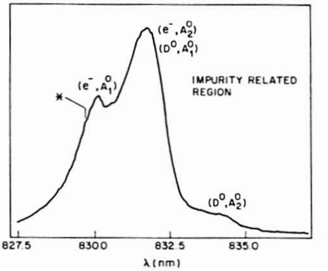

Figure 3. Spectrum of the impurity related long wavelength region of the GaAs luminescence.

RESULTS AND DISCUSSION

Details of the growth process provide a good starting place to look for information concerning the identity of impurity species in unintentionally doped material. For example, if the samples were originally prepared by organometallic chemical vapor deposition, major impurities might be expected to include carbon from the organometal, impurities in the starting materials left from the original synthesis, oxygen from the ambient if measures were not taken to exclude it, and silicon from the reactor tube itself. Other epitaxial growth techniques would result in other characteristic impurity species.

Emission features in the luminescence spectrum which embody species specific information are needed for qualitative determinations. Examination of Figures 2 and 3 shows that there are two regions in which acceptor related structure occurs. These are the (A°, X) recombination near 819.5 nm and the conduction band to acceptor (e^-, A°) band at longer wavelengths. The donor–acceptor pair band (D°,A°) is not considered because it also depends on the donor species and because its peak position is dependent on the energy of the exciting photons. The (e^-, A°) transition should provide el-

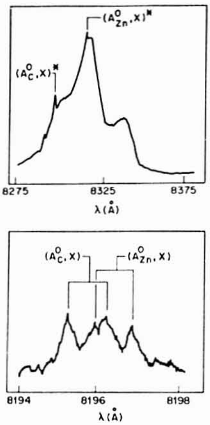

Figure 4. (Top) Spectrum of the impurity related region showing peaks resulting from relaxation of a neutral acceptor bound exciton to a final state in which the acceptor atom is excited. (Bottom) High-resolution spectrum of the (A°,X) region. Peak assignments are made on the basis of excited final state relaxation arguments.

ement specific information since the acceptor energy level in the forbidden gap is species dependent. If all transitions originated from a sharp upper state, the transition energy would yield fingerprint information about the chemical identity of the impurity. However, this band is very broad due to the spread of energies of electrons in the conduction band and the natural spread in the kinetic energy distribution of the free electrons. Such a broad spread does not lend itself to precise energy measurement and tends to increase the sample to sample variability. In addition the (e^-, A°) band of a relatively deep acceptor may overlap the (D°,A°) band of a shallower acceptor (*15*). The other possibility involves the use of the acceptor bound exciton recombination. Unfortunately the transition involving the ground state acceptor atom is only weakly dependent on chemical identity (*16, 17*). As shown in the bottom of Figure 4, the (A°,X) doublets of two different acceptors are just resolved in a favorable case.

Measurement of the excited final state relaxation energy is then the preferred method of acceptor identification. A low-resolution scan of the impurity related region in an OMCVD grown GaAs layer is shown in the top of Figure 4. Here the two spikes riding on the broad background are the excited final state relaxation peaks for two different acceptor species. By measuring the splitting between each of the (A°,X) peaks and the doublet center from the bottom spectrum in Figure 4, we made elemental identifications. Because these peaks are well separated and because the separation is much larger than the corresponding separation at the (A°,X) doublet, a facile identification is made possible. The measured values in this instance were 18.72 meV and 21.88 meV agreeing very well with the literature values for C and Zn, respectively (*10*). Values for the (e^-,A°) peak positions were also very close to previously reported values for those elements lending additional support to the assignment. The assignment of the members of the doublet of doublets in the bottom of Figure 4 was then accomplished by optimizing the intraelement j–j splitting and the fit of the internal level spacings.

A problem still exists with this type of analysis scheme. In the impurity related region the $(A^\circ,X)^*$ peaks are small and are riding on a large background. The background results from the conduction band to acceptor relaxation discussed previously. In many if not most cases the excited final state relaxation transitions are not even this well defined. The difficulty could be removed by using resonant excitation to enhance the desired process. This radiation would be sub band gap and, therefore, would not create any free electrons by one-step mechanisms. The background would be reduced and the excited final state process enhanced. This method requires radiation at the appropriate wavelength and a detection scheme to discriminate against the scattered radiation. These requirements significantly increase the experimental difficulty.

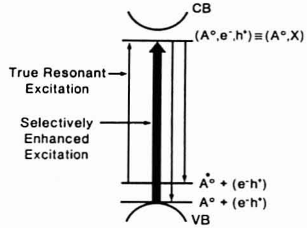

Figure 5. Energy level scheme illustrating the basis of the selectively enhanced excitation experiment.

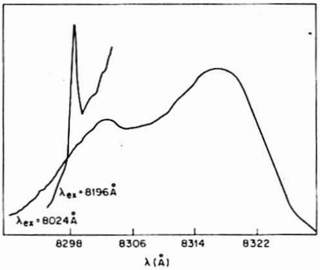

Figure 6. Spectra of the impurity related region using both above band gap radiation and ecitation designed to selectively populate the initial state of the $(A^\circ,X)^*$ transition.

An alternative approach which shares the advantages of resonant excitation but which is not as difficult to implement was adopted. As shown in Figure 5 the same effect may be obtained by selectively pumping the initial state of interest. In the present case this is the transition in which an exciton is formed and becomes bound to an acceptor. Again the formation of free electrons in the conduction band is avoided. In addition the laser radiation required is more blue and somewhat easier to produce, and the monochromator discriminates against the scattered excitation radiation. The weak dependence of the (A°,X) energy on chemical species also means that for sufficiently wide dye laser emission the same excitation conditions can be used to enhance the excited final state relaxation of several different acceptors. Results of this approach are shown for a sample containing only one acceptor in Figure 6. Excitation at 802.4 nm which is above the band gap energy produces the broad featureless spectrum with a very small feature near 829.8 nm. When 819.6-nm radiation is used to excite luminescence, however, the $(A^\circ,X)^*$ transition is dramatically enhanced. A high-resolution scan of the region with selectively enhanced excitation shows the characteristic doublet and provides a value of 18.56 meV for the internal energy level spacing. This measurement agrees

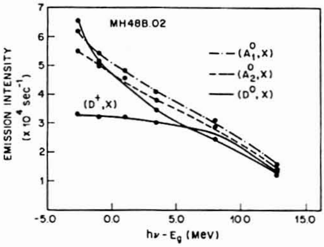

Figure 7. Plot of the dependence of emission intensity on the difference between photon energy and band gap energy for the three prominent bands in the near edge region in GaAs.

exactly with the calculated value for carbon. Thus, the technique of selectively enhanced excitation allows the observation of excited final state relaxation processes to be extended well beyond the range to which it would normally apply and allows this to be done with simpler instrumentation than would be required for strictly resonant enhancement.

It must be stated that the power of the technique is reduced when considering samples which are not crystalline semiconductors, because the special nature of the semiconductor energy band structure gives rise to the main interference from band to acceptor transitions. Within the semiconductor area, however, the technique should be quite general since complexes of impurities and excitons are observed in a wide variety of elemental, group 3–5, and group 2–6 semiconductors. For the most widely studied group 3–5 semiconductors, GaAs and InP, the limitations of the technique are clearly instrumental. The magnitude of the band gap in these compounds means that sub band gap excitation requires tunable laser radiation in the 820-nm region for GaAs and the 880-nm region for InP. The experimental difficulties in pumping dyes at these wavelengths are legion.

These results on the identification of acceptors in group 3–5 semiconductor matrices have important implications for the quantitative determination of these same species. In particular from a standpoint of understanding the sample emission the choice of the appropriate analytical emission feature is important. The best band might be defined differently for varying situations, but for any chosen line it will be important to understand how the conditions of the experiment affect the emission intensity for that line. Initial experiments have concentrated on the use of the various bound exciton lines for elemental determinations. The use of the free exciton polariton emission as an indicator of factors intrinsic to the crystal which affect luminescence efficiency is important to this approach. Thus, another prominent problem is the identification of conditions under which the free exciton emission can be easily resolved and measured.

The dependence of exciton related emission intensity on excitation wavelength is shown in Figure 7. Here the photon energy is described as the amount by which it exceeds the band gap energy. Separate plots are made for excitons bound to neutral donors (D°,X), ionized donors (D^+,X), and neutral acceptors. In each case the emission intensity increases monotonically with increasing wavelength. However, in the case of the (D^+,X) emission the intensity is fairly constant over a photon energy range extending from roughly 3 meV below band gap to 8 meV above band gap. The general trend of the data can be understood on the basis of band to band absorption near the 2 K band gap. Simple models predict an increase in the absorption coefficient with increasing photon energies above the band gap (*18*). Some of the increased free carrier concentration would then be available for exciton formation. The increased exciton population would then provide a larger pool from which bound complexes could be formed. However, increasing band to band absorption also means a shorter absorption length and should increase the surface recombination efficiency. It is this surface recombination effect which reduces the radiative relaxation efficiency at high photon energies giving rise to the observed trend.

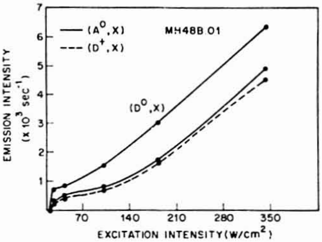

Figure 8. Plot of emission intensity vs. excitation intensity at an excitation wavelength of 814.9 nm for the three prominent bands in the near edge region in GaAs.

By use of an excitation wavelength of 814.9 nm, the variation of emission intensity with excitation intensity is plotted in Figure 8. The characteristics of the dependence are again similar for each of the bound exciton bands examined. In each case the emission intensity remains approximately constant for excitation intensities below ca. 70 W/cm^2 but increases linearly above that level. The behavior above the linearity threshold can be understood on the basis of increasing exciton generation with increasing excitation power density. It is important to note that saturation is not reached even for fairly large excitation intensities. The spectra do, however, show the expected Stark broadening from increased impurity ionization (*19*). Below the threshold the data suggest a situation in which a reasonably constant exciton population is maintained for a range of excitation powers. Above the threshold formation of bound exciton complexes is increased leading to the increased emission intensity. This behavior would be expected if there were a relatively long lifetime nonradiative process in competition with the radiative relaxation. Then at some point along the excitation intensity axis the rate of optical sampling would exceed the nonradiative relaxation rate. An Auger process, in which the energy of the annihilated exciton results in the ionization of the neutral impurity and injection of the appropriate carrier deep into the intrinsic band, would be one such nonradiative process. In addition the Auger process has been estimated to be 3 orders of magnitude more probable than radiative relaxation for excitons bound to neutral impurities in direct gap semiconductors (*20*). Experiments are in progress to discern the true nature of the competing process.

Registry No. GaAs, 1303-00-0.

LITERATURE CITED

(1) Kirkman, R. F.; Stradling, R. A. *J. Phys. C* **1973**, *6*, L324–L328.
(2) Stillman, G. E.; Wolfe, C. M.; Dimmock, J. O. *Solid State Commun.* **1969**, *7*, 921–925.
(3) Stillman, G. E.; Larsen, D. M.; Wolfe, C. M. *Phys. Rev. Lett.* **1971**, *27*, 989–992.
(4) Ozeki, M.; Kitahara, K.; Nakai, K.; Shibatomi, A.; Dazai, K.; Okawa, S.; Ryuzan, O. *Jpn. J. Appl. Phys.* **1977**, *16*, 1617–1622.
(5) Cooke, R. A.; Hoult, R. A.; Kirkman, R. F.; Stradling, R. A. *J. Phys. D* **1978**, *11*, 945–953.
(6) White, A. M.; Dean, P. J.; Ashen, D. J.; Mullin, J. B.; Webb, M.; Day, B.; Greene, P. D. *J. Phys. C* **1973**, *6*, L243–L246.
(7) Ashen, D. J.; Dean, P. J.; Hurle, D. T. J.; Mullin, J. B.; White, A. M.; Greene, P. D. *J. Phys. Chem. Solids* **1975**, *36*, 1041–1053.
(8) White, A. M. *J. Phys. C* **1973**, *6*, 1971–1974.
(9) Morgan, T. N. *J. Phys. C* **1977**, *10*, L131–L134.

(10) Lipari, N. O.; Baldereschi, A. *Phys. Rev. Lett.* **1970**, *25*, 1660–1664.
(11) Stringfellow, G. B.; Koschel, W.; Briones, F.; Gladstone, J.; Patterson, G. *Appl. Phys. Lett.* **1981**, *39*, 581–582.
(12) Tajima, M. *Jpn. J. Appl. Phys.* **1977**, *16*, 2265–2266.
(13) Tajima, M. *Appl. Phys. Lett.* **1978**, *32*, 719–721.
(14) Tajima, M.; Nomura, M. *Jpn. J. Appl. Phys.* **1981**, *20*, L697–L700.
(15) Rossi, J. A.; Wolfe, C. M.; Dimmock, J. O. *Phys. Rev. Lett.* **1970**, *25*, 1614–1617.
(16) White, A. M.; Dean, P. J.; Taylor, L. L.; Clarke, R. C.; Ashen, D. J.; Mullin, J. B. *J. Phys. C* **1972**, *5*, 1727–1738.
(17) White, A. M.; Dean, P. J.; Day, B. *J. Phys. C* **1974**, *7*, 1400–1411.
(18) Bebb, H. B.; Williams E. W. In "Semiconductors and Semimetals Volume 8: Transport and Optical Phenomena"; Willardson, R. K., Beer, A. C., Eds.; Academic Press: New York, 1972; Chapter 4
(19) Larsen, D. M. *Phys. Rev. B* **1976**, *L3* (4), 1681–1691.
(20) Nelson, D. F.; Curthbert, J. D.; Dean, P. J.; Thomas, D. G. *Phys. Rev. Lett.* **1966**, *17*, 1262.

RECEIVED for review June 13, 1983. Accepted September 23, 1983.

Fiber-Optic Probe for in Vivo Measurement of Oxygen Partial Pressure

John I. Peterson* and Raphael V. Fitzgerald

Biomedical Engineering and Instrumentation Branch, Division of Research Services, Building 13, Room 3W13, National Institutes of Health, Bethesda, Maryland 20205

Delwin K. Buckhold

Section on Laboratory Medicine and Surgery, National Heart, Lung, and Blood Institute, National Institutes of Health, Bethesda, Maryland 20205

A fiber optic probe for measuring oxygen partial pressure is described. It is based on fluorescence quenching and consists of two 250-μm strands of plastic optical fiber ending in a section of porous polymer tubing about 3 mm long and 0.6 mm in diameter. The tubing is packed with dye on an adsorptive support. The general construction is similar to a pH probe, which has previously been reported. The development required the solution of three major problems not encountered before in application of this principle. (1) A dye was needed with the combined properties of suitable oxygen quench sensitivity, excitation by visible light, and resistance to fading. (2) A hydrophobic, high-oxygen-permeability envelope was necessary. (3) An adsorptive support was required which activated the dye without sensitivity to humidity. This design provides a small-size, low-cost probe suitable for tissue and blood vessel implantation.

A suitable device is needed for the direct measurement of oxygen partial pressure of blood and tissue in a variety of clinical and research situations. Currently blood oxygen can be estimated by an in vivo optical measurement of hemoglobin saturation, by a transcutaneous sensor, or by withdrawing samples for a blood gases measurement instrument which determines the oxygen with a Clark type electrode (*1*). All of these methods have disadvantages in practicality, reliability, safety, or general applicability. It is desirable to have a very small P_{O_2} sensor which can be inserted into a blood vessel or tissue in various parts of the body with little disturbance and left there for an extended period of time, if necessary, for continuous monitoring of P_{O_2} levels. Over the years, a considerable body of literature has developed surrounding attempts to make suitable P_{O_2} electrodes, but there are two main reasons why they have not been successful. It is difficult to make a practical membrane-diffusion type of amperometric electrode in a small size, but more importantly, the diffusion dependence of the measurement is subject to calibration and drift problems. A redox or potentiometric type of electrode, as an alternative, has to be isolated to avoid specificity difficulties. In considering the problem, it appeared to us that a fiber optic sensor for measuring P_{O_2} would circumvent these problems.

We had previously developed a fiber optic probe for physiological measurement of pH (*2*, *3*), and this served as a model for future applications of the idea of a reversible indicator package at the end of an optical probe. A fiber optic sensor has the advantages, for physiological use, of very small size and flexibility, it is of sufficiently low cost and easily made that it can be considered disposable, it presents no electrical hazard, and it is an equilibrium measurement with long-term stability.

Principle of Measurement. The sensor is based upon the principle of fluorescence quenching by oxygen. The only other choice of reversible optical indicator, an absorptiometric type, offers a possible advantage over a luminescence quenching indicator in sensitivity and specificity, but a sufficiently stable metal organic compound of this type does not appear to be available. The use of luminescence quenching for oxygen measurement has been long known, but surprisingly little use appears to have been made of it. Oxygen's effect of decreasing the luminescence of dyes on an inorganic adsorbent was first observed and published in a series of papers by Kautsky and Hirsch in the early 1930's (*4*).

It was this observation and Kautsky's explanation of it in terms of formation of an active form of oxygen, by transfer of energy from the light-activated dye molecule to oxygen, which led to the recognition of singlet oxygen (*5*). The phenomenon is apparently quite general, with oxygen forming a charge transfer complex with aromatic molecules for energy transfer to oxygen (*6*, *7*). Berlman (*8*) has cataloged the oxygen-quenching sensitivities of organic molecules of interest in scintillation counting. It is interesting that the simplest aromatic, benzene, has one of the strongest sensitivities to oxygen quenching of its fluorescence. The effect is most

This article not subject to U.S. Copyright. Published 1983 by the American Chemical Society

pronounced when a dye is adsorbed on a material which suspends and exposes the molecule to the gas phase, so that the lifetime of its excited state is not made too short by transfer of the energy to a solvent and the collision rate of oxygen with the molecule is not impeded by a low permeability solid or liquid medium.

A few analytical applications of luminescence quenching for oxygen determination have been reported through the years. Kautsky (*4*) mentions phosphorescence quenching being useful for the detection of oxygen in the millitorr pressure range. Pollack et al. (*9*) used the technique to measure oxygen produced by illumination of algae. Orbán et al. (*10*) measured oxygen down to 10^{-5} torr with acriflavin on acrylic sheet. Shaw (*11*) measured the diffusion coefficient of oxygen in acrylics by observing the phosphorescence of rods. Jones (*12*) determined the oxygen permeability of acrylic films by measuring the quench rate as a function of oxygen pressure. Bergman (*13*) developed an oxygen pressure measuring instrument based on fluoranthene absorbed on plastic films and porous Vycor. Stevens (*14*) patented an instrument system based on a thin film of pyrene, either on or in a polyethylene support material. Pyrenebutyric acid was used as a probe for measuring intracellular oxygen by Knopp and Longmuir (*15*), and Lübbers and Opitz (*16*) have used solutions of pyrenebutyric acid in various membrane-enclosed forms to measure physiological oxygen pressure.

Quantitative Basis of Oxygen Quenching. Fluorescence or phosphorescence quenching is the result of a quenching decay mode competing with the luminescence decay and other decay modes of an activated molecule, thereby decreasing the overall mean lifetime of the activated state and decreasing the luminous intensity. With constant illumination, the rate of decay of the excited state is the sum of the rates of various decay modes: collision, luminescence, and vibrational. The collision quenching thus competes with the other decay modes and is proportional to the activated state mean lifetime (approximately, the fluorescence lifetime) and the collision rate, which is proportional to the pressure of the quench gas. This results in the relation derived by Stern and Volmer (*17*) for fluorescence intensity I and pressure of oxygen P_{O_2}

$$I_0/I = 1 + (P_{O_2}/P') \qquad (1)$$

where I_0 is the intensity without oxygen quenching and P' is a constant, the pressure at half-quench, and includes the rate constants for the modes of decay. The same expression can be written in terms of apparent luminescence mean lifetimes T_0 and T

$$T_0/T = 1 + (P_{O_2}/P') \qquad (2)$$

Good sensitivity to oxygen quenching requires a long natural lifetime of the excited state. Phosphorescence, with a very long lifetime (seconds), is very sensitive to quenching but is weak in intensity. Fluorescence, with a shorter lifetime relative to thermal and collisional decay, is less sensitive to quenching but has a higher brightness due to higher quantum efficiency. A dye should be chosen with P' of the order of the pressure to be measured to best compromise brightness and sensitivity, as illustrated in Figure 1. Brightness, leading to easier optical design and better signal to noise ratio in an instrument, is obtained at the expense of sensitivity or resolution.

EXPERIMENTAL SECTION

Basic Problems in Development of the Sensor. *Choice of Dye.* Although a large number of dyes and other compounds can be considered as candidates for analytical use of the oxygen quenching phenomenon, the choice is greatly limited by the particular requirements of a device for physiological and medical use. Visible wavelength excitation is dictated by the use of plastic optical fibers. These are highly flexible, do not present the risk of breakage in sharp bends, in general are much easier to work with than ceramic fibers, and allow the construction of low-cost, simple, all-plastic devices. Their disadvantage is strong attenuation of light at wavelengths shorter than 450 nm. The stability of a dye to light and aging must be sufficient for this application. The dye must be nontoxic, and it must have a sufficient oxygen quenching sensitivity to allow measurement to the nearest torr.

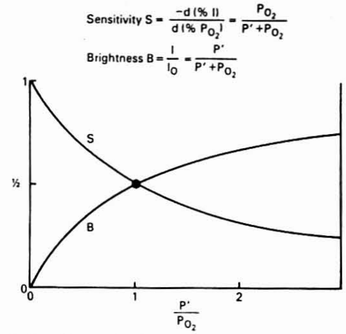

Figure 1. Sensitivity andd brightness best compromised at $P' = P_{O_2}$.

There appeared to be no very useful theoretical guidelines for relating molecular structure to the desirable dye properties, so all possible dye candidates which could be obtained, which met the wavelength requirement, were tested for oxygen quench sensitivity. Approximately 70 dyes were screened, and after considering all of the desired characteristics, the one chosen as optimum was perylene dibutyrate (solvent green 5, CI 59075) (Thermoplast Brilliant Yellow 10 G, BASF-Wyandotte). This dye has an excitation peak at 468 nm and an emission peak at 514 nm (uncorrected spectra determined on a Perkin-Elmer 650-10S spectrofluorometer). The dyes were tested dry, adsorbed from a solvent on silica gel TLC plates (Silica Gel 60, E. Merck). Some observable degree of oxygen quenching is common to many dyes tested. Poor stability or toxicity considerations rejected several of the more sensitive ones. The dye chosen, solvent green 5, is quenched on silica gel to 40% of its unquenched intensity by exposure to air and quenched to about 16% of its intrinsic intensity by oxygen at atmospheric pressure. There is no reason to expect any toxicity problem with this dye. Its stability on silica gel is better than most dyes, but not indefinite. On an organic adsorbent (to be mentioned later) the dye has not shown deterioration in 3 years of storage. The commercial form of the dye has at least eight minor impurities, which can be observed by thin-layer chromatography. The dye was purified by silica gel chromatography for testing, but there appeared to be no improvement in the characteristics or performance of the purified dye, so it has been used without purification.

Support for Dye. Classically the oxygen quenching effect has been observed on silica gel or other inorganic adsorbents, and the highest sensitivity is achieved on silica gel. A high permeability support is necessary to expose the individual dye molecules to oxygen collision. A solution of the dye in liquids or solids is insensitive because of the low oxygen permeability of such materials. Unfortunately, inorganic adsorbents are not suitable because they cause the quenching to be humidity sensitive. In general, it was found with them that quench sensitivity varies with humidity and loss of the quenching effect, or loss of fluorescence, occurs at 100% humidity, the condition for physiologic measurements. No solution could be found to the problem of humidity sensitivity of a dye on an inorganic adsorbent, although many types of adsorbents and adsorbent treatments were tested.

Organic adsorbents (porous polymers) provide a support for the dye which avoids humidity sensitivity and provides a hydrophobic indicator system. The disadvantage is that the quench sensitivity is approximately halved, relative to a silica gel support, and sensitivity of the fluorescence and quenching to organic solvent vapors occurs.

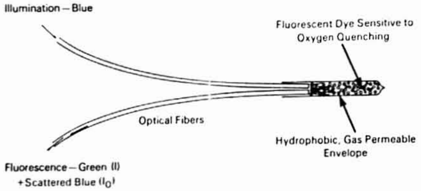
Illumination – Blue
Fluorescent Dye Sensitive to Oxygen Quenching
Optical Fibers
Hydrophobic, Gas Permeable Envelope
Fluorescence – Green (I)
+Scattered Blue (I_0)

Figure 2. Construction of fiber optic fluorescent probe.

The commonly available organic polymer adsorbents, including those used for chromatography, were tested. Amberlite XAD4 (Rohm and Haas) was found to have the best quench sensitivity with solvent green 5. The indicator packing for the sensor described in this paper was prepared by allowing the XAD4 resin beads in a filter funnel to absorb a 0.2% solution (weight/volume) of solvent green 5 in dichloromethane, drawing off the excess liquid by suction, and allowing the resin beads to dry by spreading them out on a flat surface exposed to ambient air. The resin was washed before treatment with the dye, by rinsing with water two or three times and then successively absolute ethanol and acetone, followed by drying. The first water rinse should be done by decantation to separate fine material. Cleaning the resin is good practice, but it is not certain that it is necessary. The dyed resin is ground finely with a mortar and pestle for use, producing fragments in the range of 1 to 100 μm.

Permeable Envelope. For the P_{O_2} probe we have developed, which follows the basic construction idea of the earlier pH probe, a liquid-water-impermeable but high gas permeability enclosure is required for the indicator packing at the end of the probe to protect it from contamination by exposure to blood or tissue fluids. Solid materials do not have sufficient oxygen permeability, so a microporous material is required. Metals present problems with biocompatibility, and the available porous fluorocarbon materials lack mechanical rigidity and strength. A suitable material was found to be porous polypropylene (Celgard, Celanese Corp.). This material is hydrophobic, highly permeable to gases, and furnished in 25 μm thickness with excellent strength. Some limited sizes of tubing are available, but a heat sealing technique was developed for making tubing, which allows matching of tube size to the desired probe size (*18*).

Design of the P_{O_2} Probe. The probe design, shown in Figure 2, is modeled after the pH probe we previously developed. The dye, on an adsorbent support, is contained inside a section of tubing of porous polypropylene, providing rapid equilibration with the surrounding oxygen and isolating the dye packing from contamination. Blue light illumination passes down one optical fiber to excite the dye to fluorescence. The green fluorescent light, along with scattered blue light, passes through the other fiber to a measuring instrument.

For development purposes the test probes were assembled with 0.25 mm diameter plastic optical fibers (Crofon, Du Pont). Smaller fibers can be used to make smaller probes, or a single fiber can be used with a suitable light-splitting system in the instrument to separate the excitation and emission light. A method of making bifurcated fibers has also been developed so that separate fibers leading to the light source and measurement system join and become a single fiber at the sensor end. The dual-fiber construction to be described was used generally, however, with relatively large fibers to minimize the effort involved in construction. About 20 min of work is required to completely assemble a test probe.

Test probes were made either 90 cm or 120 cm long. About 30 cm of a fiber pair was passed together through 0.6 mm inside diameter, 0.8 mm outside diameter fluorocarbon tubing filled with carbon black to make it opaque (Atlantic Tubing Co). The rest of the fibers were encased individually in the same kind of tubing of 0.4 mm inside diameter, 0.8 mm outside diameter. The joint between the two sizes of tubing where the fibers branch was joined with heat-shrink tubing. The ends of the fibers which connect to the instrument and lamp were heat flared to about twice the fiber diameter and fitted closely to the ends of the tubing. This was done after making the sensor end. The sensor end, with paired fibers, protrudes slightly from the end of the fluorocarbon tubing and is made as follows: The parallel pair of optical fibers extending from the opaque tubing are inserted into a short length of clear fluorocarbon tubing, of inside diameter slightly larger than the combined diameters of the fibers. The fibers are cut square and flush with the end of the tubing. A hot soldering iron is brought up to the ends of the fibers and they fuse together, shrink back, and expand to fill the tubing. The end of the fused fibers is cut square where the fibers are fused together but clear. Then the joint is pushed out of the fluorocarbon tubing a short distance. UV-curing optical cement (NOA 60, Norland Products, Inc.) is added to the fibers at the region of the joint and the joint is pulled back into the tubing. The liquid optical cement fills the space inside the fluorocarbon tubing for a short distance before and beyond the fiber joint. Bubbles must be avoided. Due to the nonwettability of the fluorocarbon, the cement forms a flat surface at its end. After the cement is cured by exposure to ultraviolet light (1 min exposure will set the cement but several hours are recommended for a complete cure), the joint can be removed from the tubing. A short length of porous polypropylene tubing, of an inside diameter to closely fit the joined optical fibers, is slid over the fiber joint and cemented in place with optical cement. Several hours of exposure to ultraviolet light is recommended for complete cure of the assembly. The end of the probe is packed with ground, dyed adsorbent to a depth of about 0.5 mm, which is well beyond the optical depth. Excess tubing is cut off and the open end sealed, either by heat sealing or by a plug of optical cement. It is important that the dyed adsorbent be packed tightly, with a tight seal of the tubing against it. The same general technique can be used for preparing a sensor on a single fiber end.

Design of the Optical Instrument for Use with the Probe. The excitation light for the probe was provided by a deuterium lamp (Hanau D-102, Hellma International) operated at 60 W in a specially designed aluminum housing with fan cooling. Although a deuterium lamp has relatively little of its output in the visible, it was chosen over other possible light sources because of its long life and the extremely good stability, both of position and intensity, of the 1 mm diameter bright spot. This small, stable spot allowed efficient coupling of the light into an optical fiber. A lens system was included in the lamp housing, consisting of two aspheric lenses (01 LAG 117, Melles Griot). These lenses were arranged so that the bright spot of the lamp was at the focal point of one lens, with the light traversing a short distance between the lenses and then refocusing the image of the lamp on the end of the optical fiber of the probe at the focal point of the second lens. Two filters were located in the parallel ray path of light between the lenses. The first filter was a heat reflecting filter to block red light from the lamp. The second filter was a short-pass interference filter with a nominal cutoff of 480 nm (Ditric Optics). The lamp housing provided a means of adjusting the lamp position and the position of the fiber end. A simple connector for the jacketed optical fiber consisted of a 5 cm length of hypodermic tubing of such a diameter that the fiber optic lead fitted closely inside it. The tubing was crimped slightly to hold the probe lead firmly. One end of the tubing was constricted slightly and located at the focal point of the lamp image, so that when the probe lead was inserted, the flared end of the optical fiber was located at the end of the tube at the position of the lamp image. The other end of the tubing was flared out slightly to assist insertion of the jacketed lead.

A simple analog instrument was constructed for development and evaluation of the experimental probes. Figure 3 shows the schematic outline of the measuring instrument. The optical system consists first of a connector, like the one described with the lamp, into which the second jacketed optical fiber is inserted. The tip is located at the focal point of a small collimating lens (01 LAG 002, Melles Griot). The blue and green light from the sensor end of the probe comes out of the fiber end, is made into a parallel beam by the lens, and then is split into two orthogonal beams by a dichroic filter (Ditric Optics). Light of wavelength shorter than 500 nm passes straight without reflection and light of wavelength longer than 500 nm is reflected at 90°. Two additional cleanup filters are used to make the wavelength discrimination purer. The blue and green beams of light are received by photomultiplier tubes (PF 1039, RCA). These photomultiplier tubes have the convenience of a built-in power supply and gain control.

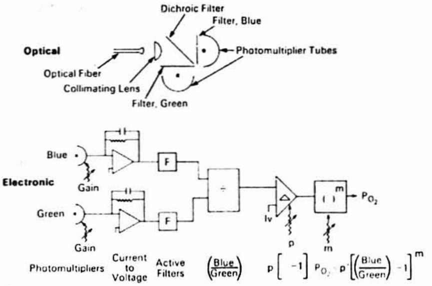

Figure 3. Outline of P_{O_2} measuring instrument.

The electronic circuit processes the blue and green signals in accord with the following relation:

$$P_{O_2} = (\text{gain})\left(\frac{(\text{blue intensity})}{(\text{green intensity})} - 1\right)^m \quad (3)$$

which is the Stern–Volmer relation rearranged, with an exponent m added for curvature. The Stern–Volmer equation provides a linear relation between quench and oxygen pressure, but a curved relation is commonly observed (a large body of literature with Stern–Volmer plotted data exists and an exponent is often attached to the oxygen pressure to fit the data to the equation). The blue signal, which is scattered and reflected excitation light, is proportional to the I_0 or intensity without quenching, and the green signal, the fluorescent light, is proportional to the I or the intensity with quenching. When the instrument is set to read zero P_{O_2} in the absence of O_2, the proportionality constants for blue and green are adjusted so that, effectively, I equals I_0.

The instrument was designed to provide digital indication of P_{O_2} to the nearest torr, over the range of 0 to 150 torr. This requires less than 0.1% error in intensity measurement. From Figure 3, the blue and green signals on the photomultipliers can be adjusted and balanced by the individual photomultiplier gain controls. The photomultiplier current is converted to a voltage signal by operational amplifiers (52K, Analog Devices). The gain of each photomultiplier is adjusted so that about 1 V is obtained at the amplifier outputs, with a probe connected. This output is observed on the P_{O_2} display by a selector switch. A 1-s time constant filtering is provided by a capacitor at this stage. The signals then pass through active filters (1 s time constant) (721L6D-1A0, Frequency devices), and then to a divider (433B, Analog Devices). At this stage the blue and green ratio, or I_0 over I, is obtained. An instrumentation amplifier (610K, Analog Devices) subtracts 1 from this ratio and multiplies the result by a variable gain or scaling factor. The resulting signal is then passed through another divider (433B, Analog Devices) for the exponent adjustment. The final signal then goes to a digital indicator (AD 2009, Analog Devices) for visual observation of P_{O_2}, and to a connector for a recorder.

To calibrate the instrument with a sensor in place, the individual photomultiplier gain adjustments are set as described. Then, with the probe in nitrogen, one of the photomultiplier gains is fine-tuned to make the P_{O_2} indication equal to 0. The probe is then exposed to a known P_{O_2} pressure and the gain (scaling factor) is adjusted so that the readout matches the known P_{O_2}. Ambient air is about 150 torr, which is a convenient value to use. The exponent adjustment must be determined by a test in which a third P_{O_2} value about halfway between (i.e., about 75 torr) is used, and the exponent setting varied until the P_{O_2} indication is correct in midscale as well as at the ends. It was necessary to use an exponent value of approximately 1.11 on the instrument to get a linear response of the fiber optic sensor. Without the use of the exponent, the sensor indicates approximately 10% high in mid-range when the instrument is adjusted to indicate correctly at 0 and 150 torr. The exponent setting is the same for different sensors and does not vary with temperature over the range from 10 to 50 °C. With typical probes, the noise level in the readout is within 1 torr.

Performance Tests of the Probe. The probe was tested in a gas stream and in water in a temperature-regulated cell. The test gas was bubbled through the water with a fritted-glass disperser and a magnetic stirrer to maximize the rate of equilibration of the water with the gas stream. Nitrogen and air at ambient pressure (approximately 150 torr P_{O_2}) were mixed with a digitally controlled valve to provide partial pressures of oxygen from 0 to 150 torr in the gas mixture. A Clark-type oxygen electrode (Yellow Springs Instruments No. 4004) was used in the gas stream to monitor the gas composition.

The electrode was tested with gas standards (Matheson) of 5, 10, and 15% oxygen in nitrogen, along with undiluted nitrogen and air. This assured that the electrode gave a linear response over this range, within an error smaller than could be observed with the fiber optic sensor. The oxygen electrode was not used directly in the water cell with the fiber optic sensor because the electrode indication is sensitive to stirring and bubbles. The sensor was tested by first calibrating as described previously. It was tested in dry gas and in water, relative to the electrode in the gas stream, with stepwise changes in oxygen composition over the 0 to 150 torr range. The fiber optic sensor indication and the electrode indication were compared simultaneously on a dual pen strip chart recorder.

Response Time. The response time of the fiber optic sensor in a gas stream was not acccurately measured due to damping by the instrument, but it is some small fraction of a second. The response time in water was measured by equilibrating the sensor in water in the temperature regulated cell and then adding water of a different P_{O_2} to make an immediate step change in the oxygen concentration of the water.

Temperature Coefficient. The temperature coefficient of the fiber optic sensor was measured in water by observing the nitrogen and air response of a sensor calibrated at 25 °C, in 5 °C steps over the range from 10 to 50 °C.

In Vivo Tests. An in vivo evaluation of the fiber optic sensor was done in the bloodstream of a 31 kg ewe. The fiber optic probe with 120 cm leads was inserted through an 18 gauge, 8 in. (20 cm) Teflon catheter (Becton Dickinson) which was inserted in the carotid artery of the sheep. The fluorocarbon jacket of the fiber optic probe closely fitted the catheter tip to prevent blood leakage. For comparison data, blood samples were removed with a syringe from a like catheter in the same artery. When blood samples were withdrawn, they were analyzed immediately on an Instrumentation Laboratories Model 713 blood gas analyzer. Before insertion in the animal, the fiber optic sensor was calibrated in water at 39 °C using nitrogen and ambient air (150 torr P_{O_2}) bubbling through the water for calibration points. Sodium thiopental was used intravenously for anesthetic induction of the animal, and anesthesia was maintained with intravenous sodium pentobarbital as needed. The breathing was maintained by a mechanical respirator supplied with nitrous oxide at a constant rate of 0.8 L/min, plus oxygen at a variable rate as described further. An initial injection of 6000 units of heparin was used for anticoagulation, followed by 3000 units hourly. After removal of the probe for cleaning and reinsertion just before 2 h of use, the heparin dosage was increased to 3000 units every half hour.

RESULTS AND DISCUSSION

In the evaluation of the probe performance in comparison with an electrode in water over the 0–150 torr range, the maximum error observed was 1 torr, which tended to occur at about three-fourths of the range in the dry gas, with the fiber optic sensor indicating higher P_{O_2}. Over most of the range in the dry gas stream and in the water test, the two sensors agreed within the noise level of a few tenths of a torr.

The time constant of the sensor (63% of an exponential response to the step change) was 0.5 min or 2 min for a 98% response at 25 °C.

The base line (nitrogen value or zero setting) does not vary with temperature. The P_{O_2} indication (in air) is approximately inversely proportional to temperature. The relation between

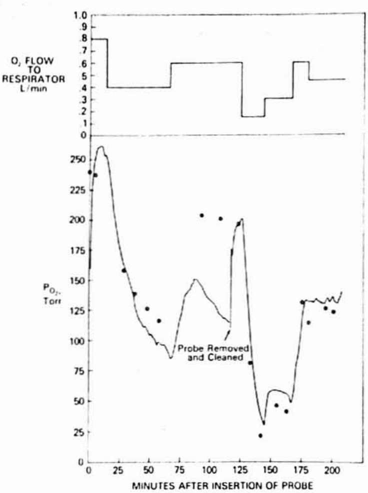

Figure 4. In vivo test of probe.

P_{O_2} and temperature (in terms of either degrees C or the inverse of absolute temperature) is curved, but a straight line fits the data with small error. A 0.6% decrease in P_{O_2} indication per C increase is observed.

Stability. The stability of the sensor over a long time is good but does not allow indefinite storage. A problem was encountered with prepared sensors, which show a typical 3% per day decrease in P_{O_2} sensitivity in dry storage. If sensors are kept in water, a loss of sensitivity of 0.1% per day over a 10-day test period is typical. Extensive tests to determine the cause of the sensitivity loss show that it must be something which diffuses out of the plastic optical fibers. The prepared reagent (dye on organic adsorbent) is stable indefinitely without change of its characteristics. Sensors which are emptied of their reagent packing after storage for a period of time, and then repacked with new reagent, show a substantially decreased loss of sensitivity. Tests of components of the sensor other than the optical fibers show that these components are not responsible for the effect.

A 5-day test showed an average loss of sensitivity of 6.5% per day due to continuous exposure to the blue excitation light when connected to a fiber optic sensor. The dye chosen for the sensor was unusually good in its stability to light, compared to other dyes tested, but intermittent exposure to the light source for pressure measurements over a long period of time is recommended.

Interference Tests. The P_{O_2} sensor was tested for interference in its response to anesthetics which are likely to appear in an in vivo application. Since the sensor is hydrophobic in construction, nonvolatile water-soluble components would not be expected to cause any interference other than possible clogging of the membrane, leading to slow response. A 1% solution of sodium thiopental in water had no observable effect on the sensor. Volatile or gaseous anesthetics can cause interference. Nitrous oxide has 2% of the effect of an equal partial pressure of oxygen on the fiber optic sensor response. This degree of interference is not important in typical in vivo applications of the sensor. A more serious problem occurs with adsorption of certain substances, particularly the halogenated anesthetics. 2-Bromo-2-chloro-1,1,1-trifluoroethane (Halothane, Halocarbon Laboratories) interferes seriously with the fiber optic sensor. The interference is cumulative, related to both concentration and time of exposure, and changes both the sensitivity and the zero adjustment of the sensor. The effect is reversible if exposure is not too severe, and it appears to be the result of adsorption by the organic adsorbent support for the dye. This is an effect analogous to the interference which water vapor causes if the dye is supported on an inorganic support.

In Vivo Evaluation. Figure 4 shows the continuous oxygen record of the fiber optic probe during the course of the experiment, lasting over 3 h, in comparison with the blood values for P_{O_2}, shown as dots. The program of variation of oxygen flow rate to the respirator, to vary the P_{O_2} of the blood over a broad range, is shown at the top of the figure. Upon the initial insertion of the fiber optic probe, the P_{O_2} indication rose rapidly to a value somewhat above the level established by the blood samples, over 250 torr. This level was substantially above the calibration point of 150 torr, so the agreement is as good as expected. Then the oxygen flow rate was halved and the blood P_{O_2} dropped rapidly into the calibration range, going below the values of the blood samples. At 66 min the oxygen flow was increased to 0.6 L/min. The probe responded to this increase in oxygen pressure immediately, but then at about 80 min, the response of the probe to the increasing oxygen pressure became poor. Clot formation around the tip of the sensor was suspected and it was removed from the catheter at 116 min. It was wiped clean and reinserted into the animal, whereupon it indicated a partial pressure of oxygen agreeing with the blood samples. The oxygen flow was then decreased to give a very low oxygen concentration in the blood. This could not be maintained for long without risking the death of the animal. The oxygen flow was then increased to a safer level and the fiber optic probe agreed reasonably well with the blood sample values.

It is not clear why difficulty with clotting occurred in the heparinized animal, because Celgard, the exterior material of the sensor, is used for other in vivo applications. A clotting problem was also encountered at the catheter used for removing blood samples. There may have been some animal-related reason for the insufficiency of what would be regarded as a suitable heparin concentration.

In conclusion, this work has demonstrated the suitability of the fiber optic P_{O_2} sensor for in vivo blood measurements where halocarbon anesthetics are not present.

ACKNOWLEDGMENT

Appreciation is due to Currie Wooten and Carter Gibson, of the Electronics Section, Biomedical Engineering and Instrumentation Branch, for their valuable advice on the design of the electronic circuit. Kenneth Breuer should be mentioned for giving much help in the unsuccessful search for a satisfactory metal–organic indicator for oxygen. We thank Joseph E. Pierce of the National Heart, Lung, and Blood Institute for providing the source of sheep and arranging the use of the Institute's surgical laboratory and staff.

LITERATURE CITED

(1) Clark, L. C., Jr. *Trans.—Am. Soc. Artif. Intern. Organs* **1956**, *2*, 41.
(2) Peterson, J. I.; Goldstein, S. R.; Fitzgerald, R. V.; Buckhold, D. K. *Anal. Chem.* **1980**, *52*, 864.
(3) Goldstein, S. R.; Peterson, J. I.; Fitzgerald, R. V. *ASME Trans. J. Biomech. Eng.* **1980**, *102*, 141.
(4) Kautsky, H. *Trans. Faraday Soc.* **1939**, *35*, 216.
(5) Ranby, B. In "Singlet Oxygen"; Ranby, B., Rabek, J. F., Eds.; Wiley: New York, 1978; Chapter 1.
(6) Evans, D. F. *J. Chem. Soc.* **1953**, 345.
(7) Tsubomura, H.; Mulliken, R. S. *J. Am. Chem. Soc.* **1960**, *82*, 5966.
(8) Berlman, I. B. "Handbook of Fluorescence Spectra of Aromatic Molecules", Academic Press: New York, 1965 (2nd ed., 1971).
(9) Pollack, M.; Pringsheim, P.; Terwood, D. *J. Chem. Phys.* **1944**, *12*, 295.
(10) Orbán, Gy.; Szentirmay, Zs.; Patko, J. *Proc. Int. Conf. Lumin. 1966* **1968**, *1*, 611.
(11) Shaw, G. *Trans. Faraday Soc.* **1967**, *63*, 2181.

Anal. Chem. 1984, 56, 67–70

(12) Jones, P. F. *Polym. Lett.* **1968**, *6*, 487.
(13) Bergman, I. *Nature (London)* **1968**, *218*, 396.
(14) Stevens, B. U.S. Patent 3 612 866, Oct 12, 1971.
(15) Knopp, J. A.; Longmuir, I. A. *Biochim. Biophys. Acta* **1972**, *279*, 393.
(16) Lübbers, D. W.; Optiz, N. *Z. Naturforsch., C: Biosci.* **1975**, *30C*, 532.
(17) Stern, O.; Volmer, M. *Physik. Z.* **1919**, *20*, 183.
(18) Peterson, J. I.; Sullivan, J. V. *Rev. Sci. Instrum.*, in press.

RECEIVED for review July 5, 1983. Accepted September 16, 1983.

Rules for Computerized Interpretation of Vapor-Phase Infrared Spectra

Sterling A. Tomellini,* James M. Stevenson, and Hugh B. Woodruff

Merck Sharp & Dohme Research Laboratories, P.O. Box 2000, Rahway, New Jersey 07065

Rules for the interpretation of vapor-phase infrared spectra have been developed for the IBM 3081 version of the Woodruff and Smith program for the analysis of infrared spectra (PAIRS) and its Nicolet 1180 version known as the Merck infrared spectral interpretation package (MISIP). Necessary changes and additions were made to the rules, rule compiler, and interpreter. Over 75 4-cm^{-1} resolution vapor-phase spectra were tested along with a number of condensed-phase spectra to ensure the proper functioning of the new rules and the uncompromised nature of the previously developed condensed-phase rules. The additional capability of the interpreter along with its availability on an instrument-based minicomputer will give those scientists employing techniques such as GC/FTIR, off-gas, and head space analysis on larger organic molecules at moderate resolution an alternative to currently available matching techniques.

The Woodruff and Smith program for the interpretation of infrared spectra (PAIRS) (*1*, *2*) was designed to aid the chemist in interpreting infrared spectra of condensed-phase (liquid or solid) compounds. Recent adaptation of this program to an instrument-based minicomputer (*3*) provided the opportunity to expand the interpretation capabilities of PAIRS. Compounds have different infrared spectra in various condensed phases and the vapor phase due to changes in hydrogen bonding, the dielectric constant of the medium, and nonpolar solvent–solute interactions. Hence, attempts to interpret vapor-phase spectra with condensed-phase interpretation rules proved to be unacceptable.

Welti (*4*) has given frequency correlation charts for some of those compounds known to have different vapor and condensed-phase spectra. Examples include alcohols, phenols, amines, amides, esters, and ketones. This book is the primary reference for the modification of previous interpretation rules and generation of new rules. Additional refinement was made by use of other recently published correlation charts of the –OH stretching region (*5*) and a number of 4-cm^{-1} resolution vapor-phase spectra. These spectra were provided by the Nicolet Instrument Corp. (Madison, WI) and were produced by Sadtler Research Laboratories Inc. (Philadelphia, PA) for Leo V. Azarraga of EPA.

This paper reports the development of vapor-phase interpretation rules for both the IBM mainframe version of PAIRS and the Nicolet 1180/1280 version known as MISIP (Merck infrared spectral interpretation package). Explanation of the programming changes necessary to utilize these new rules and examples are presented.

EQUIPMENT

A Nicolet 1180 minicomputer with 40K of 20 bit word semiconductor memory and mass storage consisting of a Diablo Model 44B dual disk system having a capacity of 4.5 megawords was used for all development work. This computer is a component of our Nicolet 7199 FTIR system. Full use was made of existing Nicolet system software.

Corresponding modifications of PAIRS software were made with an IBM 3081 computer. Transfer of interpretation rules from the Nicolet 1180 to the IBM system was made at 1200 baud with a phone modem connection through a Digital VT 125 terminal via a VAX 11/780.

PROGRAM DESCRIPTION

As described previously (*1*–*3*) the interpretation package consists of an interpreter program, a set of interpretation rules in an English-like language called CONCISE (computer oriented notation concerning infrared spectral evaluation), a rule compiler program, and a set of compiled rules used as data by the interpretation program. All components exist on both the Nicolet and IBM systems.

The interpreter is written in FORTRAN and treats the compiled rules and spectral information (peak width, position, intensity, sample state) as data. Due to the design of the interpreter, only minor FORTRAN changes were necessary to expand its capabilities to include vapor-phase spectra. Those changes consisted mainly of input and output modifications leaving the computational algorithm of the program unchanged.

The rule compiler is also written in FORTRAN and translates interpretation rules in CONCISE into more compact integer strings. Major changes were required for both the IBM and Nicolet versions of the rule compiler. Due to differences in the two versions, required by different word sizes and computational speeds of the IBM 3081 and Nicolet 1180, the changes were not identical but are entirely user transparent. Modifications were made to existing subroutines, dictionary, and internal tables to accommodate "vapor" as a sample state.

The CONCISE language was expanded to include "vapor" as a sample state, thus allowing the creation of specific vapor-phase rules and the modification of existing condensed-phase rules.

Major changes, additions and deletions, were necessary to the existing interpretation rules in CONCISE. The approach generally followed was to add specific vapor-phase conditions

0003-2700/84/0356-0067$01.50/0 © 1983 American Chemical Society

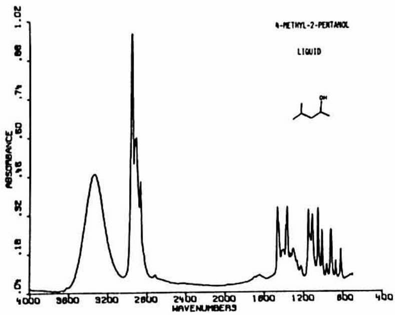

Figure 1. Liquid-phase spectrum of 4-methyl-2-pentanol.

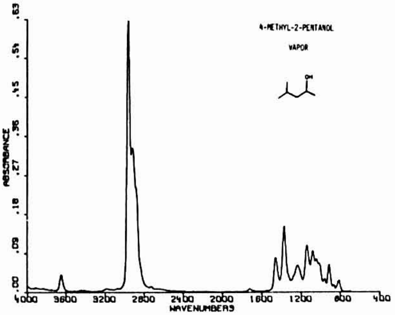

Figure 2. Vapor-phase spectrum of 4-methyl-2-pentanol.

to existing condensed-phase rules which have already undergone substantial testing and have proven to be quite useful for liquid and solid-state spectra. Thus if one requests an interpretation of a nonvapor spectrum, interpretation will be made by using essentially the same rules as were previously described (*1–3*). When a sample state of "vapor" is declared, those functionalities which show distinct spectral changes between the vapor and condensed phases and for which adequate correlation charts are available (e.g., alcohol) will be interpreted by use of the new vapor-phase rules. Those functionalities for which limited vapor correlation charts exist but which are expected to show vastly different infrared spectra on change of physical state (e.g., lactam) are disregarded when sample state is assigned as "vapor". The design of the computerized interpretation package which treats rules as data will accommodate easy rule modification with the procurement of sufficient spectral data for those functionalities to allow the development of satisfactory correlation charts.

RESULTS AND DISCUSSION

An example of the difference between vapor-phase and liquid-phase spectra of compounds which are predominately hydrogen bonded in the condensed phase can be seen in Figures 1 and 2. Both spectra are of 4-methyl-2-pentanol; one is taken as a liquid between KBr plates (Figure 1) and the other is a vapor-phase spectrum (Figure 2). Both spectra are 4 cm^{-1} resolution. The –OH stretching frequency of the liquid is 3345 cm^{-1} and is broad while the vapor spectrum shows an –OH stretching frequency of 3655 cm^{-1} with average width. Other peak intensities, widths and positions are given in Table I for the liquid-phase spectrum and Table II for the vapor-phase spectrum. The intensities are normalized from 1 to 10 with 10 being the strongest peak and the widths are given values of 1, 2, or 3 corresponding to sharp (fwhh < 12 cm^{-1}), average, or broad (fwhh > 75 cm^{-1}), respectively. The data in Table I were interpreted by use of condensed-phase interpretation rules and the results are presented in Table III. It can be seen that the interpreter correctly predicts the presence of the alcohol and methyl functionalities with high expectation values for the liquid spectrum. If the data from the vapor-phase spectrum, Table II, are interpreted by using

Table I. The 16 Largest Peaks as Determined by the Peak Picking Routine for Liquid-Phase Spectrum of 4-Methyl-2-pentanol

peak no.	position CM-1	rel intens	width
1	828	2	2
2	926	3	2
3	1017	3	2
4	1057	3	2
5	1116	3	2
6	1154	3	2
7	1275	2	2
8	1312	2	2
9	1344	2	2
10	1369	4	2
11	1412	2	3
12	1469	3	2
13	2872	5	2
14	2918	6	2
15	2960	10	2
16	3345	5	3

Table II. The 11 Largest Peaks as Determined by the Peak Picking Routine for Vapor-Phase Spectrum of 4-Methyl-2-pentanol

peak no.	position CM-1	rel intens	width
1	924	1	2
2	1025	1	2
3	1053	1	2
4	1089	2	2
5	1148	2	2
6	1244	1	2
7	1380	2	2
8	1468	1	2
9	2927	5	3
10	2969	10	2
11	3655	1	2

Table III. The Interpretation Results for Liquid-Phase 4-Methyl-2-pentanol with Condensed Phase Rules, Sample State of "Neat"

	group name	probability
1	alcohol	0.75
2	methyl	0.65
3	methylene	0.49
4	amine-tertiary	0.40
5	amine	0.40
6	amine-secondary	0.35

Table IV. The Interpretation Results for Vapor-Phase 4-Methyl-2-pentanol with Condensed-Phase Rules, Sample State of "Other"

	group name	probability
1	amine	0.40
2	amine-tertiary	0.40
3	acid	0.35
4	methyl	0.30

Table V. The Interpretation Results for Vapor-Phase 4-Methyl-2-pentanol with Modified Rules, Sample State of "Vapor"

	group name	probability
1	alcohol	0.85
2	alcohol-secondary	0.55
3	amine	0.40
4	amine-1-α-branch	0.40
5	alcohol-primary	0.35
6	amine-2-ali	0.35
7	methyl	0.30

Table VI. The 13 Largest Peaks as Determined by the Peak Picking Routine for the Vapor-Phase Spectrum of 6-Amino-2-methyl-2-heptanol

peak no.	position CM-1	rel intens	width
1	787	3	2
2	912	2	2
3	933	2	2
4	1027	1	3
5	1160	3	3
6	1215	2	3
7	1338	1	3
8	1378	4	2
9	1466	2	2
10	1621	1	2
11	2941	7	2
12	2972	10	2
13	3643	1	2

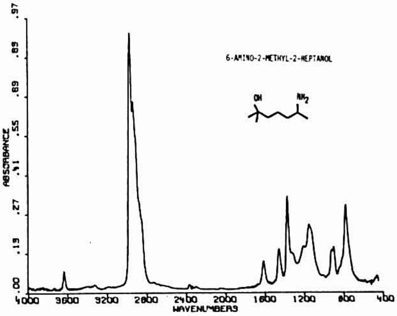

Figure 3. Vapor-phase spectrum of 6-amino-2-methyl-2-heptanol.

condensed-phase rules, the resultant interpretation is unsatisfactory and is presented in Table IV. The expectation values of 0.40 for "amine" and 0.35 for "acid" indicate that although these two functionalities are the most likely to be present in the molecule, the evidence is not overly strong. If the data in Table II are interpreted as being vapor-phase data using the modified rules containing vapor correlations, the resulting interpretation is presented in Table V. "Alcohol" is correctly predicted with a good degree of certainty and the further distinction of "secondary alcohol" is likewise correct. There is some likelihood of an amine being present, but the likelihood of an alcohol is much greater.

The vapor spectrum of 6-amino-2-methyl-2-heptanol is shown in Figure 3 with peak data presented in Table VI. Notice the lack of intensity in the NH symmetric stretching region (approximately 3300 cm^{-1}) (*4*). IR spectra of amines in the vapor state often show little evidence of NH stretching vibrations. If the data in Table VI are input into the interpreter and treated as condensed-phase data, the interpretation results shown in Table VII are returned. It is apparent that interpretation as condensed-phase data yields low expectation values for "amines" and no expectation that an alcohol is present at all. Interpretation of the data in Table VI using the modified rules with the stipulation that the spectrum was taken as a vapor yields the results presented in Table VIII. Alcohol and amine functionalities are both returned with large expectation values. In addition further distinctions are made as to the type of alcohol, tertiary, and the type of amine, primary branched (1-α-branch). In this case both subclasses

Table VII. The Interpretation Results for Vapor-Phase 6-Amino-2-methyl-2-heptanol with Condensed Phase Rules, Sample State of "Other"

	group name	probability
1	methyl	0.45
2	amine-tertiary	0.40
3	amine	0.40

Table VIII. The Interpretation Results for Vapor-Phase 6-Amino-2-methyl-2-heptanol with Modified Rules, Sample State of "Vapor"

	group name	probability
1	alcohol	0.90
2	amine	0.90
3	amine-1-α-branch	0.90
4	alcohol-tertiary	0.60
5	amine-1-*n*-ali	0.50
6	alcohol-secondary	0.50
7	methyl	0.45
8	amine-2-ali	0.40
9	alcohol-primary	0.40

Table IX. The 13 Largest Peaks as Determined by the Peak Picking Routine for the Vapor-Phase Spectrum of Heptanoic Acid

	position CM-1	rel intens	width
1	511	1	2
2	558	2	2
3	607	2	3
4	1098	5	2
5	1138	5	2
6	1282	1	3
7	1383	2	2
8	1462	1	2
9	1779	10	2
10	2877	3	2
11	2939	6	2
12	2967	5	2
13	3577	4	2

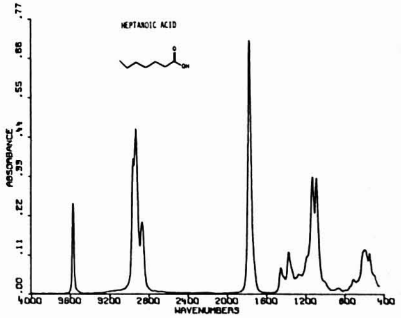

Figure 4. Vapor-phase spectrum of heptanoic acid.

Table X. The Interpretation Results for Vapor-Phase Heptanoic Acid with Modified Rules, Sample State of "Vapor"

	group name	probability
1	acid	0.90
2	acid-saturated	0.90
3	acid-α-branched	0.62
4	ester-(of-CO_2H)	0.50
5	lactone-δ-sat	0.50
6	ketone	0.47
7	ketone-5-ring	0.47
8	methyl	0.45
9	amine	0.30
10	amine-2-ali	0.30
11	ketone-sat	0.30

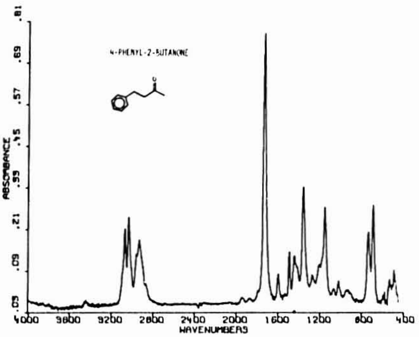

Figure 5. Vapor-phase spectrum of 4-phenyl-2-butanone.

are correct; however, the program tends to place more certainty in indicating class (e.g., alcohol) than subclass (e.g., tertiary) correctly.

Acids are another functionality which have markedly different spectra when taken in the vapor and condensed states. Figure 4 shows the vapor spectrum of heptanoic acid. Table IX contains the peak data as entered into the interpretation program. Two characteristic differences between a vapor-phase and condensed-phase acid spectrum are higher carbonyl stretching frequency (1779 cm^{-1}) and sharper hydroxyl stretch absorptions (width = 2). The interpretation results obtained by using a sample state of vapor are presented in Table X. The interpreter correctly suggests "acid", particularly "saturated acid", as being present. Also reported with some expectation are "acid-α-branched" and "ester" as well as other carbonyl containing functionalities, but all with lower expectation values. Had the data in Table IX been entered with a sample state other than vapor, the ketone functionality, especially a four-membered ring ketone, would have been predicted to be most likely present.

As a final example, the vapor spectrum of 4-phenyl-2-butanone is shown in Figure 5 with peak data presented in Table XI and interpretation results shown in Table XII. The interpreter correctly predicts the ketone and aromatic functionalities to be present with high expectation values when the sample state is entered as vapor. The only other carbonyl functionality returned is "amide" with a much lower expectation value. Had the data been entered as being a condensed-phase spectrum, "aromatic" would still have been predicted with the same expectation value, but "ketone" would have been placed below "lactam" in certainty of presence.

Table XI. The 14 Largest Peaks as Determined by the Peak Picking Routine for the Vapor-Phase Spectrum of 4-Phenyl-2-butanone

peak no.	position CM-1	rel intens	width
1	499	1	2
2	697	4	2
3	743	3	2
4	1158	4	2
5	1208	1	2
6	1363	4	2
7	1448	2	2
8	1497	2	2
9	1604	1	2
10	1734	10	2
11	2933	2	2
12	2963	2	2
13	3036	3	2
14	3072	3	2

Table XII. The Interpretation Results for Vapor-Phase 4-Phenyl-2-butanone with Modified Rules, Sample State of "Vapor"

	group name	probability
1	ketone	0.75
2	ketone-sat	0.75
3	aromatic	0.65
4	olefin-CHR=CHR(C)	0.60
5	olefin-(nonarom)	0.60
6	amide	0.50
7	amide-primary	0.50
8	methyl	0.35

These examples demonstrate the need for vapor-phase interpretation rules and are indicative of the success which we have had in developing such rules for functionalities where frequency correlations exist. The underlying philosophy of MISIP and PAIRS has been maintained with the new set of rules, namely, to aid the chemist in determining which functionalities may be present in an unknown compound. It is better to suggest more possible functionalities, i.e., have possible false positive results, than to be unrealistically restrictive giving false negative interpretations. The chemist using MISIP or PAIRS should consider the interpretation results with this philosophy firmly in mind.

PAIRS is available for distribution from the Quantum Chemistry Program Exchange, Bloomington, IN (Program number QCPE 426). MISIP is available as part of the user generated software from the Nicolet Instrument Corp.

ACKNOWLEDGMENT

We acknowledge the contributions of Graham Smith, Merck Sharp & Dohme Research Laboratories, for his valuable discussions and the staff of Nicolet Instrument Corp., especially Stephen Lowry, David Huppler, and Colleen Gilligan, for their technical support.

LITERATURE CITED

(1) Woodruff, H. B.; Smith, G. M. *Anal. Chem.* **1980**, *52*, 2321–2327.
(2) Woodruff, H. B.; Smith, G. M. *Anal. Chim. Acta* **1981**, *133*, 543–553.
(3) Tomellini, S. A.; Saperstein, D. D.; Stevenson, J. M.; Smith, G. M.; Woodruff, H. B.; Seelig, P. F. *Anal. Chem.* **1981**, *53*, 2367–2369.
(4) Welti, D. "Infrared Vapour Spectra"; Heyden: New York, 1970.
(5) Delaney, M. F.; Warren, V., Jr. *Anal. Chem.* **1981**, *53*, 1460–1462.

RECEIVED for review April 11, 1983. Accepted September 21, 1983.

Anal. Chem. 1984, 56, 71–73

Iodometric Method for Determination of Trace Chlorate Ion

Yasuhisa Ikeda, Tsung-fei Tang, and Gilbert Gordon*

Miami University, Department of Chemistry, Oxford, Ohio 45056

A modified iodometric method is reported to measure chlorate ion concentration at the sub-milligram-per-liter level with high precision and accuracy. Hexane and nitrogen are used as shielding agents to isolate the sample solution from the air phase to prevent air oxidation of iodide ion. Chlorate ion is reduced by iodide ion in 6 M hydrochloric acid. By the addition of saturated sodium phosphate, the hydrogen ion concentration is lowered to approximately 3 M, and the liberated iodine is titrated with standard sodium thiosulfate solution. The end point is detected by using Thyodene as the indicator or by the color of iodine in the hexane layer. A potentiometric end point is recommended for the determination of chlorate ion at concentrations less than 1.0 × 10^{-4} N (3.5 mg/L). By this modified iodometric method, the chlorate ion at the sub-milligram-per-liter level can be determined with a precision of better than ±1%.

Methods for chemical analysis of solutions containing chlorine-containing oxidizing agents appear to be well-defined in the chemical literature (*1–11*). Late in 1979, the *Federal Register* (*12*) published restrictions which should be placed on residual oxidants such as chlorine dioxide, chlorite ion and chlorate ion which result from the chlorine dioxide treatment of water to be used as drinking water. In the 1979 update of "Drinking Water and Health", the National Academy of Science estimated acceptable exposure values of 0.38 mg/L for chlorine dioxide and 0.21 mg/L for chlorite ion. The *Federal Register* also reports "...EPA feels that whenever chlorine dioxide is used residual oxidants should be monitored and kept below 0.5 mg/L. EPA will consider establishing an MCL for chlorine dioxide, chlorite and chlorate or the aggregate as total oxidants for inclusion in the Revised Regulations after further studies have been fully evaluated...".

At this point in time none of the analytical techniques in the literature is capable of routinely determining chlorate ion concentrations at the sub-milligram-per-liter level. It should be noted that both normality and mg/L are widely used in both the literature and in the field. In this context, mg/L is defined as [equivalents/liter (as titrated) × 35.453 g/equiv × 1000 mg/L]. The purpose of this paper is to present a revised method capable of accurately measuring chlorate ion concentrations below 100 mg/L and as low as 0.3 mg/L.

The iodometric method has been used widely to measure the concentration of various cations and anions (*3*, *4*). Oxychlorine species such as hypochlorite ion and/or hypochlorous acid and chlorite ion can be measured by the iodometric method accurately and precisely (*4*). However, the reaction of chlorate ion with iodide ion is slow under mildly acidic conditions

$$ClO_3^- + 6I^- + 6H^+ \rightarrow 3I_2 + Cl^- + 3H_2O \qquad (1)$$

According to Bray (*13*), the rate of the reaction 1 is proportional to the chlorate ion concentration and the square of the hydrogen ion concentration and is a linear function of the concentrations of chloride and iodide ions. A recent study by Hadjiioannou and co-workers (*14*) suggests that the reaction obeys the following rate law:

$$-d[ClO_3^-]/dt = k[ClO_3^-][I^-]^{1.5}[H^+]^2 \qquad (2)$$

where k is 35 ± 1.0 $M^{-3.5}\ s^{-1}$ at 30 °C and ionic strength 1.0 M.

Thus, normally the quantitative iodometric determination of chlorate ion is possible in the presence of a large excess of hydrochloric acid. Unfortunately, under these conditions iodide ion is readily oxidized by air

$$4I^- + 4H^+ + O_2 \rightarrow 2I_2 + 2H_2O \qquad (3)$$

Kolthoff (*4*) has suggested that removal of air from the sample solution by using sodium carbonate is effective to prevent the air oxidation of iodide ion. Ditz (*15*) and Rupp (*16*) have suggested using bromide ion in the presence of 7.5 M hydrochloric acid to reduce chlorate ion. The bromine produced thereby is determined iodometrically. However, these modified iodometric methods are primarily applicable to the determination of chlorate ion in the relatively high concentration range (above 0.02 N). For the determination of chlorate ion in concentrations such as in the millimolar and sub-millimolar range, additional modifications of the iodometric method are necessary in order to avoid the air oxidation of iodide ion (*5*, *9*, *17*).

A recent study (*17*) has suggested that hexane is an effective shielding agent to prevent the air oxidation of iodide ion and that the interference from air oxidation can be minimized when chlorate ion is reduced by iodide ion in 6 M hydrochloric acid followed by neutralization to approximately 3 M with either 50% (w/w) sodium hydroxide or solid sodium phosphate (Na_2HPO_4).

EXPERIMENTAL SECTION

Reagent grade chemicals and deionized distilled water were used throughout. Potassium chlorate (Matheson Coleman and Bell) was recrystallized from triply distilled water. Sodium thiosulfate solution used as the titrant was prepared in freshly boiled and cooled distilled water and was standardized with primary standard potassium iodate solution. Saturated sodium phosphate ($Na_2HPO_4 \cdot 12H_2O$, Matheson Coleman and Bell) solution was used to neutralize the acidic sample solutions. Potassium iodide (Matheson Coleman and Bell) and Spectroanalyzed grade hexane (Fisher Scientific Co.) were used without further purification. Thyodene (Fisher Scientific Co.) was used as the indicator for the iodometric end point. The nitrogen gas used for deaeration was passed through a scrubber containing 0.1 M chromium(II) in 1 M sulfuric acid to remove traces of oxygen.

The iodometric end point was detected either with Thyodene as the indicator or potentiometrically. The sodium thiosulfate solution was titrated by using a Metrohm Herisau E535 autoburet. For the potentiometric end point, a homemade combination redox electrode as shown in Figure 1 and a Metrohm Herisau Model E536 potentiometer were used. Sodium thiosulfate solution was titrated at the speed of 0.05 mL/min.

RESULTS AND DISCUSSION

In the Tang modified iodometric method (*17*), solid sodium phosphate and 50% (w/w) sodium hydroxide were used as neutralizing agents. However, a marked disadvantage of this method is that sodium phosphate does not dissolve rapidly into the sample solution and the addition of 50% sodium

0003-2700/84/0356-0071$01.50/0 © 1983 American Chemical Society

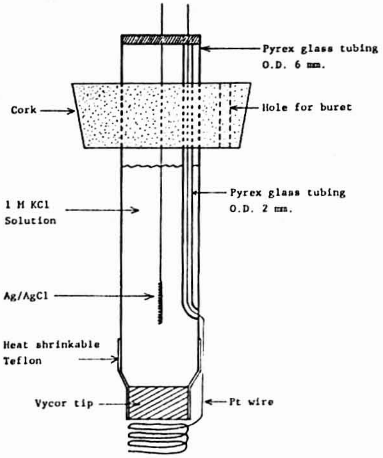

Figure 1. Combination redox electrode.

hydroxide generates a large amount of heat during the neutralization process. In this paper, a saturated sodium phosphate solution was used instead of the above mixture and hexane was used as a shielding agent.

The measurement of chlorate ion at various concentration levels with Thyodene as the indicator was carried out as follows: The sample was prepared by using a Silverman syringe (*18*) to deliver the known volumes of the standard reference potassium chlorate solution into a 60-mL glass-stoppered flask. To this sample solution, 0.25 mL of potassium iodide whose concentration varied from 0.3 M to 0.06 M depending on the chlorate ion concentration (0.1 N to 1.0×10^{-4} N) was added. This solution was bubbled with nitrogen gas for 10 min. After deaeration, approximately 1 mL of hexane was added to the sample solution. Deaerated concentrated hydrochloric acid was added to the sample solution to adjust it to 6 M in acid and immediately the flask was stoppered. After the reaction was complete (normally 20 min), deaerated saturated sodium phosphate solution was added to the sample solution to reduce the acidity to ~3 M. Finally, the liberated iodine was titrated with standard sodium thiosulfate solution and an appropriate amount of Thyodene solution was added when the yellow color of iodine in aqueous phase became pale. For concentrated solutions, the Thyodene color change was used to determine the end point. In the more dilute solutions, the titration end point was determined by comparing the color of the hexane layer of the sample solution with that of a blank solution consisting of only water and hexane. The reddish violet color of iodine in the hexane layer makes it easier to detect a titration end point because the limit of visibility of the color of hexane layer exceeds that of the Thyodene–iodine color. In each experiment, blank corrections were made for solutions of the same composition as that of the sample solution except for using deionized distilled water in place of the potassium chlorate solution.

The results are shown in Table I and indicate that the determination of chlorate ion in concentrations greater than 1.0×10^{-4} N is possible by using this modified iodometric method—with appropriate blank corrections. In these experiments, time-dependent titrations show that chlorate ion is quantitatively reduced by iodide ion within 20 min. The reproducible blank volume correction is necessary since it corresponds to 0.0–5.0% of the sample titration volume. Variations in reaction conditions such as reaction volume, elapsed time prior to titration, and the like may result in differing blank volumes. Thus the reaction blank must exactly reproduce the actual reaction conditions. Under these reaction conditions, the air oxidation of iodide ion is effectively minimized by using hexane as a shielding agent and by neutralization of the sample solution by the addition of a deaerated saturated solution of sodium phosphate.

Table I. Determination of Chlorate Ion by the Modified Iodometric Method with Hexane as a Shielding Agent

sample	equiv/L ClO_3^- added	equiv/L ClO_3^- found[a]	% error
1	1.002×10^{-1}	$(1.007 \pm 0.001) \times 10^{-1}$	0.5 ± 0.1
2	1.031×10^{-2}	$(1.033 \pm 0.005) \times 10^{-2}$	0.2 ± 0.5
3	5.035×10^{-3}	$(5.03 \pm 0.08) \times 10^{-3}$	0.1 ± 0.6
4	2.609×10^{-3}	$(2.60 \pm 0.03) \times 10^{-3}$	0.4 ± 0.5
5	6.194×10^{-4}	$(6.21 \pm 0.07) \times 10^{-4}$	0.2 ± 0.8
6	1.011×10^{-4}	$(1.00 \pm 0.02) \times 10^{-4}$	1.1 ± 1.0

[a] The uncertainties represent the standard deviation of the mean for eight replicate samples except for samples 3 and 5 which consisted of nine replicates.

Table II. Determination of Chlorate Ion at the Sub-Milligram-per-Liter Level[a]

method	shielding agent	equiv/L $ClO_3^- \times 10^5$ added	found	% error
optical end point	benzene	1.011	1.018 ± 0.094	0.7 ± 1.0
potentiometric titration	hexane	1.011	1.019 ± 0.036	0.8 ± 0.6
potentiometric titration	N_2 gas	1.011	1.023 ± 0.051	1.2 ± 1.0

[a] The uncertainties represent the standard deviation of the mean for eight replicate titrations.

On the basis of these results, the determination of chlorate ion at the level of 1.0×10^{-5} N (0.35 mg/L) was studied by using the same procedure. However, the color of iodine in the hexane layer is a very pale pink at this concentration level, and hence the end point could not be detected correctly and reproducibly. Benzene was tried as a replacement for hexane because the color of iodine in a benzene layer is more intense than in hexane. The difference in color intensity is primarily due to the fact that benzene can extract iodine more efficiently than hexane and the resulting charge-transfer complex has a higher molar absorptivity. As is shown in Table II, chlorate ion at the level of 1.0×10^{-5} N can be determined by this method with benzene as a shielding agent. However, the visual end point using benzene results in poor reproducibility in that determination of end point is difficult. Furthermore, this modification tends to depend on the investigator, resulting in possible operator bias, and benzene is a potentially hazardous solvent.

In order to improve the difficulties inherent in the visual end point methods described above for more concentrated solutions containing chlorate ion ($>1.0 \times 10^{-4}$ N ClO_3^-), the potentiometric titration method was modified and is also reported here. The effect of hexane as a shielding agent on the potentiometric end point detection was evaluated by standardizing the sodium thiosulfate solution with known volumes of potassium iodate solution which had been prepared

Table III. Standardization of Sodium Thiosulfate Solution with and without Hexane, Using Potentiometric End Point Detection

	sample 1[a] $[S_2O_3^{2-}]/10^{-4}$ N	sample 2[b] $[S_2O_3^{2-}]/10^{-4}$ N
	5.213	5.272
	5.335	5.302
	5.267	5.319
	5.292	5.320
	5.232	5.309
mean[c]	5.268 ± 0.048	5.304 ± 0.020

[a] Sample consists of 5.0066 mL of 4.239×10^{-4} N KIO_3, 0.5 mL of 0.03 M KI, 1 mL of hexane, and 2 mL of 1 M HCl. [b] Sample consists of 5.0066 mL of 4.239×10^{-4} N KIO_3, 0.5 mL of 0.03 M KI, and 2 mL of 1 M HCl (no hexane added). [c] The uncertainties represent the standard deviation of the mean.

by weight. Samples were prepared by delivering an exact volume (*18*) of potassium iodate solution (4.239×10^{-4} N) into a 60-mL glass-stoppered flask with a Silverman syringe. An appropriate amount of 0.03 M potassium iodide solution was added and the sample was acidified with 1 M hydrochloric acid to a pH less than 2. Approximately 1 mL of hexane was added and the combination redox electrode (Figure 1) was immersed under the hexane layer. The liberated iodine was titrated with sodium thiosulfate solution at a delivery speed of 0.05 mL/min. The end point was determined directly from the maximum of the first derivative titration curve as shown in Figure 2. The results in Table III for the standardization with and without hexane shielding of the sample are indistinguishable within experimental error. This result indicates that the hexane shielding has no measurable effect on the potentiometric end point.

Chlorate ion concentrations at the level of 1.0×10^{-5} N were analyzed by the potentiometric method according to the same procedure as described earlier. Exactly 10.013_2 mL of potassium chlorate stock solution and 0.5 mL of 0.015 M potassium iodide solution were used. Twelve milliliters of deaerated hydrochloric acid and 23 mL of the deaerated saturated sodium phosphate solution were added for acidification and neutralization of sample, respectively. Under these conditions of lower chlorate ion concentration, the reaction between chlorate ion and iodide ion requires 40 min for completion. The end point was detected from the first derivative titration curve. The end point is almost identical with that shown for iodate ion in Figure 2. Furthermore, the same method was investigated by using nitrogen gas rather than a layer of hexane as a shielding agent. In this method, the air space of sample flask was filled with nitrogen gas immediately after the deaerated saturated sodium phosphate solution was added to the sample solution. In both methods, blank corrections were made for solutions of the same composition as the sample solution except for using the deionized distilled water instead of potassium chlorate solution. At these low concentration levels, the blank volumes were nominally 20% and 30% of the sample titration volumes in the hexane shielding and nitrogen gas shielding experiments, respectively. This result shows that the shielding effect of nitrogen gas is perhaps somewhat less effective than that of hexane. However, and most importantly, as is noted in Table II, with appropriate blank corrections and careful shielding it is possible to accurately measure chlorate ion at the sub-milligram-per-liter level by the potentiometric method.

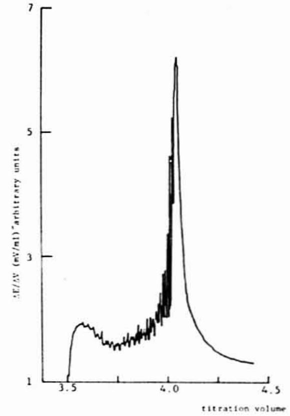

Figure 2. Derivative end-point curve.

In conclusion, the potentiometric titration method using hexane as a shielding agent is recommended for the determination of chlorate ion at low concentration levels (especially below 1 mg/L) because the blank is relatively small and no subjectivity by the investigator is involved.

LITERATURE CITED

(1) "Standard Methods for the Examination of Water and Wastewater", 14th ed.; American Public Health Association, New York, 1975.
(2) White, G. C. "Handbook of Chlorination"; Van Nostrand Reinhold: New York, 1972; pp 228–277.
(3) Vogel, A. I. "Textbook of Quantitative Inorganic Analysis", 4th ed.; Longman: New York, 1978.
(4) Kolthoff, I. M.; Belcher, R. "Volumetric Analysis"; Wiley: New York, 1957; Vol. 3.
(5) Tang, T.-F.; Gordon, G. *Anal. Chem.* **1980**, *52*, 1430.
(6) Suzuki, K.; Gordon, G. *Anal. Chem.* **1978**, *50*, 1596.
(7) Gordon, G.; Kieffer, R. G.; Rosenblatt, D. H. "The Chemistry of Chlorine Dioxide"; Lippard, S. J., Ed.; Wiley: New York, 1972; Progress in Inorganic Chemistry, Vol. 15.
(8) Noack, M. G.; Doerr, R. L. In "Kirk-Othmer: Encyclopedia of Chemical Technology", 3rd ed.; Wiley: New York, 1979; Vol. 5.
(9) Miltner, R. J. In Proceedings AWWA Water Quality Technology Conference, Dec 6–7, 1976, San Diego, CA; AWWA: Denver, CO, 1977; Paper No. 2A-5.
(10) Prince, L. A. *Anal. Chem.* **1964**, *36*, 613.
(11) Chen, T. H. *Anal. Chem.* **1967**, *39*, 804.
(12) *Fed. Regist.* **1979**, *44* (231), 68637.
(13) Bray, W. C. *J. Phys. Chem.* **1903**, *7*, 92.
(14) Nikolelis, D. P.; Karayannis, M. I.; Hadjiioannou, T. P. *Anal. Chim. Acta* **1977**, *94*, 415.
(15) Ditz, H. *Chem.-Ztg.* **1901**, *25*, 727.
(16) Rupp, E. Z. *Anal. Chem.* **1917**, *56*, 580.
(17) Tang, T.-F. M.S. Thesis, Miami University, Oxford, OH, 1980.
(18) Silverman, R. A.; Gordon, G. *J. Chem. Educ.* **1973**, *50*, 654.

RECEIVED for review July 5, 1983. Accepted October 5, 1983. Although the research described in this article has been funded in part by the U.S. Environmental Protection Agency through Cooperative Agreement No. CR808-914-010 to Miami University, it has not been subjected to agency review and, therefore, does not necessarily reflect the views of the agency and no official endorsement should be inferred.

Anal. Chem. 1984, 56, 74–77

Point-by-Point Matrix Effect Calibration for the Quantitative Analysis of Superlattices by Secondary Ion Mass Spectrometry

A. A. Galuska and G. H. Morrison*

Department of Chemistry, Cornell University, Ithaca, New York 14853

Point-by-point matrix effect calibration is applied to a variety of $Al_xGa_{1-x}As$ multilayer–multimatrix samples grown by molecular beam epitaxy. The procedure uses the linear dependence of secondary ion yields and sputtering yields on matrix composition of quantify depth profiles through matrix gradients and interfaces. The proposed method provides accurate results in the analysis of samples too complex for conventional quantitative analysis by secondary ion mass spectrometry

Secondary ion mass spectrometry (SIMS) is often used to monitor elemental depth distribution in solids and solid interfaces. The technique is highly sensitive for most elements and has good depth resolution. However, the complexity of the sputtering event has made quantitative analysis difficult. Ion implant standards (*1–3*) have been successfully used to calibrate the depth profiles of trace elements in homogeneous matrices. However, due to the variation of secondary ion yields and sputtering yields with matrix composition, matrix effects, the quantification of SIMS profiles in multimatrix samples remains a problem.

For $Al_xGa_{1-x}As$ and related matrices, it has recently been shown that practical ion yields τ (ions detected/atoms sputtered) and sputtering yields S (secondary atoms/primary ion) vary linearly with sample composition (*4*). In addition, highly precise calibration lines were obtained by use of relative ion yields Rτ and relative sputtering yields RS. These relative values were obtained by normalizing ion yields and sputtering yields from a sample matrix (τ_x and S_x) to those from a standard matrix (τ_0 and S_0) when both measurements were performed under near identical analysis conditions.

$$\mathrm{R}\tau = \tau_x/\tau_0 \tag{1}$$

$$\mathrm{RS} = S_x/S_0 \tag{2}$$

In this investigation, the application of these calibration lines to the analysis of $Al_xGa_{1-x}As$ multilayer–multimatrix samples is examined. These superlattices, as shown in Figure 1, are best characterized as a series of homogeneous matrices. A profile correction program (SLIC), which treats each point of a depth profile as a homogeneous matrix, will be presented. SLIC determines the matrix composition at each point of a depth profile and subsequently performs a point-by-point correction of the trace element distributions. The capabilities and limitations of this method will be discussed.

EXPERIMENTAL SECTION

Sample Preparation. The $Al_xGa_{1-x}As$ matrices were grown by molecular beam epitaxy (MBE) on semiinsulating GaAs substrates. The matrix compositions were determined from the MBE growth parameters and verified to an accuracy of better than 10% (*5*) with Rutherford backscattering spectroscopy (RBS). In some instances dopants were introduced during the growth process while in others, including the standards, ion implantation was used. Prior to implantation, samples were cleaned with acetone and methanol.

Instrumentation. The $Al_xGa_{1-x}As$ layers were grown in a Varian MBE-360 machine (*6*). RBS measurements were carried out on a General Ionex Tandetron Model 4110A. Analyses were performed with a 2.7 MeV He^+ ion beam with solid-state detection at a 170° angle from the incident beam path. Ion implantation was performed with a hot filament ion source and a magnet for mass separation.

SIMS analysis was carried out on a Cameca IMS-3F ion microanalyzer (*7*) interfaced to a Hewlett-Packard 9845B microcomputer for control and data acquisition. A 1.0-μA O_2^+ primary beam at an energy of 5.5 keV was rastered over a 300 × 300 μm area. Positive secondary ions were monitored from an image field 60 μm in diameter. Analyses were performed with a residual pressure of 2×10^{-8} torr and an energy window of 130 eV. A multiple sample holder was used to simultaneously mount several samples. Depth measurements of the sputtered craters were performed on a Talystep stylus device.

Software. Programs for instrumental control, data analysis, and matrix correction were written in BASIC for the HP 9845B. The program SLIC (superlattice and interface calibration) was used to correct depth profiles for matrix effects.

SLIC is a comprehensive matrix correction program. For $Al_xGa_{1-x}As$ matrices, the matrix composition and depth at each point of a depth profile is determined by an iterative process involving calibration lines for both relative sputtering yield and the relative ion yield of $^{75}As^+$. Dopant profiles are then corrected for matrix changes by use of the appropriate dopant calibration lines.

Procedure. Each sample was mounted with three standards, created by ion implantation, using a multiple sample holder. The standards, including in each case GaAs and two different $Al_xGa_{1-x}As$ matrices, and the sample were inserted simultaneously to ensure nearly identical analysis conditions. After the pressure in the sample chamber was allowed to reach a steady-state condition, the primary beam was focused to a spot of about 100 μm in diameter, and the proper mass settings were determined. Standards and sample were analyzed consecutively without changing any instrumental parameters. By using the depth profiles of the standards, matrix calibration lines were constructed and used to correct the sample depth profiles.

RESULTS AND DISCUSSION

Rτ and RS calibration lines can be used to quantify concentration and depth, respectively (*4*). With eq 3, the concentration of analyte at each point of a depth profile C_p (atoms/cm^3) can be determined.

$$C_p = I_p/\mathrm{R}\tau_x\tau_0 D_p A \tag{3}$$

Rτ_x is the relative sputtering yield determined from a calibration line for the appropriate value of x, and τ_0 is the practical ion yield of the analyte in the standard matrix (GaAs). I_p (counts) and D_p (cm) are the signal and depth increment associated with a given point of a depth profile. A is the analysis area.

Similarly, the erosion rate at a given point of a depth profile $\dot{z}_p$ (cm/s) can be determined by using eq 4.

$$\dot{z}_p = \mathrm{RS}_x\dot{z}_0 N_0/N_x \tag{4}$$

RS$_x$ is the relative sputtering yield determined from a calibration line for the appropriate value of x, and $\dot{z}_0$ (cm/s) is the erosion rate of the standard matrix (GaAs). N_0 and N_x are the atomic densities of the standard and sample matrix, respectively.

With eq 3 and 4 a multilayer–multimatrix sample can now be analyzed. The most critical ingredient of such an analysis

0003-2700/84/0356-0074$01.50/0 © 1983 American Chemical Society

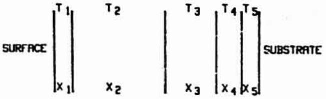

Figure 1. A hypothetical $Al_xGa_{1-x}As$ superlattice. The thickness T of the layers can vary from several angstroms to several micrometers while x can be varied from 0 to 1.

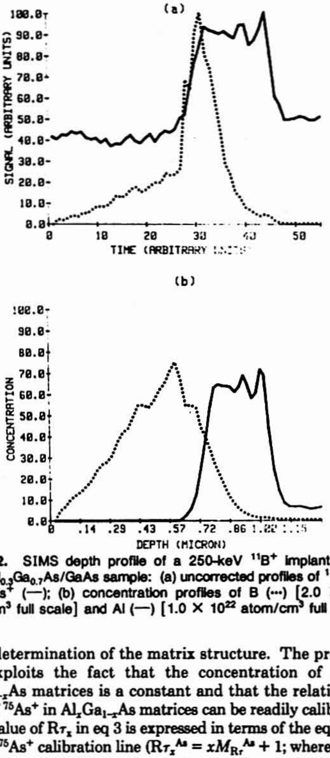

Figure 2. SIMS depth profile of a 250-keV $^{11}B^+$ implant into a $GaAs/Al_{0.3}Ga_{0.7}As/GaAs$ sample: (a) uncorrected profiles of $^{11}B^+$ (···) and $^{75}As^+$ (—); (b) concentration profiles of B (···) [2.0×10^{18} atom/cm^3 full scale] and Al (—) [1.0×10^{22} atom/cm^3 full scale].

is the determination of the matrix structure. The program SLIC exploits the fact that the concentration of As in $Al_xGa_{1-x}As$ matrices is a constant and that the relative ion yield of $^{75}As^+$ in $Al_xGa_{1-x}As$ matrices can be readily calibrated. If the value of $R\tau_x$ in eq 3 is expressed in terms of the equation for the $^{75}As^+$ calibration line ($R\tau_x^{As} = xM_{R_\tau}^{As} + 1$; where $M_{R_\tau}^{As}$ is the slope of the line), the equation can be manipulated to the followng form:

$$x = \{(I_p^{As}/C_p^{As}A\tau_0^{As}D_p) - 1\}/M_{R_\tau}^{As} \qquad (5)$$

Except for D_p, the values for all the variables on the right side of eq 5 can be readily determined. Since D_p is directly related to $\dot{z}_p$ ($D_p = \dot{z}_pT_p$; where T_p is the number of seconds per point), it can be expressed in terms of eq 4. If RS_x is replaced with the corresponding equation for the RS calibration line, eq 6 is obtained.

$$\begin{aligned} D_p &= (M_{RS}x + 1)\dot{z}_0N_0/N_xT_p \\ &= (M_{R\dot{z}}x + 1)\dot{z}_0T_p \end{aligned} \qquad (6)$$

M_{RS} is the slope of the RS calibration line, and $M_{R\dot{z}}$ is the slope of the corresponding relative erosion rate calibration line ($M_{R\dot{z}} = M_{RS}N_x/N_0$). Once again the values of D_p and x are the only unknown quantities.

For each point of a depth profile, the program SLIC determines the matrix structure by performing the following process. It initially assumes that $x = 0$. The corresponding value of D_p is determined from eq 6 and employed in eq 5 to obtain a better approximation of x. This process is reiterated until the value of x converges. In this manner, the matrix structure can be determined despite matrix gradients, interfaces, and plateaus.

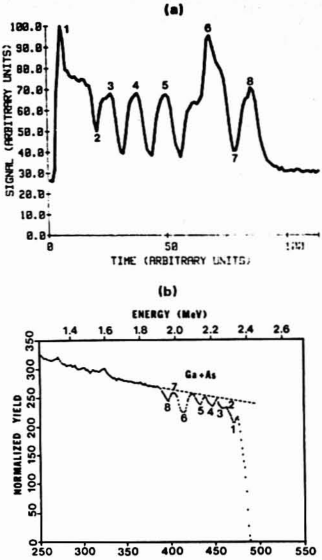

Figure 3. SIMS and RBS depth profiles of an $Al_xGa_{1-x}As$ superlattice: (a) an uncorrected $^{75}As^+$ SIMS profile; (b) an RBS profile of the total counts from Ga and As.

Capabilities and Limitations. As shown in Figure 2a, matrix effects can drastically distort SIMS analyses through multilayer–multimatrix samples. This depth profile of a boron implant through a GaAs and a $Al_xGa_{1-x}As$ layer shows a large irregularity at 31 time units. This irregularity is due to the changing matrix effects at the interface. In Figure 2b, SLIC was used to determine the Al distribution and correct the $^{11}B^+$ implant distribution. Upon correction, the implant distribution was transformed into the near Gaussian shape which was expected.

The crucial factor influencing the quality of the matrix corrections performed by SLIC is the accuracy with which the matrix structure can be determined. This accuracy can be checked with RBS. RBS analysis is accurate to about 10% and has an detection limit of 1% for $Al_xGa_{1-x}As$ matrices. In Figure 3, a complex $Al_xGa_{1-x}As$ sample was analyzed by both SIMS and RBS. The Al concentration at specific regions of the superlattice was determined by using SLIC and standard RBS techniques (5). As shown in Table I, the values determined by the two techniques agree quite well. In fact, the two sets of data are not statistically different at a 95% confidence level.

In addition to matrix composition, the point-by-point correlation between matrix structure and dopant distribution is critical. Small differences between the actual and the measured matrix structure can significantly influence the corrections performed on dopant distributions. As apparent in Figure 4, the $^{75}As^+$ signal tracks the Al distribution quite well. SLIC uses this correlation to precisely determine matrix

Table I. Point-by-Point Comparison of Al Concentrations Determined by SIMS and RBS Analyses

point	Al concn ($\times 10^{21}$ atom/cm^3) RBS	SIMS	deviation
1	12.0	13.0	−1.0
2	4.2	3.9	+0.3
3	5.1	4.8	+0.3
4	5.1	4.7	+0.4
5	5.2	4.7	+0.5
6	11.0	11.0	0.0
7	1.0	1.3	−0.3
8	4.9	5.7	−0.8

Av Deviation = −0.075

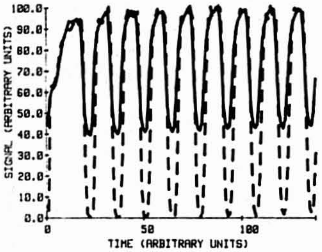

Figure 4. An uncorrected SIMS depth profile of ^{75}As$^+$ (—) and ^{27}Al^{2+} (– – –) in an Al$_x$Ga$_{1-x}$As superlattice.

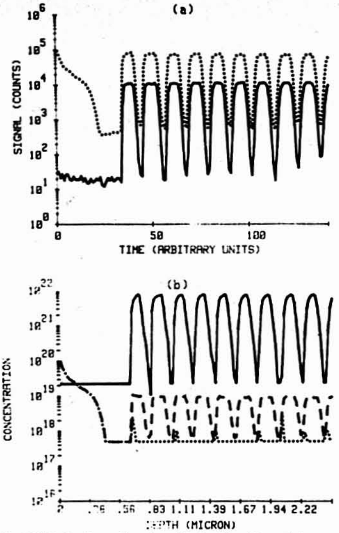

Figure 5. SIMS depth profile of an (GaAs/Al$_{0.35}$Ga$_{0.65}$As)$_n$ superlattice doped in the first 0.4 μm with Si: (a) uncorrected profiles of Al^{2+} (— and ^{28}Si$^+$ (···); (b) concentration (atom/cm^3) profiles of Al (—) and S with (···) and without (– – –) background correction.

structures. However, errors can still result from the correlation between matrix structure and dopant distribution. For example, there is a dead time between the measurement of the matrix signal and the dopant signal for each point of a depth profile. When this dead time is large compared to the abruptness of the matrix changes, the matrix and dopant signals will be obtained from different matrix regions. Consequently, the dopant signal will be calibrated for the wrong matrix composition. Fortunately, this type of error can usually be avoided by minimizing the dead time and reducing the sputtering rate.

Another obstacle to quantitative multilayer–multimatrix analysis concerns molecular interferences. Molecular ions are frequently the source of the high background signals commonly observed during elemental analysis. Molecular signals, like elemental ion yields, can change with matrix composition. When analyzing a multimatrix sample, failure to correct for the changing abundance of interfering molecular ions can lead to erroneous elemental distributions. For example, in Figure 5a, the ^{28}Si$^+$ profile (dotted line) tracks the Al^{2+} profile (solid line) through the alternating GaAs and Al$_x$Ga$_{1-x}$As layers even though this region has not been doped with Si. Fortunately, these changing background levels can often be linearly correlated to the matrix composition. For example, provided the background signals are normalized to erosion rate, a precise background signal calibration line can be obtained for Si in Al$_x$Ga$_{1-x}$As. The background signals can then be subtracted point-by-point prior to quantification. In Figure 5b, both a background corrected (dotted line) and an uncorrected (dashed line) Si concentration depth profile are presented. In the corrected version, nearly all the distortions produced by the changing background levels are removed. The doped region at the surface remains followed by a region with the Si concentration below the detection limit (5 × 10^{17} atom/cm^3) of Si in GaAs.

The full utility of SLIC can be appreciated when very complex samples are analyzed. In Figure 6, SLIC has been used to quantitatively analyze a complex Al$_x$Ga$_{1-x}$As superlattice grown by MBE with Be and Si dopants. In the uncorrected profile, Figure 6a, both the Be and Si distributions follow the

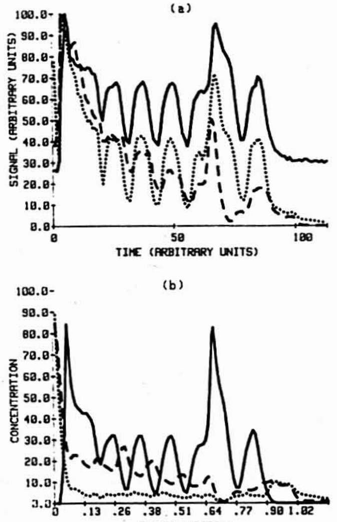

Figure 6. SIMS depth profile of an Al$_x$Ga$_{1-x}$As superlattice doped with Be and Si: (a) uncorrected profiles of ^{9}Be$^+$ (– – –), ^{28}Si$^+$ (···), and ^{75}As$^+$ (—); (b) concentration profiles of Be (– – –) [5.0 × 10^{19} atom/cm^3 full scale], Si (···) [9.0 × 10^{19} atom/cm^3 full scale], and Al (—) [1.5 × 10^{22} atom/cm^3 full scale].

Anal. Chem. 1984, 56, 77–79

$^{75}As^+$ signal due to the changing matrix effects. Upon calibration, both the Be and Si distributions have changed substantially. As expected from the growth conditions, the Be concentration generally increases as the Al concentration decreases and vice versa. In addition, excluding the surface buildup, the Si distribution has generally leveled out at 4×10^{18} atoms/cm^3. Without SLIC, this type of analysis could not have been made.

In summary, SLIC is a very precise program for applying calibration lines to the problem of matrix effects in complex samples. Although most of the work to date has been applied to $Al_xGa_{1-x}As$ matrices, this procedure can be used in related matrices, such as $In_xGa_{1-x}As$ and $GaAs_{1-x}Sb_x$. In addition, work in this laboratory indicates that similar methods can be applied to group III and V compound matrices in which several elements are changing simultaneously.

ACKNOWLEDGMENT

The authors gratefully acknowledge the assistance of C. Palmstrom and J. Mayer with the RBS measurements and B. Shaft and G. Wicks for the growth of the MBE matrices. Ion implantation was performed at the National Research and Resource Facility for Submicron Structures at Cornell.

Registry No. Al, 7429-90-5; As, 7440-38-2; Ga, 7440-55-3; Si, 7440-21-3; B, 7440-42-8; Be, 7440-41-7.

LITERATURE CITED

(1) Gries, W. H. *Int. J. Mass Spectrum. Ion Phys.* **1979**, *30*, 97–112.
(2) Leta, D. P.; Morrison, G. H. *Anal. Chem.* **1980**, *52*, 514–519.
(3) Leta, D. P.; Morrison, G. H. *Anal. Chem.* **1980**, *52*, 277–280.
(4) Galuska, A. A.; Morrison, G. H. *Anal. Chem.* **1983**, *55*, 2051–2055.
(5) Mayer, J. W.; Ziegler, J. F.; Chang, L. L.; Tsu, R.; Esaki, L. *J. Appl. Phys.* **1973**, *44*, 2322–2325.
(6) Daries, G. J.; Heckingbottom, R.; Ohno, H.; Wood, C. E. C.; Calawa, A. R. *Appl. Phys. Lett.* **1980**, *37*, 290–292.
(7) Ruberol, J. M.; Lepareur, M.; Autier, B.; Gourgout, J. M. VIIIth International Congress on X-ray Optics and Microanalysis and 12th Annual Conference of the Microbeam Analysis Society, Boston, MA, 1977; pp 133A–133D.

RECEIVED for review July 28, 1983. Accepted October 7, 1983. This work was supported by the National Science Foundation and the Office of Naval Research.

Estimation of Detection Limits in X-ray Fluorescence Spectrometry

John V. Gilfrich* and L. S. Birks

Naval Research Laboratory, Washington, D.C. 20375

The definition of minimum detection limit in instrumental analysis is frequently based on a statistical criterion. Because the magnitude of the detection limit is often derived by extrapolation from much higher concentration, the validity of the value is uncertain. An artificial analytical experiment has been conducted which allows measurement of a low-level signal both with and without contribution from any appreciable background. X-ray measurements at the low count rates expected at concentrations approaching the extrapolated X-ray fluorescence detection limit indicate that the statistical criterion provides a reasonable estimate of the minimum quantity which can be detected.

Many instrumental analytical techniques use a statistical criterion to define the minimum limit of detection, c_L. In recent years there has been general agreement that the determining factor for estimating the limit of detection is the variability of the background, or blank, contribution to the measurable. It has been commonly accepted that c_L is the concentration that produces a signal equal to some constant times the standard deviation of the blank as represented by the equation

$$c_L = ks_{bl}/H$$

where k is the constant (referred to as "k value"), s_{bl} is the standard deviation of the blank, and H is the sensitivity (slope of the calibration curve). The magnitude of the k value has been chosen by various workers to be 2 (for 95% confidence), 3 (for 99% confidence), $2 \times 2^{1/2}$ (for 95% confidence when the signal and blank require two separate measurements and the signal is approximately equal to the blank), and so forth. The International Union of Pure and Applied Chemistry (IUPAC) recommends that the k value should be 3 (*1*) and further suggests that, because the values for the blank, and the standard deviation thereof, are estimates based on limited measurements, the $3s_{bl}$ value corresponds to a confidence level of about 90%.

In X-ray fluorescence determinations, minimum detection limits, using the IUPAC criterion, are estimated to be in the range of a few nanograms per square centimeter for thin samples of many elements using commercial instrumentation (*2, 3*). Laboratory measurements under specialized conditions such as for high energy particle excitation or using synchrotron radiation sources suggest that detection of a few picograms can be achieved (*4, 5*). There has been a lingering concern in the X-ray analytical community that the estimation of c_L by extrapolation from measurements on standards containing several orders of magnitude higher concentrations may not take account of instrumental variations which are negligible at the higher concentrations. Past attempts have been made to accommodate this uncertainty by suggesting that as much as 14 times the standard deviation of the background be used as the "determination limit" (*6*) (rather than the IUPAC "detection limit" (*1*)). The American Chemical Society Guidelines (*7*) recommend a k value of 10 for the "limit of quantitation".

While in the process of attempting to design a means of producing an accurately characterized sample at a concentration which would approach detection limits estimated for synchrotron radiation excitation, a very simple experiment took shape in our minds which would test the statistics and instrumental uncertainties under conditions corresponding to nanogram quantities. This report describes that experiment and discusses its statistical significance.

This article not subject to U.S. Copyright. Published 1983 by the American Chemical Society

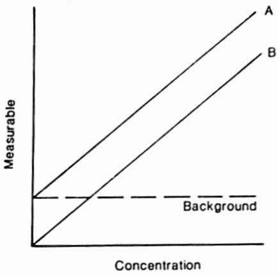

Figure 1. Straight line calibration curve, illustrated with and without background.

THEORY

A common type of straight-line calibration curve for instrumental determination is shown schematically in Figure 1. A represents the usual situation where the sensitivity (slope of the calibration curve) intersects the zero concentration axis at a value of the measurable parameter which represents the background (or blank). It is presumed that the background remains constant over the range of linearity of the calibration. B represents the more desirable situation where the background is zero (or nearly so), virtually impossible to achieve in practice. The slope of the calibration curve remains the same as A.

From the literature (*2*) it is possible to estimate the sensitivity for X-ray fluorescence measurements of thin film samples of the first period transition metals to be about 150 counts/s for each microgram of the element per square centimeter of the substrate. By optimization of the measurement conditions, it is feasible to limit the background to a few counts per second (for this exercise we shall use 5 counts/s). Using the IUPAC definition (*1*) of detection limit and 100 s counting time, we obtain a background (N_B) of 5 × 100 = 500 counts and a peak signal (N_P) including background of (150 × 100) + (5 × 100) = 15500 counts (μg/cm²) leading to the detection limit (c_L) of

$$c_L = \frac{3\sqrt{500}}{15000} = 4.5 \times 10^{-3}\ \mu g/cm^2 = 4.5\ ng/cm^2$$

The count rate for the signal at this level of the element of interest would be only 78 counts s ($3 \times 500^{1/2}$) above a background of 500 counts/100 s.

The question to be addressed, then, is as follows: Are random statistical considerations and instrumental assumptions valid when measuring X-ray signals of the order of one count per second above a background of a few counts per second? The difficulty of producing an accurately characterized standard at the level to emit that signal is quite significant. Also, measurements of the low-level signal in the absence of appreciable background are impossible. However, X-ray emitting radioisotopes are available over an activity range which should permit measurements to be made in the appropriate counting range.

EXPERIMENTAL SECTION

A Philips PW1410 X-ray fluorescence spectrometer equipped with a 0.55° 2θ blade collimator, a (200) LiF crystal, and a P-10 gas-flow proportional counter was used. An ^{55}Fe source (10 mCi as of June 1970) was positioned at the sample end of the collimator and the spectrometer set to measure the Mn Kα diffracted by the LiF crystal. To simulate background radiation at the same wavelength, a lower activity ^{55}Fe source (50 μCi, March 1960) with aluminum foil attenuators was located at the rear window of the detector. Counts of 100 s and 1000 s were taken several times to test the reproducibility of the measurements and to compare with the theoretical statistical treatment.

Table I. Measurements with no Background Source (1000 s)

	counts/1000 s		
	signal + bgd (N_P)	bgd (N_B)	signal ($N_P - N_B$)
	1305	165	1140
	1226	125	1101
	1259	149	1110
	1297	152	1145
av ($\overline{N}$)	1272	148	1124
obsd std dev	36.5	16.7	21.8
$\overline{N}^{1/2}$	35.7	12.2	37.7*
$c_L{}^b$ 0.24 ng/cm²			

[a] Because the signal is the result of *two* measurements the, parameter here is $(N_P + N_B)^{1/2}$. [b] Assuming a sensitivity of 150 (counts/s)/(μg/cm²).

One of the advantages of the use of this type of radioisotope is the elimination of any source instabilities, while maintaining any effect of variation in the spectrometer and detection system. Also, it is possible to predict the absolute intensity for such a source, as a check on the observed intensity.

The efficiency of the spectrometer can be calculated quite simply (*8*). It is the product of the integral reflection coefficient (R) of the crystal in radians, the fanning angle of the collimator ($\Delta\phi$) from the source to the detector window in radians, the detector efficiency (E_D), and a factor (amounting to about $^1/_2$) which accounts for the divergence of the collimator relative to the rocking curve of the crystal, required because the measurement is made at a fixed angle. For the instrument used

$$R = 3 \times 10^{-4}\ \text{radians}$$

$$\Delta\phi = 0.125\ \text{radians}$$

$$E_D = 0.6$$

Therefore the spectrometer efficiency (E_S) is

$$E_S = (3 \times 10^{-4}) \times 0.125 \times 0.6 \times 0.5 = 1.12 \times 10^{-5}\ \text{sr}$$

^{55}Fe has a half-life of 2.7 years. Therefore a source which was 10 mCi in June 1970 has decayed, by December 1982, to

$$12.5\ \text{years}/2.7\ \text{years} = 4.63\ \text{half-lives}$$

$$2^{-4.63} = 0.0404$$

$$0.0404 \times 10\ \text{mCi} = 0.404\ \text{mCi}$$

There are 3.7×10^{10} nuclear disintegrations per second per Curie in 4π sr and, for ^{55}Fe, 28.5% of those disintegrations produce Mn K radiation; 85% of Mn K radiation is Mn Kα. The emission rate of our ^{55}Fe source, then, is

$$(0.404 \times 10^{-3}) \times (3.7 \times 10^{10}) \times 0.285 \times 0.85/4\pi = 2.88 \times 10^5\ \text{ph s}^{-1}\ \text{sr}^{-1}$$

Combining the spectrometer efficiency with the source emission rate and including the air absorption for the 25 cm path length in the spectrometer (the ^{55}Fe was not capable of being put in a vacuum) gives us the predicted count rate

$$(1.12 \times 10^{-5})\ \text{sr} \times (2.88 \times 10^5)\ \text{ph s}^{-1}\ \text{sr}^{-1} \times 0.43 = 1.4\ \text{counts/s}$$

Initial measurements (with no background source) gave an average count rate of 1.3 counts/s with a background of 0.15 count/s. As will be seen in the tables, the signal varied between 1 count/s and 1.2 counts/s for all the measurements, in good agreement with the predictions of 1.4 counts/s.

RESULTS AND DISCUSSION

Initial measurements consisted of four 1000-s counts each with the primary source in place and without the primary source, both without the background source to illustrate the

Table II. Measurements Including Background Source (1000 s)

	counts/1000 s		
	signal + bgd	bgd	signal
	3265	1980	1285
	3322	2133	1189
	3286	1977	1309
	3235	2087	1148
	3258	2077	1181
	3301	2080	1221
av ($\overline{N}$)	3278	2056	1222
obsd std dev	31.5	63.1	62.9
$N^{1/2}$	57.3	45.3	73.0[a]
c_L[b] 0.91 ng/cm^2			

[a,b] See Table I.

Table III. Measurements Including Background Source (100 s)

	counts/100 s		
	signal + bgd	bgd	signal
	322	208	114
	337	188	149
	290	249	41
	297	229	68
	295	193	102
	322	209	113
	323	218	105
	297	224	73
	292	200	92
	315	226	89
av ($\overline{N}$)	309	214	95
obsd std dev	16.6	18.5	29.7
$\overline{N}^{1/2}$	17.6	14.6	22.9[a]
c_L[b] 2.9 ng/cm^2			

[a,b] See Table I.

low count rate with virtually zero background. Table I lists the data and the statistics. For this case where the background is very low, the square root of the number of counts is a reasonable estimate of the measured standard deviation considering the limited population. Also listed in the final column is an estimate of c_L assuming that the sensitivity of the measurement was the 150 (counts/s)/(μg/cm^2) assumed in our initial calculation.

When the background source is contributing to the total count, the situation remains the same. Table II shows six 1000-s counts and Table III ten 100-s counts. In both of these cases, even for the net signal of about 100 counts, the conventional method of estimating the standard deviation (square root of the number of counts for a single measurement or the square root of the sum of the number of counts on the peak and on the background for two measurements) seems to be a reasonable estimate of the standard deviation, ranging for this limited set of measurements from 0.72 to 1.8 times the measured values.

The value of c_L (100 s) listed in Table III is in reasonable agreement with that calculated considering that the measured background is significantly lower than that assumed in the initial calculation. This result is not unexpected but serves to indicate some degree of self-consistency.

CONCLUSIONS

From these few measurements, it seems that an X-ray analyst can have reasonable confidence, in the detection limit, c_L, which is extrapolated from standards of much higher concentrations. The experimental data include the contributions to uncertainties caused by the spectrometer and electronics but excludes any instabilities due to the X-ray generator. This latter consideration should not be a problem since modern X-ray generators are demonstrated to be very stable over both the short and long term. The significance of this fact becomes more important as technology advances to enable detection of smaller and smaller quantities and gives added confidence to our recent estimation of detection limits of a few picograms using synchrotron radiation excitation (5).

LITERATURE CITED

(1) IUPAC, Commission on Spectrochemical and Other Optical Procedures for Analysis *Pure Appl. Chem.* **1976**, *45*, 99.
(2) Wagman, Jack; Bennett, R. L.; Knapp, K. T., Environmental Protection Agency Report EPA-600/2-76-033, March 1976.
(3) Giauque, R. D.; Goulding, F. S.; Jaklevic, J. M.; Pehl, R. H. *Anal. Chem.* **1973**, *45*, 671.
(4) Johansson, T. B.; Akselsson, R.; Johansson, S. A. E. *Nucl. Instrum. Methods* **1970**, *84*, 141.
(5) Gilfrich, J. V.; Skelton, E. F.; Qadri, S. B.; Kirkland, J. P.; Nagel, D. J. *Anal. Chem.* **1983**, *55*, 187.
(6) Currie, L. A. *Anal. Chem.* **1968**, *40*, 586.
(7) ACS Subcommittee on Environmental Analytical Chemistry *Anal. Chem.* **1980**, *52*, 2242.
(8) Birks, L. S. *Anal. Chem.* **1977**, *49*, 1505.

RECEIVED for review May 2, 1983. Accepted September 1, 1983.

80 *Anal. Chem.* **1984**, *56*, 80-82

Infrared Photoacoustic Spectroscopy of Liquids with an F-Center Laser

Pao-Yuan Chen and James S. Shirk*

Department of Chemistry, Illinois Institute of Technology, Chicago, Illinois 60616

An infrared photoacoustic liquid cell with excitation by a tunable F-center laser is described. Modulation near 126 kHz excites low order, modest Q (60), radial resonance modes of the sample. The resulting photoacoustic signal is independent of sample path length over a range 0.3–4.4 cm. An absorbance of 1 × 10^{-5} provides a $S/N = 1$ with a laser power of 3.5 mW. The signal scales with laser power but the noise is dominated by detector thermal (Johnson) noise, so greater sensitivity can be achieved with more powerful lasers. The effect of sample resonances on photoacoustic experiments with pulsed laser excitation is discussed.

Photoacoustic spectroscopy (PAS) is useful for trace analysis, especially in the gas phase. It has been also widely used in the IR region; there are commercially available photoacoustic cells for some IR spectrometers (*1*). These cells are very sensitive for gaseous samples but are not particularly sensitive when used for the IR detection of trace constituents or weak absorptions in liquid phases.

The relatively low sensitivity for IR-PAS detection in liquids arises because usually the acoustic signal is detected with a capacitance microphone in the gas above the sample. Sensitivity suffers from the poor acoustic coupling of the condensed phase with a gas. Photoacoustic detection of condensed phase absorptions with microphones in the gas above the liquid is generally useful only for reasonably strong absorbances. Immersed piezoelectric detectors have better coupling to the condensed phase but suffer from a lower sensitivity (by about 2 orders of magnitude) than gas-phase microphones (*2*).

There has been some recent success at high sensitivity PAS in the visible region with piezoelectric microphones that have good acoustic impedance matching to the solution. Voigtman, Jurgensen, and Winefordner review some of the previous studies (all of these are in the visible or near-IR region) (*3*). Usually pulsed sources with gated detection (so that a true photoacoustic and not a photothermalacoustic pulse is detected) are used. For example Patel and co-workers (*4–6*) using a pulsed dye laser and measuring the height of the first acoustic peak, were able to detect molecules with absorbances of 10^{-7} cm^{-1} in liquids in the visible and near-IR regions. They were able to measure the absorption spectrum of water in the visible region.

The initial motivation for our work came from the papers of Tam and Patel. Since tunable high power pulsed lasers, analogous to dye lasers, are not available in the fundamental IR and yet trace PAS IR detection seemed a desirable goal, we decided to investigate the possibility of trading high peak power at a low repetition rate for the low peak powers at a high repetition rate which could be obtained by modulating an F-center laser.

We report here on the design, construction, and operation of an F-center laser-driven IR-PAS spectrometer for the detection of weak IR absorptions in liquids, including a comparison of pulsed modulation with sine wave modulation.

Table I. Calculated Frequency Values for Different Resonance Modes and Their Experimental Frequency Values

mode (p,m,n)	measd value, Hz	calcd value, Hz
1,0,0	1.16 × 10^4	1.05 × 10^4
2,0,0	2.75 × 10^4	2.11 × 10^4
3,0,0	3.5 × 10^4	3.17 × 10^4
0,1,0	4.1 × 10^4	4.29 × 10^4
0,2,0	7.2 × 10^4	7.12 × 10^4
0,3,0	9.7 × 10^4	9.79 × 10^4
0,0,1	8.43 × 10^4	8.93 × 10^4
0,0,2	16.05 × 10^4	16.35 × 10^4
0,1,1	12.25 × 10^4	12.35 × 10^4

EXPERIMENTAL SECTION

The IR radiation source was a computer-controlled Burleigh Model FCL-20 F-center laser, used here without an etalon, pumped by a Spectra Physics Model 164-11 Kr^+ laser. the details of this laser have been described in connection with other experiments (*7*). This laser is continuously tunable from 2.3 to 3.3 μm. The Kr^+ laser pump beam was modulated either as a sine wave or in a discrete pulsed mode using a photoacoustic modulator (Interaction Corp., Model ADM-40). We also did some experiments in which the modulated Kr^+ laser beam excited the sample directly.

The photoacoustic transducer and preamplifier were identical in design and construction with that described by Tam and Patel. The piezoelectric element was a lead zirconate–titanate cylinder made by Transducer Products. The transducer is enclosed in a housing so that only a polished stainless steel face is in contact with the sample.

A variety of sample containers were used. Most experiments were done in sample cells made of Teflon. In these cells the sample chamber was 1.3 cm in diameter and was lined with a stainless steel cylinder. One cell was 4.4 cm long. A second was 1.85 cm long; in this cell the sample length could be varied from 0.3 to 1.85 cm by adjusting a Teflon plug. The transducer assembly was inserted radially into the cell. The cell had salt or Pyrex windows sealed by an indium gasket.

The output of the microphone preamplifier was fed into a Princeton Applied Research Model HR-8 Lock-in Amplifier for modulated CW experiments. For detection of pulsed experiments the preamplifier output was amplified (×1000) and fed into a PAR Boxcar Averager Model 165 with a Model 162 plug-in module.

All liquid samples were Spectrophotometric grade dried over 4A molecular sieves and filtered through a Millipore filter. Samples were introduced into the cell under an N_2 atmosphere. Even with these precautions water estimated from the IR absorbance spectra to be in the high parts-per-billion range remained in the samples.

RESULTS AND DISCUSSION

In a reasonable sized liquid PAS sample cell with dimensions on the order of a centimeter there are a large number of closely spaced acoustic resonances in the frequency range above 10^4 Hz. For example, Table I gives the calculated resonances (*8*) for one of our sample cells and Figure 1 shows the observed acoustic response as a function of frequency for this cell; most of the maxima can be assigned to low order

0003-2700/84/0356-0080$01.50/0 © 1983 American Chemical Society

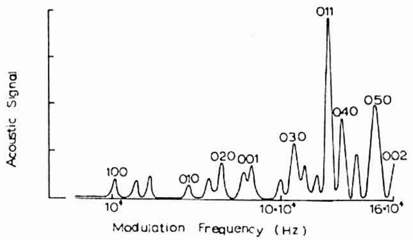

Figure 1. Acoustic response as a function of signal frequency for our approximately 1.3 cm diameter cell. The indexes of the nearest acoustic resonances are given.

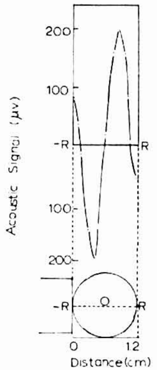

Figure 2. Acoustic signal as a function of excitation position for the 1,1,0 mode near 126 kHz.

radial and azimuthal acoustic modes.

These acoustic resonances affect the acoustic response to either pulsed or high-frequency sine wave modulated excitation. The observed frequency response, i.e., the resonance frequencies, depends upon the size and shape of the cell. In open cells, such as a cuvette of the type used in previous experiments (*3–6*), it depends on the sample volume as well, since the air/solution interface determines the boundary of the effective cell. It also depends upon the position of excitation in the cell; for maximum response the acoustic mode must have pressure maxima at both the microphone and the excitation position. Figure 2 shows the magnitude of the detected signal for the 1,1,0 mode at 126 kHz in our cell as a function of excitation position.

In pulsed experiments considerable care is necessary to achieve consistent results. In PAS with pulsed excitation the observed response for short pulses is the Fourier transform of the frequency response of the cell and the microphone. Thus the observed ringing pattern depends upon the same factors which influence the resonance frequencies of the cell–detector combination. It has been pointed out that simply measuring the initial peak is an arbitrary measure of the absorption strength (*9*). We confirmed this, for example, Figure 3 shows the pulse response of one of our samples as a function of excitation position.

The advantages attributed to pulsed excitation, high sensitivity and discrimination against window absorption, can be maintained by modulated CW excitation into one of the low order radial acoustic modes of the a sample with synchronous detection. High frequency modulated CW experiments were preferable to pulsed experiments for a variety of reasons: (1) the effective repetition rate can be higher since it is not necessary to wait for the "ringing" to die away before exciting the sample again and (2) the small signals and substantial thermal (Johnson) noise from the high-impedance detector results in low S/N ratios at the preamplifier output, sometimes as low as 1/1000. Lock-in amplifiers, which can operate at a very narrow effective band-pass, can extract a PAS signal with a better final S/N than can the boxcar integrators necessary for pulsed experiments.

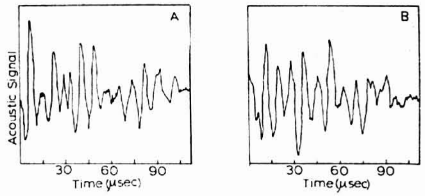

Figure 3. Pulse response of the piezoelectric detector (a) with excitation about one-third of the way across the cell and (b) with excitation about two-thirds of the way across the cell. Laser had a 1-μs pulse width at 3712 cm^{-1} and a pulse energy of 3.5 × 10^{-9} J.

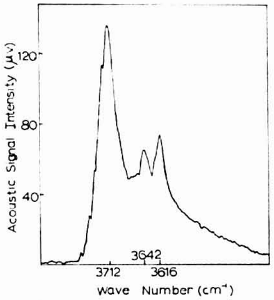

Figure 4. PAS spectrum of 4 ppm CH_3OH in CCl_4 taken at 3.5 mW laser power. The peaks at 3616 cm^{-1} and 3712 cm^{-1} are H_2O.

For the 1.3 cm diameter Teflon cells we found that the 1,1,0 mode at 126 kHz excited ca. one-third of the distance across the cell was convenient and gave a strong resonance signal. The measured Q was 60. Such modest values of Q are advantageous in that a small change in the resonance frequency does not cause large changes in the observed signal and yet the resonance enhancement provides a good signal.

Figure 4 gives a typical spectrum recorded in the long cell of 4 ppm CH_3OH in CCl_4. The bands at 3712 cm^{-1} and 3616 cm^{-1} are H_2O present as an impurity in the CCl_4. The peak laser power was about 3.5 mW. The measured S/N was 48. Since the absorbance was 8.4 × 10^{-3}, an absorbance of 1.7 × 10^{-4} would be detectable with a $S/N = 1$. Similar detection limits were obserbed on other absorptions. The PAS signal was linear with concentration and linear with laser power over the range of power available to us (~4 mW). In a separate experiment, the PAS signal from excitation of a dilute $CuSO_4$ solution in H_2O in the same cell using a modulated Kr^+ laser on the 647.1-nm line, the PAS signal was linear with laser intensity up to 700 mW. Additional experiments using the shorter, variable path length cell showed that the photoacoustic signal was approximately independent of path length over the range available to us: 0.3 cm to 4.4 cm. This was

82 *Anal. Chem.* **1984**, *56*, 82–85

expected since we were exciting into a radial acoustic resonance mode of the cell.

The long cell had the advantage that we could directly compare the PAS spectrum with an FTIR spectrum of the same sample. The PAS spectrum had about two to three times better S/N. An advantage of the PAS spectrum is that there is no interference from atmospheric absorptions such as water. The sensitivity advantage of PAS was more dramatic with shorter path length samples. Over the range 0.3–4.4 cm, the photoacoustic signal was practically independent of the sample length, so that for a 3-mm sample the detection limit ($S/N = 1$) was an absorbance of $\sim 1 \times 10^{-5}$, a factor of about 50 better than a typical FTIR spectrum. The shortest path length feasible with our current cell and microphone design was 3 mm. Presumably the sample could be made considerably thinner.

The observed noise level at the output of our lock-in amplifier was very close to the expected Johnson noise of our 22 MΩ preamplifier input resistor over the band-pass of our lock-in amplifier. This noise determines the detection limit. Higher sensitivities can be achieved by increasing the laser power or cooling the input resistor to the preamplifier.

An advantage of operating at these high frequencies is that our detector is able to operate in noisy surroundings and even with flowing samples with little interference. Furthermore using radial acoustic modes we can achieve substantial rejection of interference from window absorption.

CONCLUSIONS

IR absorption spectra of weak absorbers and trace contaminants in liquids can be observed by using a photoacoustic detection and a modest power F-center laser. The moderate Q natural acoustic resonances of typically sized liquid cells are used to enhance the signal. Even with a modest power laser (3.6 mW) absorbances in the range of 1×10^{-5} corresponding to a sample concentration for a typical absorber in the OH region of a few parts per million and a sample path of 3 mm are detectable. The current apparatus is about 50 times more sensitive than a typical FTIR.

The limiting noise is thermal (Johnson) noise in the input resistor, which is of course independent of signal. The signal scales linearly with the laser power, so the sensitivity should scale as the laser power. Thus higher sensitivities will be possible as more powerful IR lasers become available.

The high frequency used makes the technique useful in high ambient noise applications and for flowing samples. It also provides discrimination against contributions to a background signal from window absorption.

ACKNOWLEDGMENT

We thank James Mitchell and Timothy Harris for their interest and aid in obtaining a duplicate of the Tam and Patel microphone. The initial experiments which led to this research were done in collaboration with T. Harris.

LITERATURE CITED

(1) McClelland, J. F. *Anal. Chem.* **1983**, *55*, 89A.
(2) Rosencwaig, A. "Photoacoustics and Photoacoustic Spectroscopy"; Wiley-Interscience: New York, 1980.
(3) Voigtman, E.; Jurgensen, A.; Winefordner, J. *Anal. Chem.* **1983**, *53*, 1442.
(4) Patel, C. K. N.; Tam, A. C. *Rev. Mod. Phys.* **1981**, *53*, 517.
(5) Patel, C. K. N.; Tam, A. C. *Appl. Phys. Lett.* **1979**, *34*, 760.
(6) Nelson, E. T.; Patel, C. K. N. *Appl. Phys. Lett.* **1981**, *39*, 537.
(7) McDonald, P. A.; Shirk, J. S. *J. Chem. Phys.* **1982**, *77*, 2355.
(8) Morse, P. "Vibration and Sound"; McGraw-Hill: New York, 1948; p 398f.
(9) Fisher, M. R.; Fasano, D. M.; Nogar, N. S. *Appl. Spectrosc.* **1982**, *36*, 125.

RECEIVED for review August 11, 1983. Accepted October 7, 1983. This work was initially supported by the NSF under Grant No. CHE 79-09380.

Phase Plane Method for Deconvolution of Luminescence Decay Data with a Scattered-Light Component

J. C. Love and J. N. Demas*

Department of Chemistry, University of Virginia, Charlottesville, Virginia 22901

A three-parameter version of the phase-plane method for deconvolution of luminescence decay data is presented that corrects for contributions of scattered excited light in the observed decay. Through computer simulations, we tested the method with numerous combinations of lifetimes, noise levels, and scatter coefficients. The modified equation was found to be computationally rapid and yielded excellent precision and accuracy in the decay parameters.

Excited state lifetime measurements are pervasive and provide crucial information in analytical chemistry, photochemistry, photophysics, and photobiology (*1, 2*). The most common approaches to lifetime measurements involve exciting the sample with a short optical pulse and monitoring the sample decay. If the excitation source is short enough and the detection system responds quickly enough, the observed sample decay is the desired sample impulse response.

Frequently, however, the sample decays on a time scale comparable to the excitation pulse width and the response time of the detection system. The observed decay is then a complex function given by the convolution of the system response and the sample impulse (*2*). The process of extracting decay parameters from the observed excitation and decay profiles is called deconvolution.

The most important deconvolution problem involves samples with impulse responses that are single exponential decays. The observed sample decay, $D(t)$, is then given by

$$D(t) = K \exp(-t/\tau) \int_0^t E(x) \exp(x/\tau)\,dx + \alpha E(t)$$
$$E(t) = 0;\ t \le 0 \qquad (1)$$

where $D(t)$ is the observed decay signal vs. time, t, K is the proportionality constant, $E(t)$ is the observed excitation profile, and τ is the sample lifetime (*1–4*). The first term on

0003-2700/84/0356-0082$01.50/0 © 1983 American Chemical Society

the right-hand side accounts for the contribution of the sample decay. The $\alpha E(t)$ term accounts for any leakage of the scattered excitation pulse to the detector. Especially for bright emitters with a large wavelength difference between excitation and emission monitoring, α can frequently be negligibly small. In eq 1 any distortions of $E(t)$ and $D(t)$ are assumed to be linear and the same for both measurements. Furthermore, there is no time shift between $E(t)$ and $D(t)$.

A variety of methods are used to extract information from data of the form of eq 1 especially where $\alpha = 0$ (i.e., negligible scatter) (*1–5*). Many of these methods are complex and computationally time-consuming. For the $\alpha = 0$ case the phase-plane (PP) method, which was originally developed for simple exponential evaluations (*6, 7*), has proved a successful deconvolution method (*2–4*). It linearizes the data for viewing, is computationally exceptionally fast, and gives good precision and accuracy in decay parameters over a wide range of data (*2–4*).

The PP method has recently been extended to decays with a scatter contribution (i.e., $\alpha > 0$ in eq 1), a sum of two exponentials (*8*), or decays involving nonradiative intermolecular energy transfers (Förster kinetics) (*9*). Independently, we had arrived at the deconvolution of eq 1 with a scatter component. Jezquel et al. (*8*) reported only limited data on the accuracy, precision, and limitations of the PP method with a scatter correction. We report here a more extensive analysis of the limitations of the PP method with a scatter correction. In particular, we assess the accuracy and precision of the method for a range of τ, α, and K as well as for differing noise levels.

THEORY

We derive the phase-plane equations following the approach used for the normal PP equation without scatter. Taking the derivative of both sides of eq 1 with respect to t yields

$$\mathrm{d}D(t)/\mathrm{d}t = -(1/\tau)D\exp(-t/\tau)\int_0^t E(t)\exp(t/\tau)\,\mathrm{d}t + KE(t) + \alpha\mathrm{d}E(t)/\mathrm{d}t \quad (2)$$

The first term on the right is simplified by replacing it with a rearranged form of eq 1, yielding

$$\mathrm{d}D(t)/\mathrm{d}t = -(1/\tau)[D(t) - \alpha E(t)] + \alpha\mathrm{d}E(t)/\mathrm{d}t \quad (3)$$

Reintegrating eq 3 over the interval of 0 to t and rearranging yields

$$Y(t) = A_0 + A_1X_1(t) + A_2X_2(t) \quad (4a)$$

$$A_0 = K + \alpha/\tau \quad (4b)$$

$$A_1 = 1/\tau \quad (4c)$$

$$A_2 = \alpha \quad (4d)$$

$$Y(t) = W(t) = D(t)/\int_0^t E(x)\,\mathrm{d}x$$

$$X_1(t) = Z(t) = \int_0^t D(x)\,\mathrm{d}t/\int_0^t E(x)\,\mathrm{d}x \quad (4e)$$

$$X_2(t) = E(t)/\int_0^t E(x)\,\mathrm{d}x \quad (4f)$$

$Y(t)$, $X_1(t)$, and $X_2(t)$ are easily evaluated functions of the observed $D(t)$ and $E(t)$. $W(t)$ and $Z(t)$ are the original definitions given by Demas and Adamson (*3*). The use of $Y(t)$'s and $X(t)$'s here is a more consistent nomenclature for generalization. The formula is analogous to the one used by Reed and Demas (*10*) that minimized systematic errors that occur for noisy data fit by normal unweighted least squares (*11*).

Equation 4 is a linear function of two independent variables. Standard linear least-squares methods can be used to fit the observed data to obtain the desired parameters. In an unweighted least-squares sense, one strives to minimize

$$\sum\{Y(t_i) - [A_0 + A_1X_{1i} + A_2X_{2i}]\}^2 \quad (5)$$

where X_{1i} and X_{2i} are X_1 and X_2 evaluated at t_i. The summation is over all data points used in the data fitting. Taking the partial derivative with respect to A_0, A_1, and A_2 and setting them equal to zero yields the "normal" equations necessary for a minimum. In a matrix form the normal equations are

$$\begin{pmatrix} \Sigma 1 & \Sigma X_{1i} & \Sigma X_{2i} \\ \Sigma X_{1i} & \Sigma X_{1i}^2 & \Sigma X_{1i}X_{2i} \\ \Sigma X_{2i} & \Sigma X_{1i}X_{2i} & \Sigma X_{2i}^2 \end{pmatrix} \begin{pmatrix} A_0 \\ A_1 \\ A_2 \end{pmatrix} = \begin{pmatrix} \Sigma Y(t_i) \\ \Sigma Y(t_i)X_{1i} \\ \Sigma X(t_i)X_{2i} \end{pmatrix} \quad (6)$$

The summations are over the points used in the fitting. Solution of this system of normal equations yields the best A_0, A_1, and A_2 which, in turn, gives K, τ, and α from eq 4. Equation 6 is analogous to that used by Jezequel et al. (*8*).

EXPERIMENTAL SECTION

To analyze the effects of different noise levels, lifetimes, and scatter coefficients on the accuracy and precision of the new equation, we have applied the PP method to the reduction of digitally simulated decay curves. The synthetic data used had noise levels similar to that found in both single photon counting (SPC) and analog instrumentation.

Synthetic decay curves were generated by using eq 1 with $K = 1$ and a range of α's. $E(t)$ was simulated as described earlier (*2–4*) with $A = 6.0$ and $B = 6.6$ ns which yielded an $E(t)$ that peaks in ~5 ns, exhibits a full width at half maxima (fwhm) of 14 ns, and decays exponentially at long times with a 6.6-ns lifetime. The calculated decays were then scaled to give peak values in $E(t)$ and in $D(t)$ of 10^2, 10^3, and 10^4. α's used were 0.5, 2.5, 5.0, and 10.0. A total of 201 data points were generated at a 0.25-ns spacing, and τ's of 2.5 ns and 15 ns were used. These τ's were selected as representative. The short τ is much shorter than the flash width, and the long τ is appreciably longer, but $D(t)$ is still significantly affected by $E(t)$. Synthetic data were generated for all combinations of α, τ, and peak channel counts in $E(t)$ and $D(t)$.

Gaussian noise with a standard deviation equal to the square root of $D(t)$ was added to the suitably scaled $E(t)$'s and $D(t)$'s as described earlier (*4*). For values of $D(t) \geq 25$ this distribution is essentially Poisson and mimics SPC statistics. For peak values of 10^4, the data correspond to typical SPC decays. Peaks of 10^3 to 10^4 represent reasonable analog data, while peak values of 10^2 would correspond to poor analog data. Typical noise levels are shown in ref 4.

The integrals necessary for the evaluation of $Y(t)$, $X_1(t)$, and $X_2(t)$ were evaluated by the trapezoidal rule (*2–4*).

$$\int_0^{t_i} D(x)\,\mathrm{d}x = (\Delta t/2)R_i \quad (7a)$$

$$R_i = (D(t_i) + D(t_{i-1})) + R_{i-1},\ i \geq 1,\ R_0 = 0 \quad (7b)$$

$$\int_0^{t_i} E(x)\,\mathrm{d}x = (\Delta t/2)Q_i \quad (7c)$$

$$Q_i = (E(t_i) + E(t_{i-1})) + Q_{i-1},\ i \geq 1,\ Q_0 = 3 \quad (7d)$$

$$\Delta t = t_{i+1} - t_i \quad (7e)$$

$W(t)$, $Y(t)$, and $Z(t)$ are thus given as

$$Y(t_i) = 2D(t_i)/(\Delta t Q_i) \quad (8a)$$

$$X_2(t_i) = 2E(t_i)/(\Delta t Q_i) \quad (8b)$$

$$X_1(t_i) = R_i/Q_i \quad (8c)$$

The three linear equations of eq 6 were generated and solved by matrix algebra to yield the K, α, and τ values of the simulated curves. All fits were carried out from t corresponding to the peak of the noise free $D(t)$ to the 201st point. This range was selected to give as much information as possible about the sample decay while minimizing the contribution from the scatter. Further, since there is no weighting, inclusion of data from earlier times degrades the results. See the plots in ref 3 and 4. For data with a large scatter component, the observed peak of $D(t)$ will be at shorter times than the peak for the scatter free $D(t)$. With a little experience or by generating a few simulated decays, however, the

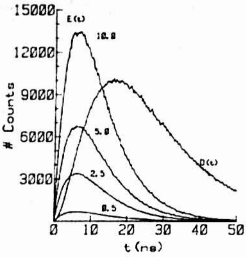

Figure 1. Scatter free $D(t)$ and $\alpha E(t)$ terms for τ = 15 ns. The α for each $E(t)$ term is indicated by the curves.

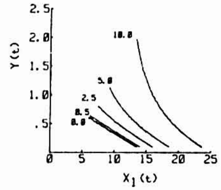

Figure 2. PP plots for the data of Figure 1. α is indicated by each curve. Data are plotted from the time of the peak of the noise and scatter free $D(t)$.

operator can easily determine where the fit should actually begin.

For every set of parameters, 20 noisy decay curves were generated and reduced. The average τ, α, and K and their respective standard deviations were calculated. For each set of decay parameters, we determined a relative error, RE, and a relative standard deviation, RSD, given by

$$\text{RE \%} = 100(\hat{V} - V)/V \qquad (9a)$$

$$\text{RSD \%} = 100\sigma/V \qquad (9b)$$

where V is the decay parameter used to simulate the decays, $\hat{V}$ is the average calculated parameter, and σ is the standard deviation. All simulations were performed on an HP-85A desktop computer.

RESULTS AND DISCUSSION

Figure 1 shows the scatter free sample decay (τ = 15 ns) and the scaled scatter contributions for different α's. Noise levels are for curves of the indicated amplitude. Note, however, that the data reduced had the noise added only after generating and scaling the composite $D(t)$. For $\alpha = 0.5$ the distortions are relatively small but the contributions to the observed decays for $\alpha \geq 2.5$ are quite serious. Figure 2 shows the corresponding normal phase plane plots of $Y(t)$ vs. $X_1(t)$ for the same data. In the absence of scatter these plots should be linear with slopes equal to $(-1/\tau)$. In the original formulation (3) these plots would be $W(t)$ vs. $Z(t)$ plots. As expected for α's $\geq \sim 0.5$, the slopes of these normal PP plots would yield inaccurate estimates of τ.

Figures 3 and 4 show corresponding data for τ = 2.5 ns. Even for $\alpha = 0.5$, significant distortions of the observed decays arise from the scatter. For $\alpha = 2.5$, the peak amplitudes of $D(t)$ and the scatter contributions are comparable. Clearly use of the normal PP method for estimating τ's is worthless. Indeed, for $\alpha = 10$ the scatter peak appears to completely overwhelm the sample decay, but, as we will show, useful information still can be extracted from such data. Figure 4 shows the $Y(t)$ vs. $X_1(t)$ plots. As expected, use of the normal PP equation without a scatter correction would not yield reliable estimates of τ for $\alpha \geq \sim 0.5$.

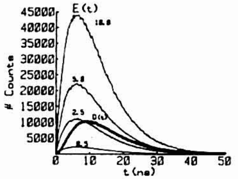

Figure 3. Scatter free $D(t)$ (X's) and $\alpha E(t)$ terms for τ = 2.5 ns. The α for each $E(t)$ term is indicated by the curve.

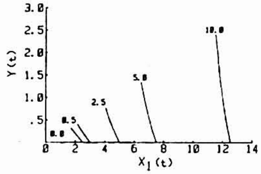

Figure 4. Normal linearized PP plots for the data of Figure 3. α is indicated by each curve. Data are plotted from the time of the peak of the noise and scatter free $D(t)$.

Table I. Relative Errors and Standard Deviations in τ

peak in $E(t)$ and $D(t)$	α	τ = 2.5 ns		τ = 15 ns	
		RE	RSD	RE	RSD
100	0.5	−0.53	19.3	−0.54	5.5
	2.5	−25.1	32.8	−2.8	5.4
	5.0	−17.0	33.7	−4.8	7.4
	10.0	−24.7	46.4	−12.0	14.4
1 000	0.5	−1.4	8.8	−0.75	2.3
	2.5	−6.1	16.5	−1.0	1.9
	5.0	−1.7	23.3	−0.98	2.1
	10.0	−16.6	38.5	−1.1	3.1
10 000	0.5	0.44	3.3	0.02	0.83
	2.5	−0.07	3.5	0.11	0.80
	5.0	0.93	9.5	−0.26	0.59
	10.0	4.0	16.3	0.06	0.80

Table I summarized our relative error and standard deviation in τ for the range of parameters. For brevity we have included only the data where the peaks in $E(t)$ and $D(t)$ were equal. Where the peak values were unequal, the results generally fell between those entries in the table for the two corresponding equal peak cases. Because the lifetime is usually the important parameter estimated, we have not reproduced our data for α and K. The full set of calculations is available on request. All the errors, however, were typically within 1–2 standard deviations of the generating parameters for the 10^3 and 10^4 peak data. Precisions in K and τ declined somewhat as the amount of scatter detected by the system rose, but acceptable fitting will occur for any reasonable degree of scatter. Single photon counting quality data typically yielded a K and τ accuracy of $\leq \sim 2\%$ or better; even noisy analog data yielded results within $\leq 9\%$ of the correct values, except for the 100 peak data and the shortest lifetime.

Precision in α improved as the precisions of K and τ declined. This is to be expected, since the exponentiality of the decay curve is influenced by the degree of scatter, yielding a somewhat more complex decay scheme (eq 4), but at the same time providing more information on the α component.

Even the apparently impossible problem of deconvoluting a 2.5-ns lifetime with $\alpha = 10$ yielded noisy but useful results. The RSD in this case was only 16% for 10^4 peak counts which

Anal. Chem. **1984**, *56*, 85–88 **85**

is the standard signal level in many SPC experiments.

We have also verified that the parameters calculated from the PP method yield statistically valid fits. Using the least squares K, τ, and α, we regenerated $D(t)$ using eq 1 and compared the resultant curve with the original data using a χ^2 test (*12*). The reduced χ^2's typically ranged from 0.9 to 1.1 which is acceptable for 200 data points (*12*).

All data fits are unweighted, and in view of the excellent results, we recommend the use of unweighted fits for the range of parameters and fits indicated. Unweighted fits are easier to do, and the much more complex weighted data treatment appears unwarranted. This conclusion is the same as that reported by Greer et al. (*4*) for deconvolution of single exponential decays using the phase-plane method and also is consistent with the results of the PP method derived for base line correction of exponential decays (*13*).

There is a potential problem with the treatment presented here when used with SPC data. These instruments actually measure the integral of the number of photons collected over the preceding time window rather than the instantaneous intensity. If too low a density of points is used, then the PP method, which is an integral method, gives systematic errors in the phase-plane plots and the evaluated parameters. However, for virtually all SPC data, the density of the data points is high enough so that the error should be negligible. Jezequel et al. (*8*) pointed out this error source and described a simple way to circumvent it should the errors ever become significant. When the PP method is used with analog data, this error source is not present.

We conclude that for a reasonable range of decay parameters and fitting regions, the modified PP equation is accurate and precise. The method can be easily programmed and is computationally very fast. These features give the PP method distinct advantages over much slower nonlinear least-squares methods, especially in view of the increasing use of microcomputers in data acquisition systems.

ACKNOWLEDGMENT

We thank J. C. Andre for providing preprints of his manuscript and J. Y. Jezequel for helpful comments.

LITERATURE CITED

(1) Birks, J. B. "Photophysics of Aromatic Molecules"; Wiley-Interscience, New York, 1970.
(2) Demas, J. N. "Excited State Lifetime Measurements"; Academic Press: New York, 1983.
(3) Demas, J. N.; Adamson, A. W. *J. Phys. Chem.* **1971**, *75*, 2463.
(4) Greer, J. M.; Reed, F. W.; Demas, J. N. *Anal. Chem.* **1981**, *53*, 710.
(5) Isenberg, I.; Dyson, R. D. *Biophys. J.* **1969**, *9*, 1337.
(6) Bernalte, A.; Lepage, J. *Rev. Sci. Instrum.* **1969**, *40*, 71.
(7) Huen, T. *Rev. Sci. Instrum.* **1969**, *40*, 106.
(8) Jezequel, J. Y.; Bouchy, M.; Andre, J. C. *Anal. Chem.* **1982**, *54*, 2199.
(9) Love, J. C.; Demas, J. N. *Rev. Sci. Instrum.* in press.
(10) Reed, F. W.; Demas, J. N. "Time Resolved Fluorescence Spectroscopy in Biochemistry and Biology", Cundall, R. B., Dale, R. E., Eds.; Plenum Press: New York, 1983; p 285.
(11) Knuth, P. E. "Seminumerical Algorithms. The Art of Computer Programming"; Addison-Wesley: Reading, MA, 1969; Vol. 1.
(12) Bevington, P. R. "Data Reduction and Error Analysis for the Physical Sciences"; McGraw-Hill: New York, 1969.
(13) Bacon, J. R.; Demas, J. N. *Anal. Chem.* **1983**, *55*, 653.

RECEIVED for review July 29, 1983. Accepted October 3, 1983. We gratefully acknowledge the donors of the Petroleum Research Fund, administered by the American Chemical Society, the Air Force Office of Scientific Research (Chemistry) (Grant AFOSR 78-3590), the Department of Energy for SERI Grant DE-FG02-CS84063, and the National Science Foundation (CHE 82-06279).

Optimization of Anion Separation by Nonsuppressed Ion Chromatography

Dennis R. Jenke and Gordon K. Pagenkopf*

Department of Chemistry, Montana State University, Bozeman, Montana 59717

The effect of eluent pH and eluent species concentration on the nonsuppressed ion chromatographic separation of anions has been studied. The retention times of Cl^-, Br^-, NO_3^-, SO_4^{2-}, and $S_2O_3^{2-}$ were determined over a large range of eluent compositions and the data were utilized to construct window diagrams. These window diagrams were used to optimize eluent composition for the separation of two or more analytes. In virtually every case resolution is limited by the separation of the NO_3^-/Br^- pair.

Since its introduction in 1975, ion chromatography has rapidly evolved into a widely accepted method for the quantitative determination of anions in aqueous samples (*1*). Single column or nonsuppressed ion chromatographic techniques have been successful in a variety of applications (*2*). As is the case with all chromatographic techniques, the most effective utilization of the ion chromatographic process requires accurate characterization of the analyte retention times and identification of analytical variables that affect the relative retention characteristics of the analytes. Of particular interest is the development of a predictive capability and optimization of ion chromatographic resolution, while minimizing analysis time. This can be complicated by the potential existence of multiple optima and the large range of eluent related variables that control chromatographic separation.

The concept of "window diagrams" has been utilized to locate optimum conditions in gas chromatography (*3, 4*). This technique also has been applied to high-performance liquid chromatographic separations (*5–8*). This study utilizes the technique to optimize the separation of inorganic ions and to predict the behavior of selected analytes under various experimental conditions.

EXPERIMENTAL SECTION

The chromatographic system employed consisted of a Perkin-Elmer Series 3B liquid chromatograph, a Vydac Model 3021 C4.6 anion separator column, a Vydac Model 6000CD conductivity detector, and a Sargent Welch XKR strip chart recorder. Injector sample loop volume was 0.10 mL and samples of 0.5 mL were injected with a Hamilton Co. Model 750 microliter syringe. Laboratory temperature was maintained at 22.5 ± 2.0 °C and the

0003-2700/84/0356-0085$01.50/0 © 1983 American Chemical Society

Table I. Legend for Analyte Pairs in Window Diagrams

diagram designation	analyte pair	diagram designation	analyte pair
1	SO_4^{2-}, Cl^-	6	$S_2O_3^{2-}$, Br^-
2	SO_4^{2-}, NO_3^-	7	$S_2O_3^{2-}$, NO_3^-
3	SO_4^{2-}, Br^-	8	NO_3^-, Cl^-
4	$S_2O_3^{2-}$, SO_4^{2-}	9	NO_3^-, Br^-
5	$S_2O_3^{2-}$, Cl^-	10	Br^-, Cl^-

active chromatographic components were thermally isolated to minimize the effect of short-term temperature fluctuations (*9*). Thirty-two phthalate eluents with a pH range of 3.8 to 6.0 and a total concentration range of 1.0 to 6.0 × 10^{-3} M were prepared from the potassium salt. KOH (0.1 M) was used for pH adjustment. Final pH measurement was made after degassing under suction. Stock analyte solutions (0.10 M) were prepared by dissolution of NaCl, $NaNO_3$, Na_2SO_4, $Na_2S_2O_3$, and KBr in doubly distilled water. Standard solutions of the analytes, 0.2, 2.0, and 10.0 × 10^{-3} M, were prepared by diluting the stock solutions with the desired eluent. This minimized the solvent dip in the chromatogram. Retention times were measured at maximum peak height of the recorded chromatogram and each analysis was done in triplicate. The retention time data have been previously presented (*10*). A flow rate of 2–3 mL/min for 1.5 h was used to allow the chromatographic system to equilibrate when the eluent was changed.

RESULTS AND DISCUSSION

By convention, window diagrams express the relationship between retention characteristics of two analyte species and an operational variable of the chromatographic system. In this study, the relationship is the relative reduced retention ratio α which is defined as

$$\alpha = \frac{t_A - t_V}{t_B - t_V} \qquad (1)$$

t_A is the retention time of analyte species A, t_B is the retention time of analyte B, and t_V is the time equivalent of the void volume. Values of t_A and t_B are readily obtained from the chromatograms while t_V is estimated from the appearance time of the solvent dip.

The operational variable is the eluent composition which, for a nonsuppressed chromatographic system, is regulated by the pH and the total phthalate concentration. Since pH and total eluent concentrations vary, three-dimensional diagrams may be generated; however, their interpretation is complicated by the large amount of data. As a consequence two-dimensional iso-pH and iso-total phthalate contours are presented.

When α equals 1.0, the two analyte peaks overlap. In addition, α is always kept greater than 1 by reversing the pairs, i.e., $t_A \geq t_B$. As α increases, the relative separation between the two pairs increases. Changes in α and the operational parameters are sizable and thus log–log diagrams are utilized.

The identification numbers for the 10 ion pairs arising from the combinations of Cl^-, Br^-, NO_3^-, SO_4^{2-} and $S_2O_3^{2-}$ are listed in Table I. A plot of log α vs. log P_T at pH 3.8 is shown in Figure 1 and the pH 6.0 data are shown in Figure 2.

The values of log α are independent of the total eluent concentrations provided that the charges of the analytes are the same (pairs 4, 8, 9, 10). This is not the case when divalent and monovalent ions are compared. Divalent retention times decrease more rapidly than the monovalent retention times as the eluent concentration increases. The slopes of the divalent–monovalent lines are the same at any given pH but they do not change with pH. This change is due to species distribution change within the eluent.

The bottom line of the window diagram identifies the pair with poorest resolution and the top line identifies the pair with best resolution. As a consequence, the bottom of the diagram limits optimization in terms of resolution whereas the top limits in terms of analysis time. The ratio of elution time for the last eluted anion and the first eluted anion will be largest and, thus will limit the analysis time. In Figure 1 the only optimization available is analysis time which decreases as total phthalate concentration increases. Resolution is limited by the NO_3^-–Br^- pair, number 9. As eluent pH increases, the divalent retention times are significantly reduced and the bottom of the diagram is determined by the separation of the SO_4^{2-}–NO_3^- pair at the highest eluent concentration; see Figure 2 (line 2). At pH 6.0 the optimum conditions occur at log P_T = −2.43, the intersection of lines 2 and 9. For P_T concen-

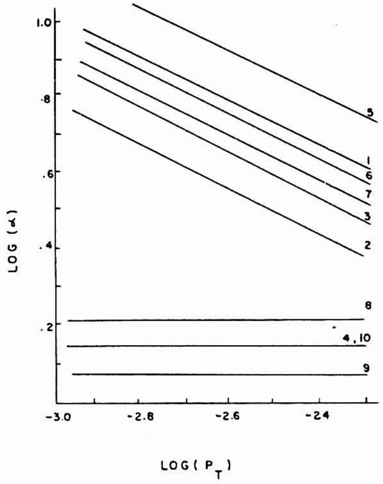

Figure 1. Window diagram for variable eluent concentration pH 3.8.

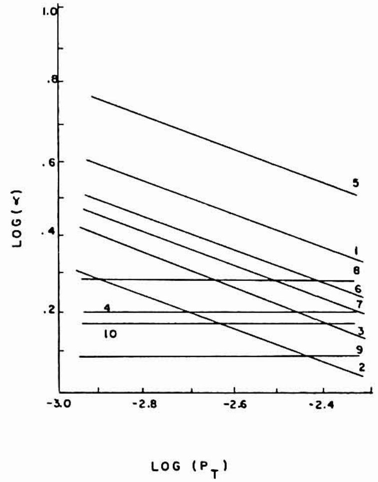

Figure 2. Window diagram for variable eluent concentration pH 6.0.

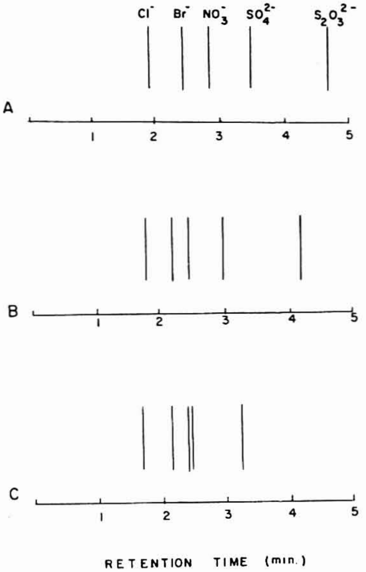

Figure 3. Calculated retention times for different total eluent concentrations, pH 6.0. For A, $P_T = 3 \times 10^{-3}$ M, for B, $P_T = 3.7 \times 10^{-3}$ M, and for C, $P_T = 5 \times 10^{-3}$ M. Typical peak widths at the base are 0.4 min. The elution order is Cl^-, Br^-, NO_3^-, SO_4^{2-}, and $S_2O_3^{2-}$.

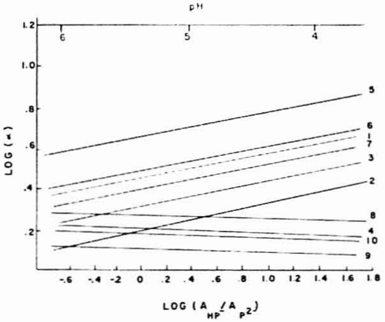

Figure 4. Window diagram for total phthalate concentration of 3×10^{-3} M, pH varies from 6.0 to 3.8.

trations greater than this value, the analysis time is reduced but resolution is sacrificed. At log P_T less than −2.43 resolution does not change whereas analysis time increases.

The absolute retention times cannot be obtained from Figures 1 and 2; however, with knowledge of the retention time of one analyte and t_V, the retention times of the other analytes may be calculated by using eq 1. A graphical presentation of the change in retention time at the P_T values cited above is shown in Figure 3. By reduction of P_T from 3.7×10^{-3} M to 3.0×10^{-3} M the analysis time increases from 4.1 min to 4.8 min with no change in resolution. When P_T increases to 5.0×10^{-3} M sulfate and nitrate peaks become indistinguishable but analysis time is reduced to 3.2 min.

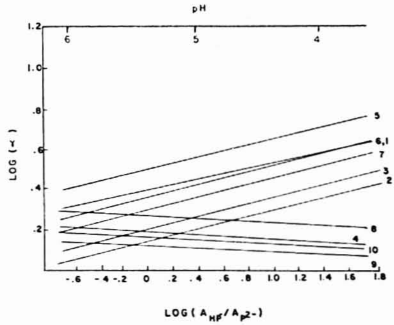

Figure 5. Window diagram for total phthalate concentration of 5×10^{-3} M, pH varies from 6.0 to 3.8.

Table II. Comparison of Predicted and Observed Retention Times

eluent	species	retention time, min	
		predicted	observed
3.5×10^{-3} M KHP pH 5.85	Cl^-	1.78	1.74
	Br^{-a}	2.16	2.16
	NO_3^-	2.45	2.45
	SO_4^{2-}	2.83	2.84
	$S_2O_3^{2-}$	3.70	3.73
1.0×10^{-3} M KHP pH 4.00	Cl^{-a}	2.65	2.65
	NO_3^-	3.74	3.58
	Br^-	3.34	3.23
	SO_4^{2-}	13.56	14.00
1.0×10^{-3} M KHP pH 4.20	Cl^{-a}	3.63	3.63
	NO_3^-	6.50	6.55
	SO_4^{2-}	18.40	18.40
1.0×10^{-3} M KHP pH 5.20	Cl^{-a}	2.00	2.00
	NO_3^-	2.72	2.63
	SO_4^{2-}	5.30	5.15

[a] Analyte used as reference peak.

Figures 4 and 5 demonstrate the change in the window diagrams as the pH varies. The conclusions are similar to those previously presented with analysis time being regulated by $S_2O_3^{2-}$–Cl^- separation (line 5).

At low pH, resolution is limited by the NO_3^-–Br^- pair (line 9) whereas at high pH, the SO_4^{2-}–NO_3^- pair (line 2) determines the resolution. Once again the intersection of lines 2 and 9 represents optimum chromatographic conditions, and as P_T increases the pH at which this interaction occurs decreases. The slopes of the lines in Figures 4 and 5 are not parallel because of the relative elution capability of HP^- and P^{2-}. As their distribution changes, so does the net elution efficiency and thus nonparallel lines.

Since the α values are relative, they should be applicable to any column with the same packing material. While the absolute magnitude of the retention times will be a function of column size and flow rate, the relative ratio is only a function of selectivity. The agreement between data obtained for two Vydan columns appears to be quite good. Linear least squares provides a slope of 0.935. The absolute retention times differed by approximately 20%.

In addition to their ability to facilitate the optimization of the chromatographic process, window diagrams provide a means of predicting the retention profile of any suite of analyte species in response to eluent compositional changes over which such diagrams are defined. The linear nature of the window diagrams for nonsuppressed ion chromatography allows for

Anal. Chem. 1984, 56, 88–91

accurate exptrapolation and interpolation of the α values. With t_V and the retention time of one analyte, t_A, the retention time of the other analytes can be predicted from eq 1. This has been done for a series of snow melt samples. The results are summarized in Table II. In all cases the agreement is within ±3% RSD which is equivalent to the experimental precision.

LITERATURE CITED

(1) Small, H.; Stevens, T.; Bauman, W. *Anal. Chem.* **1975**, *47*, 4801.
(2) Girard, J. E.; Glatz, J. A. *Am. Lab.* (*Fairfield, Conn.*) **1981**, *13* (11), 26.
(3) Laub, R. J.; Purnell, J. H. *J. Chromatogr.* **1975**, *112*, 71.
(4) Laub, R. J.; Purnell, J. H. *Anal. Chem.* **1976**, *48*, 1720.
(5) Demming, S. N.; Turoff, M. L. *Anal. Chem.* **1978**, *50*, 546.
(6) Price, W. P., Jr.; Demming, S. N. *Anal. Chim. Acta* **1979**, *108*, 22
(7) Price, W. P., Jr.; Edens, R.; Hendrix, D. L.; Demming, S. N. *Anal. Biochem.* **1979**, *93*, 233.
(8) Sachok, B.; Strawahan, J. J.; Demming, S. N. *Anal. Chem.* **1981**, *53*
70.
(9) Jenke, D. R.; Pagenkopf, G. K. *Anal. Chem.* **1982**, *54*, 2603.
(10) Jenke, D. R. Ph.D. Thesis, Montana State University, 1983.

RECEIVED for review May 31, 1983. Accepted October 11, 1983. This research was supported in part by the Office of Wat Resources Research, U.S. Department of Interior throug project A-138 MONT.

Models for Prediction of Retention in Nonsuppressed Ion Chromatography

Dennis R. Jenke and Gordon K. Pagenkopf*

Department of Chemistry, Montana State University, Bozeman, Montana 59717

The retention behavior of Br^-, NO_3^-, Cl^-, SO_4^{2-}, and $S_2O_3^{2-}$ in nonsuppressed ion chromatography is studied as a function of changing eluent composition. Three models, multiple species eluent, single species eluent, and single interaction sites, are utilized to predict chromatographic behavior. While all three are based on a thermodynamic equilibrium consideration of the ion exchange process, they differ in their characterization of the analyte/eluent competition or the ion/resin interaction. Despite this difference in approach, all three models effectively characterize the behavior of the analytes under elution conditions which are of practical importance. The relative utility of each model is discussed.

Ion chromatography has rapidly evolved into an accepted method for the determination of solute species in liquid samples (*1*, *2*), and correspondingly characterization and modeling of the separation process are critical for method optimization and subsequent development. The current models are based upon an equilibrium distribution of analyte and eluent between the mobile phase and the resin ion exchange sites (*3*, *4*). These models differ through the definition of the number of active components in the mobile phase that participate in the chromatographic separation. The single active species model (*3*) for nonsuppressed anion chromatography utilizes the phthalate dianion as the active eluent. A multiple active species model (*5*) has been used to predict the chromatography of arsenate and orthophosphate.

Three models, multiple species eluent, single species eluent, and single interaction sites have been utilized to predict the chromatographic behavior of chloride, bromide, nitrate, sulfate, and thiosulfate. These models are an extension of the ion-exchange theory developed by Mayer and Tompkins (*6*) with appropriate modifications.

Multiple Species Eluent. The equations used to model the multiple eluent treatment are similar to those previously developed for suppresed ion chromatography (*4*). There are four basic considerations.

(1) The reduced retention volume of the analyte, U, is equal to the volumetric distribution coefficient (*6*). In this case

$$U_{\mathrm{A}} = D_{\mathrm{A}} \qquad (1$$

where U_{A} is equal to the observed retention volume min the void volume. D_{A} is the ratio of analyte in the resin solution phases associated with a given theoretical pla

(2) All of the "available" exchange sites are occupi eluent anions and therefore the effective column capac given by

$$Q_{\mathrm{e}} = \sum_X m[\mathrm{E}_X{}^{m-}]$$

where m is the ionic charge.

(3) Electroneutrality is maintained during the elut process by exchange of charged species.

(4) For anions interacting with a strong base anion exchanger, the following equilibrium is established at the resin sites. The equilibrium constant for this reaction is defined as the selectivity coefficient, $K_{\mathrm{A\text{-}E}}$.

$$(\mathrm{A}^{n-}) + n/m(\mathrm{E\text{-}Rn}) = n/m(\mathrm{E}^{m-}) + (\mathrm{A\text{-}Rn}) \qquad (3)$$

$$K_{\mathrm{A\text{-}E}} = \frac{(A_{\mathrm{E}^{m-}})^{n/m}(A_{\mathrm{A\text{-}Rn}})}{(A_{\mathrm{E\text{-}Rn}})^{n/m}(A_{\mathrm{A}^{n-}})} \qquad (4)$$

Experimental observations were made with phthalate eluents. For the multiple eluent treatment, HP^- and P^{2-} are assumed to be active eluents and eq 2 becomes

$$Q_{\mathrm{e}} = A_{\mathrm{HP\text{-}Rn}} + 2A_{\mathrm{P\text{-}Rn}} \qquad (5)$$

Use of eq 4 to describe eluent/eluent and analyte/eluent exchange and substitution into eq 5 provides

$$Q_{\mathrm{e}} = A_{\mathrm{HP\text{-}Rn}} + \frac{2K_{\mathrm{P\text{-}HP}}A_{\mathrm{P}}}{(A_{\mathrm{HP}})^2}(A_{\mathrm{HP\text{-}Rn}})^2 \qquad (6)$$

The volumetric distribution coefficient for analyte A is expressed as

$$D_{\mathrm{A}} = K_{\mathrm{A\text{-}E}}(D_{\mathrm{E}})^{n/m} \qquad (7)$$

and for a monovalent eluent–divalent analyte

$$U_{2\mathrm{M}} = D_{\mathrm{A}} = K_{\mathrm{A\text{-}HP}}D_{\mathrm{E}}{}^2 = K_{\mathrm{A\text{-}HP}}\left(\frac{A_{\mathrm{HP\text{-}Rn}}}{A_{\mathrm{HP}}}\right)^2 \qquad (8)$$

0003-2700/84/0356-0088$01.50/0 © 1983 American Chemical Society

Models for Prediction of Retention in Nonsuppressed Ion Chromatography

Dennis R. Jenke and Gordon K. Pagenkopf (*Anal. Chem.* 1984, *56*, 88–91).

On page 88 eq 8 is written

$$U_{2M} = D_A = K_{A\text{-}HP}D_E{}^2 = K_{A\text{-}HP}\frac{(A_{HP\text{-}Rn})^2}{A_{HP}}$$

The parentheses in the last term should be extended to include both the numerator and denominator of that ratio, thus the final equivalence should read

$$K_{A\text{-}HP}\left(\frac{A_{HP\text{-}Rn}}{A_{HP}}\right)^2$$

While visually the change is small, it has a profound effect on the mathematical development which proceeds from that point.

In eq 9, 11, and 12 the quantity which appears under the radical sign should be

$$1 + \frac{8A_pK_{P\text{-}HP}Qe}{(A_{HP})^2}$$

(in eq 9) or in eq 11 and 12 the same form but with the equivalent substitution for A_{HP}.

Anal. Chem. 55 (7) 1984 : 1200

corrected
A.J.
270822

on

Solution of eq 6 for $A_{\text{HP-Rn}}$ and substitution into eq 8 provides

$$U_{2\text{M}} = \frac{K_{\text{A-HP}}(A_{\text{HP}})^2}{16K^2_{\text{P-HP}}(A_{\text{P}})^2}\left(\sqrt{\frac{1 + 8A_{\text{P}}K_{\text{P-HP}}Q_{\text{e}}}{(A_{\text{HP}})^2}} - 1\right)^2 \tag{9}$$

Experimental conditions are quoted in terms of total eluent concentration and hydrogen ion activity. For the phthalate system

$$E_{\text{T}} = [\text{H}_2\text{P}] + [\text{HP}^-] + [\text{P}^{2-}] \tag{10}$$

By use of the α notation, $[\text{HP}^-] = E_{\text{T}}\alpha_{\text{HP}}$, $A_{\text{HP}} = f_{\text{HP}}E_{\text{T}}\alpha_{\text{HP}}$, and $A_{\text{P}} = f_{\text{P}}E_{\text{T}}\alpha_{\text{P}}$ where f_{HP} and f_{P} are the mean ionic activity coefficients (*7*). Substitution into eq 10 and use of the second acid dissociation constant for phthalic acid provides

$$U_{2\text{M}} = \left(\frac{K_{\text{A-HP}}}{16K^2_{\text{P-HP}}}\right) \times \left(\frac{(A_{\text{H}})^2}{(K_{\text{a2}})^2}\right)\left(\sqrt{\frac{1 + 8K_{\text{P-HP}}Q_{\text{e}}f_{\text{P}}\alpha_{\text{P}}}{f^2_{\text{HP}}\alpha^2_{\text{HP}}E_{\text{T}}}} - 1\right)^2 \tag{11}$$

and in the same manner

$$U_{1\text{M}} = \left(\frac{K_{\text{A-HP}}}{4K_{\text{P-HP}}}\right)\left(\frac{A_{\text{H}}}{K_{\text{a2}}}\right)\left(\sqrt{\frac{1 + 8K_{\text{P-HP}}Q_{\text{e}}f_{\text{P}}\alpha_{\text{P}}}{f^2_{\text{HP}}\alpha_{\text{HP}}{}^2E_{\text{T}}}} - 1\right) \tag{12}$$

Single Species Eluent. When the only active eluent species is P^{2-}, Q_{e} becomes $Q_{\text{e}} = 2A_{\text{P-Rn}}$ and a derivation similar to that presented above provides

$$U_{2\text{S}} = \frac{K_{\text{A-P}}Q_{\text{e}}}{E_{\text{T}}f_{\text{P}}\alpha_{\text{P}}} \tag{13}$$

$$U_{1\text{S}} = \left(\frac{K_{\text{A-P}}Q_{\text{e}}}{2E_{\text{T}}f_{\text{P}}\alpha_{\text{P}}}\right)^{1/2} \tag{14}$$

Single Site Interaction. The resin used in these studies had a silica support and quaternary exchange sites. From the column capacity (4.9×10^{-4} mol), weight of the resin (2.9 g), and surface area 95 m^2/g, the average surface area per site is calculated to be 94 Å^2 (*8*). The area occupied by analyte and eluent anions is significantly less than this, approximately 30 Å^2, and thus if the exchange sites are evenly distributed, a divalent ion is too small to simultaneously interact with more than one adjacent site at any given time. In this situation, species charge will not affect the total number of column/species interactions which can occur but will affect the stability of the interaction. Under these conditions the effective column capacity becomes

$$Q_{\text{e}} = A_{\text{HP-Rn}} + A_{\text{P-Rn}} \tag{15}$$

which when coupled with a derivation similar to those used previously yields

$$U_{\text{A}} = \frac{K_{\text{A-HP}}Q_{\text{e}}}{E_{\text{T}}\alpha_{\text{HP}}f_{\text{HP}} + K_{\text{P-HP}}E_{\text{T}}\alpha_{\text{P}}f_{\text{P}}} \tag{16}$$

EXPERIMENTAL SECTION

The chromatographic system consisted of a Perkin-Elmer Series 3B liquid chromatograph, a Vydac Model 3021 C4.6 anion separator column, a Vydac Model 6000 CD conductivity detector, and a Sargent Welch strip chart recorder. The injection loop was 0.100 mL. The chromatographic components were thermally insulated to minimize short-term temperature variations (*9*). The eluent was prepared from reagent grade potassium hydrogen phthalate with pH being monitored after degassing under vacuum and controlled by addition of KOH. When eluent solutions were changed, the system was flushed at 2 mL/min for at least 1 h. Stock solutions (0.10 M) of NaCl, NaNO$_3$, Na$_2$SO$_4$, Na$_2$S$_2$O$_3$, and KBr were prepared from their reagent grade salts. The standard solutions were diluted with the desired eluent in order to minimize solvent dips in the chromatograms. All samples were analyzed in triplicate with a flow rate of 2–3 mL/min.

Table I. Retention Times of Analytes

total phthalate, 10^{-3} M	pH	retention time,[a] min				
		NO_3^-	Cl^-	Br^-	SO_4^{2-}	$\text{S}_2\text{O}_3^{2-}$
1.0	3.75	6.97	4.87	6.21	40.42	52.67
1.0	4.60	4.87	3.23	4.21	12.75	17.00
1.0	5.07	4.32	2.85	3.75	9.50	13.27
1.0	5.57	4.13	2.69	3.53	8.13	11.44
1.0	6.01	3.82	2.58	3.29	7.26	9.77
2.0	3.85	5.44	3.66	4.69	18.70	23.58
2.0	4.53	4.18	2.83	3.62	9.47	12.37
2.0	4.94	3.58	2.41	3.11	6.25	8.76
2.0	5.40	3.48	2.26	2.98	5.04	7.15
2.0	5.82	3.29	2.19	2.85	4.65	6.61
2.5	4.57			2.71	5.47	
2.5	5.39			2.41	3.88	
2.5	5.95			2.38	3.56	
3.0	3.82	4.02	2.79	3.53	9.37	13.65
3.0	4.54	3.30	2.32	2.90	5.76	7.45
3.0	4.80	3.09	2.16	2.71	4.71	6.39
3.0	5.42	2.91	1.96	2.53	3.52	4.80
3.0	5.89	2.82	1.93	2.47	3.42	4.68
3.5	4.61			2.41	4.33	
3.5	5.14			2.26	3.26	
3.5	5.85			2.16	2.81	
4.0	3.82	5.29	3.01	3.15	9.00	15.03
4.0	4.26	4.66	2.66	2.78	6.69	10.20
4.0	4.60	4.31	2.41	2.54	5.35	8.33
4.0	5.00	4.03	2.26	2.33	4.38	6.75
4.0	5.38	3.88	2.14	2.25	3.68	5.79
4.0	5.95	3.82	2.09	2.21	3.35	5.18
5.0	3.75	3.18	2.36	2.84	6.33	8.30
5.0	4.54	2.55	1.95	2.35	3.75	4.70
5.0	4.96	2.42	1.84	2.19	3.08	3.88
5.0	5.39	2.37	1.77	2.14	2.70	3.42
5.0	5.98	2.35	1.73	2.10	2.45	3.13
6.0	4.14			2.18	3.69	
6.0	4.60			2.08	2.98	
6.0	4.79			1.98	2.65	

[a] Flow rate of 3 mL/min.

Activity coefficients were predicted by the extended Debye–Hückel equation. The pK_{a} values for phthalic acid are 3.10 and 5.40 (*7*). The retention times for the analyte ions were obtained from the graphical display and are corrected for the dead volume equivalent. The latter was considered to be equal to the time required for the cations to move through the column. The reduced retention volume (U_i) was converted to the retention time by addition of the void volume and dividing by the eluent flow rate.

All concentrations and the column capacity are expressed in terms of interaction equivalent, the moles of exchange sites per 100 μL of sample, and moles of eluent per 100 μL.

RESULTS AND DISCUSSION

Multiple Eluent Species. The elution behavior of the five analyte anions at various elution concentrations and pH values is listed in Table I. In general the retention times decrease as pH and total eluent increase.

Modeling of the observed chromatographic behavior with eq 11 and 12 requires an evaluation of the analyte–eluent and eluent–eluent selective coefficients. These constants may be obtained from batch experiments (*10*), calculated with other mathematical theories (*11–16*), or obtained from observed retention times. The latter was used in these studies. The observed retention times and the maximum column capacity are substituted into eq 11 and 12 providing a sequence of

Table II. Selectivity Coefficients for Multiple Eluent Species Model[a]

constant	value	constant	value
$K_{Cl\text{-}HP}$	0.916 ± 0.046	$K_{HP\text{-}P}$	20.0 ± 1.0
$K_{Br\text{-}HP}$	1.384 ± 0.069	$K_{P\text{-}HP}$	0.0500 ± 0.0025
$K_{NO_3\text{-}HP}$	1.707 ± 0.085	$K_{SO_4\text{-}HP}$	0.0844 ± 0.0055
		$K_{S_2O_3\text{-}HP}$	0.125 ± 0.008

[a] See eq 4, $Q_e = 1.51 \times 10^{-5}$ mol/interaction equiv. Interaction equivalent = moles of exchange sites per sample volume (100 μL).

equations with two unknowns. This set of equations is solved by iterative minimization of the variability in $K_{A\text{-}HP}$ for a given value of $K_{HP\text{-}P}$. The values of the selective coefficients are summarized in Table II.

The magnitude of the constants increases as one goes from chloride to bromide to nitrate. This is expected since it parallels the order of elution. The greater the value of the constant, the greater the interaction with the resin and thus a longer retention time. Comparison of the divalent analyte–monovalent eluent constants indicates that P^{2-} is preferentially bound by the column with $S_2O_3^{2-}$ being retained more extensively than SO_4^{2-}. For the latter two this is in agreement with the observed retention times. Since P^{2-} is preferentially bound to the column, it takes many void volumes for the column to reach equilibrium with the eluent as the pH is lowered.

A comparision of predicted and observed retention times for bromide using the multiple species eluent treatment provides a slope of 1.00, intercept = 0.01, $R = 0.991$, and av RSD = 2.6%. A similar comparison for sulfate using the multiple species eluent treatment yields a slope of 0.96, intercept of 0.14, $R = 0.998$, and av RSD = 2.69%. The RSD values for chloride, nitrate, and thiosulfate are 2.3, 2.5, and 4.1%, respectively. The model does a particularly poor job of predicting the retention time at the lowest eluent concentrations and lowest pH values. In these cases the model predicts retention times much longer than those observed. Experimental observations indicate that the column does not have as much capacity at the low eluent, low pH conditions. This could be caused by resin swelling within a confined volume. As the resin swells some sites could become unavailable for interaction with the eluent and the analytes. Experimentally it is noted that there is a 13% decrease in void volume over the range of a eluent concentrations used and implies an increase in resin volume. It also has been observed that nonexchange adsorption and resin invasion can occur as the eluent concentration increases (*17*). In summary this model is applicable provided the total eluent concentration is greater than 2×10^{-3} M and the pH is greater than 4.

Single Eluent Species. At an eluent pH of 6, phthalate speciation is dominated by the P^{2-} ion and analyte elution can effectively be described by eq 13 and 14. Since the resin selectivity for P^{2-} vs. HP^- is large, P^{2-} controls analyte elution behavior even under conditions where the eluent is dominated by HP^-. The elution behavior of both Br^- and SO_4^{2-} approach linearity above a pH 4.6 Below this pH, HP^- contributes to analyte elution and the model becomes ineffective. Elution behavior and eluent compositions for the eluents whose pH is greater than 4.6 have been used to generate the respective selectivity coefficients. The values of $K_{A\text{-}P}$ are summarized in Table III. These coefficients cannot be directly compared to those obtained for the multiple species eluent treatment since the analytes are only related to P^{2-}. The magnitude of the coefficients for a given analyte charge accurately reflect the observed elution sequence. However, there is no continuity in trend with varying analyte charge since the mathematical forms of eq 11 and 12 differ.

Table III. Selectivity Coefficients for Single Species Eluent Model

constant	value[a]	constant	value[a]
$K_{Cl\text{-}P}$	16.2 ± 2.2	$K_{SO_4\text{-}P}$	1.48 ± 0.22
$K_{Br\text{-}P}$	34.4 ± 5.9	$K_{S_2O_3\text{-}P}$	2.14 ± 0.26
$K_{NO_3\text{-}P}$	41.7 ± 7.0		

[a] Values obtained by using data with a pH of 4.6 or greater.

Table IV. Selectivity Coefficients for Single Site Exchange Model

constant	value	constant	value
K_{CHIP}	0.80 ± 0.09	$K_{P\text{-}HP}$	2.33 ± 0.20[a]
$K_{Br\text{-}HP}$	1.21 ± 0.12		6.67 ± 0.88[b]
$K_{NO_3\text{-}HP}$	1.49 ± 0.14	$K_{SO_4\text{-}HP}$	4.93 ± 0.69
		$K_{S_2O_3\text{-}HP}$	6.82 ± 0.90

[a] Calculated by use of monovalent analyte ions.
[b] Calculated by use of divalent analyte ions.

The agreement between predicted and observed retention time for sulfate provides an av RSD = 5.0% for the data with a pH of 4.6 or greater. Extreme deviation is observed when the pH is less than 4.6 due to the contribution of HP^- to the elution process. Similar agreement was obtained for the other four anions.

Single Site Interaction. Equation 16 describes the relationship between eluent composition and retention volume under single site interaction conditions and, coupled with elution behavior and eluent composition data, can be used to generate selectivity coefficients as described previously. For a sample set which contains all analytes regardless of charge, the calculated value of $K_{P\text{-}HP}$ is (4.50 ± 0.75). Use of this value to predict analyte retention results in significantly poorer agreement than that observed with the other models. Under such conditions observed and predicted analyte retention behavior differ by ±7.7% and ±6.1% RSD for Br^- and SO_4^{2-}, respectively. If the data are divided into two sets as a function of charge, selectivity coefficients are calculated that produce better agreement between predicted and observed retention times. Once again, the magnitude of these coefficients, as documented in Table IV, accurately reflects the elution sequence of the analytes. The agreement between observed and predicted behavior using these coefficients provides a slop = 1.05, $R = 0.958$, and av RSD = 3.55% for bromide. For eluents with a phthalate concentration greater than 2×10^{-3} M, the fit is similar to that obtained with the single eluent model but is inferior to that obtained for the multiple species eluent model. Both the single site and multispecies models are unable to accurately model the chromatographic behavior at low pH and 1×10^{-3} M total phthalate eluent. As observed previously, it is suggested that this behavior reflects variability in the effective column capacity.

It is not known why two values of $K_{P\text{-}HP}$ provide a better fit for this model. Possible explainations could include the presence of charge specific sites or potassium playing a role as a counterion in the interaction between dissimilarly charged species.

CONCLUSIONS

None of the proposed models is capable of predicting chromatographic behavior under low eluent, low pH conditions. Specifically the retention times are overestimated and can be attributed to a decrease in column capacity with these conditions. The agreement between observed and predicted retention times when total phthalate concentration is greater than 2×10^{-3} M and a pH greater than 4.6 is best for the multiple species eluent model by a factor of approximately

Table V. Ratio of $K_{A\text{-}HP}$ Coefficients

	mathematical treatment used		
	multiple species eluent	single species eluent	single site
Cl^-/NO_3^-	0.54 ± 0.05	0.41 ± 0.11	0.55 ± 0.11
Cl^-/Br^-	0.67 ± 0.07	0.50 ± 0.15	0.67 ± 0.14
Br^-/NO_3^-	0.81 ± 0.06	0.86 ± 0.13	0.82 ± 0.13
$SO_4^{2-}/S_2O_3^{2-}$	0.68 ± 0.09	0.73 ± 0.17	0.75 ± 0.20

2. The single site and single eluent models are comparable; however, the applicable pH range for the single site approach is larger.

The mathematical treatments for these models provide selectivity coefficients that differ widely in magnitude. There is consistency within the models as evidenced by the ratios of the selectivity coefficients, Table V. The values for a particular pair are not statistically different. The results obtained for the other anions are comparable to those shown for bromide and sulfate.

Registry No. Br^-, 24959-67-9; NO_3^-, 14797-55-8; Cl^-, 16887-00-6; SO_4^{2-}, 14808-79-8; $S_2O_3^{2-}$, 14383-50-7; phthalic acid, 88-99-3.

LITERATURE CITED

(1) Fritz, J. S.; Gjerde, D. T.; Pohlandt, C."Ion Chromatography"; Heuthig: Heidelburg, 1982.
(2) Pohl, C. A.; Johnson, E. L. *J. Chromatogr. Sci.* **1980**, *18*, 442.
(3) Gjerde, D. T.; Schmuchkler, G.; Fritz, J. S. *J. Chromatogr.* **1980**, *187*, 35.
(4) Hoover, T. B. *Sep. Sci. Technol.* **1982**, *17*, 295.
(5) Hoover, T. B.; Yager, G. "Ion Chromatography of Anions"; EPA-600/4-80-020; Environmental Protection Agency: Washington, DC, 1980.
(6) Mayer, S. W.; Tompkins, E. R. *J. Am. Chem. Soc.* **1947**, *69*, 2866.
(7) Pagenkopf, G. K. "Introduction to Water Chemistry"; Marcel Dekker: New York, 1978.
(8) Harrison, K., The Separations Group, Vesperis, CA, personal communication, 1982.
(9) Jenke, D. R.; Pagenkopf, G. K. *Anal. Chem.* **1982**, *54*, 2603.
(10) Kunin, R. "Elements of Ion Exchange"; Reinhold: New York, 1960.
(11) Davidson, A. W.; Argerringer, W. J., Jr. *Ann. NY. Acad. Sci.* **1953**, *57*, 105.
(12) Glueckauf, E. *Proc. R. Soc. London, Ser. A* **1952**, *214*, 207.
(13) Freeman, D. H. *J. Chem. Phys.* **1961**, *35*, 189.
(14) Soldano, B. A.; Larson, Q. V.; Meyers, G. E. *J. Am. Chem. Soc.* **1953**, *77*, 1338.
(15) Marinsky, J. A.; Reddy, M. M.; Amdur, S. *J. Phys. Chem.* **1973**, *77*, 2128.
(16) Gregor, H. P. *J. Am. Chem. Soc.* **1951**, *73*, 642.
(17) Diamond, R. M.; Witney, D. C. In "Ion Exchange"; Marissky, J., Ed.; Marcel Dekker: New York, 1966; pp 227-274.

RECEIVED for review May 31, 1983. Accepted October 11, 1983.

Computer Simulation of Light Transmission through Scattering and Absorbing Chromatographic Media

I. E. Bush* and H. P. Greeley

Research Service, Veterans Administration Medical and Regional Office Center, White River Junction, Vermont 05001

Quantitative densitometry and fluorometry of thin-layer chromatograms and other planar separation media still depend for the most part on empirical management of the problems caused by light scattering. The degree of deviation from linear calibration curves reported in the literature varies considerably. To investigate this problem, a computer model was developed which simulates the Kubelka–Munk differential equations and allows a variable number of iterations. The results from this model are compared with solutions of the same equations obtained by conventional methods of integration. With simulated layers more than 100 particles thick, the results obtained are indistinguishable from the integral solutions of the Kubelka–Munk equations for scattering powers between 0 and 20. With layers thinner than 40 particles, the model predicts significant deviations from the integral solutions over the same range of scattering powers. It seems likely that thin media commonly used for paper and thin-layer chromatography are often better approximated by the discrete step model with thicknesses equivalent to 10–40 particles, thus explaining much of the reported variability in the literature.

In their classical analysis of light transmission through absorbing and scattering media, Kubelka and Munk (*1*) proposed the pair of simultaneous differential equations

$$-\mathrm{d}I/\mathrm{d}x = -(S + K)I + SJ \qquad (1a)$$

$$\mathrm{d}J/\mathrm{d}x = -(S + K)J + SI \qquad (1b)$$

where I is the intensity of light traveling inside the specimen away from its illuminated surface, J is the intensity of light traveling inside the specimen toward its illuminated surface, S is the coefficient of scatter per unit thickness, K is the coefficient of absorption per unit thickness, and x is the distance from the unilluminated surface of the specimen. Although solution of these equations is difficult and requires further simplifying assumptions (e.g., Kubelka (*2*)), the Kubelka–Munk (K-M) theory has been used extensively in industrial applications with considerable empirical success (*3*). Its applications in analytical chemistry and to luminescence in turbid materials, however, still present difficulties (e.g., ref *4*). Thus, Vaeck (*5*) first applied the K-M theory to the densitometry of chromophores on paper chromatograms, and Ingle and Minshall (*6*), Kortüm (*7*), and Goldman and Goodall (*8*) demonstrated reasonable correspondence between the concentration of material in paper and thin-layer chromatograms (TLC) and the absorbance predicted by the theory. However, Treiber (*9*) observed better correspondence with a combination of the Beer–Lambert equation with the Kubelka and Munk theory. Hurtubise (*10*) found that Goldman's later application of the K-M theory to luminescence on thin-layer chromatograms (*11*) was only partially satisfactory and pointed out the dearth of experimental work testing these and other theoretical approaches that had been suggested following Goldman's work.

Goldman and Goodall (*8*) first emphasized the theoretical weakness of direct photometry of paper and thin-layer chromatograms with the instruments then current. They suggested that two requirements were mandatory for precise measurement by this method: (1) correction of absorbances

This article not subject to U.S. Copyright. Published 1983 by the American Chemical Society

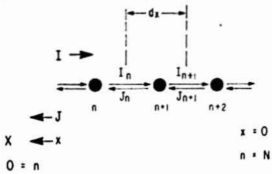

Figure 1. Schematic illustration of the Kubelka–Munk Model of light flux in a scattering medium containing chromophore: *I*, light flux away from the source of illumination; *J*, light flux in the reverse direction. Upper *n*, particle numbers and subscripts for the arrays *I*(), *J*() in the finite layer model. Lower two lines give the usual boundary conditions employed for integral solutions of eq 1 and 2 (*x*,*X*) and the finite model (*n*,*N*).

by an approximation of the K-M function; and (2) "flying spot", i.e., two-dimensional scanning in place of the usual full-width slit. Reviewing the field 10 years later, Touchstone and Sherma (*4*) described 15 commercially available TLC scanners. Only two provided two-dimensional scanning: later, a newer model of one of these was introduced which provided linearizing circuitry allowing the direct recording of absorbances corrected for scattering by an approximation of the K-M function (*12*). Touchstone and Sherma (*4*) pointed out the wide variation in the instruments available and the continuing controversy over the optimal mode of using them. Despite its popularity, this method of quantitative estimation therefore still lacks precision because it is based on empirical calibration curves for want of an agreed theoretical basis. The practical importance of the problem is considerable because the method of in situ photometry—or "scanning"—has great operational advantages over other methods of quantitative chromatography and electrophoresis (*4, 8, 13, 14*).

THEORY

The K-M theory of light scattering is the simplest of the many available (e.g., ref 8 and 15). Equation 1 describes only the two fluxes of light collinear with the incident beam and assumes two linear functions for absorption and scattering which are constant throughout the optical specimen. Thus, at any distance x, constant fractions of light traveling forward (I) are lost by scattering (SI) and absorption (KI), and another gained by the back-scatter of light traveling in the opposite direction (SJ). This is shown schematically in Figure 1. The process for the light traveling in the backward direction (J) is identical. All off-axis light is neglected.

Analytical solutions of these equations require simplifying assumptions in order to obtain expressions for transmission through, or reflection from, an actual specimen. Since *a major assumption of the K-M theory is that scattering and absorption occur at infinitesimal distances*, the equations have usually been solved by standard integration techniques (i.e., $dx \rightarrow 0$). The major factors affecting the approximations used for particular analytic solutions are (a) the thickness of the specimen and (b) whether the properties of the transmitted or reflected light are to be measured (*2, 7, 8*). The general solution of eq 1 for transmitted light, I_t, in thin layers (*8*) is

$$I_t = A \sinh [bSX] + B \cosh [bSX] \tag{2a}$$

$$J_0 = (aA - bB) \sinh [bSX] + (aB - bA) \cosh [bSX] \tag{2b}$$

where $a = (S + K)/S$ and $b = (a^2 - 1)^{1/2}$. A and B are arbitrary constants.

For transmittance, T $(= I_t/I_0)$, the boundary conditions are as follows: at $x = 0$, $I = I_0T$ and $J = 0$; at $x = X$, $I = I_0$. Thus

$$T = b/(A \sinh [bSX] + B \cosh [bSX]) \tag{3}$$

where absorbance D is

$$D = \log (A \sinh [bSX] + B \cosh [bSX]/b) \tag{4}$$

In the case of thin-media chromatograms, we are interested in obtaining an accurate measure of KX from the light absorbed by a chromophore assumed to be uniformly distributed across the light beam and through the thickness of the scattering medium. For simplicity, it is also assumed that the chromophore is uniformly distributed microscopically (i.e., within each scattering element). However, the optical specimen in a planar chromatogram is not only very thin but contains relatively few scattering particles in the light path. Thus, a typical TLC layer is 0.25 mm thick with silica gel particles of 10–30 μm diameter. With spheres of this size in close hexagonal packing, such layers would contain approximately 14–41 particles in a light path normal to the layer. Microphotographs of typical chromatographic filter papers show bundles of irregular fibers 5–20 fibers thick (*16*). Although these structures are not necessarily identical with the scattering points of theoretical models, they probably approximate them quite closely. It therefore seemed possible that the conventional integration methods ($dx \rightarrow 0$) used in practical applications of the K-M theory might well be invalid for the case of typical thin-media chromatograms. We wished to examine this point before investigating the more complex variants of the theory which have been proposed for the measurement of luminesence (*10, 17*).

METHODS

Attempts to simulate K-M eq 1a and 1b using the DYNAMO language (Dartmouth Time Sharing System version) failed because it permits boundary conditions at only one surface (*18*). The power series used to overcome this limitation gave poor approximations for J with moderately large values of SX and KX, despite promising simulations at lower values.

We therefore devised a program in BASIC (DTSS) which computed I and J for each scattering element by using eq 1 serially through the *whole* layer and *successively* in opposie directions for I and J. The process was repeated until the corrections to the I_n from the new estimates of J_n fell below a prescribed limit (usually $\sum \Delta I/I < 0.005$). A flow chart of the kernel is shown in Figure 2. A complete listing may be obtained on request. Another program was written to generate tables of values for absorbance by using eq 4 and the identities

$$\sinh (x) = \frac{e^x - e^{-x}}{2} \text{ and } \cosh (x) = \frac{e^x + e^{-x}}{2} \tag{5}$$

This "brute force" model works surprisingly well, achieving very close approximation to values given by eq 4 for $0.001 \leq SX \leq 15$ and $0 \leq KX \leq 2.0$ with layers of $200 \leq N \leq 400$ scattering elements. To facilitate comparison with earlier work, results were expressed as net chromophore absorbance (i.e., $\log (I'_0/I_t)$ where $I'_0 = I_t$ at $KX = 0$). Only the behavior of transmitted light was examined, although reflectance measures are also provided by the model.

RESULTS

Typical outputs of the two computer programs are shown in Tables I and II. In order to minimize execution time of the simulation program, we omitted overflow checks required for the unique case of $SX = 0$. Thus, to compare the results of the two programs for this case in which eq 4 reduces to the Beer–Lambert law, we used approximations for SX (<0.001) (Table I). For the same reason, we used a simple division by N (the number of particles in the simulated layer) to obtain K and S from the initial values of KX and SX selected by the operator. This gives correct values for K for all values of N since KX is the (mass × molar absorptivity) of chromophore in a layer x units thick. However, the scattering power, SX, of the whole layer is only a linear function of S, the fractional scattering coefficient per particle, when $dx \rightarrow$

Table I. Typical Output of the Computer Model

initial $SX = 6$ $N = 100$

$A'0 = 0.86994$ true $SX = 6.41474$

KX	$I(X)/I(0)$	$J(0)$	OD	log $J(0)$	tries	limit
0.000 00	0.134 87	0.864 02	0.000 00	−0.063 46	34	0.000 48
0.100 00	0.102 82	0.809 90	0.117 79	−0.091 55	31	0.000 42
0.200 00	0.080 00	0.766 46	0.226 78	−0.115 49	28	0.000 44
0.300 00	0.063 27	0.730 42	0.328 64	−0.136 40	26	0.000 41
0.400 00	0.050 67	0.699 71	0.425 06	−0.155 06	24	0.000 43
0.500 00	0.041 03	0.673 03	0.516 73	−0.171 94	23	0.000 37
0.600 00	0.033 48	0.649 44	0.605 02	−0.187 43	21	0.000 46
0.700 00	0.027 54	0.628 36	0.689 85	−0.201 76	20	0.000 45
0.800 00	0.022 79	0.609 30	0.772 00	−0.215 13	19	0.000 46
0.900 00	0.018 96	0.591 93	0.851 83	−0.227 69	18	0.000 50
1.000 00	0.015 87	0.575 98	0.929 24	−0.239 55	18	0.000 36
1.100 00	0.013 32	0.561 24	1.005 22	−0.250 81	17	0.000 42
1.200 00	0.011 23	0.547 55	1.079 25	−0.261 53	17	0.000 32
1.300 00	0.009 50	0.534 78	1.152 18	−0.271 78	16	0.000 40
1.400 00	0.008 06	0.522 81	1.223 49	−0.281 60	16	0.000 31
1.500 00	0.006 85	0.511 56	1.293 96	−0.291 05	15	0.000 42

[a] A'0, attenuance due to scattering alone (i.e., at $KX = 0$); OD, absorbance due to the chromophore (i.e., total attenuance minus $A'0$); tries, the number of iterations required; limit, the final value of E of Figure 2. $I(X)/I(0)$, the transmittance of the simulated layer (i.e., I_t/I_0 due to both scattering and absorption).

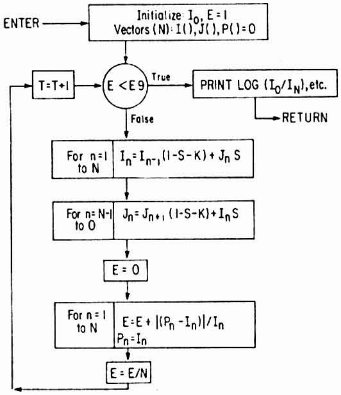

Figure 2. Kernel of the computer model for discrete step simulation of light transmission in finite layers using eq 1 and 2. I_n is the intensity of the forward light after the nth particle and J_n the back scattered light reaching the nth particle in the layer. S and K are the fractional loss at each particle by scattering and absorption, respectively. T is a control variable indicating the number of iterations required to reach the limit E. The first two loops below "False" compute eq 1a and 1b.

0 and $N \rightarrow \infty$. As expected, the results given by the discrete model for SX only correspond with the selected initial values when N is large (≥ 200). To compare the results of the two programs for small values of N, therefore, we ran the model with typical initial values of SX and then used the final values obtained (computed as $(I_0 - I_t)/I_t$) for the case $KX = 0$) as inputs to the second program to give absorbance plots by eq 4.

Case of $SX \rightarrow 0$ (Beer–Lambert Law) The first column of Table III and Figure 3 show the results obtained for this important case in which the Beer–Lambert law is shown to be a special case of the Kubelka-Munk (K-M) equation (8). It is seen that the results with the discrete model correspond very closely with those of eq 4 for $N \geq 100$ particles in the layer. Unexpectedly, the deviation from linearity is relatively small even when N was reduced to 20.

Table II. Typical Output from the Second Program Which Tabulates Values for Chromophore Absorbance Calculated by the Integral Solution of the Kubelka-Munk Equations

	absorbance at the following SX(calcd)			
KX	5.0007	6.0007	6.4155	7.0007
0.00	0.0001	0.0000	0.0000	0.0000
0.10	0.0999	0.1127	0.1181	0.1255
0.20	0.1932	0.2169	0.2267	0.2404
0.30	0.2814	0.3145	0.3281	0.3470
0.40	0.3652	0.4067	0.4236	0.4473
0.50	0.4455	0.4945	0.5145	0.5423
0.60	0.5228	0.5787	0.6014	0.6330
0.70	0.5976	0.6597	0.6850	0.7201
0.80	0.6701	0.7381	0.7657	0.8041
0.90	0.7406	0.8141	0.8439	0.8853
1.00	0.8095	0.8880	0.9199	0.9642
1.10	0.8768	0.9602	0.9940	1.0409
1.20	0.9427	1.0307	1.0663	1.1158
1.30	1.0073	1.0997	1.1371	1.1891
1.40	1.0709	1.1674	1.2065	1.2608
1.50	1.1334	1.2339	1.2746	1.3311

[a] The values given are for $D - D_0$ using eq 4, where D_0 is the attenuance due to scattering alone (i.e., with $KX = 0$).

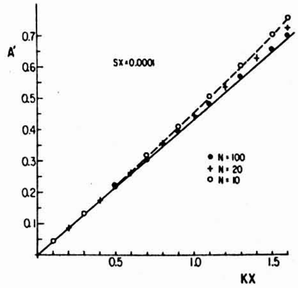

Figure 3. Results of simulating layers with $SX \rightarrow 0$ (quasi-Beer–Lambert law). The solid line is the linear relationship of the Beer–Lambert law. Other symbols and the dashed curve are for layers with the number of particles shown (N).

Table III. Comparison of Chromophore Absorbance Functions Obtained with the Kubelka-Munk Equation (KM) and Those Given by the Discrete Model for a Layer N Particles Thick

	SX = 0.00001		5		10		15	
KX	KM	model N = 200	KM	model N = 400	KM	model N = 400	KM	model N = 400
0.0	0.0000	0.000 00	0.0000	0.000 00	0.0000	0.000 00	0.0000	0.000 00
0.1	0.0434	0.043 43	0.0999	0.098 83	0.1634	0.162 78	0.2243	0.213 34
0.2	0.0868	0.086 89	0.1932	0.192 02	0.3087	0.305 76	0.4162	0.401 40
0.3	0.1303	0.130 36	0.2814	0.280 66	0.4411	0.435 56	0.5870	0.568 50
0.4	0.1737	0.173 86	0.3652	0.365 61	0.5638	0.558 13	0.7426	0.721 56
0.5	0.2171	0.217 38	0.4455	0.444 40	0.6789	0.674 98	0.8868	0.867 11
0.6	0.2605	0.260 92	0.5228	0.523 41	0.7878	0.782 68	1.0221	1.001 60
0.7	0.3040	0.304 48	0.5976	0.597 23	0.8915	0.886 30	1.1500	1.130 90
0.8	0.3474	0.348 07	0.6701	0.671 94	0.9909	0.986 41	1.2719	1.250 53
0.9	0.3908	0.391 68	0.7406	0.741 87	1.0866	1.083 47	1.3886	1.371 55
1.0	0.4342	0.435 31	0.8095	0.810 40	1.1791	1.177 91	1.5008	1.483 78
1.1	0.4776	0.478 96	0.8768	0.880 28	1.2687	1.265 33	1.6091	1.592 87
1.2	0.5211	0.522 63	0.9427	1.945 95	1.3558	1.355 13	1.7139	1.699 45
1.3	0.5645	0.566 32	1.0073	1.010 60	1.4406	1.443 28	1.8157	1.803 51
1.4	0.6079	0.610 04	1.0709	1.074 30	1.5234	1.524 63	1.9148	1.905 41
1.5	0.6513	0.653 78	1.1334	1.139 75	1.6043	1.604 67	2.0113	1.999 35
1.6	0.6947	0.697 54	1.1950	1.201 42	1.6836	1.687 73	2.1056	2.097 23
1.7	0.7382	0.741 32	1.2558	1.262 37	1.7614	1.764 85	2.1978	2.193 60
1.8	0.7816	0.785 13	1.3158	1.322 65	1.8377	1.845 55	2.2881	2.282 20
1.9	0.8250	0.828 95	1.3750	1.382 30	1.9127	1.920 10	2.3767	2.375 47
2.0	0.8684	0.872 80	1.4336	1.441 37	1.9866	1.993 75	2.4636	2.461 22

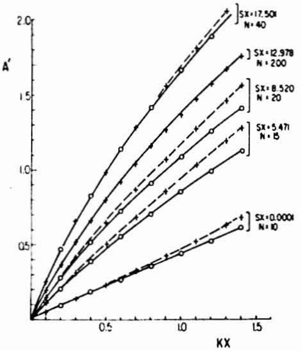

Figure 4. Simulations by the model of layers of varying thickness with SX at various values within the range usually encountered with paper and thin-layer chromatograms. The examples are chosen for convenient illustration, with the Beer-Lambert case of Figure 5 superimposed to indicate the scale. In each case the solid line with open circles is the integral solution given by program 2 using eq 4; the dashed line with crosses indicates the results given by the simulation for the values of N shown alongside.

Case of $SX > 0$ (Kubelka-Munk Equation). In Table III the values obtained with the discrete model at $N = 400$ for $SX = 5$, 10, 15 and $0 \leq KX \leq 2.0$ are compared with the values obtained by using eq 4. In each case the absorbance values are for the chromophore alone; i.e., $D' = D - D_0$, where D_0 is the absorbance due to scattering alone (i.e., log (I_0/I_t) at $KX = 0$). The correspondence between the K-M equation and the model is seen to be excellent over the range of SX and KX commonly observed in practice with paper and silica gel TLC chromatograms (*4*, *6–8*, *10*).

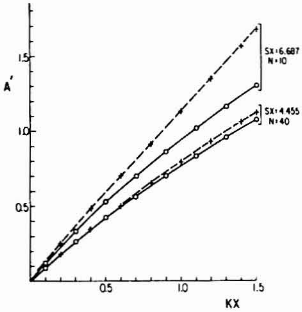

Figure 5. Simulation of two cases in the range of SX probably found with paper and some thin-layer plates without binder. The deviation from the Kubelka-Munk equation (circles and solid line) is very small with $N = 40$ but striking with $N = 10$. The simulation for the latter (upper dashed line) gives an almost linear relationship.

In Figures 4 and 5 the effects of reducing N are shown. It is clear that for any SX, close correspondence between the model and eq 4 is obtained for values of N much greater than 40. At this value a clear divergence becomes apparent and increases steadily as N is reduced to 10. Thus, the few-particled layers give absorbance functions of similar initial slope to those of eq 4 but increasingly smaller curvature. The case of $SX \to 0$ (Figure 3) suggests that some, but not all, of this is due to the positive curvature of the discrete approximation to the Beer-Lambert law with small N. Thus, for the case $N = 10$ and $SX = 6.687$, which is typical of many paper chromatograms (*6*, *7*, *19*, *20*), the greater part of the function ($KX \geq 0.1$) is linear, and the intercept of this part of the function with the D' axis is only 0.045 absorbance units (Figure 5).

DISCUSSION

The validity of the model is suggested by: its direct use of eq 1a and 1b without approximations or use of assumptions additional to those of Kubelka and Munk (1); its correct simulation of the Beer-Lambert law when SX approximates 0 and $N \geq 200$ (*5*); its monotonic convergence to the values given by eq 4 for $5 \leq SX \leq 15$ as N increases to 200 or more. We could find no artifactual reason for such convergence.

The model uses two modes of iteration which can be varied independently: (a) the number of scattering points, N in the simulated layer; (b) the number of iterations back and forth through the layer required to reach a solution within the prescribed limit, $E9$ (Figure 2). As expected, the number of the latter iterations increases as N is reduced and decreases as KX increases (Table I).

The increased light absorbance of a chromophore in the presence of scattering particles has been well established in biochemistry since Keilin and Hartree first noted the phenomenon in frozen extracts of cytochromes (*21*). The Kubelka–Munk equations described both this "hyperchromic" effect for chromophores embedded in the scattering particles and a nonlinear, negative deviation from the Beer–Lambert law (*1*, *8*). Both effects were noted by workers attempting to measure substances in situ on paper or other thin media by absorptiometry after chromatographic or electrophoretic separation (*5–9*, *14*). Detailed quantitative analysis of the phenomenon in silica gel TLC plates was first made by Goldman and Goodall, who claimed close agreement with an approximation of the K-M equations (*4*, *8*). Since then, Pollak (*22*) investigated an electrical analog model and derived equations which closely simulated the K-M equation for $0 \le SX \le 5$.

Although Goldman and Goodall's studies have had a profound influence on the field (*4*, *10*), only one TLC scanner specifically based on their recommendations is available commercially (*12*). Most workers use empirical calibration curves and two major points of controversy remain unresolved. These concern (a) the relative merits of reflectance vs. transmission densitometry (*4*, *8*, *9*) and (b) the apparent conflict of the last 3 decades between those studies reporting linear and those reporting nonlinear absorbance/concentration curves with transmission densitometry (*4*, *6*, *8*, *9*, *13*, *14*, *23–29*). With fluorometry, Goldman predicted bilinear emission/concentration curves: but most results suggest linear functions (e.g., ref 4 and 29) and Hurtubise (*10*) obtained only partial experimental agreement with Goldman's theory. It is generally agreed that in the absence of a resolution of these uncertainties, the empirical calibration curves used by most workers are critically dependent for their precision on the uniformity of the thin layer (*4*, *8*, *10*, *25*), and the reproducibility of sample deposition and the running of the chromatogram, among other factors (*4*, *7*, *14*, *29*). The results obtained from the computer model appear to offer a possible basis for understanding the second of the above controversies.

Thus, the most striking finding with the discrete model is that the "hyperchromic effect" of scattering (*7*, *8*, *14*, *21*) is not only retained but slightly increased with small N, while the negative curvature is reduced (Figure 5). Previously, it had seemed inconceivable on the basis of the K-M theory that one could exist without the other. The discrete model predicts, on the basis of the K-M model itself (eq 1a, 1b), that thin layers with $SX \le 6$ and $N \le 15$ will give almost linear absorbance/concentration curves with initial slopes close to those predicted by eq 4. With larger values, $SX > 8$ and $N > 40$, the slopes *and* curvatures will be barely distinguishable from eq 4. It is unlikely that such small differences would have been detected by Goldman and Goodall, who used a second degree polynomial to approximate eq 4 and whose experimental results fitted this polynomial with a relative standard deviation of ±2.7% (*8*). Their later work with a two-dimensional scanner obtained similar results (*23–25*). As they carefully implied (*8*), their results constituted a necessary but not a sufficient proof of the validity of eq 4 itself.

The values of SX in typical planar chromatographic media are uncertain because of (1) optical variations in the instruments used over the past 3 decades (*4*, *7*, *14*); (2) the currently unexplored role of Fresnel reflection (significant at both surfaces) (*14*, *15*); and (3) the uncertain size distribution and refractive indexes of particles in the layer, which affects both N and SX (*7*, *8*). The last (3) is complex, depending on the main medium (SiO_2, cellulose, etc.), binders (*8*, *25*), color reagents (*14*, *29*), and the degree of solvation and interpenetration of the chromophore and the above components (*7*, *8*). It is to be expected that SX will increase with the refractive index and the presence of gypsum binders and reagent precipitates and that solvation will reduce the refractive index of the main medium (*8*, *25*). With these reservations however, it seems likely that the media commonly used in planar chromatography lie awkwardly across the range of N and SX in which the model predicts a change from absorbance functions indistinguishable from eq 4 to those barely distinguishable from linear ones ($5 \le N \le 10$ and $2 \le SX \le 10$).

Thus, some of the most strikingly linear absorbance/concentration curves reported are those of Touchstone's group with ketosteroid dinitrophenylhydrazones (*28*) and diazotized estrogens (*30*), using the Schoeffel SD 3000 scanner and 0.25-mm SiO_2 layers *without binder*. From Hurtubise's (*10*) values for SX in such layers *with binder* using the same instrument (2.9–6.6), it is probable that SX in Touchstone's studies was <5. With a particle size of 10–30 μm and no binders or color reagents in these studies, N would be less than 14–41 calculated on the basis of close hexagonal packing. By contrast, Goldman and Goodall (*8*) reported values of SX of 6.6–19 for their instrument with 0.25-mm SiO_2 layers and obtained their well-known results approximating to eq 4.

Other results in the literature are of less certain interpretation due to various factors, mainly, variations in the optics employed, absence of actual measurements of SX, or the uncertain physical state of color reagents used. It is clear, however, that linear absorbance/concentration functions would be expected more commonly from paper chromatograms in which SX is approximately 3–7 for the thicknesses usually employed (*8*, *19*, *20*), and Lugg's microphotographs (*16*) suggest that N is of the order of 15. It should be emphasized that in challenging the general applicability of eq 4 to transmission densitometry of thin chromatographic layers, we are *not* disputing the validity of the K-M model itself which is based on eq 1a, 1b and the original assumptions underlying them (*1*). What the model shows is that discrete solutions of these equations for small values of N and SX *are significantly different from the usual analytical solution* (eq 4). The available experimental data suggest that these values are within the range found in many published analytical methods that use paper or TLC, and may, therefore, be of significance in the design of instruments and procedures for quantitative thin layer densitometry.

One important observational fact suggests that the discrete model may be preferable for the majority of chromatographic thin layers. Thus, N is uncertain because one cannot identify particular structures with the scattering points of the K-M theory, particularly in the presence of binders and reagents. However, SX is well-known to be largely independent of the wavelength of light outside the range in which the scattering medium itself shows significant absorbance (*5*, *7*, *8*, *14*, *15*, *22*, *24*). Precise agreement with eq 4 would imply that typical thin layers contained at least 200–400 scattering elements in 0.19–0.25 mm, at which density their mean diameters would be, at most, 1–2 μm. This is sufficiently close to the wavelengths of light studied that Rayleigh scattering would be observed with its strong dependence on wavelength (*7*, *31*).

LITERATURE CITED

(1) Kubelka, P.; Munk, F. *Z. Tech. Phys.* **1931**, *12*, 593.
(2) Kubelka, P. *J. Opt. Soc. Am.* **1948**, *38*, 448.
(3) Judd, D. B. "Color in Business, Science and Industry"; Wiley: New York, 1952; p 314.
(4) Touchstone, J. C.; Sherma, J. "Densitometry in Thin Layer Chromatography"; Wiley: New York, 1979.
(5) Vaeck, S. V. *Anal. Chim. Acta* **1954**, *10*, 48.
(6) Ingle, R. B.; Minshall, E. *J. Chromatogr.* **1962**, *8*, 369.
(7) Kortüm, G. "Reflectance Spectroscopy"; Springer-Verlag: New York, 1969.
(8) Goldman, J.; Goodall, R. R. *J. Chromatogr.* **1968**, *32*, 24.

(9) Treiber, L. R. *J. Chromatogr.* **1974**, *100*, 123.
(10) Hurtubise, R. J. *Anal. Chem.* **1977**, *49*, 2160.
(11) Goldman, J. *J. Chromatogr.* **1973**, *78*, 7.
(12) Yamamoto, H.; Kurita, T.; Suzuki, J.; Hira, R.; Nakamo, K.; Makabe, H. *J. Chromatogr.* **1976**, *116*, 29.
(13) Bush, I. E. *J. Chromatogr.* **1967**, *29*, 157.
(14) Bush, I. E. In "Methods of Biochemical Analysis"; Glick, D., Ed.; Wiley: New York, 1963; Vol. 11, p 149.
(15) Duntley, S. Q. *J. Opt. Soc. Am.* **1942**, *32*, 61.
(16) Lugg, J. W. H. *J. Chromatogr.* **1963**, *10*, 272.
(17) Spitzer, D.; Ten Bosch, J. J. *Appl. Opt.* **1976**, *15*, 934.
(18) Forrester, J. W. "Principles of Systems"; Wright Allen Press: Cambridge, MA, 1968; Chapter 8.
(19) Bush, I. E., unpublished results.
(20) Goldman, J., Imperial Chemical Industries, Pharmaceutical Division, Macclesfield, U.K., personal communications.
(21) Keilin, D.; Hartree, E. F. *Nature (London)* **1949**, *164*, 254.
(22) Pollak, V. *Adv. Chromatogr.* **1979**, *17*, 1.
(23) Goldman, J.; Goodall, R. R. *J. Chromatogr.* **1969**, *40*, 345.
(24) Goldman, J.; Goodall, R. R. *J. Chromatogr.* **1970**, *47*, 386.
(25) Goodall, R. R. *J. Chromatogr.* **1975**, *103*, 265.
(26) Treiber, L. R.; Örtengren, B.; Lindsten, R.; Örtengren, T. *J. Chromatogr.* **1972**, *73*, 135.
(27) Touchstone, J. C.; Levin, S. S.; Murawec, T. *Anal. Chem.* **1971**, *43*, 858.
(28) Knapstein, P.; Touchstone, J. C. *J. Chromatogr.* **1968**, *37*, 83.
(29) Boulton, A. A. In "Methods in Biochemical Analysis"; Glick, D., Ed.; Wiley: New York, 1968; Vol. 16, p 327.
(30) Rayleigh, Lord *Proc. R. Soc. London, Ser. A* **1914**, *90*, 219.

RECEIVED for review June 29, 1983. Accepted October 12, 1983.

Linear and Helical Flow in a Perfluorosulfonate Membrane of Annular Geometry as a Continuous Cation Exchanger

Purnendu K. Dasgupta

Department of Chemistry, Texas Tech University, Box 4260, Lubbock, Texas 79409

Flow through an annulus, especially helical flow through an annulus, permits highly efficient mass transfer to the walls of a tube and can be constructed in low dead volume configurations. Mass transfer efficiency has been studied with K^+ and NEt_4^+ as diffusing species, as a function of annular gap and helix diameter, in helices of nylon monofilament filled Nafion perfluorosulfonate membrane tubing. Penetration of common acid regenerants through Nafion membrane, used for proton exchange, has been studied in detail and may be predicted as a function of concentration. Mass transfer to, through, and from the wall has been considered in detail. In regard to mass transfer to the wall, annular helical flow was found to be highly efficient.

Our original interest in continuous ion exchange stemmed from extending the concept of "diffusion denuding" of gases. Diffusion denuders are widely used in atmospheric analysis for discriminating between gaseous and aerosol species where a chemical discrimination is difficult (*1*). When the mixture of a gas and particles (e.g., atmospheric NH_3 and aerosols containing NH_4^+) is passed through a suitably long tube whose walls act like a perfect sink for the gas (e.g., coated with oxalic acid), the NH_3 is selectively removed by diffusion to the wall because of the 4 orders of magnitude higher diffusion coefficient for the gas compared to a micrometer sized atmospheric particle (*2*). The classical equation that describes mass transfer to the walls of a cylindrical tube from a stream flowing through the tube is due to Gormley and Kennedy (*3*) and has been verified experimentally by a number of workers. The sole parameter governing mass transfer under laminar flow conditions is $\pi DL/F$ where D is the diffusion coefficient of the species to be removed, L is the length of the tube, and F is the flow rate. Although diffusion coefficients of ions in the liquid phase are much smaller than gaseous diffusion coefficients, a comparable and compensating difference exists between air sampling and chromatographic flow rates. The concept of ion exchange by diffusion denuding (IEDD) with an ion exchanger tubing was then tested successfully with perfluorosulfonate Nafion tubing which were in use in this laboratory for the removal of water vapor by diffusion denuding. Similar to the use of dry airflow outside the tube to maintain its sink capacity for use as a dryer (*4*), a flow of dilute acid was used outside the tubing for maintaining proton exchange capacity. A principal objective of such a continuous proton exchanger was utilization in ionic chromatography. Although quantitative IEDD was accomplished, we deemed the band dispersion in such hollow tubes (700 μm diameter) too large to be useful for chromatographic purposes. The Gormley–Kennedy equation states that the mass transfer efficiency is independent of tube diameter. In contrast, relative band dispersion is proportional to the fourth power of diameter (*5*). Thus, dispersion problems should be greatly reduced, without affecting ion exchange efficiency, by a reduction of diameter. At this time, we noted the prior and independent work of Stevens et al. (*6*), describing a "hollow fiber suppressor" which utilized 300 μm diameter sulfonated polyethylene tubing as the ion exchange membrane tube. This work also describes the detailed principle of operation of the continuous cation exchanger, which is therefore not repeated here. Interestingly, even though the tube diameter was lower by more than a factor of 2 compared to the tube diameter used by us, the band dispersion was greater than what we were observing. Apparently, this dispersion was due to the much longer tube lengths that were required.

Any of the following may limit the overall exchange rate observed with the system described above: (a) mass transfer to the wall, (b) mass transfer through the wall, and (c) mass transfer from the wall (regenerant flow/concentration insufficient).

Assuming that sufficient exchange sites were present and regenerant flow was adequate, the only possible explanation is limitation of exchange by (b). Mass transfer through the wall is rate limited by the diffusion coefficient of the ion through the wall matrix and the wall thickness. Since the wall thickness of the perfluorosulfonate tubing was nearly double that of the polyethylene tubing, ion transport through the hydrophilic perfluorosulfonate must be far more facile. Having failed to persuade the manufacturer toward making smaller diameter perfluorosulfonate tubing available (*7*), we sought alternatives for reducing band broadening problems with available perfluorosulfonate tubing.

Theoretical and experimental studies on flow through an open tubular helix are not new (*8–13*). The helical structure leads to the development of a secondary flow perpendicular

© 1983 American Chemical Society

to the axial flow. This secondary flow flattens the parabolic profile of the flow velocity observed in a linear tube and also leads to both reduced axial dispersion and increased mass transfer to the walls of the tube. Following the pioneering work of Dean (*8, 9*), the most important parameter in helical flow, $\mathrm{Re}(d_t/d_c)^{1/2}$, has been designated the Dean number (Re is Reynold's number and d_t and d_c are the diameters of the tube and the coil, respectively). The differences between helical and linear flow increase with increasing Dean number. The rigorous analytical solution for the hydrodynamics of helical flow is complex. Although numerical methods have recently become available (*14, 15*), certain approximations are necessary and such methods apply to a limited, albeit useful, range of Dean numbers.

For annular flow, mass transfer studies have not received much attention. However, the analogous case for heat transfer has been studied in detail (*16*) and predicts that transfer should be more efficient compared to flow through an open tube, the difference being significant for small values of r_o/r_i where r_o and r_i are the radii of the outer and inner cylinder, respectively. Very recently, mass transfer in an annular diffusion denuder has been studied both theoretically and experimentally (*17*). In this study, although both the surfaces defining the annulus act as sinks, a clear relationship between increased mass transfer efficiency and decreasing annular gap (low r_o/r_i) was established. Additionally, the advantages of small annular gap systems in promoting mass transport in boundary layers have been recognized for a long time in designing efficient dialyzers (*18*).

During the course of our study, the work of Stevens et al. (*19*), which employed Nafion tubing packed with inert beads of optimized size, was published. We pursued our investigations because it was clear that helical flow through an annular geometry may be a significant improvement over the bead packed configuration. Comparison of the annular helical device with the packed bead device, as suppressors in anion chromatography, appears in a companion paper (*20*).

EXPERIMENTAL SECTION

All reagents used in this work were of analytical reagent grade. The water used was distilled and deionized but not free from CO_2. Solutions to be ion exchanged were thermostated at 30 ± 0.1 °C and pumped by an Altex Model 110A reciprocating pump (Berkeley, CA) through a pulse dampener (Handy and Herman Tube Co., Norristown, PA) into the device under test. The effluent conductivity was measured with a Wescan Model 213 conductivity detector (Santa Clara, CA). The attendant detector cells (nominal volume 2 or 20 μL, cell constants as determined with 0.01 D KCl solution were 34.1 and 0.117, respectively) were thermally insulated by polyurethane foam molds. The reported conductance values are corrected to 25 °C. The regenerant solution, also thermostated at 30 °C, was pumped by an Eldex Model E-120-S reciprocating pump (Menlo Park, CA) or allowed to flow under gravity.

Construction of Devices. Nafion 811x perfluorosulfonate membrane tubing (Du Pont Polymer Products Division, Wilminton, DE) was used as the cation exchanger membrane tubing. The nominal dimensions of this tubing are 875 μm o.d. and 625 μm i.d. in the dry state. The hydrophilic material expands significantly upon wetting. Two separate batches of tubing were used during the course of this study; their diameters were perceptibly different although both were within the usual manufacturing tolerance. Devices otherwise identical, except for the batch of tubing, produced significantly different results. The bulk of the data reported in this paper are typical among several dozen individual devices fabricated with the smaller diameter tubing, which is at the lower end of the diameter distribution of the manufacturer's product (*21*).

Options for leak-free connections (to withstand several hundred pounds per square inch) for membrane tubing with 75 μm wall thickness are limited. Because of wide interest in the potential application of Nafion membranes (*22, 23*), sealing techniques developed during the course of this work may be useful to others.

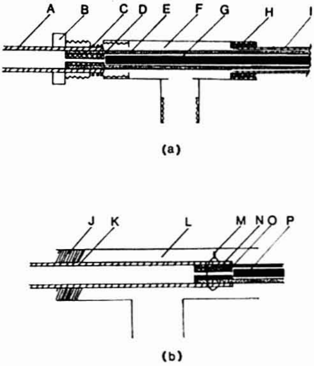

(a)

(b)

Figure 1. Inlet/outlet designs: A,K, inlet/outlet PTFE tube; B, 1/4-28 male nut; C, O-rings; D,O, microbore PTFE insert; E,N, Nafion membrane tubing; F, 1/4-28 threaded T; L, polypropylene T; G,P, nylon monofilament; M, nichrome wire crimp; J, H, adhesive filler; I, jacket tubing.

The swell-seal method (*19, 23*) which takes advantage of the hydrophilic expansion of Nafion, could not be easily applied to filament filled Nafion tubing. Much initial work was done with a flange seal technique in which the open end of the tubing is brought close to a flame whereupon it softens, rolls back upon itself and produces a ring like flange. While with appropriately constructed fittings a good seal could be obtained, commercially available T-fittings with 1/4-28 thread (made for $^1/_{16}$ in. tubing) frequently have interconnecting holes that are too large for this purpose. Also, very small homemade washers were needed for sealing. Although this technique has some distinct advantages, this approach was discontinued in favor of the following. A small section (0.5–1 cm) of microbore PTFE tubing (0.3 mm i.d., 0.75 mm o.d.) was forced into the Nafion tubing and then the Nafion tubing was inserted into the connecting PTFE tubing (0.3 mm i.d., 1.5 mm o.d.; the tubing was enlarged at the end with a suitable tool to accommodate the Nafion tubing; if dead volume considerations are unimportant, 0.8 mm i.d., 1.6 mm o.d. PTFE tubing is more convenient) to no further depth than the microbore insert. Sealing was then accomplished either by compression with O-rings (Figure 1a) or by crimping with 28 gauge nichrome wire (Figure 1b).

Monofilament nylon lines (fishing lines) were used for insertion into the Nafion tubing. Three different filament diameters were investigated: 0.52 mm (Sigma, 25 lb strength line), 0.56 and 0.66 mm (Stren, Du Pont, 30 and 40 lb strength lines, respectively). If the membrane is thoroughly wet, insertion of the 0.52- or 0.56-mm filaments into the Nafion tubing is facile. The direct insertion of the 0.66-mm filament (which actually exceeds the dry inside diameter of the tubing) is however, very difficult. Initially we accomplished this by splicing the filament onto a narrower filament which has already been inserted into a desired length of the Nafion tubing and pulling it through. This was found to be very difficult for lengths exceeding 0.5 m and a better method was found. After insertion of the microbore PTFE tubing and establishment of a leak-free connection at one end, this end was connected to a pump and water was pumped through the Nafion tubing. The filament was pushed from the open end of the Nafion tubing inward. A flow rate of 1 mL/min produced a pressure drop about 200 psi which adequately expanded the tubing for smooth passage of the filament. When the filament was all the way in and butting the microbore tubing, the tubing and filament were gripped from the insertion end and the pressure was released by discontinuing flow. Excess filament was then cut off flush with the tubing. Gentle stretching of the membrane tubing then produced enough void space at the insertion end for inserting a small section of microbore tubing for connections, as at the other end.

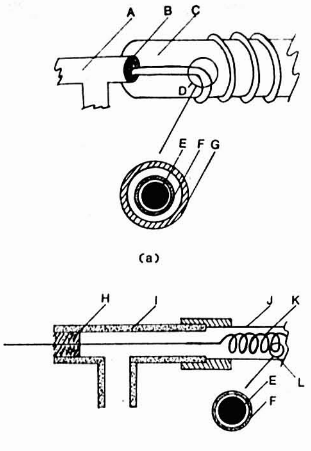

(a)

(b)

Figure 2. Device designs: A, 1/4-28 T; B, adhesive filler; C, support rod; D, enlarged cross section below; E, filament; F, Nafion tubing; G, jacket tubing; H, adhesive; I, polypropylene T; J, jacket tube; K, filament filled helix; L, enlarged cross section below; E, filament; F, Nafion tubing.

Compared to the original unstretched dry lengths, the longitudinal expansion of the Nafion tubing as a result of the above operations is significant and can be as large as 10%. The tubing lengths reported in this paper refer to the original dry lengths.

Coiling was then accomplished to produce the filament filled helix (FFH). Two basic types of device construction were studied. In the first design, the jacket tubing for regenerant flow outside the membrane tubing was concentric with the membrane tubing and filament, i.e., the jacket formed an outer helix (Figure 2a). In this design, used with the inlet connection depicted in Figure 1a, jacket inside diameter only slightly larger than the membrane outside diameter were practical. Vinyl tubing (1–1.25 mm i.d.) was used as jacket and was sealed in place with a suitable adhesive. For larger diameter helices, 3 mm o.d. PTFE tubing, which could be conveniently flange sealed, were used as jacket tubing. The support rod and the inlet/outlet T's were cemented together. Although the concentric design permits the most efficient use of the regenerant flow, the attainable lower limit of helix diameter was poor. Additionally, attempts to obtain low diameter helices with small diameter support rods (e.g., 1.5 mm o.d. metal tubing) were frequently foiled by the membrane tubing biting into the jacket and effectively losing the surface area of the membrane in such contact from an active role. The advantage of this design was that with a closely fitting jacket, the membrane tubing tolerated, under dynamic conditions, relatively high absolute pressures (studied up to the limit of the fitting used, ~700 psi). Since significant pressures were involved for the regenerant flow (up to 300 psi for 5 mL/min) with this design, the actual pressure differential experienced by the membrane tubing was substantially less than the absolute pressure.

In the second design, the jacket was concentric with the FFH (Figure 2b). The FFH was made first by tying one end of the filament filled tubing to a suitable support rod, coiling it around the support, and then trying the other end to the support. The whole assembly was then put in boiling water for 30 min to 1 h. The thermal treatment set the filament in shape. Ties and support rods were next removed. The coils expanded slightly upon removal of support, the extent of this expansion decreased with decreasing coil diameter and increasing filament diameter. For most of our experiments, support rods 1.5 mm (chromatography tubing) and 0.6 mm (guitar string) in diameter were used; these led to helix diameters in the actual operating devices of about 4 and 2 mm, respectively. Helices with much larger diameters did not retain their shapes very well and had to be studied by the first design. For operation, the FFH was enclosed in a suitable jacket with inlet/outlet T's depicted in Figure 1b. Tygon or glass tubing was used for the jacket. A closely fitting jacket made efficient use of the regenerant flow; care was taken however to ensure that the FFH did not contact the jacket walls and was stretched very slightly to prevent succeeding turns of the coil from touching each other. In both designs, during coiling, the minimum possible pitch (with turns touching each other) was used.

During operation, the regenerant solution was pumped countercurrent to the flow in the FFH. For most of our experiments with design (b), the regenerant solution was alllowed to flow by gravity and, when unimpeded, resulted in a maximum flow rate of 15 mL/min. With design (a), the maximum flow rate of the pump (5.75 mL/min) was used.

Table I. Regenerant Penetration[a]

external liquid	conductance, μS	external liquid	conductance, μS
H_2O	5.3	H_2SO_4, 0.5 mM	6.2
HCl, 1 mM	6.4	H_3PO_4, 0.33 mM	20.0
$HClO_4$, 1 mM	6.3	HOAc, 1 mM	32.6
HNO_3, 1 mM	6.7	HOAc, pH 3	1400

[a] Internal liquid water, flow rate 1 mL/min. External flow rate 2 mL/min. Membrane tube length 20 cm. Detector cell 20 μL.

RESULTS AND DISCUSSION

Regenerant Penetration. At low regenerant concentrations, the Donnan potential effectively prevents the penetration of the regenerant anion through the cation exchange membrane into the inner stream. However, when the concentration of the solution to be ion exchanged is high, regenerant concentration also needs to be relatively high to prevent the mass transport from the outer wall of the membrane to be rate limiting. Under such conditions, the ionic concentration differential between the two sides of the membrane is sufficient to overcome the Donnan potential and penetration of the regenerant anion into the inner flowstream is significant. We compared a number of regenerant solutions with respect to penetration into a water flowstream; the results are reported in Table I.

The high penetrations of H_3PO_4 and HOAc are clearly due to the efficient transport of the un-ionized uncharged species, not subject to the Donnan barrier. Perchloric and sulfuric acids were studied further, at higher and more practical concentrations, up to 75 mN; the results are shown in Figure 3. Cation transport through perfluorosulfonate membranes has been studied (*24*), but anion transport has not been addressed. Clearly, the relationship between penetration rate and regenerant concentration is nonlinear. Likewise, no simple relationship between penetration and osmolality was observed. In our system, the penetration rate was found to be limited by sorption rate at the outer wall or rate of transport through the wall, because under conditions of significant penetration (>10 mN acid), the effluent conductance (directly related to the permeate concentration) was linearly related to the reciprocal of the internal flow rate (data not shown). Helfferich (*25*) describes the equation governing the equilibrium concentration of a sorbed ion in an ion exchanger bearing fixed charges of the same sign as

$$\bar{m}/m = (\bar{m}_{\mathrm{R}}/2zm) + (a^2b^p) - \bar{m}_{\mathrm{R}}/2zm \qquad (1)$$

where $\bar{m}$ and m are the molality of the ion of charge magnitude z in ion exchanger and solution, respectively, $\bar{m}_{\mathrm{R}}$ is the molality of ion exchange groups in ion exchanger, a is the ratio of the activity coefficient of the ion in solution to that in exchanger, b is the ratio of activity of water in exchanger to that in

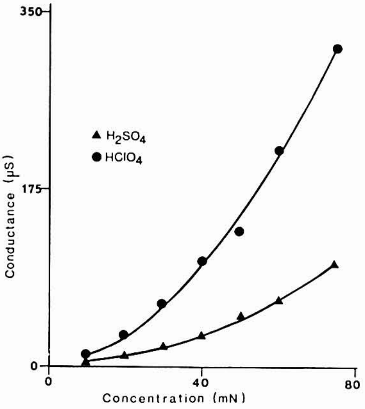

Figure 3. Effect of regenerant concentration on penetration. Conditions are the same as those given in Table I.

solution, and p is the ratio of partial molar volume of the electrolyte to partial molar volume of water. In our systems, a, b, m, p, and z may all be regarded as constants as a first approximation. Assuming that the permeate concentration (directly proportional to the observed conductance) is linearly related to m, eq 1 reduces to a much simpler form

$$\alpha A^2 + \beta A = m^2 \qquad (2)$$

where A is the observed conductance. In Figure 3, the symbols represent the experimental points (molarity rather than molality has been used, the difference is not significant at these concentrations) while the solid lines depict the best fit curve for eq 2 obtained by second-order regression analysis (*26*). Concentrations lower than 10 mN were omitted from data analysis due to the significant background conductance of the water employed. The fit was good for both $HClO_4$ and H_2SO_4; the respective best fit equations were $m^2 = (3.07 \times 10^{-3})A^2 + 17.16A - 84.58$ ($R^2 = 0.995$) and $m^2 = (4.30 \times 10^{-2})A^2 + 53.24A - 166.70$ ($R^2 = 0.996$) where m is in units of milliequivalents per liter and A is in microsiemens. The appearance of the constants in the best fit equations is primarily due to the significant conductance of the water used. If lower concentration data are excluded, the magnitude of the constant term is reduced drastically. The reduced penetration of H_2SO_4 compared to $HClO_4$ is probably related to differences in charge and hardness (lipophilicity) of the two anions, aside from the incompleteness of the second dissociation step in the case of H_2SO_4. Note that unlike H_3PO_4 or HOAc, incomplete dissociation of H_2SO_4 leaves HSO_4^- which is still subject to the Donnan barrier. On the basis of the above results, H_2SO_4 solutions were used exclusively as regenerant. It should be pointed out that if an electrolyte solution constitutes the inner flowstream, observed penetration appears to be somewhat smaller but occurs nevertheless. The interpretation of the experimental data is however more complex and was not pursued.

The Annular Geometry. The regularity of the annular geometry (i.e., does the filament touch the walls of the tube?) is subject to question. Photomicrography of the linear devices or the FFH under operating conditions did not reveal any such irregularity. Inasmuch as the flowing fluid essentially inflates the membrane to create a passage for itself, this is to be expected. However, to determine the nature of mass transfer to the walls of the tube, solutions of cationic dyes (crystal violet and malachite green) that bind very strongly to Nafion, were injected into linear and FFH devices. The device was then taken apart and short longitudinal sections, representing equal portions of the tube perimeter, were cut from the membrane tube. The dye was extracted from each section by strongly acidic methanol. Spectrophotometric determination of the dye indicated uniform deposition across the perimeter. Similar experiments with axial cross sections of the membrane tube as a function of the distance from the inlet indicated that the extent of deposition decreased exponentially with increasing distance from the inlet, except in the immediate vicinity of the inlet where the deposition was much higher than that predicted by the exponential relationship.

For the three linear annular flow systems (filament radius r_i = 0.26, 0.28, and 0.32 mm, respectively) the mean annular gap, $r_o - r_i$, was calculated from

$$r_o - r_i = [r_i^2 + (V/\pi L)]^{1/2} - r_i \qquad (3)$$

where V is the dead volume of the device as obtained from residence time measurements (see ref 20 for details). At a flow rate of 2 mL/min, the mean annular gaps were found to be 0.130, 0.108, and 0.064 mm, respectively, for the three systems. The outer radii, r_o, were then calculated to be 0.390, 0.388, and 0.384 mm, respectively, indicating absence of any large changes in the diameter of the membrane tube between the three systems. However, these values are significantly higher than the mean radius of the hollow tube, determined in an analogous fashion to be 0.350 mm. The annular gap as determined above decreases slightly with decreasing flow rate. Also, the increase in the pressure drop with flow rate is less than linear, suggesting increases in the annular gap with increasing pressure; albeit the effect is small. For the helical devices, the annular gaps, determined as above, were found to be slightly smaller than the corresponding linear devices. The pressure drops at a given flow rate were always larger for the helical devices compared to their linear analogues. For a hollow tube, this increase in pressure drop upon introducing a helical configuration is well-known (*10, 11*).

Mass Transfer to the Wall: Linear Devices. To avoid saturation of the exchange sites, dilute (1 mM) solutions of KNO_3 and NEt_4ClO_4 were used as solutions to be ion exchanged. These cations were chosen to explore the effects of varying ionic size and thus the diffusion coefficient. Five millimolar H_2SO_4 was used as regenerant, at an adequate flow rate, to minimize regenerant penetration. The fraction exchanged, f, was calculated from

$$f = (Y - X)/(Z - X) \qquad (4)$$

where X is the conductance of the original solution, Y is the conductance of the solution after passage through the device under test, and Z is the conductance of the solution after passage through a conventional packed column exchanger. The accuracy of this calculation is limited by the pressure-induced water loss from the inside to the outside of the membrane and regenerant penetration, both of which tend to exaggerate the actual efficiency. The results are reported in Table II. For the NEt_4^+ case, the initially stable conductance reading decreases eventually to a lower value, due to wall saturation arising from the very slow transport of this ion through the wall. The values reported in Table II are the initial values. Some values of f, especially those at the lowest flow rate, were calculated to be higher than 1 (up to 1.04) due to regenerant penetration but are reported as unity for consistency. Improvement of efficiency with decreasing annulus width is evident from Table II and is observed for both K^+ and NEt_4^+. In quantitatively assessing the increase in efficiency, it is convenient to relate the improvement of performance in terms of decreased device length necessary for a given application. As long as the rate of mass transfer to

Table II. Efficiency of Mass Transfer to the Wall: Fraction Ion Exchanged[a]

device type	solution	flow rate, mL/min			
		0.5	1.0	2.0	4.0
hollow	KNO_3	0.94	0.64	0.54	0.38
	NEt_4ClO_4	0.70	0.57	0.36	0.29
annular linear, 0.52 mm filament	KNO_3	0.94	0.83	0.72	0.54
	NEt_4ClO_4	0.93	0.77	0.58	0.39
annular linear, 0.56 mm filament	KNO_3	1	0.97	0.90	0.67
	NEt_4ClO_4	0.97	0.91	0.75	0.46
annular linear, 0.66 mm filament	KNO_3	1	1	0.98	0.75
	NEt_4ClO_4	1	0.97	0.76	0.56

[a] Tubing length 50 cm in all cases.

the wall is the limiting factor in controlling the observed extent of exchange and irregularities of transport at the inlet/outlet of the device are ignored, an exponential relationship between the device length and the observed extent of exchange may be assumed as a first approximation (analogous to the attenuation of light as a function of path length), such that

$$\ln (1 - f) = kL \qquad (5)$$

where L is the device length and k is a proportionality constant. Thus, a convenient way to consider the increase in efficiency in terms of length is to consider the efficiency factor E

$$E = \ln (1 - f')/\ln (1 - f) \qquad (6)$$

where f is the extent of exchange observed with the hollow tube and f' is the extent observed with a more efficient device of the same length at the same flow rate. Limiting our attention to the data for the highest flow rate (4 mL/min) only, the efficiency factors for the 0.52, 0.56, and 0.66 mm filament filled systems are 1.6, 2.3, and 2.9 for the K^+ case and 1.4, 1.8, and 2.4 for the NEt_4^+ case, respectively. Values of E calculated with high values of f are likely to be less reliable due to inaccuracies involved in evaluating f. As discussed in the foregoing section, changes in the annular gap occur for a given system as a function of flow rate. This makes it difficult to carry out theoretical interpretation of the experimental data. Plotting of f vs. F for the data in Table II (and other data at intermediate flow rates not presented here) show that f is a single valued monotonic function of F for all the systems. The Gormley–Kennedy equation is an infinite series; a valid three term approximation is

$$1 - f = 0.8191e^{-3.657\mu} + 0.0975e^{-22.3\mu} + 0.0325e^{-57\mu} \qquad (7)$$

where $\mu = \pi DL/F$, these terms having been defined previously. While the data for the hollow tube fit reasonably well to eq 7, the calculated values of D from the best fit equations are much larger (by as much as a factor of 4) than the known diffusion coefficients of K^+ and NEt_4^+. Several factors may be responsible for the observed enhancement of transport: pump pulsations, turbulence at inlet/outlet, turbulence induced by the surface roughness of the tubing, and the finite length necessary for the development of laminar flow. For the filament filled systems, these factors contribute increasingly to the departure from theoretical models, especially with very small annular gaps. Even though the work of Possanzini et al. (*17*) for annular systems suggests that the Gormley–Kennedy equation should be applicable to such systems (with the modification that μ should be multiplied by a factor determined by the geometry of the annulus), our data for the annular systems do not fit well to eq 7.

Helical Devices. For a given filament, the annular gap may be considered a constant. At constant rates of flow, the Dean no., $Re(d_t/d_c)^{1/2}$, will vary inversely as the square root of the coil diameter, $d_c^{1/2}$. Since the Reynold's no., Re, is a constant, d_t, which, in the annular case, is the hydraulic radius rather than the tube radius, is also a constant. Plots of fraction exchanged vs. $1/d_c^{1/2}$ are shown in Figures 4 and 5 for K^+ and NEt_4^+, respectively, for 0.66 mm diameter filament filled helices. To obtain a large spread in the value of f, device lengths chosen for the KNO_3 and the NEt_4ClO_4 study were 25 and 35 cm, respectively. If the data for the linear devices are excluded, the plots appear to be monotonous single valued functions with the mass transfer efficiency to the wall being

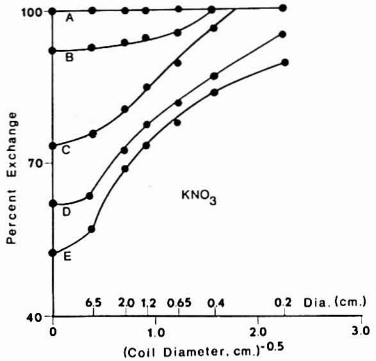

Figure 4. Exchange efficiency in helical devices as a function of coil diameter, 1 mM KNO_3: flow rate (A) 0.5, (B) 1.0, (C) 2.0, (D) 3.0, (E) 4.0 mL/min. Device length was 25 cm and filament diameter 0.66 mm.

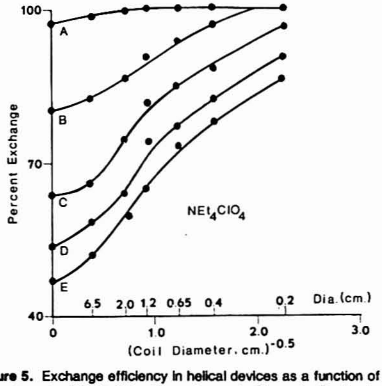

Figure 5. Exchange efficiency in helical devices as a function of coil diameter: 1 mM NEt_4ClO_4, flow rates as in Figure 4. Device length was 35 cm and filament diameter 0.66 mm.

acutely dependent on the coil diameter. For K^+, the efficiency factor E may be calculated from the data presented in Figure 4 to be 3.1 in going from a linear to helical ($d_c = 0.2$ cm) 0.66 mm diameter filament filled device (curve E, flow rate 4 mL/min). Comparison with data presented in Table II for the hollow tube (and recognizing the differences in device lengths employed), the efficiency factor for the 0.2 cm diameter helix is then calculated to be 9.5 relative to the hollow tube. The analogous value for NEt_4^+ at the same flow rate is 8.3 for the 0.66 mm diameter filament filled helix ($d_c = 0.2$ cm) relative to the hollow tube. Experiments with hollow helices as a function of coil diameter show the expected increase in efficiency of mass transfer with decreasing coil radius. However, the effect is substantially lower than that represented by the data for the annular helical case presented above. Within the annular helical geometry, the efficiency was observed to increase with decreasing annular gap (increasing filament diameter), at any given coil diameter. The effect of pitch (defined as the distance between successive turns of the coil divided by the circumference of the coil) at a given coil diameter is increasing efficiency with decreasing pitch, short of the coil turns touching each other during operation. It has been argued that the effect of moderate values of pitch is the same as that due to a small change in the effective coil diameter (*10*).

Mass Transfer through the Wall. As was noted in the introduction, the outstanding advantage of Nafion perfluorosulfonate membrane is small resistance to cation transport. Consider the limiting case wherein mass transfer to and from the wall are infinitely efficient; the resistance to mass transfer through the wall is the limting factor. This situation plays a significant role in continuous ion exchange of solutions of relatively high concentration such as the eluents used in nonsuppressed ion chromatography (*20*).

For illustrative purposes, consider the ion exchange of a C molar solution of NaX where transport of Na^+ through the wall is the only limiting factor. An adequate regenerant flow and concentration is assumed and the rejuvenation of exchange sites by the fast diffusing proton is not considered to be rate limiting. The selectivity coefficient, S, of Nafion for Na^+ has been measured by Yeager and Steck (*27*) to be 1.22; where S is defined as

$$S_{Na^+} = X_{Na^+}[H^+]/X_{H^+}[Na^+] \tag{8}$$

where X_i is the fraction of ion exchange sites occupied by ion i and $[i]$ represents the molarity of i in solution. (S_i increases at very low values of X_i and a more rigorous analysis will need to take this into account.) Recognizing that the concentration of ion exchange sites is fixed for a given membrane material, eq 8 may be rewritten as

$$S_{Na^+} = M_{Na^+}[H^+]/((\rho/\mathrm{EW}) - M_{Na^+})[Na^+] \tag{9}$$

where M_i is the concentration of ion i in the exchanger phase in mol/cm³, EW is the equivalent weight of the exchanger, and ρ is its density; ρ/EW represents total exchange site concentration in mol/cm³. Rearrangement of eq 9 yields a more convenient form:

$$M_{Na^+} = S(\rho/\mathrm{EW})[Na^+]/([H^+] + S[Na^+]) \tag{10}$$

Consider now an infinitesimally small segment of the device of length dL cm, such that by passage through this section, dC molar Na^+ is exchanged at the wall for H^+. We assume $C \gg \mathrm{d}C$, such that the entire length dL of the segment may be considered to be in equilibrium with C molar Na^+. We assume, for simplicity, that the concentration of Na^+ outside the membrane (and therefore at the outer surface of the membrane) is essentially zero. If the thickness of the membrane, t, is small, the transport flux of Na^+, Q, through the membrane is given by Fick's first law (*28*)

$$Q = M_{Na^+}D_m/t \tag{11}$$

where Q is in mol cm^{-2} s^{-1}, t is in cm, and D_m is the diffusion coefficient of Na^+ in the Nafion membrane (measured to be 9.44×10^{-7} cm²/s, ref 29). The flux through the membrane for the segment is

$$Q' = 2\pi r_i M_{Na^+} D_m \mathrm{d}L/t \tag{12}$$

where $2\pi r_i \mathrm{d}L$ is the inner surface area of the segment. At steady state with a solution flow rate of F mL/s, the decrease in concentration of Na^+ by ion exchange at the wall, $-\mathrm{d}C$, is

$$-\mathrm{d}C = 1000Q'/F \tag{13}$$

and the effluent concentration C' is given by

$$C' = C - \mathrm{d}C \tag{14}$$

Using a new value of C equal to C' and iterating calculations through eq 10–14, we can evaluate the unexchanged concentration after any number of such segments. However, the change in $[H^+]$ needs to be taken into account. From charge balance requirements, at any point in the system

$$[Na^+] + [H^+] = [OH^-] + [X^-] \tag{15}$$

Upon substitution of $[Na^+] = C$ where C is the current unexchanged concentration and $[X^-] = C_o(K/(K + [H^+])$ where C_o is the original concentration of Na^+ and K is the dissociation constant of HX, eq 15 yields

$$[H^+]^3 + (C + K)[H^+]^2 + (KC - K_w - KC_o)[H^+] - KK_w = 0 \tag{16}$$

Equation 16 may be solved by the Newton–Raphson method (*29*) at each iteration step and the value fed back in eq 10 for the subsequent cycle. In these calculations, we have assumed $t = 0.0075$ cm, $r = 0.035$ cm, and $\rho = 1.98$ g/cm³ (the dependence of ρ on present and past hydration history of the membrane as well as the nature of its ionic content as detailed in ref 30 has been ignored). The numerical solution stabilized at dL = 0.01 cm and thus no further reduction in dL was attempted. Note that for strong acids, eq 16 simplifies to

$$[H^+] = C_o - C \tag{17}$$

and an analytical solution is possible. Equations 10–13 combine to

$$-\mathrm{d}C = \frac{C}{[H^+] + SC}\theta \mathrm{d}L \tag{18}$$

where $\theta = 2000\pi r_i D_m S\rho/(Ft\mathrm{EW})$. Substituting eq 17 into eq 18 and integrating

$$C = C_o \exp[-((S - 1)/f + (\theta L/C))] \tag{19}$$

which can be solved numerically.

Figure 6 shows the effect of the dissociation constant of HX upon the fraction exchanged. The variation of pH with f is the same as that during the titration of NaX with a strong acid. Consequently, the more facile exchange with decreasing acidity of HX is notable and is particularly important if quantitative or near-quantitative exchange is to be accomplished.

Figure 7 shows the effect of varying the concentration of the solution to be ion exchanged (salt of a strong acid). At high concentrations, mass transfer to the wall will clearly be the limiting factor.

Figure 8 shows the effect of varying the flow rate of the influent solution (strong acid salt) upon the overall exchange rate. Note that variation of D_m, r_i, t, or EW lead to similar results.

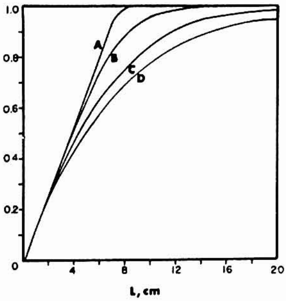

Figure 6. Effect of the dissociation constant of HX on the wall transport limited ion exchange of NaX: (A) $pK = 8$, (B) $pK = 5$, (C) $pK = 2$, (D) strong acid. Influent concentration was 0.01 M; flow rate was 2 mL/min.

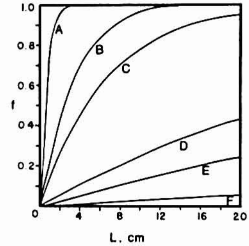

Figure 7. Effect of the influent concentration on the wall transport limited ion exchange of NaX (HX is strong acid): (curves A–F) 0.001, 0.005, 0.01, 0.05, 0.1, and 0.5 M influent NaX. Flow rate was 2 mL/min.

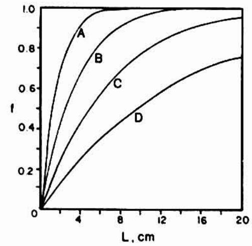

Figure 8. Effect of flow rate on the wall transport limited ion exchange of NaX (HX is strong acid): (curves A–D) 0.5, 1.0, 2.0, and 4.0 mL/min. Influent concentration was 0.01 M.

Table III. Effect of Regenerant Concentration on Ion Exchange Efficiency[a]

regenerant (H_2SO_4) concn, mM	conductance, μS, at the indicated flow rate (mL/min) 0.5	1.0	2.0	4.0
12.5	0.62	1.77	7.72	8.25
25	0.70	0.88	3.05	6.45
50	0.99	0.73	2.30	4.85
100	2.80	1.07	2.39	4.83

[a] Influent solution 2.4 mM Na_2CO_3 + 3 mM $NaHCO_3$; tube length 50 cm; filament diameter 0.66 mm; coil diameter 4 mm; design b; jacket i.d. 1 cm; regenerant flow rate 5 mL/min; direct conductance of this solution is 20.8 μS; completely exchanged (packed column) conductance is 0.690 μS.

Mass Transport from the Wall. Adequate flow rate and concentration of regenerant are necessary to prevent mass transfer from the outer wall of the membrane from becoming a limiting factor. The maximum permissible degree of regenerant penetration, which must be decided for a specific application, sets an upper limit on the regenerant concentration. Other than the convenience of gravity flow and practicality of maintaining the flow rate, there are no restrictions on increasing the flow rate. The regenerant solution may also be recycled through a large bed exchanger. The geometry of the jacket is obviously a very important factor in determining how efficiently the regenerant flow is utilized. When the influent ionic concentration is high, mass transfer from the outer wall may become a significant factor. Data for overall exchange observed with a solution containing 3 mM $NaHCO_3$ + 2.4 mM Na_2CO_3 are presented in Table III as a function of regenerant concentration. These data represent an interplay of two opposing factors on the effluent conductance; regenerant penetration and mass transfer inefficiency at the outer wall. Thus, the data in the second column, where the mass transfer efficiency is not limiting, shows increasing conductance with increasing regenerant concentration; this is due to regenerant penetration. In contrast, the data in the last column show the opposite trend; here mass transfer efficiency is the limiting factor. Note also for carbonate containing solution, quantitative cation exchange through the devices often leads to an effluent conductance significantly lower than that obtained with a packed bed exchanger. This is due to facile loss of CO_2 through the membrane. Since the loss must obviously be much greater with increasing distance from the inlet (as the amount of free H_2CO_3 increases), no simple method has proved feasible for calculating the fraction exchanged.

Overall Exchange Rate. Since the rate of mass transport from the wall can be prevented from limiting the overall exchange rate by proper choice of regenerant concentration and flow rate, effects due to mass transport from the wall may be disregarded. In general, for most solutions to be ion exchanged, the observed exchange rate will be dependent on mass transfer through the wall for the initial part of the device. This will continue until the concentration drops to a level where the flux brought to the wall falls below the amount that can be transported through the wall. Past this point, the wall will behave as a perfect sink and the exchange rate will be controlled by the rate of mass transport to the wall. Due to the complexity of the hydrodynamics involved, we are presently unable to formulate an analytical expression for the rate of mass transport during helical flow through an annulus. However, as a first approximation, an exponential depletion with length may be assumed under conditions of mass transport to the wall being the limiting factor, for a given flow field. Thus, we may assume that a fraction, k, of the influent flux is capable of reaching the wall during passage through a segment of length dL. The calculations for f as performed in the section on mass transport through the wall then need to be modified only in that

$$-dC = kCdL \qquad (20)$$

which is eq 5 in differential form. At each iteration step, either eq 18 or 20 is used depending on which produces the limiting value. The net effect of decreasing k for a given set of wall transport parameters is then manifested in divergence from the wall transport limited exchange curve at lower and lower values of L. Note that k depends on the assumed value of dL, the maximum permissible value being $1/dL$. However, for realistic values of the influent concentration, the transfer through the wall is likely to become rate limiting long before this maximum value can be attained.

CONCLUSIONS

Although we have focused our attention in this article on the use of the FFH as an efficient continuous cation exchanger, mass transfer efficiency and low dead volume considerations are of paramount importance in many other systems, including dialyzers in artificial kidney machines. Detailed theoretical considerations on the hydrodynamics of helical flow through an annulus are clearly necessary. We believe that such a flow configuration will be of utility in a large number of membrane-based separation systems. The computational approach presented here can be extended to other systems. For example, in designing dialyzers with porous membranes, the density of pore distribution is analogous to exchange site density of an ionomeric membrane, while the selectivity coefficient will be controlled by the pore size distribution and the size of the molecule to be dialyzed.

Additionally, in open tubular capillary LC, the generation of active sites in the walls of such small capillaries is a significant task. It is considerably easier to produce such sites on a filament. A thermally shrinkable jacket could then be shrunk down on the filament, yielding very small annular gaps. With appropriate membrane material, an FFH could be used for efficient mixing in of a reagent without large band dispersions. We hope that the considerations outlined in this paper will promote the use of annular and annular helical flow in analytical chemistry.

ACKNOWLEDGMENT

Discussions with Daniel P. Y. Chang, Department of Civil Engineering, University of California at Davis, were invaluable during all phases of this work. The author is indebted to Donald Chinn, Lubbock High School, for carrying out the bulk of the experimental work. Wescan Instruments is thanked for the gift of the conductivity detector used in this work.

Registry No. K, 7440-09-7; NEt_4^+, 66-40-0; H_3PO_4, 7664-38-2; HOAc, 64-19-7; $HClO_4$, 7601-90-3; H_2SO_4, 7664-93-9.

LITERATURE CITED

(1) Braman, R. S.; Shelley, T. J.; McClenny, W. A. *Anal. Chem.* **1982**, *54*, 358–364.
(2) Ferm, M. *Atmos. Environ.* **1979**, *13*, 1385–1393.
(3) Gormley, P. G.; Kennedy, M. *Proc. R. Ir. Acad., Sect. A* **1949**, *52A*, 163–169.
(4) D'Ottavio, T.; Garber, R.; Tanner, R. L.; Newman, L. *Atmos. Environ.* **1981**, *15*, 197–203.
(5) Snyder, L. R.; Kirkland, J. J. "Introduction to Modern Liquid Chromatography", 2nd ed.; Wiley: New York, 1982; p 87.
(6) Stevens, T. S.; Davis, J. C.; Small, H. *Anal. Chem.* **1981**, *53*, 1488–1492.
(7) Kirkland, J. J., E.I. du Pont de Nemours and Co., personal communication, Sept 1981.
(8) Dean, W. R. *Philos. Mag.* **1927**, *4*, 207–223.
(9) Dean, W. R. *Philos. Mag.* **1928**, *5*, 673–695.
(10) Truesdell, L. C., Jr.; Adler, R. J. *AIChE J.* **1970**, *16*, 1010–1015.
(11) Austin, L. R.; Seader, J. D. *AIChE J.* **1973**, *19*, 85–93.
(12) Janssen, L. M. *Chem. Eng. Sci.* **1976**, *31*, 215–218.
(13) Deelder, R. S.; Kroll, M. G. F.; Beeren, A. J. B.; Van den Berg, J. H. M. *J. Chromatogr.* **1978**, *149*, 669–682.
(14) Trivedi, R. N.; Vasudeva, K. *Chem. Eng. Sci.* **1974**, *29*, 2291–2295.
(15) Trivedi, R. N.; Vasudeva, K. *Chem. Eng. Sci.* **1975**, *30*, 317–325.
(16) Lundberg, R. E.; Reynolds, W. C.; Kays, W. M. NASA Technical Note D-1972, Aug 1963.
(17) Possanzini, M.; Febo, A.; Liberti, A. *Atmos. Environ.*, in press.
(18) Craig, L. C.; Chen, H. C.; Taylor, W. I. *J. Macromol. Sci., Chem.* **1969**, *A3*, 133–149.
(19) Stevens, T. S.; Jewett, G. L.; Bredeweg, R. A. *Anal. Chem.* **1982**, *54*, 1206–1208.
(20) Dasgupta, P. K. *Anal. Chem.*, following paper in this issue.
(21) Esaylan, M., E. I. du Pont de Nemours and Co., personal communication, 1982, 1983.
(22) Eisenberg, A., Yeager, H. L., Eds. *ACS Symp. Ser.* **1982**, *No. 180*.
(23) Cox, J. A.; Litwinski, G. R. *Anal. Chem.* **1983**, *55*, 1640–1642.
(24) Yeager, H. L. *ACS Symp. Ser.* **1982**, *No. 180*, 41–64.
(25) Helfferich, F. "Ion Exchange"; McGraw-Hill: New York, 1962; p 143.
(26) Poole, L.; Borchers, M. "Some Common BASIC Programs", 3rd ed.; Osborne/McGraw-Hill: Berkeley, 1979.
(27) Yeager, H. L.; Steck, A. *Anal. Chem.* **1979**, *51*, 862–865.
(28) Stumm, W.; Morgan, J. J. "Aquatic Chemistry", 2nd ed.; Wiley: New York, 1981; p 212.
(29) Eberhart, J. G.; Sweet, T. R. *J. Chem. Educ.* **1966**, *37*, 422–425.
(30) E. I. du Pont de Nemours and Co., product information literature, Nafion perfluorosulfonic acid products, 1976.

RECEIVED for review September 15, 1983. Accepted October 7, 1983. This work was supported partially by the Water Resources Center, Texas Tech University, and by the NIH Biomedical Research Support Program at TTU. D.C. was supported by a minority high school student research internship program.

Annular Helical Suppressor for Ion Chromatography

Purnendu K. Dasgupta

Department of Chemistry, Texas Tech University, Box 4260, Lubbock, Texas 79409

A nylon monofilament filled Nafion perfluorosulfonate cation exchanger membrane tubing functions as an efficient suppressor of low dispersion and dead volume for anion chromatography.

Since its introduction in 1975 (*1*), ion chromatography (IC) with eluent conductance suppression and conductometric detection has established itself as a singularly important and powerful tool, especially in anion analysis. The facility of such analysis as demonstrated by commercially available instrumentation is, at least in part, responsible for resurgent interest in ionic analysis by chromatography. The modern practice of ion chromatography includes alternative detection methods (*2–11*). Nonsuppressed single column IC with conductometric detection has also been shown to be useful (*12–16*). The advantages and disadvantages of nonsuppressed vs. suppressed IC have been discussed in the literature (*12, 15, 17*). In essence, the advantages of suppressed IC include wide dynamic range (large column exchange capacity, low probability of column overloading), rapid equilibration, high sensitivity (good base line stability and low drift), and a wide choice of eluents. It suffers from (a) the need to regenerate the suppressor column, (b) variable retention of weak acids by the suppressor column as a function of its degree of exhaustion, and (c) band broadening induced by the suppressor. With the introduction of the continuously regenerated hollow fiber suppressor (*18*) which is always in the same state of regeneration, problems (a) and (b) have been effectively solved. The rather large

0003-2700/84/0356-0103$01.50/0 © 1983 American Chemical Society

dispersion caused by the original version of the continuous suppressor has since been reduced by a packed bead configuration (*19*). In view of continuing advances in improving column efficiency (*20*), the band broadening introduced by this modified version is still significant. In a companion paper (*21*), we have introduced the concept of helical flow through an annulus as a highly efficient way to conduct mass transport to the walls of a tube. In the present article, the use of a filament-filled helix (FFH) as an IC suppressor of low dead volume and dispersion is described and the performance is compared with a continuous suppressor of packed bead configuration.

EXPERIMENTAL SECTION

Construction of devices and other experimental details have been described in ref 21. The devices used in this work consist of 0.66 mm diameter nylon monofilament (40 lb strength fishing line, Stren, Du Pont) filled Nafion 811X (Du Pont Polymer Products Division, Wilmington, DE) perfluorosulfonate cation exchanger membrane tubing (~0.7 mm i.d.) coiled into a helix with a coil diameter of 2 mm. The helix was enclosed in a glass jacket (3 mm i.d.) provided with inlet/outlet T's for flow of regenerant solution (design b in ref 21). Sulfuric acid solution (12.5 mM) was used as regenerant, the choice being dictated by considerations outlined in ref 21. The regenerant solution was allowed to flow by gravity countercurrent to the flow in the helix. The reported conductance data refer to a cell constant of 34.1. The experiments were carried out at 30 °C; the conductance data are corrected to 25 °C. The packed bead suppressor described in ref 19 was obtained as its commercial version (Dionex Corp., Sunnyvale, CA). Apparently the use of glass rather than poly(styrene–divinylbenzene) beads is the only major difference from the literature description of this device. Two solutions, 3 mM $NaHCO_3$ + 2.4 mM Na_2CO_3 and 8 mM $NaHCO_3$ + 6 mM Na_2CO_3, which are widely used in anion chromatography, were used in this work for testing ion exchange efficiency and are designated as E1 and E2, respectively. Dead volume and band dispersion experiments were carried out with water pumped at 2 mL/min through the device, injecting 20 μL of 1 mM KNO_3 solution with a loop injector (Altex Model 210, Berkeley, CA), and recording the optical absorbance as determined at 230 nm by a Schoeffel Model 770 detector (Kratos Inc., Westwood, NJ) with a time constant of 0.5 s at a chart rate of 25 cm/min. In all cases, values for connections only were also determined and were significant. The dead volume of the device under study was taken to be $F(t - t')$ less half the injection volume (10 μL) where F is the flow rate and t and t' are the retention times of the KNO_3 slug for the device (including terminating connections) and connections only. The band broadening introduced by the device was calculated as $(W^2 - W'^2)^{1/2}$ where W and W' are the respective band volumes (twice the peak width at half height) for the device plus terminations and terminations only (*22*).

RESULTS AND DISCUSSION

Quantitative exchange is essential for proper operation in IC. Unfortunately, with Nafion membrane based continuous exchangers, the degree of cation exchange observed with carbonate solutions is difficult to evaluate accurately due to the facile loss of CO_2 through the membrane. Thus, such membrane-based continuous exchangers often lead to suppressed eluent conductances significantly below those obtained with a conventional packed column suppressor. It is therefore important to realize that the attainment of the packed suppressor conductance does not guarantee quantitative exchange. A lack of quantitative exchange manifests itself in serious loss of sensitivity in determining sample ions. The calibration plot (peak conductance vs. concentration of sample ion injected) becomes highly nonlinear at low sample ion concentrations, the linear portion suggesting a negative intercept on the conductance axis at zero sample ion concentration. With E1, we have found that if the suppressed eluent conductance is 95% or below that of the conductance obtained after passage through a conventional packed column suppressor, calibration plots for the chloride ion at the 0.1–1 ppm level is linear. In terms of molarities, 0.1 ppm Cl^- is 2.8 μM while E1 is 7.8 mM Na^+. These results therefore suggest that under these conditions, the eluent is at least 99.97% exchanged. This is suggested as an arbitrary level of acceptable completeness of exchange.

Table I. Performance as an IC Suppressor

flow rate, mL/min	E1[a] conductance, μS			50 cm,[b] Dionex
	50 cm	75 cm	100 cm	
0.5	0.48–0.59	0.56–0.59	0.56–0.84	0.50–0.53
1.0	0.47–0.56	0.54–0.66	0.54–0.66	0.80–0.85
1.5	0.52–1.00	0.45–0.46		
2.0	0.54–1.30	0.50–0.54	0.50–0.51	1.20–1.65
2.5	0.77–1.80	0.65–0.80	0.50–0.52	
3.0	1.29–2.29	0.84–1.06	0.45–0.50	2.00–3.40
3.5			0.50–0.55	
4.0	2.20–3.00	1.18–1.60	0.48–0.62	3.10–5.20

flow rate, mL/min	E2[c] conductance, μS		
	50 cm	75 cm	100 cm
0.5	0.47–0.78	0.85–1.08	0.83–1.25
1.0	0.77–0.96	0.74–0.92	0.85–1.12
1.5	1.10–1.51	0.91–1.15	
2.0	3.70–4.75	1.50–2.31	0.75–0.86
2.5			0.84–1.15
3.0	10.6–12.2	3.71–6.23	1.22–1.69
4.0	16.3–22.0	6.30–11.6	2.66–4.90

[a] Direct conductance 20.8 μS. Completely exchanged conductance 0.69 μS. [b] 50 cm length from commercially available packed bead suppressor. [c] Direct conductance 65.2 μS; completely exchanged conductance 1.05 μS.

The effluent conductances for E1 and E2 at various flow rates for annular helical devices of different lengths are shown in Table I. These data represent the observed range of results for a number of devices made in this laboratory. As has been noted in ref 21, annular helical exchangers excel in their efficiencies of mass transport to the wall. However, mass transport to the wall is only one of the factors in the observed overall efficiency for solutions of such concentrations ($[Na^+]$ = 7.8 and 20 mM for E1 and E2, respectively). We believe that the variation of the wall thickness of the membrane tube among different devices (as well as among different regions of the same device) is the primary reason for the variance of the data reported in Table I. Even with a given device, merely changing the direction of flow (while maintaining countercurrent regenerant flow) often produces a significant change in the effluent conductance. This is not observed when a more dilute solution (e.g., 1 mM KNO_3) is ion exchanged under the same conditions. With such dilute solutions mass transport through the wall is a less important factor (*21*).

The general conclusion that can be reached from Table I is that with E1, 50-cm devices are adequate for flow rates up to 1 mL/min; many perform well up to 2 mL/min. Devices 75 cm in length are adequate for flow rates up to 2 mL/min; many perform well up to 3 mL/min. Devices 1 m long will exchange E1 up to 4 mL/min and, more often than not, up to 5 mL/min (data not shown). We have not carried out detailed studies on minimum regenerant flow requirements since it is so dependent on the exact jacket design and dimensions. However, for the dimensions of the device given in the Experimental Section, 12.5 mM H_2SO_4 flowing at 5 mL/min is sufficient to completely exchange E1 at 4 mL/min through the 100-cm device.

The commercial packed bead suppressor is 150–155 cm long. As have been pointed out by Stevens et al. (*19*), the diameter

Table II. Dispersion Data

device	dead vol, μL	band vol, μL	dispersion, μL
connections only	125	180	
50 cm annular helix	90	200	90
75 cm annular helix	135	220	130
100 cm annular helix	180	234	150
150 cm packed bead supressor	935	421	380

of the packing beads has been optimized in their design and it is indeed an efficient configuration. Since the 1.5 m length results in complete exchange even at 4 mL/min, the performance of this device could not be compared with the FFH devices without altering the length. Fifty-centimeter sections of the packed bead device were utilized for comparison and the results appear in Table I. The FFH is more efficient compared to the packed bead device of the same length. It is however, important to recognize that, over a significant portion of the device, the rate of exchange is controlled by mass transport through the wall, which is not dependent on the nature of the flow field. As such, the differences in mass transfer efficiencies (to the wall) between the two configurations are not reflected in these data. The differences decrease even further with the higher concentration eluent E2. Conversely much larger differences are observed with eluents of lower concentration.

One of the disadvantages that we have found with the packed bead suppressor is the deterioration of performance, especially with respect to band broadening and dead volume, with use. The beads are reportedly packed by suction, without pressure. Under use, pressure expands the elastomeric membrane allowing the mobile beads to pack down densely and less uniformly, leaving large voids in the tube. Additionally, the mobility of the beads contributes to pressure-induced rupture of the membrane at lower pressures than that observed with the FFH, presumably by creating local pressure points. From standard ASTM procedures, Esayian (*23*) estimates the burst pressure of the Nafion 811X tubing to be 400 psi when wet. We suspect that the actual burst pressure is probably somewhat higher since our 1-m devices are in continued operation at 350–400 psi (4 mL/min) for extended periods of time. Concerning pressure drops, the increase in pressure drop with flow rate is less than linear.

When the FFH is first used, the flow rate must be brought up slowly, allowing the fluid to force open its passageway. It is also good practice not to allow the FFH to become completely dry. If these precautions are taken, the FFH suppressor provides a long trouble-free life. Occasionally, after continued use, a small gap develops between the microbore insert and the filament (see Figure 1 in ref 21). If dead volume and dispersion considerations are important, the inlet needs to be disassembled, the microbore insert is pushed in, excess membrane is cut off, and the device is reassembled.

It is important to emphasize that devices much longer than necessary for a given application are undesirable, especially if weak acid anions are to be analyzed. Analogous to the CO_2 loss, loss of the weak acid occurs through the membrane, resulting in diminished analyte signals and increased nonlinearity in calibration plots.

Dispersion and dead volume data are reported in Table II; here the superiority of the FFH is clearly evident. The extent of the increase in dispersion with device length suggests that a significant portion of the observed broadening is due to the terminations integral to the device and not the FFH itself.

ACKNOWLEDGMENT

This research was supported partially by the Water Resources Center at Texas Tech University.

Registry No. Nafion 811X, 65666-67-3.

LITERATURE CITED

(1) Small, H.; Stevens, T. S.; Bauman, W. C. *Anal. Chem.* **1975**, *47*, 1801–1809.
(2) Girard, J. E. *Anal. Chem.* **1979**, *51*, 836–839.
(3) Ricci, G. R.; Shepard, L. S.; Colovos, G.; Hester, N. E. *Anal. Chem.* **1981**, *53*, 610–613.
(4) Zenki, M. *Anal. Chem.* **1981**, *53*, 968–971.
(5) Small, H.; Miller, T. E., Jr. *Anal. Chem.* **1982**, *54*, 462–469.
(6) Denkert, M.; Hackzell, L.; Schill, G.; Sjogren, E. *J. Chromatogr.* **1981**, *218*, 31–43.
(7) Reeve, R. N. *J. Chromatogr.* **1979**, *177*, 393–397.
(8) Buytenhuys, F. A. *J. Chromatogr.* **1981**, *218*, 57–64.
(9) Cortes, H. J. *J. Chromatogr.* **1982**, *234*, 517–520.
(10) Bond, A. M.; Heritage I. D.; Wallace, G. G.; McCormick, M. J. *Anal. Chem.* **1982**, *54*, 582–585.
(11) Williams, R. J. *Anal. Chem.* **1983**, *55*, 851–854.
(12) Molnar, I.; Knauer, H.; Wilk, D. *J. Chromatogr.* **1980**, *201*, 223–240.
(13) Gjerde, D. T.; Fritz, J. S.; Schmuckler, G. *J. Chromatogr.* **1979**, *186*, 509–519.
(14) Gjerde, D. T.; Schmuckler, G.; Fritz, J. S. *J. Chromatogr.* **1980**, *187*, 35–45.
(15) Gjerde, D. T.; Fritz, J. S. *Anal. Chem.* **1981**, *53*, 2324–2327.
(16) Okada, T.; Kuwamoto, T. *Anal. Chem.* **1980**, *55*, 1001–1004.
(17) Pohl, C. A.; Johnson, E. L. *J. Chromatogr. Sci.* **1980**, *18*, 442–452.
(18) Stevens, T. S.; Davis, J. C.; Small, H. *Anal. Chem.* **1981**, *53*, 1488–1492.
(19) Stevens, T. S.; Jewett, G. L.; Bredeweg, R. A. *Anal. Chem.* **1982**, *54*, 1206–1208.
(20) Stevens, T. S.; Langhorst, M. A. *Anal. Chem.* **1982**, *54*, 950–953.
(21) Dasgupta, P. K. *Anal. Chem.*, preceding paper in this issue.
(22) Snyder, L. R.; Kirkland, J. J. "Introduction to Modern Liquid Chromatography", 2nd ed.; Wiley: New York, 1982.
(23) Esayian, M., E. I. Du Pont de Nemours Co., personal communication, 1982.

RECEIVED for review September 15, 1983. Accepted October 7, 1983.

Ion Chromatographic Determination of Morpholine and Cyclohexylamine in Aqueous Solutions Containing Ammonia and Hydrazine

Roland Gilbert* and **Reynald Rioux**

Institut de recherche d'Hydro-Québec (IREQ), 1800 Montée Sainte-Julie, Varennes, Québec, Canada J0L 2P0

Souheil E. Saheb

Gentilly 2 Nuclear Power Plant, Gentilly, Québec, Canada G0X 1G0

In this paper the analysis by ion chromatography (IC) has been successfully applied for the quantification of morpholine (C_4H_9NO) and cyclohexylamine ($C_6H_{11}NH_2$) in aqueous solutions containing parts-per-million amounts of ammonia (NH_3) and hydrazine (N_2H_4). The method is proven to be sensitive and selective at the concentration ranges normally found during water treatment of steam-generating systems. The column length, eluent flow rate, and eluent ionic strength have been optimized to obtain satisfactory resolution of the peaks of the four cations $C_4H_{10}NO^+$, $C_6H_{11}NH_3^+$, NH_4^+, and $N_2H_5^+$ under three analytical modes. The analysis time for all those modes is approximately 50 min. The detection limits are better than those obtained with conventional methods, being 0.1 ppm for both morpholine and cyclohexylamine. None of the water constituents known to interfere with the conventional technique hampers the IC determination. Furthermore, under the amine analytical conditions, this technique allows determination of concomitant species present as impurities in steam–water cycles.

Volatile amines are widely used as corrosion inhibitors in the steam–water cycles of fossil and nuclear power stations. They are usually added to the feedwater to raise the pH of the condensate, feedwater, and drainwater to the level of 9.0–9.5 in order to counteract the corrosive action of any carbon dioxide present in the system. The amine distribution in the steam and condensate sections is obtained by volatilization or steam distillation from the steam generator or boiler. The two amines most widely used for this purpose are morpholine and cyclohexylamine, which in many cases are employed simultaneously. Along with these, hydrazine is injected to scavenge dissolved oxygen and passivate metal surfaces. All of these compounds are subject to thermal–hydraulic decomposition at the temperature and pressures of a medium-pressure steam generator, where the prevailing conditions are such that the major breakdown product is ammonia.

Quantification of these additives and ammonia is an essential step in determining the appropriate amounts to use for maximum protection. Until recently, low levels of morpholine and cyclohexylamine in demineralized water were quantified by such conventional means as gas chromatography (*1, 2*), direct titration (*3, 4*), and colorimetric tests (*5*) (commonly known as the carbon disulfide method for morpholine and the diazotization of *p*-nitroaniline method for cyclohexylamine). However, gas chromatography using flame ionization detection calls for a threshold of 1 ppm for both amines, a limit which unfortunately is a decade higher than the values expected in some critical parts of the steam–water cycle. On the other hand, direct titration, based on determination of the total alkalinity of a sample, gives no information on specific contributors, e.g., ammonia, hydrazine, morpholine, and cyclohexylamine. Finally, when more than one of the amine species are present together, colorimetric procedures are of limited value and are applicable only at higher limits of detection.

There is clearly a need for a specific, interference-free, and more sensitive analytical method for the detection of morpholine and cyclohexylamine in aqueous solutions containing parts-per-million levels of ammonia and hydrazine. Those volatile amines are added to process waters contaminated by cation impurities such as Na^+, K^+, Ca^{2+}, and Mg^{2+} which, since they can cause corrosion of system components, are governed by water quality specifications. In the search for a suitable analytical technique for evaluating the presence of morpholine, cyclohexylamine, ammonia, hydrazine, and the major impurities, the authors report herein upon the possibilities of ion chromatography (IC) as it applies to these amines in the lower concentration ranges found in various systems. The use of IC in power plants for the analysis of steam-condensate purity has already been reported in the literature (*6–10*), while an on-line mode of analysis is currently under development to control high-pressure boilers by blowdown adjustment (*11, 12*).

EXPERIMENTAL SECTION

Apparatus. A Dionex Model 16 ion chromatograph (Dionex Corp., Sunnyvale, CA) equipped with a HP 3390A reporting integrator (Hewlett-Packard Canada, Ltd.) was used for all analyses. The major components of this instrument are an eluent reservoir, a pumping system, a sample-introduction loop, a cation-exchange separator column, and an ion-exchange suppressor column for conversion of the eluent to a nonconductive form. A conductivity cell detector was used for all analyses except for N_2H_4 where the outlet of the separator column was fed through a Dionex electrochemical detector (potentiostat). Disposable plastic 3-mL syringes were used for sample loading in conjunction with an Acrodisc-CR 0.45-μm filter available from Gelman Sciences Inc.

Reagents. Commercially available reagent-grade chemicals were used to prepare the eluents (HCl and HCl/L-lysine) and the cation stock solutions. Standard solutions of each cation of interest and of mixed cations were obtained by diluting aliquots of stock solutions. The sodium hydroxide regenerant (0.5 N) was prepared by using NaOH reagent-grade pellets. Extremely low conductivity water (≃ 0.15 μmhos/cm) obtained by polishing demineralized water through an organic removal cartridge (Barnstead D8904) and an ultrapure mixed-bed ion exchange cartridge (Barnstead D8902) was used for all those preparations.

Procedure. The separator and suppressor columns were first equilibrated with the eluent to be used by maintaining a pump flow rate of 0.7–1.9 mL/min for 45 min; the background conductivity due to the eluent was then electronically offset. The separator column was rinsed at the end of each day by recircu-

0003-2700/84/0356-0106$01.50/0 © 1983 American Chemical Society

Table I. Optimum Instrument Conditions for the Quantification of Ammonia, Hydrazine, Cyclohexylamine, and Morpholine by Ion Chromatography

conditions	mode A	mode B	mode C
analytical column	4 mm × 200 mm Dionex Normal Cation Separator 30831	4 mm × 400 mm Dionex Normal Cation Separator 30831	4 mm × 200 mm Dionex Normal Cation Separator 30831
suppressor column	9 mm × 100 mm Dionex Normal Cation Suppressor 30834	9 mm × 100 mm Dionex Normal Cation Suppressor 30834	none
eluent	0.005 M HCl	0.003 M HCl + 0.0025 M L-lysine	0.003 M HCl + 0.0025 M L-lysine
flow rate, mL/min	1.92	1.30	0.77
sample volume, μL	100	100	100
detection	conductivity	conductivity	electrochemical
ions quantified	$C_4H_{10}NO^+$, NH_4^+, Na^+, K^+	$C_6H_{11}NH_3^+$	$N_2H_5^+$

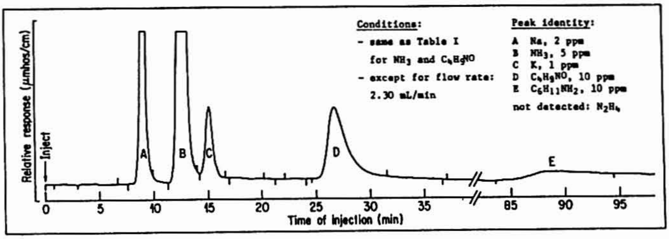

Figure 1. Typical ion chromatogram of a mixture of Na, NH_3, K, N_2H_4, C_4H_9NO, and $C_6H_{11}NH_2$ under optimum conditions for quantification of NH_3 and C_4H_9NO.

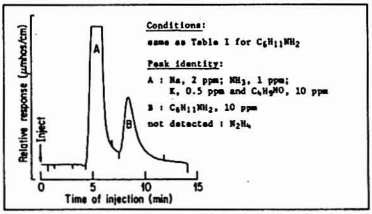

Figure 2. Typical ion chromatogram of a mixture of Na, NH_3, K, N_2H_4, C_4H_9NO, and $C_6H_{11}NH_2$ under optimum conditions for quantification of $C_6H_{11}NH_2$.

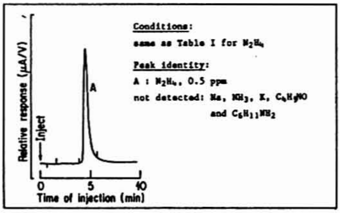

Figure 3. Typical ion chromatogram of a mixture of Na, NH_3, K, N_2H_4, C_4H_9NO, and $C_6H_{11}NH_2$ under optimum conditions for quantification of N_2H_4.

lating the eluent for a period of 1 h. This was followed by regeneration of the suppressor column by back-flushing with the NaOH regenerant at a flow rate of 3.5 mL/min and then rinsing with low-conductivity water. Mixed standard cations were used to optimize the instrument conditions for the quantification of each ion. Species were identified according to their retention times with respect to standard solutions. The calibration data were obtained under the final set of conditions: column length, eluent ionic strength, eluent flow rate, etc.

Table II. Calibration Data for Morpholine, Cyclohexylamine, Hydrazine, and Ammonia—Concentration of Standard Solutions vs. HP 3390A Integrator Signal (Arbitrary Units)

ppm injected	morpholine integrator counts × 10^4	cyclohexylamine integrator counts × 10^4
0.1	0.456	0.400
0.25	1.038	1.063
0.50	1.940	2.065
1	3.764	4.073
2	7.813	8.709
5	20.190	23.519
10	36.784	45.783
20	63.840	99.015
ppm injected	**hydrazine integrator counts × 10^4**	**ammonia integrator counts × 10^4**
0.001	0.048	
0.005	0.242	
0.01	0.493	
0.02		0.541
0.025	1.272	
0.05	2.526	
0.1	5.110	2.837
0.2		5.998
0.25	11.894	
0.5	22.602	15.691
1	39.259	30.321

RESULTS AND DISCUSSION

The separation of amines is illustrated in Figures 1, 2, and 3. Figure 1 shows an ion chromatogram of a mixture of C_4H_9NO, $C_6H_{11}NH_2$, NH_3, N_2H_4, Na and K ions in which all the peaks are well resolved. This separation was obtained with

Table III. Typical Water Chemistry Specifications in the Secondary Cycle of Steam-Generating Systems: Volatile Amines, Hydrazine, and Ionic Impurities

parameter	location	permissible range	first action limit
hydrazine, ppb	CEP[a]	50–100	50
	SGB[b]	50–200	200
NH_4^+, ppm	CEP	<0.8	2
Na^+, ppb	CEP	<1	2
	SGB	<70	70
Cl^- and F^-, ppb	SGB	<100	100
Mg^{2+}, ppb	condenser	<5	5
morpholine, ppm	feedwater	4–17	
	steam and condensate	1–2	
cyclohexylamine, ppm	steam and condensate	1–2[c]	

[a] CEP, condensate extraction pumps. [b] SGB, steam generator blowdown. [c] Not official values.

the columns at room temperature under the instrument conditions shown in Table I, mode A, which were selected for the quantification of C_4H_9NO, NH_3, and the alkali metals Na and K. As shown in Figure 1, the $C_6H_{11}NH_3^+$ ion is eluted as a very wide peak in about 90 min and is detectable only as a minor base line drift. The ion chromatogram of Figure 2 shows two well-defined peaks under the conditions optimized for the quantification of the cyclohexylammonium ion (see Table I, mode B). The length of the analytical column was increased to 400 mm and the eluent flow rate reduced to 1.30 mL/min to obtain the optimum compensation for the accelerating elution effect obtained by the addition of L-lysine to the eluent. The time required for the elution of the $C_6H_{11}NH_3^+$ ion decreased from 90 min (Figure 1, peak E) to 8.45 min (Figure 2, peak B); the broad peak of Figure 2 at 5.23 min (peak A) corresponds to the unresolved ion conductivity signals for Na, C_4H_9NO, NH_3, and K. Under the conditions of modes A and B the hydrazinium ion is virtually undetectable. Hydrazine is rather weakly dissociated and its detection, by conductivity, calls for a more sensitive device. A Dionex electrochemical detector (ECD) was therefore coupled between the IC separator and suppressor column, as recommended by the manufacturer. Figure 3 shows a chromatogram of the mixture recorded from the ECD signal under the conditions specified in Table I, mode C. The peak at 4.77 min corresponds to N_2H_4, which is the only electrochemically active species at the applied potential of +0.6 V by the potentiostat. The eluent at a flow rate of 0.77 mL/min was formulated with the L-lysine component, which here significantly reduces the elution time and allows under mode B the sensitive determination of $C_6H_{11}NH_3^+$.

The HP 3390A integrator signals measured at various cation concentrations of standard solutions are given in Table II. These standards were chromatographed in triplicate runs for each concentration in order to validate its reproducibility. A 10-μmhos/cm full-scale conductivity setting was found suitable for calibration down to sensitivities of 0.1 ppm for morpholine, 0.1 ppm for cyclohexylamine, and 0.02 ppm for ammonia. The hydrazine calibration data were obtained with an ECD setting at 1 μA/V, full-scale, and the sensitivity is such that 0.001 ppm can be determined readily. The four calibration curves that can be obtained from the data of Table II pass through zero, indicating good linearity at the low-concentration range studied, but deviate from linearity as the ionic strength increases. Typical concentrations of morpholine and cyclohexylamine required in feedwater, steam, and condensate to maintain the pH at an appropriate level are given in Table III along with specifications concerning hydrazine, ammonia, and some ionic impurities. As can be seen from the data, the detection limits achieved by IC are below the morpholine and cyclohexylamine prescriptions. For the four cations studied here, the upper limits of the permissible ranges are almost always before the point where the calibration curves deviate from linearity. As shown by Bouyoucos (*13*), the detector deviations from linearity for weak bases such as morpholine, cyclohexylamine, ammonia, and hydrazine could be eliminated if necessary by introducing a short column of chloride-form resin between the suppressor and the conductivity detector. It is even possible to improve the IC detection for more dilute concentrations of morpholine and cyclohexylamine by adding a cation concentrator column and/or a hollow fiber suppressor (*14*) to the analytical system.

To investigate whether these amines interfere with each other when determined by IC, a series of solutions of different cation/interferent ratios in the parts-per-million range were examined. Sodium and potassium were also included as possible interferents because of their close elution with some amines. A sample of a standard cation was chromatographed, followed by a mixture made up from the same standard cation and an interferent. The percentage recoveries observed by comparing the peak area of the standard to that of the mixture are reported in Table IV. None of the constituents known to interfere with the conventional methods indicates a sig-

Table IV. Cation Interference

interferent (C)	morpholine: ppm ratio $C:C_4H_9NO$	morpholine: % recovery	cyclohexylamine: ppm ratio $C:C_6H_{11}NH_2$	cyclohexylamine: % recovery	hydrazine: ppm ratio $C:N_2H_4$	hydrazine: % recovery
$C_6H_{11}NH_2$	10:10	103.8			10:1	97.5
	1:10	94.4			1:1	99.2
	1:1	102.5			10:0.2	102.3
					1:0.2	95.7
C_4H_9NO			10:10	95.9	10:1	96.8
			1:10	98.0	1:1	96.4
			1:1	102.8	10:0.2	106.9
					1:0.2	106.8
NH_3	1:10	107.0	1:10	93.0	1:0.2	101.6
	0.3:10	105.8	0.3:10	97.9	0.5:0.5	96.2
	1:1	101.2	1:1	99.4		
N_2H_4	0.5:10	104.6	0.5:10	94.8		
	0.2:10	95.9	0.2:10	98.5		
	0.2:1	102.0	0.1:1	103.6		
Na	1:10	102.8	1:10	46.8	1:0.2	100.8
	1:1	93.4	1:1	94.4		
K					0.5:0.2	101.5

nificant effect on the percentage recovery by IC.

Variations in the retention times and peak areas were noted during the course of this study: retention times tend to be shortened and peak areas increased with the use of a given separator column. Consequently, the peaks of Figures 1 and 2 were not satisfactorily resolved after a certain number of column loads, apparently because of inorganic and organic cations being absorbed into the column, leading to a reduction in resin capacity. However, the effective lifetime of a separator can easily be extended by following a recommended cleanup procedure, such as recirculating a solution of 0.1 M sodium tartrate into the column for 15 min at 2.3 mL/min as employed in this work. The column to be reconditioned is placed in the suppressor line and the solution is injected from the regeneration system (*15*).

In a subsequent paper, the distribution pattern of these amines between the aqueous and the steam phases will be treated.

ACKNOWLEDGMENT

The assistance and the support provided by the Chemical Division at Hydro-Québec's Gentilly 2 Nuclear Power Station are gratefully acknowledged.

Registry No. C_4H_9NO, 110-91-8; $C_6H_{11}NH_2$, 108-91-8; NH_3, 7664-41-7; N_2H_4, 302-01-2.

LITERATURE CITED

(1) Malaiyandi, M.; Thomas G. H.; Meek, M. E. *J. Environ. Sci. Health, Part A* **1979**, *A14* (7), 609.

(2) Sharif'yanova, L. N. *Metody Anal. Kontrolya Kach. Prod. Khim. Promsti.* **1978**, *6*, 6. *Chem. Abstr.* **1979**, *90*, 214789*w*.

(3) Przybylenski, J. L. *Mater. Perform.* **1979**, *18* (9), 49.

(4) Cuisia Dionesio G. *Mater. Perform.* **1977**, May, 21.

(5) Standard Test Method for Cyclohexylamine in Water, ASTM D2909-74; Standard Test Method for Morpholine in Water, ASTM D1942-74.

(6) Stevens, T. S. *Anal. Chem.* **1977**, *49*, 1176.

(7) Rawa, J. A. In "Ion Chromatography Analysis of Environmental Pollutants"; Mulik, J. D., Sawicki, E., Eds.; Ann Arbor Science: Ann Arbor, MI, 1979; Vol. 2, p 245.

(8) Peterson, S. H.; Bellows, J. C.; Pensenstadler, D. F.; Hickam, W. M. "Proceedings of 40th International Water Conference"; Engineers' Society of Western Pensylvania: Pittsburgh, PA, 1979; p 201.

(9) Brown, J.; Massey, R. E. "Proceedings of 41st International Water Conference"; Engineers' Society of Western Pennsylvania: Pittsburgh, PA, 1980; p 151.

(10) Roberts, K. M. *Anal. Chem.* **1981**, *53*, 1691.

(11) Mansfield, G. H. In "Ion Chromatography Analysis of Environmental Pollutants"; Mulik, J. D., Sawicki, E., Eds.; Ann Arbor Science: Ann Arbor, MI, 1979; p 271.

(12) Hickam, W. M.; Peterson, S. H.; Pensenstadler, D. F.; Bellows, J. C. *Advan. Instrum.* **1981**, *2*, 591.

(13) Bouyoucos, S. A. *Anal. Chem.* **1977**, *49*, 401.

(14) Stevens, T. S.; Jewett, G. L; Bredeweg, R. A. *Anal. Chem.* **1982**, *54*, 1206.

(15) Dionex Ion Chromatography Systems, Technical Note 2R, 1980.

RECEIVED for review July 25, 1983. Accepted September 30, 1983.

CORRESPONDENCE

Direct Analysis of Thin-Layer Chromatography Spots by Fast Atom Bombardment Mass Spectrometry

Sir: Thin-layer chromatography (TLC) is a simple and effective method for the separation of mixtures. Among the techniques available for the identification of fractions after TLC separation, mass spectrometry is especially attractive because of the sensitivity provided. However, the transfer of the separated material from the TLC plate to the mass spectrometer is a laborious, time-consuming procedure which is also subject to certain problems. Usually this transfer is accomplished by scraping the TLC spot from the substrate and either (a) introducing the adsorbent directly into the ion source (*1–4*) or (b) eluting the adsorbed material from the adsorbent with a suitable solvent and evaporating the resulting solution prior to introduction into the mass spectrometer (*4–10*). Various devices have been described for performing these operations on a microscale. Other approaches have included more elaborate systems for locally heating a TLC plate which is directly coupled to the mass spectrometer (*11*, *12*).

Conventional ionization methods (e.g., electron impact or chemical ionization) are limited to samples which can be vaporized without decomposition. However, because gas chromatography is not feasible, TLC is frequently used to separate nonvolatile or thermally labile materials. Although such materials can be ionized by field desorption (FD), the elution procedure is still required in order to transfer the TLC fraction to the FD emitter. It is desirable to avoid the elution step because of possible solubility problems and because severe contamination can be introduced.

We have developed a direct method for obtaining mass spectra of TLC spots which eliminates the above problems. Fast atom bombardment (FAB) ionization (*13*) appeared to be ideally suited for this purpose because adsorbed materials, including those that are nonvolatile or thermally labile, can be ionized directly while on the adsorbent, i.e., without elution. To facilitate the procedure, a simple technique was devised for transferring TLC spots to a FAB probe.

The proposed method involves the following basic steps: (1) After completion of the TLC separation, the spots are located in the usual manner, preferably by ultraviolet fluorescence. (2) The FAB probe tip is covered with a strip of double-faced masking tape and the tip of the probe is merely pressed against the TLC spot of interest in order to transfer the coated adsorbent (Figure 1). (3) About 1–2 μL of a suitable solvent (usually dichloromethane or methanol) and 2–5 μL of FAB matrix liquid (e.g., glycerine or thioglycerine) are added to the TLC adsorbent adhering to the probe tip. (4) The probe tip is then introduced into the mass spectrometer to acquire FAB spectra in the usual manner.

In step (2) the longer dimension of the probe tip is usually placed on the TLC spot parallel to the direction of solvent flow as shown in Figure 1. If a larger flake is removed, the excess can be trimmed. With the probe tip placed at a right angle to the direction of solvent flow, adjacent areas of a single spot may be studied; if the contact area is first lightly scored, excess adsorbent will not be removed.

The application of the method described will be illustrated below using three commercially available coccidiostats.

EXPERIMENTAL SECTION

A Kratos MS-50 high-resolution mass spectrometer was used

0003-2700/84/0356-0109$01.50/0 © 1983 American Chemical Society

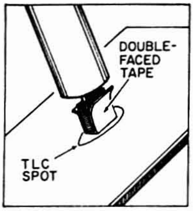

Figure 1. Process for transferring TLC spot to the FAB probe tip.

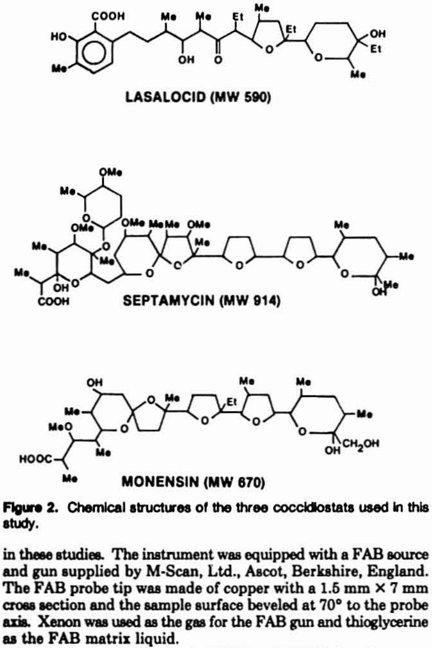

Figure 2. Chemical structures of the three coccidiostats used in this study.

in these studies. The instrument was equipped with a FAB source and gun supplied by M-Scan, Ltd., Ascot, Berkshire, England. The FAB probe tip was made of copper with a 1.5 mm × 7 mm cross section and the sample surface beveled at 70° to the probe axis. Xenon was used as the gas for the FAB gun and thioglycerine as the FAB matrix liquid.

Plastic-backed TLC sheets, 1B2-F and 1B2 Baker-flex, were from J. T. Baker Chemical Co., Phillipsburg, NJ, and glass-backed TLC plates, silica gel 60F-254, 0.25 mm, were from MCB Manufacturing Chemists, Inc. (associate of E. Merck, Darmstadt, Germany) Cincinnati, OH. Prior to spotting, all TLC plates were cleaned by solvent development and drying. Lasalocid, septamycin, and monensin are commercially available poultry coccidiostats.

To demonstrate the method, a dichloromethane solution was prepared containing 60 μg/μL of a mixture consisting of equal amounts of lasalocid, septamycin, and monensin. About 0.3 μL of this solution was spotted on a TLC plate alongside 1 μL of a 20 μg/μL solution of each of the three individual products. The plate was developed with 70/30 ethyl acetate/dichloromethane.

RESULTS AND DISCUSSION

The structures of the three coccidiostats used to demonstrate the method are shown in Figure 2. Preliminary FAB spectra of the three individual products gave pseudomolecular ions such as MH^+, MNa^+, MK^+, etc., with MNa^+ being the most prominent. Septamycin also gave an intense fragment ion at m/z 875. The chromatogram of the mixture is shown in Figure 3, together with those of the three separate products run in parallel. This TLC plate was charred with sulfuric acid for visualization. R_f values were 0.89, 0.79, and 0.27 for lasalocid, septamycin, and monensin, respectively. Although minor impurities were observed in septamycin, they were not studied.

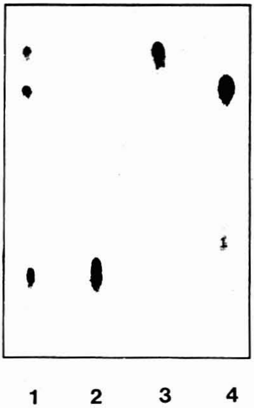

Figure 3. Thin-layer chromatograms of (1) mixture of lasolocid, septamycin, and monensin (6 μg of each); (2) monensin (20 μg); (3) lasalocid (20 μg); and (4) septamycin (20 μg).

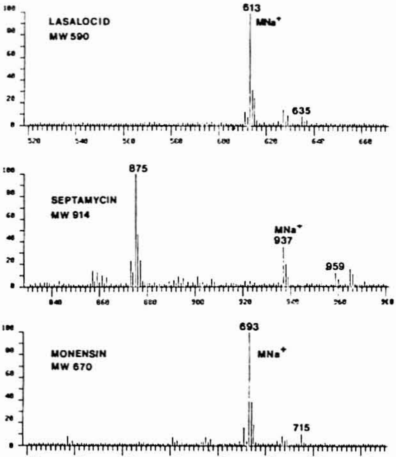

Figure 4. FAB mass spectra obtained from the TLC spots after separation of a mixture of lasalocid, septamycin, and monensin.

The FAB spectra shown in Figure 4 were obtained for each of the three TLC fractions after separation of the mixture by using the procedure previously described. Each fraction is readily identified based on the pseudomolecular ion(s). These FAB spectra are comparable to those obtained with the individual products prior to mixing. Minor differences are attributable to the separation of impurities and to the partial neutralization of the carboxyl functionality. The latter change is indicated, e.g., by the presence of a small peak at m/z 635 in the spectrum of lasalocid, which is assigned to (M − H + Na)Na$^+$. With monensin spotted on a TLC plate, the sensitivity of detection was established as well below 0.1 μg.

A major concern was the possible interference related to the components in the TLC adsorbent and the masking tape. However, no background interference was observed in the mass range of interest based on blank tests of both fluorescent and nonfluorescent TLC plates and direct tests of the masking tape. Also, contamination of the ion source by the TLC adsorbent, i.e., silica gel, was not observed. However, after the depletion of the FAB matrix liquid, the flake of adsorbent from plastic-backed TLC sheets appeared to remain intact while that from glass TLC plates tended to disintegrate. For this reason we favor the use of plastic-backed TLC sheets.

In conclusion, we have demonstrated a simple and rapid method for directly obtaining FAB spectra of TLC fractions which circumvents the problems associated with the previously cited methods.

ACKNOWLEDGMENT

We wish to thank D. B. Borders and M. T. Lee of Lederle Laboratories, American Cyanamid Company, for providing the coccidiostats and the TLC separation procedure.

LITERATURE CITED

(1) Deverse, F. T.; Gipstein, E.; Lesoine, L. G. *Instrum. News* **1967**, *18*, 16.
(2) Down, G. J.; Gwyn, S. A. *J. Chromatogr.* **1975**, *103*, 208–210.
(3) Kraft, R.; Otto, A.; Makower, A.; Etzold, G. *Anal. Biochem.* **1981**, *113*, 193–196.
(4) Nilsson, C. A.; Norstrom, A.; Andersson, K. *J. Chromatogr.* **1972**, *73*, 270–273.
(5) Rix, M. J.; Webster, B. R.; Wright, I. C. *Chem. Ind. (London)* 1969, 452.
(6) Clemett, C. J. *Anal. Chem.* **1971**, *43*, 490.
(7) Clarke, R. L. *Chem. Ind. (London)* **1971**, *1434*–1435.
(8) Koehler, M. *Chromatographia* **1975**, *8*, 685–689.
(9) Dekker, D. *J. Chromatogr.* **1979**, *168*, 508–511.
(10) Unger, S. E.; Vincze, A.; Cooks, R. G.; Chrisman, R.; Rothman, L. D. *Anal. Chem.* **1981**, *53*, 976–981.
(11) U.S. Patent 3 896 661, 1975.
(12) Ramaley, L.; Vaughan, M. A.; Jamieson, W. D.; Burnett, N. H. 30th Annual Conference on Mass Spectrometry and Allied Topics, Honolulu, HI, June 6–11, 1982.
(13) Barber, M.; Bordoli, R. S.; Elliott, G. J.; Sedgwick, R. D.; Tyler, A. N. *Anal. Chem.* **1982**, *54*, 645A–657A.

Ted T. Chang*
Jackson O. Lay, Jr.
Rudolph J. Francel

Chemical Research Division
American Cyanamid Company
P.O. Box 60
1937 West Main Street
Stamford, Connecticut 06904

RECEIVED for review June 20, 1983. Accepted August 18, 1983.

Electrokinetic Separations with Micellar Solutions and Open-Tubular Capillaries

Sir: The applicability of the solubilization by micelles to chromatography as a distribution process has briefly been discussed by Nakagawa (*1*). The point of his discussion may be summarized as follows: Micelles of an ionic surfactant can migrate in an aqueous solution by electrophoresis. When a solubilizate is added into a micellar solution, some portion of the solubilizate may be solubilized into the micelle. Thus the solubilization by micelles can constitute a mechanism of retention in chromatography. The distribution ratio of a solubilizate will increase with an increase of the micellar concentration but will be constant regardless of the concentration of the solubilizate. If a solubilizate is soluble in an aqueous solution to a certain extent, the distribution equilibrium is considered to be established very rapidly because, e.g., the stay time of benzene in the micelle of sodium dodecyl sulfate has been estimated to be less than 10^{-4} s (*2*).

The electrokinetic separation method described in this paper may be classified as a type of liquid–liquid partition chromatography requiring no solid support to hold the stationary liquid phase, although micelles are considered to be a pseudophase. It should be noted that this technique is distinctly different from the reversed-phase liquid chromatography with micellar mobile phase (*3*): In the latter, the separation is based on distribution processes among three phases, stationary bonded phase, micelle, and water, and micelles migrate with water as an aqueous pseudophase.

This paper presents the results of some preliminary studies on electrokinetic separation with micellar solution in open-tubular capillaries, in which use was made of the technique of free zone electrophoresis in open-tubular capillaries (*4*, *5*).

EXPERIMENTAL SECTION

Apparatus. Electrokinetic separation was performed in microbore vitreous silica tubing, 650 or 900 mm long, 0.05 mm i.d. (Scientific Glass Engineering Inc.), with a Model HSR-24P regulated high-voltage dc power supply (Matsusada Precision Devices, Otsu, Japan) delivering +3 to +25 kV. Each end of the capillary tube was dipped in a small glass beaker containing a surfactant solution covered with a silicone–rubber stopper having two small-bore holes, one for a platinum electrode and the other for the capillary tube. The electric current was monitored between the negative electrode and the negative terminal of the power supply with an ammeter throughout the operation. Detection was carried out by on-column measurement of UV absorption through a slit of 0.05 mm × 0.75 mm, the long axis of which was placed parallel to the column axis at a position 150 mm from the negative end of the tube. The polymer coating of the vitreous silica tubing was partly burned out at the detection point of the tube to make an on-column UV cell. A Jasco UVIDEC-100-II spectrophotometric detector (Tokyo, Japan) was used with minor modification to obtain a higher amplifier gain and a shorter response time than the conventional one.

Reagent. Sodium dodecyl sulfate (SDS) of protein-research grade purchased from Nakarai Chemicals (Kyoto, Japan) was used as it was received. Water was purified with a Milli-Q system. Other reagents were of analytical-reagent grade and were used without further purification. Borate–phosphate buffer solution, pH 7.0 was prepared by mixing a 0.025 M sodium tetraborate solution and a 0.05 M sodium dihydrogen phosphate solution in an appropriate ratio to indicate pH 7.0. An SDS solution was prepared by dissolving 1 mmol of SDS in 20 mL of the borate–phosphate buffer solution followed by filtration of the solution through a membrane filter of 0.5-μm pore size.

Procedure. A capillary tube was filled with an SDS solution by use of a microsyringe and 1.5 mL each of the same SDS solution was introduced in two beakers placed at the same level. For the sample injection, the positive end of the tube was moved into a vessel containing a sample solution and the level of the sample solution was raised about 4 cm higher than that of the SDS

© 1983 American Chemical Society

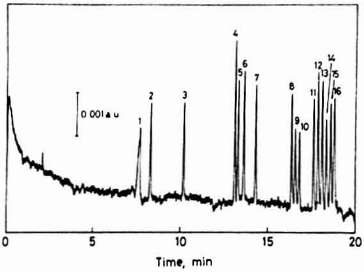

Figure 1. Electrokinetic separation of phenols with an SDS solution: (1) water, (2) acetylacetone, (3) phenol, (4) *o*-cresol, (5) *m*-cresol, (6) *p*-cresol, (7) *o*-chlorophenol, (8) *m*-chlorophenol, (*9*) *p*-chlorophenol, (10) 2,6-xylenol, (11) 2,3-xylenol, (12) 2,5-xylenol, (13) 3,4-xylenol, (14) 3,5-xylenol, (15) 2,4-xylenol, (16) *p*-ethylphenol; micellar solution, 1 mmol of SDS in 20 mL of borate–phosphate buffer, pH 7.0; current, 28 μA; detection wavelength, 270 nm; temperature, ca. 25 °C.

solution to allow the sample solution to flow downward into the capillary tube. After 5 to 90 s depending on the desired amount of injection, the end of the tube was returned to the beaker and a high voltage was applied.

RESULTS AND DISCUSSION

The chromatogram shown in Figure 1 illustrates the high resolution obtained by electrokinetic separation with micellar solution. The applied voltage between both ends of 900 mm tube was ca. 25 kV. The separation performed in the 750 mm portion from the injection end to the detector cell was recorded by the on-column detection technique. Fourteen phenol derivatives injected as a water solution were completely resolved within 19 min. The injected amount of each phenol was estimated to be 0.7–1 ng and the total injection volume about 12 nL. Theoretical plate numbers calculated from the chromatogram were 210 000 for phenol, 260 000 to 350 000 for cresols and chlorophenols, and 300 000 to 400 000 for xylenols and *p*-ethylphenol, corresponding to plate height equivalent to a theoretical plate of 1.9–3.6 μm. Lower plate numbers observed for the peaks at shorter retention times may be attributable to the adverse effect of the large sample volume.

It has been reported that the electroosmotic flow is much stronger than the electrophoretic migration of an ion in the case of electrophoresis in open-tubular glass capillaries (*5*). Similar results were observed in this study: The SDS solution as a whole was carried from the positive electrode to the negative one and negatively charged micelles of SDS also migrated toward the negative electrode as opposed to the electrophoretic attraction. This means that every sample injected at the positive end of the tube can be detected at the negative side of the tube. When a cationic surfactant such as cetyltrimethylammonium bromide was employed instead of an anionic one, the situation was reversed and hence the inversion of polarities of electrodes was needed.

The volume flow by electroosmosis in a narrow cylindrical capillary increases linearly with the applied electric field and also with the current (*6*). When the electrokinetic radius κa is larger than 50, where κ is the reciprocal of the Debye length and a is the radius of the capillary tube, the velocity profile has been calculated to be flat in the range $0 \leq r \leq 0.9a$ by Rice and Whitehead (*6*), where r is the point distance from the axis. The value κa is estimated much larger than 50 under the conditions employed in this study. Therefore, the plug-shape flow of electroosmosis is one of the reasons for the high efficiency attained in this study. The linear relationship between the electroosmotic migration velocity v_{EO} and the current was always recognized. However, the plot of the velocity v_{EO} vs. the total applied voltage showed a positive deviation from linearity at higher voltages, although the actual strength of the applied field in the tube was not measured.

The retention parameters in electrokinetic separation are different from those in the conventional elution chromatography, because the retention time of any sample, if it is electrically neutral, should fall between the retention times of an insolubilized solute and a micelle itself in this method. Two assumptions are made for simplicity of the discussions below. One is that solute molecules are electrically neutral under the separation conditions. The other is that the electroosmotic velocity is larger than the electrophoretic velocity of a micelle and that their migrating directions are opposite.

A solute which is not solubilized by micelles at all should migrate with the same velocity as the electroosmotic flow v_{EO} and be eluted first at the retention time t_0. On the other hand, a solute which is completely solubilized with micelles should migrate with the same velocity as that of a micelle v_{MC} and be eluted last at the retention time t_{MC}. The velocity v_{MC} is the difference between v_{EO} and the electrophoretic velocity of a micelle v_{EP}, or $v_{MC} = v_{EO} - v_{EP}$. The retention time of an ordinary sample should depend on the capacity factor k', which is given by the ratio of the total moles of the solute in the micelle n_{MC} to those in the aqueous phase n_W, or $k' = n_{MC}/n_W$. The retention time t_R should appear in the range $t_0 \leq t_R \leq t_{MC}$. The R value, the fraction of the solute in the aqueous phase, is given by

$$R = \frac{v_S - v_{MC}}{v_{EO} - v_{MC}} \tag{1}$$

where v_S is the migration velocity of the solute. Now, the R value can be related to k' by (*7*)

$$R = \frac{1}{1 + k'} \tag{2}$$

Inserting the relationship, $v_{EO} = L/t_0$, $v_{MC} = L/t_{MC}$, and $v_S = L/t_R$, where L is the tube length from the injection end to the detector cell, into eq 1, followed by combination with eq 2 gives

$$k' = \frac{t_R - t_0}{t_0(1 - (t_R/t_{MC}))} \tag{3}$$

The term $(1 - (t_R/t_{MC}))$ comes from the retention behavior characteristic of electrokinetic separations. When t_{MC} becomes infinite, eq 3 is equivalent to the well-known equation for conventional chromatography.

The chromatogram shown in Figure 2 clearly reflects the situation described above. Methanol was chosen as an insolubilized solute to measure t_0 and Sudan III to determine t_{MC}. The capacity factors of the solutes in Figure 2 are 0, 0.49, 1.28, 2.27, 3.08, and infinity in the order of elution. A capacity factor of infinity means the solute will not be eluted by traditional chromatography and it also means that the solute is totally associated with the micelle in this case. The linear decrease of k' with the increase of the current or v_{EO} was observed although slopes of the plots k' vs. v_{EO} were different among solutes. The reason for this dependence remains to be clarified but can probably be found in the increase of the solution temperature by Joule heating with increasing applied voltage and/or the possible change in the physical property of a micelle by the strong external electric field.

Electrokinetic separations with micellar solutions in open-tubular capillaries have been proved to be a high-resolution chromatographic method. It is limited to an analytical application because of a small sample size at present, but the zone electrophoretic technique with some kinds of stabilizing media widely utilized in the field of electrophoresis may be

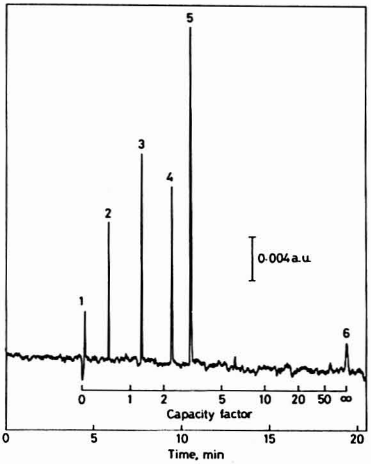

Figure 2. Chromatogram by electrokinetic separation indicating the total range of elution: (1) methanol, (2) phenol, (3) *p*-cresol, (4) 2,6-xylenol, (5) *p*-ethylphenol, (6) Sudan III; total tube length, 650 mm; tube length from the injection end to the detector cell, 500 mm; total applied voltage, ca. 20 kV; current, 33 μA; detection wavelength, 220 nm. Other conditions are the same as in Figure 1.

employed for preparative purposes in electrokinetic separations. The use of a surfactant solution in an aqueous organic solvent will expand the applicability of this method to water-insoluble compounds. Electrokinetic separations with micellar solutions would be useful for studying chemistry of micelles as well as for analytical purposes. Further extensive investigations are being continued to develop the possibilities of this technique.

ACKNOWLEDGMENT

We thank T. Nakagawa who has proposed the application of solubilization by micelles to chromatography and H. Jizomoto for their helpful suggestions and discussions.

LITERATURE CITED

(1) Nakagawa, T. *Newsl., Div. Colloid Surf. Chem., Chem. Soc. Jpn.* **1981**, *6*, No. 3, 1.
(2) Nakagawa, T.; Tori, K. *Kolloid Z. Z. Polym.* **1964**, *194*, 143–147.
(3) Armstrong, D. W.; Nome, F. *Anal. Chem.* **1981**, *53*, 1662–1666.
(4) Mikkers, F. E. P.; Everaerts, F. M.; Verheggen, Th. P. E. M. *J. Chromatogr.* **1979**, *169*, 11–20.
(5) Jorgenson, J. W.; Lukacs, K. D. *Anal. Chem.* **1981**, *53*, 1298–1302.
(6) Rice, C. L.; Whitehead, R. *J. Phys. Chem.* **1965**, *69*, 4017–4024.
(7) Karger, B. L.; Snyder, L. R.; Horvath, C. "An Introduction to Separation Science"; Wiley: New York, 1973; Chapter 5.

Shigeru Terabe*
Koji Otsuka
Kunimichi Ichikawa
Akihiro Tsuchiya
Teiichi Ando

Department of Industrial Chemistry
Faculty of Engineering
Kyoto University
Sakyo-ku, Kyoto 606, Japan

RECEIVED for review July 8, 1983. Accepted September 19, 1983.

Electrodeposition of Actinides in a Mixed Oxalate–Chloride Electrolyte

Sir: The increasing number of analyses of environmental and biological samples along with a greater need for more sensitivity have made almost impossible demands upon electrodeposition procedures. Electrodeposition has virtually become a requirement for high-quality isotopic identification and quantification of the α-emitting actinides, often under the most severe conditions. Increased sensitivity requires larger samples, and this, short of extensive separations, means more impurities during deposition. Because most deposition procedures are extremely sensitive to hydrolytic losses, even microgram amounts of impurities can cause problems with yield and resolution. However, by merely increasing the acidity immediately prior to the beginning of the deposition, losses have been substantially decreased, and the tolerance to impurities has been improved for all the actinides without the addition of hydrofluoric acid as previously required (*1*). Previously, the pH was adjusted by addition of ammonium hydroxide and hydrochloric acid to a pH of about 4 using methyl red indicator. To eliminate this pH adjustment and the possibility of local hydrolysis around the drops of ammonium hydroxide, the sample is dissolved in a preadjusted electrolyte. A final pH adjustment is made with hydrochloric acid to a pH of ~1.6–1.8, the salmon pink end point of thymol blue indicator. To ensure complete dissolution of extremely hydrolytic nuclides such as protactinium and thorium, the sample, in sodium acid sulfate crystals, is heated in a hydrochloric acid–sulfuric acid mixture to sulfuric acid fumes just before deposition. The above-named changes markedly improved the reliability of all of our actinide analyses.

EXPERIMENTAL SECTION

Apparatus. Early depositions were made with an Eberbach electroanalysis apparatus modified to maintain a constant preset current, with the motor replaced to reduce the speed of the anode to about 30 rpm. Subsequent depositions were made with an apparatus designed and fabricated in our own laboratory with characteristics similar to the Eberbach apparatus. The 20-mm i.d. glass cells described in a prior publication (*1*) are no longer available and have been replaced with disposable polyethylene cells molded in our laboratory. The brass bases and polyethylene collars have been modified to accommodate the new cells. A water-cooling jacket is no longer required in the base as the brass holder on the apparatus is water cooled and serves as a heat sink as well as an electrical conductor. The platinum anode and stainless steel disks are the same as before. The stainless steel disks are boiled in 16 M nitric acid for about 5 min, rinsed with distilled water, blotted, and air-dried. The α-emitting nuclides were deposited from solutions of approximately 2×10^4 dpm and were counted for 10 min by alpha scintillation as described by Sill (*2*). α-energy analyses were obtained with a 450-mm^2 solid-

This article not subject to U.S. Copyright. Published 1983 by the American Chemical Society

state surface barrier detector in conjunction with a 400-channel pulse-height analyzer. All γ counting was done in a 3 by 3 in. thallium-activated sodium iodide well crystal for 5 min on solutions of approximately 10^4 cpm to give an error of <1% at the 95% confidence level.

Reagents. *Preadjusted Electrolyte.* Dissolve 30 g of ammonium oxalate monohydrate, 51.4 g of ammonium chloride, 0.9 g of hydroxylamine hydrochloride, and 3.3 mL of a 1 M solution of the ammonium salt of diethylenetriaminepentaacetic acid (DTPA) (*1*) in 900 mL of boiling water. Cool to about 35 °C and add 12 M hydrochloric acid to a pH of 3.5 as measured with a pH meter. Cool to room temperature and dilute to 1000 mL with water.

Procedure. Heat the sample with 100 mg of sodium acid sulfate and 0.5 mL of 18 M sulfuric acid to near absence of fumes in a 250-mL Erlenmeyer flask on an asbestos-covered hotplate. At this point, the sample can be stored almost indefinitely without risk of loss due to hydrolysis. Just before the deposition, dissolve the crystals with 10 mL of 6 M hydrochloric acid 0.06 M in sulfuric acid and heat to sulfuric acid fumes.

Deposition of Th, Pa, Np, and Pu. Using a total of 15 mL of preadjusted electrolyte, transfer the sample to the cell in the following manner. Add about 5 mL of the electrolyte and 2 drops of thymol blue indicator and heat to dissolve the sample. For protactinium, neptunium, and thorium depositions, add 2 drops of 4.7 M hydrofluoric acid. Add 12 M hydrochloric acid dropwise to a pink end point (pH ~1.6–1.8), and add the solution to the electrodeposition cell. Make two rinses, without heating, with the remaining electrolyte. Position the cell in the electrodeposition apparatus so that the platinum anode is about 5 mm above the cathode and turning at about 30 rpm. Deposit the sample onto a 19-mm diameter cathode at 1.8 A (0.63 A/cm^2) for 70 min. Continue as below.

Deposition of Am, Cm, Cf, and U. Using a total of 20 mL of preadjusted electrolyte, transfer the sample in the following manner. Add about 15 mL of the electrolyte and 2 drops of thymol blue and heat to dissolve the sample. Add 12 M hydrochloric acid dropwise to a pink end point. Boil the solution gently for 4 min and add the solution to the cell. Rinse the flask with the remaining electrolyte. For Am, Cm, and Cf, deposit 90 min at 2.2 A, and for U, deposit 90 min at 2.0 A. Adjust the flow rate of the cooling water so that the temperature of the electrolyte is warm, 25 to 35 °C. Because of the evolution of chlorine gas, the deposition must be performed in a fume hood. At the end of the deposition, forcefully add 3 to 5 mL of 14 M ammonium hydroxide to the cell from a wash bottle. After about 30 s, turn the stirrer off and remove the cell from the apparatus. Discard the electrolyte and rinse the cell with approximately 0.01 M ammonium hydroxide. Dismantle the cell and wash the plate with the 0.01 M ammonium hydroxide by directing the rinse at the unplated portion of the disk. Wash the plate with 95% ethanol in the same manner, and dry the plate on a bare hotplate for 5 min to fix or volatilize any polonium-210 and prevent subsequent contamination of the detector (*3*).

RESULTS AND DISCUSSION

Electrodeposition is probably the most critical step in actinide analysis. These extremely hydrolytic nuclides, with microgram quantities of impurities, can often deposit on the glass cell or the anode or even precipitate in the electrolyte during the deposition. When serious losses do occur, most of the undeposited activity is usually found in the electrolyte, probably due to hydrolysis and precipitation of the actinides with the impurities.

The problems associated with impurities and hydrolysis are probably common to all electrodeposition procedures. However, the extent of the impurity problem is somewhat dependent upon the method of separation used prior to the electrodeposition step. Many analytical procedures separate the actinides from various sample matrices with ion exchange techniques, thereby minimizing the amounts of impurities accompanying the actinides. We use the faster liquid–liquid extraction in our laboratory for most of our separations and, consequently, have had to accommodate our electrodeposition method to relatively substantial amounts of impurities. Although the interference study in the previous procedure (*1*) indicated we should have few problems from the most common impurities, we did have some severe yield problems with our soil analyses. However, the addition of more acid at the beginning of the deposition dissolves and keeps dissolved the total sample, preventing hydrolysis and loss within the electrolyte.

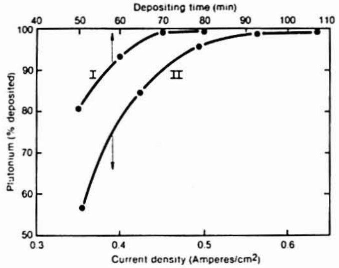

Figure 1. Effect of time and current density on the deposition of plutonium: (I) variable depositing time at 0.63 A/cm^2; (II) variable current density, 70-min depositions.

Rather than prepare the electrolyte by separate additions of each component and a pH adjustment with ammonium hydroxide and hydrochloric acid for each deposition, the electrolyte ingredients were combined and adjusted as a single reagent before the deposition. The combination of the ingredients in their original concentrations would not stay in solution at room temperature. Therefore, the concentrations in this single reagent were reduced to approximately 75% of those published. Previously, where the components were added separately, solubility was not a problem as the components were added hot and remained hot throughout the deposition. At this new concentration level and pH of 3.5, the electrolyte is quite stable and remains soluble at room temperature. However, much variation of the pH either way from 3.5 can cause solubility problems.

New time and current curves were determined for the new electrolyte as shown in Figure 1. Although good yields were obtained at lower current densities, the higher value of 0.63 A/cm^2 for a 70-min deposition is recommended in order to discharge more rapidly any excess hydrogen ion that might be added during pH adjustment.

Table I shows the effect of some commonly encountered cations on electrodeposition yields and α peak resolution using a preadjusted electrolyte and higher acidity. As before (*1*), the major emphasis was placed on plutonium with the yield values determined by analyzing the minor fractions on $BaSO_4$ (*2*). As iron is common to almost every kind of sample, it was examined at greater length than the other cations. Aluminum is almost equally important as aluminum nitrate salting solutions are used in many extractions of the actinides. Both iron and aluminum showed considerably less interference at the higher acidity and without the need of hydrofluoric acid as previously described (*1*). Titanium, calcium, lanthanum, cerium, thorium, and uranium are all found to some extent in soils. With the exception of cerium, small amounts of these elements do not greatly affect the yield. Cerium is probably oxidized to the tetravalent state at the anode subsequently hydrolyzing and carrying activity out of solution.

The platinum that is dissolved off the platinum dishes used for pyrosulfate fusions, and the lead impurity that is frequently found in reagents such as aluminum nitrate, do not seem to lower the yield seriously. However, the lead did have a very bad effect on the resolution, plating with or onto the activity.

Table I. Yields and Resolution of Nuclides Deposited in the Presence of Various Cations

		percent deposited[a]			
cation	µg	thorium-230	uranium-233	plutonium-239	americium-241
Fe^{3+}	500			77.1 (42)[b]	
	250			92.3 (49)	
	100			98.1 (41)	
	50	99.0	97.2	99.3 (40)	99.1
Al^{3+}	200			96.3 (36)	
	100	97.0	95.5	98.0 (36)	91.7
Ti^{4+}	100			85.9 (59)	
	50	92.9	92.4	99.5 (49)	97.2
Th^{4+}	200			92.9 (64)	
	100	93.0	93.1	97.8 (58)	98.3
Ca^{2+}	1000			95.3 (35)	
	500	97.8	98.4	99.6 (38)	98.3
La^{3+}	100			85.6 (64)	
	50	99.2	81.8	95.3 (49)	99.0
Ce^{3+}	100			70.9 (39)	
	50	99.2	55.2	92.6 (45)	74.6
U^{6+} (as UO_2^{2+})	500			77.6 (73)	
	250			91.5 (86)	
	100	98.3	93.8	96.4 (52)	96.2
Pt^{4+}	1000	99.2	97.5	99.3 (36)	99.4
Pb^{2+}	1000	71.8	99.6	92.2 (67)	95.6
(10 µg each of 10 cations above)[c]				99.4 (66)	
Al^{3+} Fe^{3+} Ti^{4+} Ca^{2+}	50 ea 25 ea 25 ea[c]	98.5	99.3	93.4 (45) 99.6 (42) 99.5 (56)	

[a] Deposited from solutions of ~2 × 10^4 dpm with uncertainties of ±0.2% based on counting statistics. [b] Resolution, keV, fwhm. [c] Flamed with a Fisher blast burner to dry crystals.

Good resolution expressed in keV full width at half maximum peak height (fwhm) is almost as important as good yields, as a broad energy peak can obscure a closely neighboring peak. Had both plutonium-239 and protactinium-231 been deposited with the lead, the protactinium-231 could quite easily have been overlooked completely. Substantial amounts of any material that deposit on or with an actinide will seriously affect the resolution. Therefore, it is important that the total mass deposited be kept at a minimum.

Heating the sample to sulfuric acid fumes in the presence of sodium acid sulfate just prior to the deposition ensures that the nuclides, as well as any impurities present, can be easily and quickly dissolved in the electrolyte. Equally important, the nuclides will be in the proper ionic form to undergo the chemistry of deposition and will not remain even partially hydrolyzed. This treatment has proven to be a very important step, particularly for thorium depositions.

In most depositions, impurities will probably occur in combination, not singly, so their effects on yield and resolution would be at least additive if not worse. Therefore, to show just how effective and necessary the presence of sodium acid sulfate is, two plutonium-239 samples, of about 2 × 10^4 dpm, with a total of 0.100 mg of various impurities, 100 mg of sodium acid sulfate, and sulfuric acid, were heated to dry crystals in the high temperature flame of a Fisher blast burner. Such vigorous treatment should markedly enhance the effect of any impurities present. However, no major loss of activity resulted from this treatment, only deterioration of resolution due to self-absorption from codeposited material. Both yields were greater than 99% as seen in Table I.

The small amount of sulfuric acid remaining after heating the sample to fumes is not sufficient to lower the pH to ~1.6. Obviously, more sulfuric acid could be added for this purpose, thus obviating the need for any pH adjustment at all. However, this kind of treatment has consistently resulted in lower yields. As it is highly possible for hydrolysis and precipitation to occur even during the dissolution and transfer with the electrolyte, the addition of 12 M hydrochloric acid is almost mandatory to redissolve any even partially hydrolyzed material and lower the pH before deposition.

Table II. Depositions of Actinides[a]

	percent deposited[b]	
nuclide	w/o HF	w/HF[c]
^{230}Th	98.8 (99.0)[d]	98.2 (98.5)
^{231}Pa	97.8	96.6
^{233}U	98.4 (100)	96.2 (98.9)
^{237}Np	93.3 (92)	99.2 (99.4)
^{239}Pu	99.3 (100)	96.9 (99.3)
^{241}Am	98.4 (100)	87.7 (99.2)
^{244}Cm	98.8 (96)	83.4 (99.2)
^{252}Cf	98.6 (92)	81.8 (99.3)

[a] Approximately 2 × 10^4 dpm. [b] Uncertainties are ±0.2% based on counting statistics. [c] [HF] = 0.03 M. [d] Numbers in parentheses are published values from *Anal. Chem.* 1972, *44*, 284.

With the exception of neptunium, all the actinides deposited with good yields in the absence of fluoride as seen in Table II. However, neptunium was also low previously (*1*) in the absence of fluoride. Fluoride is known to have a catalytic effect on the oxidation or reduction of NpO_2^+ (*4*) which probably accounts for the increased yield with fluoride. The concentration of fluoride used was nearly the same as that in the published procedure. Lower volume and electrolyte concentrations, which resulted in decreased complexing ability and competition with the fluoride, probably caused the tervalent actinides to precipitate as insoluble fluorides. Though there was little difference in the thorium yields with and without fluoride, 2 drops of 4.7 M hydrofluoric acid is recommended for thorium depositions, particularly for those analyses that use organic phosphates for liquid–liquid extractions. With the increased tolerance to impurities at the lower pH, it is doubtful that fluoride will ever again be used routinely, except for thorium, protactinium, and neptunium.

The distribution of activity within the deposited area greatly influences the counting efficiency of the solid-state detector used to identify and quantify a given nuclide. The shape of the anode and its proximity to the cathode, to some extent, determine this distribution. However, by use of internal tracers for yield determination such as ^{236}Pu, ^{243}Am, and ^{232}U, the anomalies of distribution become insignificant.

Rotation of the anode is not needed to obtain a good yield, but a moderate rotation speed does have some advantage. A rotating anode will prevent the accumulation of gas bubbles and assure an even current flow. Additionally, rotation should accommodate wobble and imperfections of shape, thereby evening out any incorrect attitudes of the anode with respect to the cathode. The gauze anode used in this procedure, rotating at about 30 rpm, seems to give the best yields with the most uniform distribution of activity. A faster rotation speed does not improve the distribution or yield but could possibly dislodge microgram amounts of deposited material.

Registry No. ^{230}Th, 14269-63-7; ^{231}Pa, 14331-85-2; ^{233}U, 13968-55-3; ^{237}Np, 13994-20-2; ^{239}Pu, 15117-48-3; ^{241}Am, 14596-10-2; ^{244}Cm, 13981-15-2; ^{252}Cf, 13981-17-4.

LITERATURE CITED

(1) Puphal, K. W.; Olsen, D. R. *Anal. Chem.* **1972**, *44*, 284.
(2) Sill, C. W. *Health Phys.* **1969**, *17*, 89.
(3) Sill, C. W.; Olson, D. G. *Anal. Chem.* **1970**, *42*, 1596.
(4) Hyde, E. K. "Proceedings of the International Conference on the Peaceful Uses of Atomic Energy"; United Nations, NY 1956; Vol. 17, p 292.

[1] Present address: Los Alamos National Laboratory, Health Division H-7, Los Alamos, NM 87544.

[2] Present address: P.O. Box 1785, Liberty Lake, WA 99019.

Kenneth W. Puphal*
Terry D. Filer[1]
Gerald J. McNabb[2]
Radiological and Environmental Sciences Laboratory
U.S. Department of Energy
550 Second Street
Idaho Falls, Idaho 83401

RECEIVED for review March 2, 1983. Accepted October 3, 1983.

AIDS FOR ANALYTICAL CHEMISTS

Modified Polishing Equipment for Voltammetric Electrodes

Mary Schreiner, John J. O'Dea, Neal Sleszynski, and Janet Osteryoung*

Department of Chemistry, State University of New York at Buffalo, Buffalo, New York 14214

Various authors have cited the requirement that solid electrodes for voltammetry need to be well polished and have clean, reproducible surfaces (*1–5*). Usually, polishing is done manually with a polishing cloth or by using a rotating polishing wheel. The second method is especially useful for major alterations in the surface of the electrode. These same procedures are required when manufacturing one's own electrodes in the laboratory. Since these methods are also used for the preparation of polished samples in metallography, it seemed logical to draw on the technology in that area for a means of providing an automated or semiautomated method for polishing solid electrodes reproducibly.

Automated polishing provides the following advantages over the manual method. The polishing parameters, and therefore the entire process, are controllable. Once a specific scheme is devised, for example, for a final polishing of a glassy carbon rotating disk electrode, one can be assured that everytime that electrode is mechanically polished with the same combination of abrasive, cloth, polishing time, load, etc., that its surface is as reproducible as possible. In addition, the procedure is transferable, that is, the resulting finish on the surface of the electrode is to a large degree independent of the person operating the polisher. Lastly, it eliminates or reduces the tedium that accompanies manual polishing over extended periods and allows for more efficient use of one's time. This is especially important in situations where best results are achieved by polishing with the finest abrasive (or no abrasive), small loads, and extended polishing times (e.g., overnight).

Here we describe our use of a Minimet Specimen Polisher manufactured by Buehler, Ltd. (41 Waukegan Rd., P.O. Box 1, Lake Bluff, IL 60044), for this purpose. The Minimet is a table top model which polishes samples held by a variably loaded arm. This arm moves the specimen in a geometrical pattern within a stationary bowl containing the abrasive materials. In conventional use, a hole drilled into the back of the sample provides the means by which the sample is linked to the load arm. The pattern produced by the movement of the load arm is shown in Figure 1. In addition, the sample is able to pivot about the load arm. These two motions, occurring simultaneously, increase the degree to which the sample is exposed to fresh, clean abrasive. Since a considerable number of the electrodes we use are fabricated in the laboratory, it was possible in some instances to alter their design to fit the original configuration of the Minimet. For the remaining electrodes the goal was to modify the Minimet to accept the electrodes or electrode components without losing the patterns of rotation and revolution.

EXPERIMENTAL SECTION

In order to use the Minimet in its original configuration, we designed the two-component electrode system shown in Figure 2. The long barrel consisted of coaxial cable imbedded in slow setting Buehler epoxide (no. 20-8130-032) with the electrical connection to the lower segment provided by a screw-connecter. The barrel mold was a section of Tygon tubing. The billet containing the elecrode material was constructed in a three-step process by using molds of Teflon. The active material was first imbedded in epoxy. Next this was connected to the nut with silver epoxy (Eccobond solder 57-C supplied by Emerson & Cuming, Inc., Canton, MA). Finally, this assembly was repotted in Buehler epoxy so that the connector was insulated from the solution. These two pieces then were screwed together with a rubber O-ring wound with Teflon tape as a seal. The billet containing the electrode surface is the approximate size and shape of typical metallographic samples and thus is readily polished in the unmodified polishing machine.

0003-2700/84/0356-0116$01.50/0 © 1983 American Chemical Society

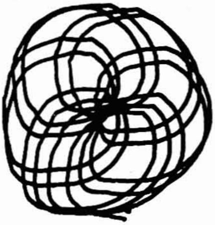

Figure 1. Pattern traced by arm of Minimet Polisher/Grinder.

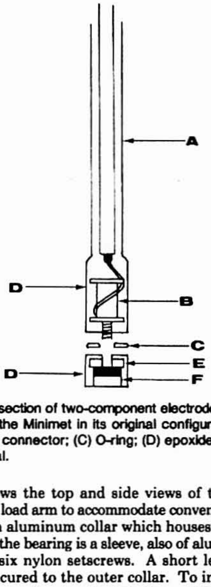

Figure 2. Cross section of two-component electrode system designed to be used with the Minimet in its original configuration: (a) coaxial cable; (B) screw connector; (C) O-ring; (D) epoxide; (E) nut; (F) electroactive material.

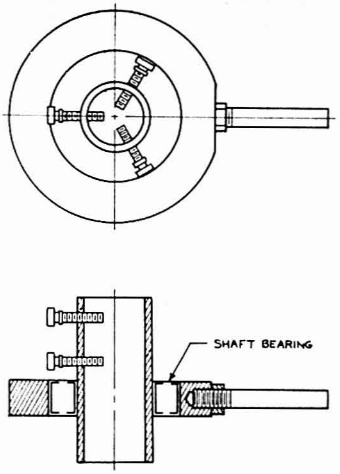

Figure 3. Top view and cross section of modified arm assembly.

Figure 3 shows the top and side views of the modification designed for the load arm to accommodate conventional electrodes. It consists of an aluminum collar which houses a standard 1-in. bearing. Inside the bearing is a sleeve, also of aluminum, in which are positioned six nylon setscrews. A short length of shaft is permanently secured to the outer collar. To install this on the Minimet, the tip and approximately 8 cm of the load arm were removed. A sleeve accommodating two small setscrews was attached to the shortened end of the load arm. The bearing assembly was fitted into the load arm sleeve and secured by the setscrews. A groove, into which the setscrews fit, was subsequently machined into the shaft to facilitate aligning the bearing assembly.

As one might expect, the modified load arm was much heavier than the original one. Good polishing technique requires that a minimum force be exerted downward on the electrode surface, especially in the final stages of polishing. Therefore, a Plexiglas and Teflon outrigger was attached to the bottom of the aluminum collar. This outrigger rested on the lip of the polishing bowl which then absorbed the weight of the load arm. When using the modified load arm the outrigger supported the weight of both the load arm and the electrode itself. As long as the electrode is not removed from the load arm, the force exerted at the electrode surface becomes less through successive polishing stages as material is worn away. The speed and additional load set on the front panel must be adjusted to give the proper drag so that the electrode will rotate.

In addition, other changes were made to the body of the Minimet: (1) the opening on the face plate was made larger so that the sleeve and setscrews on the load arm would not hit the face plate, (2) the cover was hinged to the cabinet frame, and (3) the top of the slide channel was removed, and its front sides were flared out. These last two changes were made to facilitate frequent inspection of the electrode surface without removing the electrode from the load arm assembly. A Plexiglas cover was also fabricated to keep the area clean during the polishing process.

All reagents used were reagent grade. Cyclic voltammograms were run with an IBM 225 Voltammetric Analyzer.

Minimet, Carbimet, Microcloth, Texmet, and Metadi are registered trademarks of Buehler, Ltd.

RESULTS AND DISCUSSION

The variables associated with the polishing process include types of abrasives and their sequencing, thickness of nap on the polishing cloth, polishing time, speed, and load. The variety of these parameters prevents one from defining a polishing routine too specifically. However, this same variety has the potential advantage of accommodating a wide diversity in electrode materials. The bonded abrasives available at present include Carbimet (silicon carbide) paper available in 180, 240, 320, 400, and 600 grit sizes. Of these only the last two appear to have practical value in polishing electrodes. In addition, polishing compounds employing both natural and synthetic diamond are available in particle sizes ranging from 45 μm to 0.25 μm. Overlapping this range are alumina polishing powders with particle sizes from 5.0 μm to 0.05 μm. Relatively new products, deagglomerated alumina abrasives, appear promising for polishing relatively soft metals like gold and silver. Adhesive-backed polishing cloths come in three different types. Microcloth has a deep nap; Texmet has a shallower nap. In addition, nylon polishing cloths are available which have no nap.

We have generally polished electrodes by using 400 and then 600 grit Carbimet paper with water as lubricant, followed by diamond paste (45, 15, 6, and 1 μm) on Microcloth with Metadi extender fluid. Final polishing or renewal of the surface of a used electrode is done with 0.3 and 0.05 μm alumina on Microcloth. Final polishing is done for ca. 15 min, but the entire polishing time is at least several hours. Figure 4 compares cyclic voltammetric background currents for solutions of borate buffer and sodium hydroxide at a Pine rotating disk silver electrode. Voltammograms 1 and 3 illustrate background currents on the electrode "well polished" by hand and 2 and 4 for the same electrode after polishing mechanically

Anal. Chem. 1984, 56, 118–119

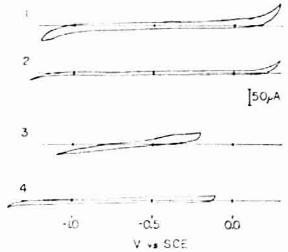

Figure 4. Cyclic voltammograms of background currents (standard Pine rotating disk silver working electrode, area 0.0442 cm^2, vs. SCE): (1) hand-polished electrode, pH 9.4 borate buffer; (2) mechanically polished electrode, pH 9.2 borate buffer; (3) hand-polished electrode, 0.2 M NaOH; (4) mechanically polished electrode, 0.1 M NaOH.

with 0.3 and 0.05 µm alumina for at least 15 min. In both cases, background currents were decreased substantially by the use of automated polishing methods.

In polishing relatively soft metals like gold and silver, one must be especially careful to keep all materials scrupulously clean. Also, one must pay particular attention to match the hardness of the electrode material with the hardness of the abrasive. In cases where the electrode material is harder than the insulating material, the insulating material can be worn away preferentially. As a result the electrode protrudes out of the insulating material. This leads to varying degrees of nonlinear diffusion when the electrode is being used. To minimize these problems, we switched to a nylon polishing cloth. The incorporation of the outrigger described previously also helped to minimize this problem.

For both soft materials and electrodes for which the insulator and active area differ in hardness, the modified Minimet makes it possible to polish for very long times using very gentle conditions. During long unattended periods of polishing, the heat generated by friction tended to evaporate the lubricant. To prevent this the polishing bowls were modified to hold dry ice. A small opening was made in the lip and the underside of the collar of the bowl was closed off by using a snugly fitting piece of plastic tubing. Crushed dry ice placed in the opening just under the glass plate kept the area cold.

If electrodes are small or light, it may be difficult to get them to rotate. In such cases, the electrode should be secured off center in the sleeve. In addition, a clamp holder or hose clamp attached to the top of the electrode can provide a moment of inertia large enough for rotation with no compromise in the quality of the polished surface. Narrow-barreled electrodes posed one other problem: that of proper alignment of the surface with the polishing cloth. Care must be taken that they are exactly perpendicular to one another. Construction of a collar/roller bearing assembly employing a smaller diameter roller bearing would eliminate this problem.

ACKNOWLEDGMENT

The authors wish to thank Gary Sagerman for constructing the modified load arm, Jerry Ptak for providing a technical drawing of the same, and Mizuho Iwamoto for supplying the cyclic voltammograms.

LITERATURE CITED

(1) Vydra, F.; Stulik, K.; Julakova, E. "Electrochemical Stripping Analysis"; Wiley: New York, 1976.
(2) Bard, A. J., Ed. "Electroanalytical Chemistry"; Marcel Dekker: New York, 1973; Vol. 6.
(3) Ewing, G. W. "Instrumental Methods of Chemical Analysis", 3rd ed., McGraw-Hill: New York, 1960.
(4) Bard, A. J; Faulkner, L. R. "Electrochemical Methods"; Wiley: New York, 1980.
(5) Delahay, P. "Double Layer & Electrode Kinetics"; Wiley-Interscience: New York, 1965.

RECEIVED for review June 27, 1983. Accepted October 3, 1983. This work was supported by the National Science Foundation under Grant No. CHE 7917543 and CHE 8305748.

Rotating Ring–Disk Electrode with Wide Temperature Range

David K. Roe* and Mario Aparicio-Razo

Department of Chemistry, Portland State University, Portland, Oregon 97207

With few exceptions, rotating ring–disk electrodes have been constructed from organic polymers and metals, a combination that has a ratio of thermal expansion coefficiences between 5 and 10. Deformation of the polymer usually occurs at 10 to 20 °C above room temperature resulting in solution penetration along the sides of the metal electrode. This problem restricts all electrochemical experiments to a narrow temperature range when this type of electrode is used. Phillips et al. (*1*) were successful in construction of a glassy carbon electrode assembly using borosilicate glass to insulate the ring and the disk. In this case, the coefficients of thermal expansion are sufficiently close that the electrode was usable in fused salts up to 450 °C. By properly selecting the type of glass, a few other electrode materials could be used.

Two recent electrode designs (*2*, *3*) appear to avoid extreme sensitivity to temperature of the seal between insulator and electrodes by employing heat shrinkable polyolefin tubing. Operation at 100 °C was said to be possible with the one design (*2*) and may also apply to the other (*3*) due to similarity of sealing technique. A rotating disk electrode made by thermal compression (*4*) of a platimum disk in Kel-F has been used in aqueous solutions up to 60 °C without leakage problems (*5*). In principle, the assembly technique could be extended to include a ring electrode.

A quite different approach to the design of a ring–disk electrode assembly has been used in our laboratory to permit use over a wide temperature range. The body of the electrode assembly is fabricated from a machinable ceramic and coated by thermal evaporation or sputtering to form the conductive surface that becomes the ring and the disk. Electrical contact to the two electrodes is provided by a simple and reliable means: a platinum rivet.

EXPERIMENTAL SECTION

Details of the major features of the ceramic ring–disk electrode are given in Figure 1a. The electrode body is a piece of ceramic machined from Macor (Corning Glass Works) with an internal thread that mates with a shaft of stainless steel tubing. A length of Macor rod of nominal 0.5 in. diameter was turned to 12 mm and cut into 20 mm lengths. Each piece was drilled and tapped with a $^1/_4$ × 28 thread to a depth of about 15 mm. The top 5 mm

0003-2700/84/0356-0118$01.50/0 © 1983 American Chemical Society

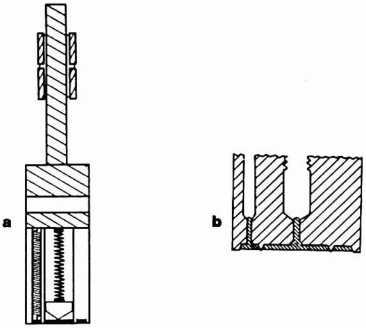

Figure 1. (a) Partial cross section of electrode and shaft. (b) Enlarged view of lower end of electrode body. Drawings are not to scale.

of the hole was machined to a diameter of 6.5 mm to provide accurate centering with the shaft. A second 2 mm hole was drilled in the wall directly above the intended ring location, again to a depth of 15 mm. Both this hole and the center one were continued to the lower end at a diameter of 0.5 mm and the exit hole was slightly flared. Platinum wire of the same diameter was stretched slightly to provide a tight fit and then one end was melted to form a small ball. After threading the wire through one of the holes, it was cut off at a distance of 0.5 mm from the ceramic surface and the end peened flat to finish the rivet. During this step, the ball-end of the platinum wire was supported on a steel rod. After installation of the second rivet, the end of the ceramic was machined in the form shown in Figure 1b. Ring and disk diameters were defined in this step by cutting into the surface to a depth of about 0.1 mm, leaving a ridge with a base width of about the same dimension. This surface was then polished to a mirror finish with 0.5-μm alumina.

Metalization of the lower end of the ceramic was by thermal evaporation under vacuum or by sputtering; both methods have been used successfully. Good adherence depends upon applying first an intermediate layer of chromium or titanium, about 1 to 5 nm thick, followed by the desired metal, in this case gold, to a thickness of 10–50 nm. A number of ceramic pieces can be metalized at the same time. When properly applied, the metal layer resisted the pull of adhesive tape. Next, the gold was removed from the outside and intermediate ridges by a very thin cut on a lathe. The depth of this cut determines the space between disk and ring and it has been made as small as 0.025 mm.

Electrodeposition was used to build up the thickness of the ring and disk areas. For gold, a 0.1 F solution of $AuCl_3$ in 1 F HCl was found to produce pure, dense deposits at 50 °C and a current density of 1 mA cm^{-2}. Several steps of plating followed by polishing produced a surface that was flush with the edges of the ridges that defined the areas of the ring and disk, as is illustrated in Figure 1b.

Electrical contact to the platinum rivets was provided by springs, as shown in Figure 1a. The upper end of the spring from the ring contacted a stainless steel disk centered on a ceramic hub for insulation and a wire from the disk was connected to a brass slip ring on the shaft. This arrangement allows easy removal of the electrode body yet reliable electrical contact.

Collection efficiencies were measured with $Fe(CN)_6^{3-}$ in 0.1 F H_2SO_4 over the range of rotation rates from 500 to 5000 rpm. The rotator and dual potentiostat were designed and constructed in this laboratory.

RESULTS AND DISCUSSION

Calculated collection efficiency for an electrode assembly with a disk radius of 0.381 cm, inner ring radius 0.407 cm, and outer ring radius of 0.597 is 0.488 according to the method of Albery and Hitchman (*6*). Measured efficiency at room temperature with $Fe(CN)_6^{3-}$ was 0.493 and it remained constant within 1% over the entire rotation rate range.

This electrode design has also been used extensively over the past 2 years in a study of sulfur and selenium electrochemistry using dimethyl sulfoxide as solvent. In these experiments, temperatures up to 125 °C were used with no apparent failure due to thermal changes. Details of these measurements will soon be published.

The sucess of this electrode design rests upon the nearly perfect match of thermal expansion coefficients of platinum ($(9.7 \times 10^{-7})/°C$) and Macor ($(9.4 \times 10^{-7})/°C$), providing a leak-free electrical contact to the electrode surface. Gold and most other metals have different expansion coefficients but in thin layers on the ceramic the dimensional changes can be accommodated to some degree. We have not yet prepared electrodes of metals other than gold and so cannot comment on their properties. It is obvious that the critical step is evaporation or sputtering of the intermediate metal layer; lack of adhesion is always due to poor surface preparation or improper conditions during this operation. Through a series of empirical tests, conditions for good adhesion were finally obtained. This seems to be the usual approach in thin film preparation by these techniques.

In comparison with other designs, this electrode assembly appears to be simpler and more easily made. One shaft assembly can be used with a variety of electrode bodies and their exchange is very simple. A number of metals can be electroplated in satisfactory purity, so there are no serious limitations in choice of materials. It is also possible to deposit carbon on inert substrates in the pyrolytic form, although we have not as yet explored this technique. Finally, it should be noted that very narrow disk-to-ring gaps are possible and, with modification of the ring contact, multiple, thin rings can also be made.

ACKNOWLEDGMENT

Many of the details of this electrode design as well as the construction were the result of the ingenious efforts of the late Thomas B. Hutchins, III.

Registry No. Gold, 7440-57-5.

LITERATURE CITED

(1) Phillips, J.; Gale, R. J.; Wier, R. G.; Osteryoung, R. A. *Anal. Chem.* **1976**, *48*, 1266.
(2) Rowley, P. G.; Osteryoung, J. G. *Anal. Chem.* **1978**, *50*, 1015.
(3) Geiger, T.; Anson, F. C. *Anal. Chem.* **1980**, *52*, 2448.
(4) Tench, D.; Odgen, C. *J. Electrochem. Soc.* **1978**, *125*, 194.
(5) Haak, R. P.; Ogden, C. Rockwell International Science Center, Thousand Oaks, CA, personal communication, 1981.
(6) Albery, W. J.; Hitchman, M. L. "Ring-Disc Electrodes"; Clarendon Press: Oxford, 1971.

RECEIVED for review July 29, 1983. Accepted September 16, 1983.

120 *Anal. Chem.* **1984,** *56,* 120–122

Optimization of Electrothermal Atomization–Inductively Coupled Plasma Atomic Emission Spectrometry for Simultaneous Multielement Determination

Hassan M. Swaidan[1] **and Gary D. Christian***

Department of Chemistry, BG-10, University of Washington, Seattle, Washington 98195

Inductively coupled plasma atomic emission spectrometry (ICP-AES) is an attractive analytical tool for the simultaneous determination of major, minor, and trace elements in various samples (*1–5*). The use of direct vaporization of the sample has been described previously in various reports (*6–14*). Recent modifications of commercial electrothermal atomizers have been described for application to ICP-AES. Crabi et al. (*15*) modified the HGA 500 electrothermal atomizer to be used as an introduction device to the ICP-AES. They used the L'vov platform to improve the tolerance of their system for variations in matrix composition. Aziz et al. (*16*) used the HGA 74 graphite furnace atomizer with a modified gas system in the analysis of small-volume biological samples. They indicated that a gas circulation system will minimize memory effects in routine application. Recently (*17*), we reported the use of the HGA 2000 graphite atomizer in combination with an ICP (GA-ICP). The combination of a graphite furnace and microwave induced plasma atomic emission spectrometer for the multielement analysis of small volume liquid samples has been described (*18*). Grabau and Fassel (*19*) have demonstrated the ability of the photodiode array detector as an alternative to the polychromators commonly used with the ICP-AES. In all the previous techniques, detection limits have been reported to be several orders of magnitude better than those obtained under similar conditions with conventional ICP.

Compromised conditions for simultaneous multielement analysis by ICP have been reported (*20*). In use of the HGA-ICP system, compromised conditions must be accommodated for both the graphite atomizer and the inductively coupled plasma in order to obtain the lowest relative detection limits for most elements and to minimize interelement effects, both chemical and spectral. In this paper, we describe optimization of parameters for the HGA-ICP system and explore its applicaton for simultaneous multielement analysis of microsamples, utilizing direct readout of the transient signals by the Jarell Ash Model 955 inductively coupled plasma spectrometer. Elements are arranged by groups for simultaneous determination in mixtures, based on their arrival time in the plasma and compromised operation parameters.

EXPERIMENTAL SECTION

Apparatus. A modified Perkin-Elmer HGA 2000 graphite furnace was employed as a sample introduction source. The furnace was modified and connected to the ICP torch of a Jarrel Ash Model 955 Plasma Atomcomp inductively coupled plasma spectrometer through a modified spray chamber as previously described (*17*). Graphite tubes were coated with a thin pyrolytic film using 0.05 L/min mixture gas (10% methane and 90% argon) by heating at the charring temperature of 2100 °C for 10 min. The operating conditions are described in Table I. Signals were monitored with the polychromator of the Model 955, by commanding the computer to look at the specific channel or channels of interest, and were recorded on a teletype as digital readouts. Samples were introduced into the furnace with a 10-µL syringe micropipet with disposable polypropylene tips.

After signals were recorded for the blank and the sample, the graphite atomizer was purged by maximizing the temperature and running the cycle with argon only.

Table I. Operating Conditions

Jarrel-Ash Model 955 Plasma Atomcomp		
incident rf power		1 kW
reflected rf power		≤10 W
coolant argon flow rate		18 L/min
plasma argon flow		0.0–0.5 L/min
Direct Reader		
dispersion		0.55 nm/mm
entrance slit width (fixed)		25 µm
exit slit width (fixed)		50 µm
observation height		10–20 mm
Perkin-Elmer HGA 2000		
argon carrier flow rate		1–2.5 L/min
cycle	temp, °C	time, s
drying	400	20
charring	800	2–5
atomizing	2400	5–10

Data were treated with an Apple II Plus computer with software from Interactive Microware, Inc., State College, PA, for plotting the graphs using scientific plotter and curve fitting programs.

Reagents. Stock solutions of 1000 ppm were obtained from Fisher Scientific Co. Working standard solutions were prepared by fresh dilution of the stock solutions with deionized water. Volumes of 10 µL were used throughout the experiment for measurements.

RESULTS AND DISCUSSION

Optimization Routine. After the plasma was ignited and stabilized, the optimal conditions of flow rate, height above the coil, and the reflected power for an element or mixture of elements were obtained as follows. The graphite cycle was adjusted for 400 °C drying for 20 s, 800 °C charring for 5 s, and 2400 °C atomizing for 10 s. A 10-µL aliquot of a blank (deionized water) or sample was injected into the atomizer. Studying one element at a time (either alone or in mixture), we measured the arrival time (the time from the beginning of the atomization cycle of the atomizer to the rise of the galvanometer on the 955 spectrometer) and the lifetime in the plasma (exposure time) with a timer by observing the rise and fall of the galvanometer on the spectrometer. From this information, the computer was programmed to measure the plasma emission signal over a set observation period (exposure time), adjusting for the arrival time to minimize background recording, i.e., to observe primarily the duration of the atomic emission signal. A digital readout was recorded on a teletype for each channel. By use of the appropriate exposure times, the operating parameters were optimized for each element from maximum signal-to-noise ratios. A similar procedure was adopted for the mixed groups, selecting the compromized conditions that give the best detection limits for the most elements.

Operating Conditions. Simultaneous multielement analysis is best approached by considering the various parameters that affect optimization for each element. The optimal parameter for each element will necessarily be compromised in exchange for a common set of operating conditions

---

[1] Present address: Chemistry Department, Faculty of Science, King Saud University, Riyadh, Saudi Arabia.

0003-2700/84/0356-0120$01.50/0 © 1983 American Chemical Society

Table II. Optimal Conditions for Single Elements

element	optimal height, mm	optimal carrier flow rate, L/min	arrival time, s	exposure time, s
Cd	12	1.0	6	7
Mn	12	1.5	4	7
Ni	12	2.5	4	4
Cr	12	2.5	3	6
Al	12	2.0	6	4
Zn	12	1.0	7	4
Pb	14	2.0	3	7
Sb	14	1.5	4	7
Si	14	2.0	4	4
Co	14	2.5	3	6
Fe	14	2.0	4	5
Ag	14	2.0	4	6
Cu	18	2.5	3	4
Ba	18	2.5	6	10
Ca	16	2.0	7	4

that give the lowest detection limits for the mixture. Several parameters may influence the HGA-ICP system, not only the magnitude of the detection limits but also interelement interferences. These include the power of the ICP, the observation height above the coil, the flow rate of the carrier gas which transports the sample aerosol into the plasma, the graphite atomizer temperature and cycle time, the deterioration and aging of the graphite tube, the length of the transport tube to the ICP, and the arrival and the exposure times for the elements of interest.

The graphite tube will deteriorate after a limited number of firings and the signal intensity will diminish. A pyrolitically coated tube provides a barrier between vapor phase atoms and the graphite substrate (*21*). Hence, we coated the graphite tube with a thin pyrolytic layer to improve aging of the tube and obtain a steady signal for a longer period of firings.

The arrival time (the time from the beginning of the atomization cycle of the graphite atomizer to the deflection of the galvanometer on the spectrometer) and the exposure time (the time from the rise to the end of the fall of the galvanometer on the spectrometer) were measured for each of the 15 elements. Results are given in Table II. The effect of the observation window on the intensity of the recorded signal and the signal-to-noise ratio is very significant for transient signals, and the observation time should be adjusted to correspond to just the peak width to the extent possible. The background reading from the plasma increases in proportion to the observation time. However, the observation window must be sufficiently broad that slight variations in sample arrival time will not affect the observed analyte signal or that multiple elements that arrive at slightly different times can be observed.

The flow rate and the observation height above the coil were optimized for maximum signal-to-noise ratio for each of 15 elements (Table II). On the basis of optimal conditions for individual elements, the 15 elements were arranged into three different groups according to their observation heights. Group one consists of cadmium, manganese, nickel, chromium, aluminum, and zinc with a height of 12 mm. Group two consists of lead, antimony, silicon, cobalt, iron, and silver with a height of 14 mm. Group three consists of copper, barium, and calcium with a height of 18 mm. The elements tend to fall into patterns on the basis of "hard" and "soft" lines as noted by Blades and Horlick (*22*), i.e., those whose spatial behavior is relatively insensitive to operating parameters (group one) and those that are sensitive to operating parameters (group three). Blades and Horlick found the spatial behavior of the "soft" line elements to be correlated with plasma temperature.

The flow rate dependence, arrival time, and exposure time were determined for each element in the different mixtures, and compromised conditions were selected to provide the best compromised detection limits for simultaneous determinations. The optimal observation heights above the coil, flow rates, arrival times, and exposure times were, respectively, 12 mm, 1.8 L/min, 4 s, and 7 s for group one, 14 mm, 2.0 L/min, 4 s, and 6 s for group two, and 18 mm, 2.5 L/min, 3 s, and 7 s for group three.

Detection Limits. Detection limits were determined by using 1 ppm concentrations of the analytes and represent the concentrations which give a net signal equal to three times the experimentally determined standard deviation of the blank for each element. Table III lists the detection limits obtained for single elements and compares the values obtained via peak height measurement of the recorded signal (*17*). The present detection limits are poorer due to the substantial background signal included in the observation window. Detection limits for each element were determined in mixtures for the three groups and are also summarized in Table III. Results are generally comparable to those for single elements, although there is some substantial enhancement in the mixtures, particularly for chromium and iron, possibly due to formation of alloys of enhanced volatility in the mixtures. Table III also compares the present detection limits with those of previous workers utilizing combined electrothermal atomizer/plasma spectrometry and various volume samples. The precisions for the various elements in the group mixtures were determined by using 1 ppm concentrations and seven readings. Relative standard deviations were better than 10%, with 5% or less

Table III. Detection Limits (ng/mL)

element	wavelength, nm	single (this work) (10 μL)	mixture (this work) (10 μL)	peak height measurement (*17*) (10 μL)	HGA74-ICP (*16*) (50 μL)	HGA74-MIP (*18*) (50 μL)	HGA500-ICP (*15*) (20 μL)
Cd	228.8	50	20	4	8	35	2
Mn	257.6	2	3	0.9		7	0.4
Ni	231.6	90	50			76	
Cr	205.5	20	5		4 (Cr II)	84 (Cr II)	0.7
Al	308.2	60	170				3
Zn	213.8	10	7	8	6	10	
Pb	220.3	40	50		130 (Pb I)	50 (Pb I)	
Sb	217.5	160	250	10			
Si	251.6	80	50				
Co	228.6	30	20	4			
Fe	259.9	70	10		2	90	
Ag	328.0	30	10	0.8			
Cu	324.7	20	10		10	18	0.1
Ba	493.4	70	150				
Ca	396.8	60	30			77 (Ca I)	

for most elements.

Dynamic Range and Relative Sensitivities. The net intensity readings for concentrations ranging from 0.1 ppm to 30 ppm for the elements in the three mixtures were determined. Measurements beyond 10 ppm concentrations for group two were difficult due to apparent reaction between the elements or from anion/cation effects in the mixture which resulted in loss of analyte element, for example, through vaporization of molecular halide species (*23*). In addition, concentrations in excess of 10 ppm require extensive cleaning of the graphite atomizer between readings, necessitating several purgings which in turn will accelerate the decrease in the intensities of signals by aging the graphite tube. Measurements could be made over at least 2 orders of magnitude for all the elements. The correlation coefficient for signal vs. analyte concentration was 0.992 or better for all the elements tested in group two.

ACKNOWLEDGMENT

The assistance and discussions of Steven Hartenstein are gratefully acknowledged.

Registry No. Cd, 7440-43-9; Mn, 7439-96-5; Ni, 7440-02-0; Cr, 7440-47-3; Al, 7429-90-5; Zn, 7440-66-6; Pb, 7439-92-1; Sb, 7440-36-0; Si, 7440-21-3; Co, 7440-48-4; Fe, 7439-89-6; Ag, 7440-22-4; Cu, 7440-50-8; Ba, 7440-39-3; Ca, 7440-70-2.

LITERATURE CITED

(1) Kniseley, R. N.; Fassel, V. A.; Butler, C. C. *Clin. Chem.* (*Winston-Salem, N.C.*) **1973**, *19*, 807.
(2) Subramanian, K. S.; Meranger, J. C. *Sci. Total Environ.* **1982**, *24*, 147.
(3) Winge, R. K.; Fassel, V. A.; Kniseley, R. N.; DeKalb, E.; Hass, W. J., Jr. *Spectrochim. Acta, Part B* **1977**, *32B*, 327.
(4) Dahlquist, R. L.; Knoll, J. W. *Appl. Spectrosc.* **1978**, *32*, 1.
(5) Barnes, R. M. "Application of Plasma Emission Spectroscopy"; Heyden & Son Inc.: Philadelphia, PA, 1979.
(6) Kleinmann, I.; Svoboda, V. *Anal. Chem.* **1969**, *41*, 1029.
(7) Nixon, D. E.; Fassel, V. A.; Kniseley, R. N. *Anal. Chem.* **1974**, *46*, 210.
(8) Human, H. G. C.; Scott, R. H.; Oakes, A. R.; West, C. D. *Analyst* (*London*) **1976**, *101*, 265.
(9) Gunn, A. M.; Millard, D. L.; Kirkbright, G. F. *Analyst* (*London*) **1978**, *103*, 1066.
(10) Millard, D. L.; Shan, H. C.; Kirkbright, G. F. *Analyst* (*London*) **1980**, *105*, 502.
(11) Kirkbright, G. F.; Snook, R. D. *Anal. Chem.* **1979**, *51*, 1938.
(12) Salin, E. D.; Horlick, G. *Anal. Chem.* **1979**, *51*, 2284.
(13) Mermet, J. M.; Hubert, J. *Prog. Anal. At. Spectrosc.* **1982**, *5*, 1.
(14) Kirkbright, G. F.; Walton, S. J. *Analyst* (*London*) **1982**, *107*, 276.
(15) Crabi, G.; Cavalli, P.; Achilli, M.; Rossi, G.; Omenetto, N. *At. Spectrosc.* **1982**, *3*, 81.
(16) Aziz, A.; Broekaert, J. A. C.; Leis, F. *Spectrochim. Acta, Part B* **1982**, *37B*, 369.
(17) Swaidan, H. M.; Christian, G. D. *Can. J. Spectrosc.*, in press.
(18) Aziz, A.; Broekaert, J. A.; Leis, F. *Spectrochim. Acta, Part B* **1982**, *37B*, 381.
(19) Grabau, F.; Fassel, V. A. "Book of Abstracts"; 184th National Meeting of the American Chemical Society, Kansas City, Sept 12–17, 1982; American Chemical Society: Washington, DC, 1982.
(20) Berman, S. S.; McLaren, J. W. *Appl. Spectrosc.* **1978**, *32*, 372.
(21) Slavin, W.; Manning, D. C.; Carnrick, G. R. *At. Spectrosc.* **1981**, *2*, 137.
(22) Blades, M. W.; Horlick, G. *Spectrochim. Acta, Part B* **1981**, *36B*, 861.
(23) Fuller, C. W. "Electrothermal Atomization for Atomic Absorption Spectrometry", Billing & Sons Ltd.: Great Britain, 1977.

RECEIVED for review March 21, 1983. Resubmitted June 24, 1983. Accepted September 26, 1983. We appreciate the financial support of King Saud University and the Arabian American Oil Company for this research.

CORRECTION

Performance Characteristics of a Continuum-Source Wavelength-Modulated Atomic Absorption Spectrometer

J. D. Messman, M. S. Epstein, T. C. Rains, and T. C. O'Haver (*Anal. Chem.* **1983**, *55*, 1055–1058).

There are several typographical errors in this paper. On page 1056, under "Instrumentation", a R374 photodetector was used for WM-AAC measurements of potassium and sodium instead of a R372 photodetector. In Table I on page 1057, the WM-AAC detection limit for Cd should read 0.09 mg/L. In the same table, the wavelength for Tl should read 276.787 nm.

MANUSCRIPT REQUIREMENTS

The following guide is published by the Editors of ANALYTICAL CHEMISTRY *to aid authors in writing, and editors and reviewers in expediting review and publication of manuscripts.*

SCOPE. The journal is devoted to the dissemination of knowledge concerning all branches of analytical chemistry. Articles either are entirely theoretical with regard to analysis or are reports of laboratory experiments that support, argue, refute, or extend established theory. Articles may contribute to any of the phases of analytical operations, such as sampling, preliminary chemical reactions, separations, instrumentation, measurements, and data processing. They need not refer to existing or even potential analytical methods in themselves, but may be confined to the principles and methodology underlying such methods.

In addition to regular research papers, *Correspondence* and *Aids* are published. *Correspondence* may be brief disclosures of new analytical concepts of unusual significance. They may also represent important comments on the work of others, in which case the authors of the work being discussed will, ordinarily, be allowed to reply. *Aids for Analytical Chemists* should be brief descriptions of novel apparatus or techniques, requiring real ingenuity on the author's part, which offer definite advantages over similar ones already available.

Papers involving extensive use of computers will be judged by the usual criteria of originality, technical content, and value to the field. They should include a statement of the objectives and the procedural steps to the objective, and the results. However, *details* of procedural steps, including programs, should be omitted. Availability of the latter through commercial collections or by writing to the author should be clearly indicated in the text. Computational techniques for calculations of well-known analytical methods cannot be considered.

Papers involving experimental data should offer a new or modified approach to analysis in a particular field, not just extend the existing library of data.

SUBMISSION OF MANUSCRIPTS. Papers submitted to ANALYTICAL CHEMISTRY are considered with the understanding that they have not been published and are not under consideration elsewhere.

Four complete copies of the manuscript are required. All copy must be typed double- or triple-spaced on 22 × 28 cm ($8^1/_2 \times 11$ in.) or A4 paper, with text, tables, and illustrations of a size that can be mailed to reviewers under one cover.

Reviewers suggested by authors may be used at the discretion of the editors.

Send all copies of the manuscript with cover letter to ANALYTICAL CHEMISTRY, 1155 Sixteenth St., N.W., Washington, DC 20036.

TITLE. Use specific and informative titles with a high keyword content. Avoid unnecessary phrases ("on the", "a study of") and articles (a, an, the), as well as words that are either obvious (new, novel, useful, improved) or relative (versatile, rapid, simple, inexpensive, sensitive). Indicate, where applicable, compound or element determined, method, and special reagents—e.g., "Spectrophotometric Determination of Thallium in Zinc and Cadmium with Rhodamine B". Do not use symbols, abbreviations, or series designations. Use one complete title rather than a title and subtitle. Be informative but brief. Careful attention should be paid to the choice of words—e.g., *trace* or *micro*, *determination* or *analysis*, etc.—to reflect correct usage.

AUTHORSHIP. Give authors' names in as complete a form as possible. First names, initials, and surnames should be included. Omit professional and official titles. Give complete mailing address for place where work was done and include telephone number of the corresponding author. Add current address of each author, if different, on the title page of the manuscript with a numerical superscript and footnote. Corresponding author is indicated by an asterisk.

ABSTRACT. Abstracts are required for all manuscripts, but will not be published with *Correspondence* and *Aids*. (Put on separate page for these categories.) The abstract is to be self-explanatory and suitable for reproduction by abstracting services without rewriting. It indicates what is new, different, and significant. State the objectives of the study, the limits of detection, the degree of accuracy and precision, and the major unique reagents, times, and temperatures, but avoid the lengthy stepwise recipe. The length of the abstract should reflect the content and length of the manuscript, but should not exceed 150 words.

TEXT. Consult the publication for general style. Write for the specialist. Do not include information and details or techniques that should be common knowledge to the specialist.

General Organization. Indicate the breakdown among and within sections with center heads and side heads. Results and Discussion follow Experimental Section. Keep all information pertinent to a particular section within that section—e.g., do not present results in the Experimental Section. Avoid repetition. Do not use footnotes for descriptive or explanatory information; include the information at an appropriate place in the text.

INTRODUCTION

Discuss the relationship of your work to previously published work, but do not repeat published information. If a recent article has summarized work on the subject, cite this article rather than repeating individual citations.

EXPERIMENTAL SECTION

Use complete sentences—i.e., do not use outline form. Be consistent in voice and tense.

APPARATUS. List only devices of specialized nature. Do not include equipment that is standard in an analytical laboratory and used in the normal way.

REAGENTS. List and describe preparation of special reagents only. Do not list reagents normally found in the laboratory and preparations described in standard handbooks and texts.

PROCEDURE. Omit details of procedures that are common knowledge to those in the field. Describe pertinent and critical factors involved in reactions so that the method can be reproduced, but avoid excessive description. Brief highlights of published procedures may be included; details should be left to references.

Caution: Describe any procedures that are hazardous and list any reagents that are toxic.

RESULTS AND DISCUSSION

Be complete and relevant but concise. Omit calculations that are well-known to the specialist.

CONCLUSIONS

Use Conclusions only when necessary for interpretation and not to summarize information already given in the text *or* abstract.

ACKNOWLEDGMENT

Acknowledge professional technical assistance and source of special materials only. Do not use professional titles and avoid wordy sentences.

LITERATURE CITED. References that are considered part of the permanent literature are to be numbered in one consecutive series by order of mention in the text. However, the complete list of literature citations is placed on a separate page at the end of the manuscript. Reference numbers in the text are in parentheses and on line. Repetition is avoided by using the number corresponding to the original reference. Descriptive or explanatory (footnote) material is not given a reference number or included in the literature cited. This material must be included in the body of the text.

Use *Chemical Abstracts Service Source Index* abbreviations for journal names and include publication year, volume, and page number (inclusive pagination is recommended). Include *Chemical Abstracts* reference for foreign publications that are not readily available. List submitted articles as "in press" *only if* formally accepted for publication, and give the volume number and year if known. Otherwise use "submitted to" or "unpublished work" with place where work was done and date. Include name, affiliation, and date for "personal communications".

Please use the format given in the following examples.

(1) Koile, Ross C.; Johnson, Dennis C. *Anal. Chem.* **1979**, *51*, 741–744.

(2) Willard, Hobart H.; Merritt, Lynne L., Jr.; Dean, John A.; Settle, Frank A., Jr. "Instrumental Methods of Analysis", 6th ed.; Van Nostrand: New York, 1981; Chapter 2.

CREDIT. On a separate page, give credit for financial support, meeting presentation information, and auspices under which work was done, including permission to publish. In the JOURNAL this information will immediately follow the received and accepted dates, and is not a part of the Acknowledgment.

FIGURES AND TABLES. Do not use figures or tables that duplicate each other or material already in the text. ***Omit straight line graphs***; give information in a table, or in a sentence or two in the text. Do not include tables or figures found elsewhere in the literature.

Tables. Prepare tables in a consistent form, furnish each with an appropriate title, and number consecutively with Roman numerals in the order of reference in the text. Type each table on a separate page, and collate at end of manuscript.

Figures. Submit original drawings (or sharp glossy prints) of graphs and diagrams prepared on tracing cloth or plain white paper. If structures are given in the text, original drawings are to be provided. All lines, lettering, and numbering should be sharp and unbroken. If coordinate paper is used, use nonphotographic blue cross-hatch lines. Use black India ink and a lettering set for all letters, numbers, and symbols. Do *not* use a typewriter to letter illustrations.

Design illustrations to fit the width of one journal column (8.3 cm). The width of original drawings should be twice the publication size. Letters and symbols should be about 4 mm high on the original (2 mm in reduced journal version). Lines should be drawn with a light (#1 Leroy for graph grids), medium (#2 Leroy for graph borders or reference lines), or heavy (#5 Leroy for graph curves or emphasis) thickness on the original. Lettering on copy should be in proportion. Label ordinates and abscissas of graphs along the axes and outside the graph proper.

Supply glossy prints of photographs. Sharp contrasts are essential. Label each figure on the back with the name of the corresponding author and the figure number.

Number all figures consecutively with Arabic numerals in the order of reference in the text.

If drawings are mailed under separate cover, identify by name of author and title of manuscript.

Figure Captions. Include, on one page, a list of all captions and legends for illustrations. Make the legend a part of the caption rather than inserting it within the figure. Keep captions as brief as possible and include detailed information in the text.

BRIEF. On a separate page, state in 30 words or less the significant results obtained, emphasizing precision and accuracy data when possible. Do not repeat the title. No Briefs are necessary for *Correspondence* or *Aids*.

NOMENCLATURE. Nomenclature conforms with rules established by the International Union of Pure and Applied Chemistry, the Nomenclature Committee of the American Chemical Society, and the Chemical Abstracts Service. Consult Kurt Loening, P.O. Box 3012, Chemical Abstracts Service, Columbus, OH 43210, for advice.

Avoid trivial names. Well-known symbols and formulas may be used (write out in title and abstract) if no ambiguity is likely. Define trade names and abbreviations at point of first use. First letter of trade names is capitalized.

Use SI units of measurement (with acceptable exceptions) and give dimensions for all terms. If nomenclature is specialized, as in mathematical and engineering reports, include a Nomenclature section at end of paper, giving definitions and dimensions for all terms. Write out names of Greek letters and other special symbols in margin of manuscript at point of first use.

Type all equations and formulas clearly and number all equations in consecutive order. Place superscripts and subscripts accurately, indicate capital letters, and distinguish between characters which are alike on the keyboard—e.g., one and the letter "el", zero and the letter "oh". Avoid superscripts that may be confused with exponents.

For numbers less than one, a zero precedes the decimal point.

For specialized nomenclature used by this JOURNAL, see "Guide for Use of Terms in Reporting Data in ANALYTICAL CHEMISTRY", "Spectrometry Nomenclature", and "SI Units", which appear annually, with the "Manuscript Requirements", at the end of the technical section in the January issue. From time to time, ANALYTICAL CHEMISTRY publishes special nomenclature guides promulgated by various organizations.

General information about American Chemical Society publications, including preparation of manuscripts, is given in the "Handbook for Authors of Papers in American Chemical Society Publications", available from Distribution Office, American Chemical Society, 1155 16th St., N.W., Washington, DC 20036.

Analysis, Identification, Determination, and Assay

While most chemists probably realize the difference among the terms *analyze*, *identify*, and *determine*, they are frequently careless when using them. Most frequently the term *analysis* is used when *determination* is meant.

A study of the nomenclature problem indicates that only samples are *analyzed*; elements, ions, and compounds are *identified* or *determined*. The difficulty occurs when the sample is nominally an element or compound (of unknown purity). "Analysis of —" (an element or compound) must be understood to mean the identification or determination of impurities. When the intent is to determine how much of such a sample is the material indicated by the name, *assay* is the proper word.

Guide for Use of Terms in Reporting Data in ANALYTICAL CHEMISTRY

It is important to know the meaning of the terms an author uses. For publications in ANALYTICAL CHEMISTRY, the following definitions are applicable and it is understood that they are used with a series of normally distributed replicate results with no prior information on bias of the method. They are endorsed by members of the Advisory Board. The Guide is necessarily incomplete, and it should be used only with an understanding of its limitations; one is that a value obtained for a term is usually based on a relatively small number of observations, and it is therefore to be regarded as an estimate of the parameter. For appropriate background, the reader should consult a reputable text on the subject of data evaluation.

Set refers to a number n of independent replicate measurements of some property. Authors are encouraged to report this number n.

Precision relates to the reproducibility of measurements within a set, that is, to the scatter or dispersion of a set about its central value.

Accuracy normally refers to the difference (error or bias) between the mean, $\bar{X}$, of the set of results and the value $\hat{X}$, which is accepted as the true or correct value for the quantity measured. It is also used as the difference between an individual value X_i and $\hat{X}$. The *absolute accuracy* of the mean is given by $\bar{X} - \hat{X}$ and of an individual value by $X_i - \hat{X}$. The *relative accuracy* of the mean is given by $(\bar{X} - \hat{X})/\hat{X}$, and the percentage accuracy $100(\bar{X} - \hat{X})/\hat{X}$.

Measures of the Central Value of a Set. MEAN (or Average or Arithmetic Mean) is the sum $\sum_{j=1}^{n} X_i$ of the values of individual results divided by the number, n, of results in the set. The mean is given by

$$\bar{X} = (X_1 + X_2 + \ldots X_i + \ldots X_n)/n = \sum_{i=1}^{n} X_i/n$$

MEDIAN is the middle result of an odd number of results, or the average of the central pair for an even number, when they are arranged in order of magnitude. The median is less affected by extreme values than is the mean.

Measures of Precision within a Set. STANDARD DEVIATION is the square root of the quantity (sum of squares of deviations of individual results from the mean, divided by one less than the number of results in the set). The standard deviation, s, is given by

$$s = \sqrt{\sum_{i=1}^{n} (X_i - \bar{X})^2/(n-1)}$$

Standard deviation has the same units as the measurement. It becomes a more reliable expression of precision as n becomes large. When the measurements are independent and normally distributed, the most useful statistics are the mean for the central value and the standard deviation for the dispersion.

VARIANCE, s^2, is the square of the standard deviation.

RELATIVE STANDARD DEVIATION is the standard deviation expressed as a fraction of the mean, $s/\bar{X}$. It is sometimes multiplied by 100 and expressed as a percentage. Relative standard deviation is preferred over "coefficient of variation".

MEAN (or AVERAGE) DEVIATION is the mean of the deviations of the individual measurements from the mean of the set without regard to sign. It is given by $\sum_{i=1}^{n} |X_i - \bar{X}|/n$. The mean deviation is not recommended as a measure of precision except when the set consists of only a few measurements.

RANGE is the difference in magnitude between the largest and smallest results in a set. The range is not recommended as a measure of precision except when the set consists of only a few measurements. If range is used, the number of measurements in the set must be indicated.

Measure of Precision of a Mean. CONFIDENCE LIMITS (or Interval) are the limits around the measured mean within which the mean value for an infinite number of measurements can be expected to be found with the stated level of probability. Confidence limits for independent normally distributed measurements are given by

$$\text{confidence limits} = \bar{X} \pm ts/\sqrt{n}$$

where s is the standard deviation and t is the t-table value at the stated confidence level. The use of standard error, $s/n^{1/2}$, to express precision of a mean is acceptable only if the authors clearly make the distinction from standard deviation.

Spectrometry Nomenclature

We have compiled the following list of terms, their definitions, and abbreviations, which occur most frequently in papers on spectrometry. The list indicates our preferred usages in an attempt to obtain some consistency in a field where much discrepancy exists.

Absorbance, A (not optical density, absorbancy, or extinction). Logarithm to the base 10 of the reciprocal of the transmittance $A = \log_{10}(1/T)$.

Absorptivity, a (not k). (Not absorbancy index, specific extinction, or extinction coefficient.) Absorbance divided by the product of the concentration of the substance and the sample path length,

$$a = \frac{A}{bc}$$

Absorptivity, Molar, ϵ (not molar absorbancy index, molar extinction coefficient, or molar absorption coefficient). Product of the absorptivity, a, and the molecular weight of the substance.

Angstrom, Å. Unit of length equal to 1/6438.4696 of wavelength of red line of Cd. For practical purposes, it is considered equal to 10^{-8} cm.

Beer's Law (representing Beer–Lambert law). Absorptivity of a substance is a constant with respect to changes in concentration.

Concentration, c. Quantity of the substance contained in a unit quantity of sample. (In absorption spectrometry it is usually expressed in grams per liter.)

Frequency. Number of cycles per unit time.

Infrared. The region of the electromagnetic spectrum extending from approximately 0.78 to 300 μm.

Micrometer, μm. Unit of length equal to 10^{-6} m. (Do not use micron.)

Nanometer, nm. Unit of length equal to 10^{-9} m. (Do not use millimicron.)

Sample Path Length, b (not l or d). Internal cell or sample length, usually given in centimeters.

Spectrograph. Instrument with an entrance slit and dispersing device that uses photography to obtain a record of spectral range. The radiant power passing through the optical system is integrated over time, and the quantity recorded is a function of radiant energy.

Spectrometer, Optical. Instrument with an entrance slit, a dispersing device, and with one or more exit slits, with which measurements are made at selected wavelengths within the spectral range, or by scanning over the range. The quantity detected is a function of radiant power.

Spectrometry. Branch of physical science treating the measurement of spectra.

Spectrophotometer. Spectrometer with associated equipment, so that it furnishes the ratio, or a function of the ratio, of the radiant power of two beams as a function of spectral wavelength. These two beams may be separated in time, space, or both.

Transmittance, T (not transmittancy or transmission). The ratio of the radiant power transmitted by a sample to the radiant power incident on the sample.

Ultraviolet. The region of the electromagnetic spectrum from approximately 10 to 380 nm. The term without further qualification usually refers to the region from 200 to 380 nm.

Visible. Pertaining to radiant energy in the electromagnetic spectral range visible to the human eye (approximately 380 to 780 nm).

Wavelength (one word). The distance, measured along the line of propagation, between two points that are in phase on adjacent waves—units Å, μm, and nm.

Wavenumber (one word). Number of waves per unit length. The usual unit of wavenumber is the reciprocal centimeter, cm^{-1}. In terms of this unit, the wavenumber is the reciprocal of the wavelength when the latter is in centimeters in vacuo.

SI Units

The move toward the usage of the International System of Units (SI) has been agreed to by ACS editors as general ACS policy. Although, in principle, the change to strict SI usage is desirable, necessary adjustments dictated by practical reality must be considered. This guide gives authors an idea of what exceptions are acceptable in articles published in ANALYTICAL CHEMISTRY. Also included are the SI base units, derived units, and prefixes. Units that are not compatible with SI or the acceptable exceptions, but which must be used in a manuscript, should be followed by the SI equivalent in parentheses, e.g., 1-in. (2.5 cm) tubing *or* 1-in. (2.54 cm) tubing. The number in the SI equivalent should include only as many digits as are significant for any particular use.

SI Base Units

Length	meter	m
Mass	kilogram	kg
Time	second	s
Electric current	ampere	A
Thermodynamic temperature	kelvin	K
Amount of substance	mole	mol
Luminous intensity	candela	cd

(supplementary units)

Plane angle	radian	rad
Solid angle	steradian	sr

SI Derived Units

Area	square meter	m^2
Concentration	mole per cubic meter	mol/m^3
Density	kilogram per cubic meter	kg/m^3
Velocity	meter per second	m/s
Volume	cubic meter	m^3
Wavenumber	1 per meter	m^{-1}

(with special names)

Capacitance	farad	F
Conductance	siemens	S
Electric charge, quantity of electricity	coulomb	C
Electric potential, potential difference, electromotive force	volt	V
Energy, work, quantity of heat	joule	J
Force	newton	N
Frequency	hertz	Hz
Illuminance	lux	lx
Inductance	henry	H
Luminous flow	lumen	lm
Magnetic flux	weber	Wb
Magnetic flux density	tesla	T
Power	watt	W
Pressure	pascal	Pa
Radioactive activity	becquerel	Bq
Resistance	ohm	Ω

SI Prefixes

10^{18}	exa	E
10^{15}	peta	P
10^{12}	tera	T
10^{9}	giga	G
10^{6}	mega	M
10^{3}	kilo	k
10^{2}	hecto	h
10^{1}	deka	da
10^{-1}	deci	d
10^{-2}	centi	c
10^{-3}	milli	m
10^{-6}	micro	μ
10^{-9}	nano	n
10^{-12}	pico	p
10^{-15}	femto	f
10^{-18}	atto	a

Acceptable Exceptions

Area	barn
Concentration	molal = mole per kilogram (m = mol kg^{-1}) molar = mole per liter (M = mol L^{-1}); *not* formal or normal
Conductance	mho (Ω^{-1})
Density	gram per cubic centimeter (g/cm^3)
Energy	electronvolt (eV); also keV, MeV
Length	angstrom (Å)
Plane angle	degree (°), minute (′), second (″)
Pressure	atmosphere (atm), bar, torr
Radioactivity of radionuclides	disintegrations per second (dps)
Second-order rate constants	1 per (mole per liter) per second (M^{-1} s^{-1})
Temperature	degree Celsius (°C)
Time	minute (min), hour (h), day (d), etc.
Volume	liter (L), milliliter (mL), microliter (μL)
Wavenumber	1 per centimeter (cm^{-1})

COPYRIGHT STATUS FORM

Name of American Chemical Society Publication

Author(s)

Ms No.

Ms Title

Received

This manuscript will be considered with the understanding you have submitted it on an exclusive basis. You will be notified of a decision as soon as possible.

Print or
Type
Author's
Name and
Address

[THIS FORM MAY
BE REPRODUCED]

COPYRIGHT TRANSFER

The undersigned, with the consent of all authors, hereby transfers, to the extent that there is copyright to be transferred, the exclusive copyright interest in the above cited manuscript (subsequently referred to as the "work") to the **American Chemical Society** subject to the following (Note: if the manuscript is not accepted by ACS or if it is withdrawn prior to acceptance by ACS, this transfer will be null and void and the form will be returned.):

A. The undersigned author and all coauthors retain the right to revise, adapt, prepare derivative works, present orally, or distribute the work provided that all such use is for the personal noncommercial benefit of the author(s) and is consistent with any prior contractual agreement between the undersigned and/or coauthors and their employer(s).

B. In all instances where the work is prepared as a "work made for hire" for an employer, the employer(s) of the author(s) retain(s) the right to revise, adapt, prepare derivative works, publish, reprint, reproduce, and distribute the work provided that all such use is for the promotion of its business enterprise and does not imply the endorsement of the American Chemical Society.

C. Whenever the American Chemical Society is approached by third parties for individual permission to use, reprint, or republish specified articles (except for classroom use, library reserve, or to reprint in a collective work) the undersigned author's or employer's permission will also be required.

D. No proprietary right other than copyright is claimed by the American Chemical Society.

E. For works prepared under U.S. Government contract or by employees of a foreign government or its instrumentalities, the American Chemical Society recognizes that government's prior nonexclusive, royalty-free license to publish, translate, reproduce, use, or dispose of the published form of the work, or allow others to do so for noncommercial government purposes. State contract number: ____________________.

SIGN HERE FOR COPYRIGHT TRANSFER [Individual Author or Employer's Authorized Agent (work made for hire)]

Print Author's Name

Print Agent's Name and Title

Original Signature of Author on Behalf of All Authors (in Ink)

Date

Original Signature of Agent (in Ink)

CERTIFICATION AS A WORK OF THE U.S. GOVERNMENT

This is to certify that **ALL** authors are or were bona fide officers or employees of the U.S. Government at the time the paper was prepared, and that the work is a "work of the U.S. Government" (prepared by an officer or employee of the U.S. Government as a part of official duties), and, therefore, it is not subject to U.S. copyright. (This section should NOT be signed if the work was prepared under a government contract or coauthored by a non-U.S. Government employee.)

INDIVIDUAL AUTHOR **OR** AGENCY REPRESENTATIVE

Print Author's Name

Print Agency Representative's Name and Title

Original Signature of Author (in Ink)

Date

Original Signature of Agency Representative (in Ink)

FOREIGN COPYRIGHT RESERVED (NOTE: If your government permits copyright to be transferred, refer to section E and sign this form in the top section.)

☐ If **ALL** authors are employees of a foreign government that reserves its own copyright as mandated by national law, **DO NOT SIGN THIS FORM. Please check this box as your request for the FOREIGN GOVERNMENT COPYRIGHT FORM (Blue Form) which you will be required to sign. If you check this box,** mail this form to: Copyright Administrator, Books and Journals Division, American Chemical Society, 1155 Sixteenth Street, N.W., Washington, D.C. 20036, U.S.A.

AUTHOR INDEX

Admasu, A., 30
Ando, T., 111
Aparicio-Razo, M., 118

Bhat, R., 58
Birks, L. S., 77
Blakley, C. R., 2
Bohn, P. W., 58
Buckhold, D. K., 62
Bush, I. E., 91

Cantillo, A. Y., 33
Chandravanshi, B. S., 30
Chang, T. T., 109
Chen, P.-Y., 80
Chen, T. I., 19
Christian, G. D., 120
Crow, F. W., 8

Dasgupta, P. K., 96, 103
Demas, J. N., 82

Eldan, M., 43
Epstein, B. D., 21
Epstein, M. S., 122

Fan, T. P., 2
Filer, T. D., 113
Fitzgerald, R. V., 62
Francel, R. J., 109

Galuska, A. A., 74
Gilbert, R., 106
Gilfrich, J. V., 77
Goldbart, Z., 37, 43
Gordon, G., 71
Greeley, H. P., 91
Gross, M. L., 8

Hara, S., 24
Hardin, E. D., 2
Harnly, J. M., 48
Harris, T. D., 58
Helz, G. R., 33

Ichikawa, K., 111
Ikeda, Y., 71
Irimajiri, S., 24

Jenke, D. R., 85, 88

Kane, J. S., 48
Kono, M., 24
Kuwabara, H., 14

Lay, J. O., Jr., 109
Lippstreu, D. L., 8
Lorber, A., 37, 43
Love, J. C., 82
Lyon, P. A., 8

Matsuoka, Y., 24
McNabb, G. J., 113
Messman, J. D., 122
Minagawa, K., 24
Mok, W. M., 27
Morris, M. D., 19
Morrison, G. H., 74

Noguchi, M., 24

O'Dea, J. J., 116
O'Haver, T. C., 122
Oka, K., 24
Osteryoung, J., 116
Otsuka, K., 111

Pagenkopf, G. K., 85, 88
Peterson, J. I., 62
Puphal, K. W., 113
Rains, T. C., 122
Rioux, R., 106
Roe, D. K., 118

Saheb, S. E., 106
Schreiner, M., 116
Shirk, J. S., 80
Sinex, S. A., 33
Sleszynski, N., 116
Stebbings, W. L., 8
Stevenson, J. M., 67
Streckert, H. H., 21
Swaidan, H. M., 120
Swartzfager, D. G., 55

Tang, T.-f., 71
Terabe, S., 111
Tomellini, S. A., 67
Tomer, K. B., 8
Tsuchiya, A., 111
Tsuchiya, M., 14

Vestal, M. L., 2

Wai, C. M., 27
Woodruff, H. B., 67

Future Articles

Preparation of Chlorophylls and Phenophytins by Isocratic Liquid Chromatography
Tadashi Watanabe, Akinori Hongu, Kenichi Honda, Masataka Nakazato, Mitsuo Konno, and Sadao Saitoh

Solvatochromic Investigation of Polarizable Polymeric Liquids
James E. Brady, Dale Bjorkman, Christian D. Herter, and Peter W. Carr

Determination of Dialkyllead, Trialkyllead, Tetraalkyllead, and Lead(II) Compounds in Sediment and Biological Samples
Y. K. Chau, P. T. S. Wong, G. A. Bengert, and J. L. Dunn

Analysis of Hazardous Waste by Fused Silica Capillary Gas Chromatography/Fourier Transform Infrared Spectrometry and Gas Chromatography/Mass Spectrometry
K. H. Shafer, T. L. Hayes, J. W. Brasch, and R. J. Jakobsen

Determination of One-Carbon to Three-Carbon Alcohols and Water in Gasoline/Alcohol Blends by Liquid Chromatography
Mikio Zinbo

Evaluation of a Thermionic Ionization Detector for Nitrated Polycyclic Aromatic Hydrocarbons
Curt M. White, Albert Robbat, Jr., and Randall M. Hoes

Nonreactive Coadsorption of Solutes on a Sampling Adsorbent
Karen J. Hyver and Jon F. Parcher

Characterization and Determination of Formaldehyde Oligomers by Capillary Column Gas Chromatography
David F. Utterback, David S. Millington, and Avram Gold

Multiple Peak Formation in Reversed-Phase Liquid Chromatography of Papain
S. A. Cohen, K. P. Benedek, Shannian Dong, Yitzhak Tapuhi, and B. L. Karger

Laser-Induced Fluorescence of Flowing Samples as an Approach to Single-Molecule Detection in Liquids
Norman J. Dovichi, John C. Martin, James H. Jett, Mitchell Trkula, and Richard A. Keller

Characterization of Electrochemically Pretreated Glassy Carbon Electrodes
Royce C. Engstrom and Vernon A. Strasser

Pulsed Thermal Atom Source for Resonance Ionization Mass Spectrometry
J. D. Fassett, L. J. Moore, R. W. Shideler, and J. C. Travis

Stability and Chaos in a Voltage-Thresholded High-Voltage Spark Source
Billy R. Hardas and Alexander Scheeline

Weighs and means.

sartorius
1.1602 g
Now
$1,995

Priced so low even the budget committee will love it!

Sartorius Series 1600 electronic analytical balances for as little as $2,195.

It's time to change your old mechanical weighs for the new electronic weighs—Sartorius Series 1600 Analytical Balances with advanced high-technology electronics. And planning the 1984 budget will be easier on everyone because you're getting so much for so little: 0.2-second update speed, expanded weighing capacities, widest stability range, one-button control of balance functions, and virtually no downtime or maintenance.

Figure out for yourself just how affordable the new electronic weighs are. With the expanding use of electronic balances in industry and research, you can't afford not to.

For more information or a demonstration, call or write:
Brinkmann Instruments Co., Division of Sybron Corporation,
Cantiague Road, Westbury, NY 11590 • Tel: 800-645-3050,
in New York: 516-334-7500.

Sartorius electronic
weighing systems
Brinkmann

SYBRON

BRK 5011

CIRCLE 30 ON READER SERVICE CARD